

Slide sets of team meeting at Fudan University

From 2016-2020 (7 terms)
Zhou Ying

Preface

This slide set primarily consists of slides used during team meetings at Fudan University. They are included here to showcase the progress made in reading, thinking, and studying at this stage. The slides are organized by term and timeline. During this period of study, I participated in two projects. The first project focused on the study of stem cells in the cortex gyri of developmental ferrets, which is reflected in the first four sets of slides. The second project involved the classification of interneurons and is represented in the last three sets of slides. Through the first project, I acquired a foundational understanding of brain development, including concepts such as neural progenitors and the cellular organization of the cerebral cortex, as well as various wet experimental techniques. Additionally, during the second project, I gained a deeper comprehension of the complexity of neurons in the brain, as well as familiarity with data formats related to electrophysiology and morphology, their analysis, and some data mining methods. The knowledge and skills I acquired during this stage have provided a solid foundation for my future studies. Furthermore, the second project has been [published](#) and summarized on a [poster](#). Although the first project took more time and is currently under submission, a poster related to my work is available [here](#). **For easy navigation, all slides are listed in the 'Contents' page, with clickable links directing to the corresponding slide covers.**

Content

Sep. 2016-Feb.2017

**Study on stem cell in the cortex
gyri of developmental ferret**

Zhou Ying
18th Jan. 2017

2024/4/7

4

Mar. 2017-Jul.2017

**Study on stem cell in the cortex
gyri of developmental ferret**

Zhou Ying
16th Jul. 2017

2024/4/7

28

Feb. 2018-Jul.2018

**Study on stem cell in the cortex
gyri of developmental ferret**

Zhou Ying
23rd Jul. 2018

2024/4/7

90

Sep. 2018-Dec.2018

Interneuron Classification

Zhou Ying
18th Dec. 2018

2024/4/7

145

Sep. 2019-Feb.2020

Interneuron Classification

Zhou Ying
2nd Aug. 2019

2024/4/7

184

Sep. 2017-Nov.2017

Data Presentation

Zhou Ying
28th Nov. 2017

2024/4/7

60

Deb. 2019-Jul.2019

Interneuron Classification

Zhou Ying
2nd Aug. 2019

2024/4/7

184

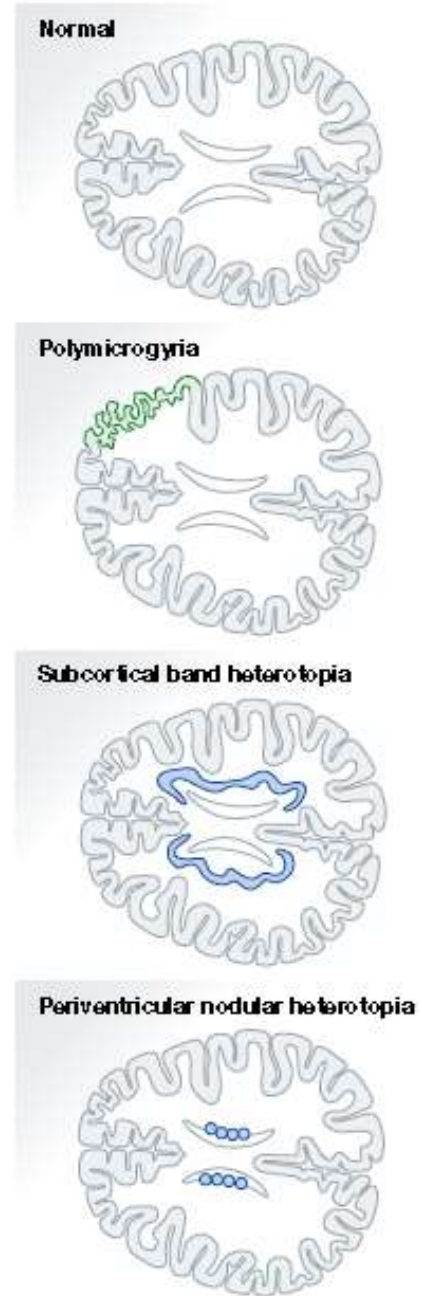
Study on stem cell in the cortex gyri of developmental ferret

Zhou Ying

18th Jan. 2017

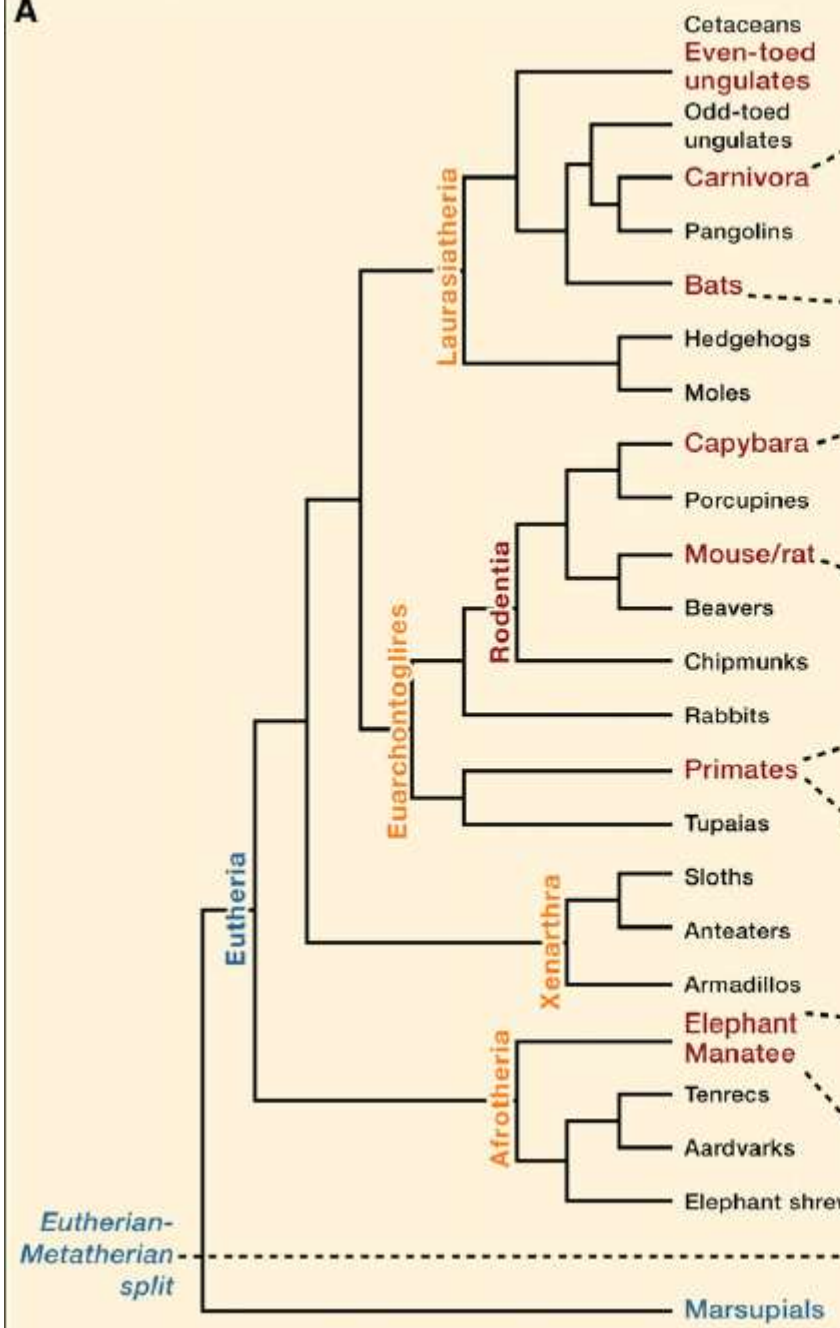
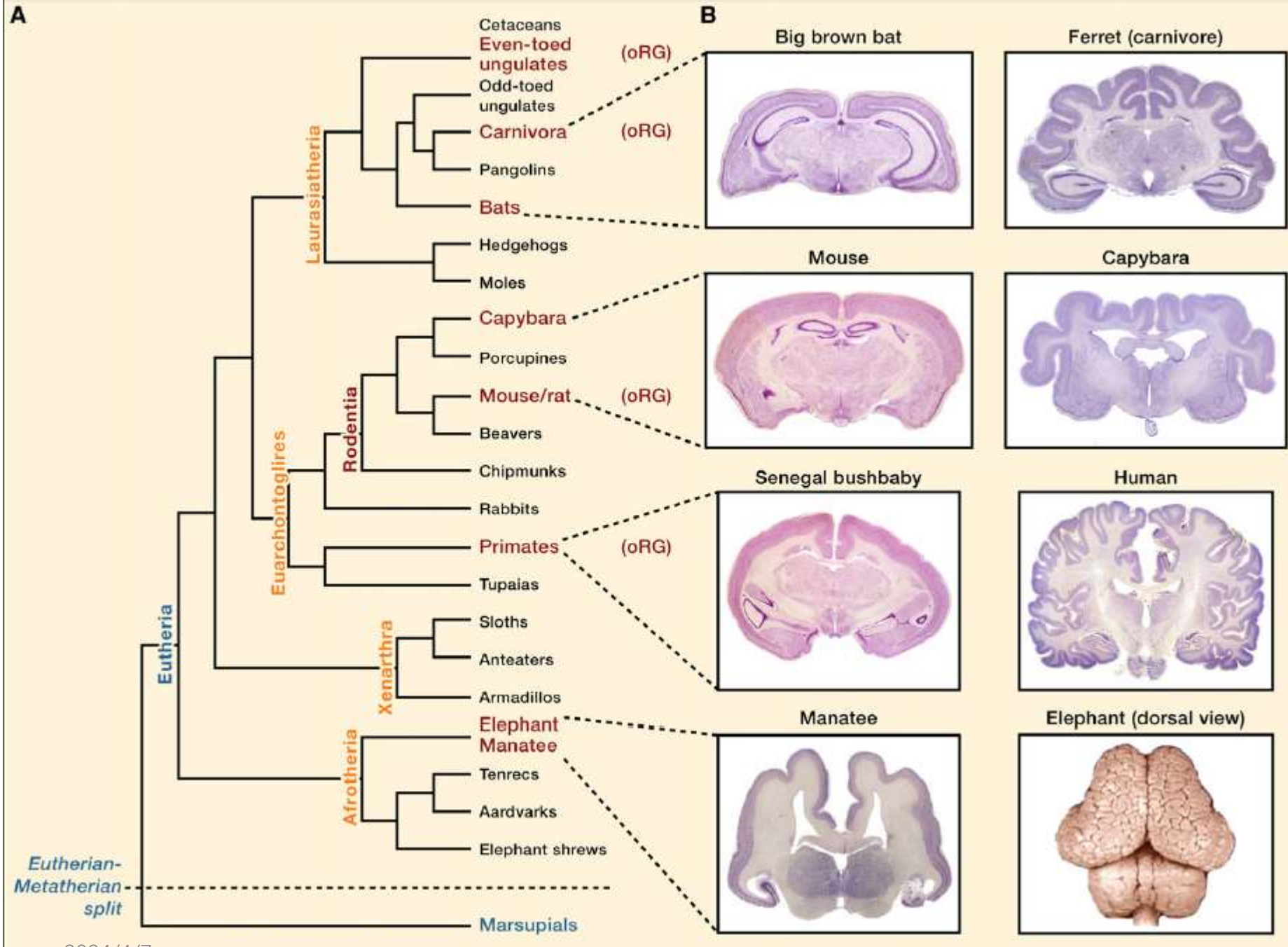
Background

Defects of cortical folding:
human disease



MALFORMATION	SIZE	FOLDING	ECTOPIA
Microcephaly	Reduced	Mild – Normal	No
		Severe – Altered	Yes
Megalencephaly	Increased	Mild – Normal	No
		Severe – Altered	No
Dysplasia	Altered	Increased	Abnormal layers
Lissencephaly type I	Normal	Reduced	Abnormal layers
	Reduced		
Lissencephaly type II Cobblestone	Normal	Increased	Cortical surface
Polymicrogyria	Increased	Increased	Abnormal layers
	Reduced		
Subcortical band heterotopia Double cortex	Reduced	Normal	White matter
Periventricular heterotopia	Normal	Normal	Periventricular
	Reduced		

Virginia et al.(2016)*The EMBO Journal*

A**B**

Liu et al.(2011) Cell

B

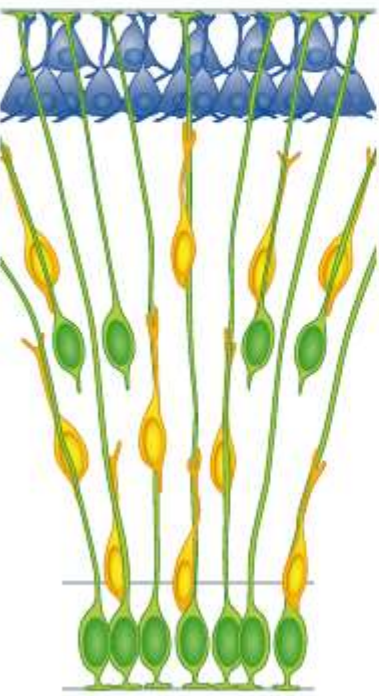
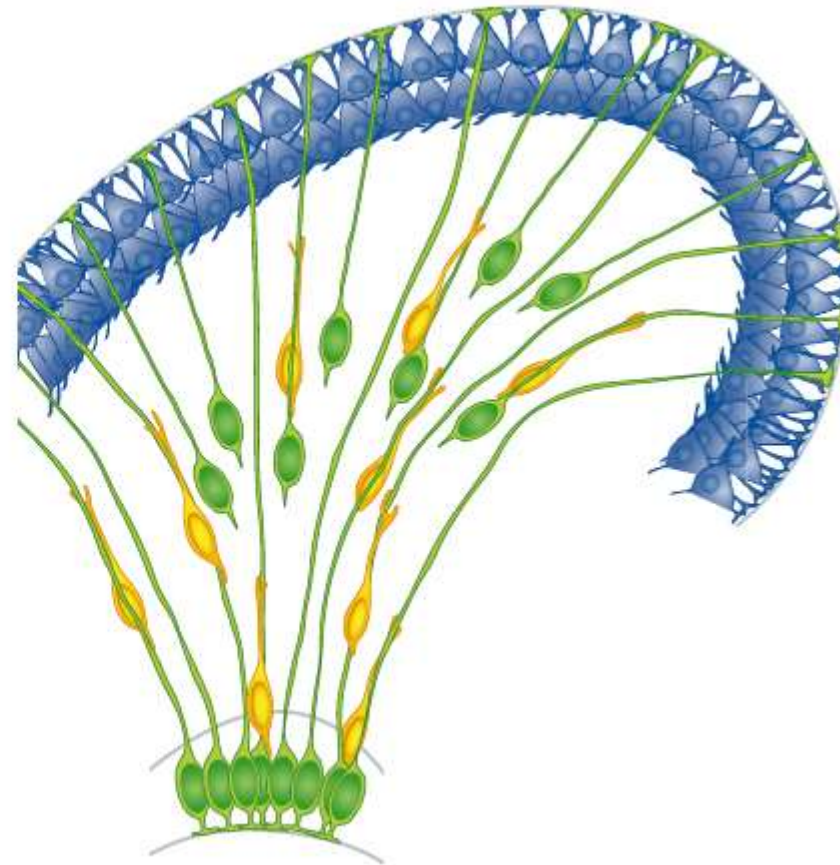


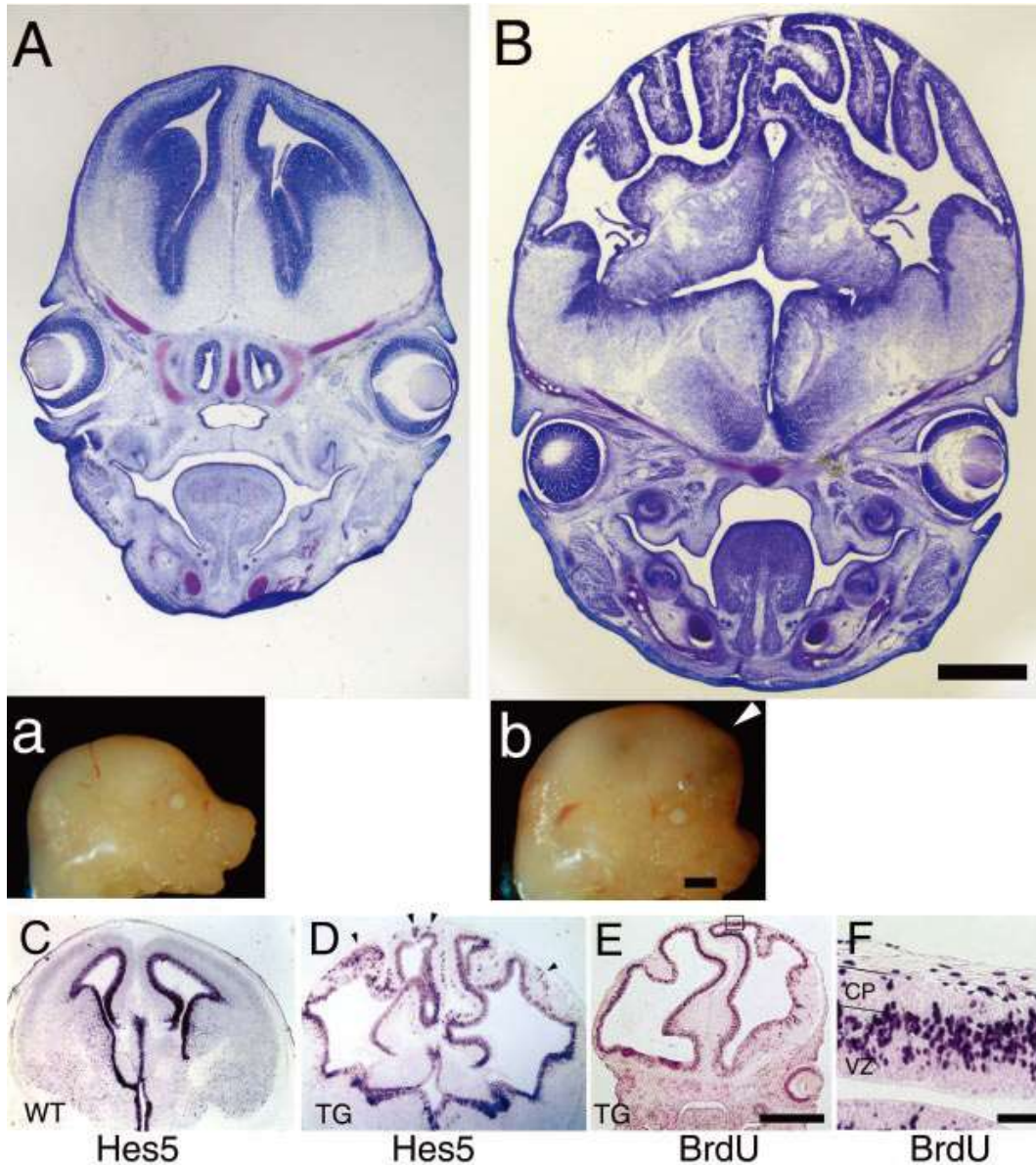
Figure 2.

lissencephalic species



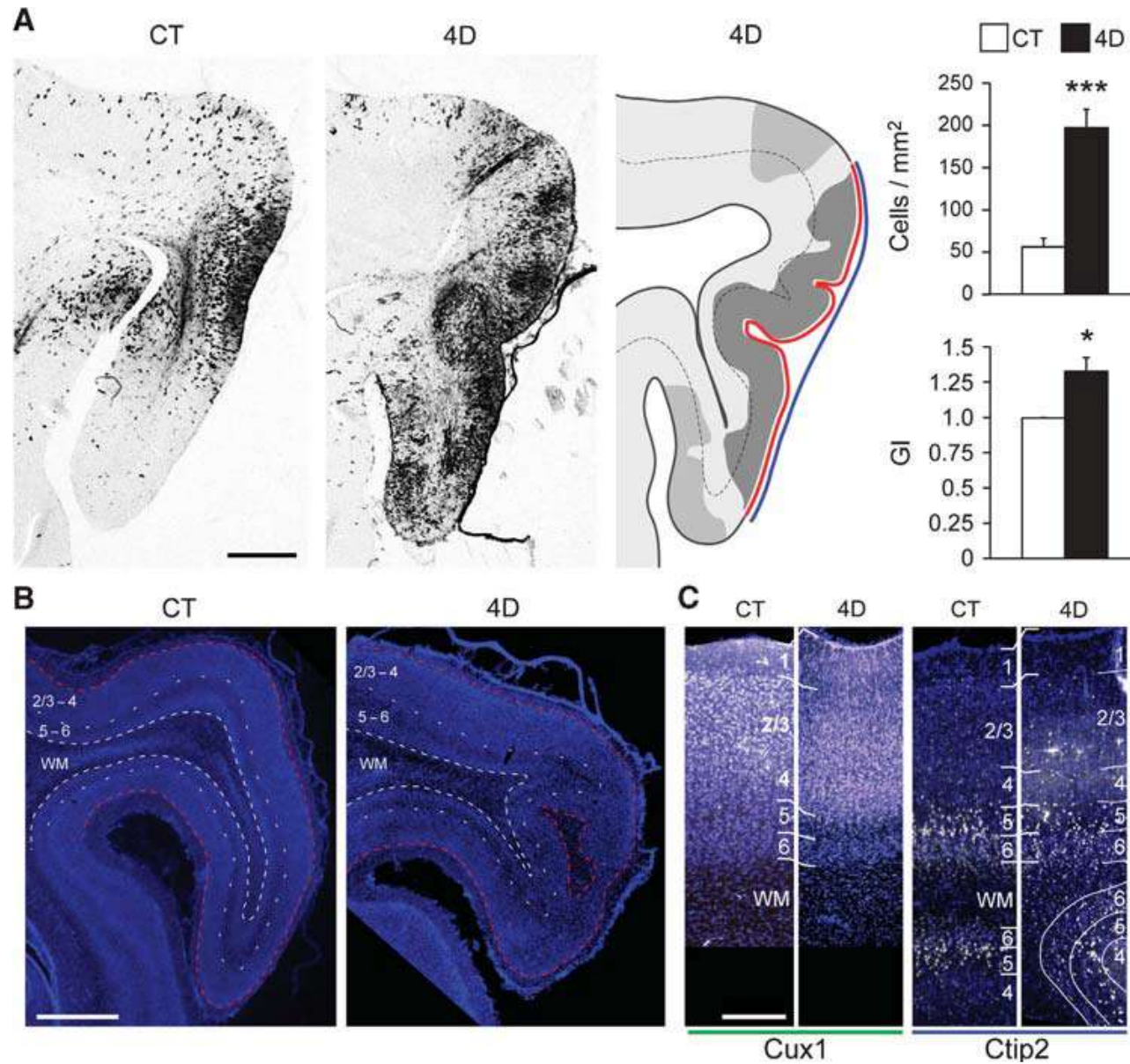
gyrencephalic species

Virginia et al.(2016)The EMBO Journal



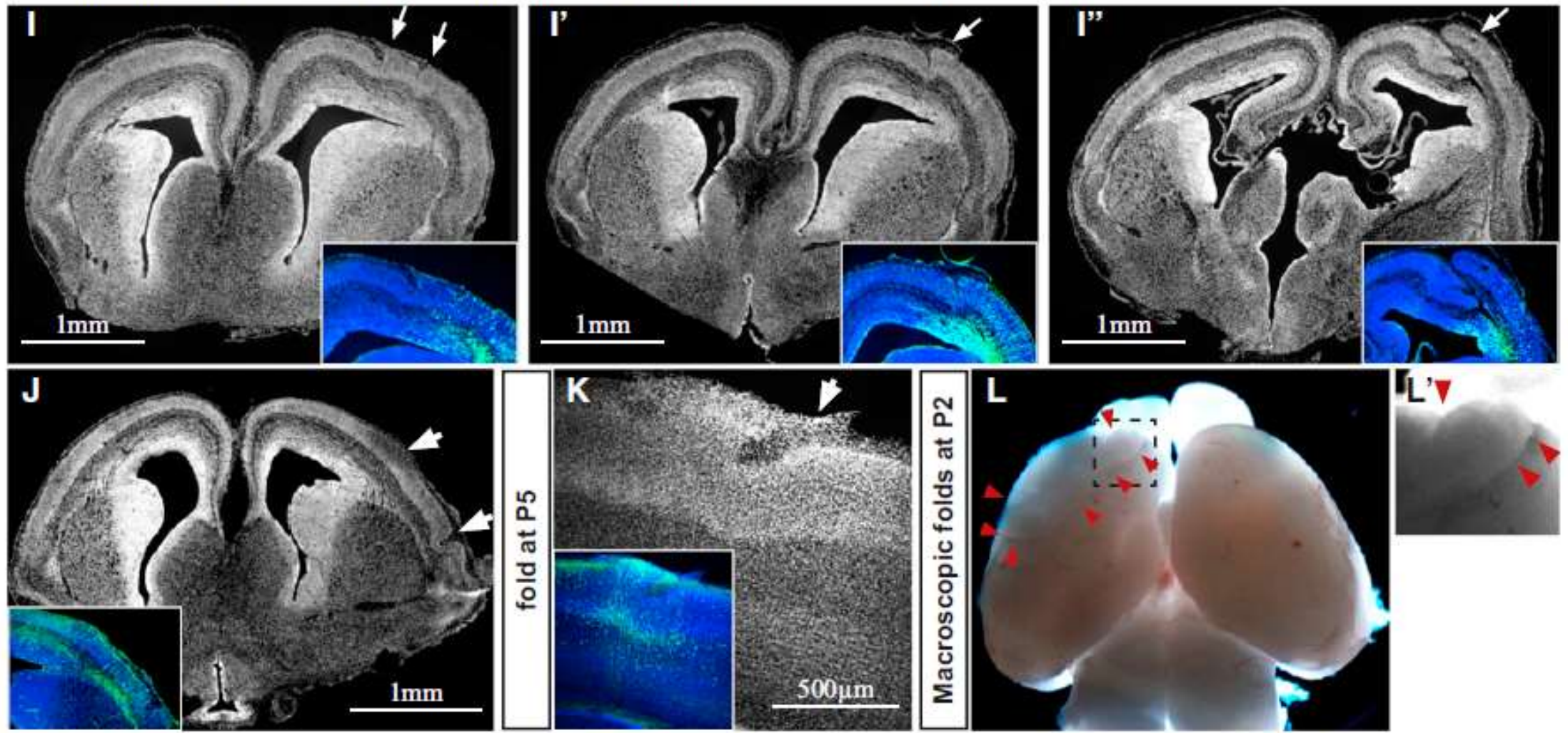
By changing β -catenin,
the cell cycle of transgenic
mice was altered to make
the cortex fold

Anjen Chenn et al.(2002)Science

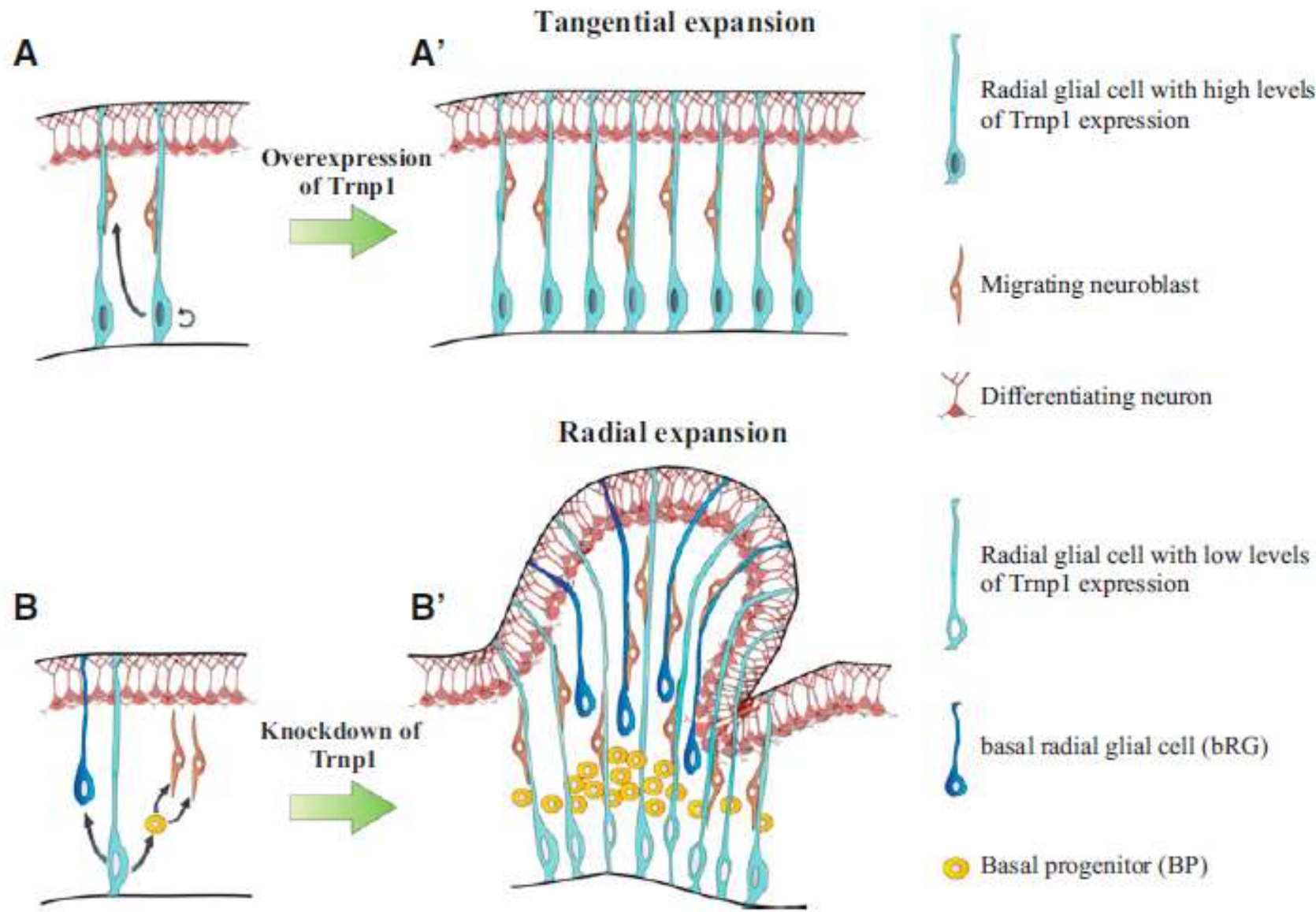


Increasing bRGCs by increasing Cdk4/CyclinD1 resulted in an increase in ferret gyrus

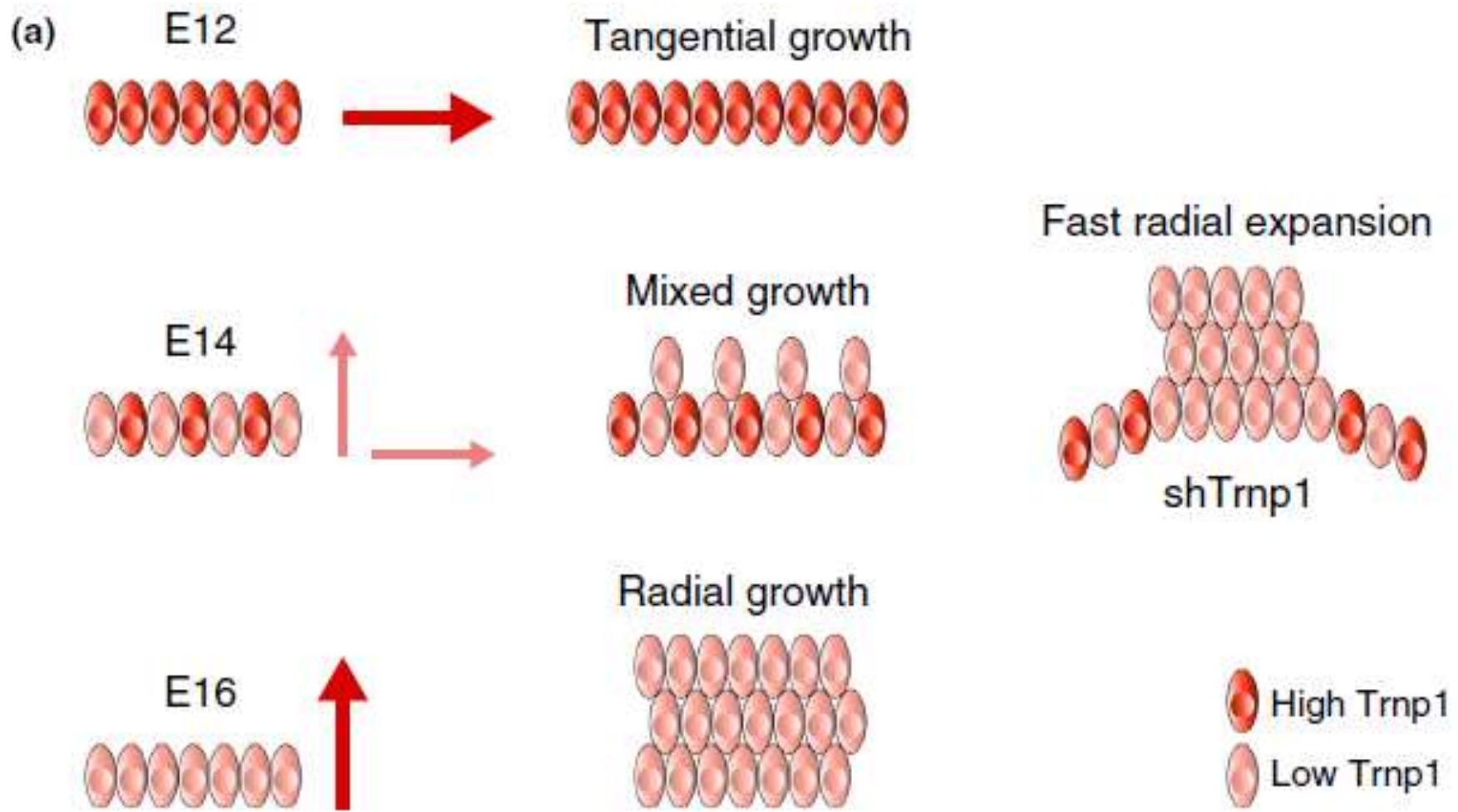
Miki Nonaka-Kinoshita et al.(2013)*The EMBO Journal*



Ronny Stahl et al.(2013)cell

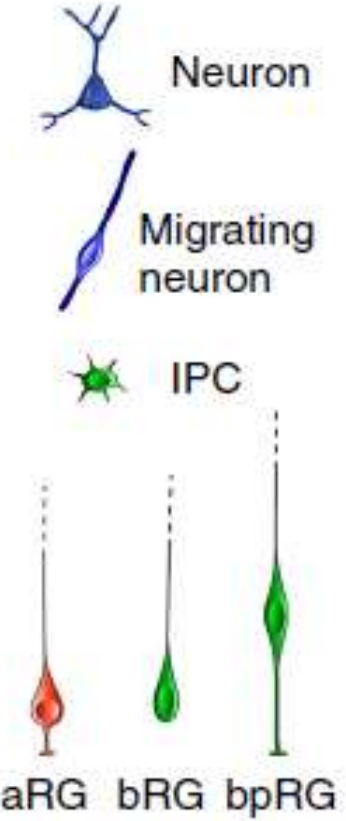
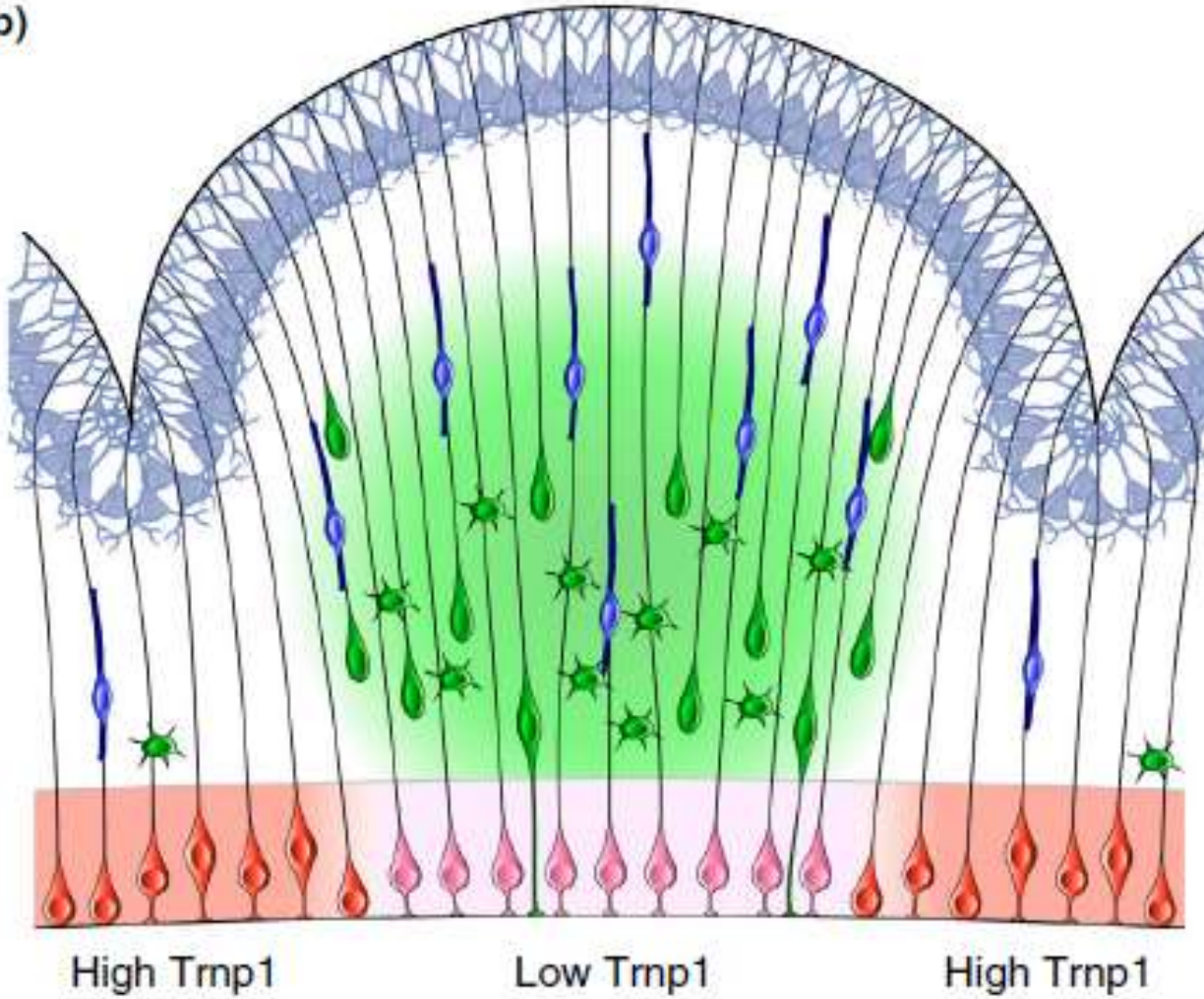


Ronny Stahl et al.(2013)*cell*



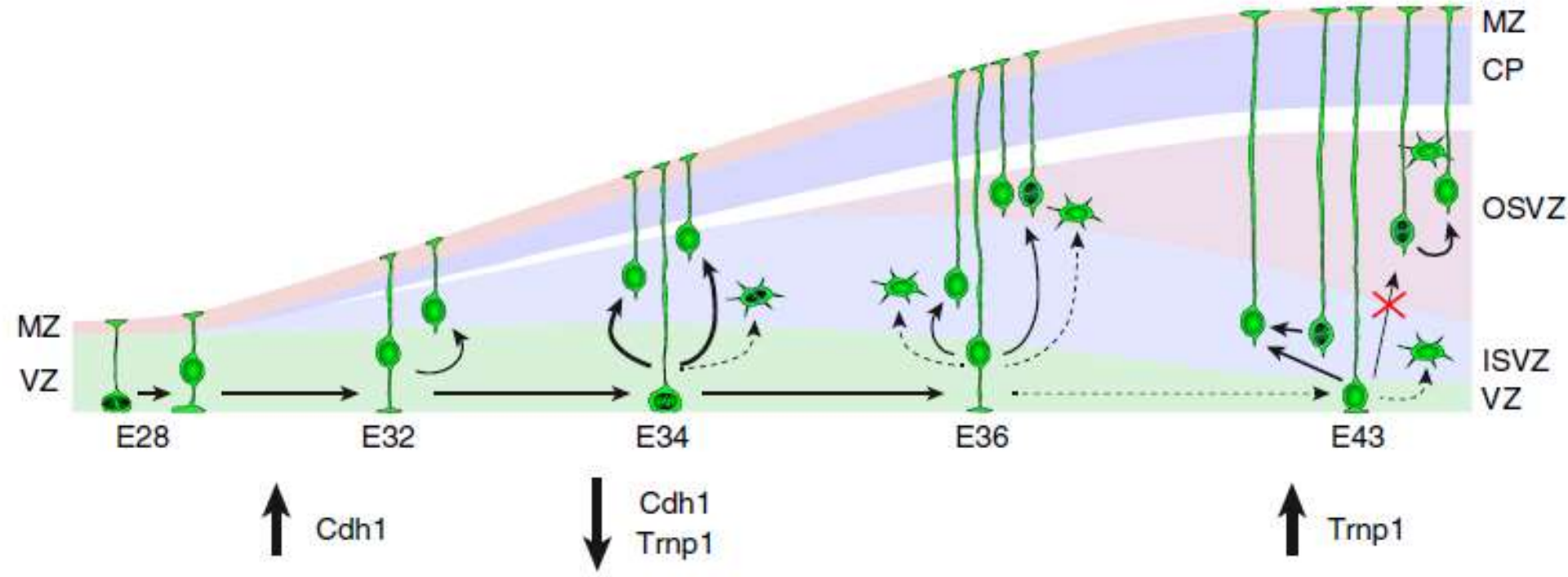
Victor Borrell et al.(2014) *Current Opinion in Neurobiology*

(b)

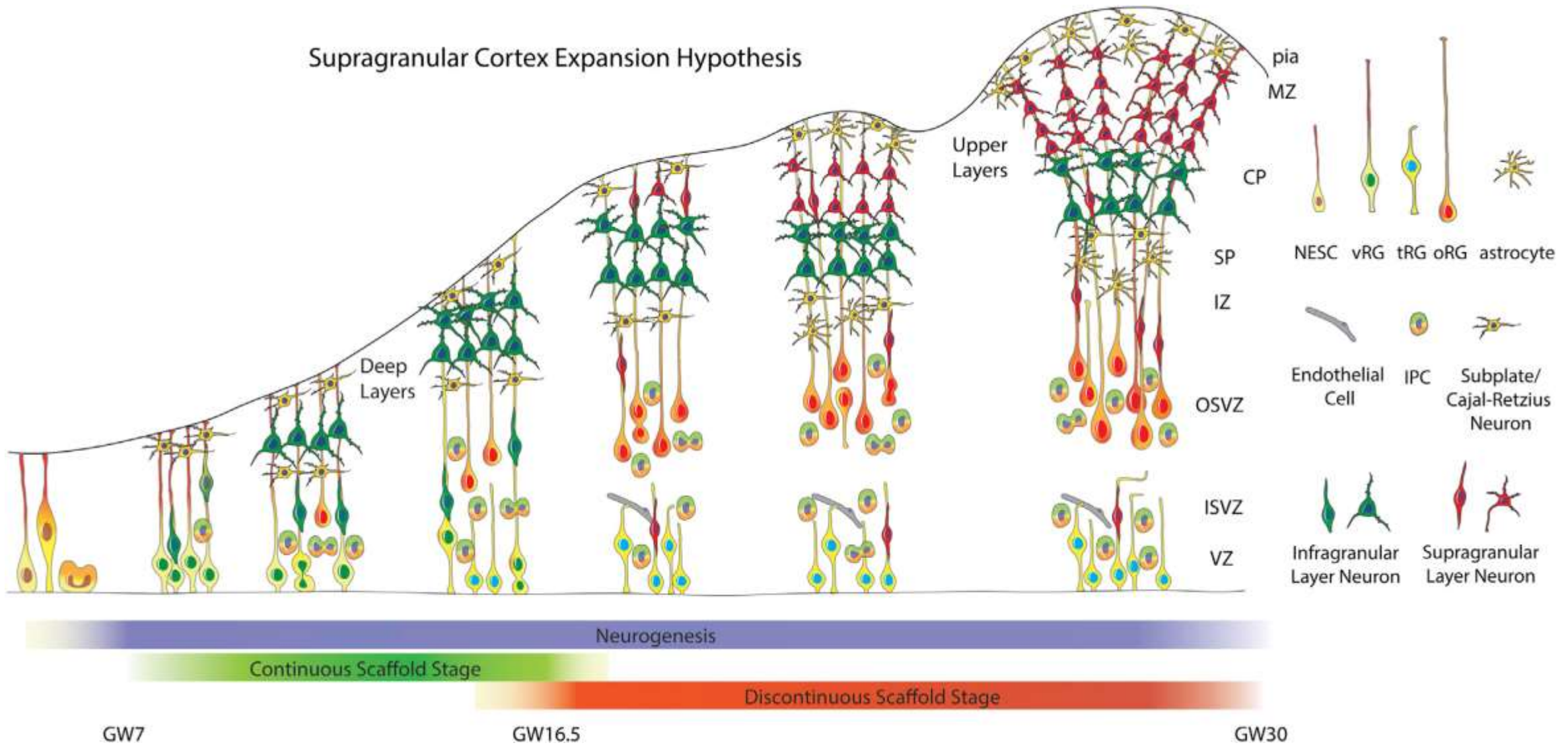


Current Opinion in Neurobiology

Victor Borrell et al.(2014) *Current Opinion in Neurobiology*

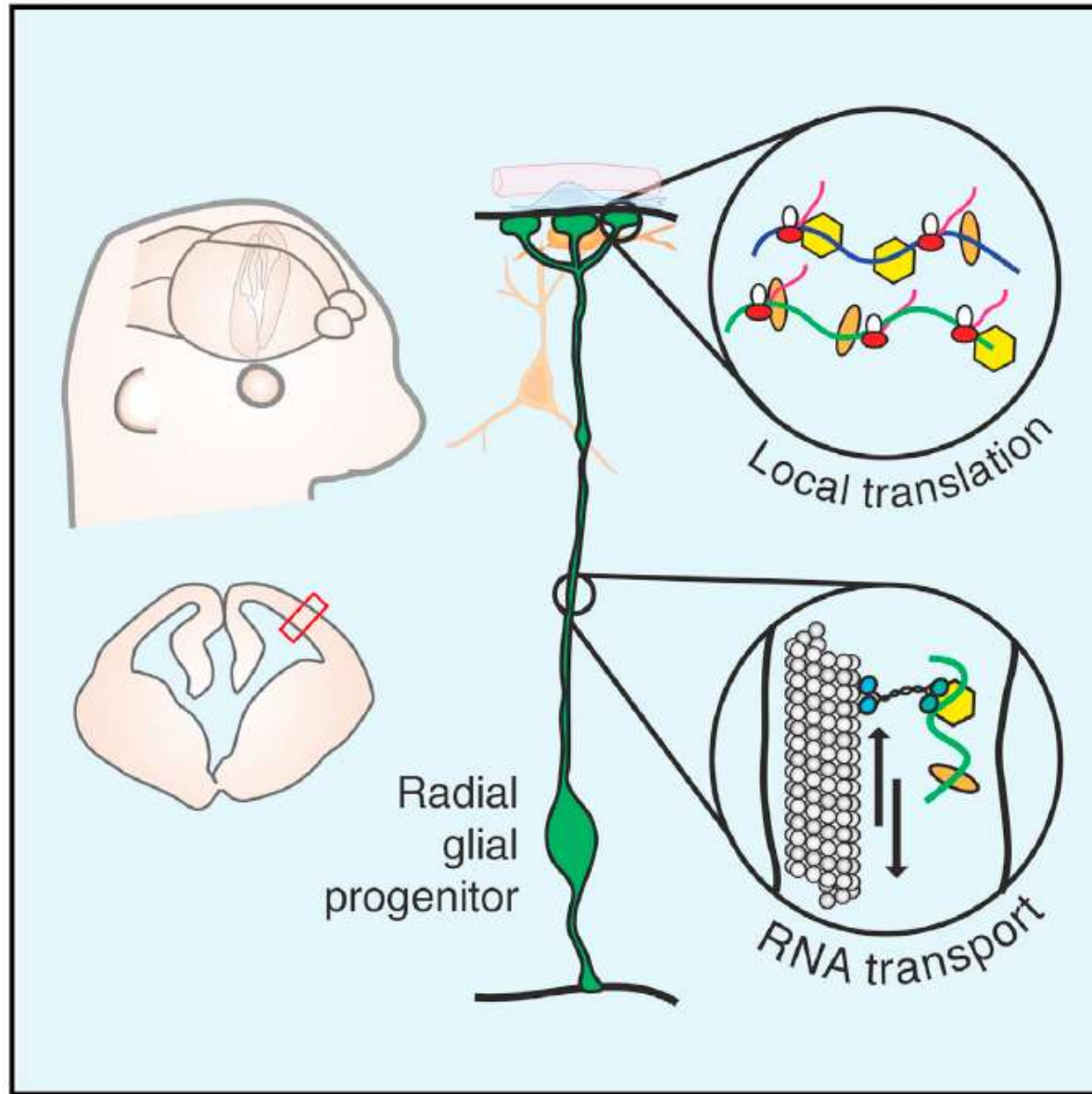


Maria Ángeles Martínez-Martínez et al. (2016) Nature Communications



Tomasz J et al.(2016) *Neuron*

Graphical Abstract



Authors

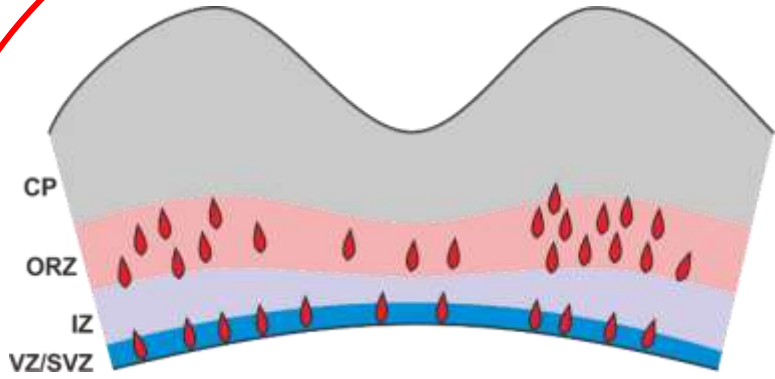
Louis-Jan Pilaz, Ashley L. Lennox,
Jeremy P. Rouanet, Debra L. Silver

Correspondence

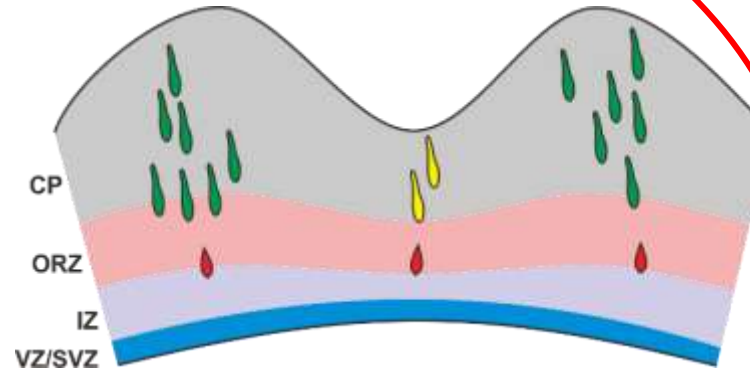
debra.silver@duke.edu

In Brief

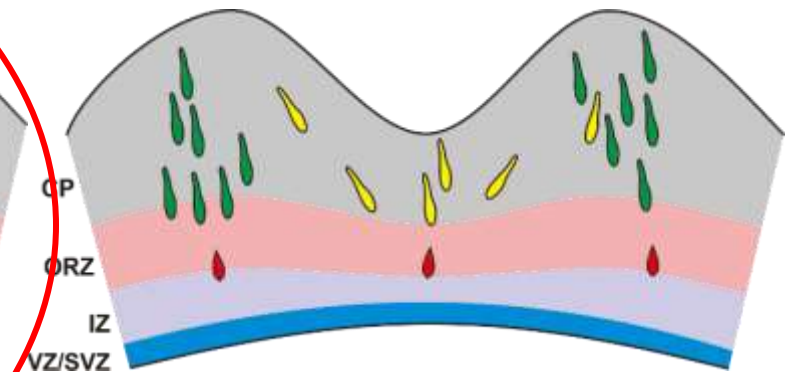
Pilaz et al. use live imaging in mouse embryonic brain tissue to visualize active RNA movement and local translation in radial glia basal processes and distal endfeet. They identify an endfoot FMRP-bound transcriptome enriched for signaling and cytoskeletal regulators. This study exposes dynamic RNA mechanisms in stem cells of the developing brain.



**Hypothesis 1: Differences in
stem cell distribution**



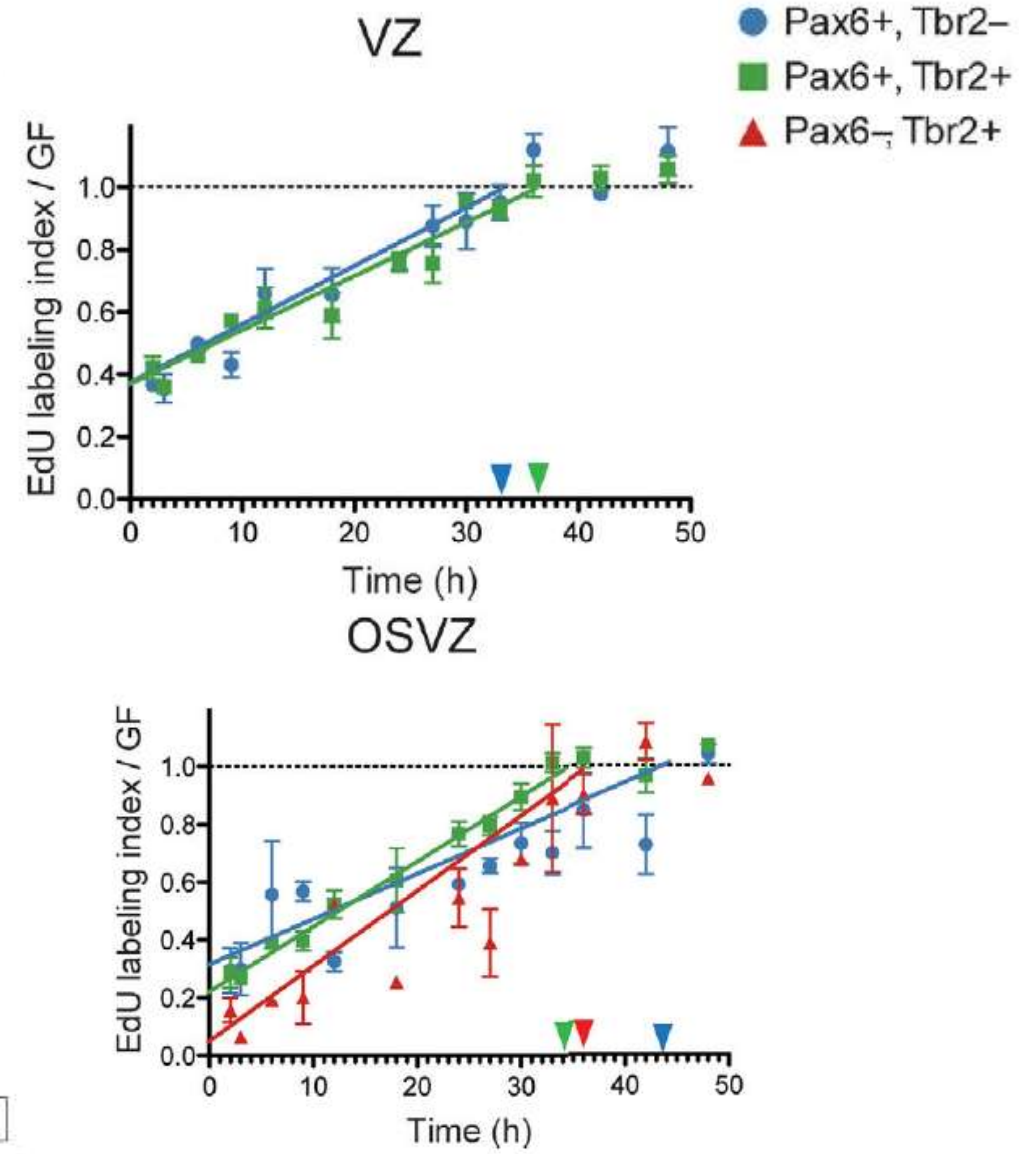
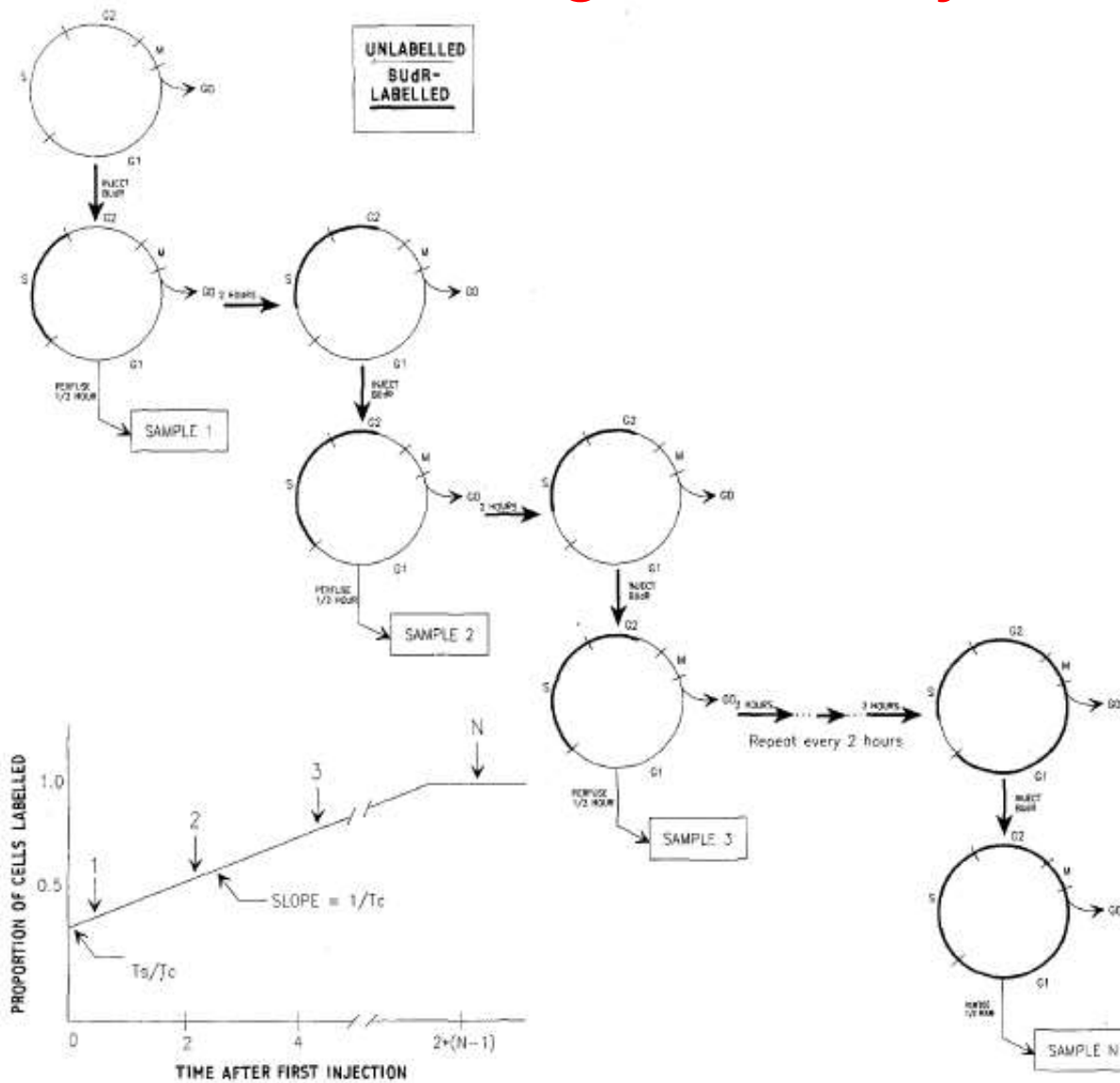
**Hypothesis 2: Differences in
time of cell cycle**



**Hypothesis 3: Differences in
neuronal migration**

目前研究内容

Length of cell cycle estimation



R. S. NOWAKOWSKI et al.(1989) *Journal of Neurocytology*

Differentiation of stem cell types (vRG、oRG、IP)

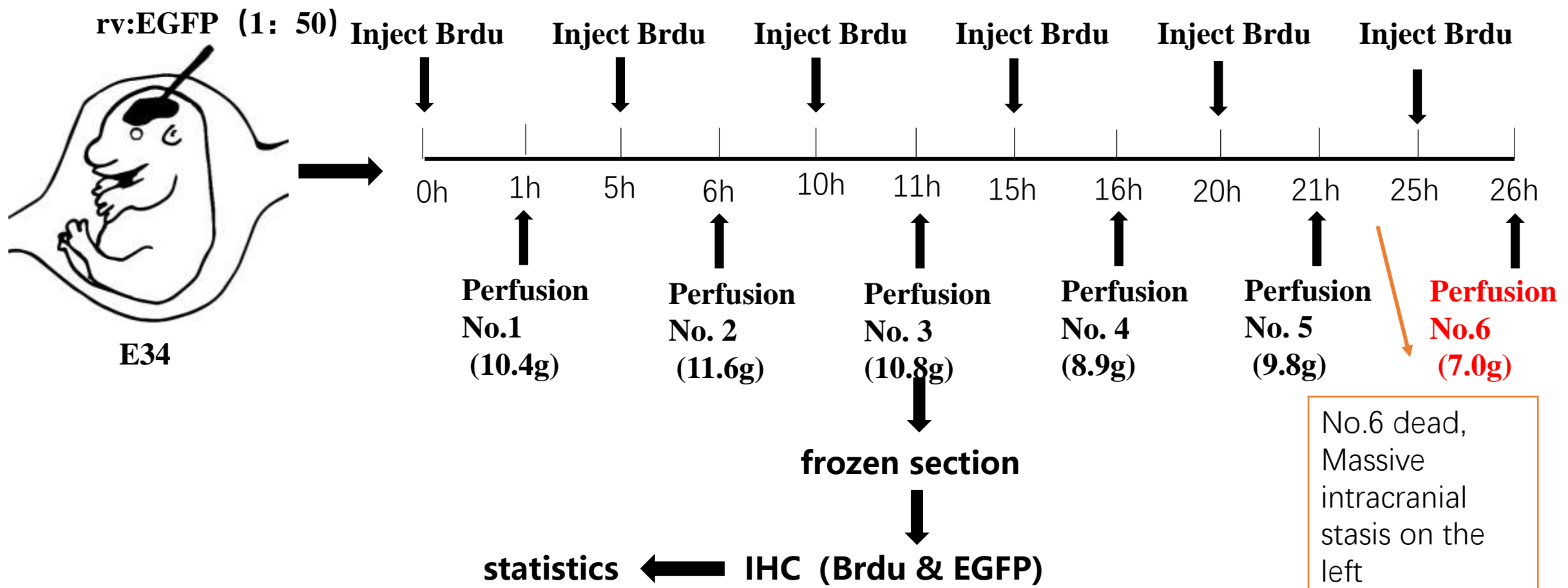
The cell cycle was calculated by statistical analysis

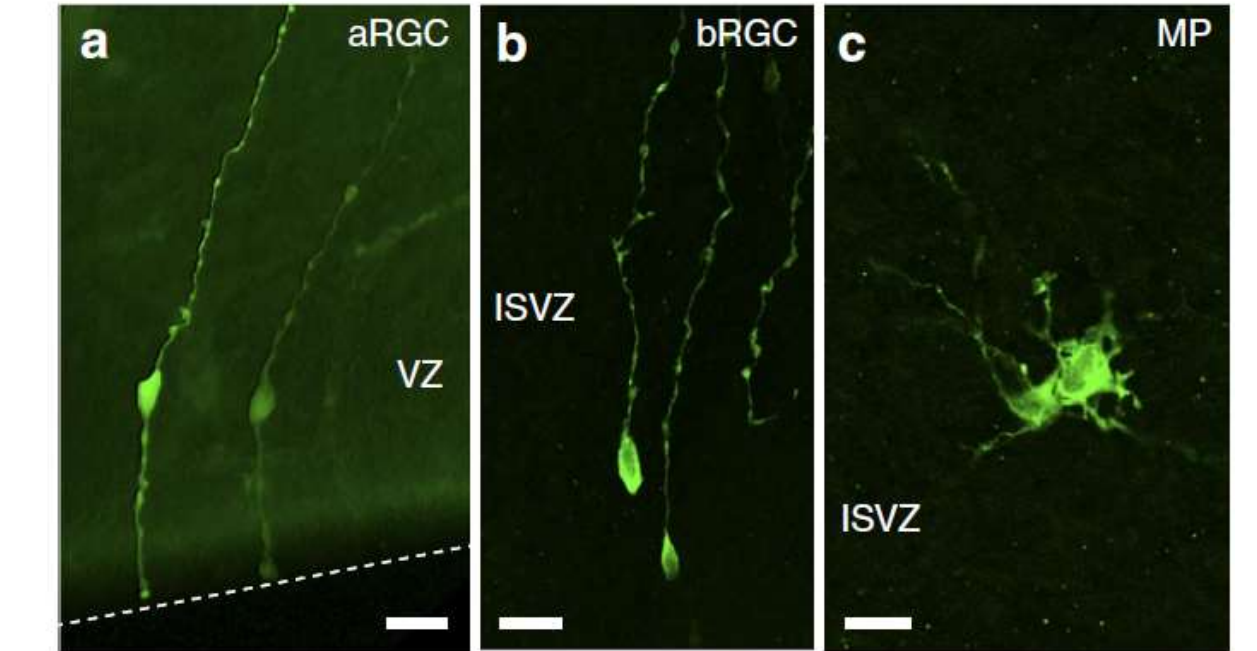
Specific antibodies were used as markers

By virus injection, different types of stem cells were distinguished according to their morphology and location

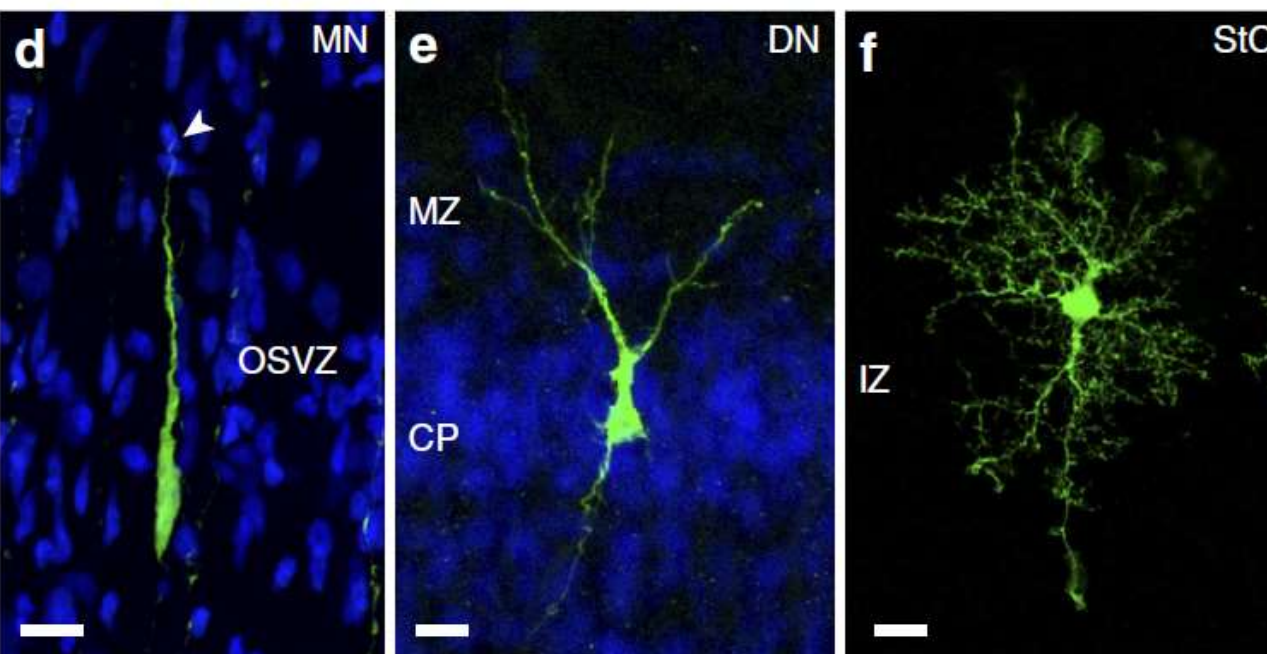


Reasonable gyrus zoning

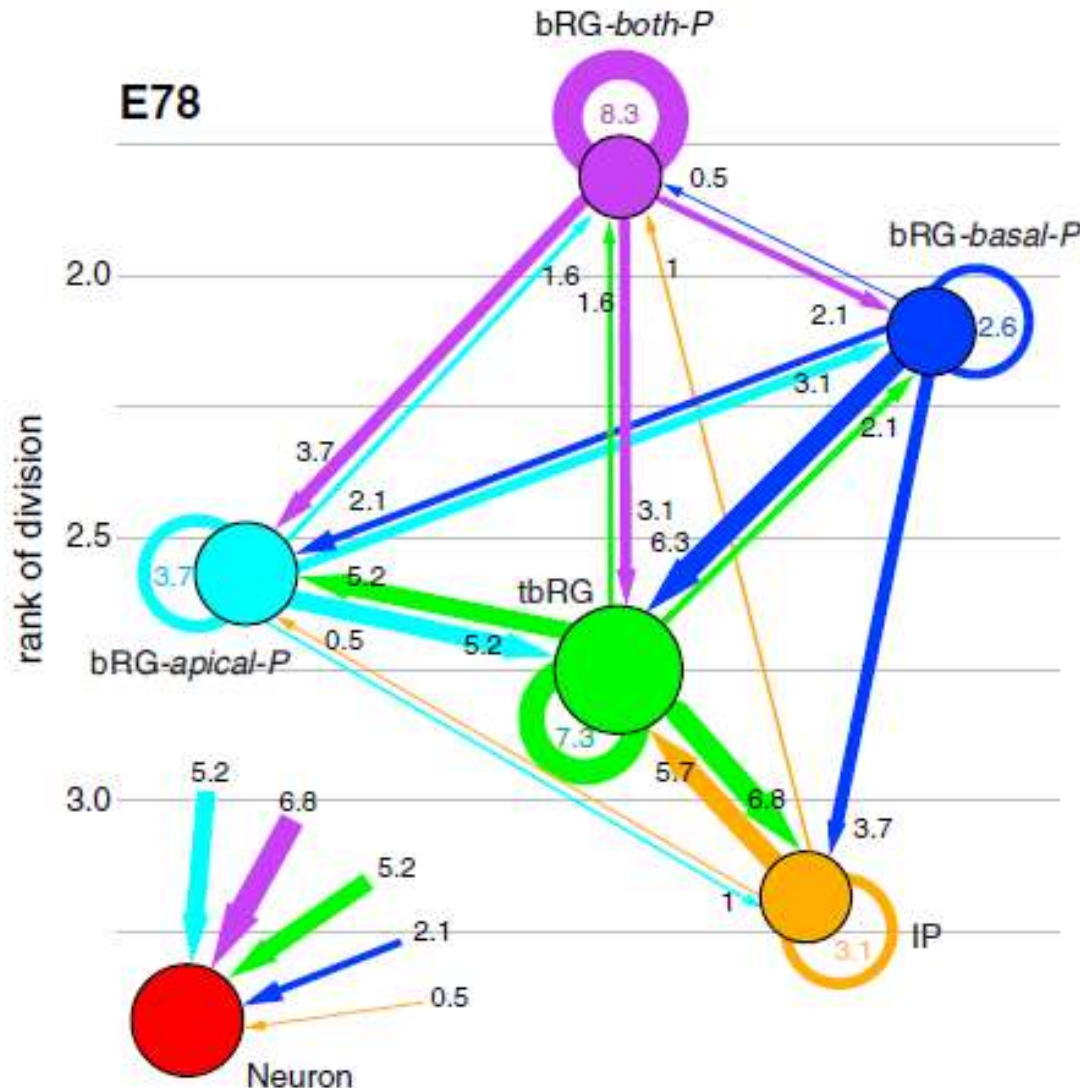




Morphologies of neural cells during development



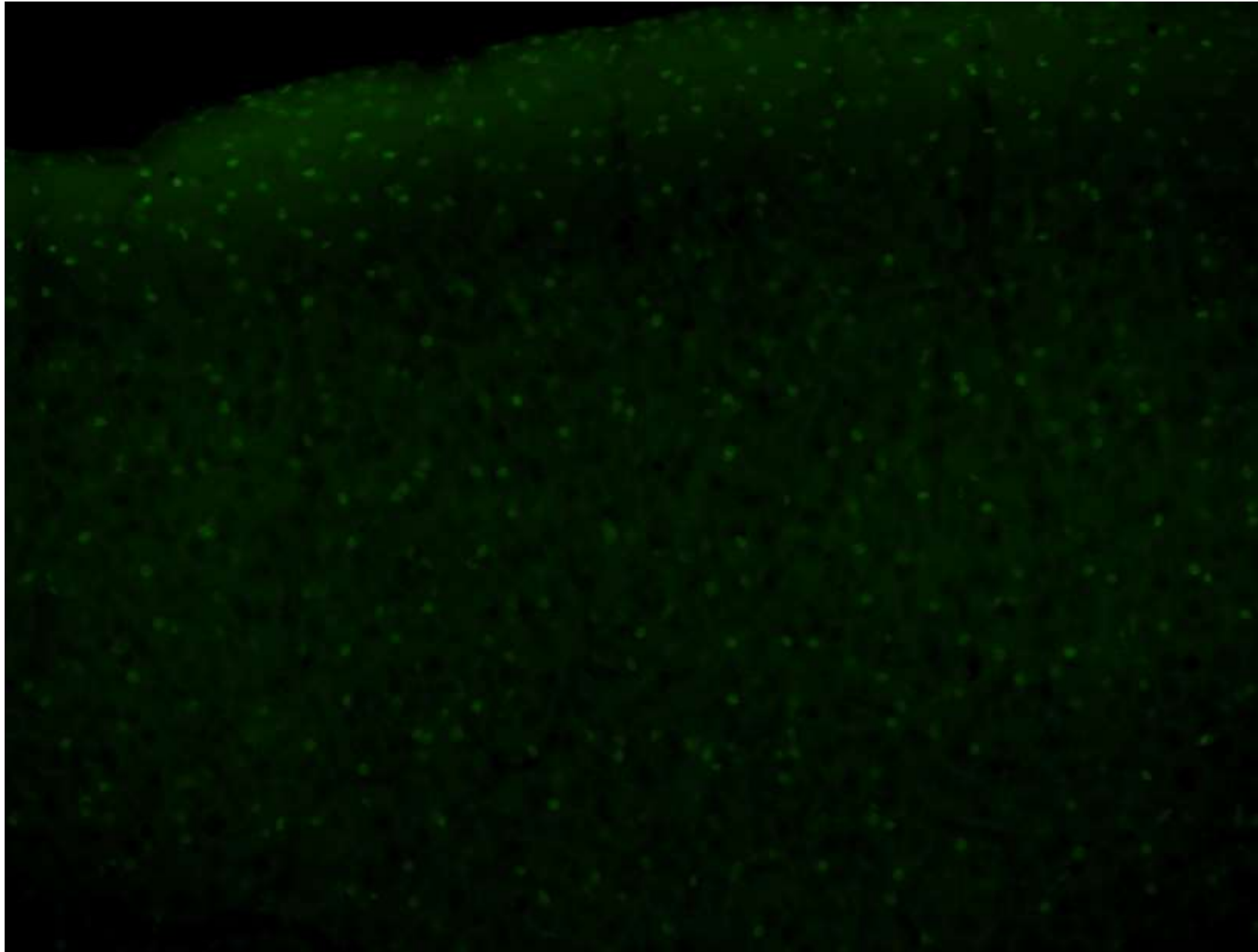
*Maria Angeles Martínez-
Martínez et al. (2016) Nature
Communications*



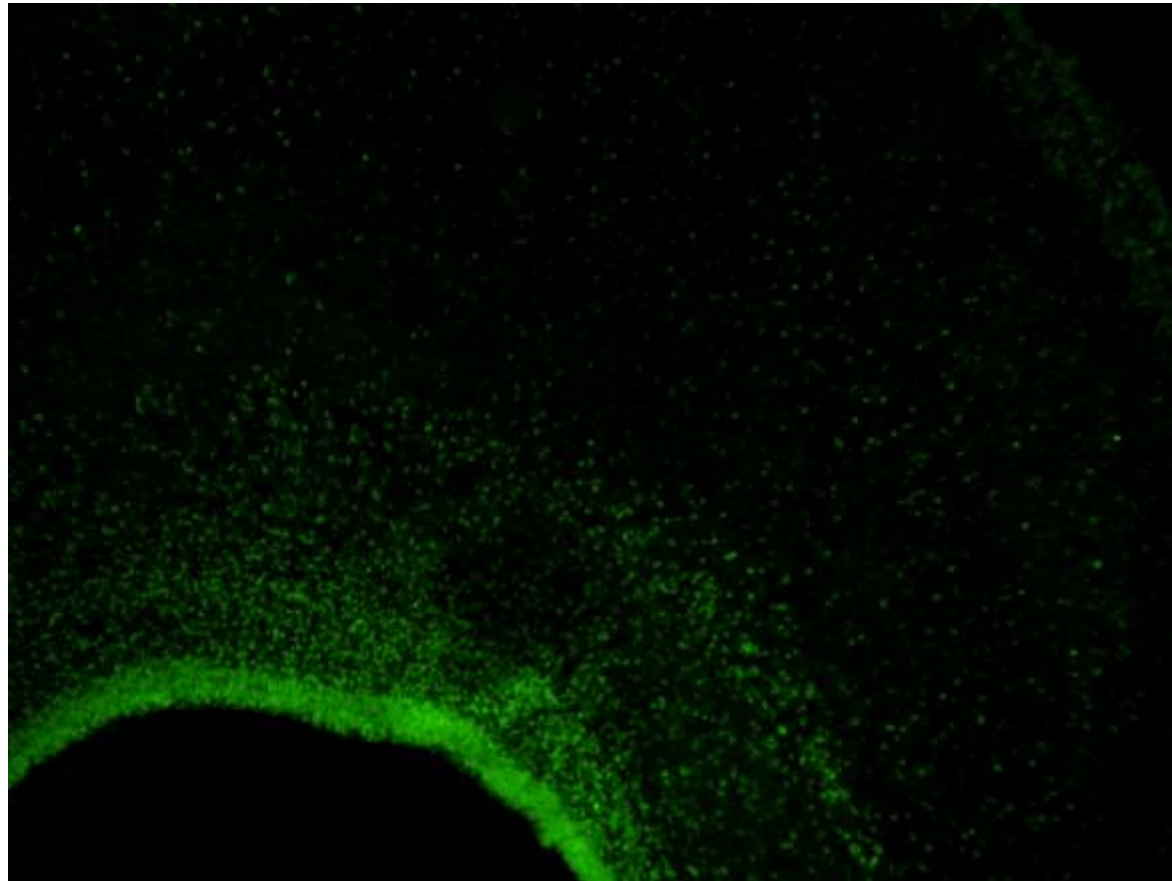
If bRG has apical-P, basal-P, and both-P, is it possible to differentiate vRG from oRG using only morphological position?

Marion Betizeau et al.(2013)*neuron*

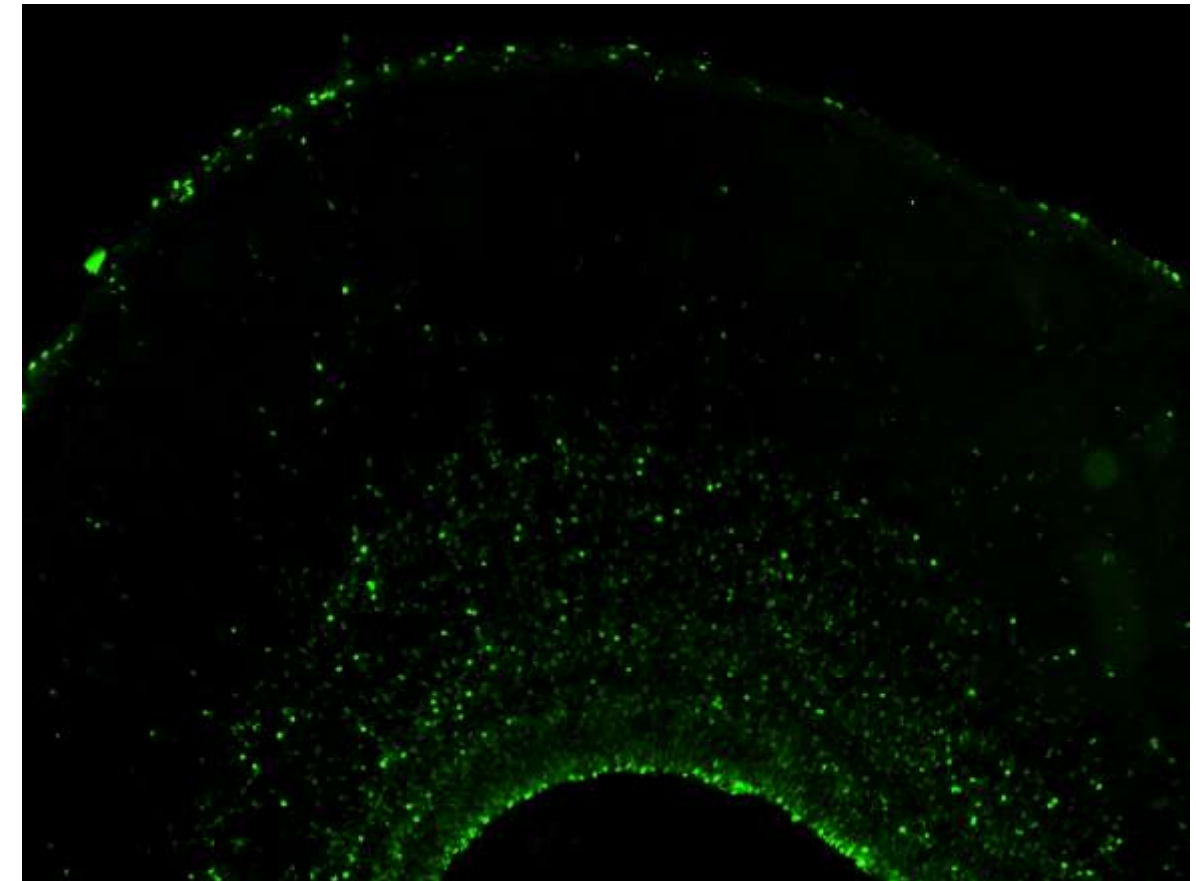
Can vRG and oRG be color-distinguished
and morphologically displayed by virus injection
or embryo electrotransfer?



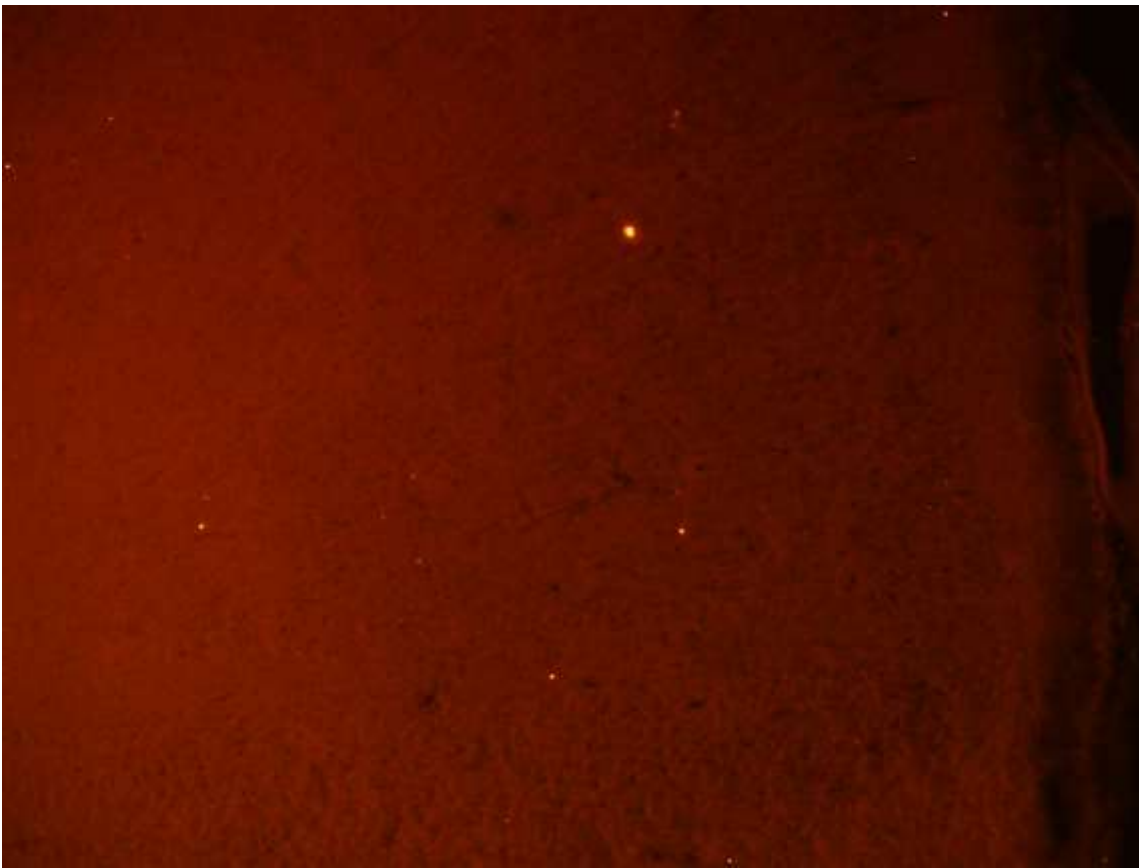
Adult mouse cortex Sox2(original)



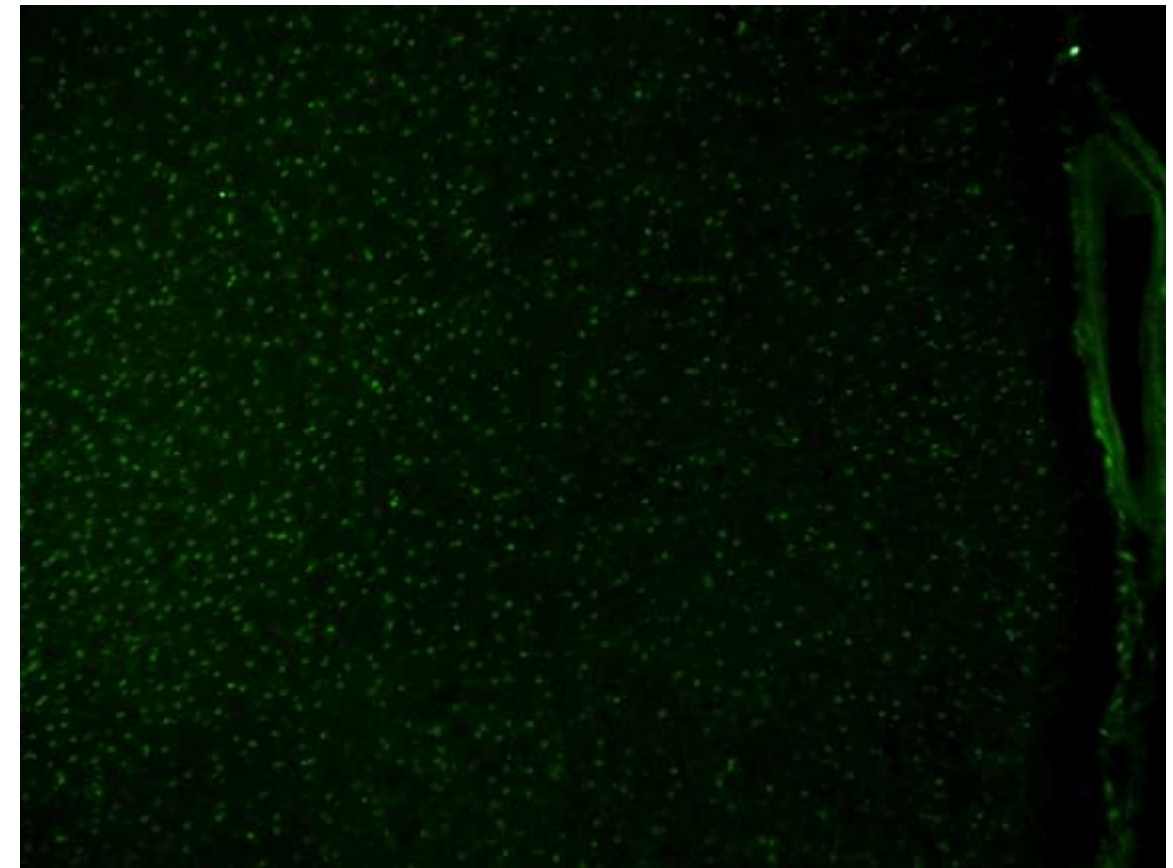
Ferret P1 Sox2



Ferret P1 Ki67



Ferret P35 Ki67

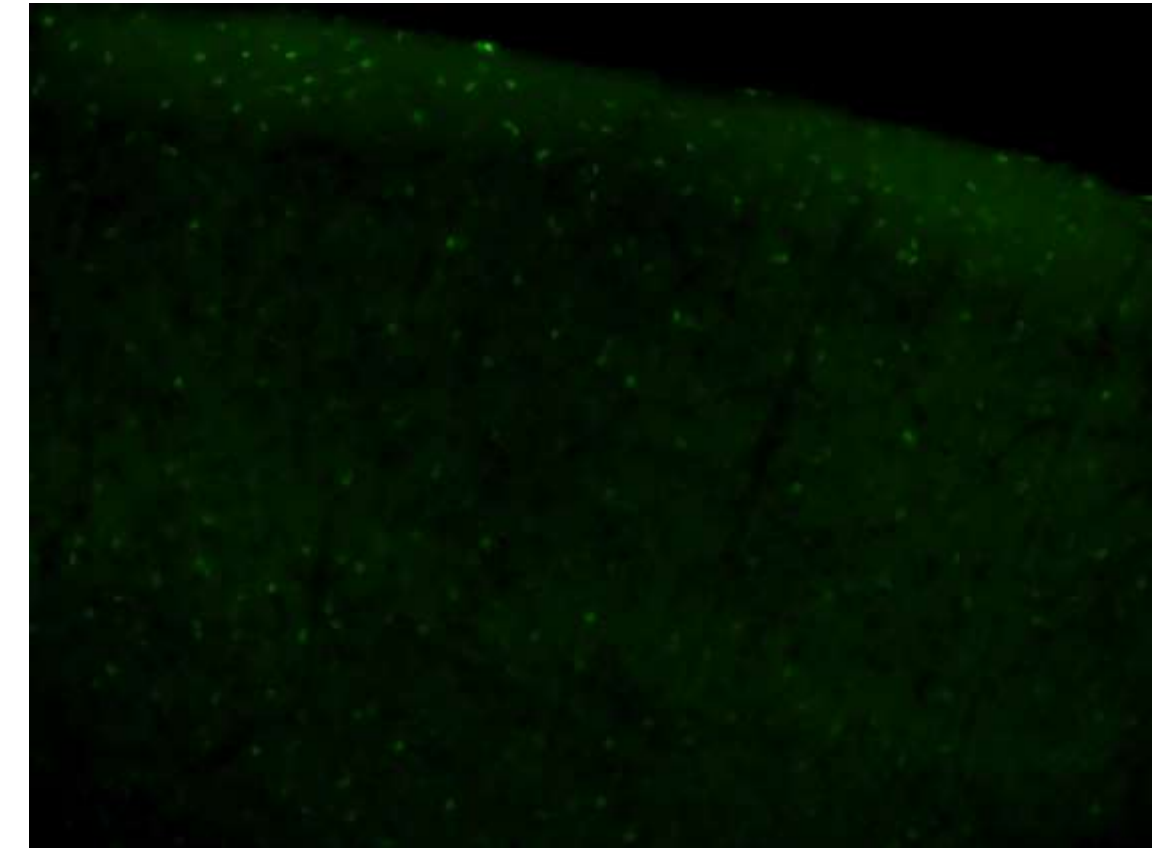


Ferret P35 Sox2



Adult mouse Ki67

2024/4/7



Adult mouse Sox2

Content			
Sep. 2016-Feb.2017	Study on mice until the status got to be determined	Mar. 2017-Jul.2017	Study on mouse under control with the same condition
Feb. 2018-Jul.2016	Data on mice for the study got to be determined	Sep. 2018-Dec.2018	Data Presentation
Sep. 2019-Feb.2020	Unknown or Classification	Sep. 2019-Jul.2019	Unknown or Classification
Sep. 2019-Feb.2020	Unknown or Classification	Sep. 2019-Jul.2019	Unknown or Classification

27

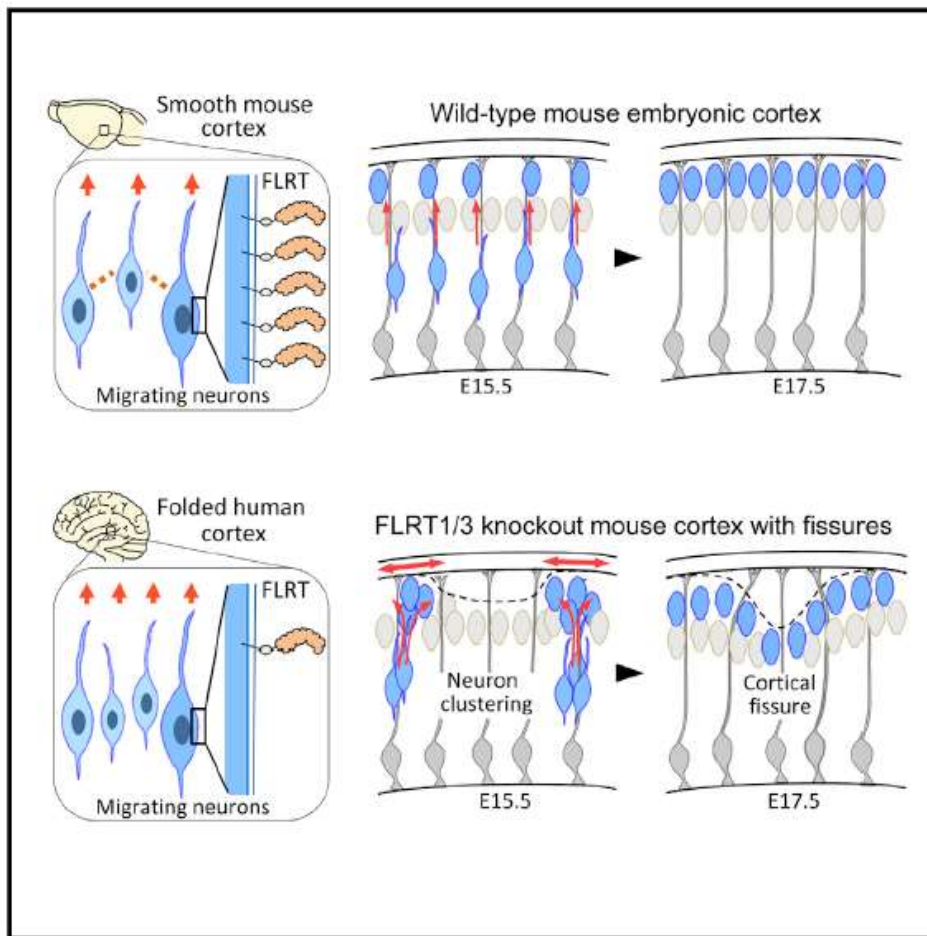
Study on stem cell in the cortex gyri of developmental ferret

Zhou Ying

16th Jul. 2017

Regulation of Cerebral Cortex Folding by Controlling Neuronal Migration via FLRT Adhesion Molecules

Graphical Abstract



Authors

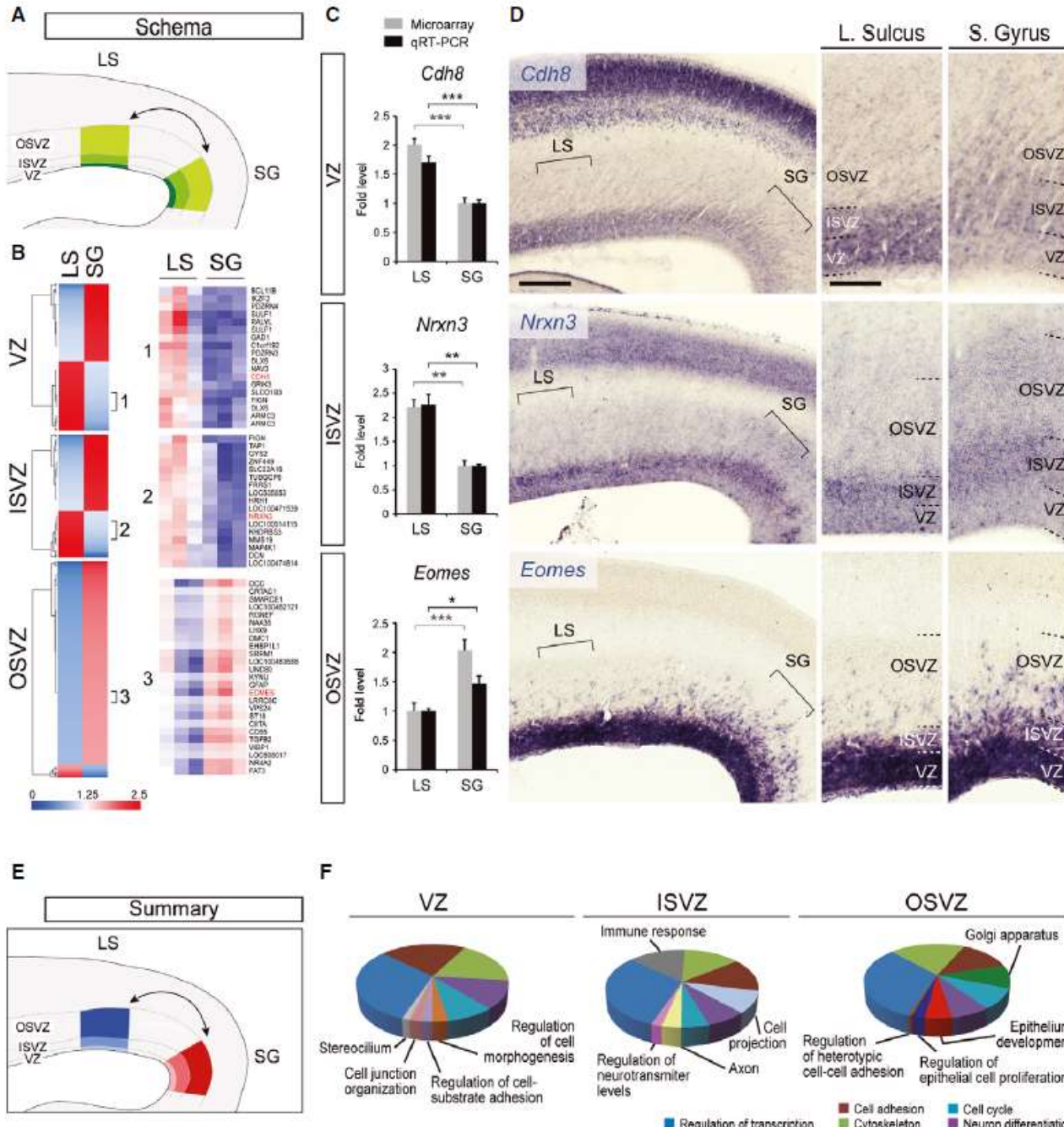
Daniel del Toro, Tobias Ruff,
Erik Cederfjäll, Ana Villalba,
Gönül Seyit-Bremer, Víctor Borrell,
Rüdiger Klein

Correspondence

rklein@neuro.mpg.de

In Brief

Physical migration of neurons can create the folded cortical surface characteristic of primate brains.



- The gene expression in the cortex VZ&SVZ of ferret, sulcus and gyrus regions exhibits significant differences.
- Microarray analysis was conducted using tissue samples, primarily indicating differential gene expression between the sulcus and gyrus regions.
- The analysis method was imprecise, merely identifying some differentially expressed genes without conducting dynamic expression analysis at different developmental time points or mechanistic analysis.

Published online: April 26, 2015

Resource



THE
EMBO
JOURNAL

Discrete domains of gene expression in germinal layers distinguish the development of gyrencephaly

Camino de Juan Romero¹, Carl Bruder^{2,†}, Ugo Tomasello¹, José Miguel Sanz-Anquela³ & Víctor Borrell^{1,*}

REVIEW

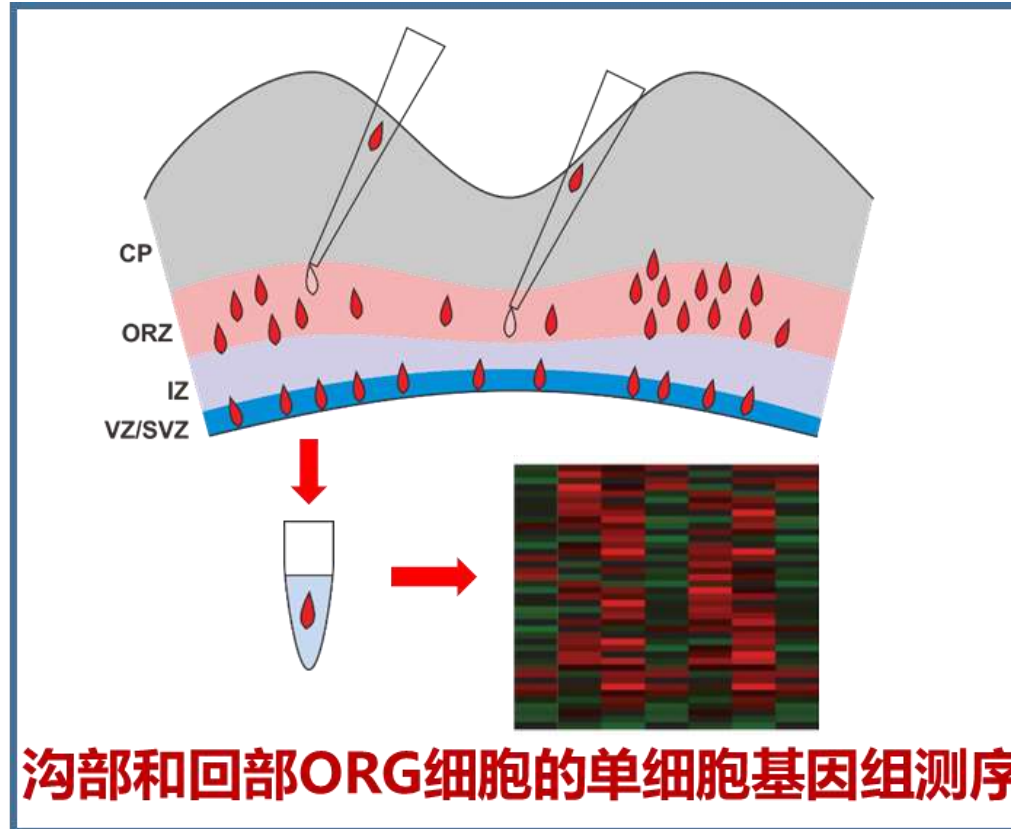
Open Access



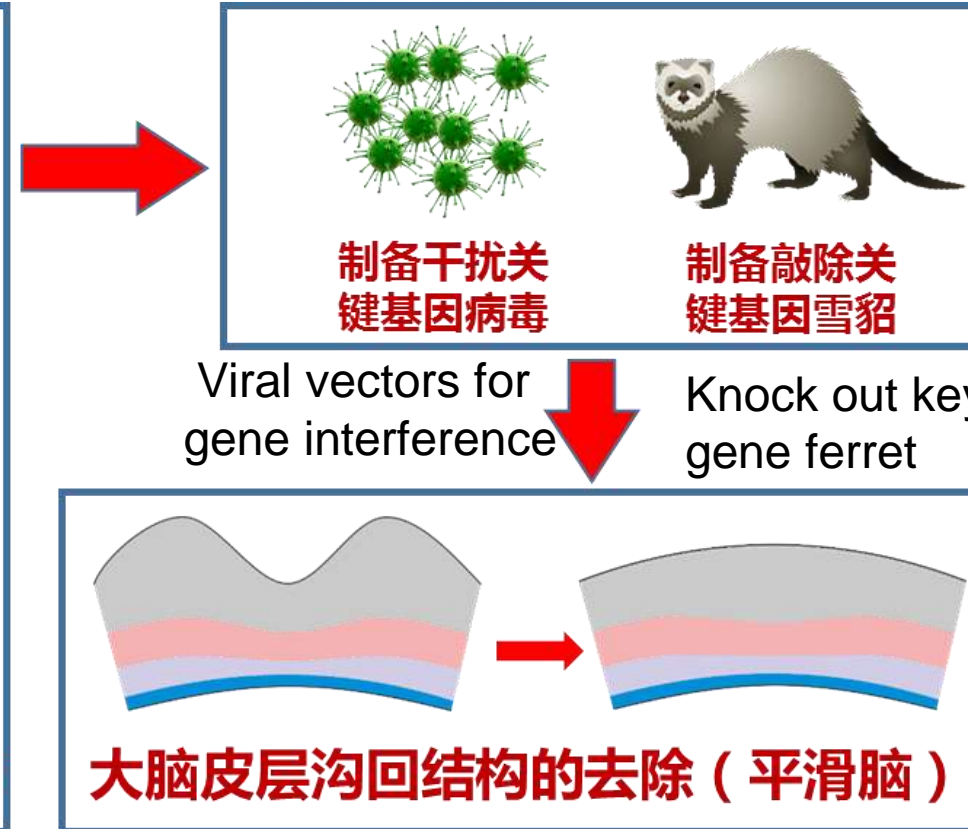
Single-cell RNA-sequencing of the brain

Raquel Cuevas-Diaz Duran^{1,2†}, Haichao Wei^{1,2†} and Jia Qian Wu^{1,2*}

- The gene expression analysis obtained from RNA-seq is based on an bulk cells or tissue, which masks the heterogeneity within the cell population.
- Single-cell RNA sequencing (scRNA-seq) technology enabling the analysis of gene expression in single cells level.
- The mammalian brain is an extremely complex structure, containing a vast array of different cell types. Therefore, scRNA-seq technology has become increasingly important in neuroscience research.

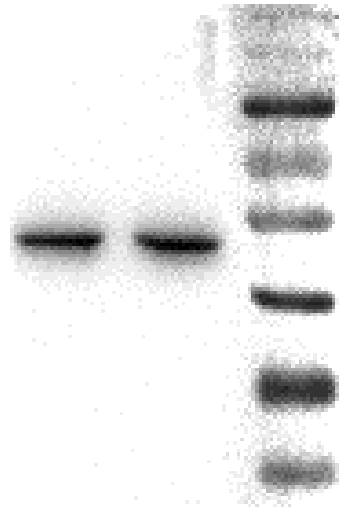


scRNA-seq to oRGCs from sulcus and gyrus

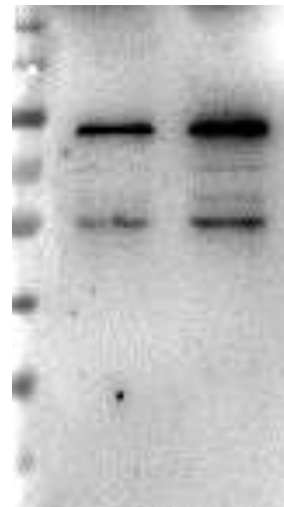


Found key gene that changing gyrus structure, which potential relevant with defects of cortical folding

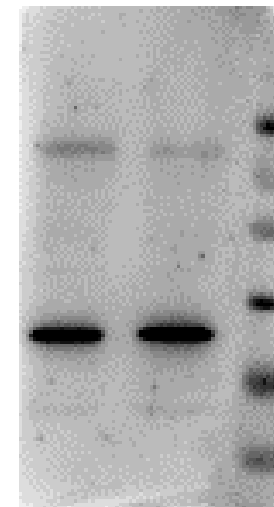
WB antibody verification of P1 ferret brain tissue



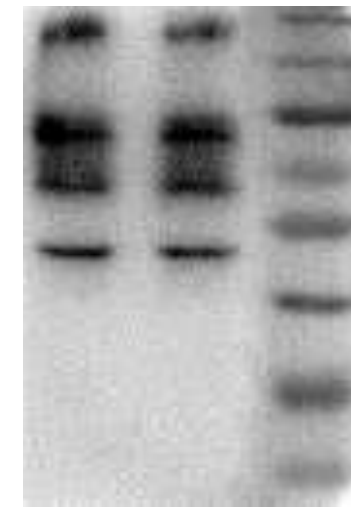
Pax6(Rb)



PTPRZ1



Tbr2



Hopx

Conclusion

- The injection of embryo virus leads to severe brain malformation.
- Cells labeled with the virus show a low distribution in the ventricular zone (VZ) and outer subventricular zone (OSVZ), and hardly co-localize with BrdU.
- The uneven distribution of virus-labeled cells complicates cell cycle analysis.
- WB results confirm poor specificity of Hopx and PTPRZ1 in ferret.
- Tbr2 appears acceptable based on WB results, while Pax6 shows specificity.

Next work

- Testing Different Antigen Retrieval Methods for Tbr2 Staining
- Converting Images to Density Distribution Heatmaps
- Addressing Alignment Issues Between Heatmaps and Marker Signal Images
- Implementing Partitioning and Binning in MATLAB

Antigen retrieval for Tbr2 staining

- Sodium citrate buffer solution microwave-heated for 20 minutes or more

(Can be stained, weak signal, severe section detachment, bubbling)

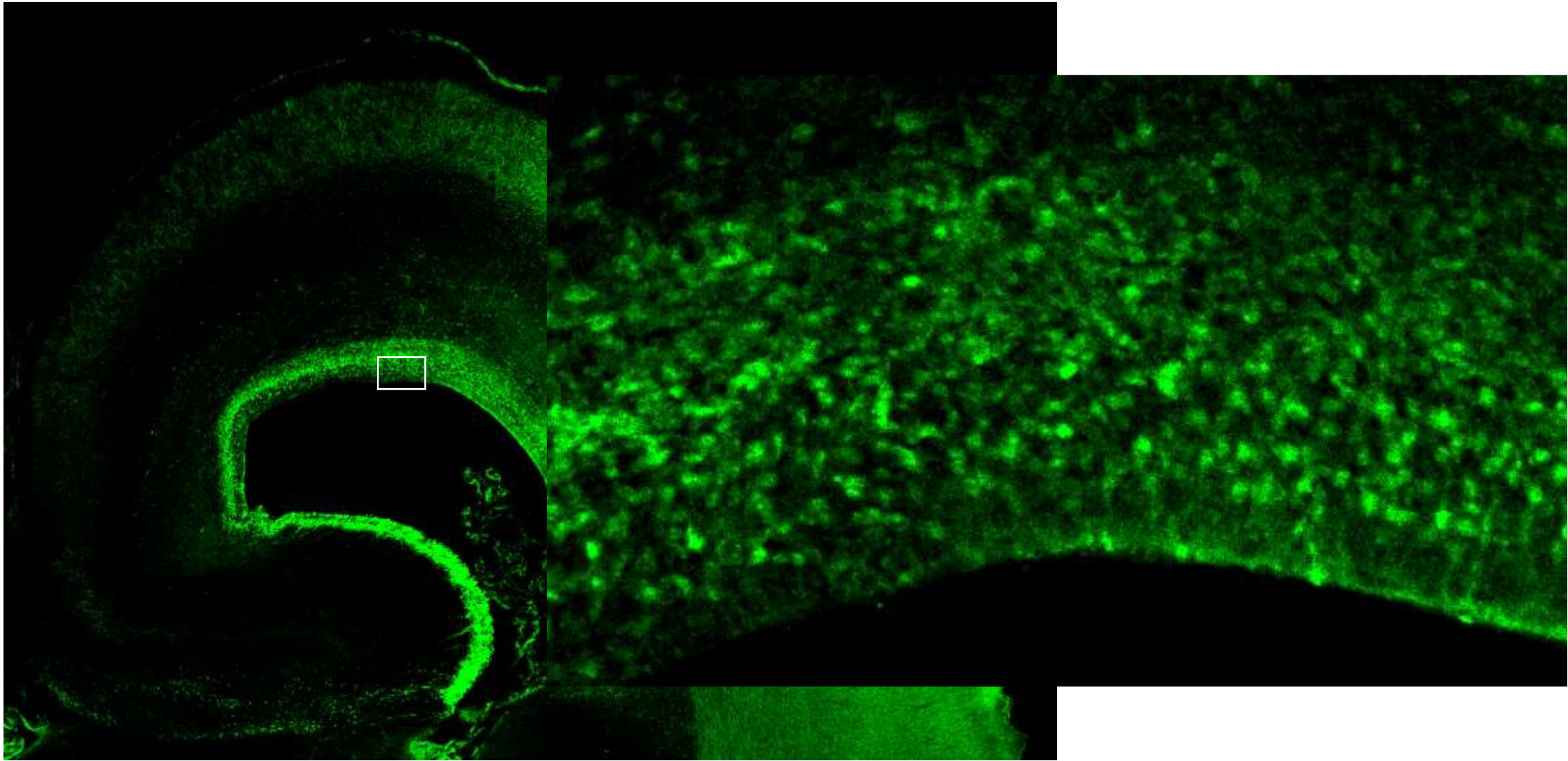


- Frozen section quick antigen retrieval solution (SDS) incubated at room temperature for 5 minutes

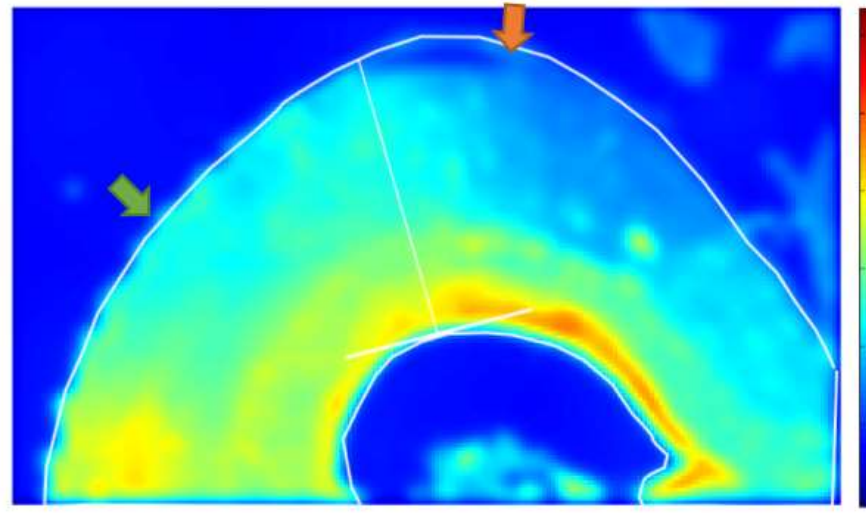
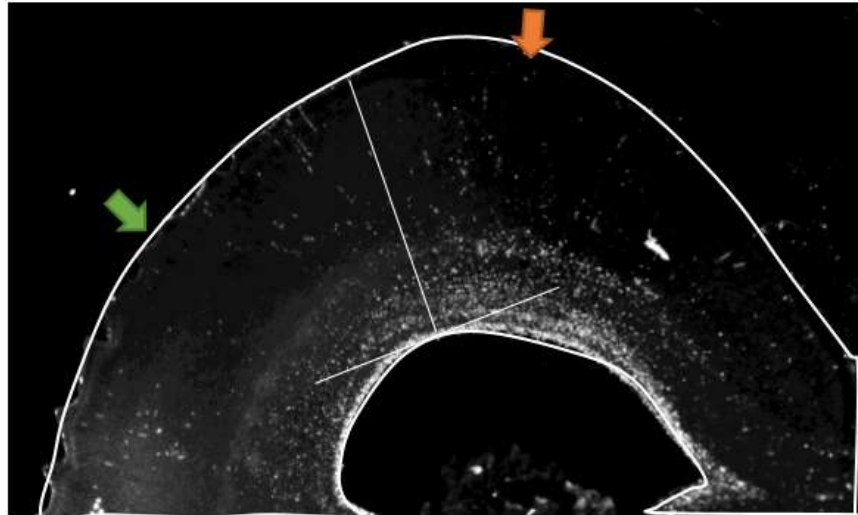
(Can be stained, somewhat unstable, no heating required, no section detachment, no bubbling)

- Universal high-efficiency quick antigen retrieval solution (decrosslinking agent) microwave-heated for 20 minutes or more

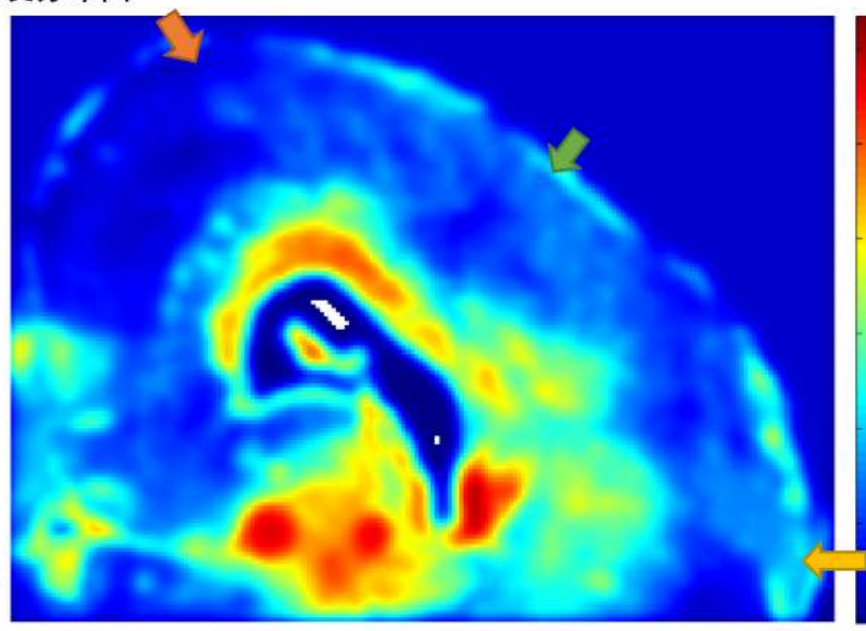
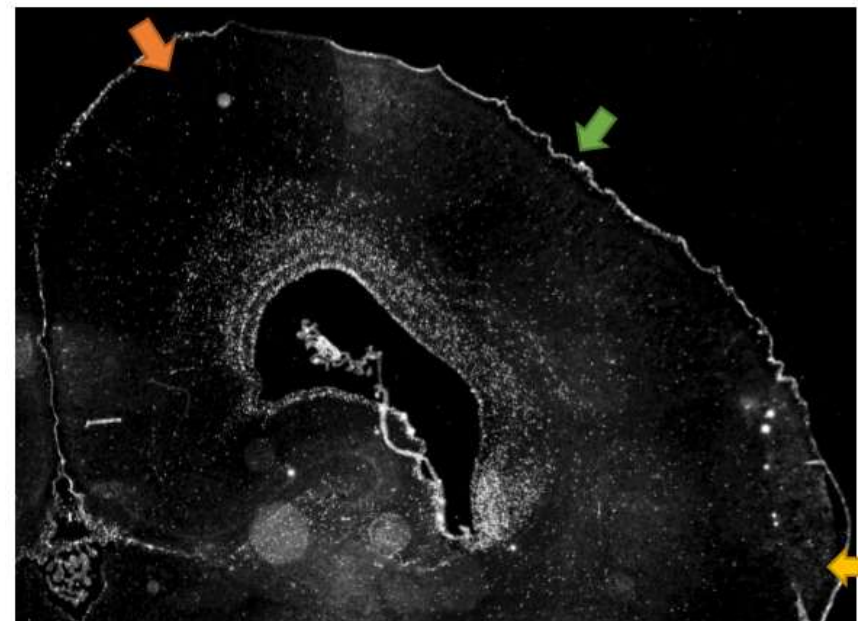
(Produces better staining results, prone to section detachment, bubbling)



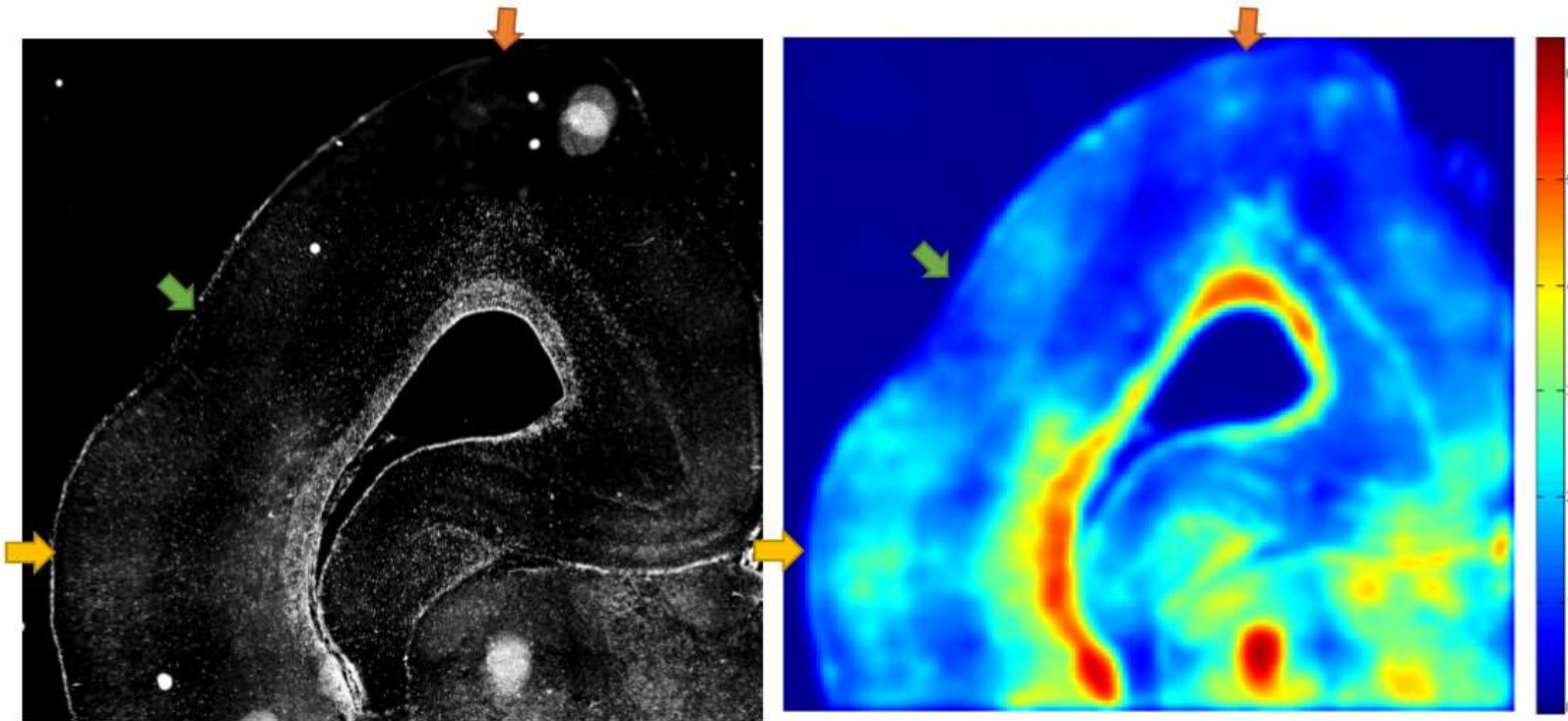
Tbr2



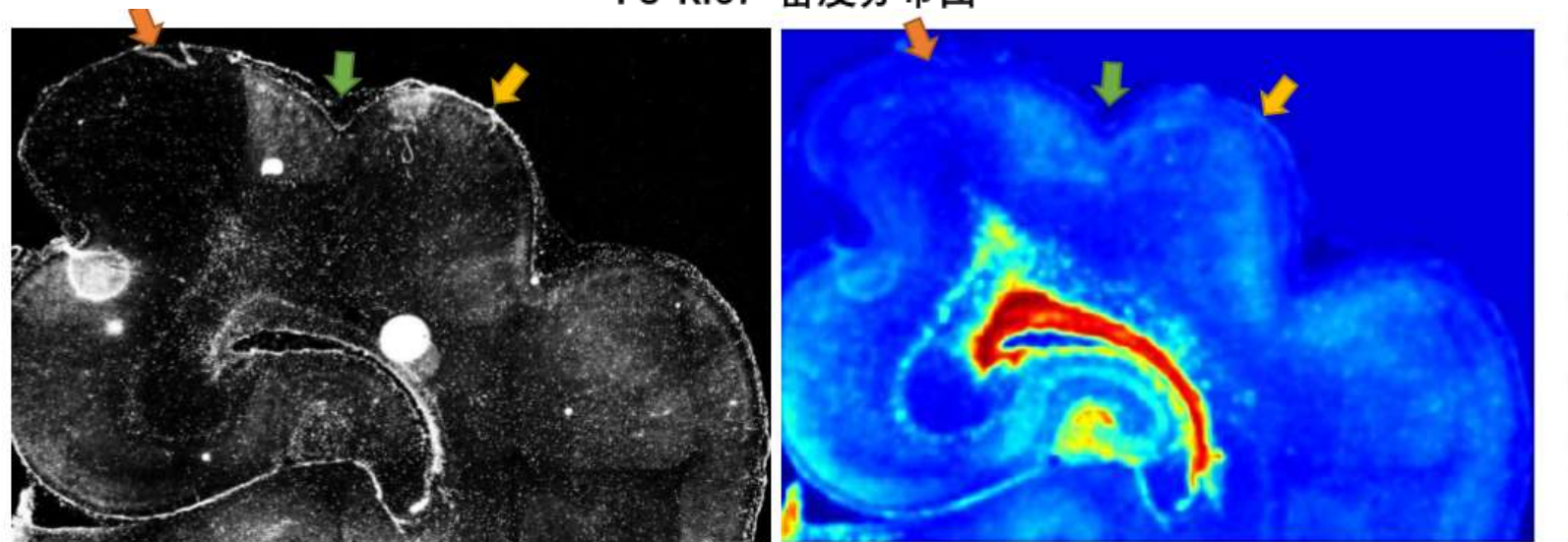
P2 KI67 密度分布图



P4 KI67 密度分布图

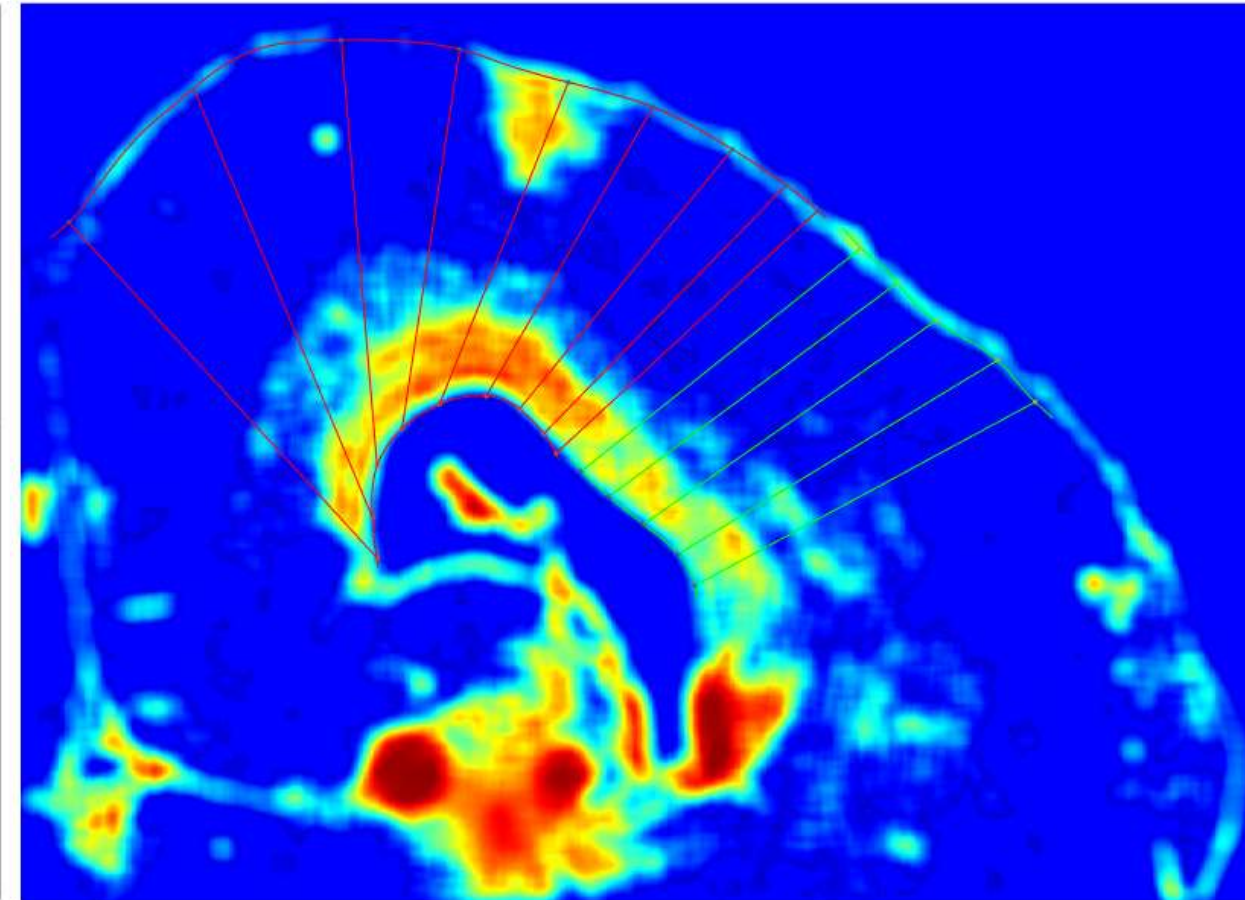
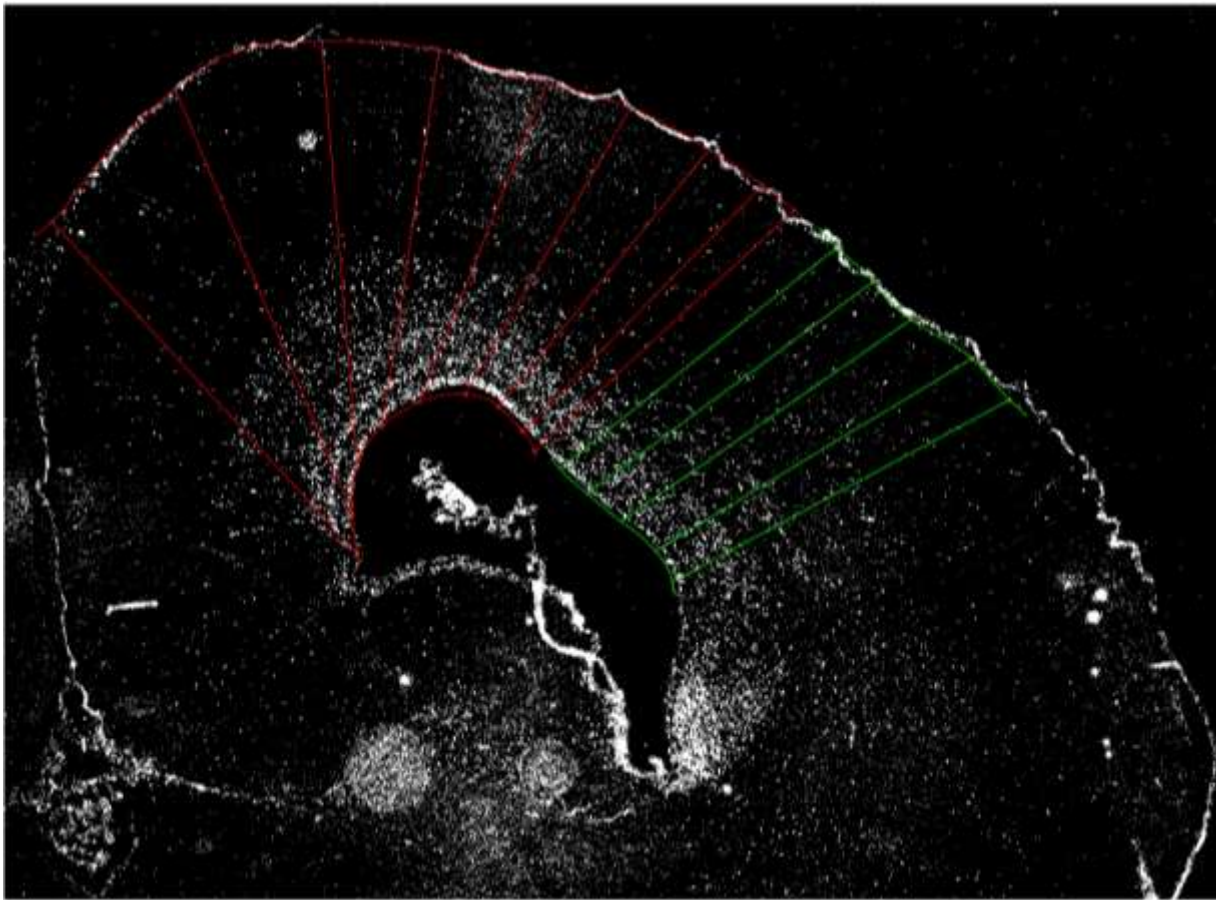


P8 KI67 密度分布图

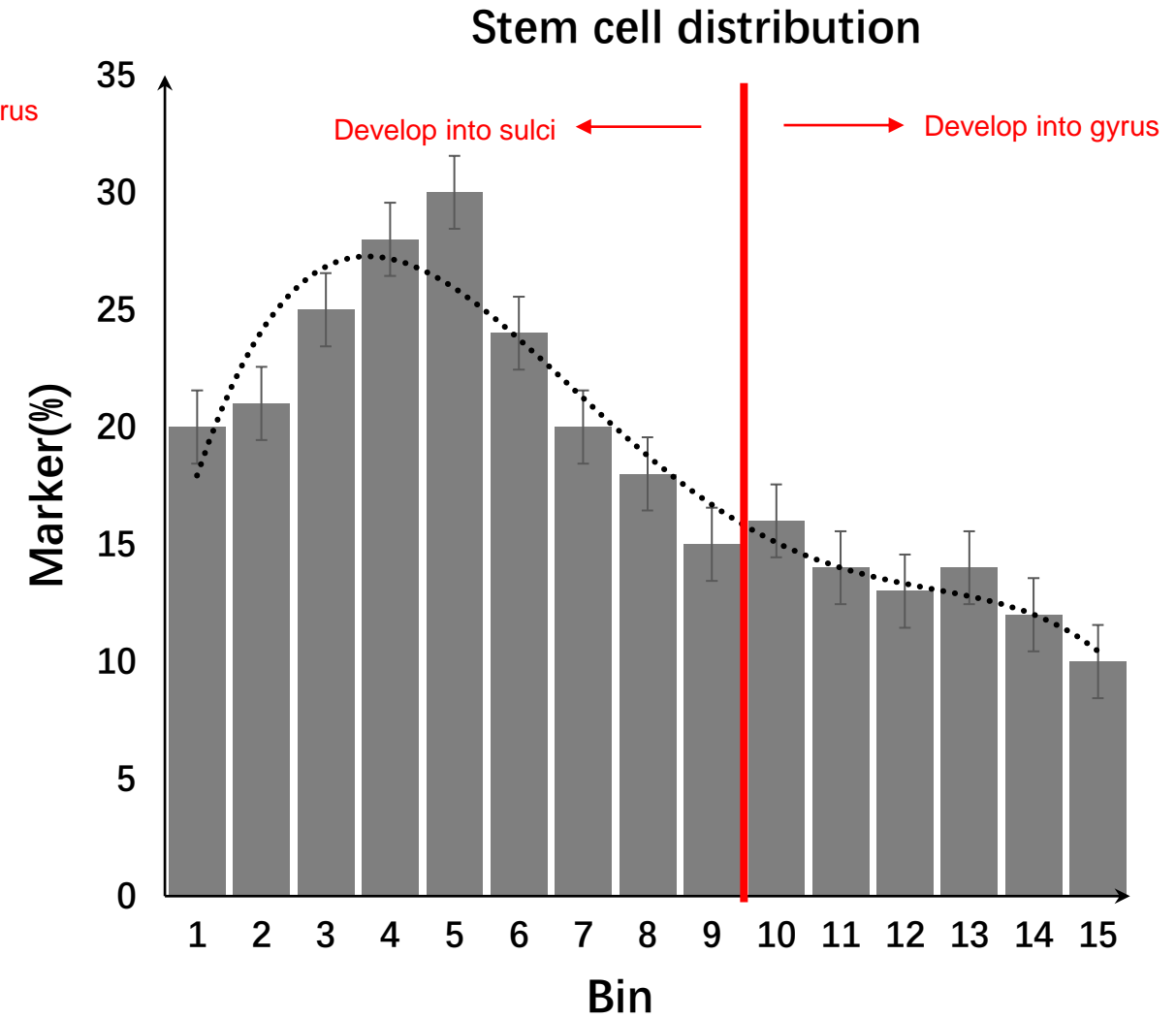
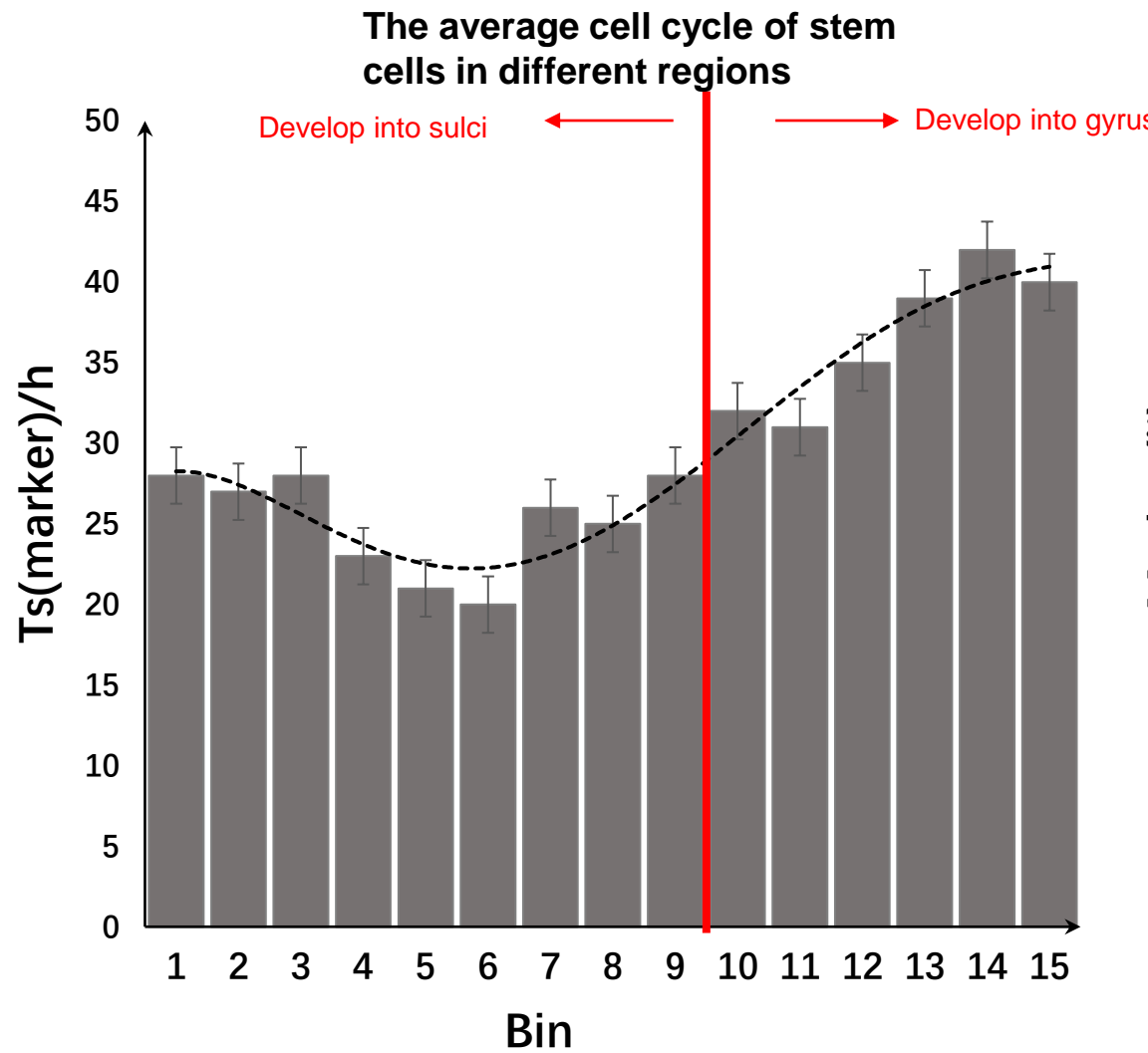


P11 KI67 密度分布图

Plotting Binning Graph



Simulating Expected Statistical Graph by Binning



The current status of antibodies

Antibodies	Results
Pax6 (santa-cruz ,Gt)	Unable to achieve staining
Pax6 (MBL ,Rb)	The results are satisfactory; staining can be achieved using conventional methods.
Tbr2 (abcam , Rb)	Unable to achieve staining
Tbr2 (Millipore , Rb)	Staining can be achieved through antigen retrieval
Tbr2 (Millipore , Ck)	Various fixation methods, different concentrations, and staining protocols described in literature have been attempted, but staining remains unsuccessful.
Pax6(santa-cruz ,Ms)	Tried different concentrations without obtaining any signal.

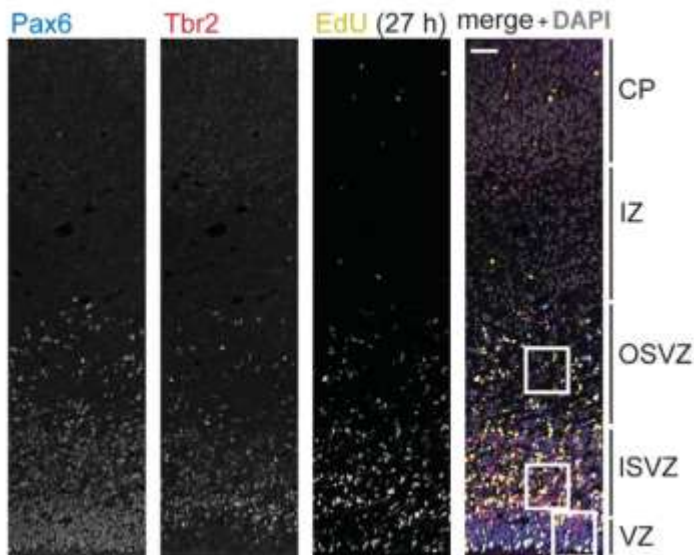
- The major issue currently lies in species conflict among available antibodies, preventing dual labeling.
- Most antibodies for Tbr2 are derived from the rabbit species across various companies, while Santa Cruz's antibody is mouse-derived, suitable only for immunoprecipitation (IP) and Western blotting (WB).

TABLE 2.

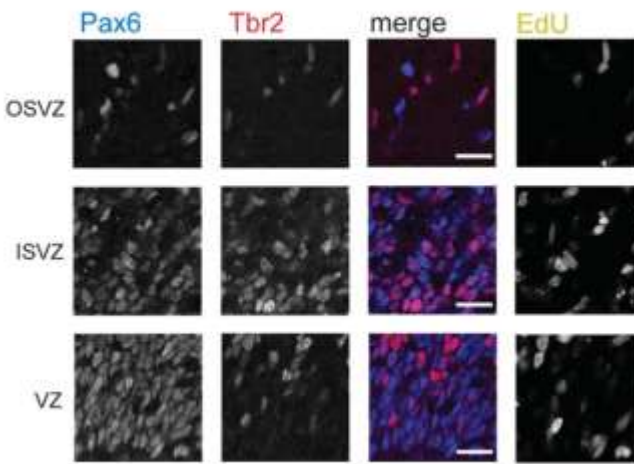
Primary Antibodies Used in This Study

Antigen	Description of Immunogen	Source, cat. #, RRID, host species	Dilution
Anti-Pax6	Peptide (QVPGSEPDMMSQYWPRLQ) derived from the C-terminus of the mouse Pax-6 protein	Covance PRB-278P, RRID: AB_2313780, rabbit polyclonal	1:200
Anti-Tbr2	Synthetic peptide conjugated to KLH derived from within residues 650 to the C-terminus of mouse TBR2/Eomes	Abcam ab23345, RRID: AB_778267, rabbit polyclonal	1:200
Anti-Tbr2	KLH-conjugated linear peptide corresponding to mouse Tbr2	Millipore AB15894, RRID: AB_10615604, chicken polyclonal	1:500
Anti-Tbr2	<i>E. coli</i> -derived recombinant human EOMES, Gly471-Pro686	R&D AF6166, RRID: AB_10569705, sheep polyclonal	1:200
Anti-Ki67	Human recombinant peptide corresponding to a 1002-bp Ki-67 cDNA fragment	Dako M7240, clone MIB-1, RRID: AB_2142367, mouse monoclonal	1:200
Anti-PCNA	Rat PCNA made in the protein A vector pR1T2T	Millipore MAB424, clone PC10, RRID: AB_95106, mouse monoclonal	1:200
Anti-PH3	Synthetic peptide conjugated to KLH, corresponding to amino acids 23–35 of human histone H3	Abcam ab10543, RRID: AB_2295065, rat monoclonal	1:500

A



B



Miguel Turrero García et al. (2016)

immunofluorescence staining, cryosections were washed in PBS; heat-induced antigen retrieval was then performed at 70°C for 1 hour, in a sodium citrate solution (0.01 M in water, pH 6.0) containing glycerol (10% v/v). The slides were allowed to cool down to room temperature for 10–15 minutes, and then washed with PBS, permeabilized with 0.3% (v/v) Triton X-100 in PBS for 30 minutes, and quenched with 0.1 M glycine-Tris (pH 7.4) for 30 minutes. The sections were then washed with Tx buffer (300 mM NaCl, 0.2% v/v gelatin, 0.3% v/v Triton X-100 in PBS). Primary antibodies were diluted in the same buffer, and the sections were incubated with them overnight at 4°C. The sections were then washed with Tx, and incubated with secondary antibodies and DAPI, diluted in the same buffer, for 1–2 hours at room temperature. The slides were mounted with a coverslip, using either Mowiol or ProLong Gold Antifade Reagent (Molecular Probes, Eugene, OR), and stored at 4°C in the dark. Primary antibodies and dilutions are listed in Table 2. Donkey (1:500) or goat (1:1,000) secondary antibodies coupled to Alexa 488, Alexa 555, or Alexa 647 were used. For EdU detection, the Click-iT EdU Alexa Fluor 647 Imaging Kit (Invitrogen, Carlsbad, CA) was used, according to the supplier's instructions with slight modifications (Arai et al., 2011).

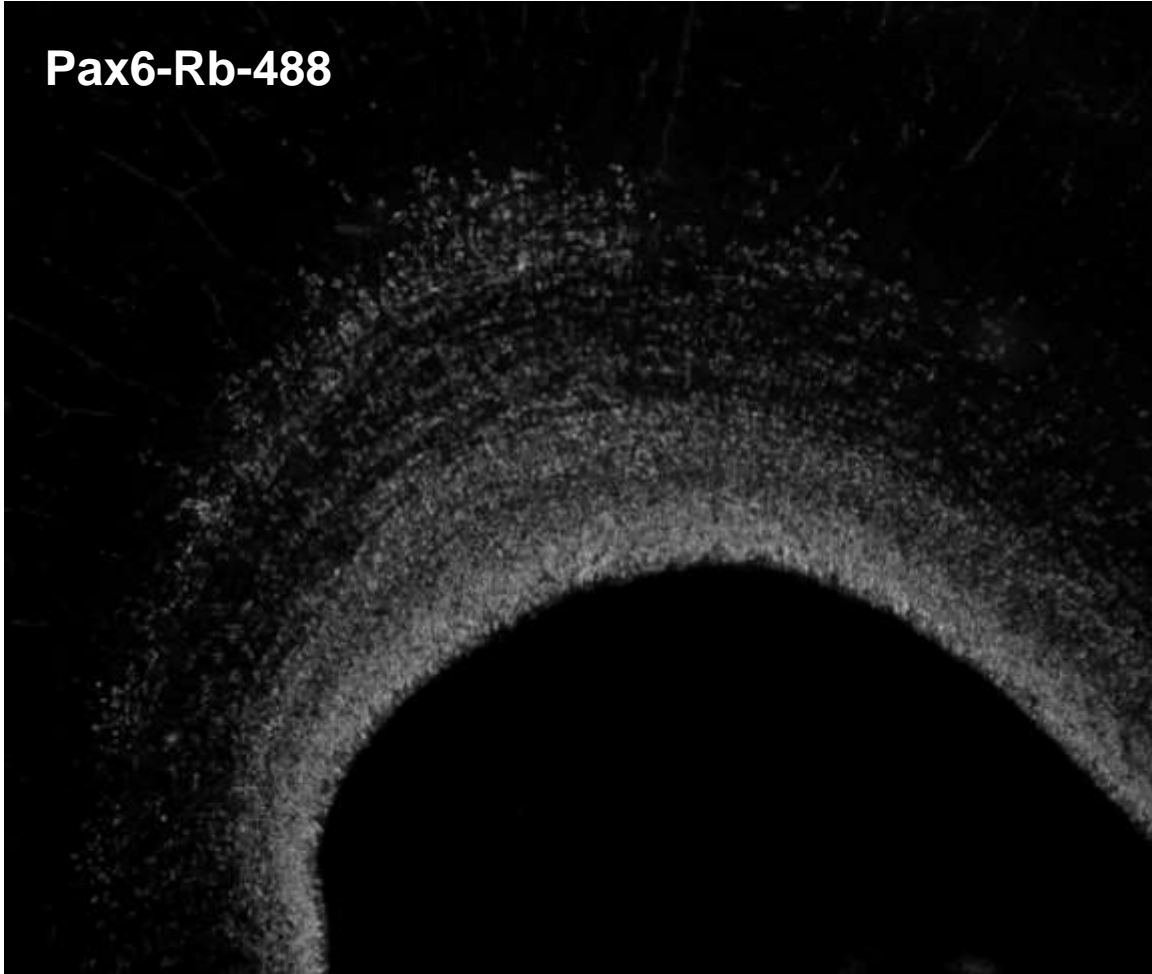
The current antibody strategy

- Based on the existing ability to stain Tbr2 and Pax6 with rabbit (Rb) antibodies separately, one approach to achieving dual labeling with antibodies of the same species involves utilizing sequential staining techniques.
- for Tbr2 and Pax6 staining, exploring non-rabbit species antibodies may offer a solution. By identifying and testing antibodies from different species
- Regarding preparing antibodies specifically for ferret

Dual labeling with antibodies of the same species (Rb) for Tbr2 and Pax6

- **Sequential staining with two antibodies**
 - Can be attempted based on existing well-staining antibodies
 - May result in slight cross-reactivity
 - Immunohistochemistry staining is time-consuming
 - Conditions are difficult to optimize
- **Zenon® labeling technology**
 - Rapid staining
 - Requires purchase of related reagent kits
 - Requires optimization of conditions

Pax6-Rb-488

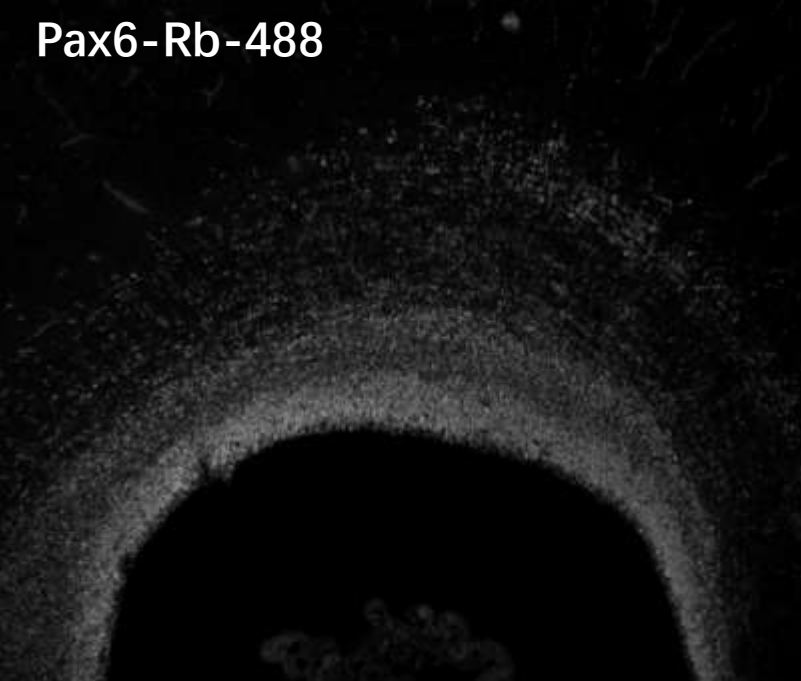


Pax6-Rb-555



Pax6 primary antibodies → Rb-488 → Rb-555

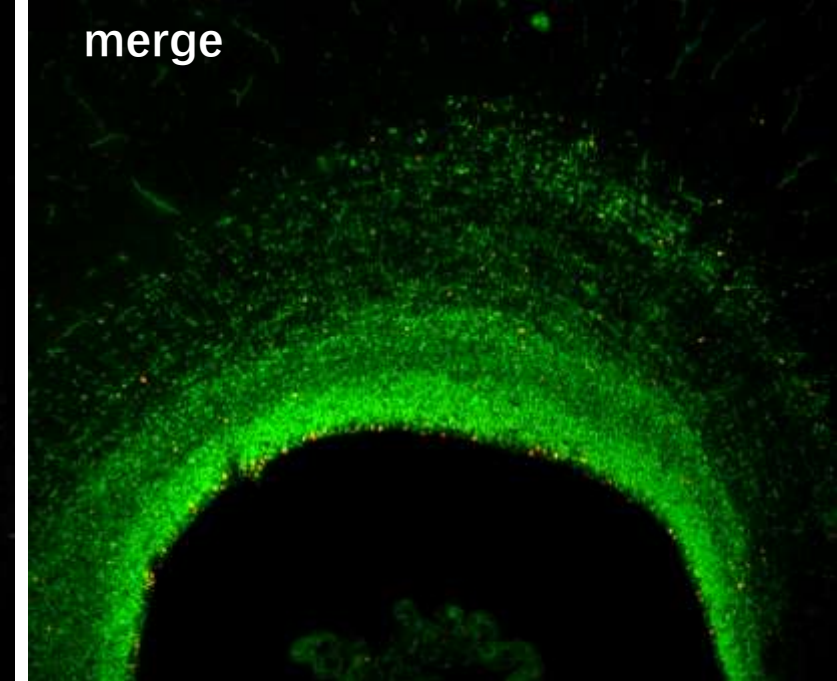
Pax6-Rb-488



PH3-Rb-555



merge



Pax6(Rb) primary → Rb-488 → PH3(Rb) Primary → Rb-555

The main reason for cross-reactivity when sequentially staining with two antibodies

- When the secondary antibody A is insufficient to bind with primary antibody A, the remaining Fc segment of primary antibody A may bind with secondary antibody B.

to determine the appropriate working concentration of secondary antibody A

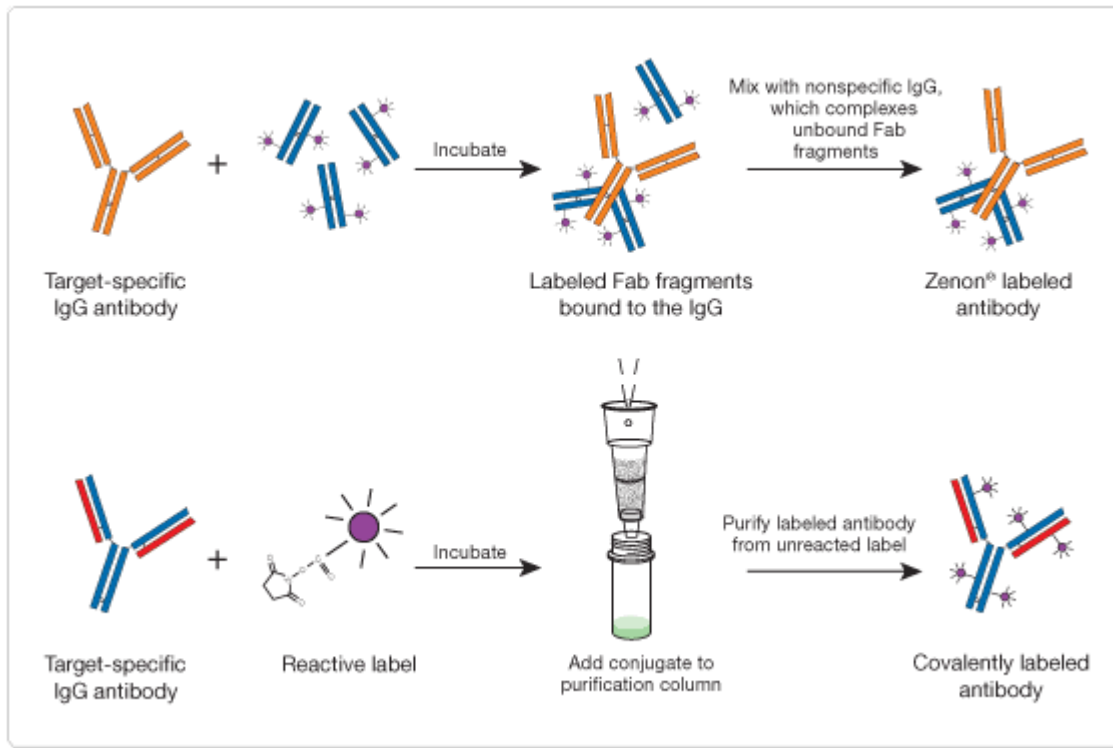
- Excessive secondary antibody A may not be thoroughly washed away, resulting in residual secondary antibody A binding with primary antibody B.

to determine the appropriate working concentration of secondary antibody A and optimize the washing conditions to thoroughly remove residual secondary antibody A.

- multiple binding sites for antibody binding, secondary antibody B can bind to the unoccupied binding sites of primary antibody A

to find a method to block the binding sites of primary antibody A.

Zenon® labeling technique



NIH Public Access

Author Manuscript

Microsc Res Tech. Author manuscript; available in PMC 2011 November 28.

Published in final edited form as:

Microsc Res Tech. 2010 June ; 73(6): 623–630. doi:10.1002/jemt.20803.

A Reproducible Technique for Specific Labeling of Antigens Using Preformed Fluorescent Molecular IgG-F(ab')₂ Complexes From Primary Antibodies of the Same Species

GETHIN RH, OWEN, LARI HÄKKINEN, CHUANYUE WU, and HANNU LARJAVA*

Laboratory of Periodontal Biology, Faculty of Dentistry, Department of Oral, Biological and Medical Sciences, University of British Columbia, Vancouver, Canada V6T 1Z3

- Pre-labeled with specially designed Zenon® fragments, which only bind to the Fc fragment of the primary antibody.
- The primary antibody labeled with Zenon® fragments binds to the target protein.
- Rapid reaction, compatible with antibodies of the same species, flexible labeling, and stronger immunohistochemical signals compared to direct methods.

Antibody preparation targeting ferret

- Without the purification technology for the target protein, only the gene information and protein sequence of the target protein can be provided to the company.
- Due to the relatively unique species of ferret, the company needs to assess the feasibility of antibody preparation.
- The ferret-related cDNA information available on NCBI is mostly predicted and needs validation.
- Monoclonal antibody preparation has a longer cycle, requiring 6 months, but it may solve the issue of flow cytometry. However, the current problem may have a slightly longer cycle.

- PREDICTED: [Mustela putorius furo](#) protein DEK (LOC101676431), partial mRNA
12. 852 bp linear mRNA
Accession: XM_013051010.1 GI: 859970044
[GenBank](#) [FASTA](#) [Graphics](#)
- PREDICTED: [Mustela putorius furo](#) uncharacterized LOC106004733 (LOC106004733). ncRNA
13. 484 bp linear ncRNA, lncRNA
Accession: XR_001177749.1 GI: 859970039
[GenBank](#) [FASTA](#) [Graphics](#)
- PREDICTED: [Mustela putorius furo](#) uncharacterized LOC101675936 (LOC101675936). ncRNA
14. 490 bp linear ncRNA, lncRNA
Accession: XR_201486.2 GI: 859970034
[GenBank](#) [FASTA](#) [Graphics](#)
- PREDICTED: [Mustela putorius furo](#) atherin-like (LOC106004732), partial mRNA
15. 912 bp linear mRNA
Accession: XM_013051009.1 GI: 859970028
[GenBank](#) [FASTA](#) [Graphics](#)
- PREDICTED: [Mustela putorius furo](#) uncharacterized LOC106004731 (LOC106004731). ncRNA
16. 509 bp linear ncRNA, lncRNA
Accession: XR_001177748.1 GI: 859970023
[GenBank](#) [FASTA](#) [Graphics](#)
- PREDICTED: [Mustela putorius furo](#) aldehyde dehydrogenase, dimeric NADP-preferring-like (LOC101674738), partial mRNA
17. 600 bp linear mRNA
Accession: XM_004782616.2 GI: 859970012
[GenBank](#) [FASTA](#) [Graphics](#)
- PREDICTED: [Mustela putorius furo](#) probable ATP-dependent RNA helicase DDX5 (LOC106004729), partial mRNA
18. 765 bp linear mRNA
Accession: XM_013051007.1 GI: 859970001
[GenBank](#) [FASTA](#) [Graphics](#)
- PREDICTED: [Mustela putorius furo](#) probable ATP-dependent RNA helicase DDX5 (LOC106004728), partial mRNA
19. 675 bp linear mRNA
Accession: XM_013051006.1 GI: 859969995
[GenBank](#) [FASTA](#) [Graphics](#)
- PREDICTED: [Mustela putorius furo](#) molybdenum cofactor biosynthesis protein 1 (LOC101673878), mRNA
20. 819 bp linear mRNA
Accession: XM_004782613.2 GI: 859969985
[GenBank](#) [FASTA](#) [Graphics](#)

PREDICTED: [Mustela putorius furo](#) eomesodermin (EOMES), mRNA

NCBI Reference Sequence: XM_004754370.2

[FASTA](#) [Graphics](#)

Go to:

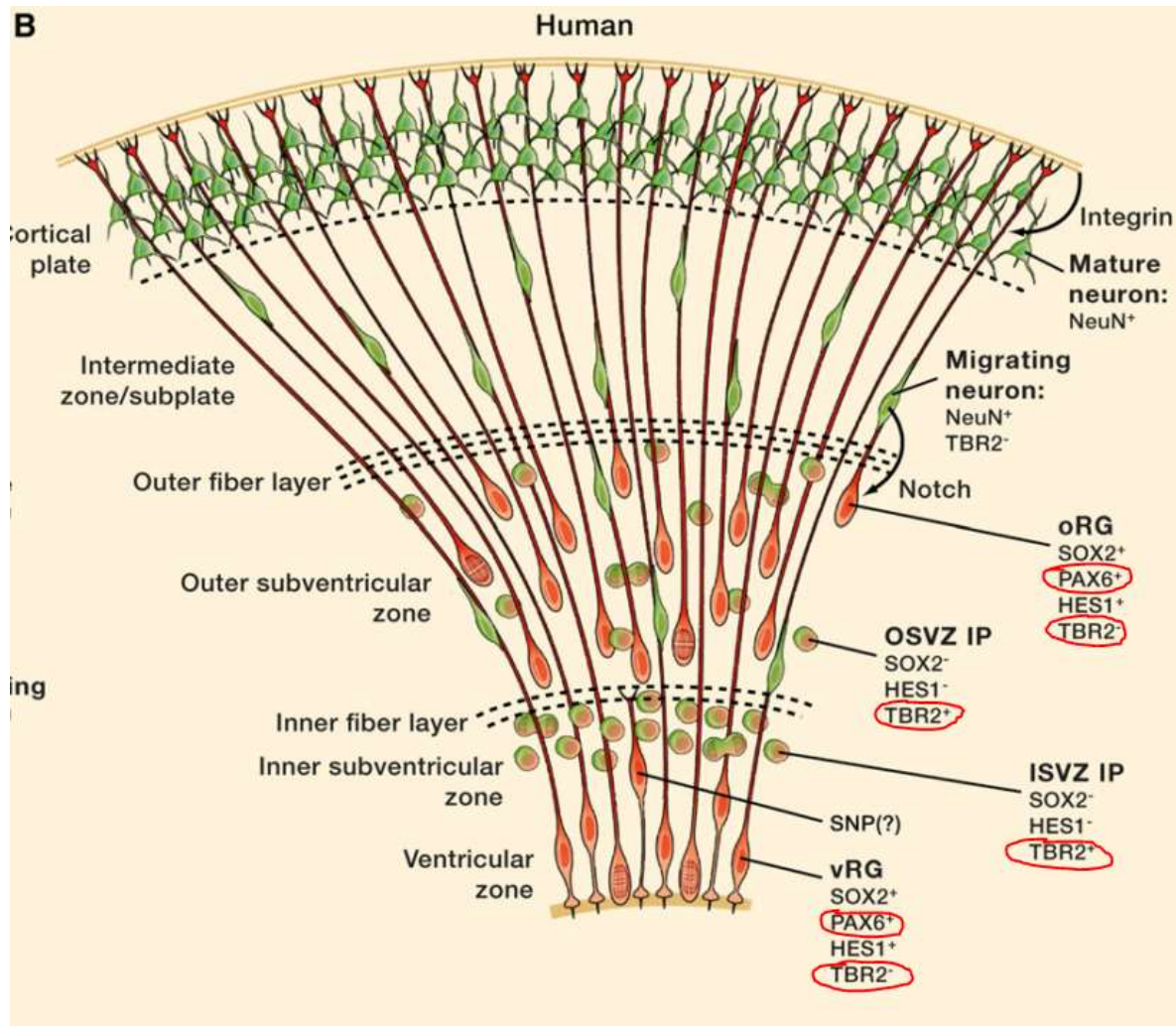
LOCUS XM_004754370 3528 bp mRNA linear MAM 01-JUL-2015
DEFINITION PREDICTED: [Mustela putorius furo](#) eomesodermin (EOMES), mRNA
ACCESSION XM_004754370
VERSION XM_004754370.2
DBLINK BioProject: [PRJNA158527](#)
KEYWORDS RefSeq.
SOURCE Mustela putorius furo (domestic ferret)
ORGANISM [Mustela putorius furo](#)
Eukaryota; Metazoa; Chordata; Craniata; Vertebrata; Euteleostomi;
Mammalia; Eutheria; Laurasiatheria; Carnivora; Caniformia;
Mustelidae; Musteliniae; Mustela.
COMMENT MODEL [REFSEQ](#): This record is predicted by automated computational
analysis. This record is derived from a genomic sequence
([NW_004569185.1](#)) annotated using gene prediction method: Gnomon.
Also see:
[Documentation of NCBI's Annotation Process](#)

- The mink-related cDNA sequences found on NCBI are mostly predicted
- require validation to confirm their accuracy
- it may have implications for downstream single-cell data analysis.

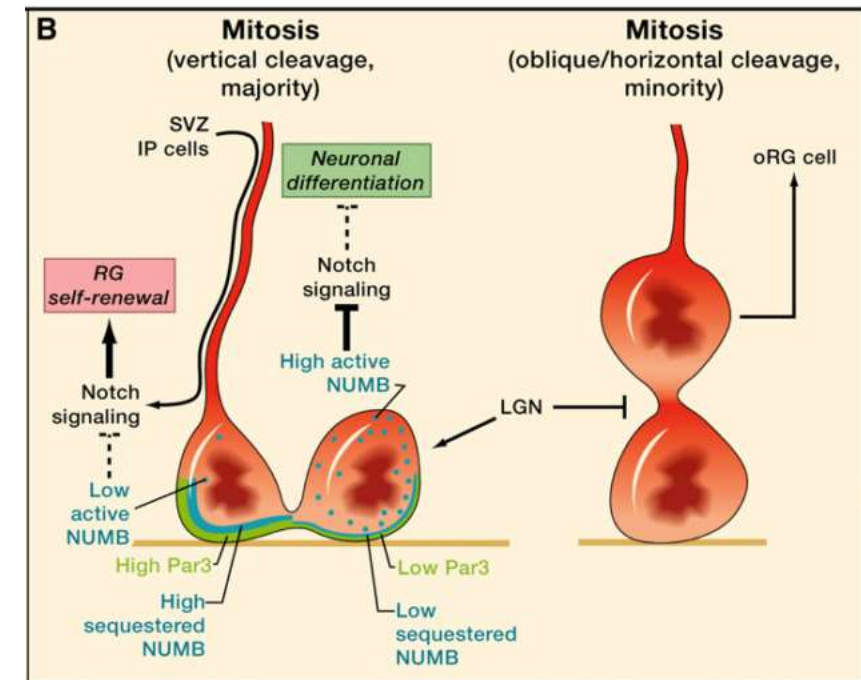
Conclusion

- The randomness in antibody switching is too high
- Dual labeling with antibodies from the same species presents technical challenges
- Developing ferret-specific antibodies has a long cycle and cannot address immediate issues due to uncertainties in nucleic acid and protein information
- Currently, several strategies are being pursued simultaneously

干细胞分布与周期差异统计的思考



- IP: Pax6-&Tbr2+
- RG: Pax6+&Tbr2-
- Pax6+&Tbr2+ cells were present, which may be new IP cells
- There are new neurons in Pax6-&Tbr2+ cells, which need to be removed



ARTICLE

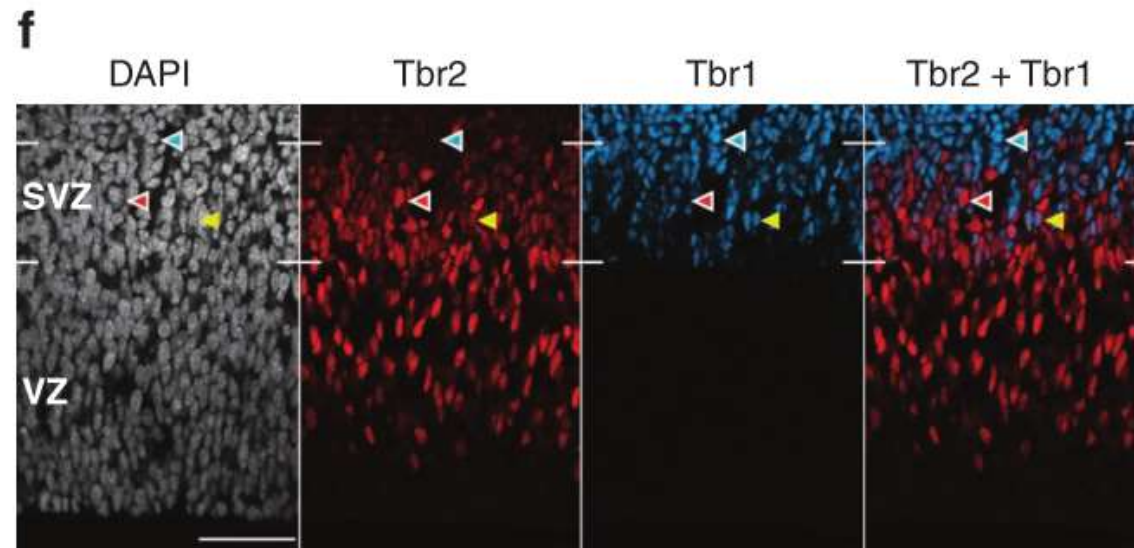
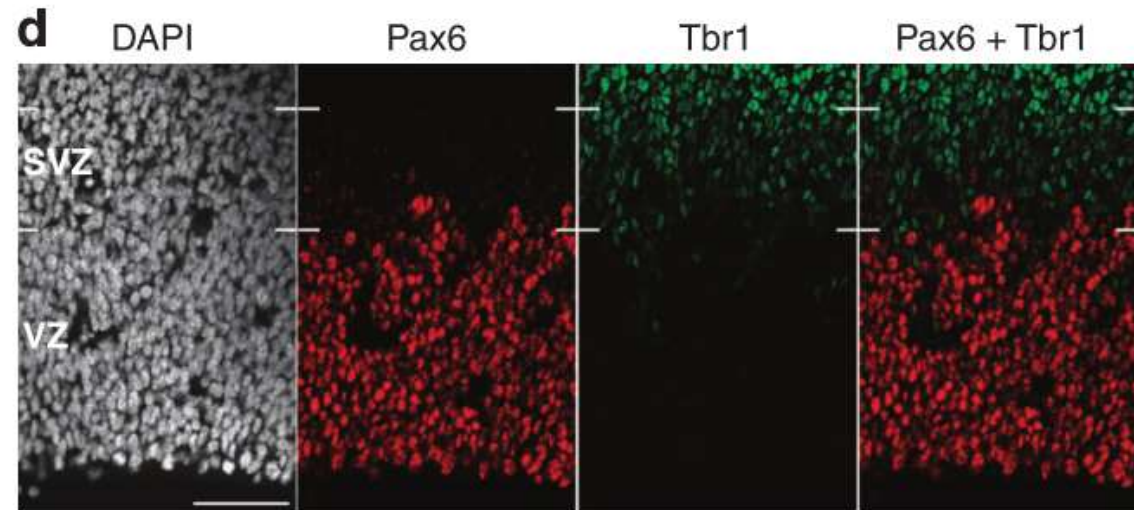
Received 29 Sep 2010 | Accepted 2 Dec 2010 | Published 11 Jan 2011

DOI: 10.1038/ncomms1155

Neural stem and progenitor cells shorten S-phase on commitment to neuron production

Yoko Arai¹, Jeremy N. Pulvers¹, Christiane Haffner¹, Britta Schilling¹, Ina Nüsslein¹, Federico Calegari² & Wieland B. Huttner¹

- IP cells: Cells that are positive for Tbr2 and negative for Tbr1.
- Is Tbr1 expressed in all newborn neurons?
- Do RG cells not directly generate neurons?
- Is NeuN a more representative marker for neurons?
- Can Ki67 be used to exclude newborn neurons?
(Reducing channel occupancy)



关于scRNA-seq

1. scRNA-seq or qRT-PCR?

Cell-cycle regulation	<i>Cdkn1c</i>	Cyclin-dependent kinase inhibitor 1C (p57)	Antiproliferative gene	+3.0	0.022
	<i>Ccng2</i>	Cyclin G2	Mid/late S-phase cyclin	+2.4	0.007
	<i>Rb1</i>	Retinoblastoma 1	G1/S transition regulator	+2.4	0.013
	<i>Cdk2ap1</i>	Cdk2 (cyclin-dependent kinase 2)-associated protein 1	Cdk2 inhibitor	+1.7	0.011
	<i>Cdc25a</i>	Cell division cycle 25 homolog A (<i>Schizosaccharomyces pombe</i>)	Activator of S-phase progression, regulator of DNA checkpoints	+1.6	0.027
	<i>Cdk4</i>	Cyclin-dependent kinase 4	G1/S transition	+1.5	0.012
	<i>Erf</i>	Ets2 repressor factor	Repressor of c-Myc and cdc2	-3.0	0.039
	<i>Cdkl2</i>	Cyclin-dependent kinase-like 2	Cyclin-dependent kinase	-2.5	0.042
	<i>Fbxw7</i>	F-box and WD-40 domain protein 7	Subunit of ubiquitin ligase complex promoting degradation of cell cycle-positive regulators	-1.9	0.019
	<i>E2f1</i>	E2F transcription factor 1	Positive regulator for S-phase progression	+2.2	0.016
DNA replication and repair	<i>Fen1</i>	Flap structure-specific endonuclease 1	Positive regulator of Okazaki fragment maturation and base excision repair	+2.0	0.039
	<i>Fancf</i>	Fanconi anemia, complementation group F	Positive regulator of translesion synthesis	+1.7	0.031
	<i>Rnaseh2b</i>	Ribonuclease H2, subunit B	Positive regulator of Okazaki fragment	+1.5	0.016
	<i>Top2a</i>	Topoisomerase (DNA) II alpha	Regulator of DNA checkpoints, relaxing supercoiled DNA	+1.5	0.046
	<i>Tdg</i>	Thymine DNA glycosylase	Initiator of base excision repair	+1.3	0.041
	<i>Chd1l</i>	Chromodomain helicase DNA-binding protein 1-like	Positive regulator of chromatin relaxation for DNA repair	-2.2	0.031
	<i>Parp16</i>	Poly(ADP-ribose) polymerase family, member 16	Positive regulator of DNA repair	-1.9	0.042
Chromatin remodeling	<i>Gadd45g</i>	Growth arrest and DNA-damage-inducible 45 gamma	DNA demethylase	+4.1	0.032
	<i>Cbx2</i>	Chromobox homolog 2 (<i>Drosophila</i> Pc class)	Polycomb repressive complex subunit	+1.9	0.007
	<i>Phc2</i>	Polyhomeotic-like 2 (<i>Drosophila</i>)	Polycomb repressive complex subunit	+1.6	0.020
	<i>Kdm1a</i>	Lysine (K)-specific demethylase 1A	Histone modifier	+1.6	0.042
	<i>Hdac2</i>	Histone deacetylase 2	Histone modifier	+1.5	0.030
	<i>H3f3b</i>	H3 histone, family 3B	Chromatin component	+1.5	0.031
	<i>Kdm2b</i>	Lysine (K)-specific demethylase 2B	Histone modifier	+1.5	0.046
	<i>Brd3</i>	Bromodomain containing 3	Histone modifier	+1.4	0.026
	<i>Bmi1</i>	Bmi1 polycomb ring finger oncogene	Polycomb repressive complex subunit	+1.3	0.033
	<i>Sin3a</i>	Transcriptional regulator, SIN3A (yeast)	Regulator of histone modification	+1.3	0.040
	<i>Hils1</i>	Histone H1-like protein in spermatids 1	Chromatin component	-3.6	0.010
	<i>Hmga2</i>	High-mobility group AT-hook 2	Chromatin component	-3.4	0.037
	<i>Pcgf5</i>	Polycomb group ring finger 5	Polycomb repressive complex subunit	-2.1	0.049
	<i>Mbd2</i>	Methyl-CpG-binding domain protein 2	Histone modifier	-1.9	0.024

- Genes related to cell division speed are numerous.
- Apart from directly regulating the cell cycle, genes associated with DNA repair, chromatin remodeling, microtubule and microfilament regulation, adhesion factors, and signaling pathway regulators are all involved in cell cycle regulation.
- qRT-PCR is not suitable for this purpose.
- After screening, further validation can be done through qRT-PCR and in situ hybridization.

2. RNA-seq or microarray?

RNA-Seq	microarray
<ul style="list-style-type: none">➤ Broader coverage➤ Possibly detecting unknown genes➤ Large dataset, difficult analysis➤ Can only be sent to sequencing companies, difficult quality control➤ Difficult to achieve dynamic detection of gene expression at developmental time points	<ul style="list-style-type: none">➤ The coverage area is relatively small.➤ The detected genes are all known.➤ After designing the reaction plate and hybridization conditions, the operation is convenient.➤ It is easy to achieve dynamic detection of gene expression at different developmental time points.

Published online: April 26, 2015

Resource



TRANSPARENT
PROCESS



OPEN
ACCESS

THE
EMBO
JOURNAL

Discrete domains of gene expression in germinal layers distinguish the development of gyrencephaly

Camino de Juan Romero¹, Carl Bruder^{2,†}, Ugo Tomasello¹, José Miguel Sanz-Anquela³ & Víctor Borrell^{1,*}

RESEARCH ARTICLE | OPEN ACCESS

Transcriptome sequencing and development of an expression microarray platform for the domestic ferret

Carl E Bruder , Suxia Yao, Francis Larson, Jeremy V Camp, Ronald Tapp, Alexis McBrayer, Nicholas Powers, Willy Valdivia Granda and Colleen B Jonsson

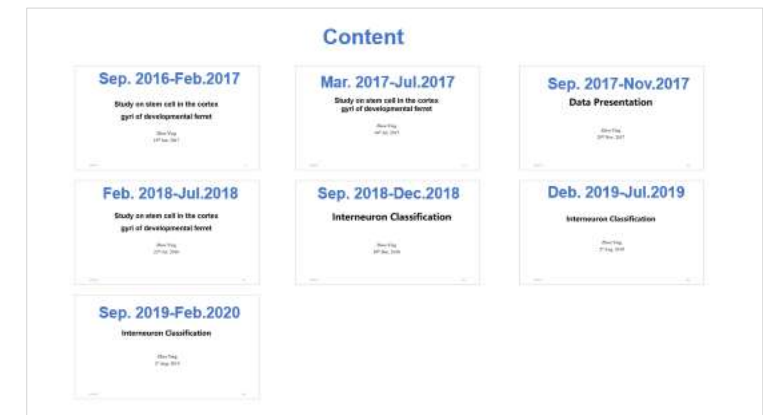
BMC Genomics 2010 11:251 | DOI: 10.1186/1471-2164-11-251 | © Bruder et al; licensee BioMed Central Ltd. 2010

Received: 17 December 2009 | Accepted: 19 April 2010 | Published: 19 April 2010

- The limited information available in ferret-related gene databases poses challenges for alignment, making it difficult to analyze sequence results effectively
- the lack of background knowledge about expressed genes may also hinder analysis
- Techniques for analyzing sequence results, such as quality control of raw data and assessment of gene expression, require careful consideration and expertise

Next stage plan

- Priority is to address the antibody issue
- Once resolved, promptly obtain data on the distribution and cycle differences of stem cells
- Experiment with the precision of microdissection on P2 mink brain slices
- Experiment with individualized cells and conduct immunohistochemistry



Data Presentation

Zhou Ying

28th Nov. 2017

Content

- Current work
- Problems of RNA-Seq experiment and data analysis
- Literatures and thinking
 - Folding of the Cerebral Cortex Requires Cdk5 in Upper-Layer Neurons in Gyrencephalic Mammals (Hiroshi Kawasaki)
 - Gyrification of the cerebral cortex requires FGF signaling in the mammalian Brain (Hiroshi Kawasaki)
- Next plan

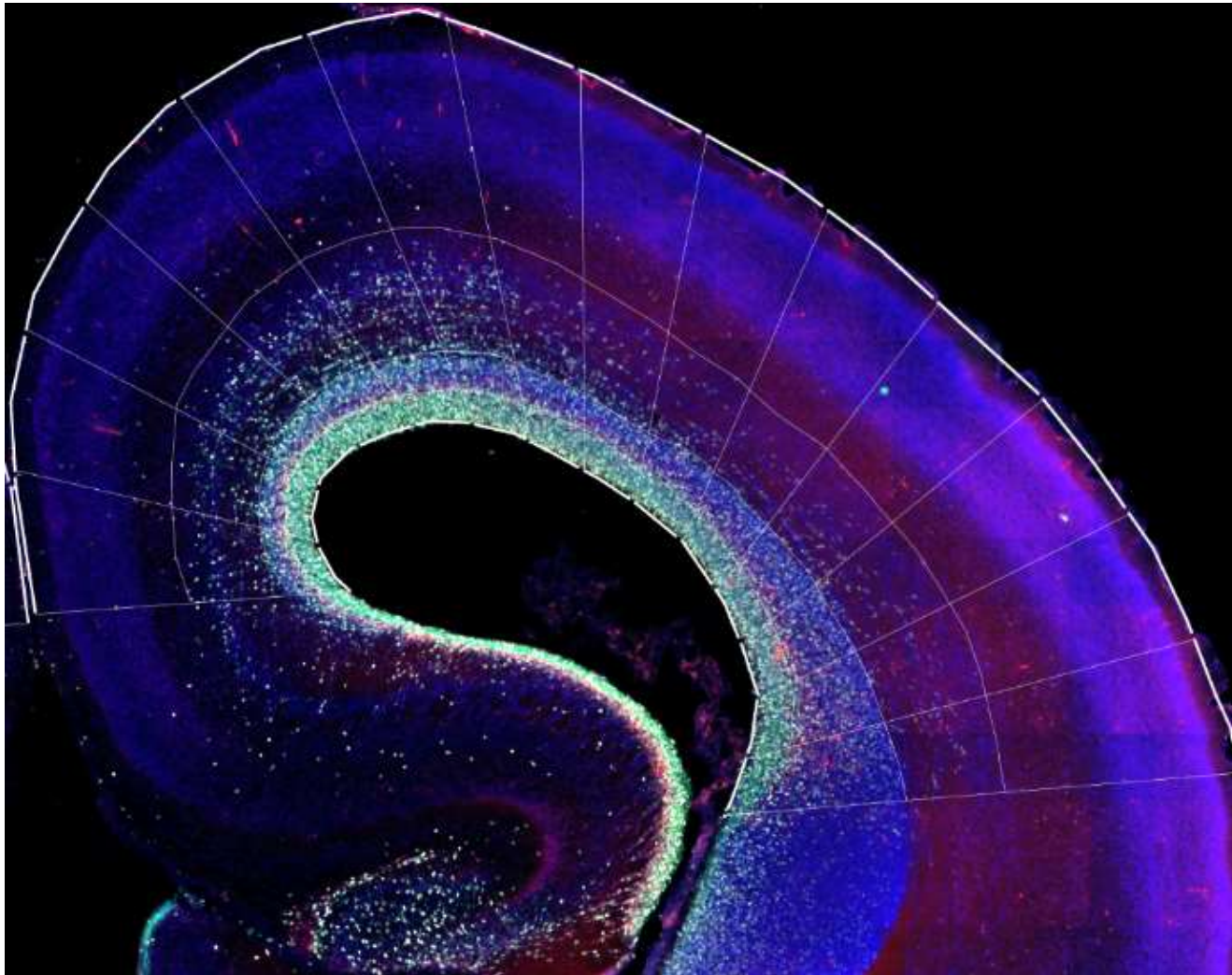
Current work

The progress of sampling and image acquisition for P2-P3 juvenile ferrets.

Brdu injection	0h(P2)	5h(P2)	10h(P2)	15h(P2)	20h(P2)	25h (P3)	30h (P3)	35h (P3)	40h (P3)	45h (P3)
1 st group	分区完成，统计部分	分区完成	分区完成	分区完成	分区完成	分区完成	分区完成	发育有些不正常	干细胞分布统计	-
2 nd group	图像采集	图像采集	图像采集	图像采集	图像采集	图像采集	图像采集	发育有些问题	干细胞分布统计	染色没染好

Current work

- Adjust the Tbr2 staining protocol to enhance Tbr2 signal and reduce background.
- Compile the distribution data of stem cells at P3 (P2+40h, near P4).
- Organize the heatmap of stem cell distribution for P2, P3 (P2+40h, near P4), and P4.
- Extract total RNA from mink cortex together with Luo Yuhui.



Merge+DAPI



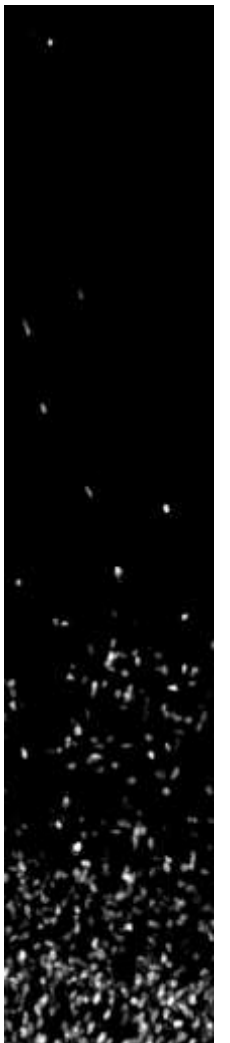
Pax6

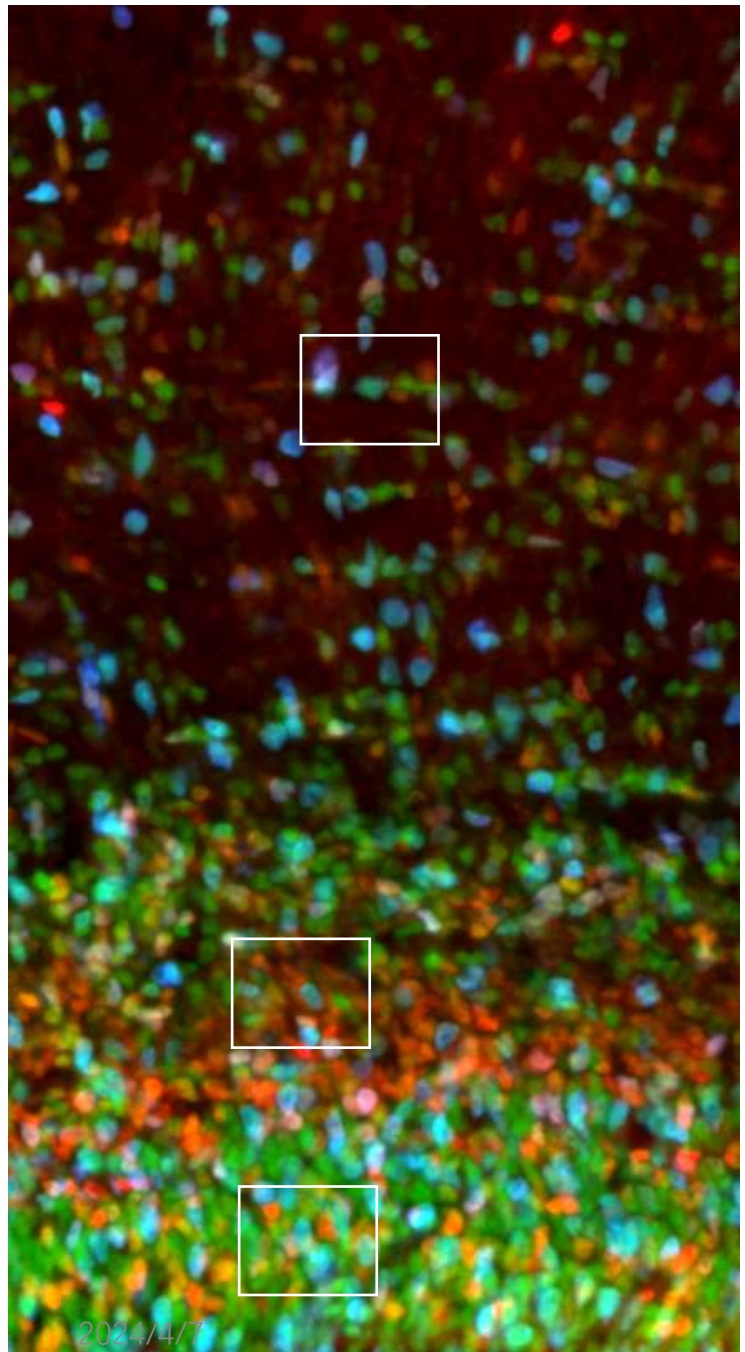


Tbr2



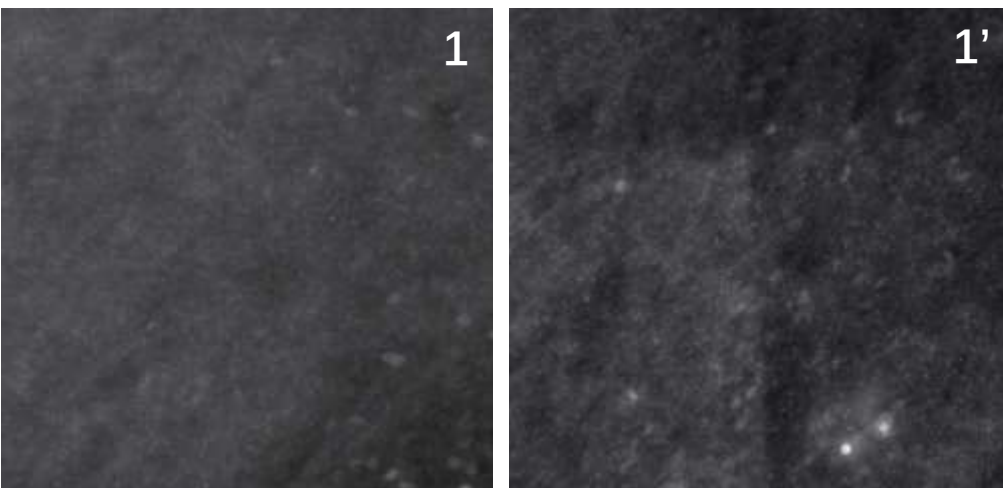
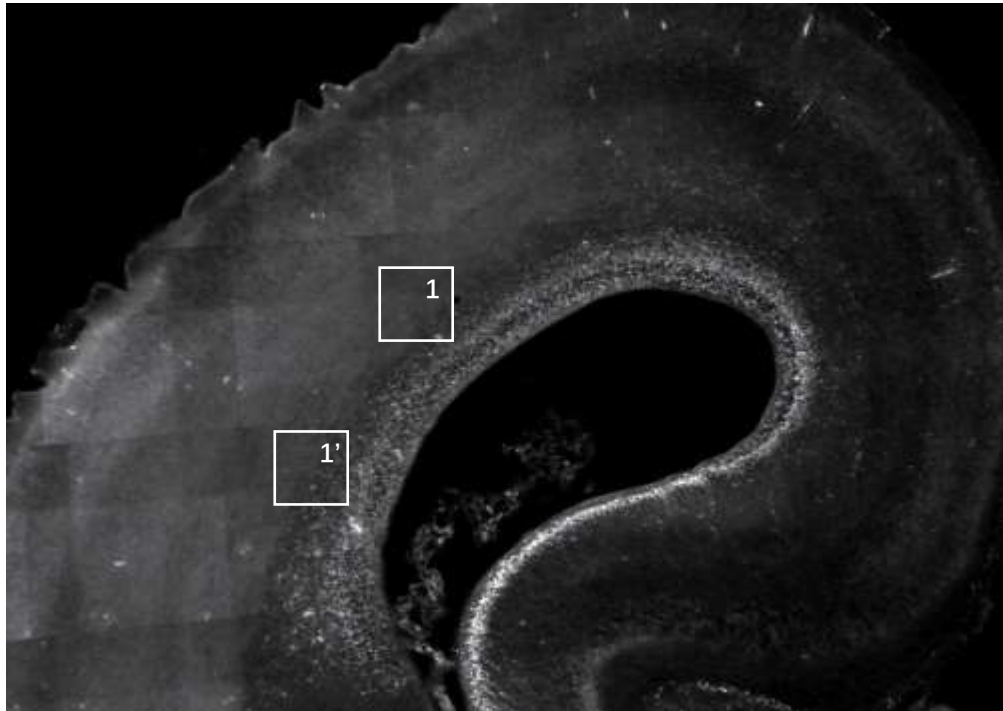
BrdU



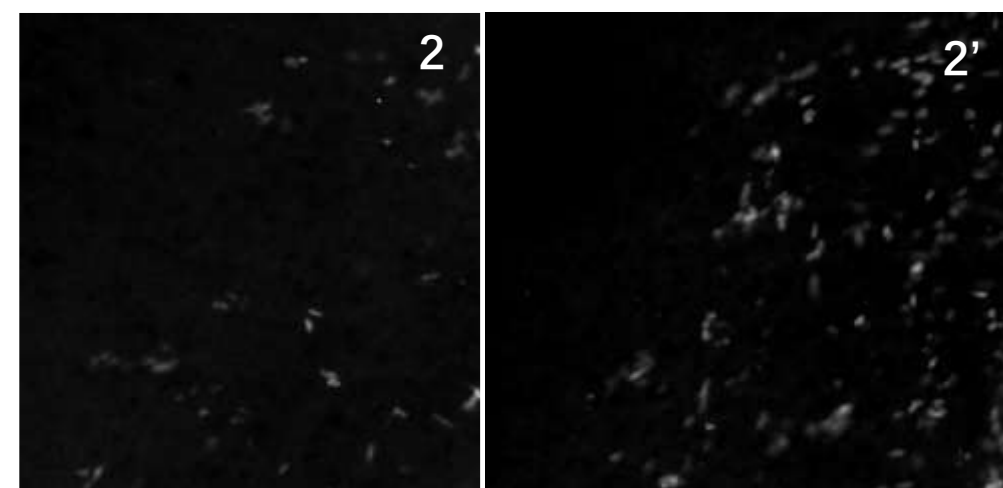
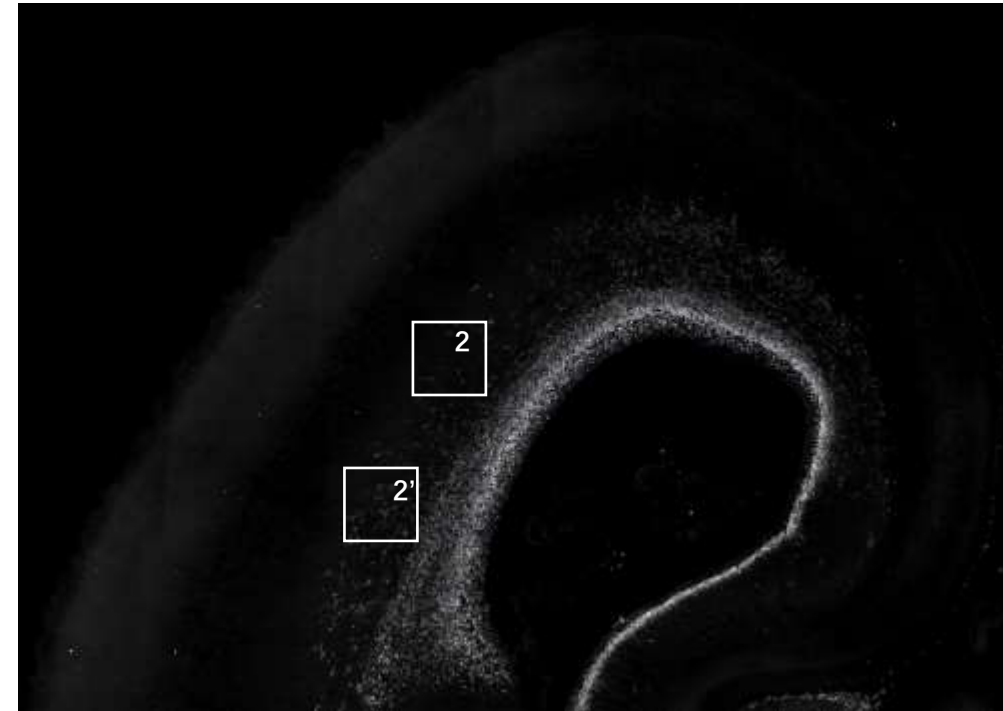


The improved Tbr2 staining protocol

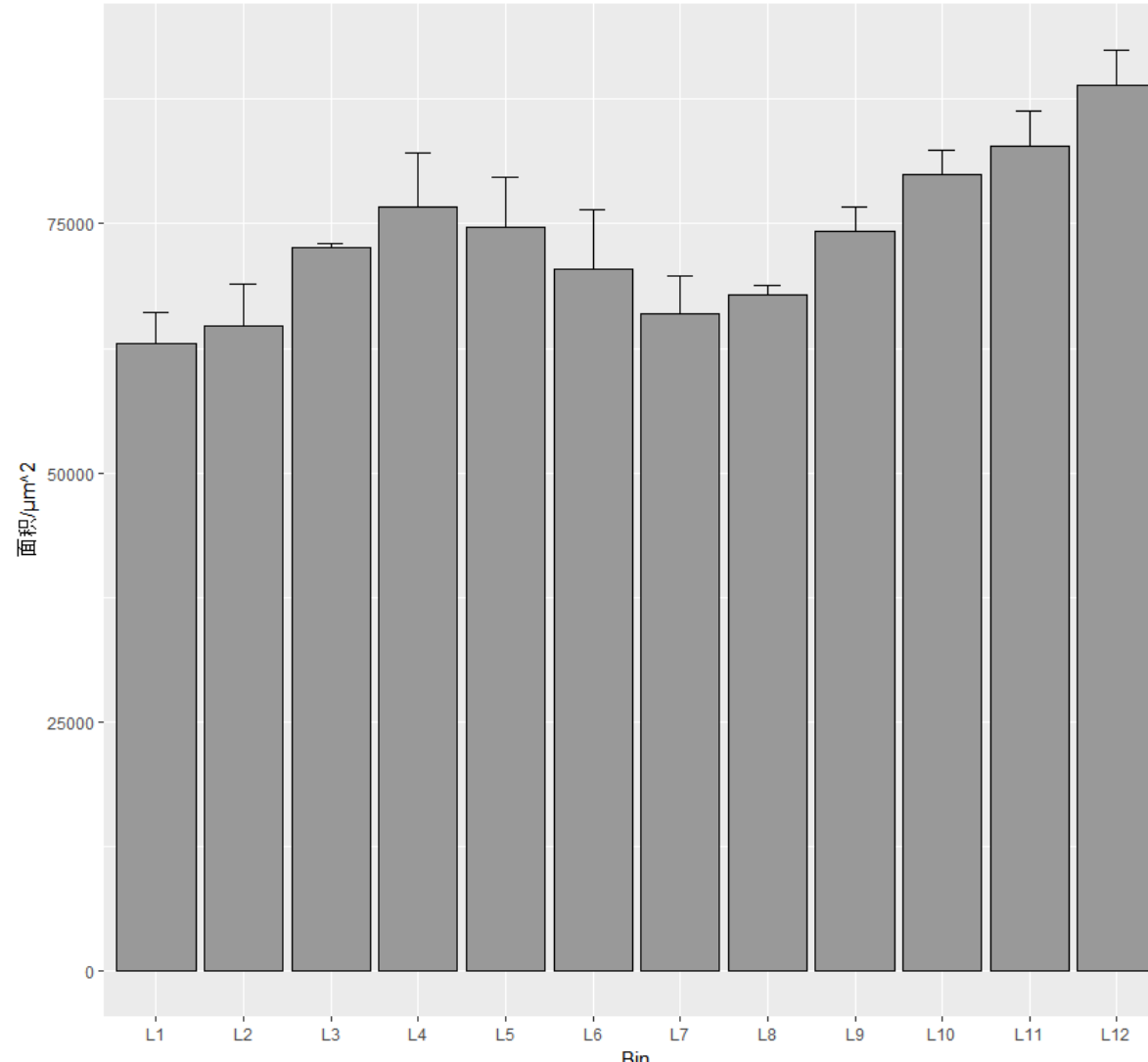
- After washing away OCT, incubate in 0.3% PBST at room temperature for 30 minutes or more to thoroughly permeabilize the membrane.
- Antigen retrieval at room temperature for 5 minutes.
- Incubate in Tris-Glycine at room temperature for 30 minutes to quench the spontaneous fluorescence of PFA aldehyde groups.
- Proceed with standard immunohistochemistry



Before stanning methods of Tbr2



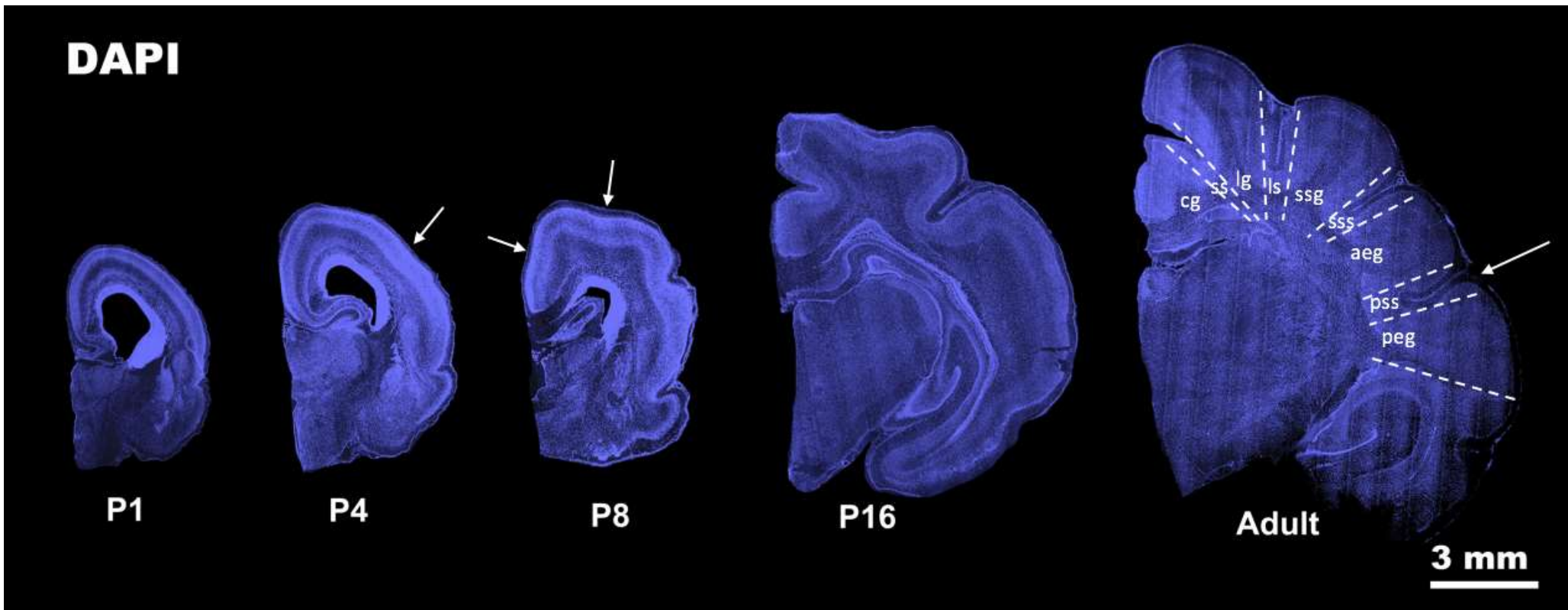
Improved stanning methods of Tbr2



At the same developmental time and position, the area difference of bin values is not significant.

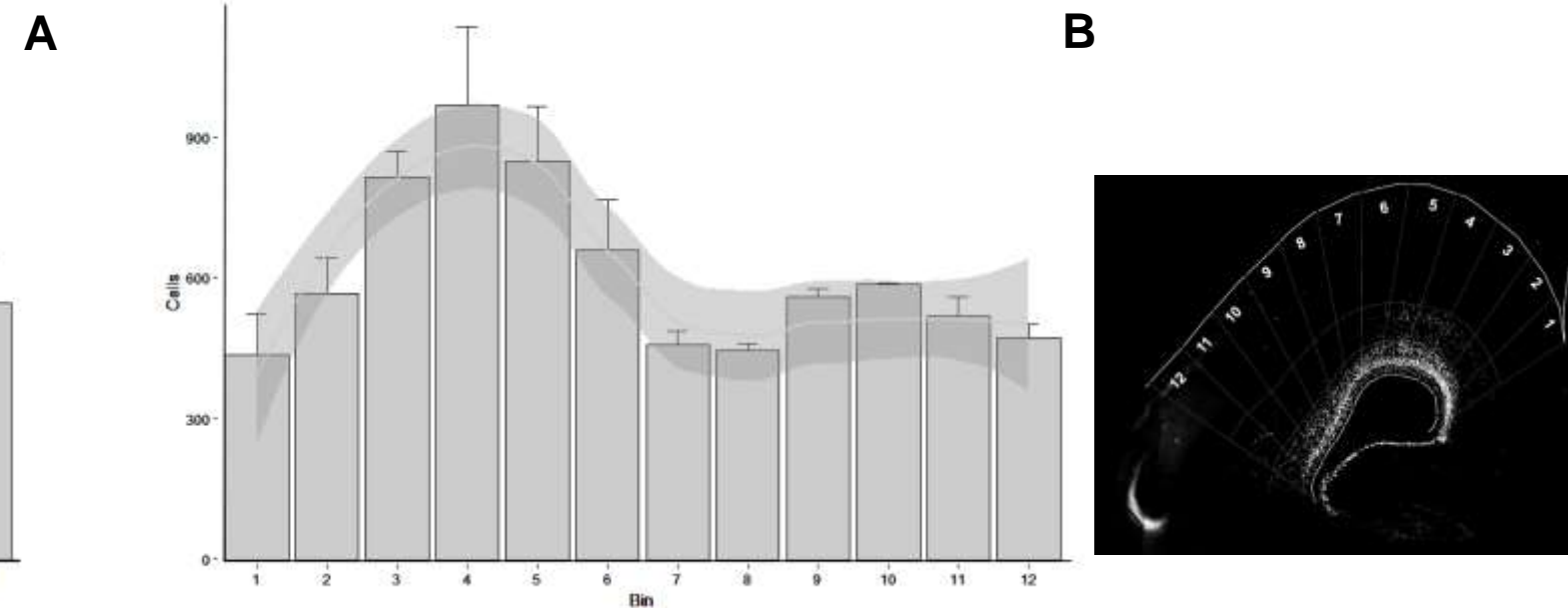
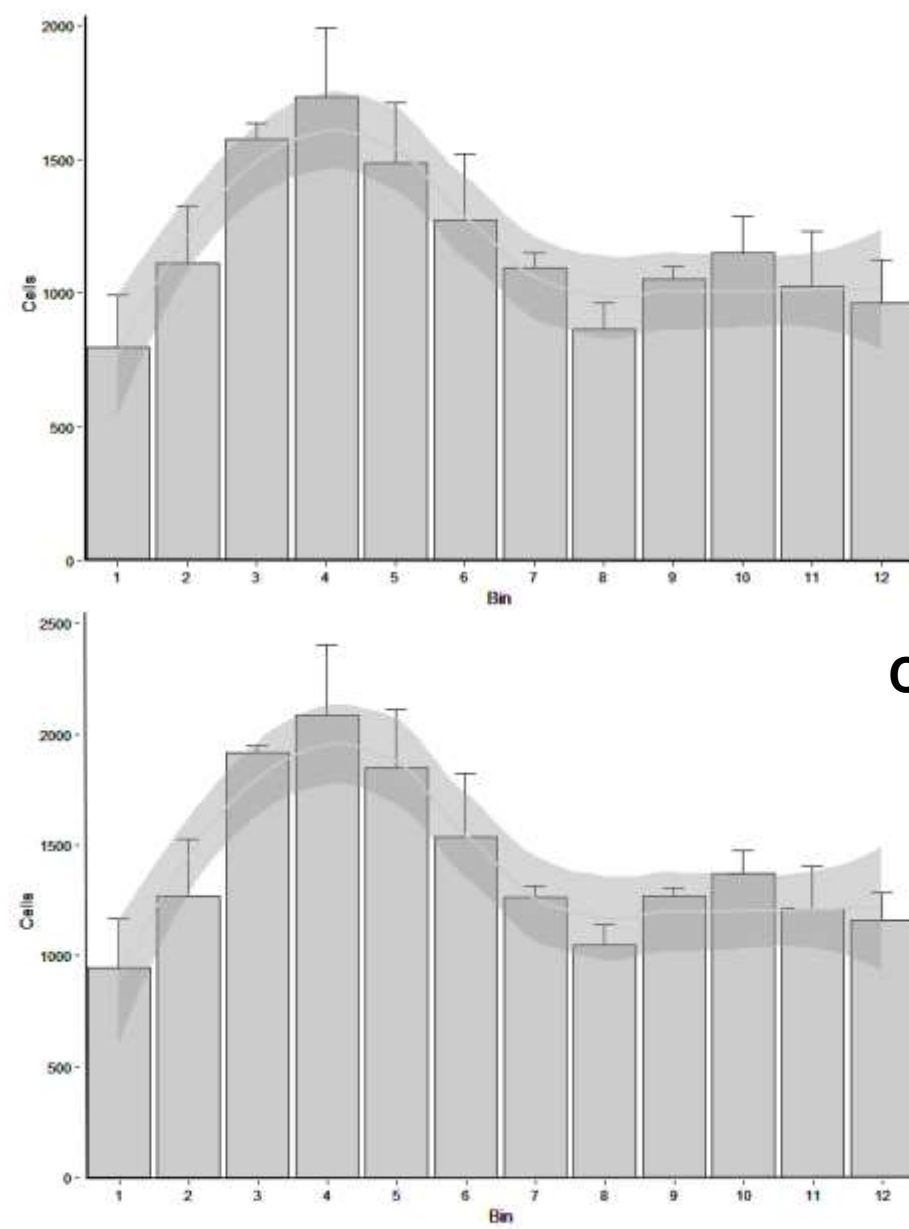
P3(P2+40), n=2 ferret, Bar present mean \pm SEM

- Control the positioning and size of the bins.
- Establish the starting position of the first bin uniformly based on the main distribution of the marker.
- The outer contour is approximately 400 μm , and the inner contour is approximately 150 μm to define the boundary. Connect the lines to form the boundary of the bins. Divide the layers based on DAPI density.



林攸宁, 罗宇慧 (标注沟回名称)

A: Distribution of Pax6+ cells B: Distribution of Tbr2+ cells C: Distribution of Pax6+ & Tbr2+ cells P3 (P2+40h), n=2 ferrets

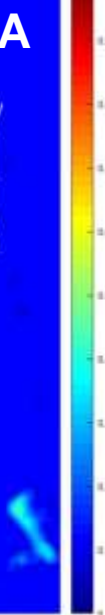
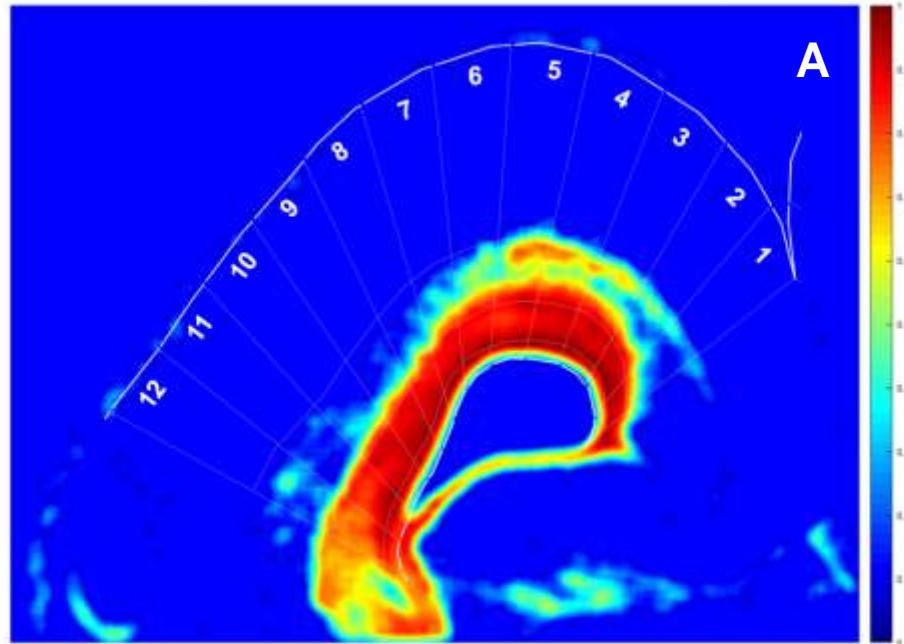


A: Distribution of Pax6+ cells

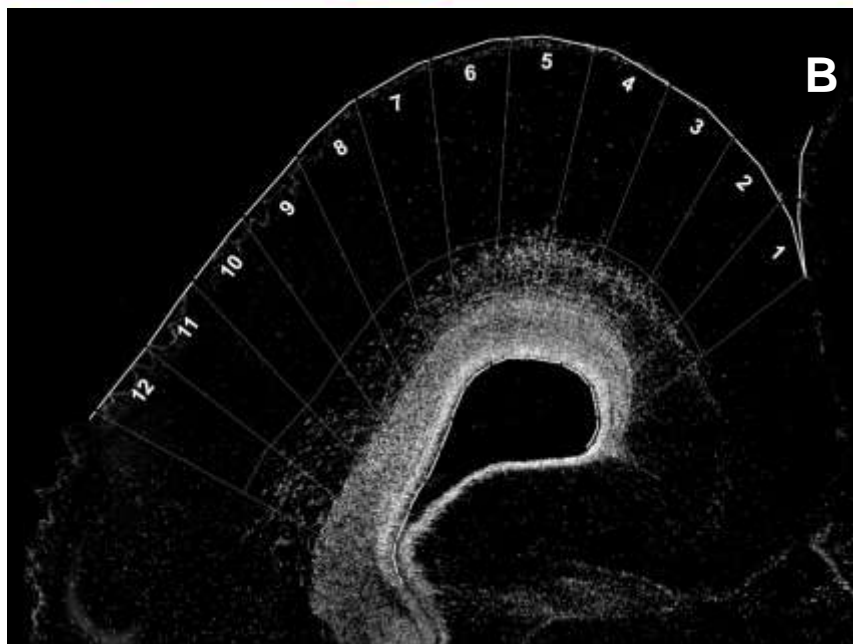
B: Distribution of Tbr2+ cells

C: Distribution of Pax6+ & Tbr2+ cells

P3 (P2+40h), n=2 ferrets, Bar represents mean \pm SEM



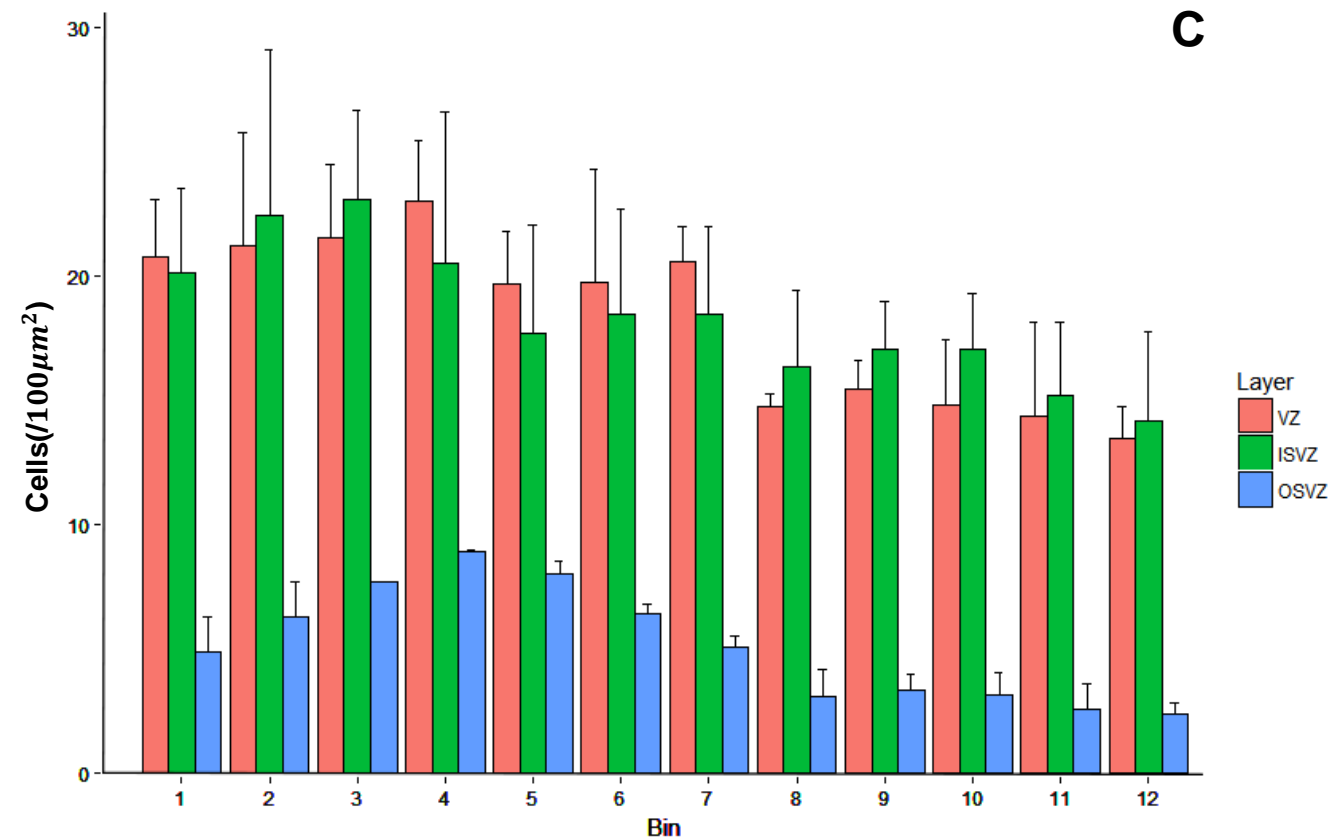
A: Density distribution plot of Pax6 at P3



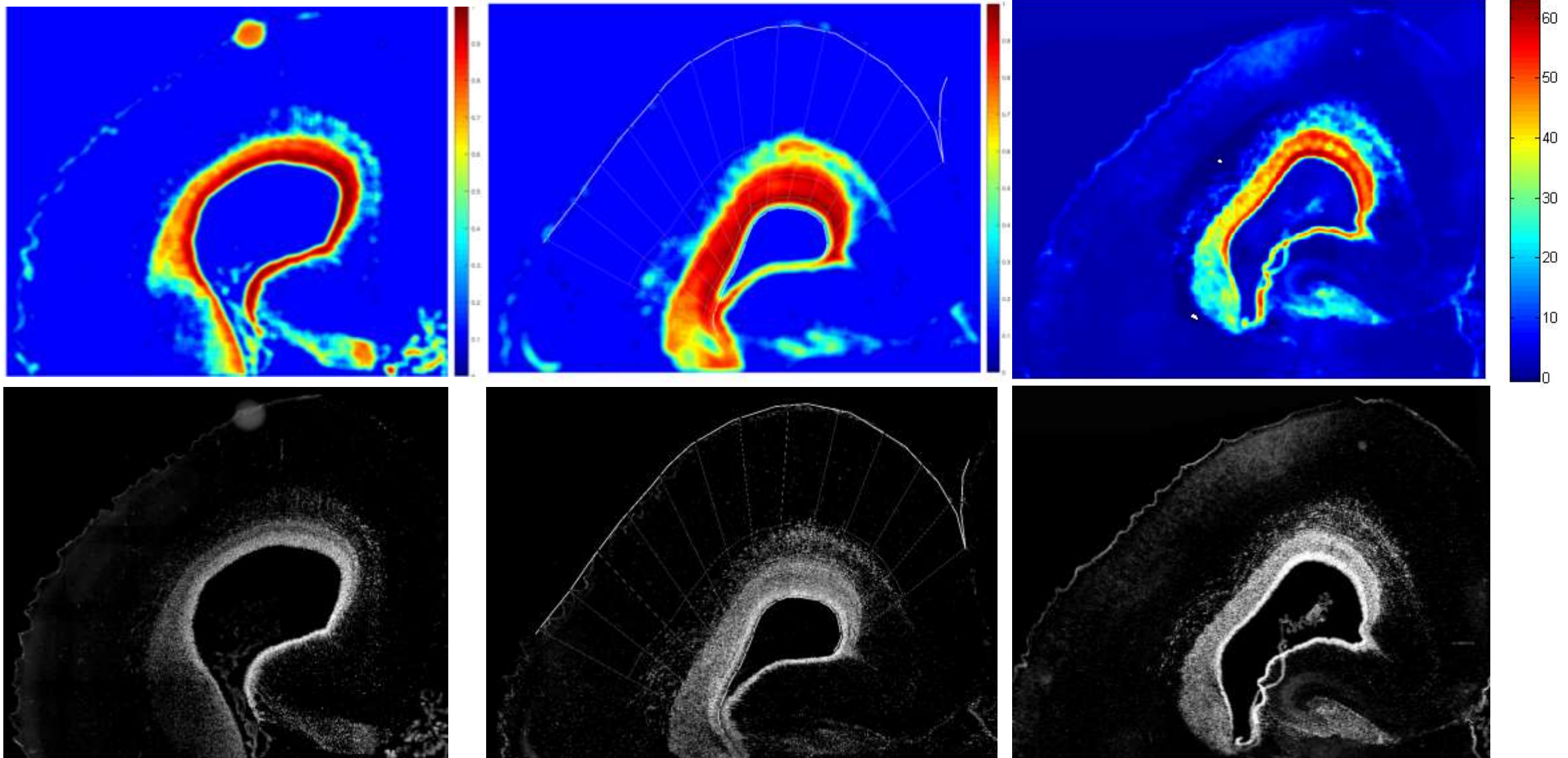
B: Pax6 IHC at P3

C: Density distribution statistics of Pax6 in different layers

n=2 ferrets, Bar represents mean \pm SEM



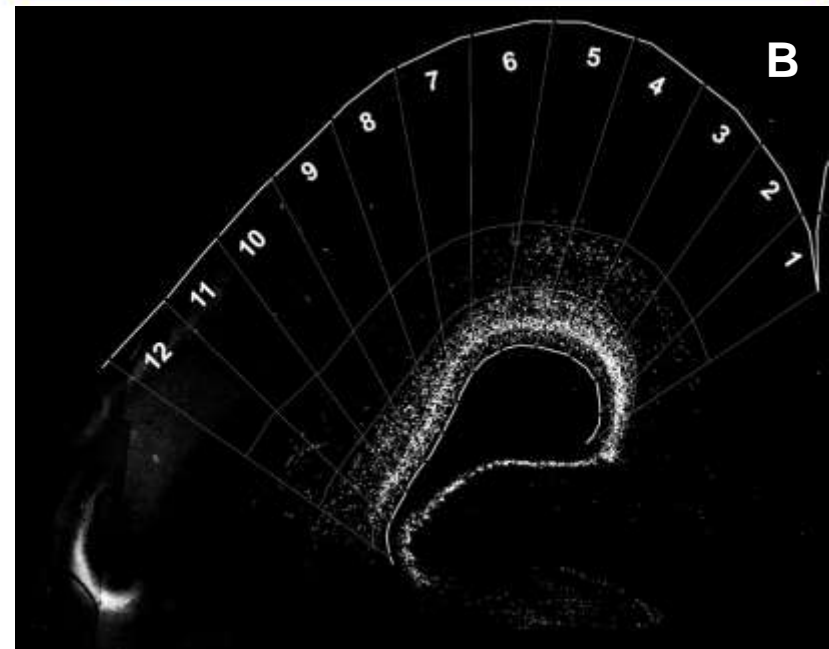
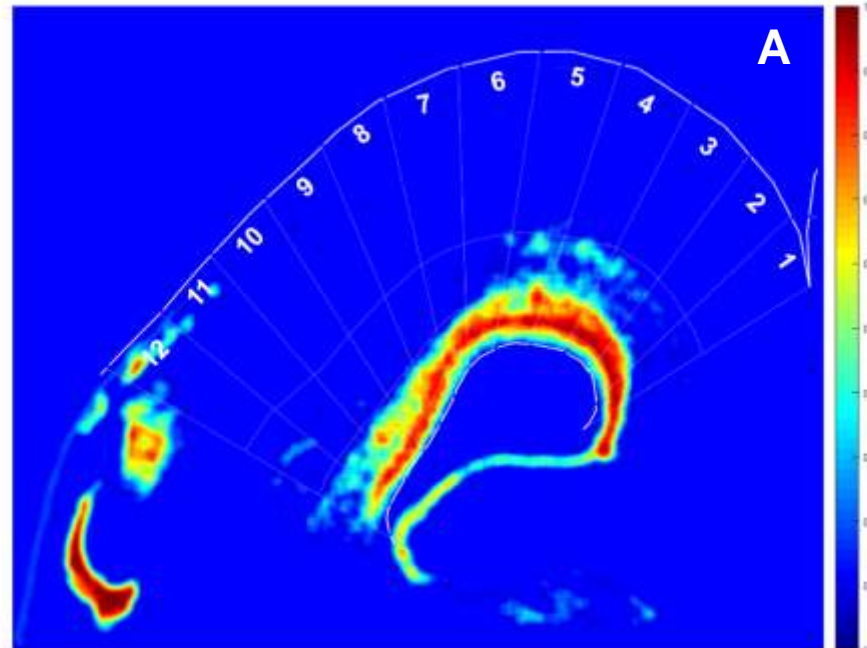
Layer
 VZ
 ISVZ
 OSVZ



P2 Pax6

P3 (P2+40h) Pax6

P4 Pax6

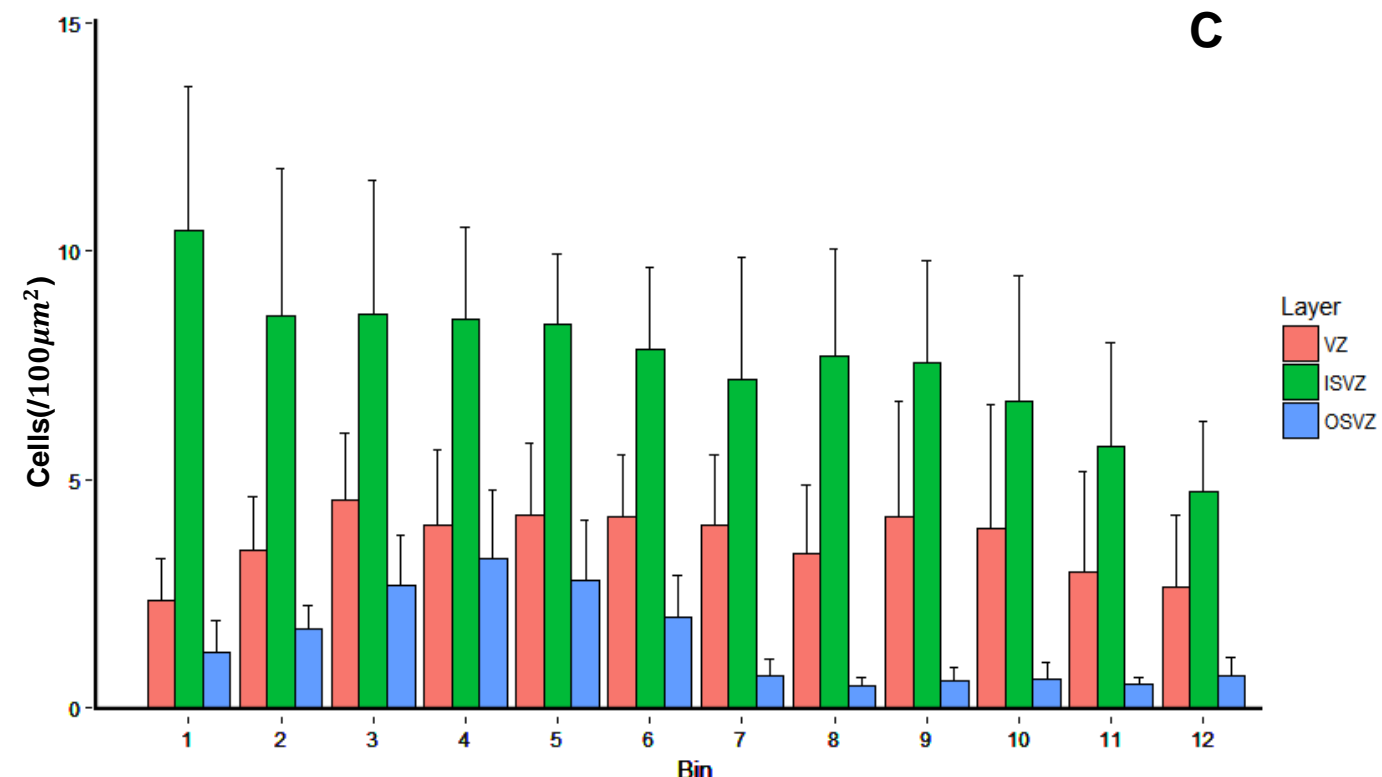


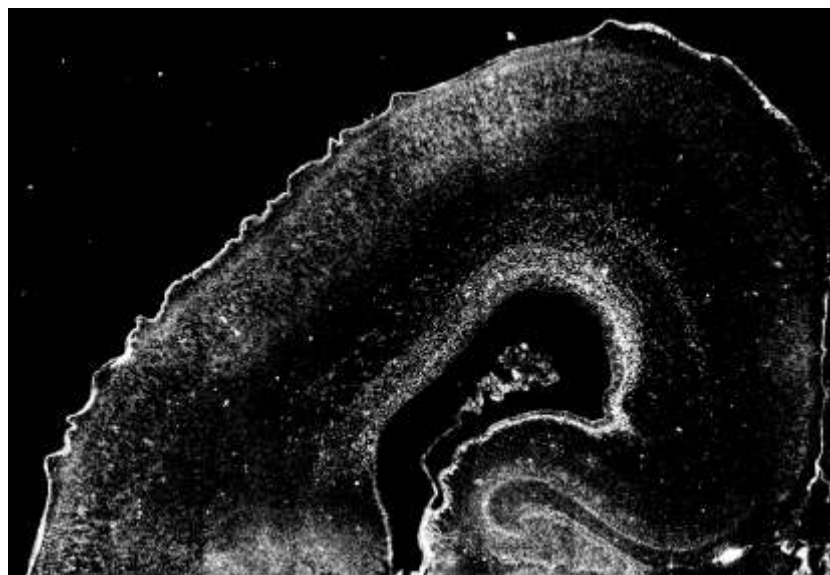
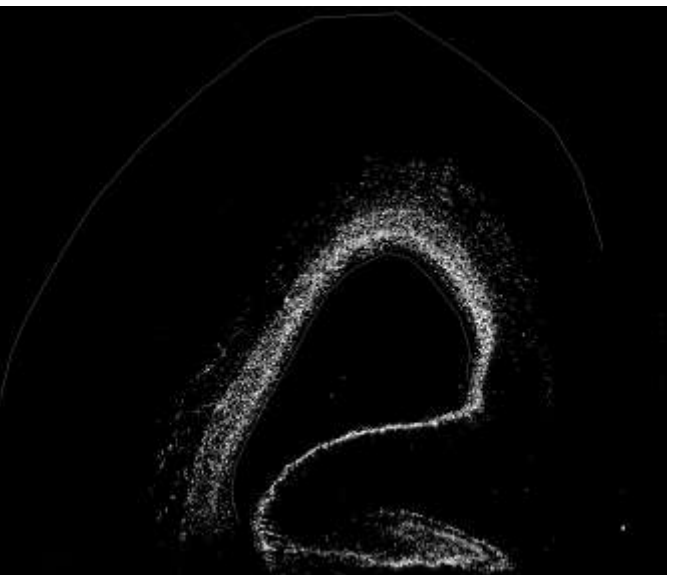
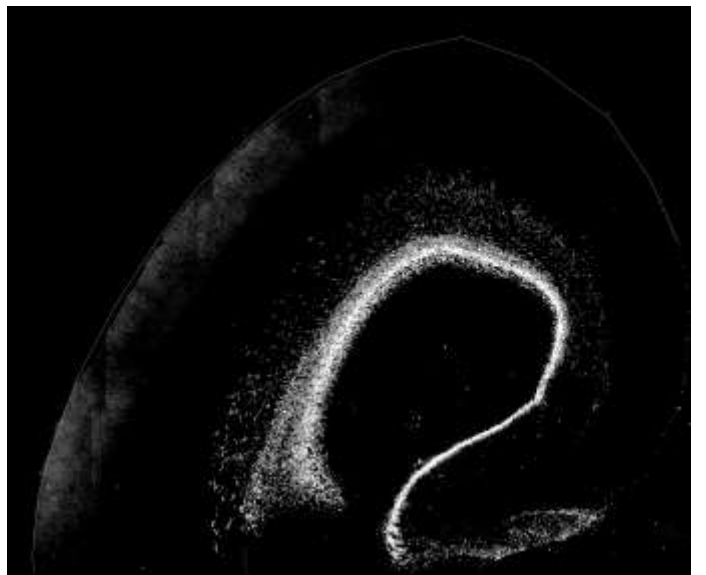
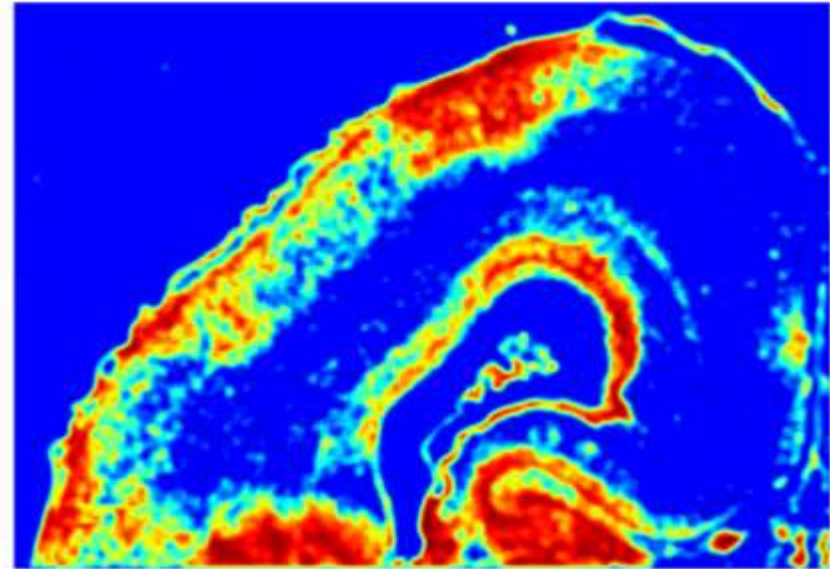
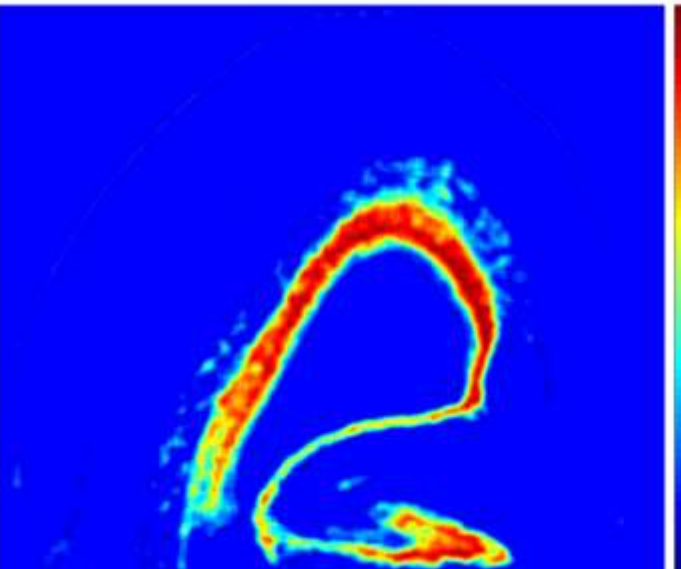
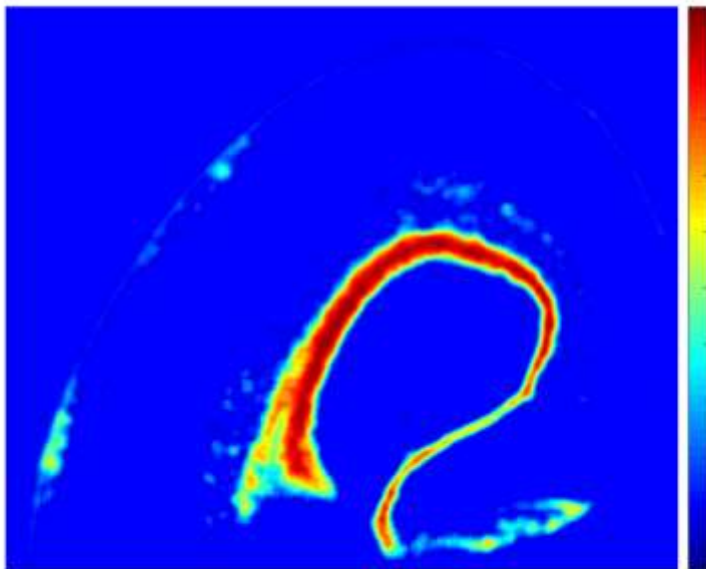
A: Density distribution plot of Tbr2 at P3

B: Tbr2 immunohistochemistry at P3

C: Density distribution statistics of Tbr2 in different layers

n=2 ferrets, Bar represents mean \pm SEM

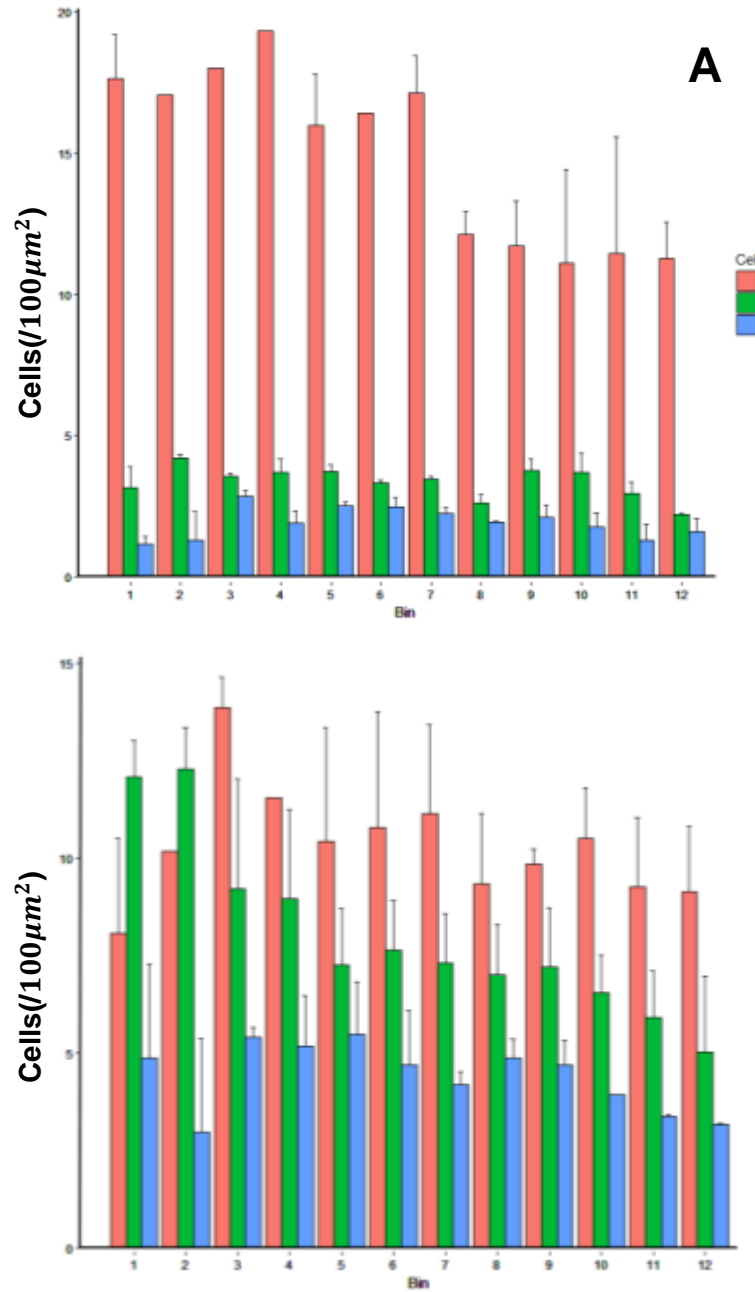




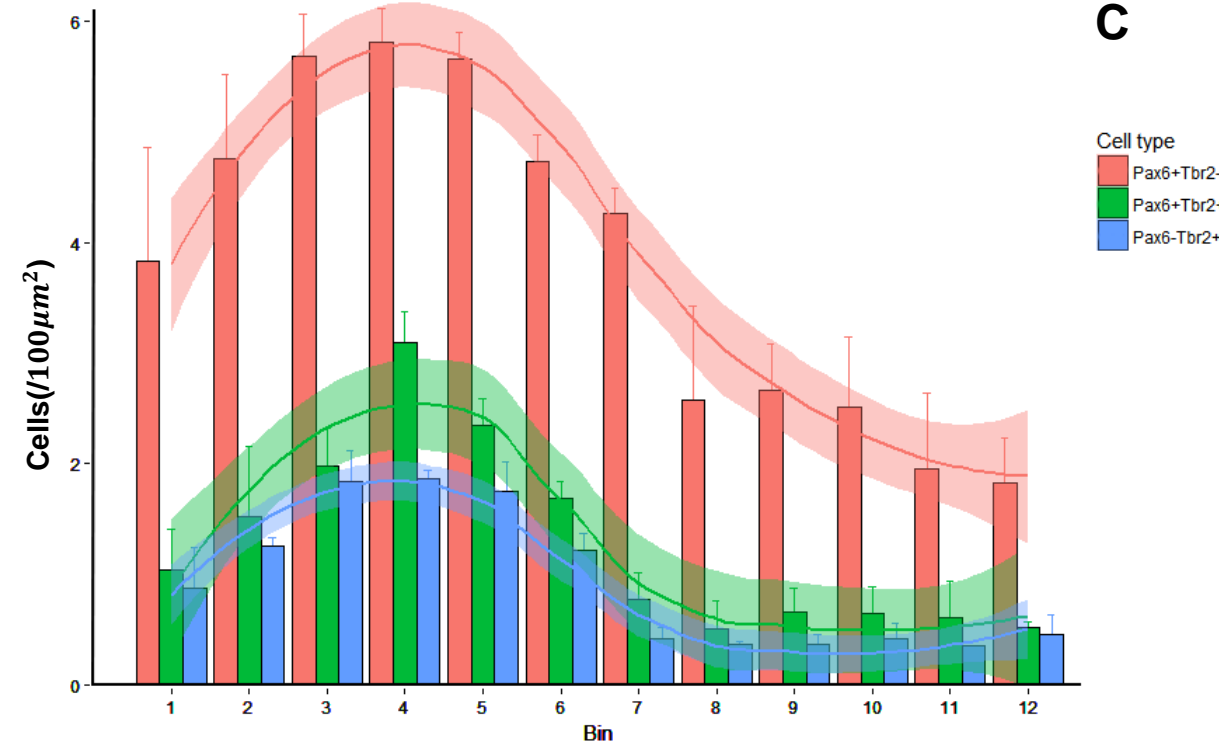
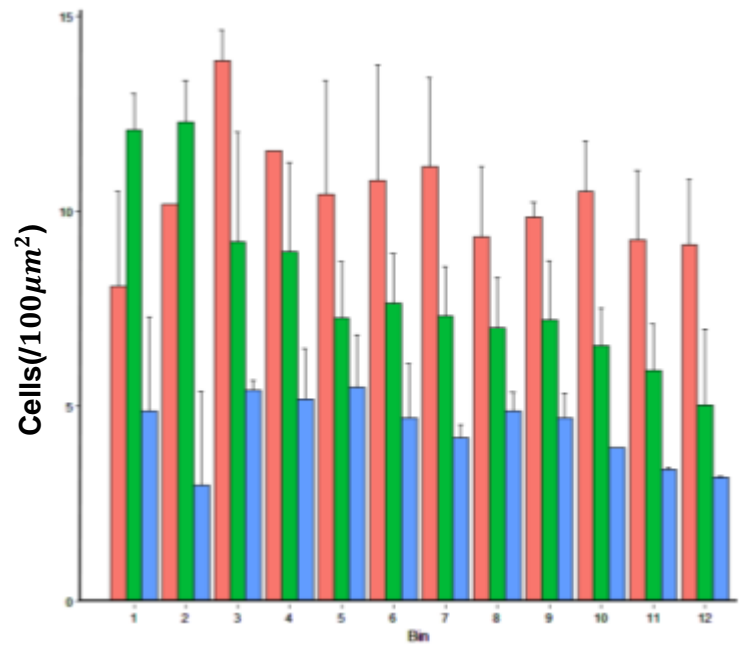
P2 Tbr2

P3 (P2+40h) Tbr2

P4 Tbr2

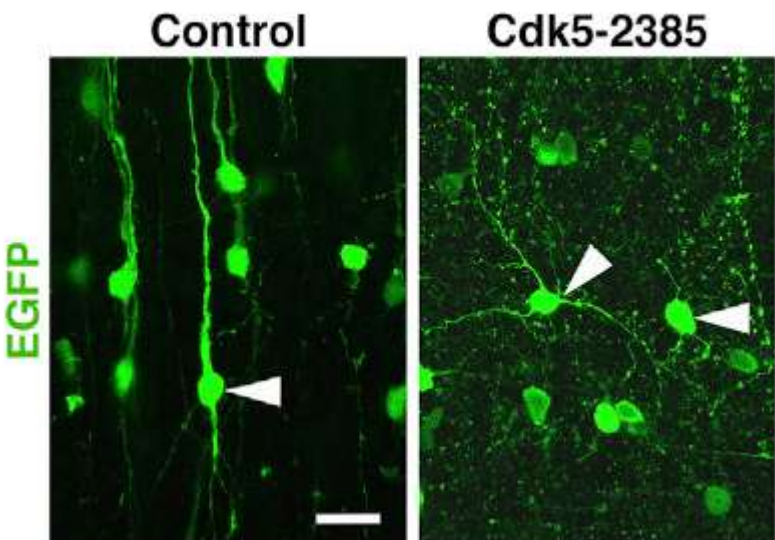
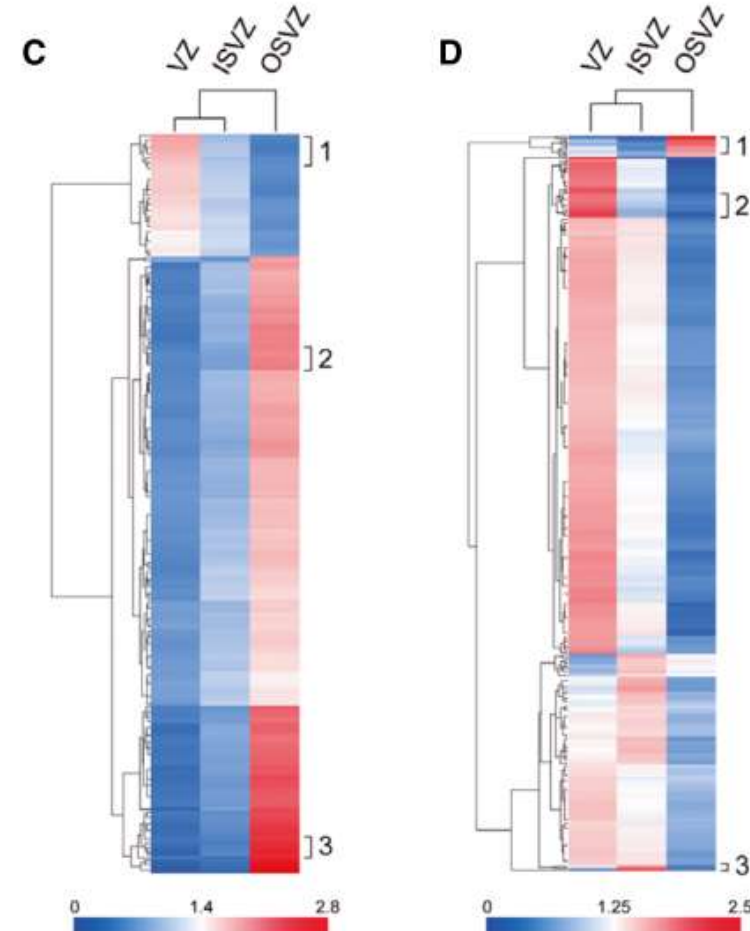
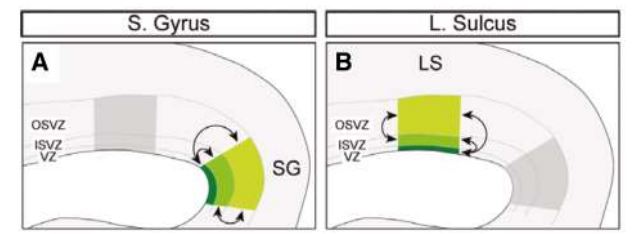
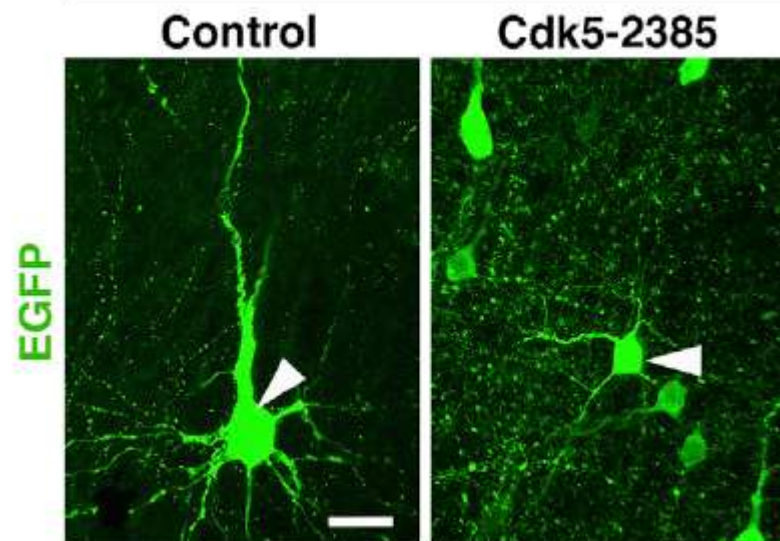


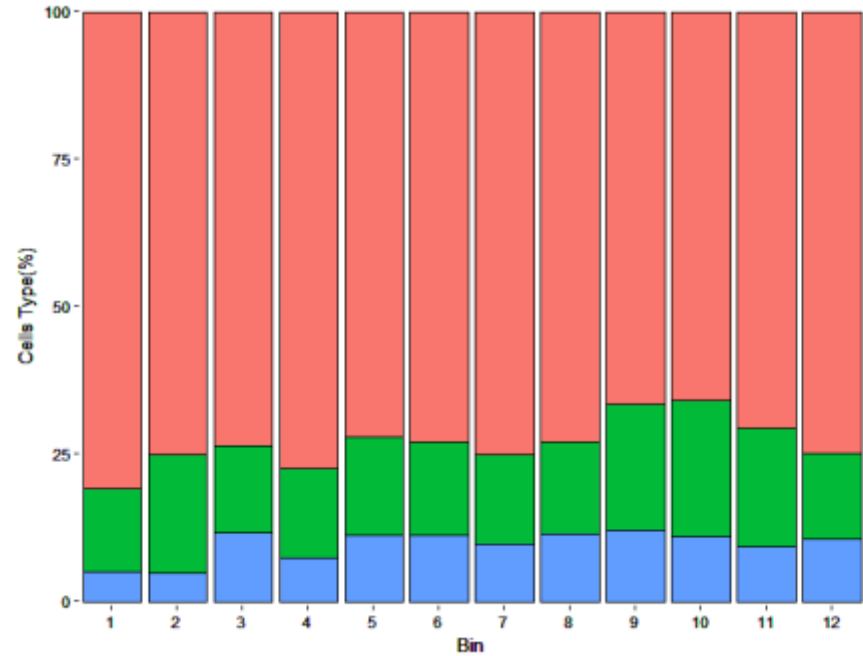
A: Density distribution of different stem cells in VZ at P3
B: Density distribution of different stem cells in ISVZ at P3
C: Density distribution of different stem cells in OSVZ at P3
n=2 ferrets, Bar represents mean \pm SEM



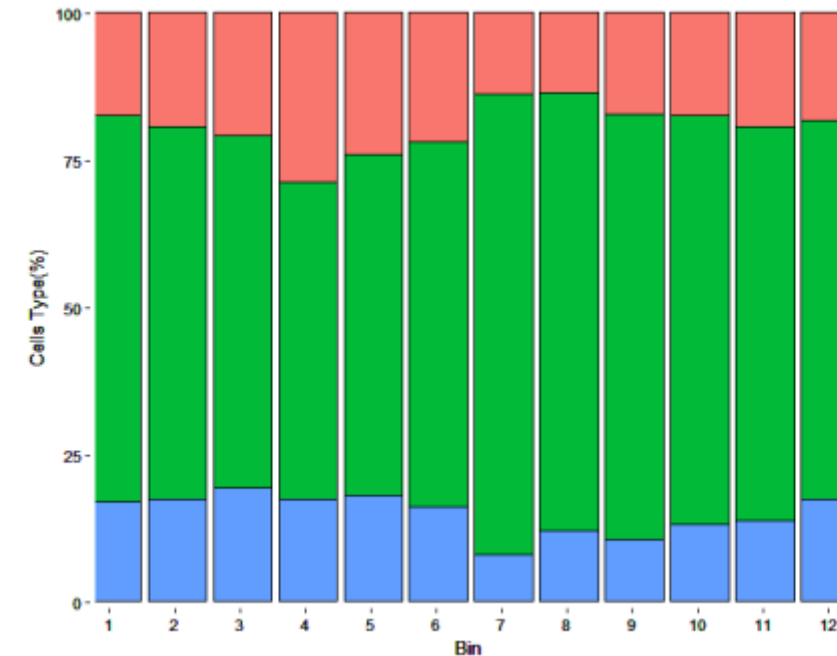
Summary

- Overall, in terms of stem cell distribution, there is a higher density of stem cells in the location where the LG develops.
- Pax6 is primarily distributed in the VZ/ISVZ, while Tbr2 is mainly distributed in the ISVZ.
- Regarding layer-specific distribution, the OSVZ layer exhibits the greatest differences, with a higher density of stem cells at the LG location, and the distribution trend corresponds to the subsequent formation of LG and SSS.
- From density distribution plots at different time points, it can be observed that positions with higher stem cell density in the OSVZ tend to shift towards the midline, aligning with the developmental trend of the LG.

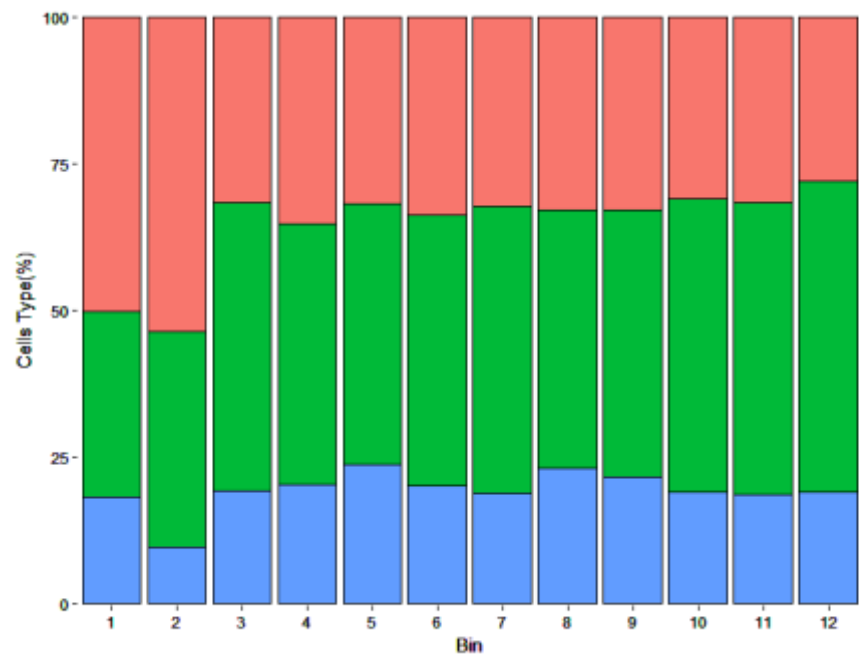
D**P6****E****P16**



A



C



B

Stem cell type preferences at different locations

- A: Distribution proportions of stem cells in VZ at P3
 - B: Distribution proportions of stem cells in ISVZ at P3
 - C: Distribution proportions of stem cells in OSVZ at P3
- n=2 ferrets, Bar represents mean \pm SEM

- Based on observed differences in nuclear morphology during the statistical process and hints from the literature, it is suggested that there may be variations in cell maturity between the sulcus and gyrus regions.
- Although there is a slight trend in stem cell distribution proportions between OSVZ and VZ, it is not significant (possibly due to the statistical proportion being based only on cells marked by the marker, which may lower the proportion).
- Different regions seem to have inherent differences in DAPI density. Normalizing solely based on density distribution and using area normalization may not provide high comparability. Considering incorporating DAPI for normalization.
- Statistical analysis of large areas with high DAPI density poses significant challenges.

Statistical strategy

- Collect high-quality DAPI images, perform statistical analysis for each region, identify proportional patterns, and convert them into correction factors.
- Standardize the statistical results to represent proportions relative to DAPI.
- Estimate the proportion of Pax6-Tbr2- cells.

Verify if cells in the sulcus mature earlier than those in the gyrus

- Calculate the proportion of Pax6-Tbr2- cells, which can be considered predominantly neurons, and examine their distribution.
- Ratio of cells in the S phase and G1 phase of the cell cycle to the total cell cycle.
- Search for appropriate markers for newborn neurons and examine their distribution.

Problems of RNA-Seq mapping

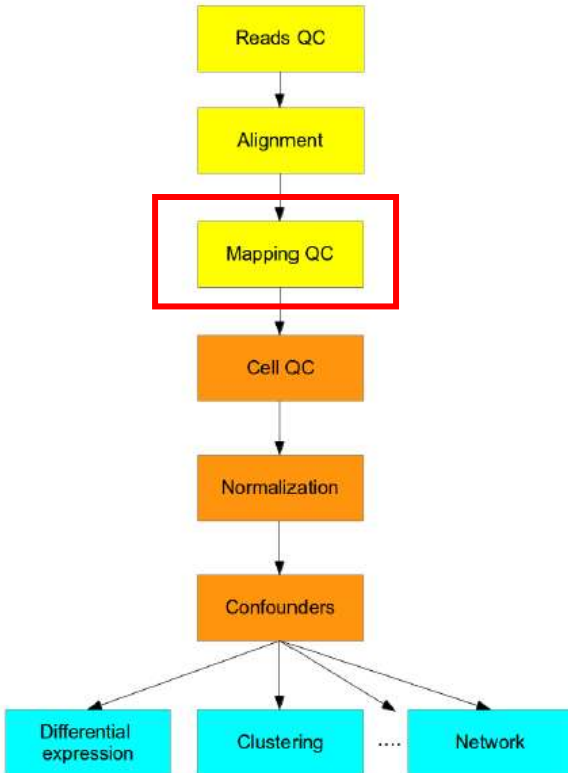


Figure 2.2: Flowchart of the scRNA-seq analysis

Identifying expressed transcripts:

- Aligning to the reference genome (advantageous for discovering new genes, but requires substantial computational resources).
- Aligning to the reference transcriptome (easy alignment, but unable to identify new genes).
- In the absence of a reliable reference genome or transcriptome, transcriptome assembly can be performed from scratch.

Issues with the ferret reference genome and reference transcriptome

Mustela putorius furo (domestic ferret)Representative genome: [Mustela putorius furo \(assembly MusPutFur1.0\)](#)

Download sequences in FASTA format for genome, transcript, protein

Download genome annotation in GFF, GenBank or tabular format

BLAST against Mustela putorius furo genome

All 2 genomes for species:

[Browse the list](#)[Download sequence and annotation from RefSeq or GenBank](#)

Display Settings: Overview

Send to:

[Organism Overview](#) ; [Genome Assembly and Annotation report \[2\]](#) ; [Organelle Annotation Report \[1\]](#)

ID: 3295

**Mustela putorius furo (domestic ferret)**

domestic ferret

Lineage: Eukaryota[2586]; Metazoa[855]; Chordata[366]; Craniata[358]; Vertebrata[358]; Euteleostomi[352]; Mammalia[150]; Eutheria[145]; Laurasiatheria[69]; Carnivora[15]; Caniformia[11]; Mustelidae[2]; Mustelinae[1]; Mustela[1]; Mustela putorius[1]; Mustela putorius furo[1]

The domestic ferret (*Mustela putorius furo*), is a weasel-like mammal that is distantly related to other carnivores like dogs, cats, bears, and otters. The domestic ferret is a subspecies of the European polecat (*Mustela putorius*). Ferrets are important model organisms in the study of influenza, coronavirus transmission in severe acute [More...](#)

SummarySequence data: genome assemblies: 2 (See [Genome Assembly and Annotation report](#))

Statistics: median total length (Mb): 2405.53

median protein count: 48107

median GC%: 41.8

NCBI Annotation Release: 101

Publications

1. The draft genome sequence of the ferret (*Mustela putorius furo*) facilitates study of human respiratory disease. Peng X, et al. *Nat Biotechnol* 2014 Dec
2. Sequencing, annotation, and characterization of the influenza ferret infectome. León AJ, et al. *J Virol* 2013 Feb
3. De-novo transcriptome sequencing of a normalized cDNA pool from influenza infected ferrets. Camp JV, et al. *PLoS One* 2012
4. Transcriptome sequencing and development of an expression microarray platform for the domestic ferret. Bruder CE, et al. *BMC Genomics* 2010 Apr 19
5. Layer-specific expression of multiple cadherins in the developing visual cortex (V1) of the ferret. Krishna-K, et al. *Cereb Cortex* 2009 Feb
6. Molecular characterization and expression pattern of the equine lactate dehydrogenase A and B genes. Echigoya Y, et al. *Gene* 2009 Nov 1
7. Regulation of Ca²⁺/calmodulin kinase II by a small C-terminal domain phosphatase. Gangopadhyay SS, et al. *Biochem J* 2008 Jun 15
8. Untranslated region-dependent exclusive expression of high-sensitivity subforms of alpha4beta2 and alpha3beta2 nicotinic acetylcholine receptors. Briggs CA, et al. *Mol Pharmacol* 2006 Jul
9. tRNAscan-SE: a program for improved detection of transfer RNA genes in genomic sequence. Lowe TM, et al. *Nucleic Acids Res* 1997 Mar 1

NCBI Resources[Genome Data Viewer](#)[Map Viewer](#)**Tools**[BLAST Genome](#)**Related information**[Assembly](#)[BioProject](#)[Gene](#)[Components](#)[Protein](#)[PubMed](#)[Taxonomy](#)**Search details**["Mustela putorius furo" \[Organism\]](#)[Search](#)[See more...](#)**Recent activity**[Turn Off](#) [Clear](#)[Mustela putorius furo](#)

Genome

[Mustela putorius furo\[orgn\] \(1\)](#)

Genome

[Pathophysiological analyses of cortical malformation using gyrencephalic](#)[Pathophysiological analyses of cortical malformation using gyrencephalic](#)

PubMed

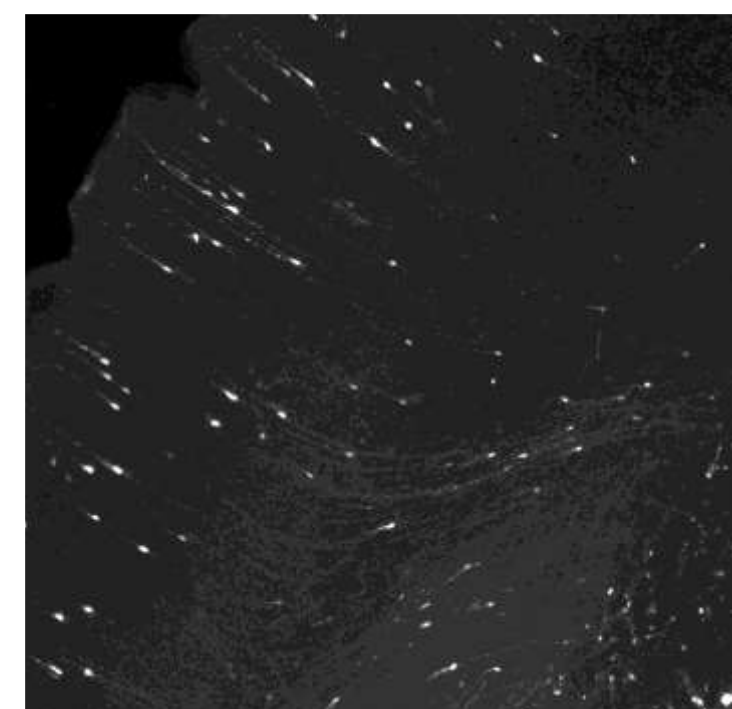
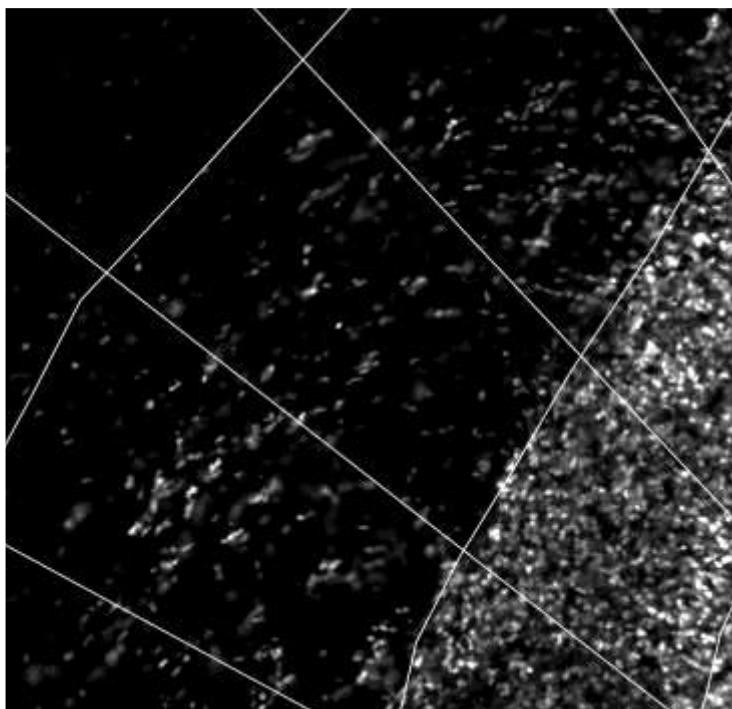
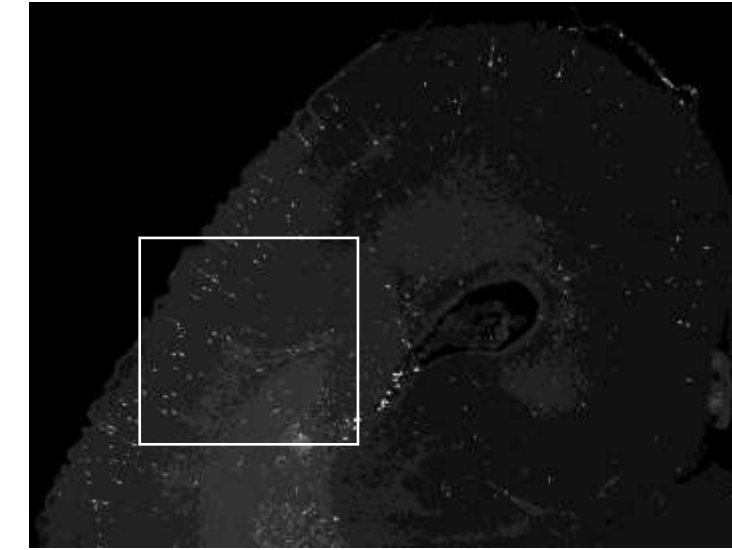
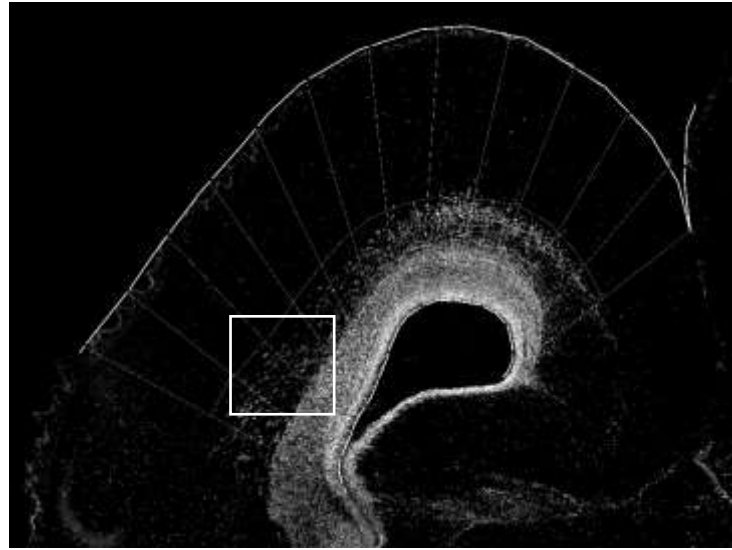
[Pathophysiological analyses of periventricular nodular heterotopia](#)

PubMed

[See more...](#)

Problems

- Due to the limited availability of reference databases related to ferret genes, is it necessary to perform de novo transcriptome assembly?
- Should we choose single-end or paired-end sequencing for our sequencing? What should be the fragment length? Does the company have any recommendations? (Is paired-end sequencing more advantageous for de novo transcriptome assembly?)
- For single-cell sequencing, what library preparation schemes and quality control-related sequences such as ERCC and UMI should be used? Does the company have any suggestions?



P3 Tbr2

P2 Pax6

P2 EGFP

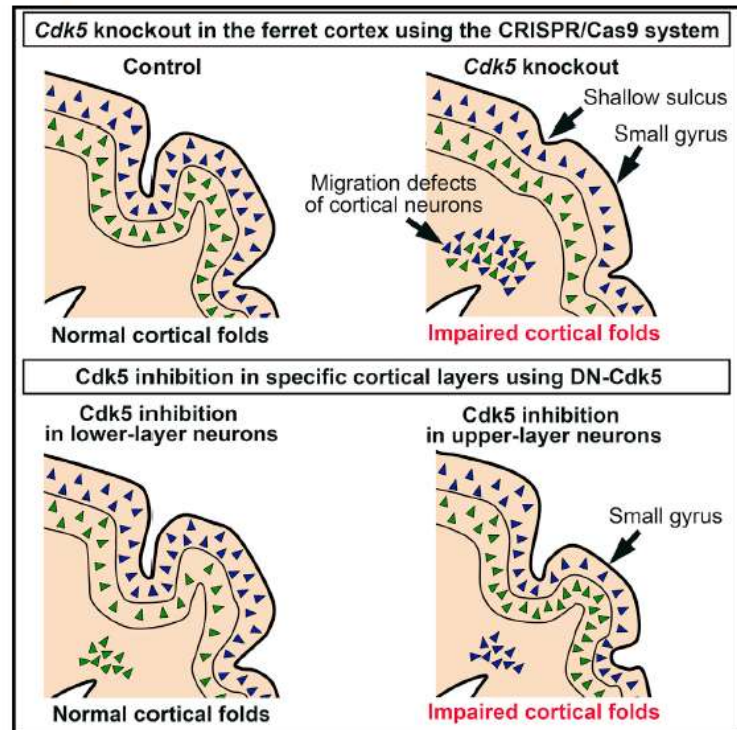
Thoughts on the microdissection locations

- From the heatmap, there appears to be some difference between LG and LS. Based on the current experimental conditions, it may be feasible to sample both LG and LS, but I still feel they are somewhat close in proximity.
- From various experimental observations, the most apparent differences seem to be between LG and SSS in the early stages, despite not ultimately developing into adjacent sulci and gyri.
- Would it be possible to postpone stem cell classification and instead perform bulk-Seq on tissues from different layers of LG, LS, and SSS?"

Cell Reports

Folding of the Cerebral Cortex Requires Cdk5 in Upper-Layer Neurons in Gyrencephalic Mammals

Graphical Abstract



Authors

Yohei Shinmyo, Yukari Terashita,
Tung Anh Dinh Duong, ...,
Kazuyoshi Hosomichi, Atsushi Tajima,
Hiroshi Kawasaki

Correspondence

hiroshi-kawasaki@umin.ac.jp

In Brief

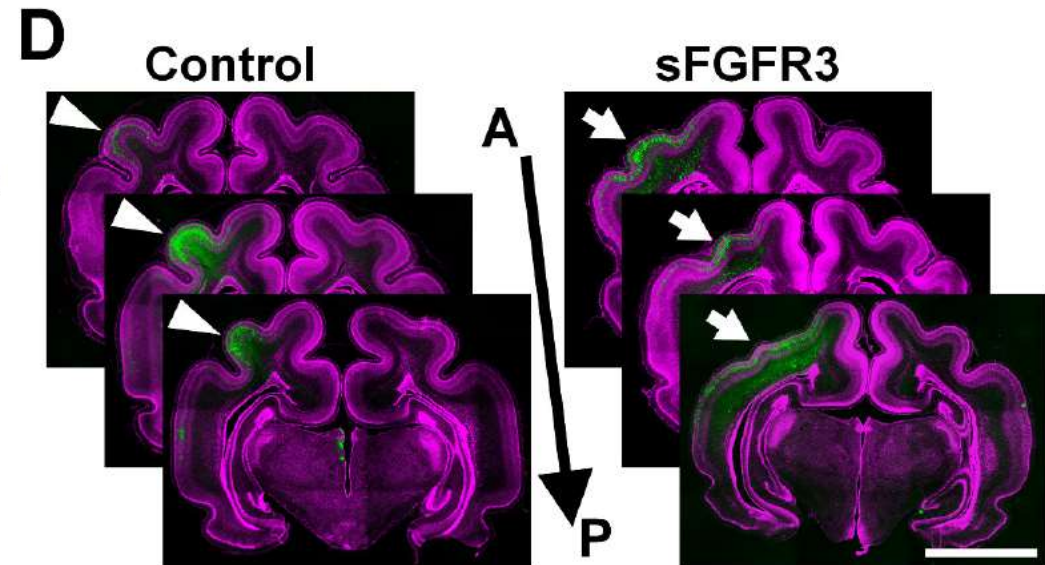
Shinmyo et al. describe a highly efficient gene knockout method for the folded cerebral cortex of ferrets using the CRISPR/Cas9 system. Loss-of-function studies of the *Cdk5* gene suggest that appropriate positioning of upper-layer neurons is crucial for cortical folding.

Article

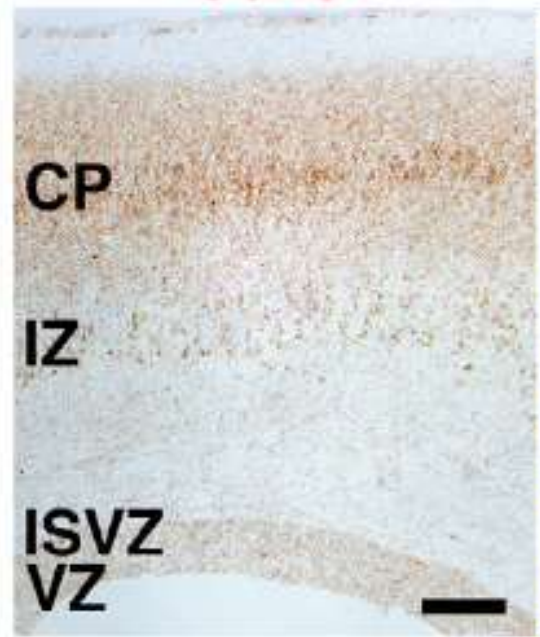
Gyrification of the cerebral cortex requires FGF signaling in the mammalian brain

Naoyuki Matsumoto, Yohei Shinmyo, Yoshie Ichikawa, Hiroshi Kawasaki*

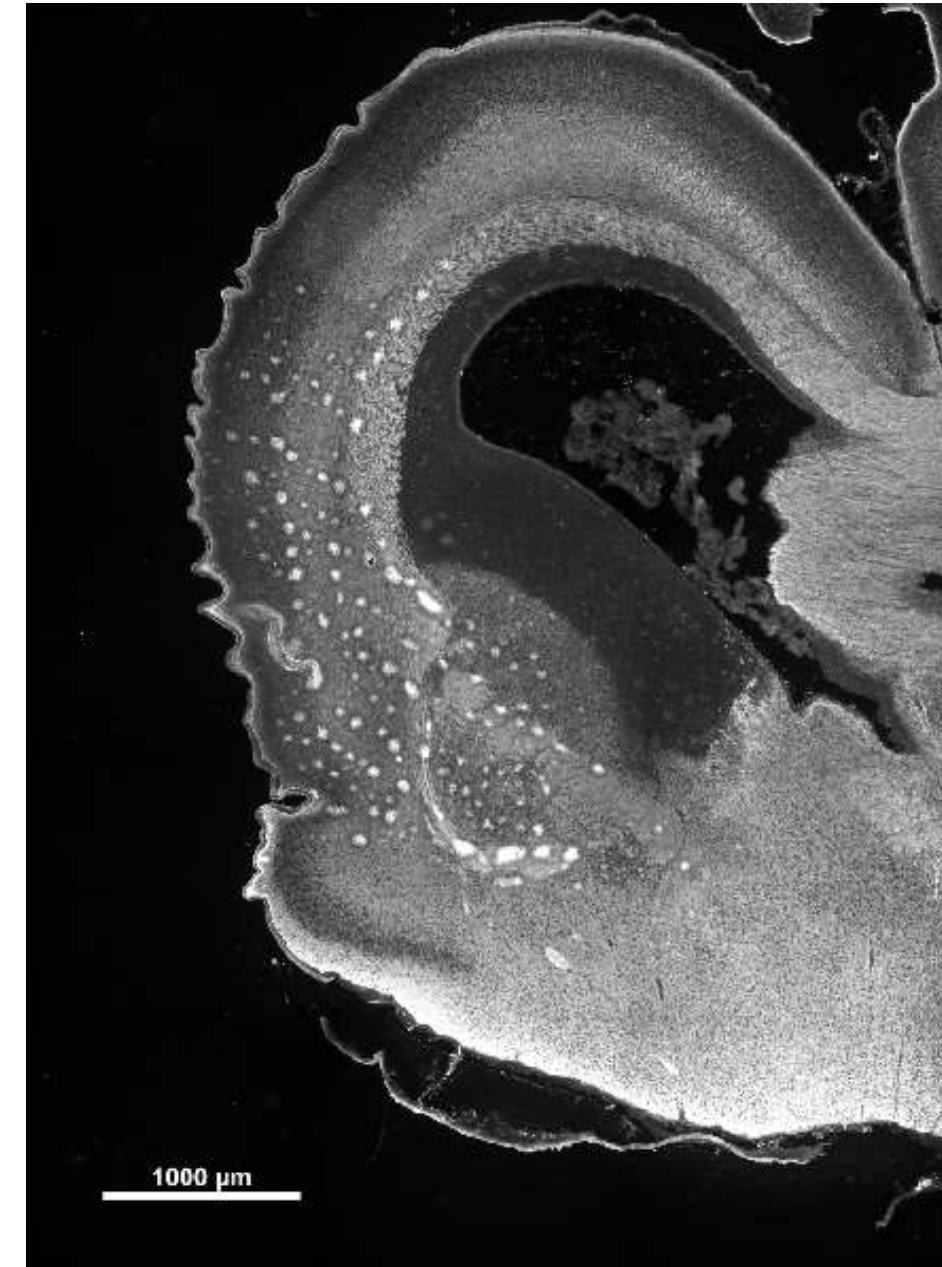
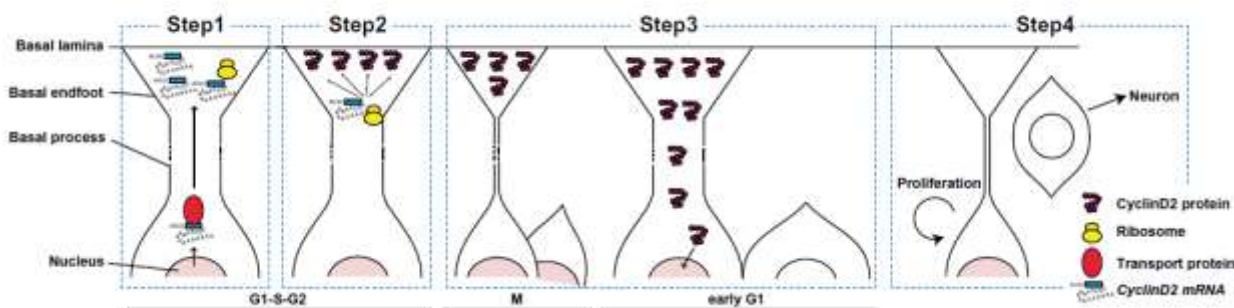
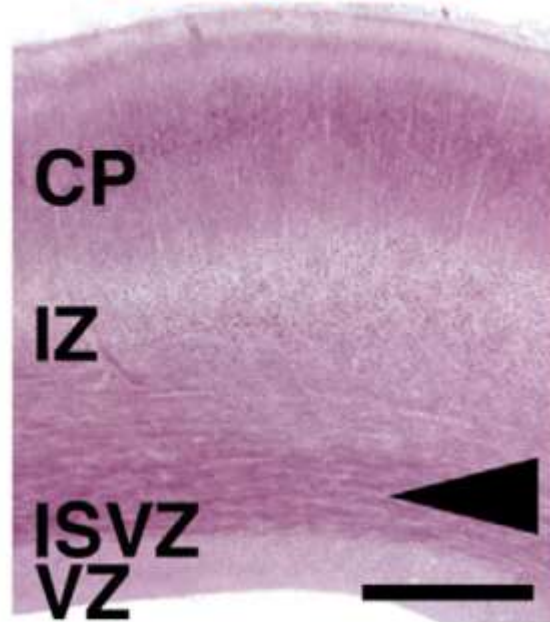
Department of Medical Neuroscience, Graduate School of Medical Sciences,
Kanazawa University, Ishikawa, Japan



A *Cdk5*



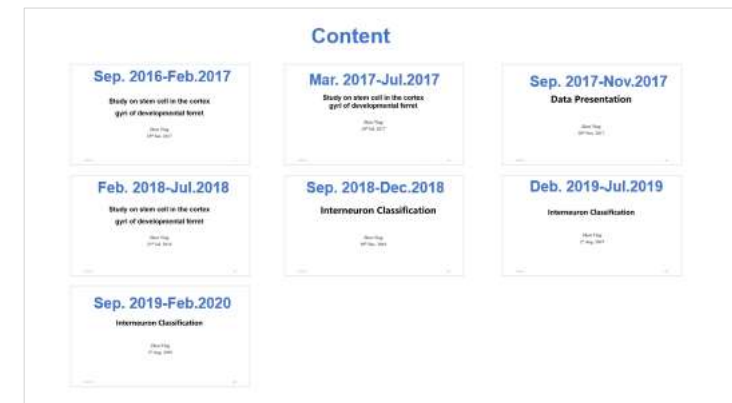
D *Cdk5 protein*



Cyclin D2

Next Plan

- P4 BrdU injection, tissue collection, staining, and image acquisition (2 batches) [3-4 weeks].
- Collect high-quality DAPI images, perform regional statistics, and determine correction factors.
- Statistical analysis of BrdU accumulation distribution, cumulative curves, and cell cycle-related marker expression.
- Gain understanding of RNA-Seq-related knowledge (principles, workflow, experimental design, and quality control).
- Establish Ferret qPCR experimental techniques.



Study on stem cell in the cortex gyri of developmental ferret

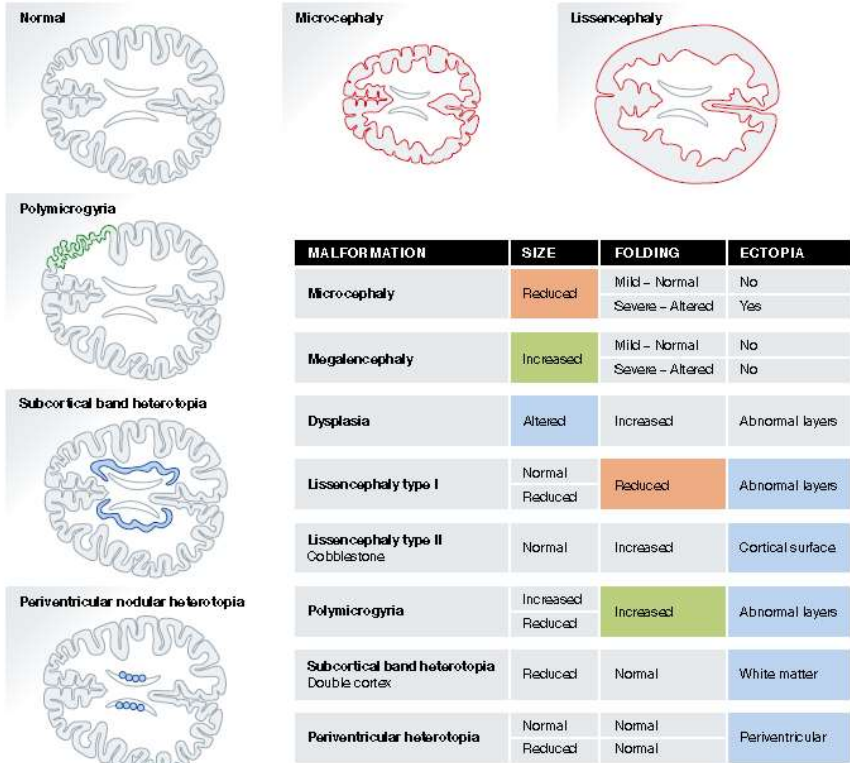
Zhou Ying

23rd Jul. 2018

Content

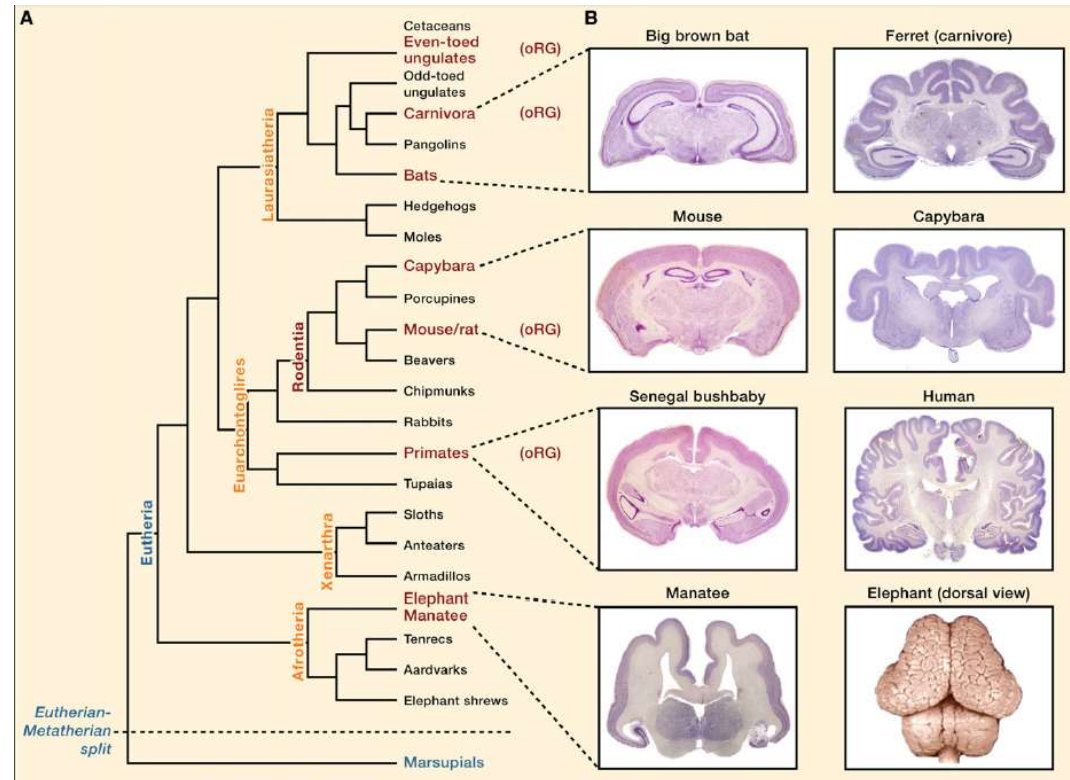
- Background
- Current work
- Distribution of stem cells
- Present data of cell cycle
- Current thinking and reflection
- Next Plan

Background

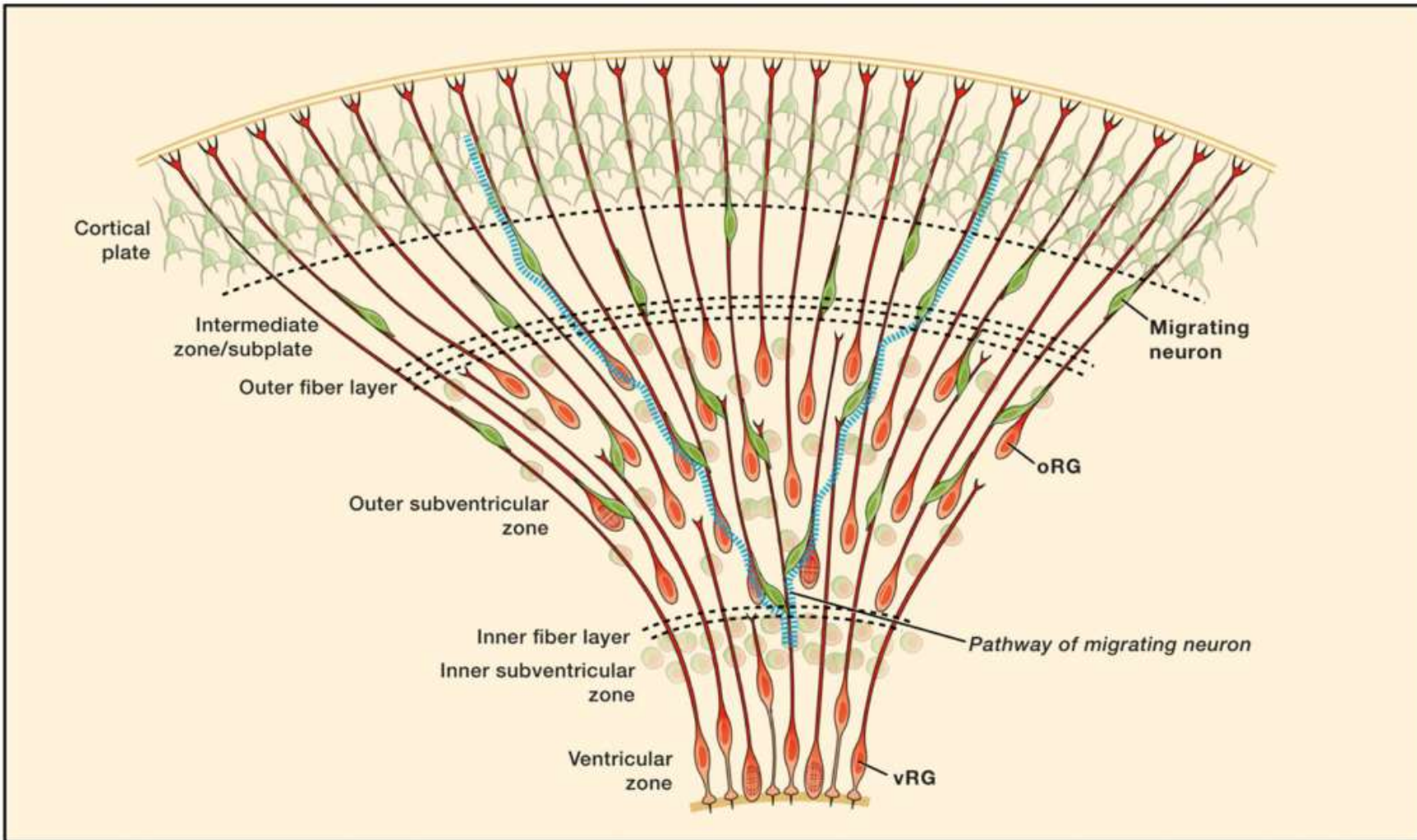
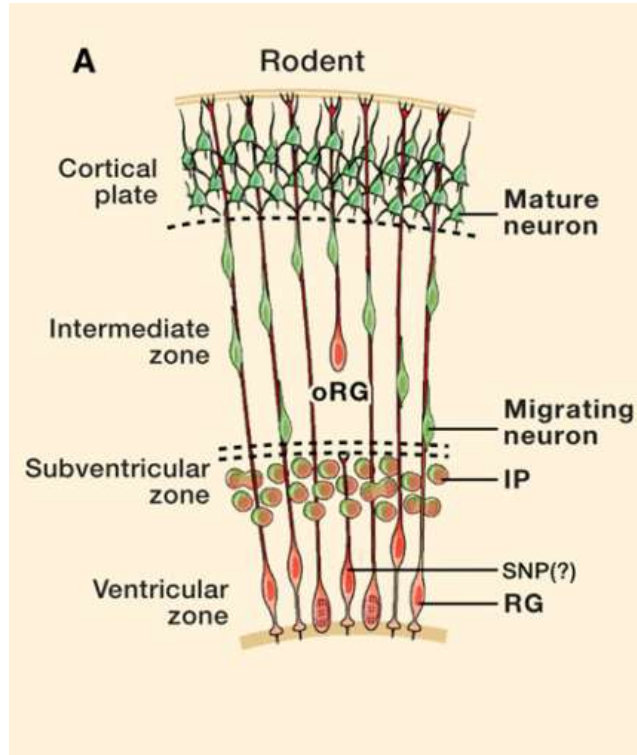


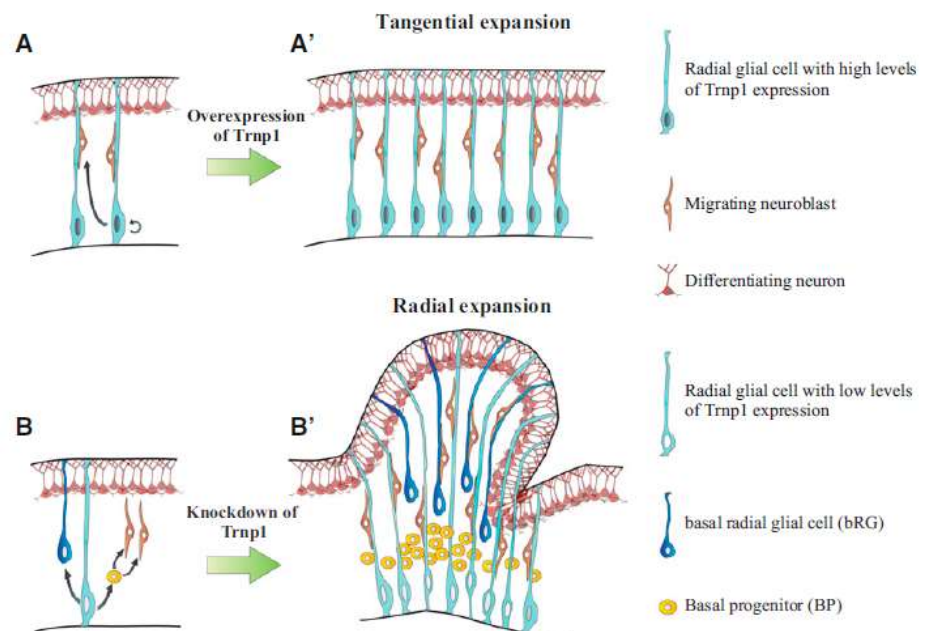
Virginia et al.(2016) *The EMBO Journal*

How are cortical sulci and gyri structures formed?



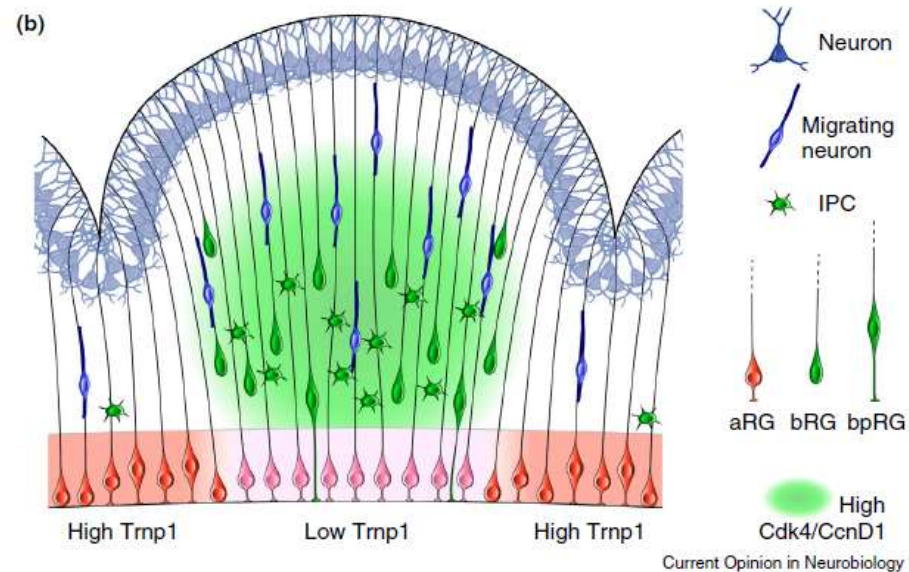
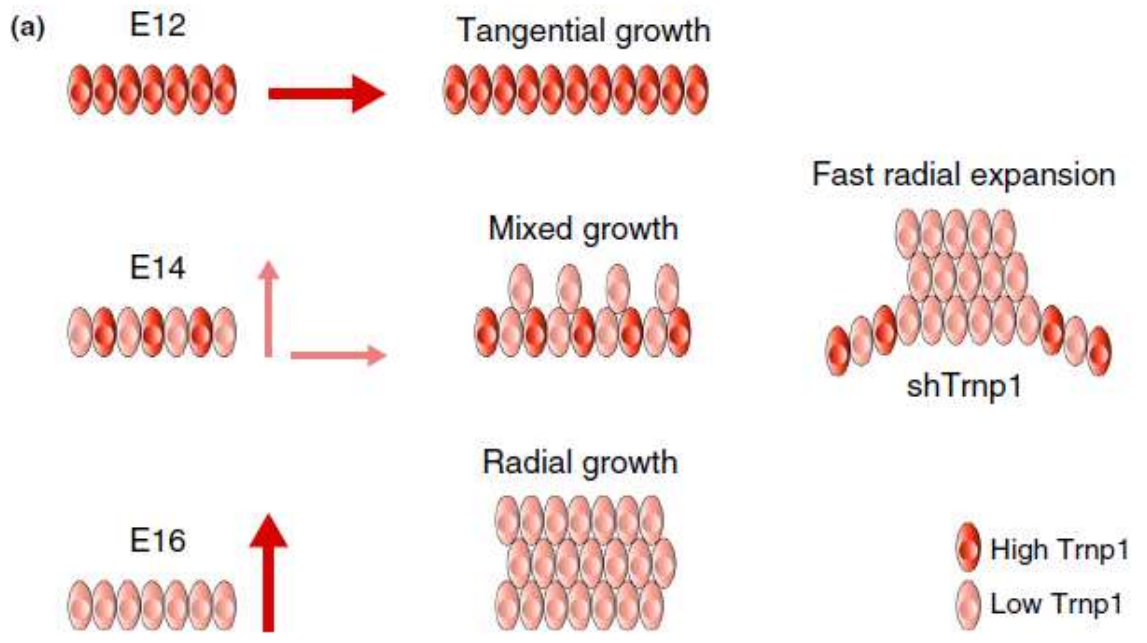
Liu et al.(2011) *Cell*



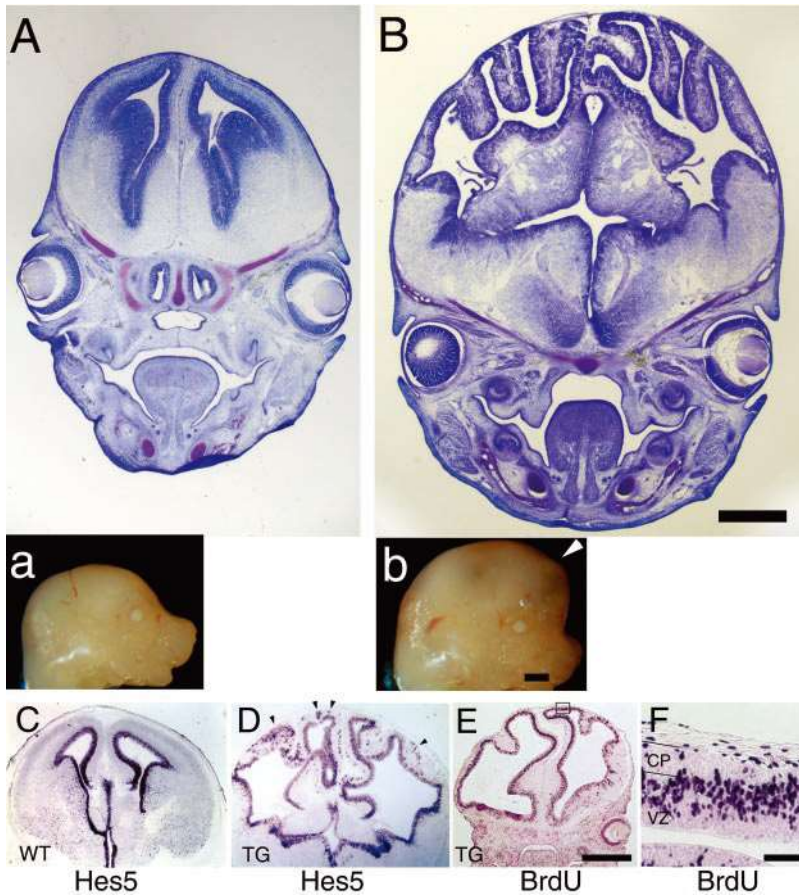


Ronny Stahl et al.(2013) *cell*

The uneven distribution of stem cells may lead to the formation of sulci and gyri.



Current Opinion in Neurobiology

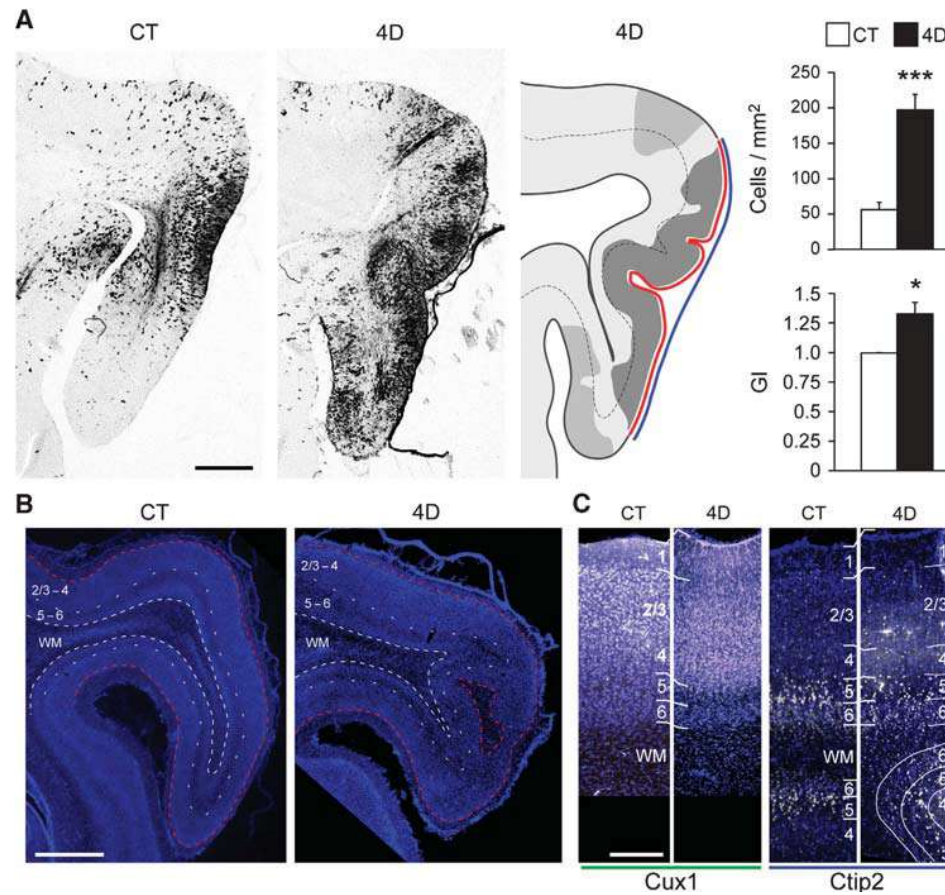


Modulating β -catenin alters the cell cycle of transgenic mice, resulting in cortical folding.

Anjen Chenn et al.(2002)Science

2024/4/7

The unevenness of stem cell cell cycles may lead to the formation of sulci and gyri.



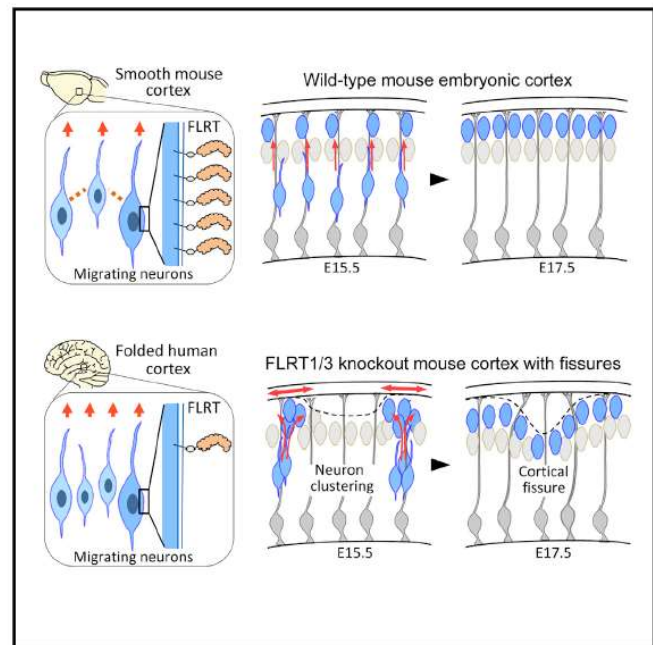
Increasing Cdk4/CyclinD1 enhances bRGCs, leading to an increase in sulci and gyri in ferret.

Miki Nonaka-Kinoshita et al.(2013)The EMBO Journal

95

Regulation of Cerebral Cortex Folding by Controlling Neuronal Migration via FLRT Adhesion Molecules

Graphical Abstract



Authors

Daniel del Toro, Tobias Ruff,
Erik Cederfjäll, Ana Villalba,
Gönül Seyit-Bremer, Víctor Borrell,
Rüdiger Klein

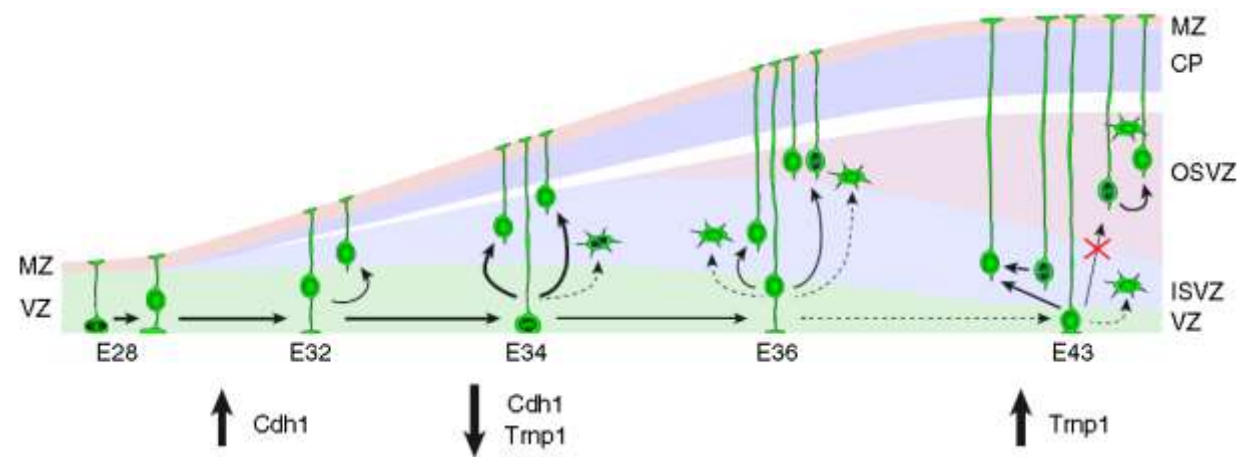
Correspondence

rklein@neuro.mpg.de

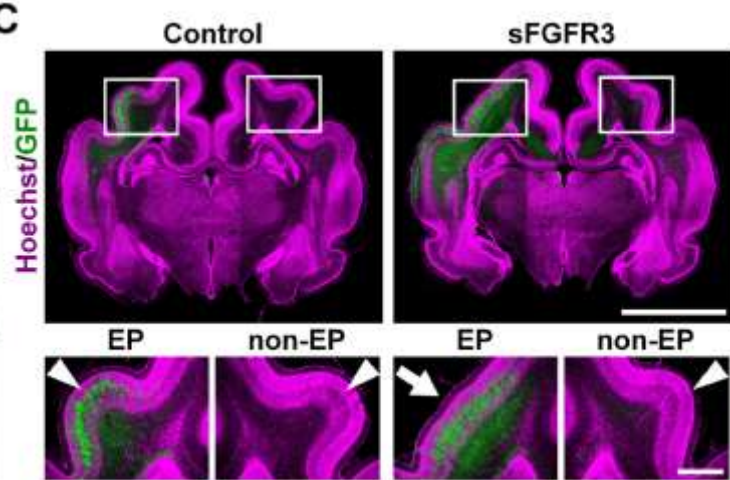
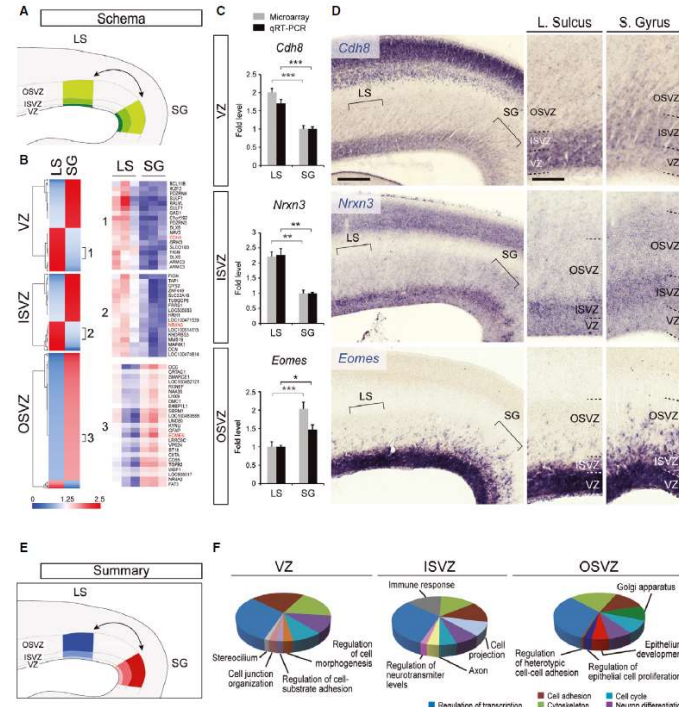
In Brief

Physical migration of neurons can create the folded cortical surface characteristic of primate brains.

The migratory activity of stem cells may lead to the formation of sulci and gyri



Maria A'ngel Martínez-Martínez et al.(2016) Nat.communications

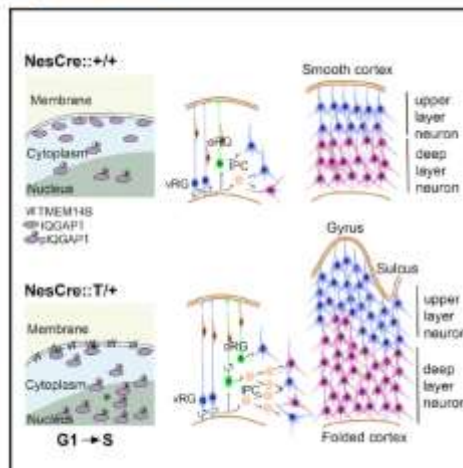


2024/4/7

Cell Stem Cell

The Primate-Specific Gene *TMEM14B* Marks Outer Radial Glia Cells and Promotes Cortical Expansion and Folding

Graphical Abstract



Authors

Jing Liu, Wensu Liu, Lu Yang, ..., Jun Zhang, Fuchou Tang, Xiaoqun Wang

Correspondence
drzhang@outlook.com (J.Z.), tangfuchou@pku.edu.cn (F.T.), xiaoqunwang@ibp.ac.cn (X.W.)

In Brief

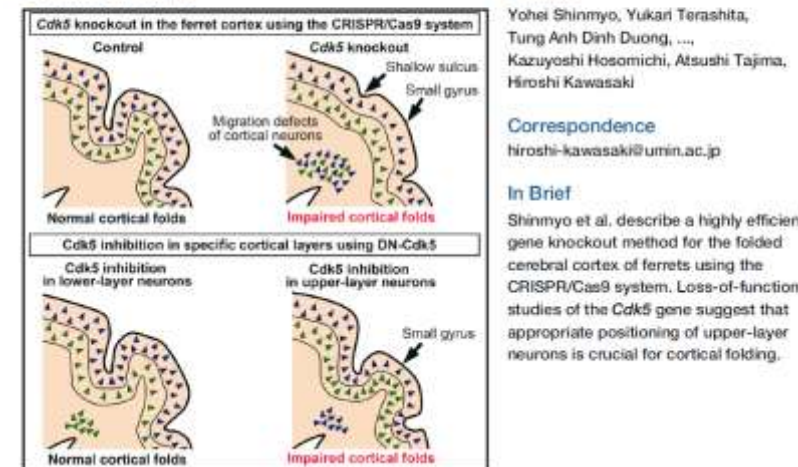
Wang and colleagues show that the primate-specific gene *TMEM14B* marks a subset of human neural progenitors and induces cortical folding, providing insights into human brain evolution. Expressing *TMEM14B* in the fetal mouse brain increases proliferation of progenitor subsets and cortical thickening through nuclear shuttling of IQGAP1, which promotes G1/S transitions.

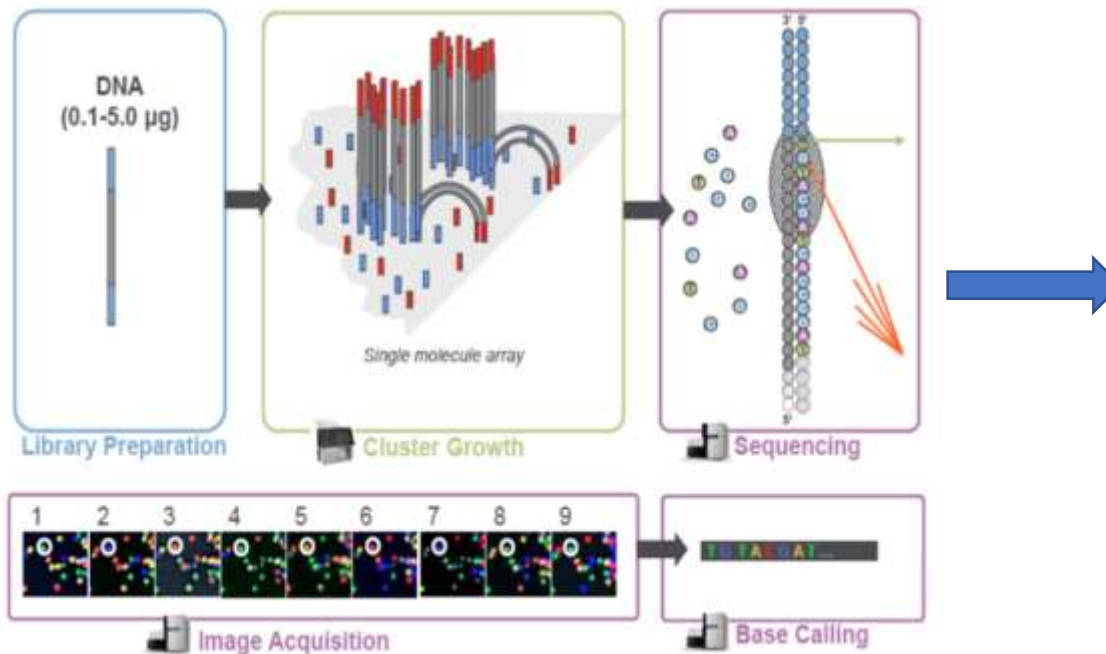
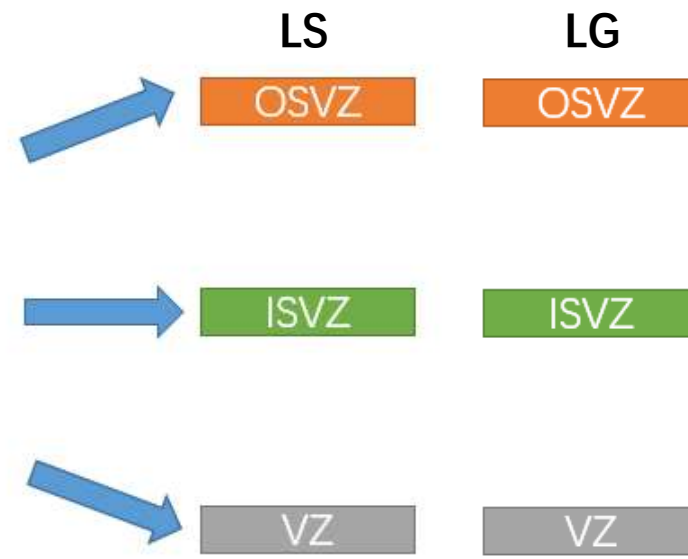
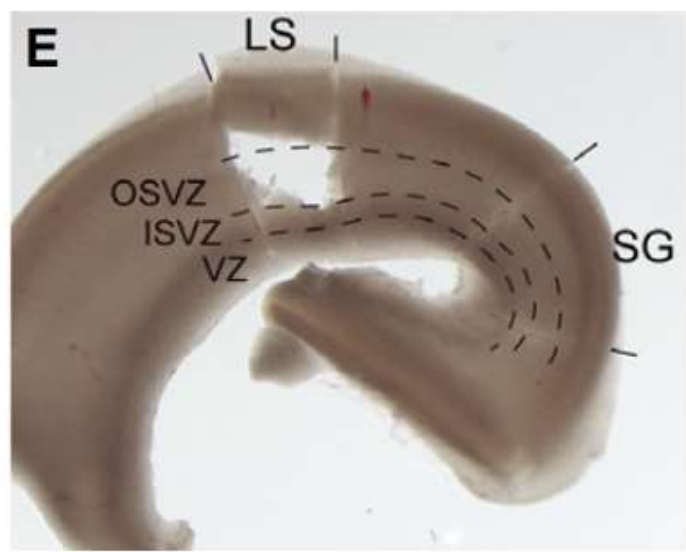
During the development of sulci and gyri, there are significant molecular differences that regulate cell activities, thereby influencing the formation of sulci and gyri

Cell Reports

Folding of the Cerebral Cortex Requires *Cdk5* in Upper-Layer Neurons in Gyrencephalic Mammals

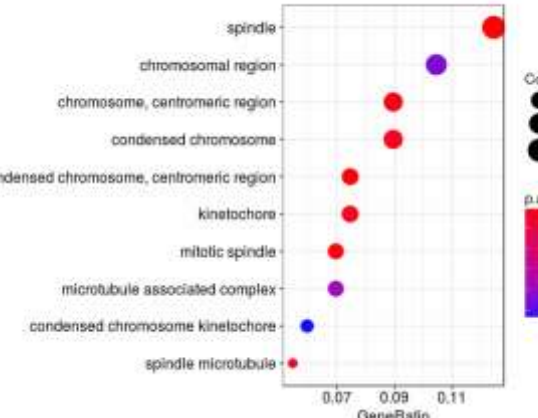
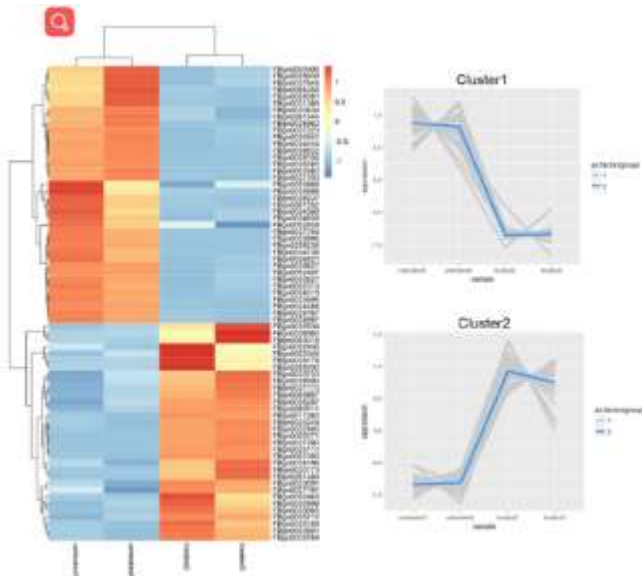
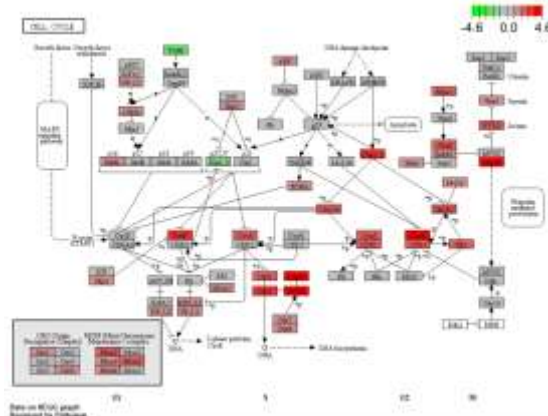
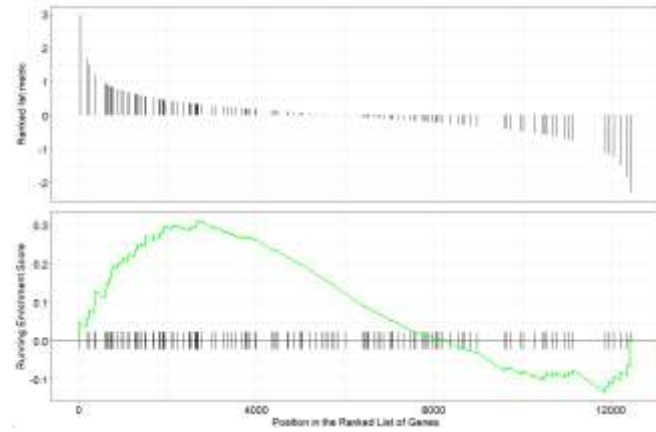
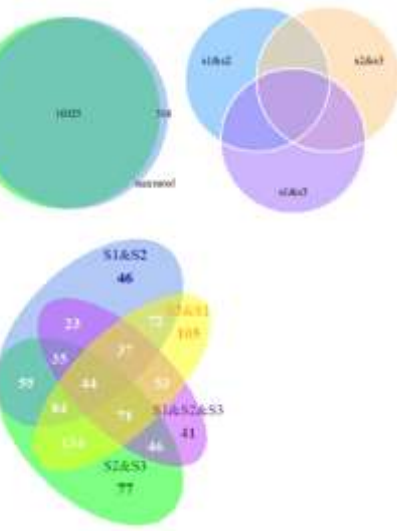
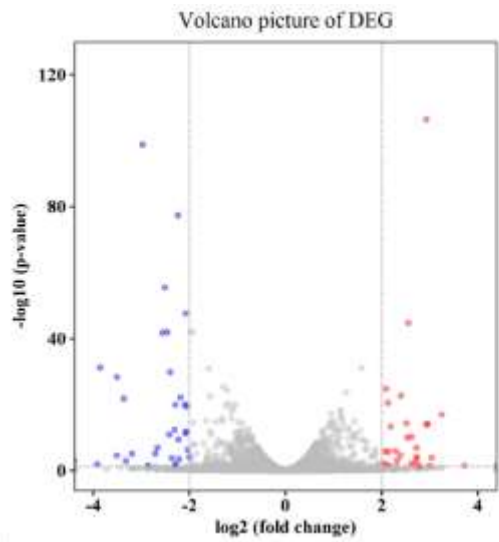
Graphical Abstract



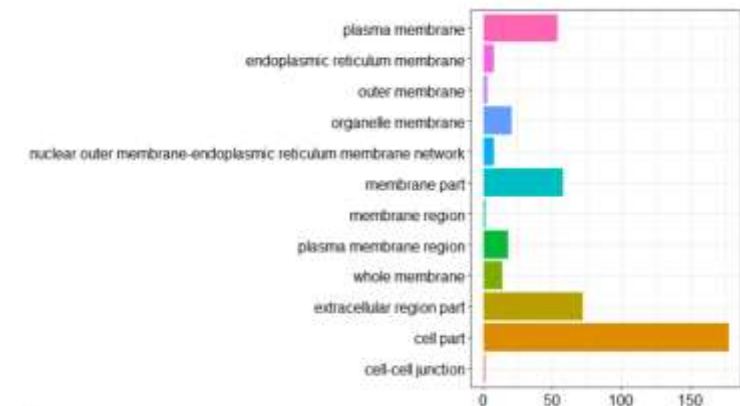


Current work

RNA-Seq data analysis	Learning of RNA-Seq data analysis Selection and testing of reference genomes in ferrets P2 stem cell cycle collation in layers P4 different types of stem cell distribution data statistics P4 statistical data of stem cell cycle in layers P6 Brdu Injection, sample, slice (8 brains)
Cell cycle and distribution of stem cells	P4 optimization of RNA extraction quality in gyrus tissue
RNA-Seq samples	



GO over-representation test



GO classification

Ferret reference genome and sequence alignment

/pub/release-92/fasta/mustela_putorius_furo/dna/ 的索引

 [上级目录]

	名称	大小	修改日期
	CHECKSUMS	451 B	2018/4/24 下午4:23:00
	Mustela_putorius_furo.MusPutFur1.0.dna.nonchromosomal.fa.gz	670 MB	2018/4/24 下午4:24:00
	<u>Mustela_putorius_furo.MusPutFur1.0.dna.toplevel.fa.gz</u>	670 MB	2018/4/24 下午4:24:00
	Mustela_putorius_furo.MusPutFur1.0.dna_rm.nonchromosomal.fa.gz	446 MB	2018/4/24 下午4:24:00
	Mustela_putorius_furo.MusPutFur1.0.dna_rm.toplevel.fa.gz	446 MB	2018/4/24 下午4:24:00
	Mustela_putorius_furo.MusPutFur1.0.dna_sm.nonchromosomal.fa.gz	716 MB	2018/4/24 下午4:24:00
	Mustela_putorius_furo.MusPutFur1.0.dna_sm.toplevel.fa.gz	716 MB	2018/4/24 下午4:24:00
	README	4.8 kB	2018/4/24 下午4:23:00

- .toplevel - Includes haplotype information
- .primary_assembly - Single reference base per position
- toplevel format contain haplotype information, which will result in increasing of calculation, primary is optimized
- _sm and _rm both label highly repetitive sequences, especially _rm replaces highly repetitive sequences with N, which is not conducive to subsequent analysis.
- The reference genome and annotation files should be aligned with the coordinate system.

/pub/release-92/gtf/mustela_putorius_furo/ 的索引

[ 上级目录]

	名称	大小	修改日期
	CHECKSUMS	142 B	2018/3/11 上午6:06:00
	Mustela_putorius_furo.MusPutFur1.0.92.abinitio.gtf.gz	3.3 MB	2018/3/9 上午11:47:00
	<u>Mustela putorius furo.MusPutFur1.0.92.gtf.gz</u>	7.7 MB	2018/3/9 上午11:42:00
	README	9.2 kB	2018/3/9 上午11:42:00

The GTF file with the .abinitio suffix includes annotation information predicted by Genscan and other tools, which may be more comprehensive. However, it may not necessarily be reliable.

Sample name	Bulk_neuron_1	Bulk_neuron_2	Bulk_progenitor_1	Bulk_progenitor_2
Total reads	48704440	34138714	59935529	52044691
Total mapped reads	42968029	30099137	53256828	46109194
Uniquely mapped reads	42091359	29486919	52130536	45118534
Multiple mapped reads	876670	612218	1126292	990660
Total mapping rate	88%	88%	89%	89%
Uniquely mapping rate	86%	86%	87%	87%
Multiple mapping rate	2%	2%	2%	2%

gene_id	Gene name	bulk_neuron_rep	bulk_neuron_rep2	bulk_progenitor	bulk_progenitor	sum_count
ENSMPU00000011610	ACTG1	32571	24771	33545	26791	117678
ENSMPU0000004478	EEF2	24966	16954	36045	28358	106323
ENSMPU0000014466	FABP7	11709	9065	42023	40272	103069
ENSMPU0000015433	NCAN	19338	12586	35359	29053	96336
ENSMPU0000015264	SRRM2	18261	12622	31649	26757	89289
ENSMPU0000000862	DPYSL2	21938	15129	20360	18119	75546
ENSMPU0000000462	TUBB2B	25970	19010	15758	12226	72964
ENSMPU0000015774	STMN1	27306	19716	14081	11761	72864
ENSMPU0000012886	EIF4G2	20086	14515	19289	17745	71635
ENSMPU0000009153	FOS	763	732	37269	32722	71486
ENSMPU0000015046	SLC1A3	75	46	36083	34384	70588
ENSMPU0000012592	HSP90AB1	15133	10612	22911	21105	69761
ENSMPU0000009039	DPYSL5	22379	15532	17187	12656	67754
ENSMPU0000011602	VIM	180	116	35273	31130	66699
ENSMPU0000014406	MAP1B	13194	10388	18444	18775	60801
ENSMPU0000006874	PTPRZ1	8033	5558	23419	22506	59516
ENSMPU0000015734	ZBTB18	21080	15005	11713	9838	57636
ENSMPU0000005308	PTPRS	16184	10477	16673	11851	55185
ENSMPU0000008861	CHD3	21704	14841	10455	8095	55095
ENSMPU0000004325	NFIX	16047	11374	14878	10666	52965
ENSMPU0000004426	GDPD2	72	35	29436	23244	52787
ENSMPU0000011319	PRRC2A	11962	9052	17431	14202	52647
ENSMPU0000009343	EGR1	2325	2500	27164	20089	52078
ENSMPU0000010680	LENG8	15746	9629	15603	10735	51713
ENSMPU0000012044	GPM6A	18968	13268	8617	8207	49060
ENSMPU0000001687	TNC	1405	888	24300	21790	48383

Gene name: 16,761

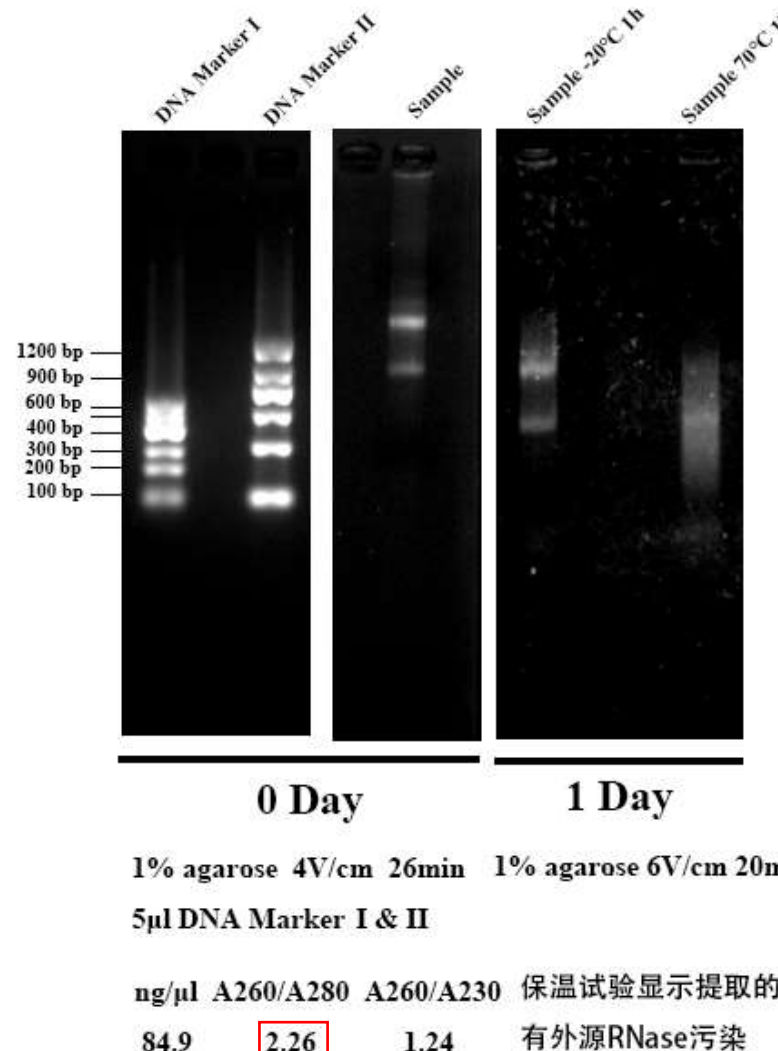
No corresponding gene name: 15,298

Total: 32,059

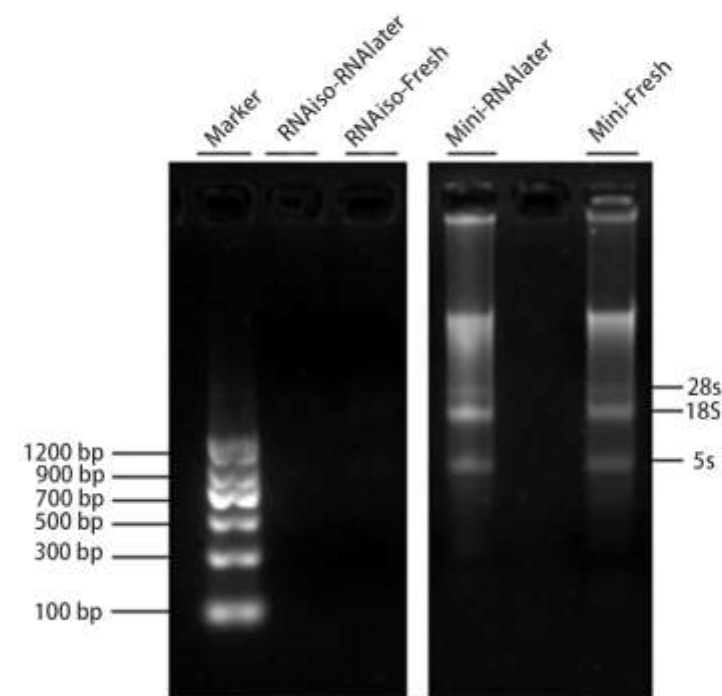
Summary

- Downloaded bulk-seq data for mink neurons and progenitors.
- Bowtie2 and bwa index are fine. Alignment was done using Bowtie2, and quantification using HTSeq.
- Encountered memory overflow with Hisat2 index, added memory, successfully obtained index, and performed quantification using HTSeq.
- Only about half of the ensemble IDs were successfully converted to gene names.

Mouse cortex RNA Used RNAlater 0 Day (20180611)



Mouse cortex total RNA RNAiso vs Mini &RNAlater vs Fresh (20180613)

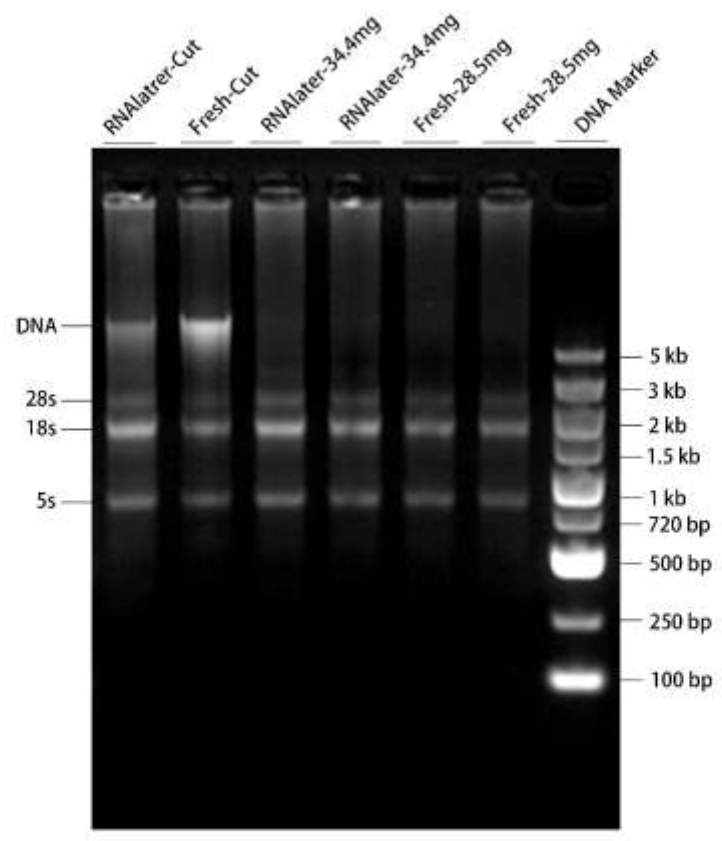


	A280/A260	A260/A230	提取量(μ g)
RNAiso-RNAlater	1.52	0.22	0.135
RNAiso-Fresh	0.81	0.11	0.120
Mini-RNAlater	2.07	0.97	1.371
Mini-Fresh	2.04	0.90	0.885

提取的样品均有DNA污染

RNAlater的组织均4°C浸泡3天

RNAlater浸泡4天的组织与新鲜切割的组织RNA含量的对比 (20180615)



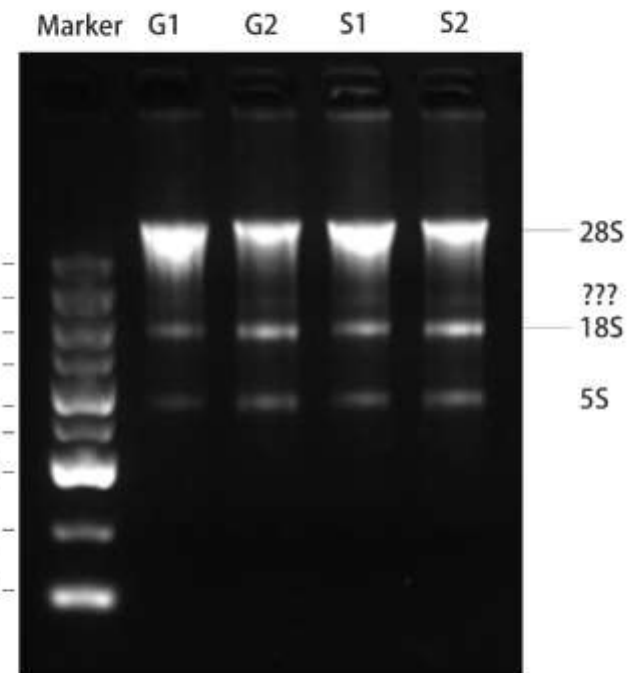
	A280/A260	A260/A230	提取量(μg)	组织RNA含量(μg/mg)
RNAlater-Cut	2.07	1.23	1.473	—
Fresh-Cut	2.08	0.68	0.894	—
RNAlater-32.4mg	2.10	2.07	16.824	0.5193
Fresh-28.5mg	2.11	1.21	12.336	0.4328

切割后的组织有DNA污染

RNAlater浸泡4天的组织，比新鲜切割的组织所含的RNA多，说明RNA稳定处理的组织更有利于RNA提取

2024/4/7 上样量：9 μl, 9 μl, 1 μl, 1 μl 样品, 10 μl 体系 (四个样品依次) Marker 3.5 μl 除 500 bp 70 ng 其他条带 35ng

P4 Ferret LG & LS Total RNA (20180621)



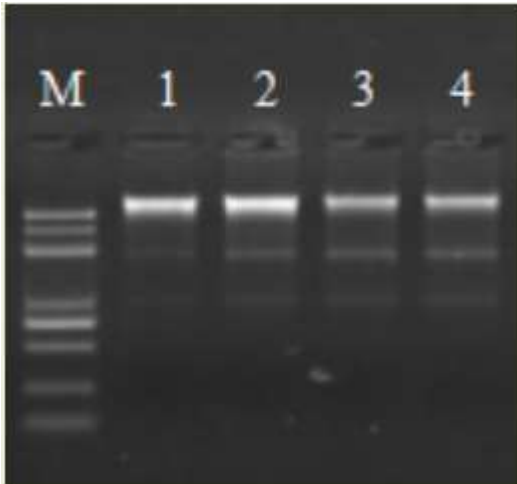
1% agarose 6V/cm 15min

G1、G2 —— LG 不同雪貂

S1、S2 —— LS不同雪貂

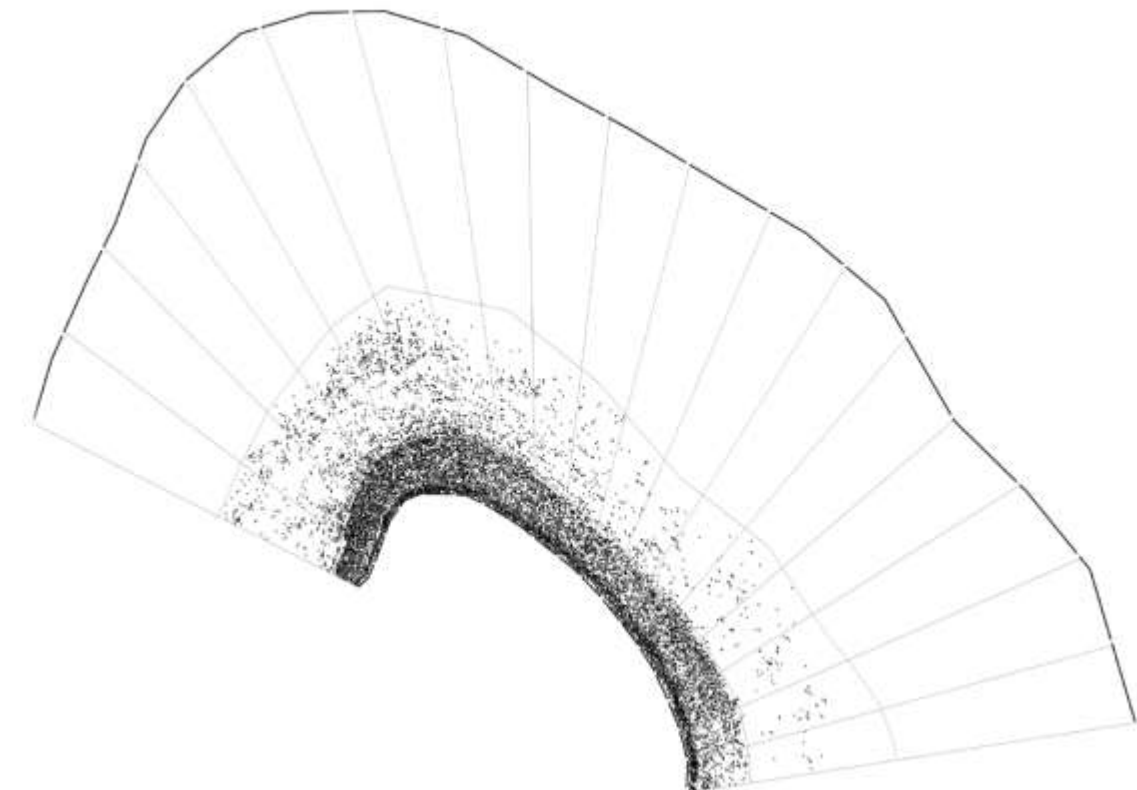
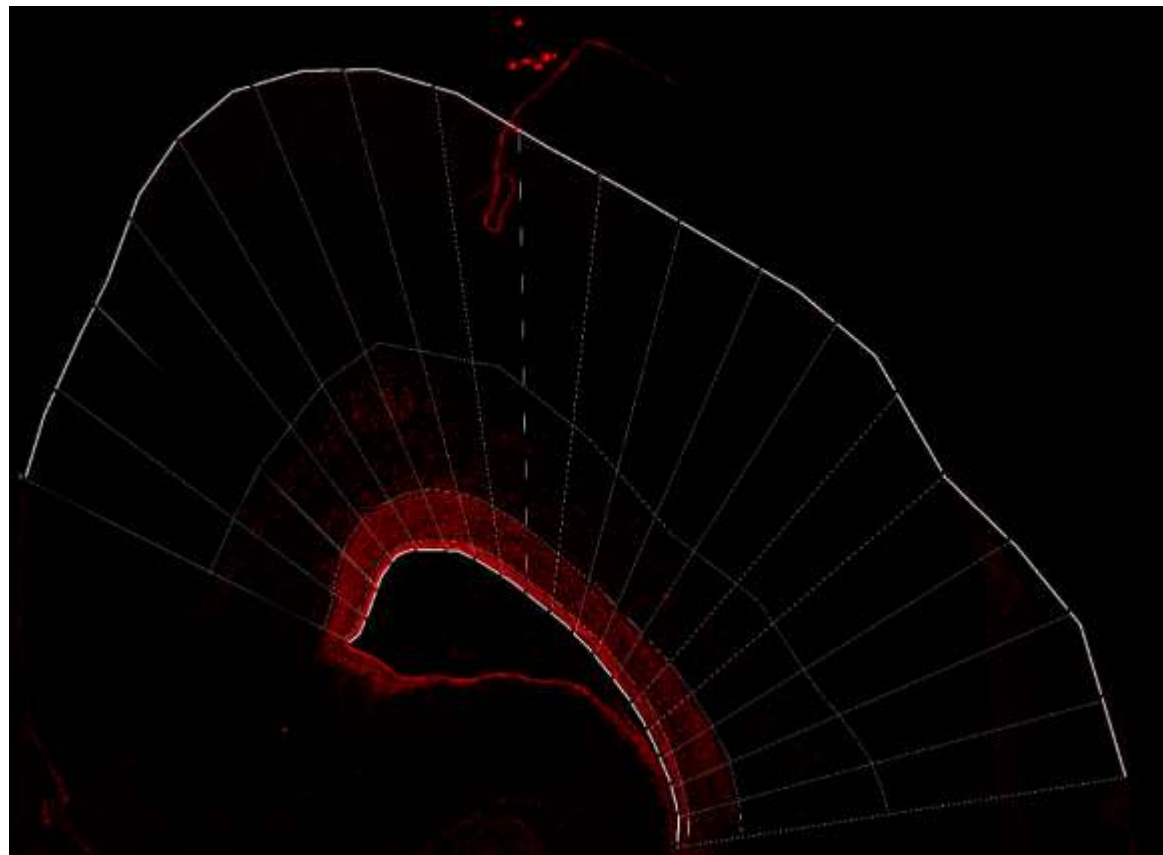
	A260/A280	A260/A230	浓度 (ng/μl)	提取量(μg)
G1	1.92	1.02	74.1	2.223
G2	2.00	1.07	75.1	2.253
G3	1.94	1.78	99.4	2.982
G4	2.00	1.43	80.3	2.409

Summary

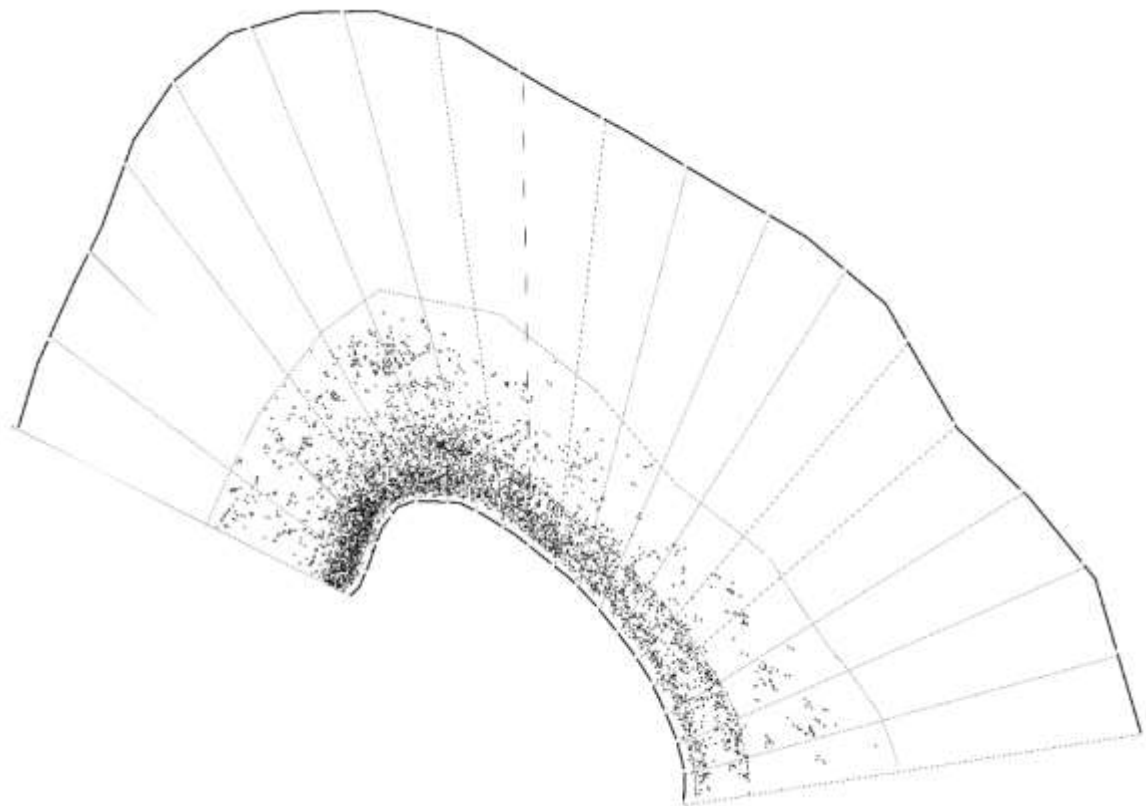
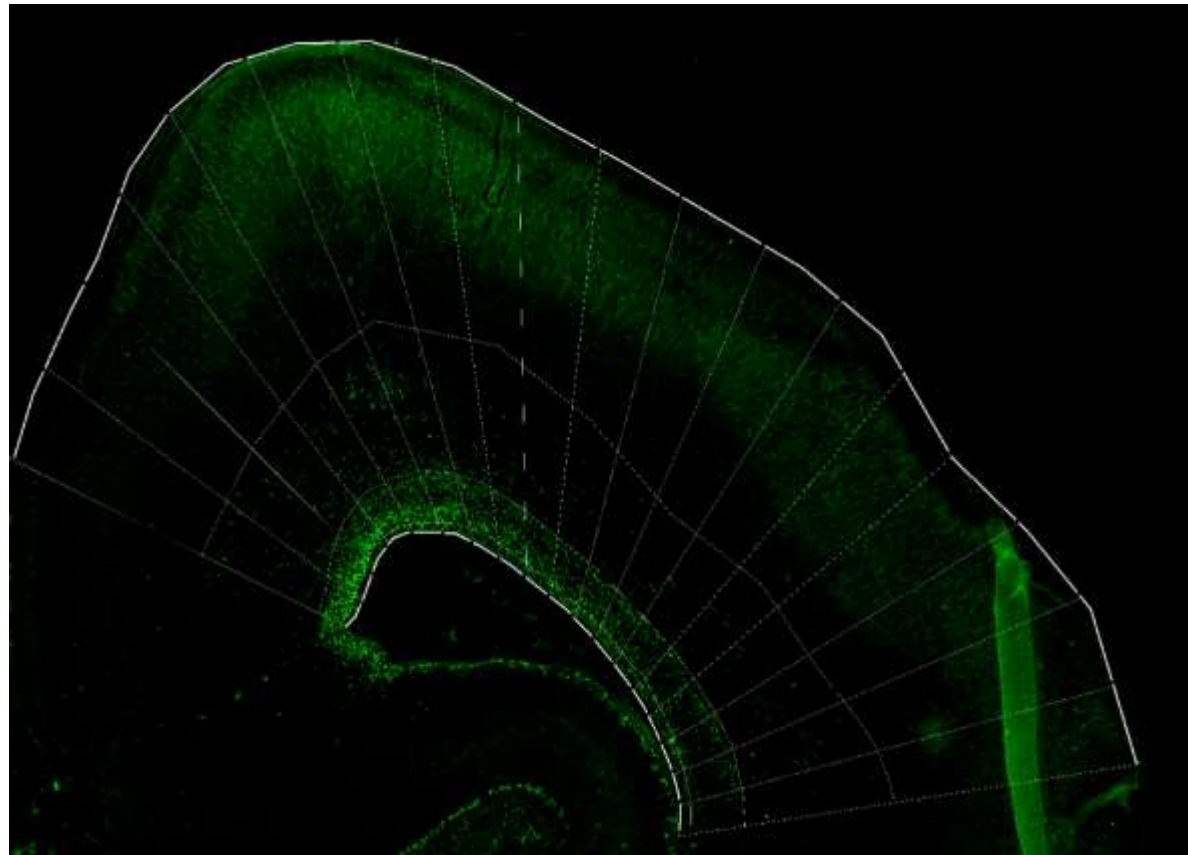


The second sample

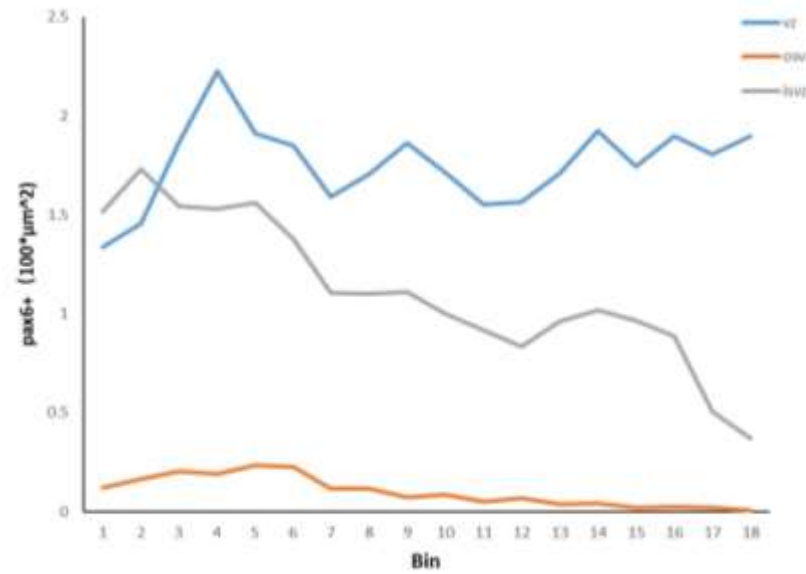
- The issue of RNA degradation in the second sample has been controlled.
- The main discrepancy with the company lies in the significant difference between the assessment of DNA contamination and the values measured by Nanodrop.
- The main problem lies in the insufficient quantity of RNA samples.



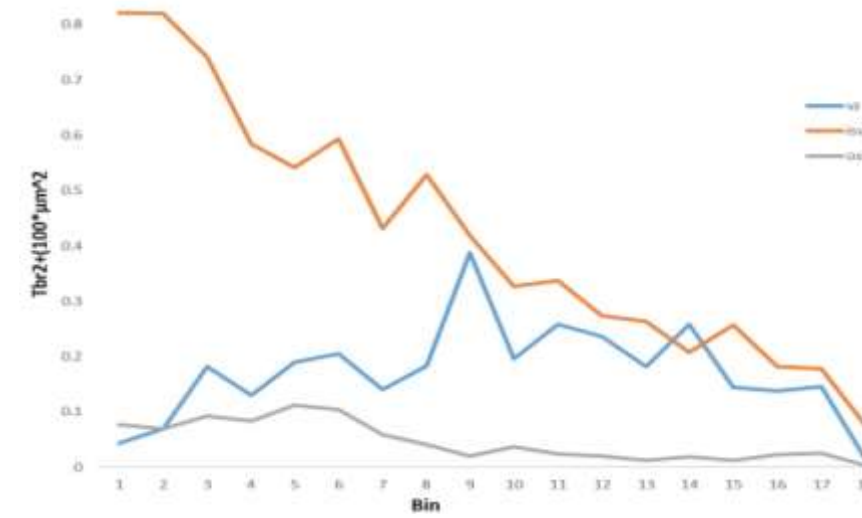
P8 Pax6+ cell density distribution



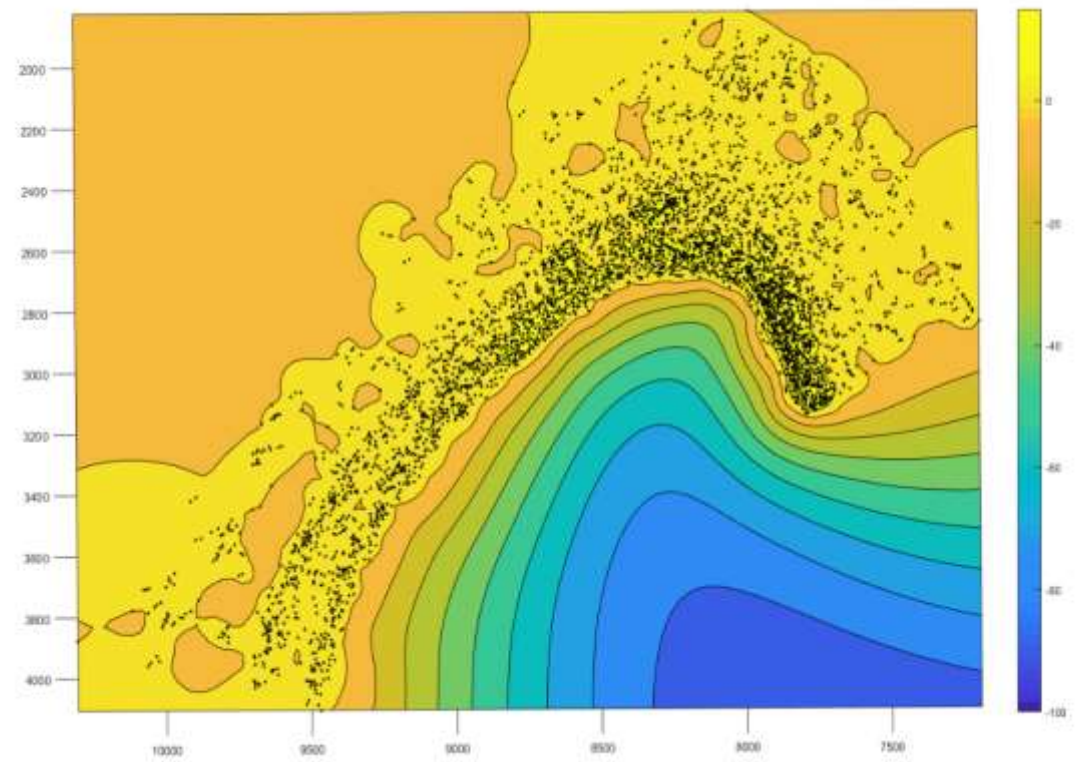
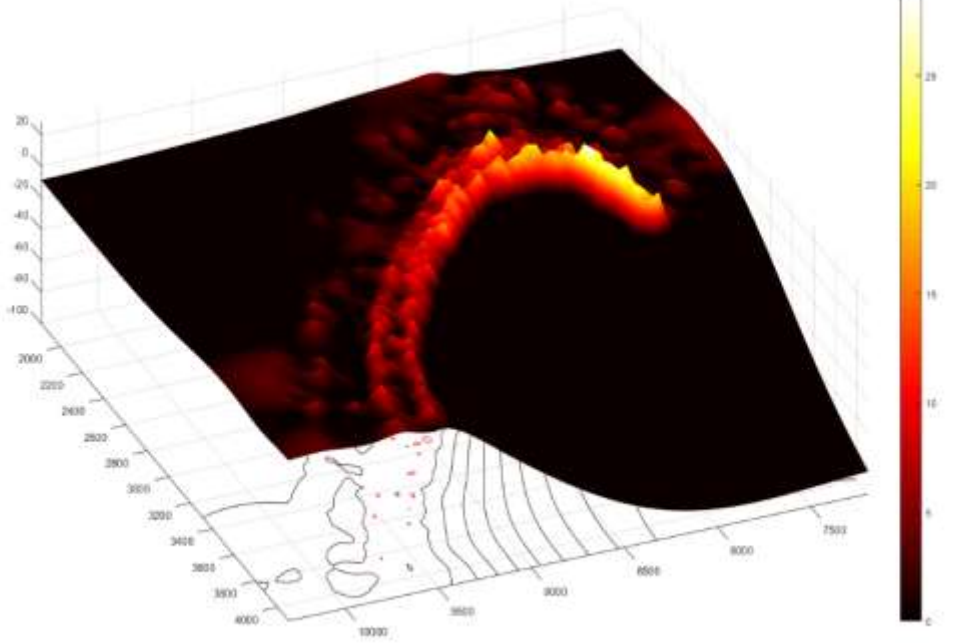
P8 Tbr2+ cell density distribution

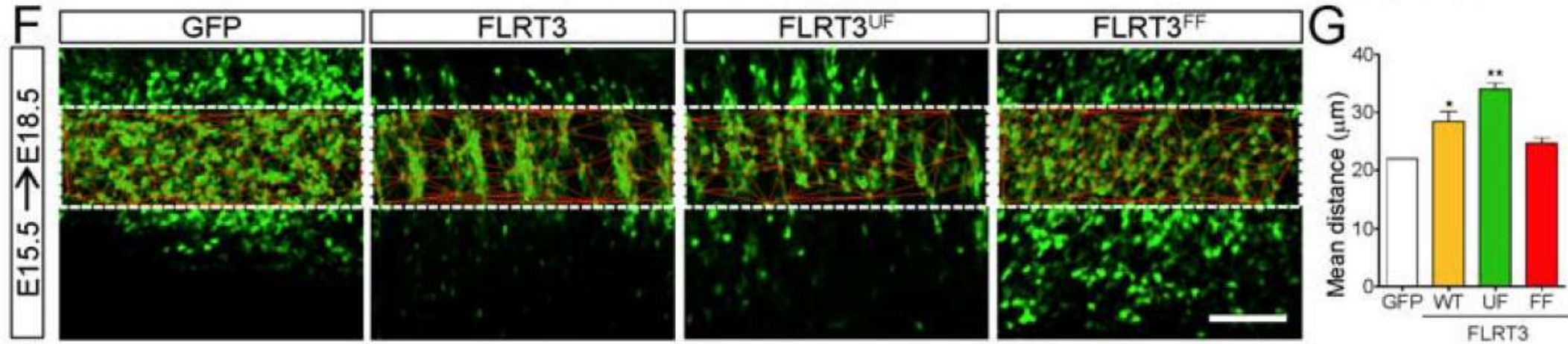


P8 Pax6+ cell density distribution



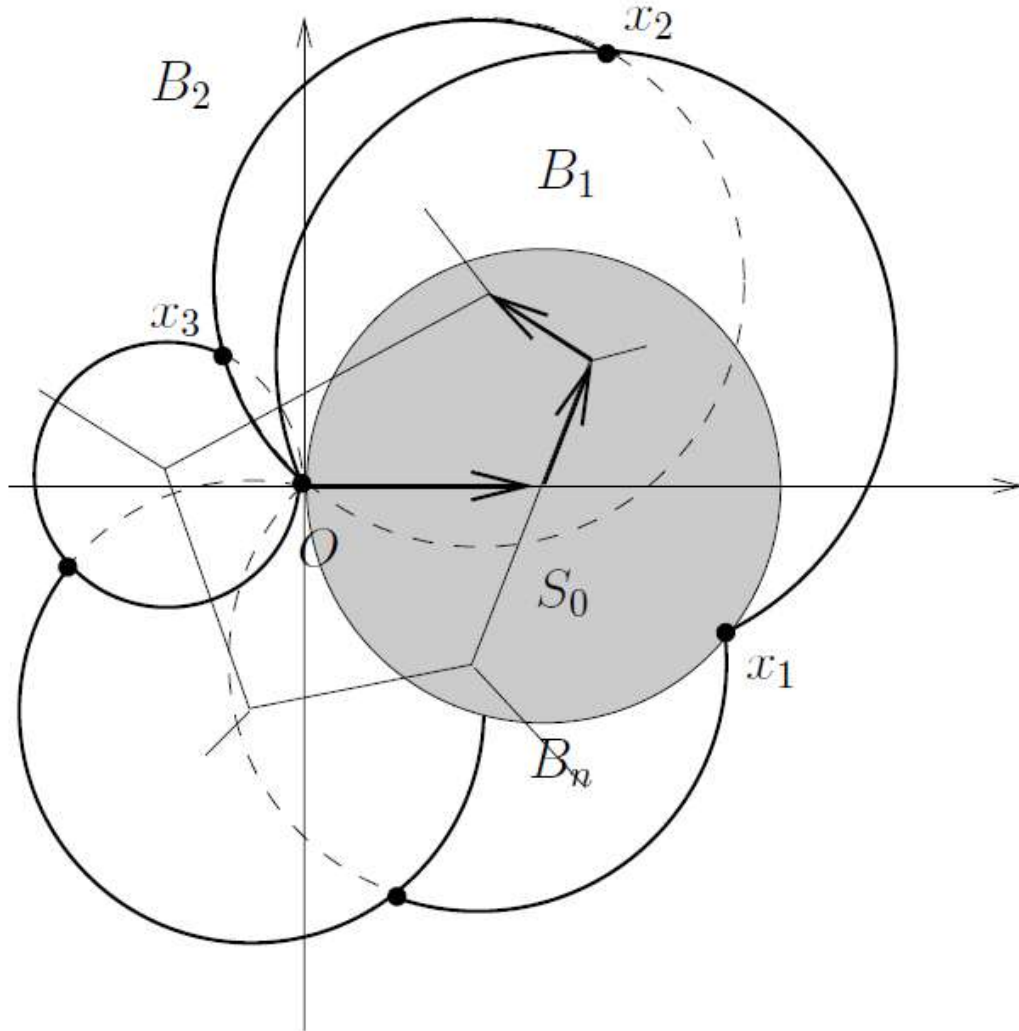
P8 Tbr2+ cell density distribution





Voronoi(维诺图/泰森多边形)

Elena Seiradake et al.(2014) Neuron



Case Studies in Spatial Point Process Modeling

$$L(X)^2 - 4\pi A(X) \geq 0$$

等周不等式：所有周长相等的封闭图形中，圆包围的面积最大

$$\text{RFav} = \frac{1}{N} \sum_{i=1}^N \frac{4\pi A(X_i)}{L(X_i)^2} \quad (0 < \text{RFav} \leq 1)$$

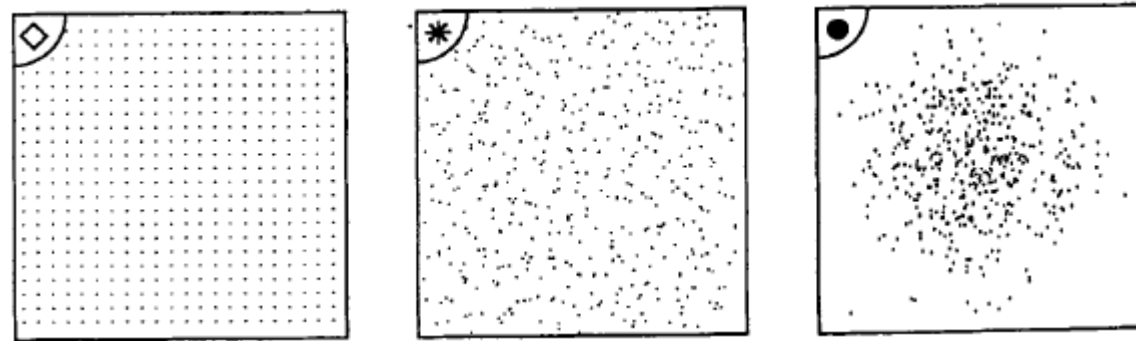
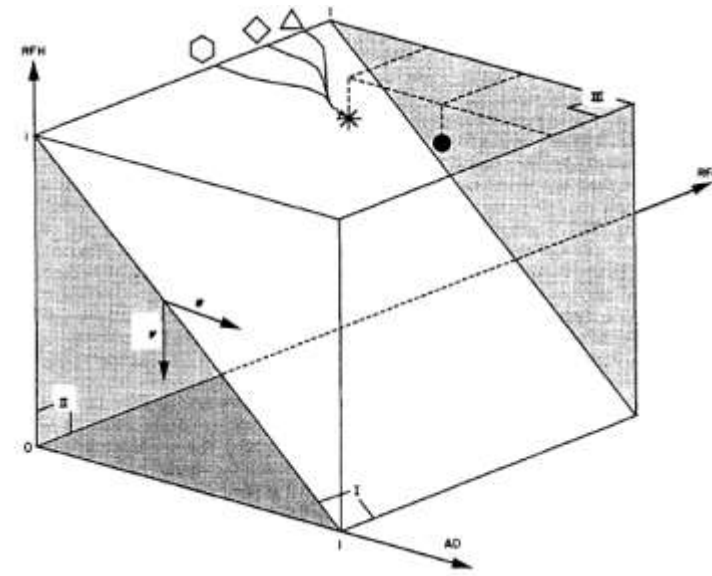
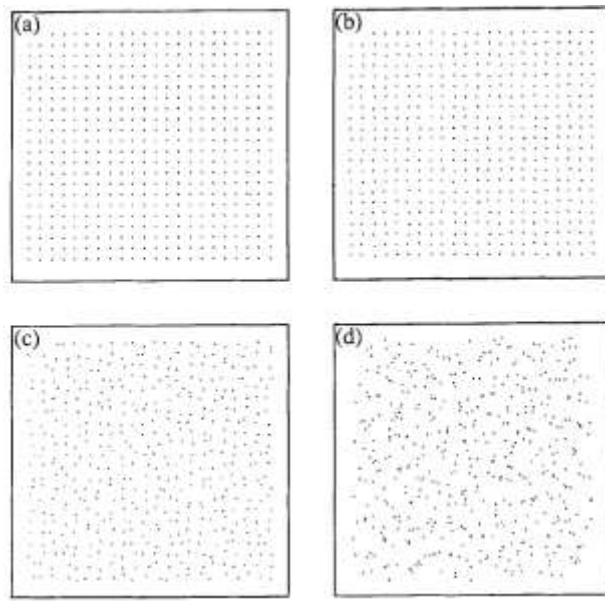
RFav越接近1说明多边形越圆

$$\text{AD} = 1 - \left(1 + \frac{\sigma_A}{A_{\text{av}}} \right)^{-1} \quad \text{RFH} = \left(1 + \frac{\sigma_{\text{RF}}}{\text{RF}_{\text{av}}} \right)^{-1}$$

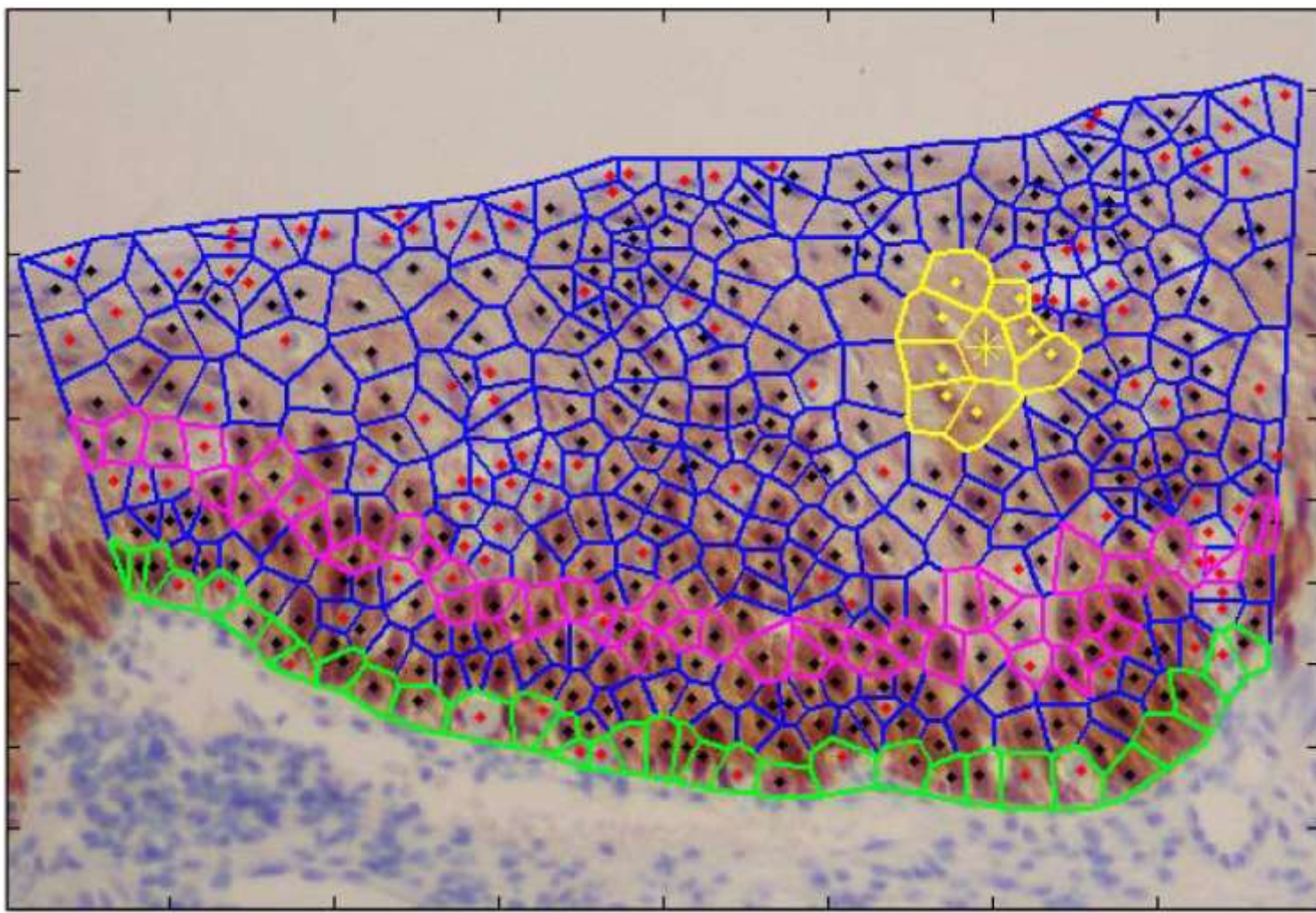
属于[0,1]，越接近0面积越均质，越接近1面积越异质

属于[0,1]之间，越接近0形状越均质，越接近1，形状越异质

R. MARCELPOIL et al.(1992) J. theor. Biol.

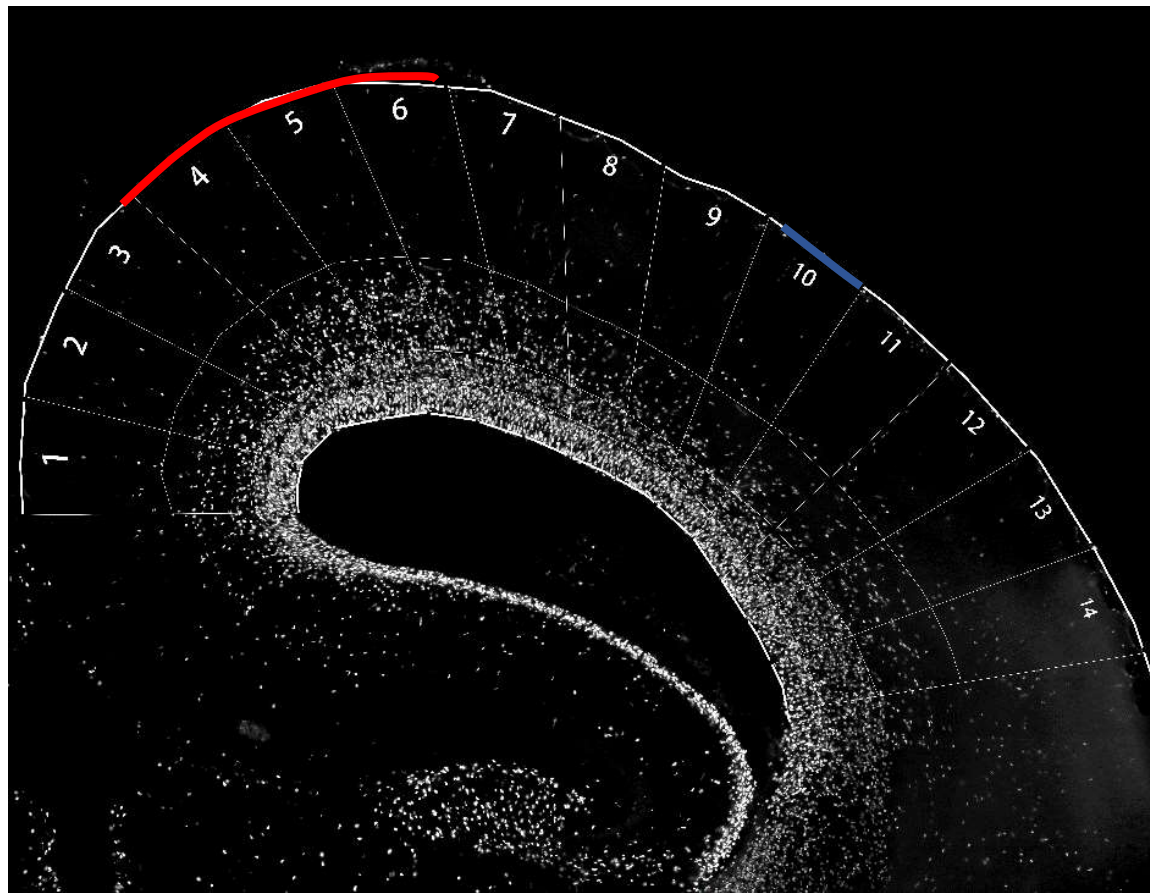


R. MARCELPOIL et al.(1992) J. theor. Biol.

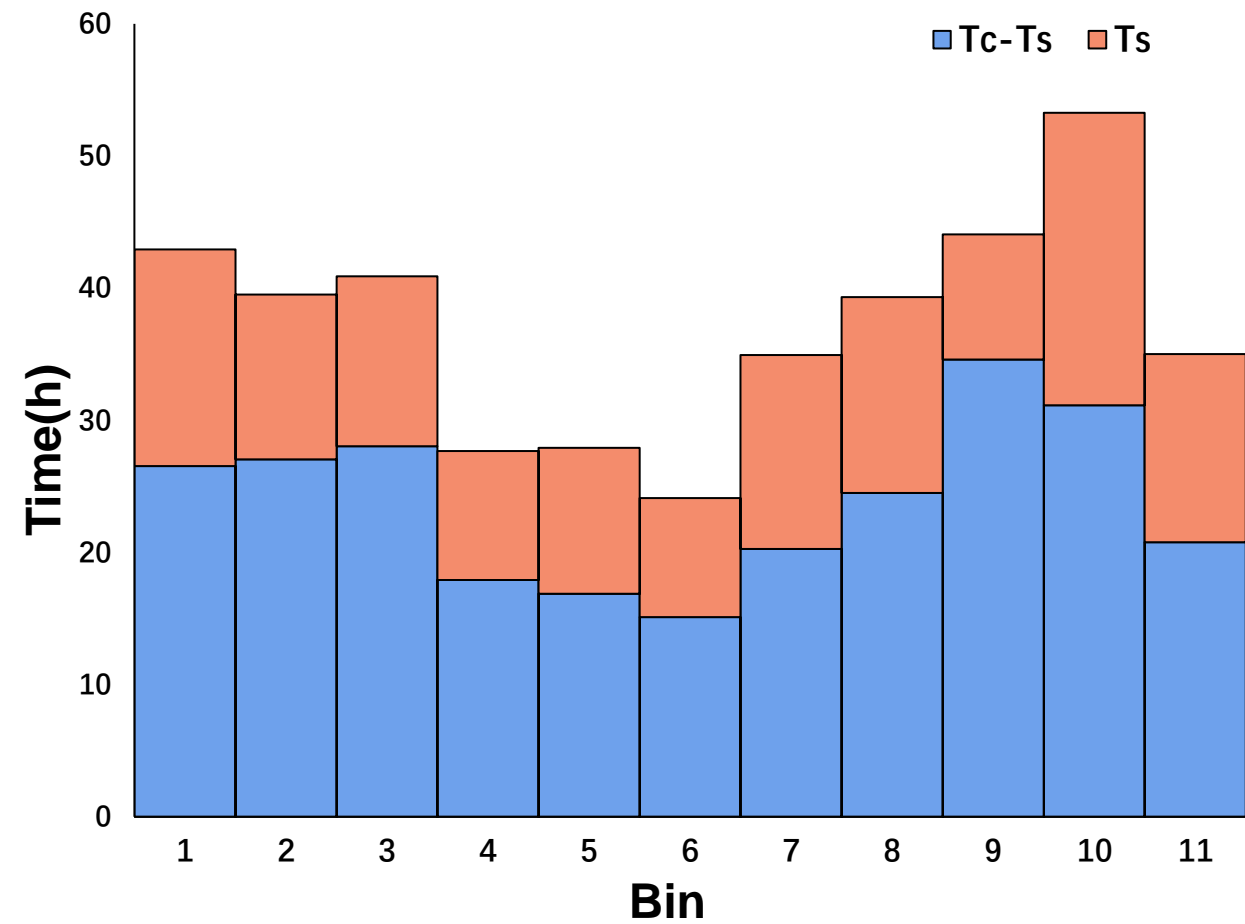


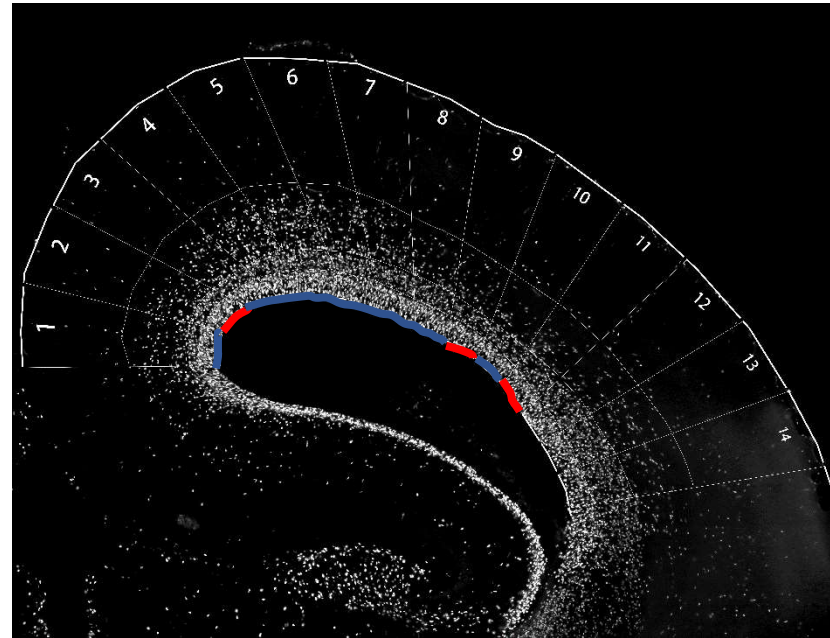
Mehrnoosh Khojasteh-Lakelayeh, 2012

Stem cell distribution and cell cycle

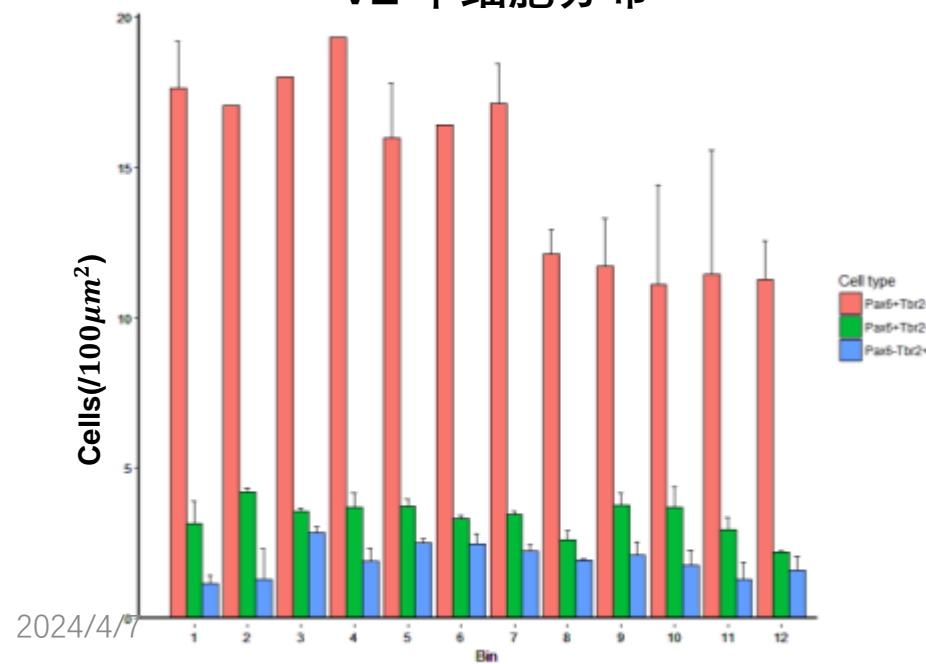


P2 average of cell cycle

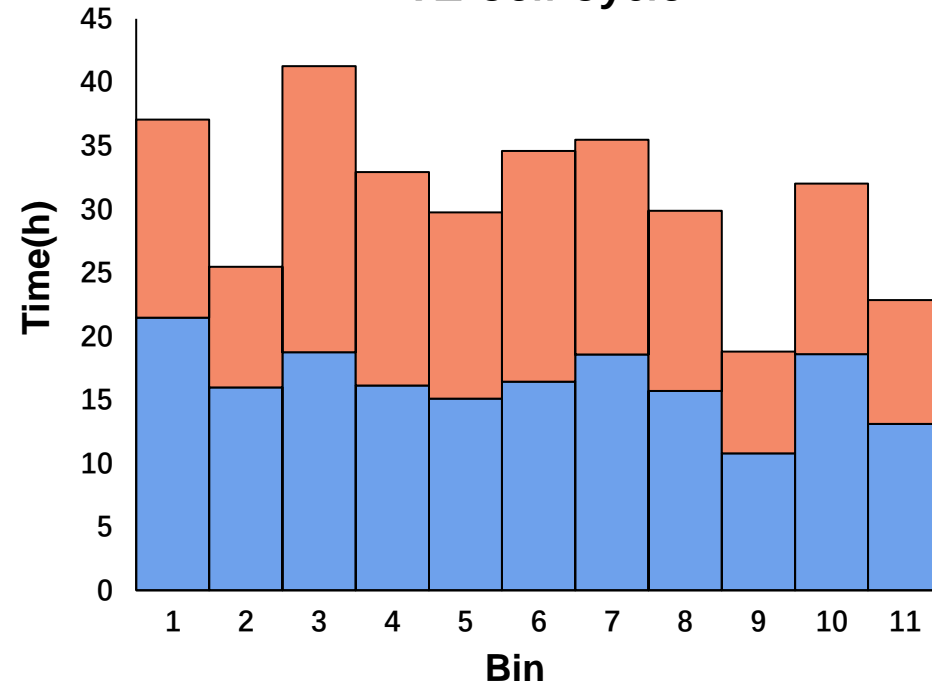




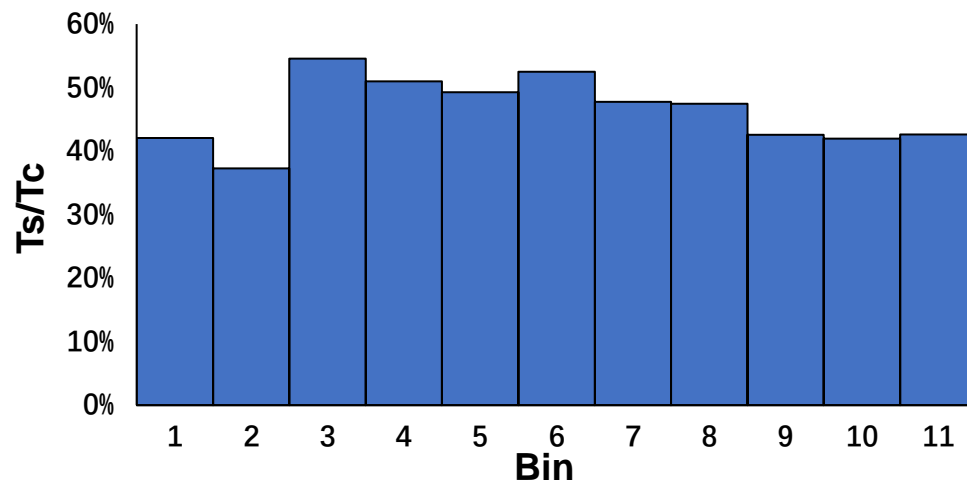
VZ 干细胞分布

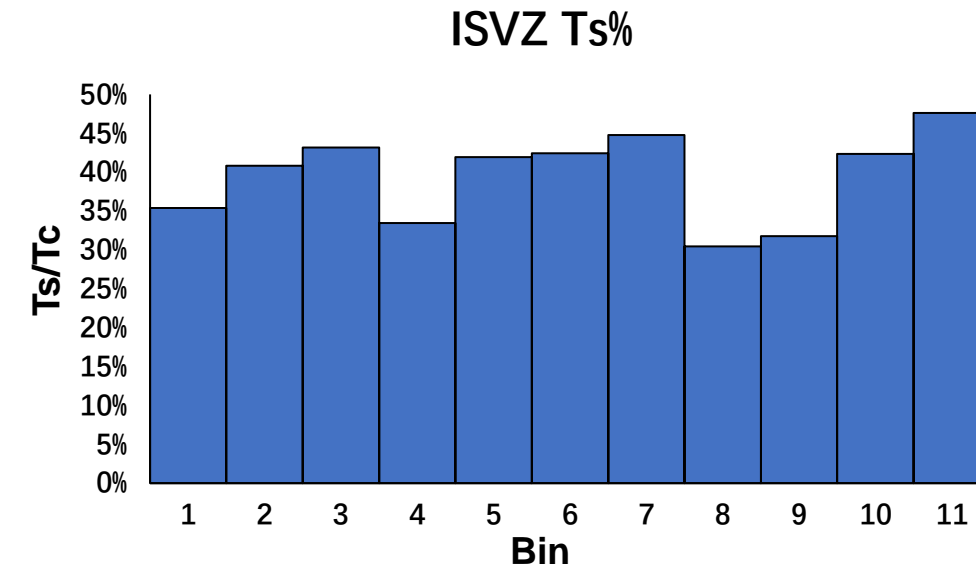
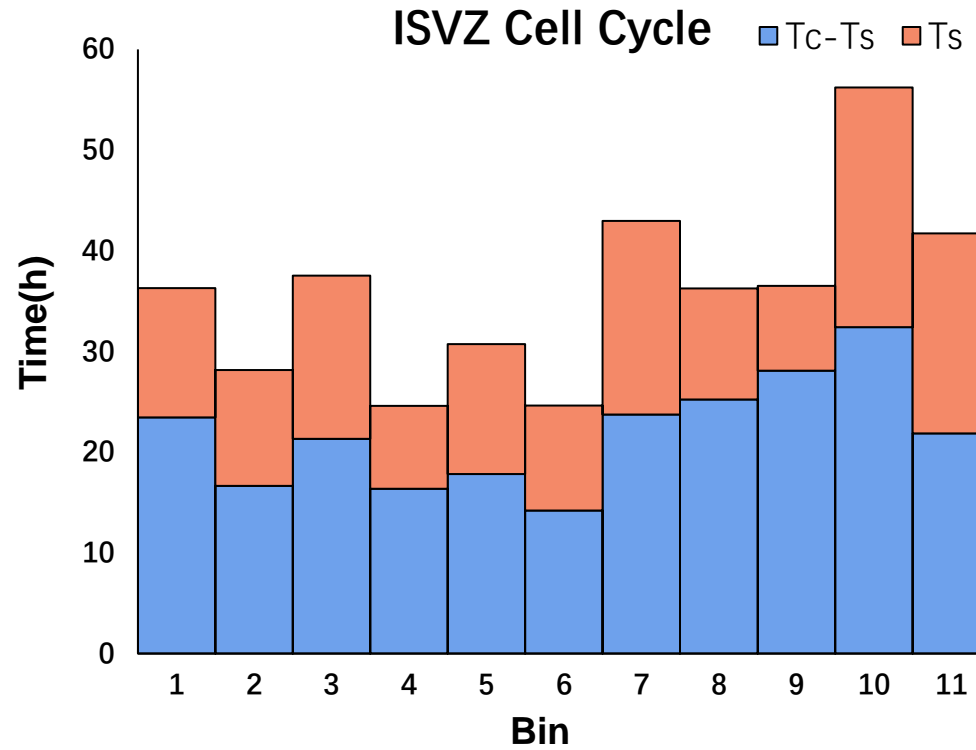
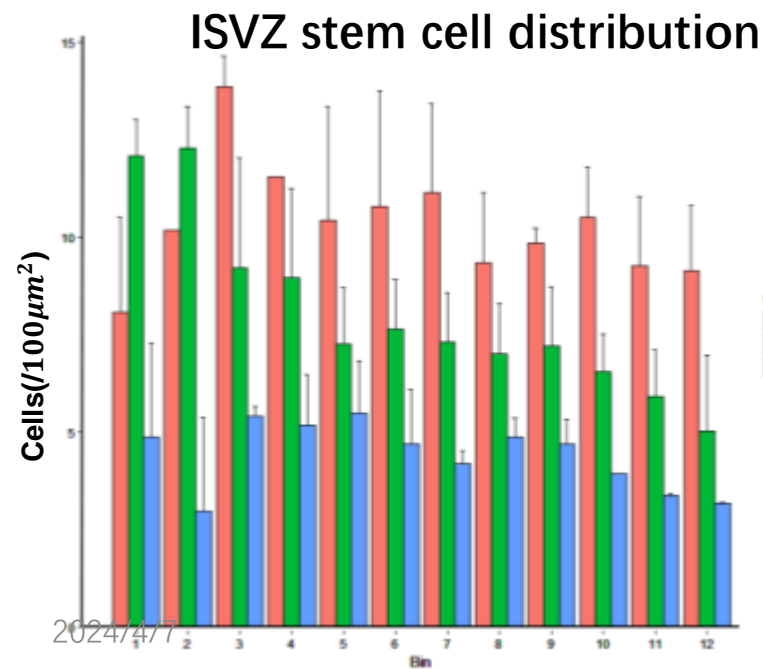
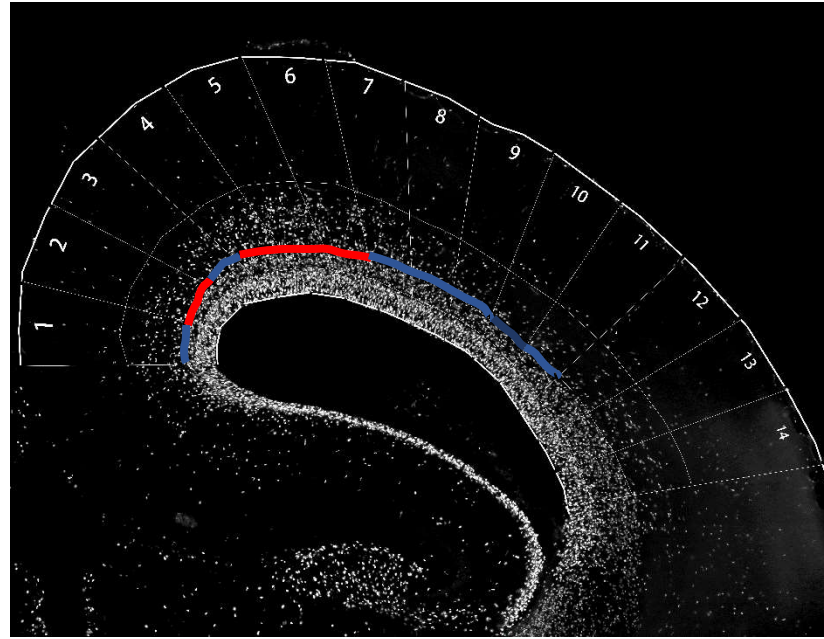


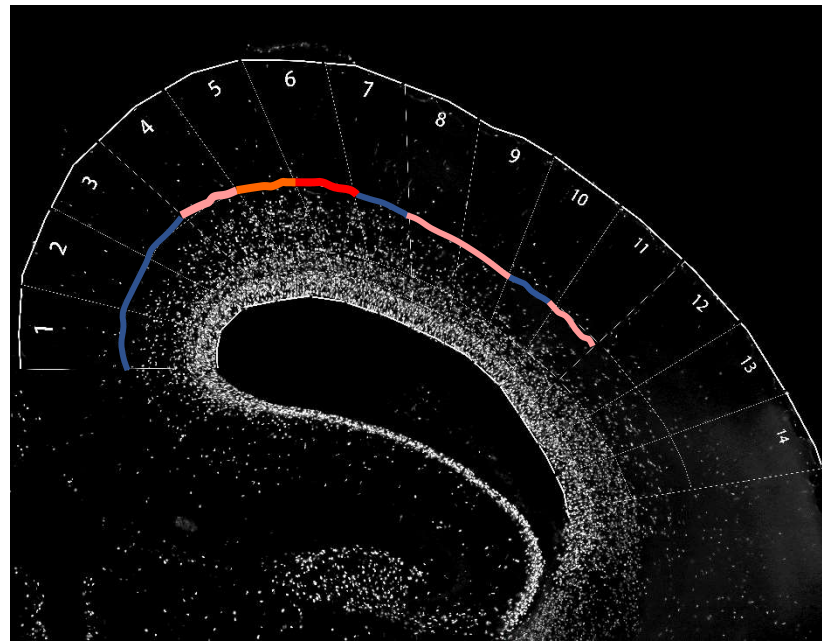
VZ Cell Cycle



VZ Ts%

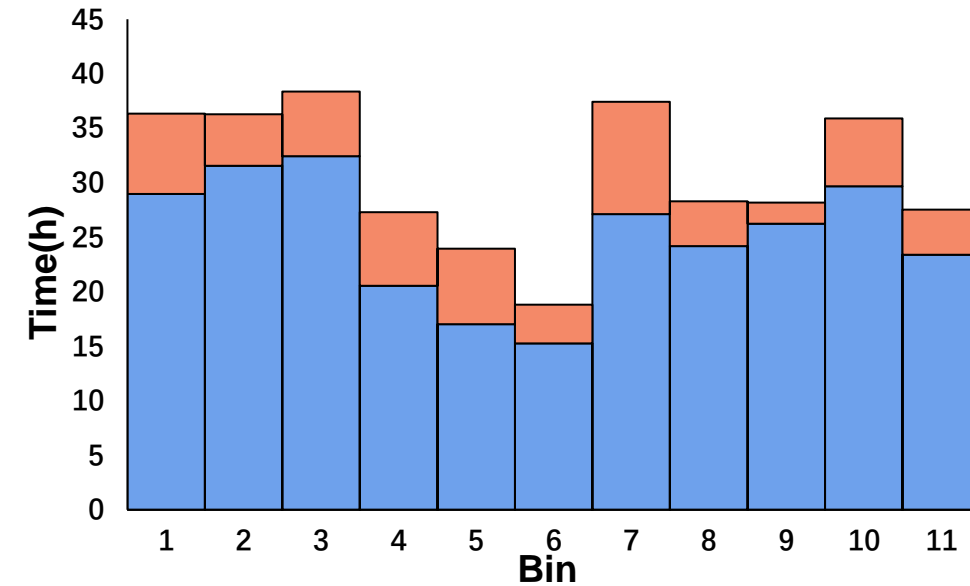




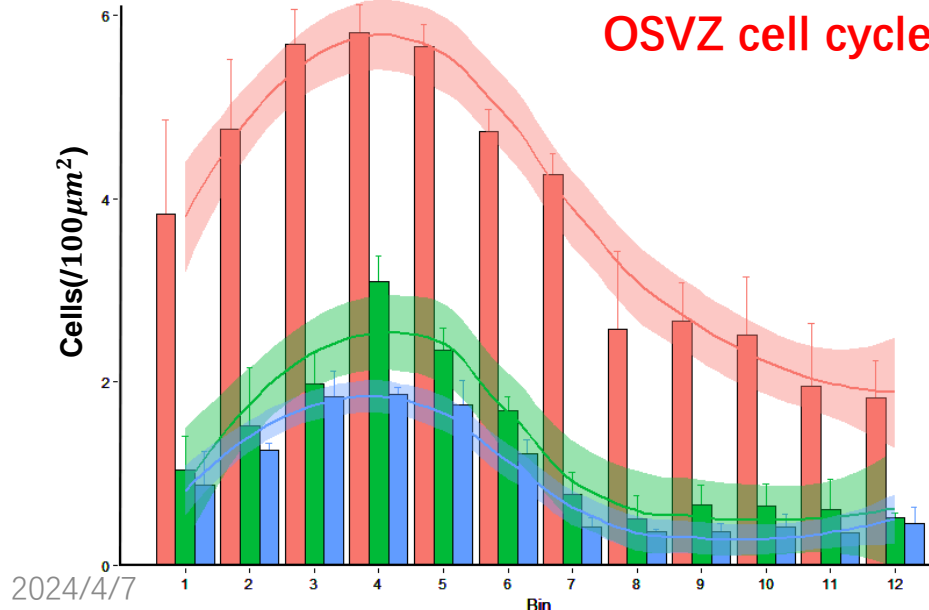


OSVZ Cell Cycle

■ Tc-Ts ■ Ts



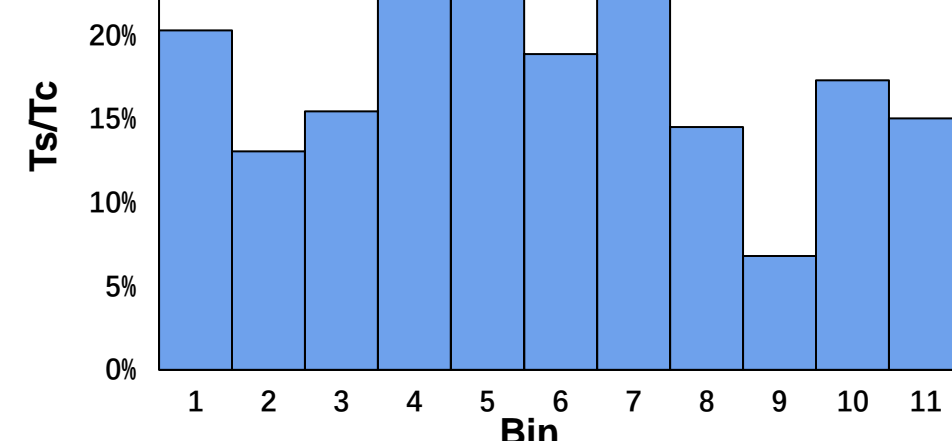
OSVZ stem cell distribution

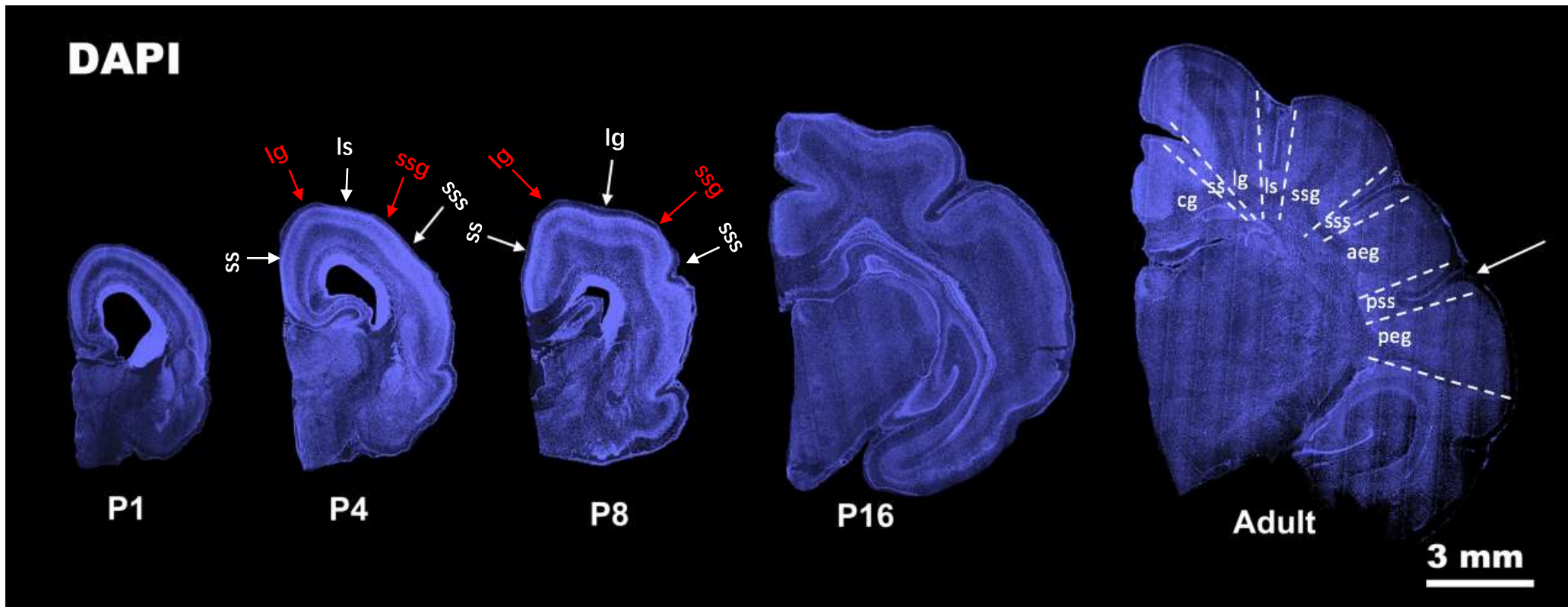


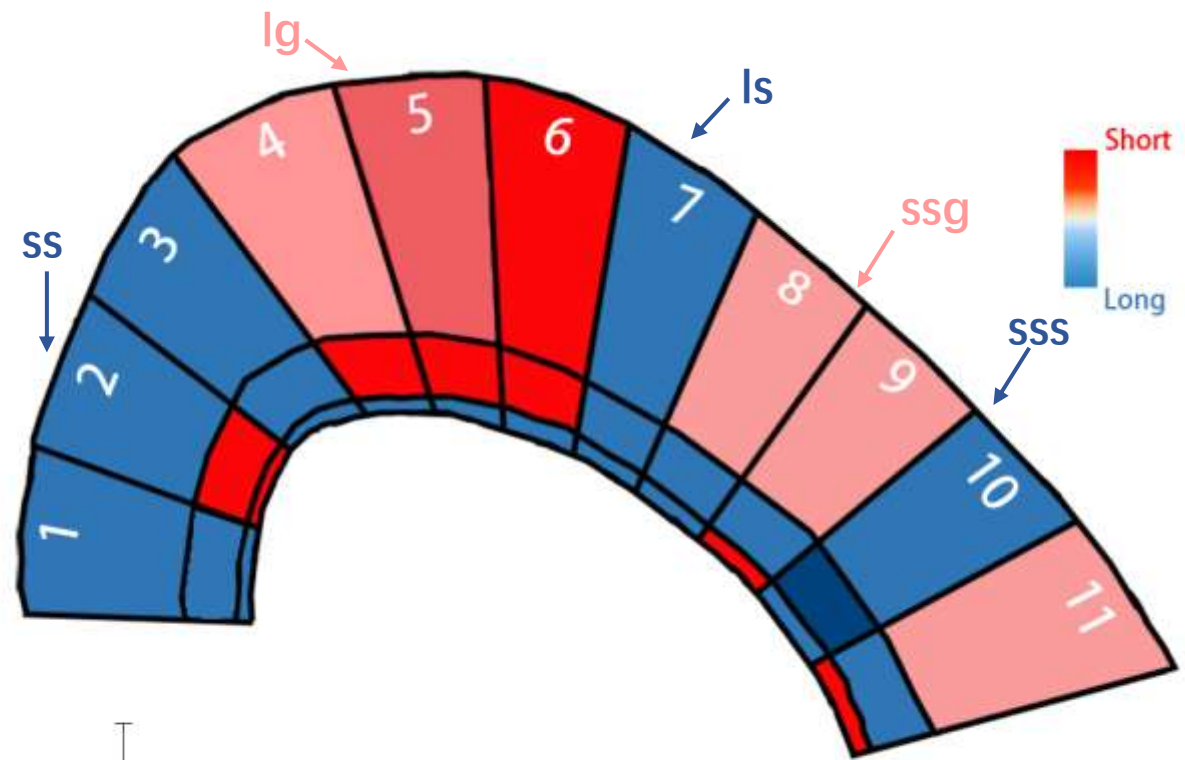
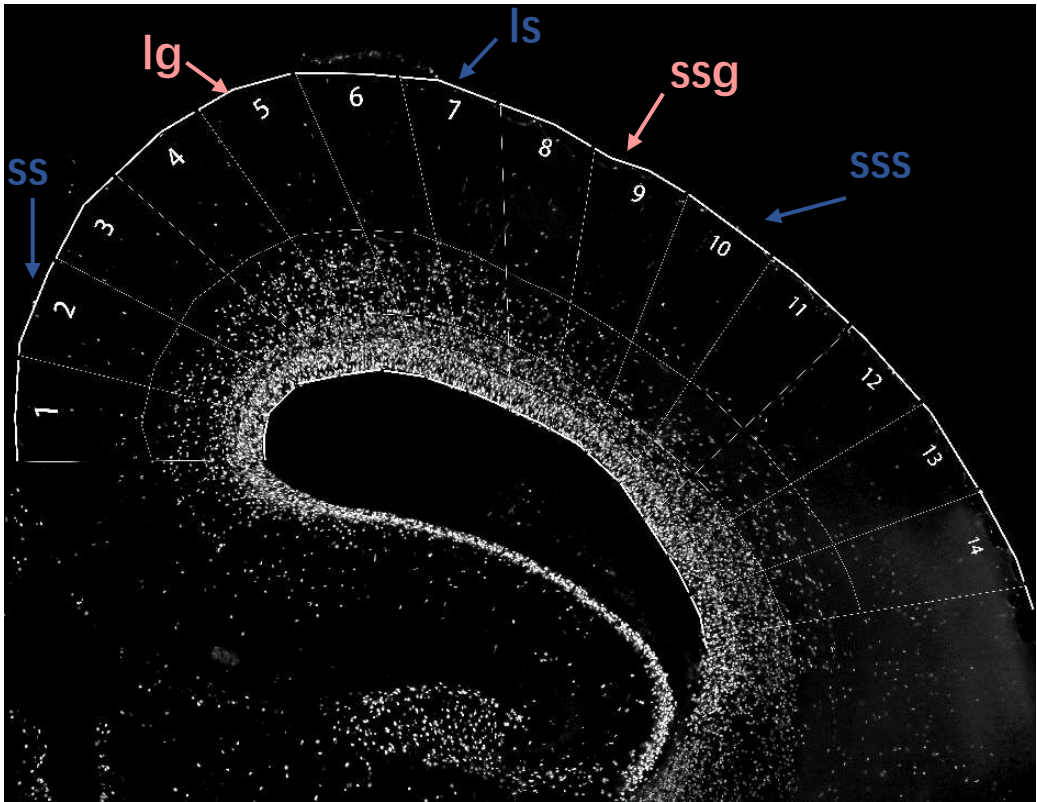
OSVZ cell cycle shows the apparent difference

Cell type
Pax6+Tbr2-
Pax6+Tbr2+
Pax6-Tbr2+

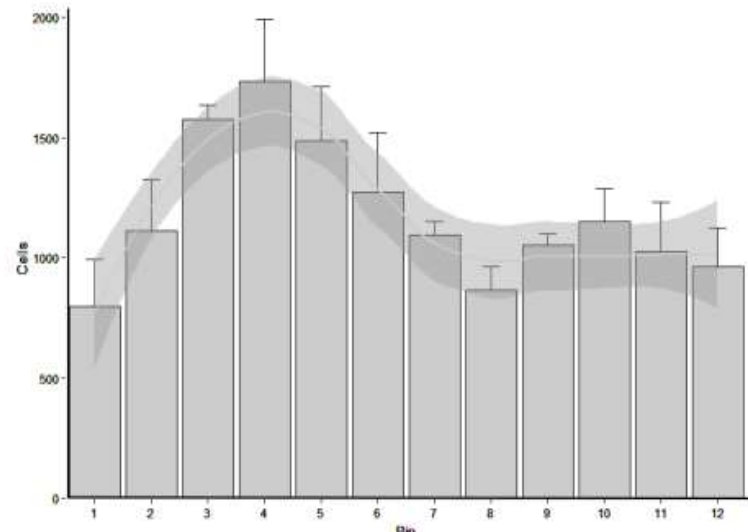
OSVZ Ts%



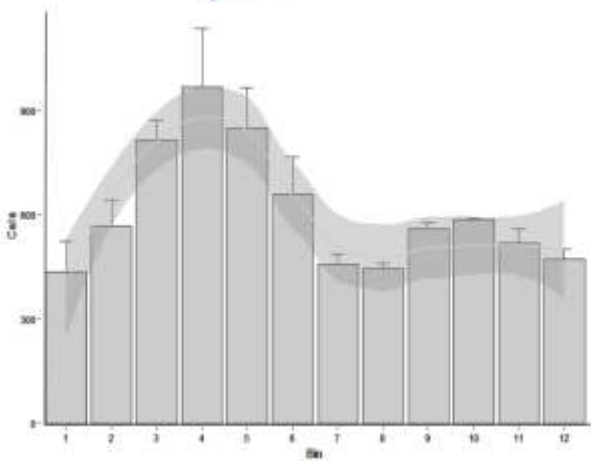


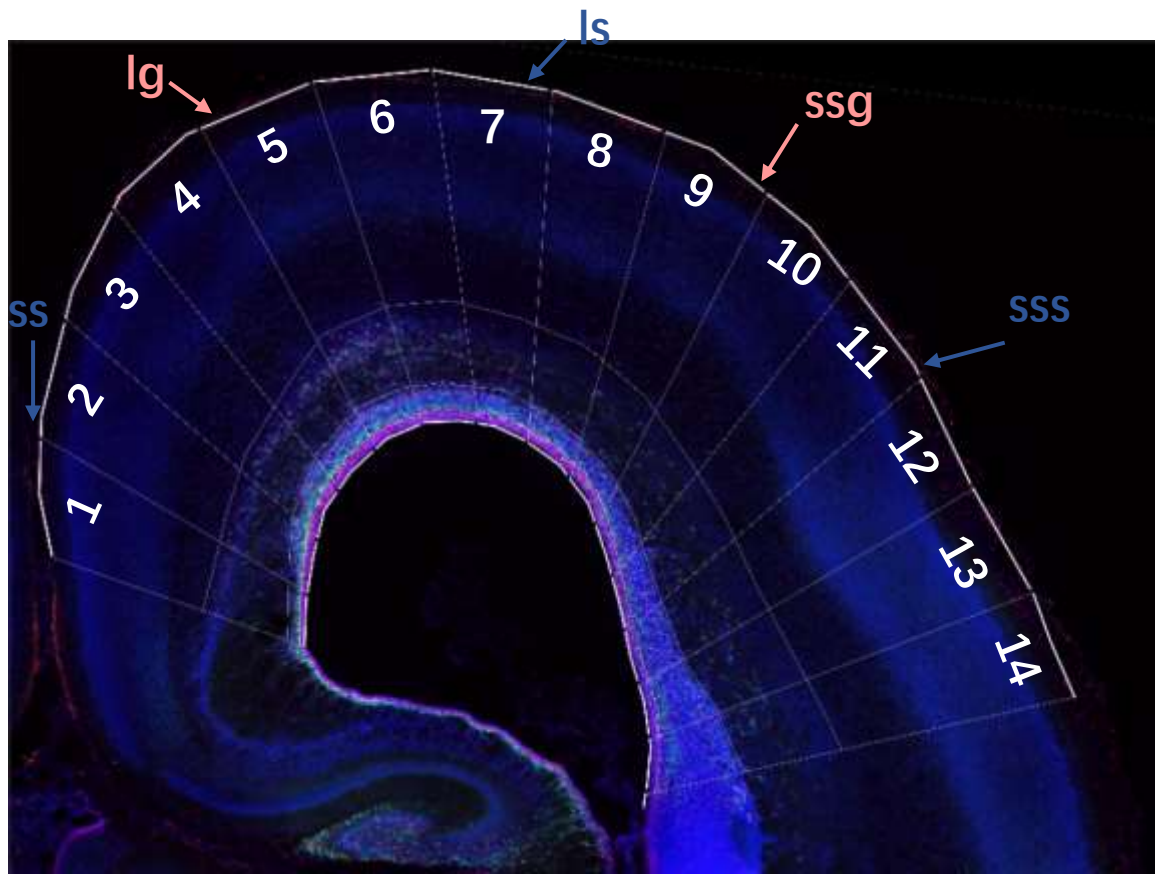


- The distribution of cell cycle lengths generally aligns with the development of sulci and gyri.
- In the locations where sulci are forming, the VZ and ISVZ exhibit faster cell cycle progression.

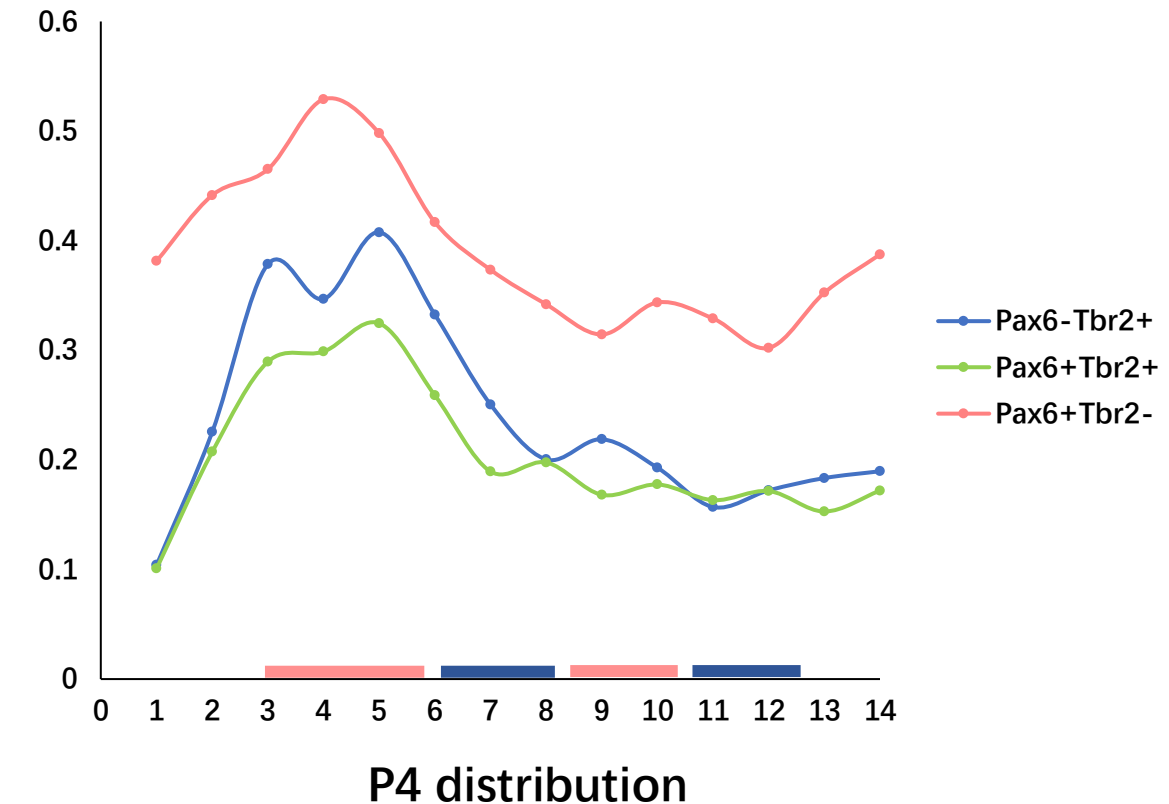


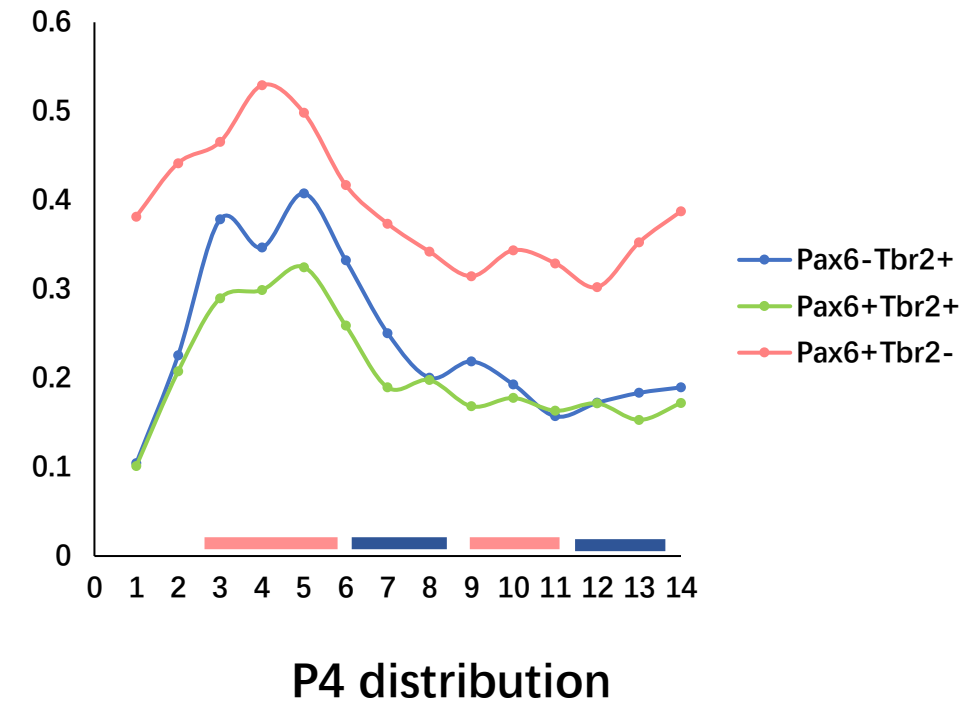
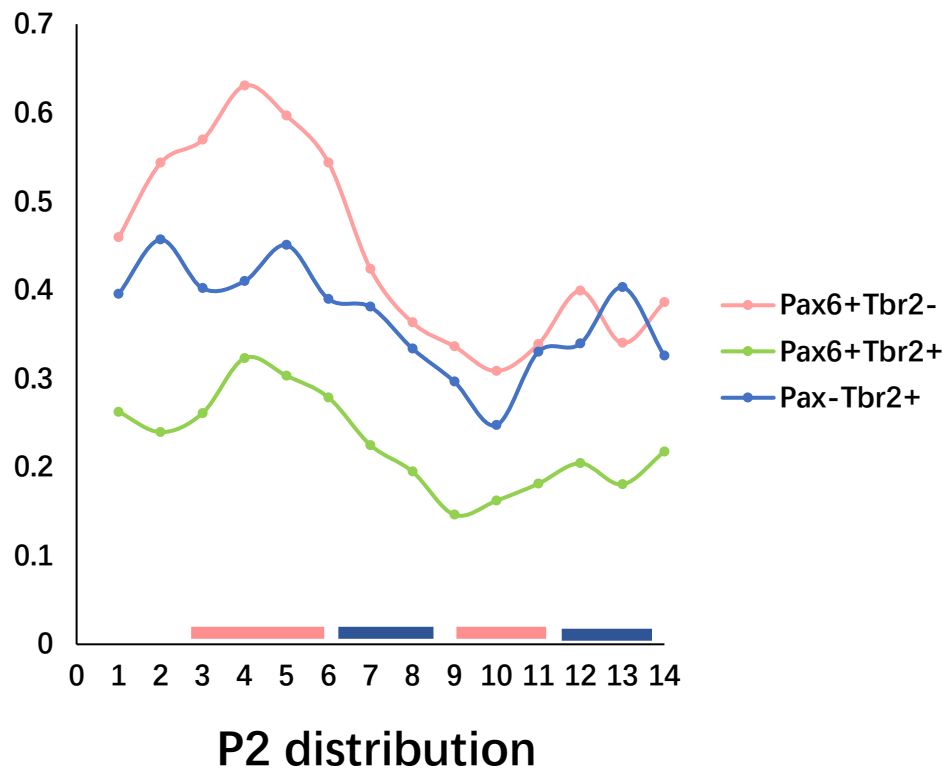
Tbr2+ distribution

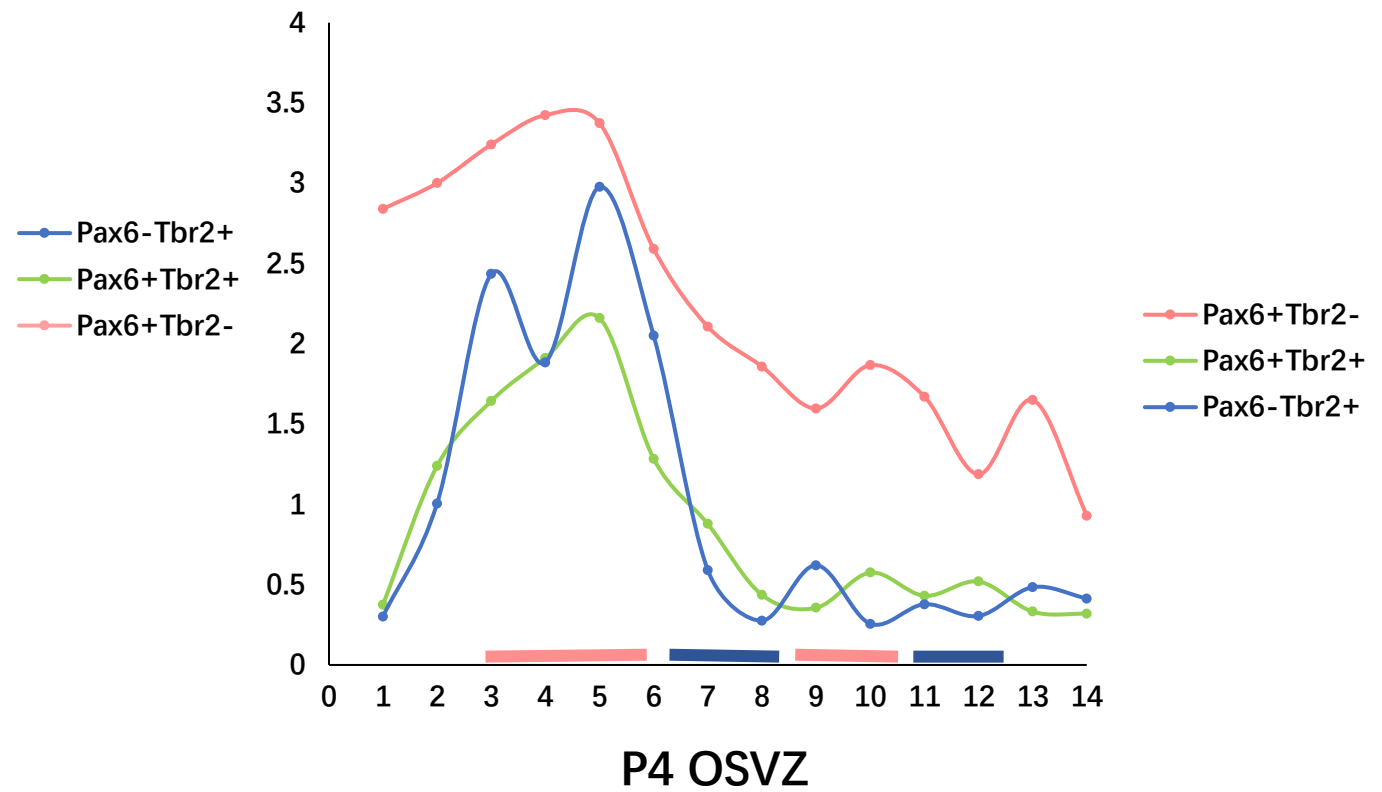
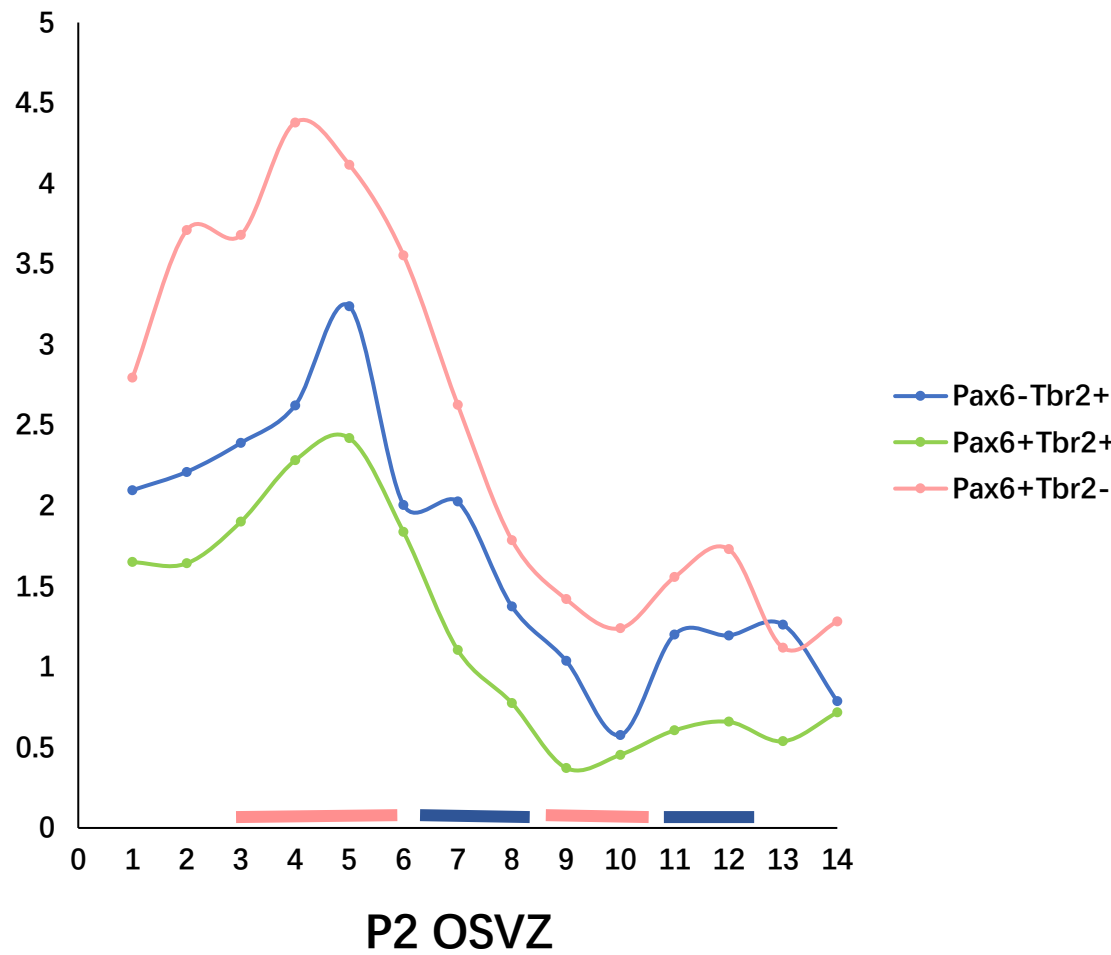


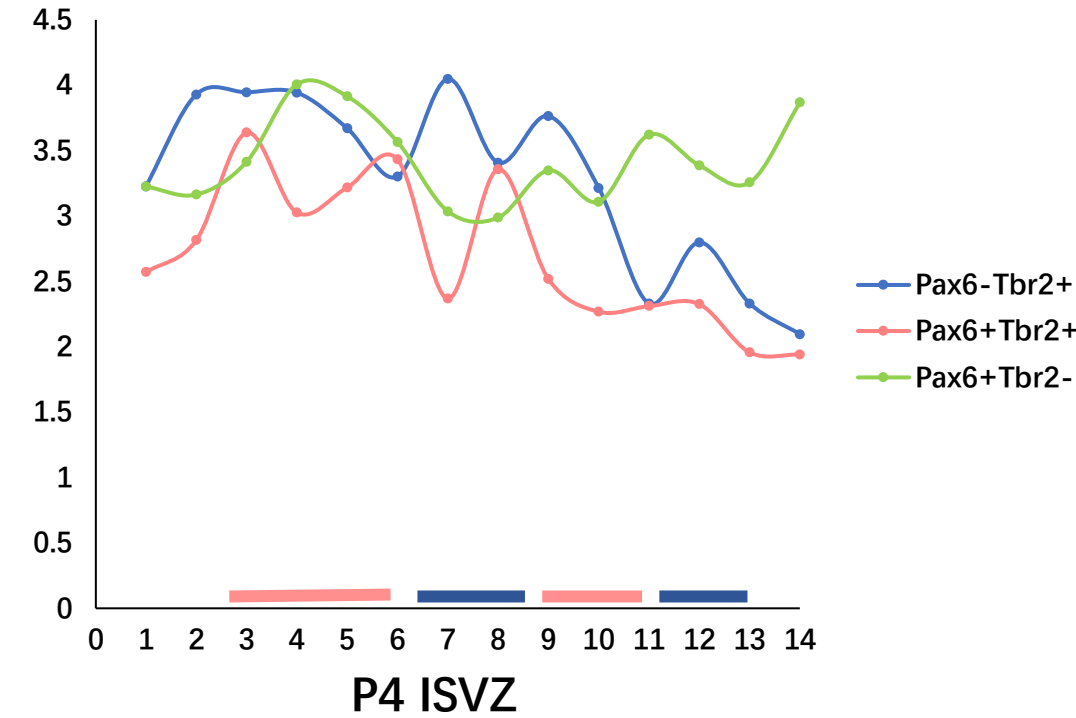
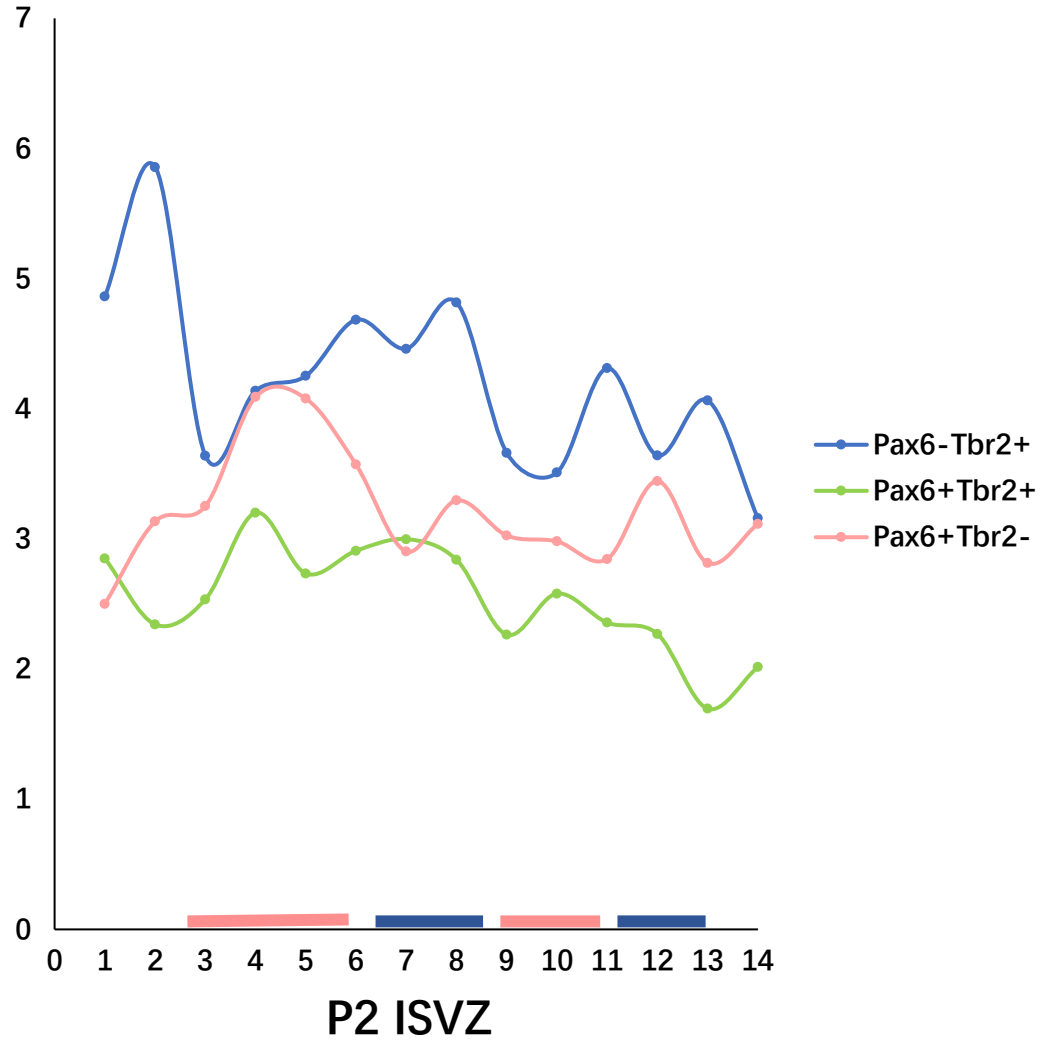


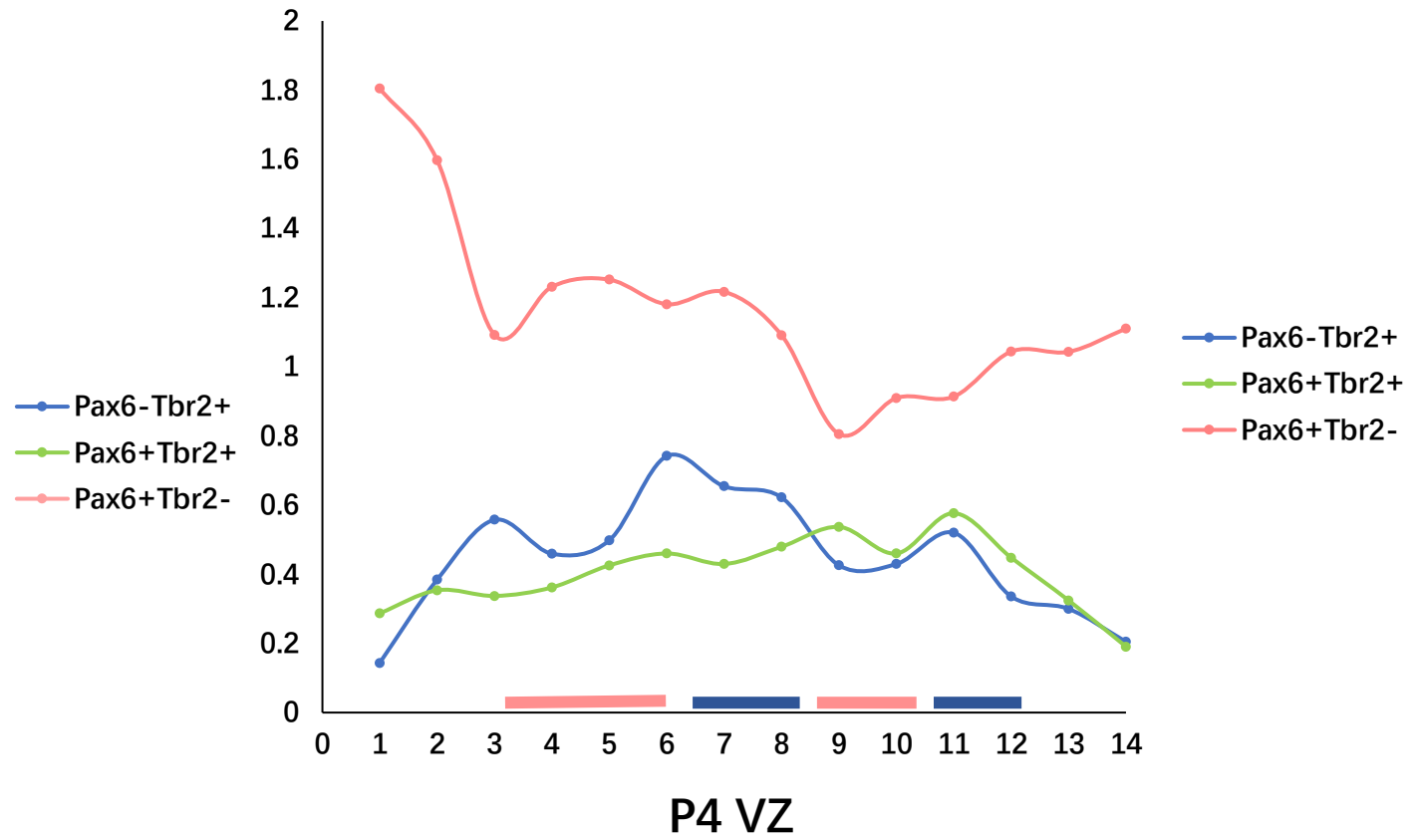
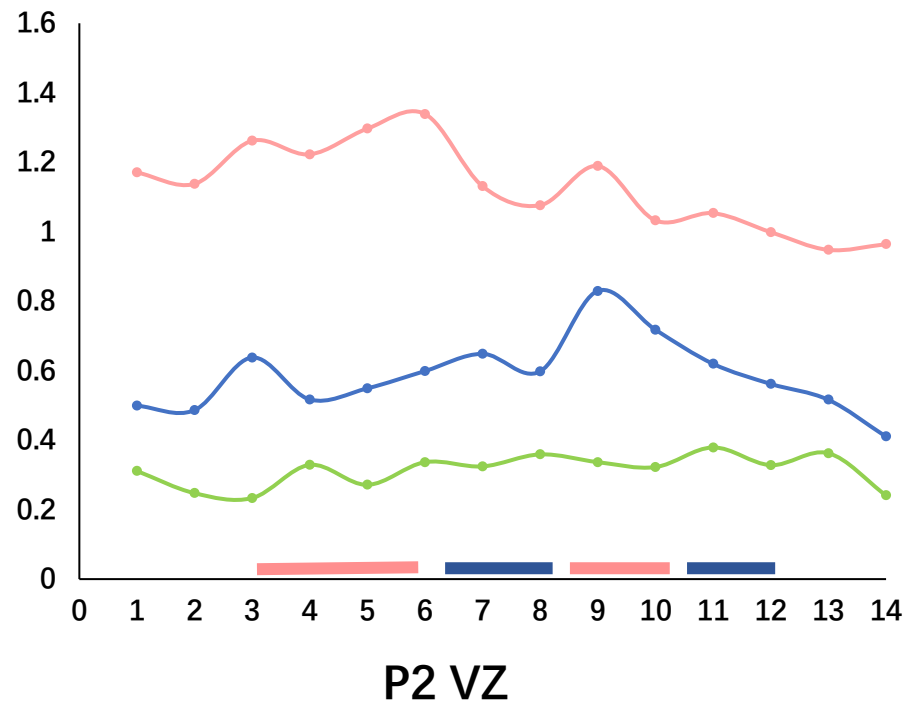
P4 distribution

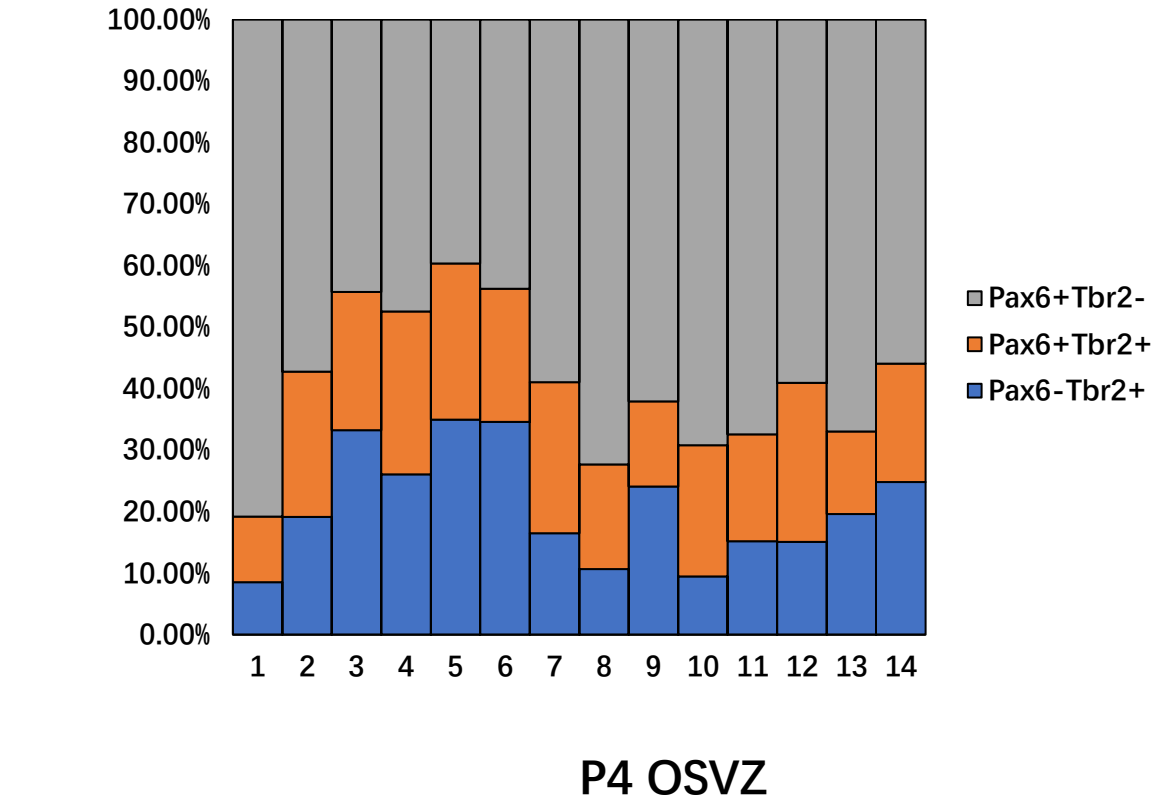
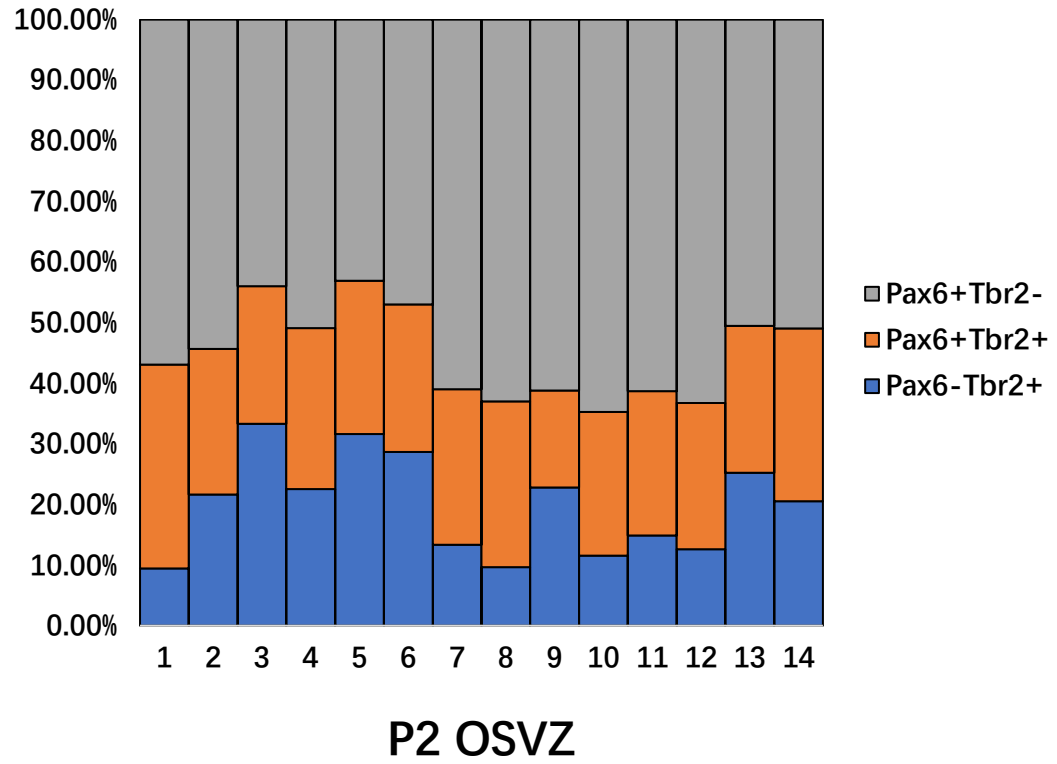


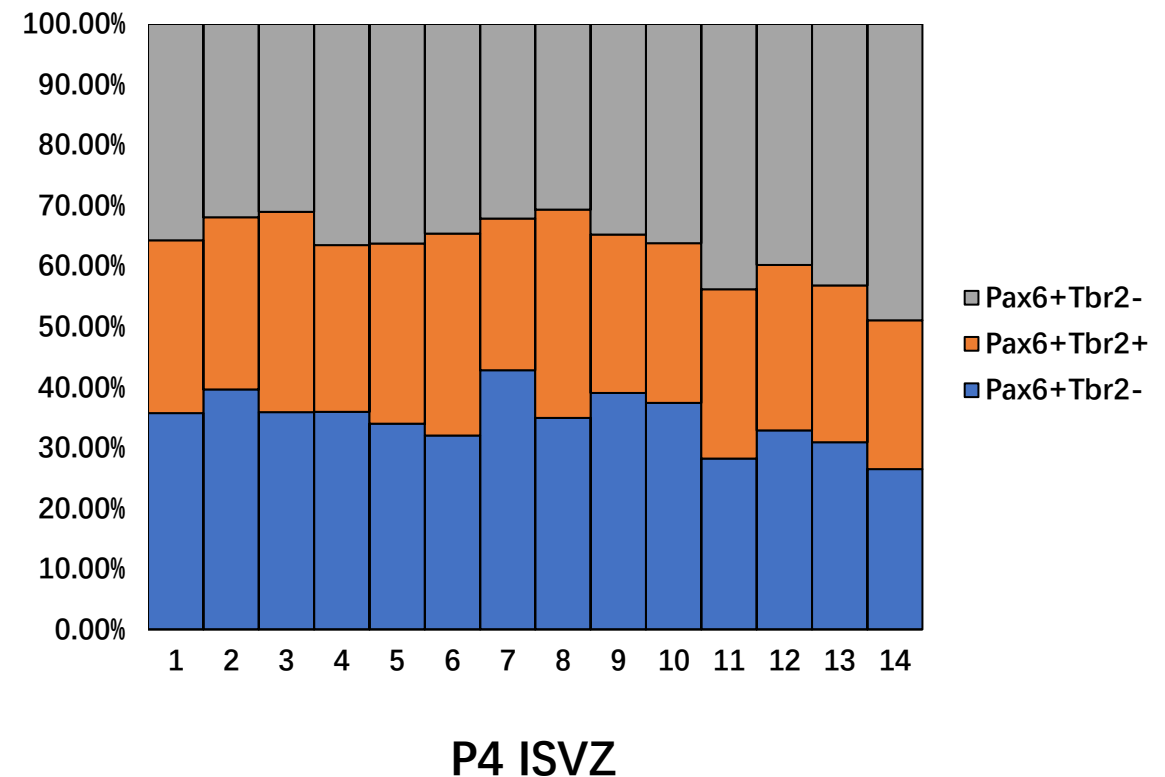
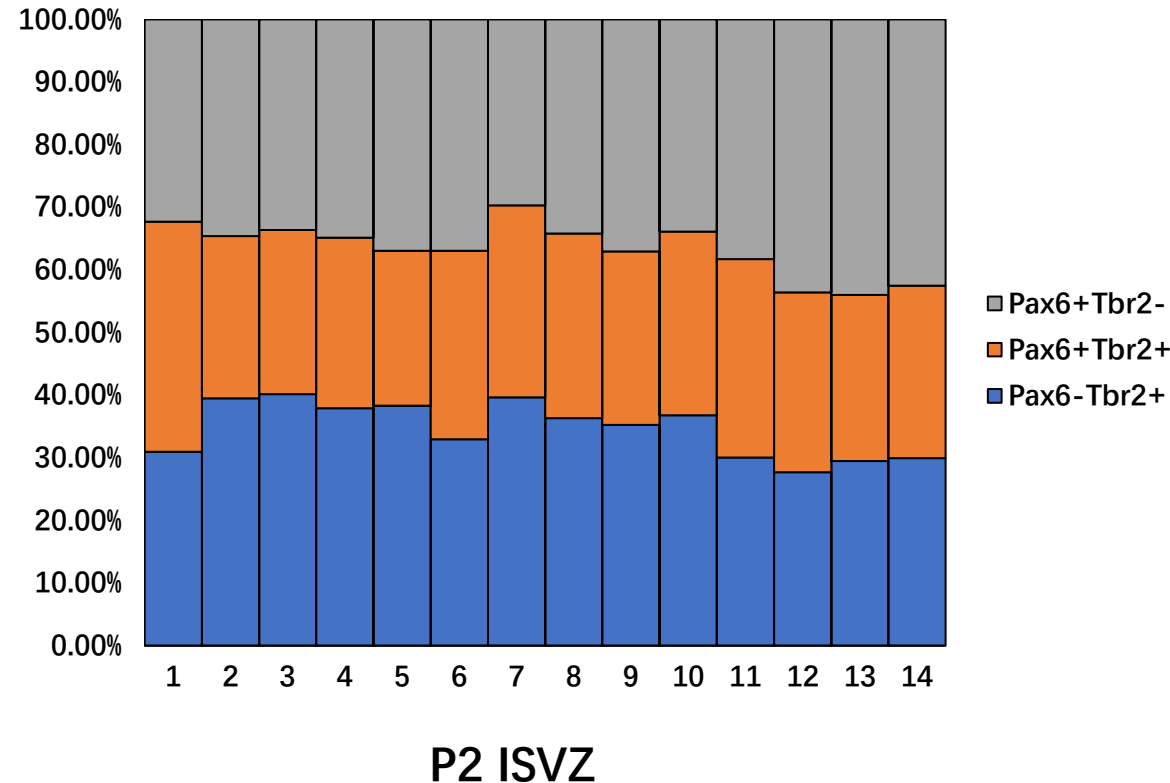


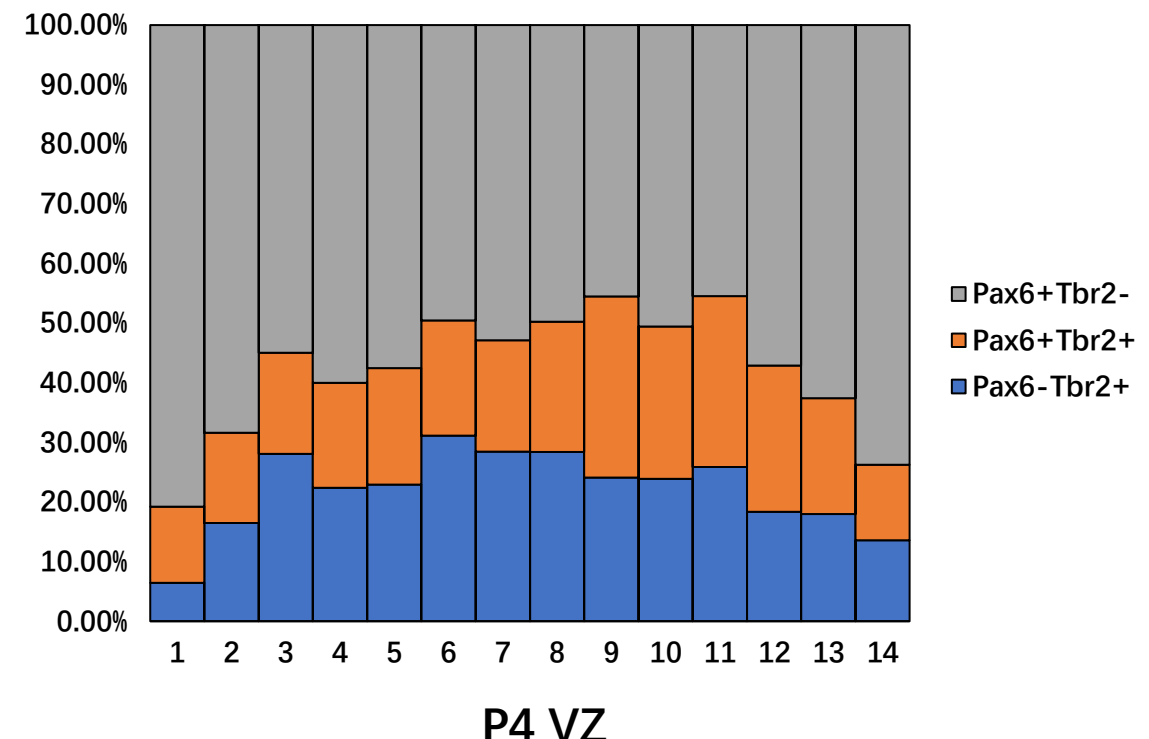
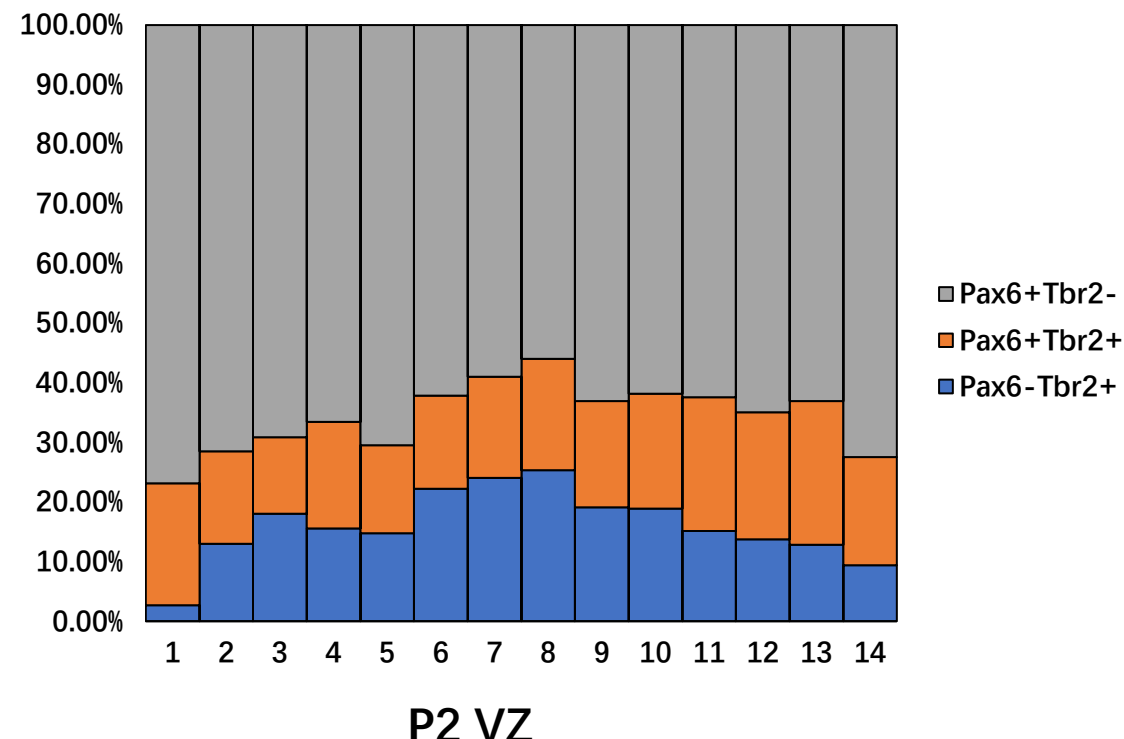




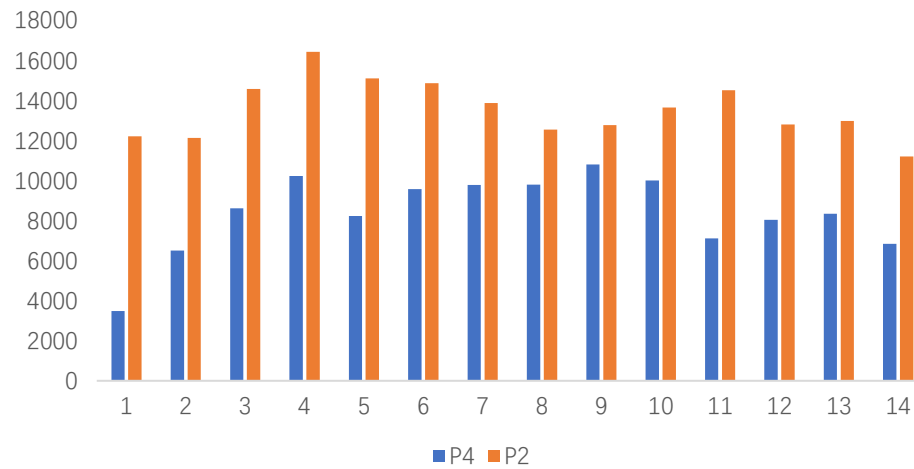




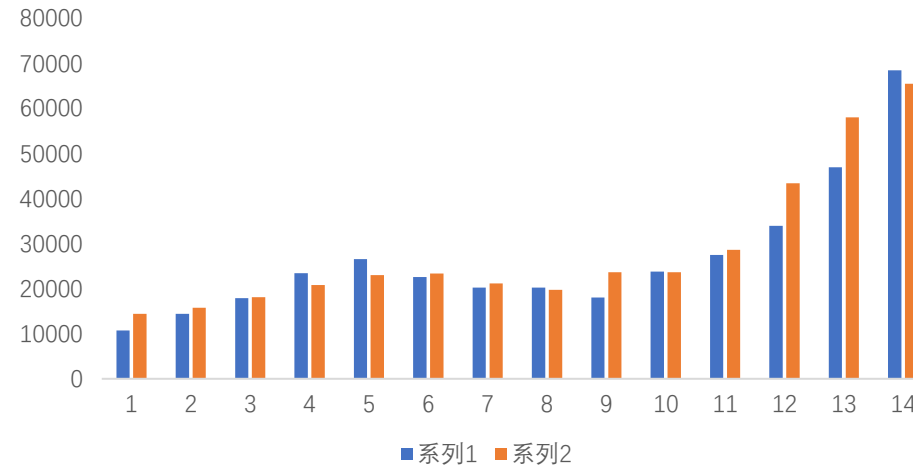




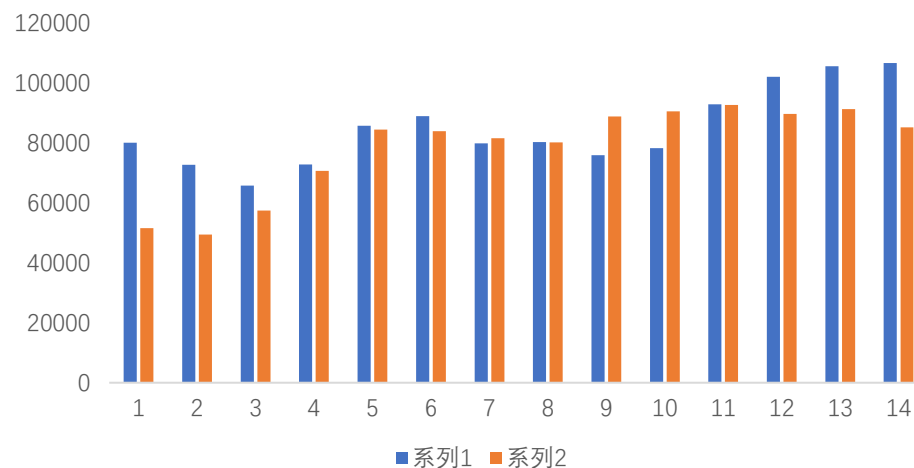
VZ



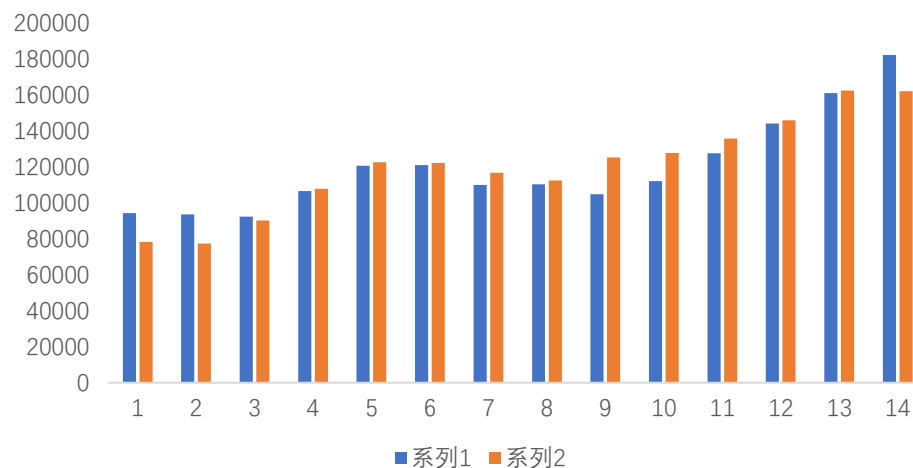
ISVZ



OSVZ

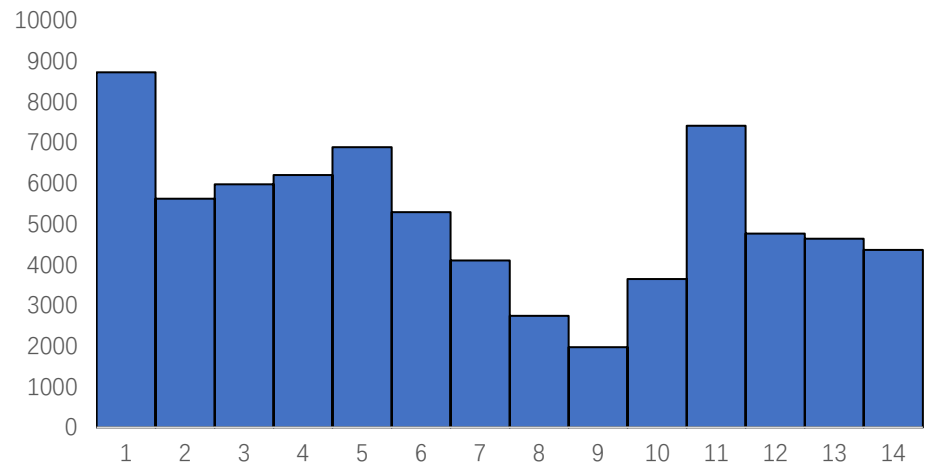


total

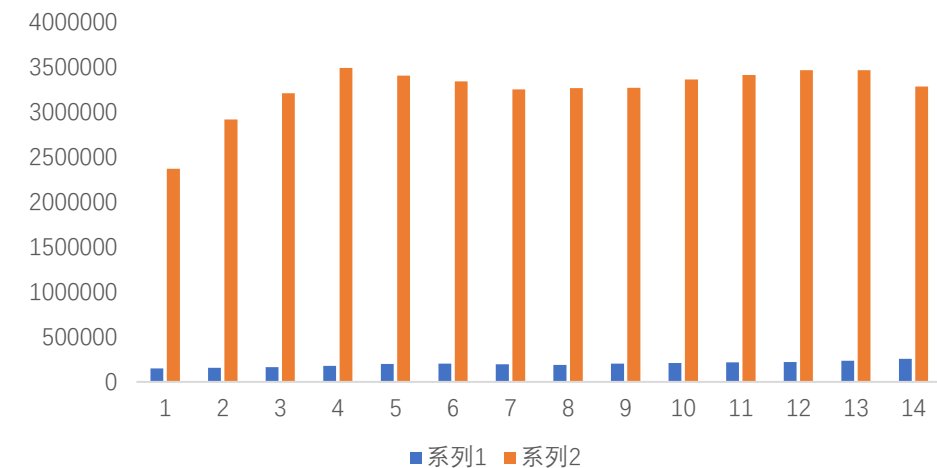


P2 P4 area comparison

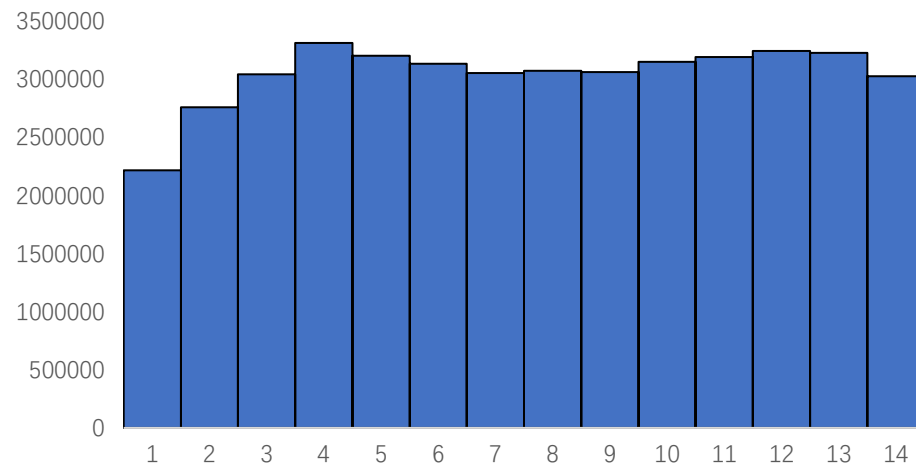
vz p2-p4

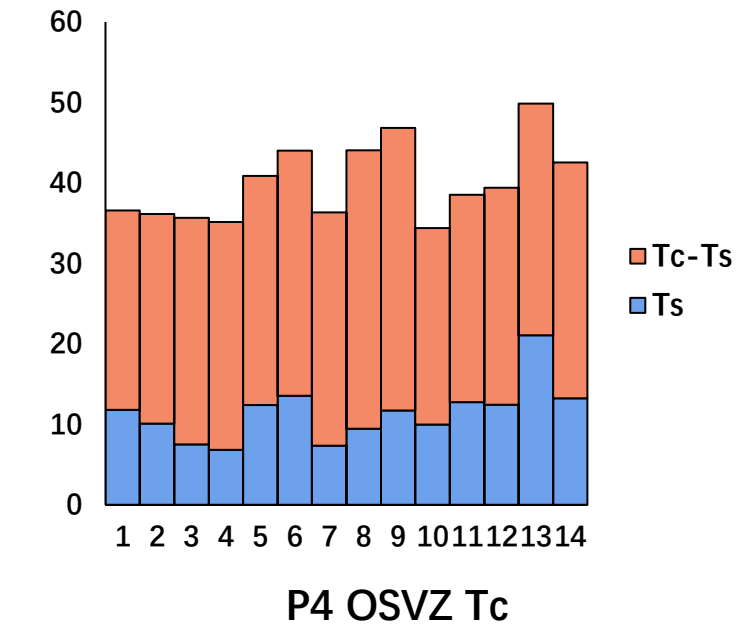
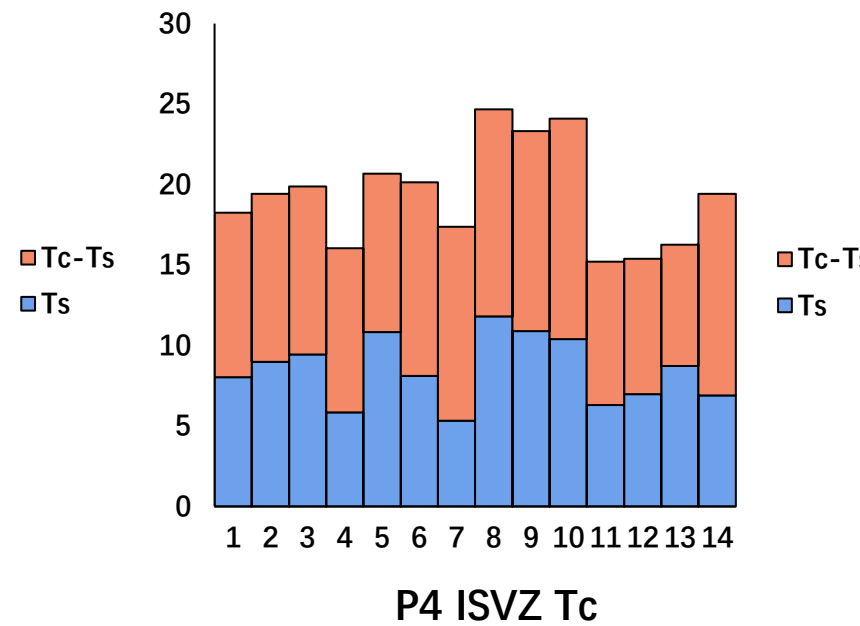
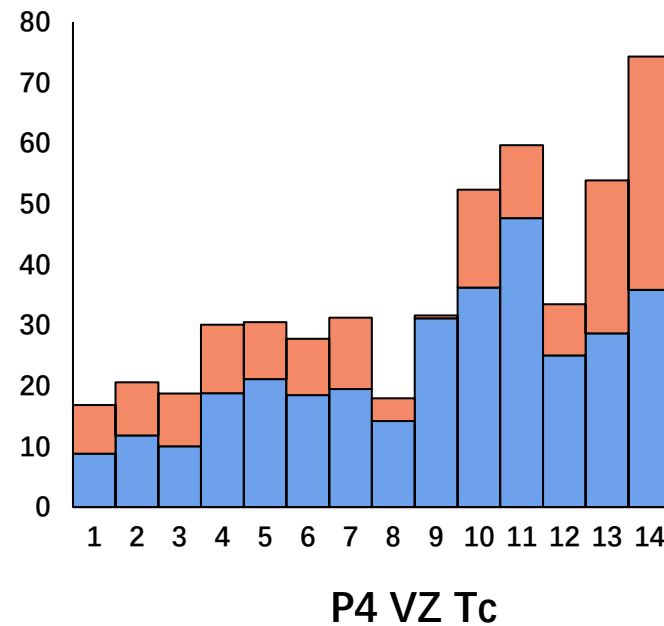


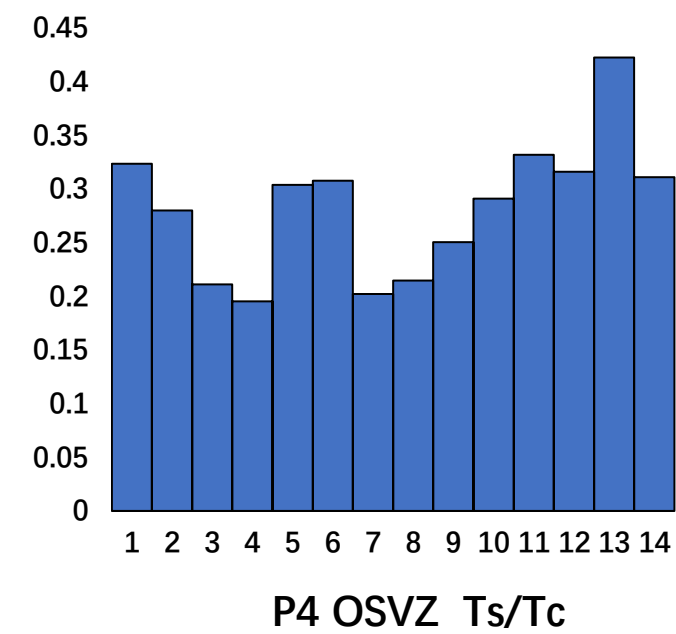
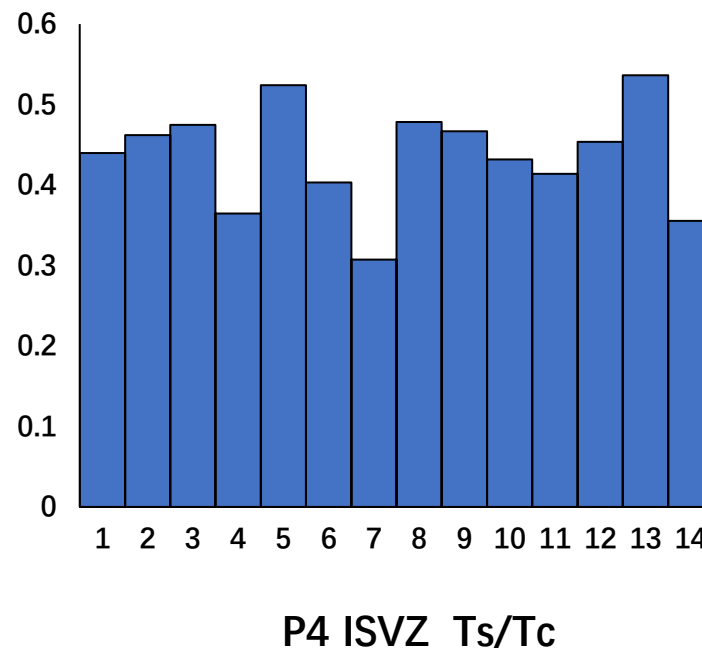
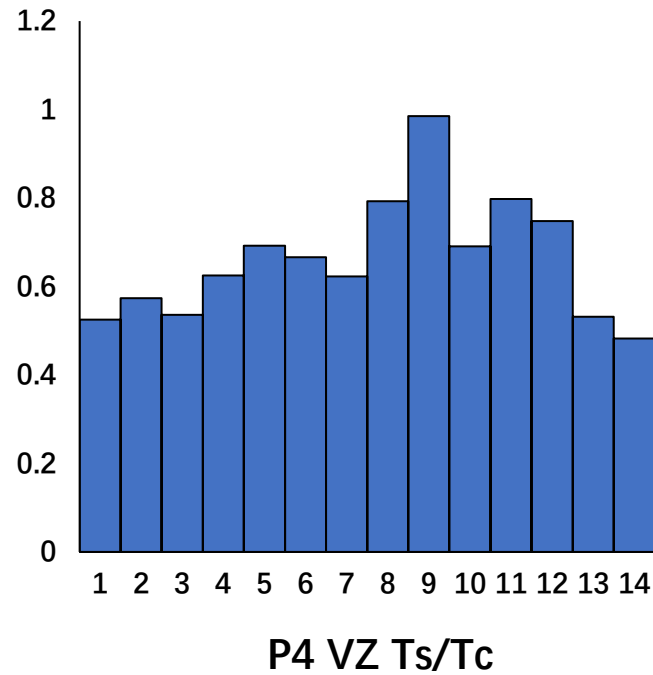
MZ CP IZ area

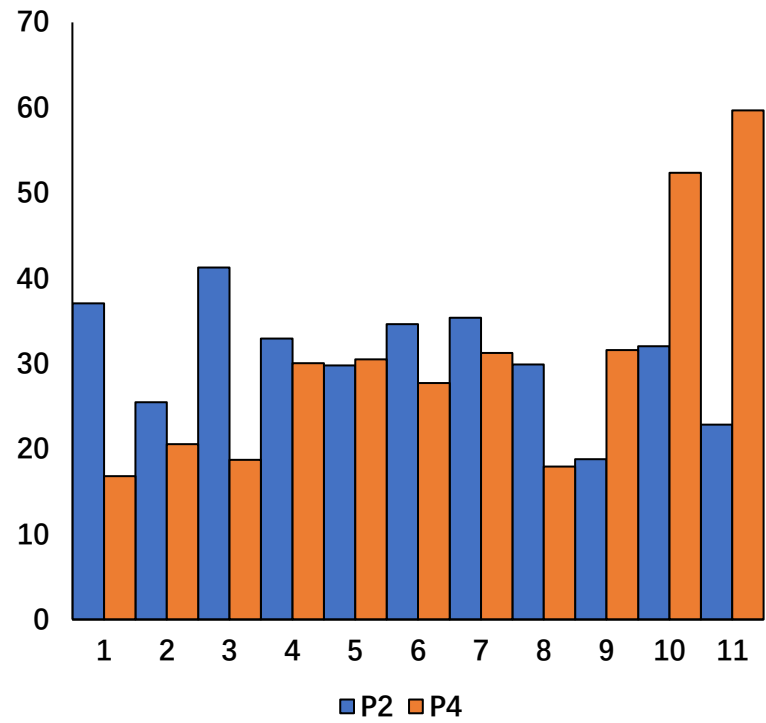


Mz cp iz p4-p2

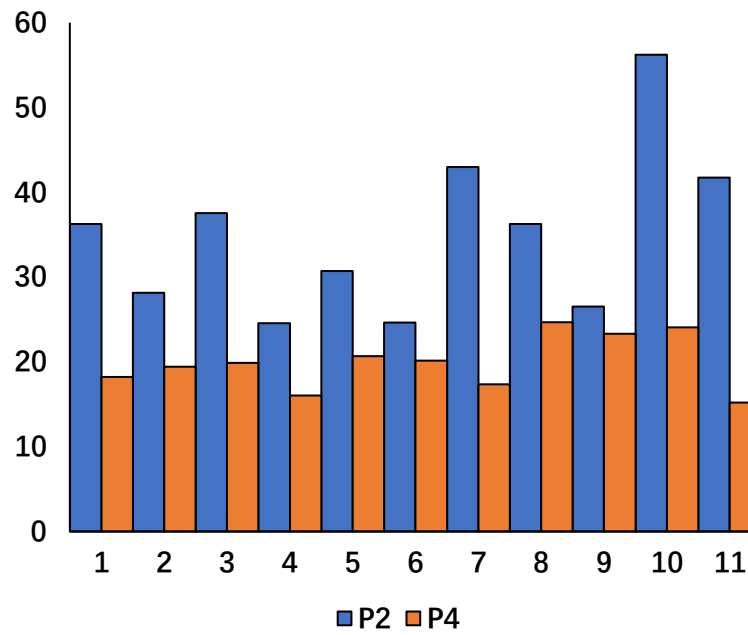




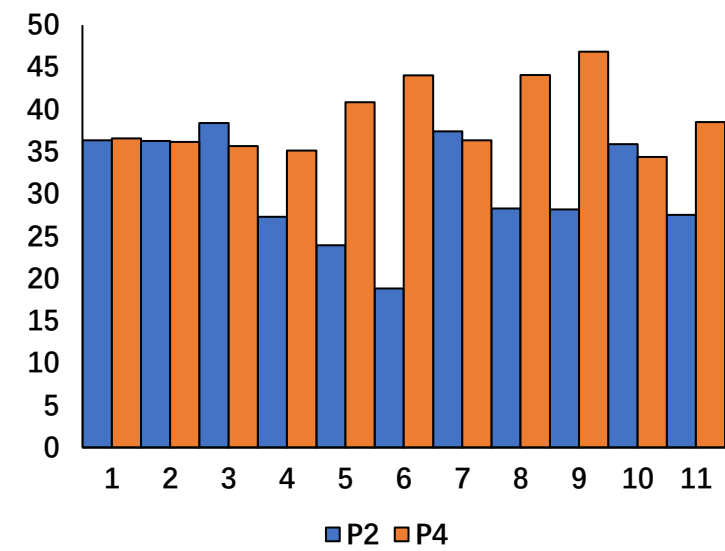




P2&P4 VZ Tc



P2&P4 ISVZ Tc



P2&P4 OSVZ Tc

Summary

- There was no noticeable trend in the total length of the cell cycle at P4.
- During the statistical process, there was a significant fluctuation in the number of BrdU-labeled cells in each bin at P4.
- This could be influenced by cell migration or individual differences.
- After performing repetitions, a clearer trend may emerge.
- Currently, the data collection is fragmented, and there is a need for summarization and consolidation.

Questions and Reflections: Integration of Mechanisms and Anatomy of Sulcus and Gyrus Structures

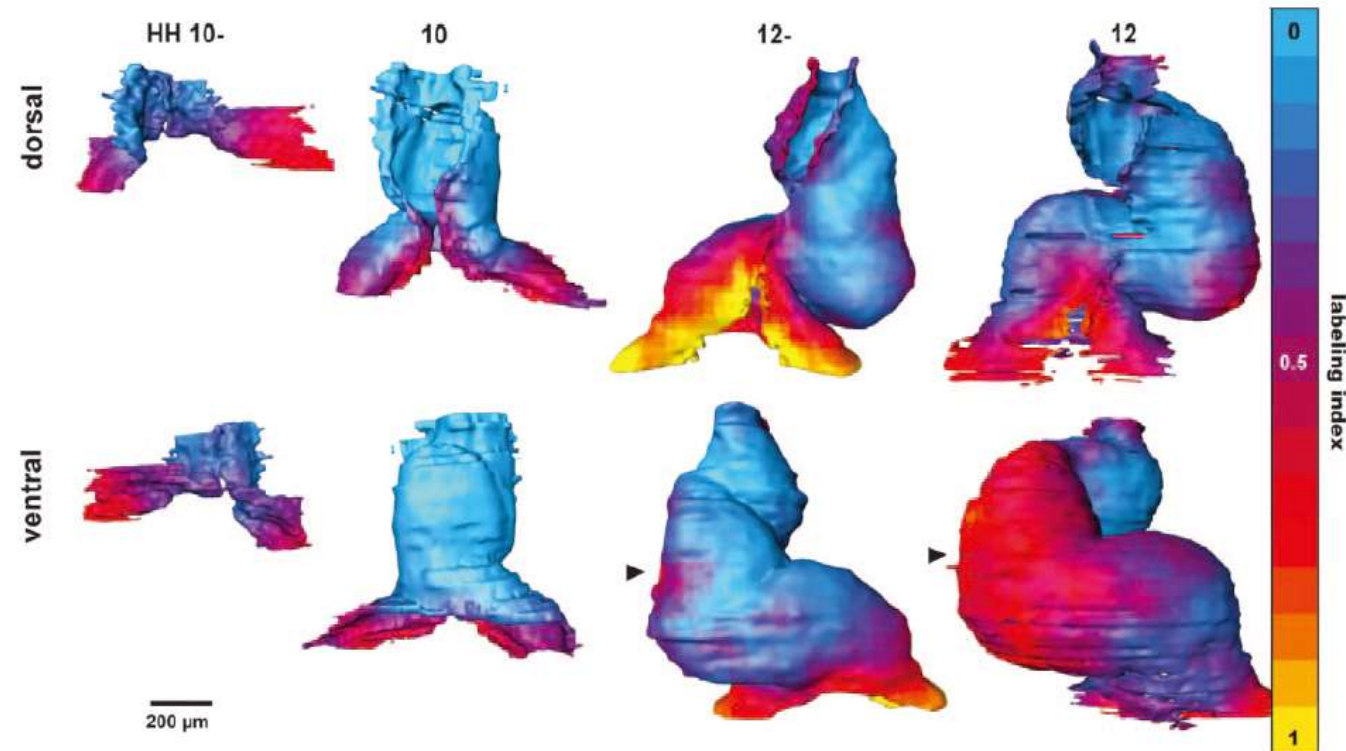
Regionalized Sequence of Myocardial Cell Growth and Proliferation Characterizes Early Chamber Formation

Alexandre T. Soufian,[#] Gert van den Berg,^{*} Jan M. Ruijter, Piet A.J. de Boer,
Maurice J.B. van den Hoff, Antoon F.M. Moorman

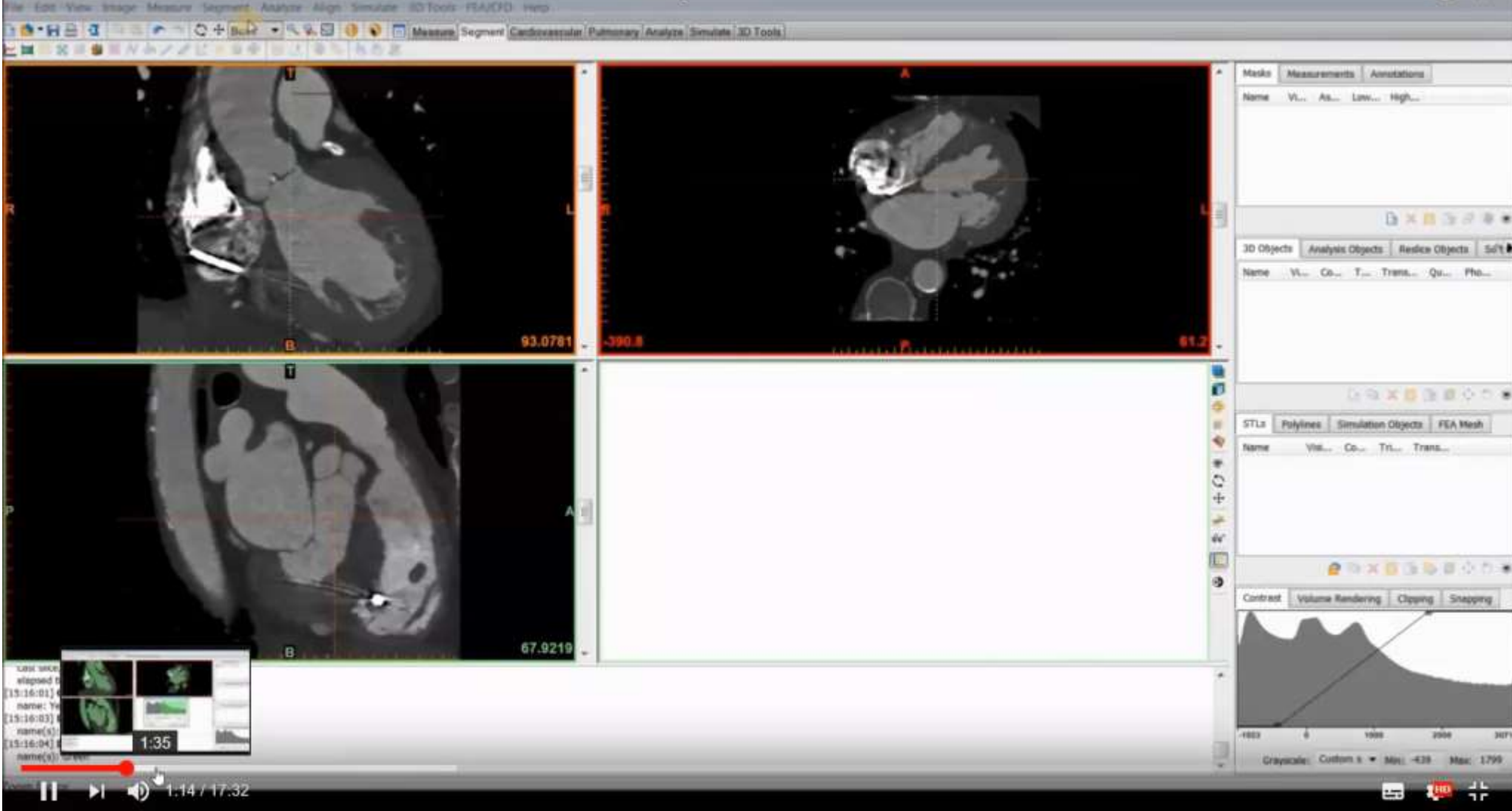
Abstract—Increase in cell size and proliferation of myocytes are key processes in cardiac morphogenesis, yet their regionalization during development of the heart has been described only anecdotally. We have made quantitative reconstructions of embryonic chicken hearts ranging in stage from the fusion of the heart-forming fields to early formation of the chambers. These reconstructions reveal that the early heart tube is recruited from a pool of rapidly proliferating cardiac precursor cells. The proliferation of these small precursor cells ceases as they differentiate into overt cardiomyocytes, producing a slowly proliferating straight heart tube composed of cells increasing in size. The largest cells were found at the ventral side of the heart tube, which corresponds to the site of the forming ventricle, as well as the site where proliferation is reinitiated. The significance of these observations is 2-fold. First, they support a model of early cardiac morphogenesis in 2 stages. Second, they demonstrate that regional increase in size of myocytes contributes significantly to chamber formation. (*Circ Res*. 2006;99:545-552.)

Key Words: 3D visualization ■ quantitative reconstruction ■ embryology ■ heart development

The study of heart development models is currently one of the better research methods for integrating anatomical structures with cell proliferation.



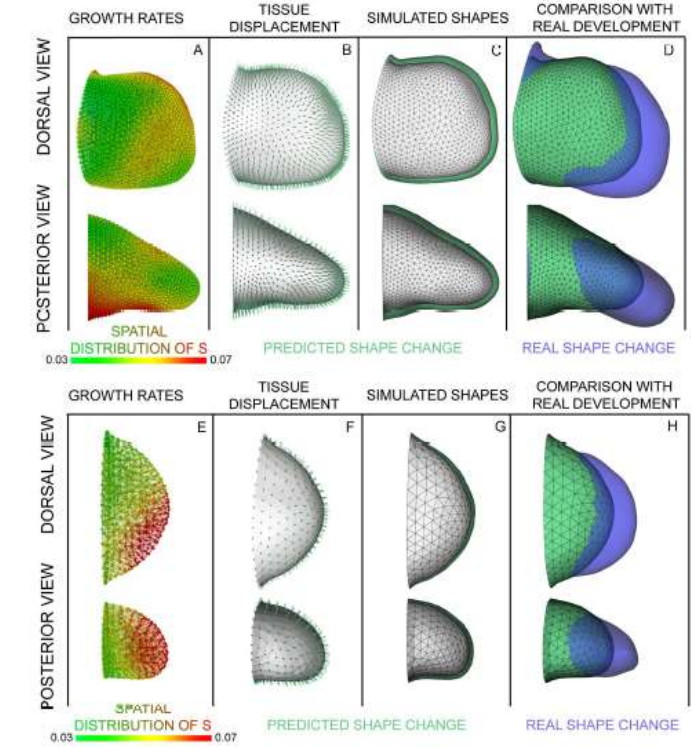
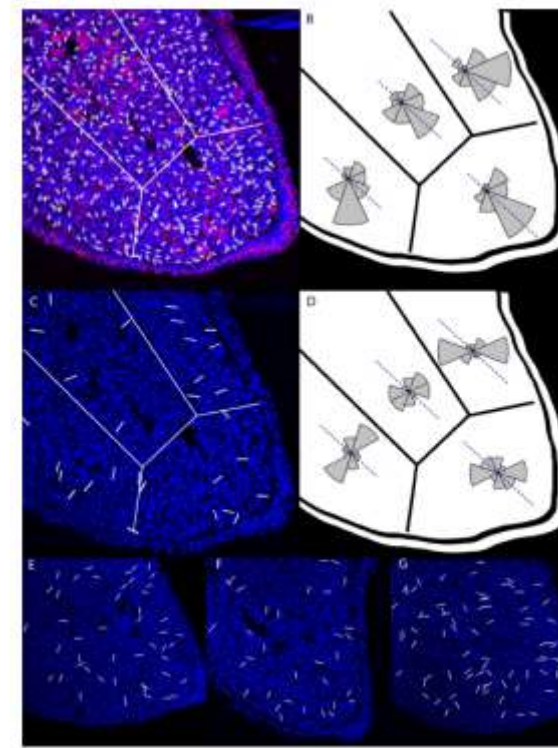
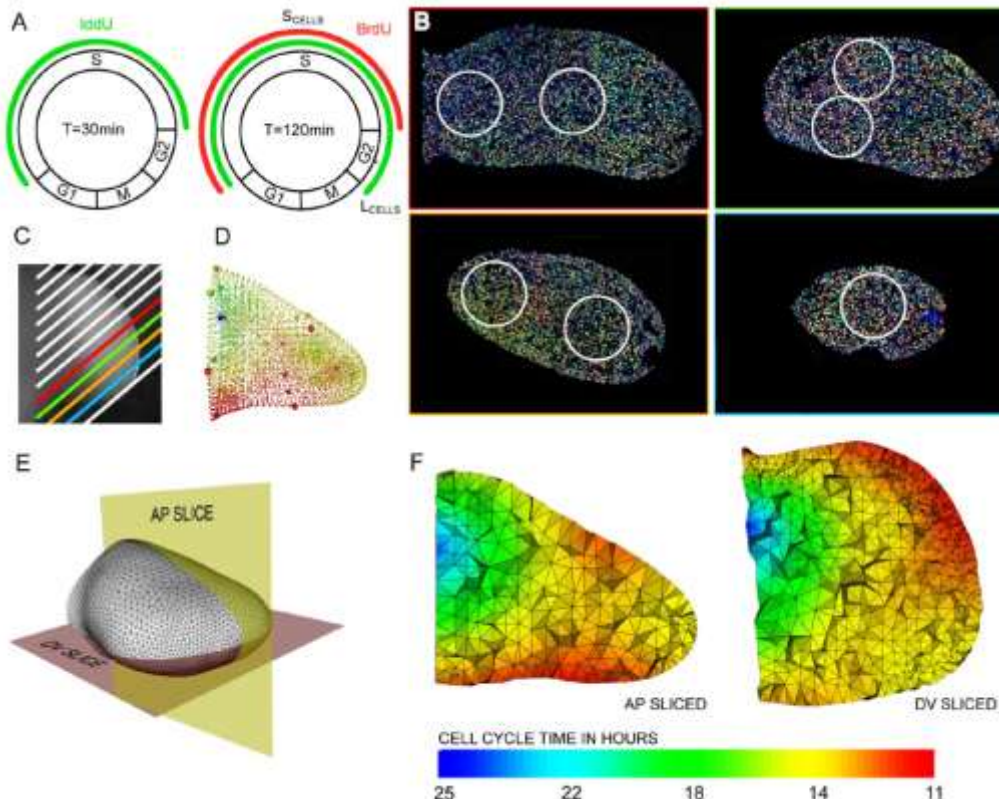
Tutorial: Mimics Innovation Suite - Create a Heart Model for 3D Printing



The Role of Spatially Controlled Cell Proliferation in Limb Bud Morphogenesis

Bernd Boehm¹, Henrik Westerberg¹, Gaja Lesnicar-Pucko¹, Sahdia Raja^{1,2}, Michael Raatschka¹, James Cotterell^{1,2}, Jim Swoger¹, James Sharpe^{1,3*}

1 EMBL-CRG Systems Biology Research Unit, Centre for Genomic Regulation (CRG), UPF, Barcelona, Spain, **2** MRC Human Genetics Unit, Edinburgh, Scotland, United Kingdom, **3** ICREA Professor, Centre for Genomic Regulation (CRG), UPF, Barcelona, Spain

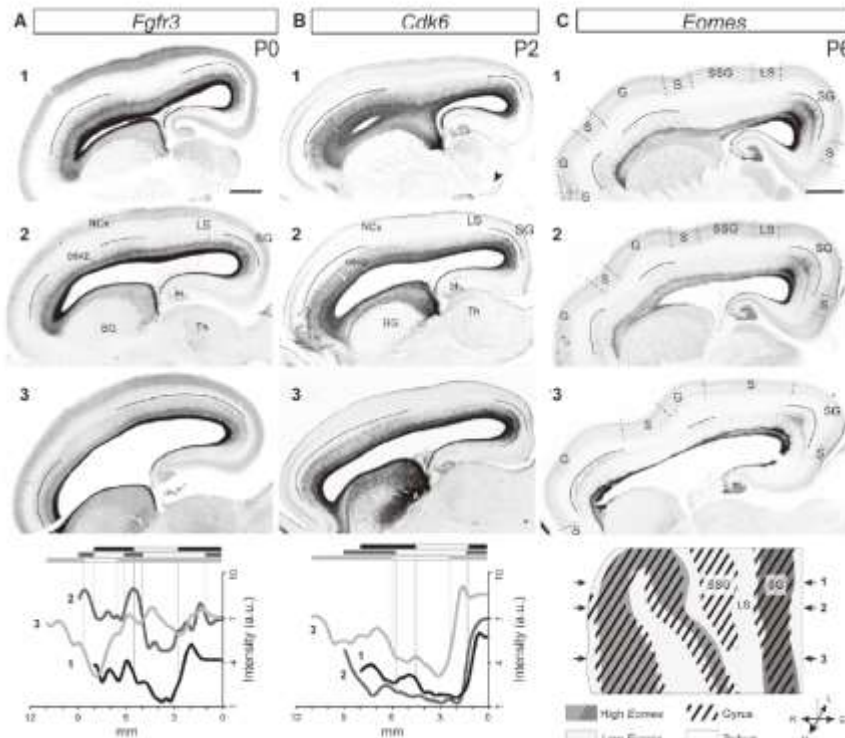


Three-dimensional reconstruction of gene expression patterns during cardiac development¹

Alexandre T. Soufan, Jan M. Ruijter, Maurice J. B. van den Hoff,
Piet A. J. de Boer, Jaco Hagoort, and Antoon F. M. Moorman

Experimental and Molecular Cardiology Group, Academic
Medical Center, 1105 AZ, Amsterdam, The Netherlands

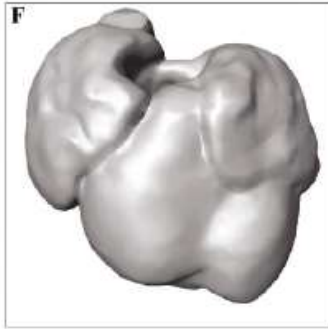
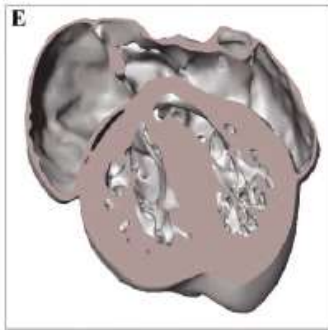
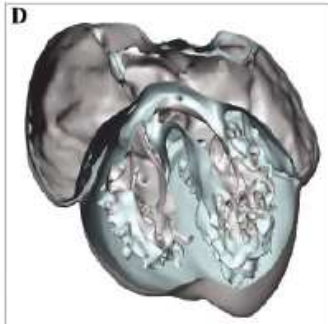
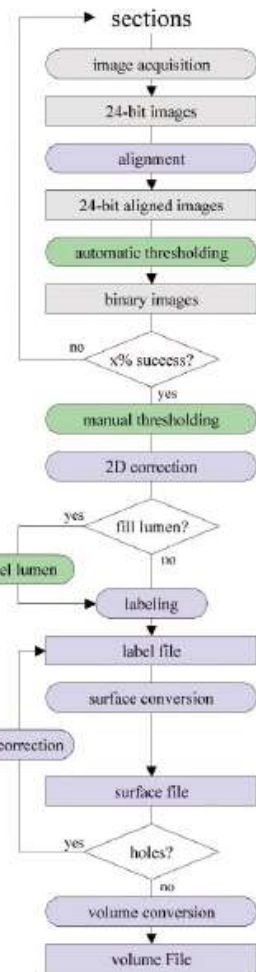
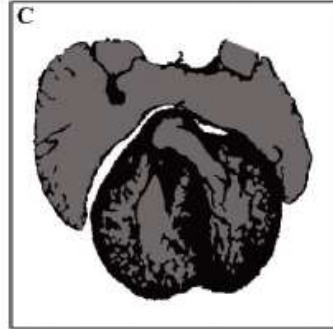
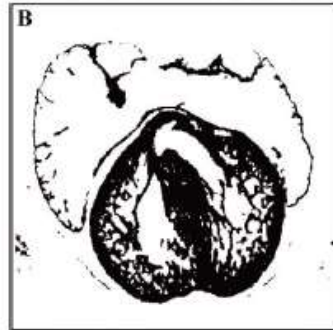
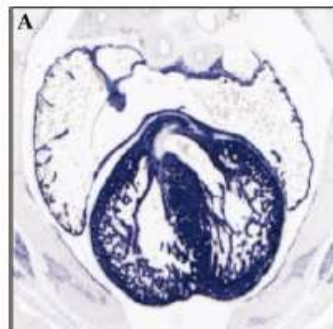
Submitted 19 December 2002; accepted in final form 23 January 2003



Camino de romero et al.(2015) EMBO

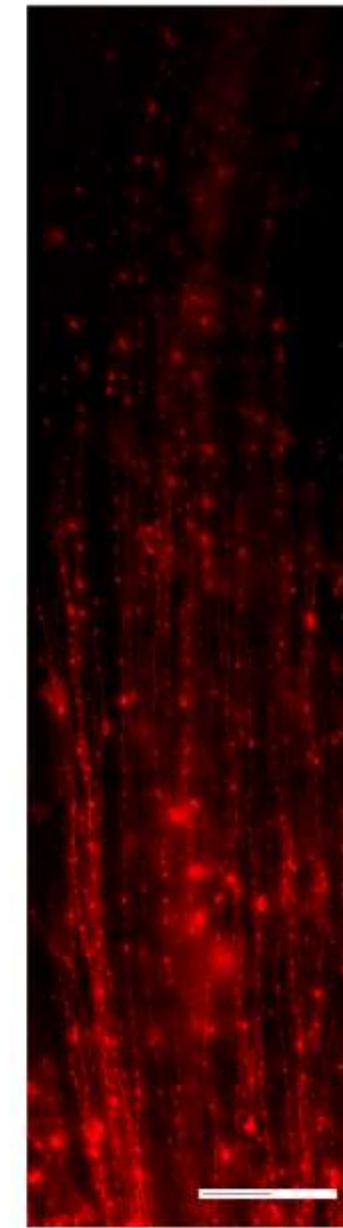
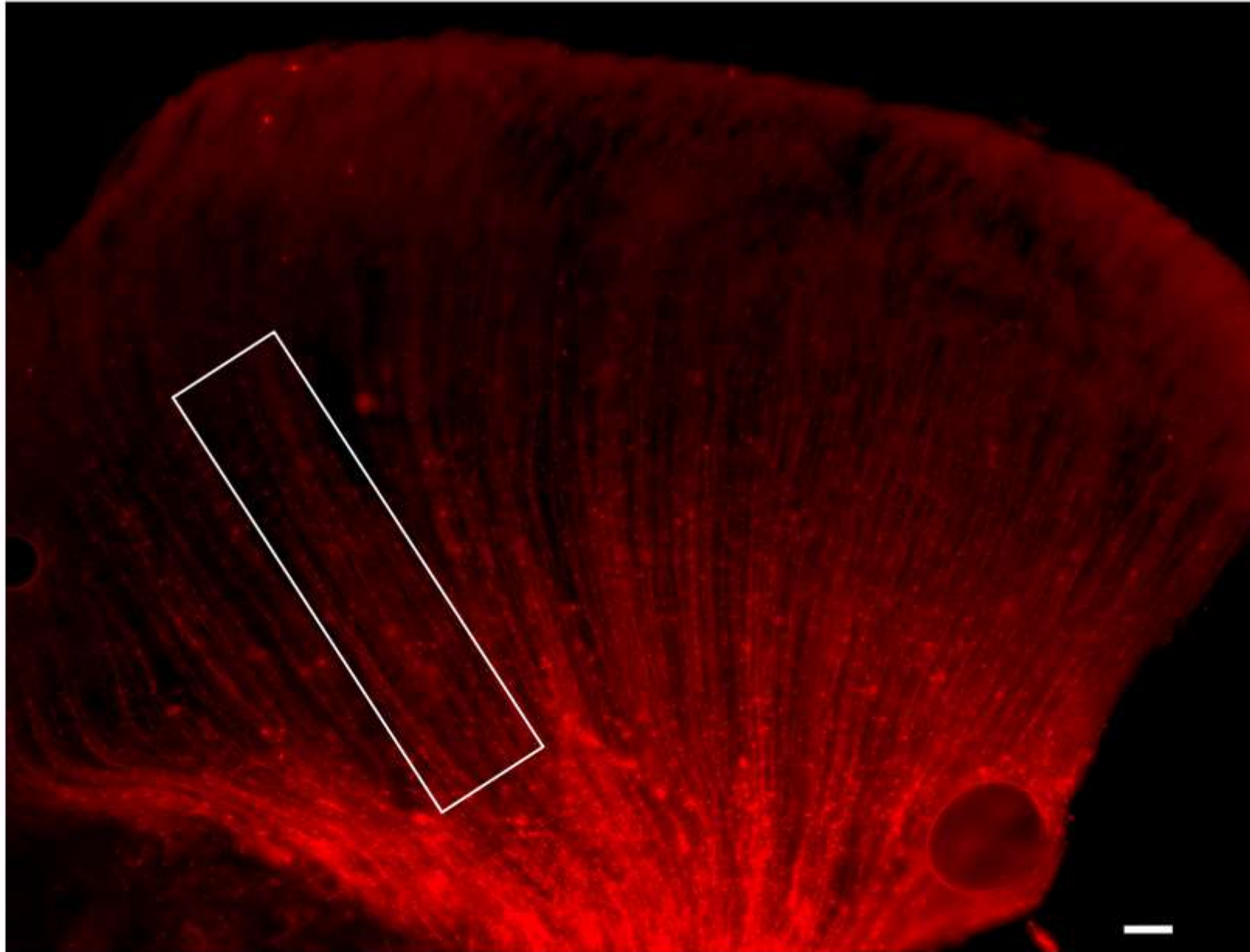
190

REVIEW: 3D RECONSTRUCTION OF CARDIAC GENE EXPRESSION



Next Plan

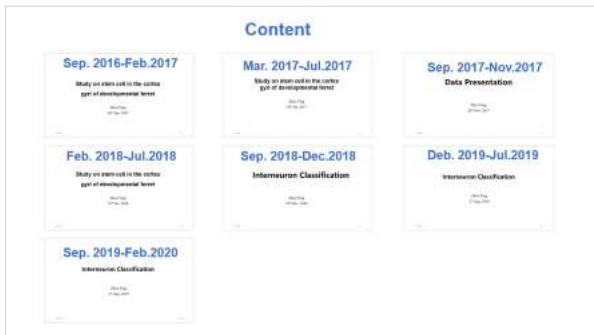
- the statistical analysis of the P6 data.
- Thoroughly analyze and summarize the trends in data from each developmental stage.
- Attempt to integrate information using 3D modeling.
- Address the issues with RNA-Seq sample submission for sequencing, and proceed with sequencing as soon as possible.



P6 ferret Dil 脑室注射 RT 14 days

Dil标记process关键：

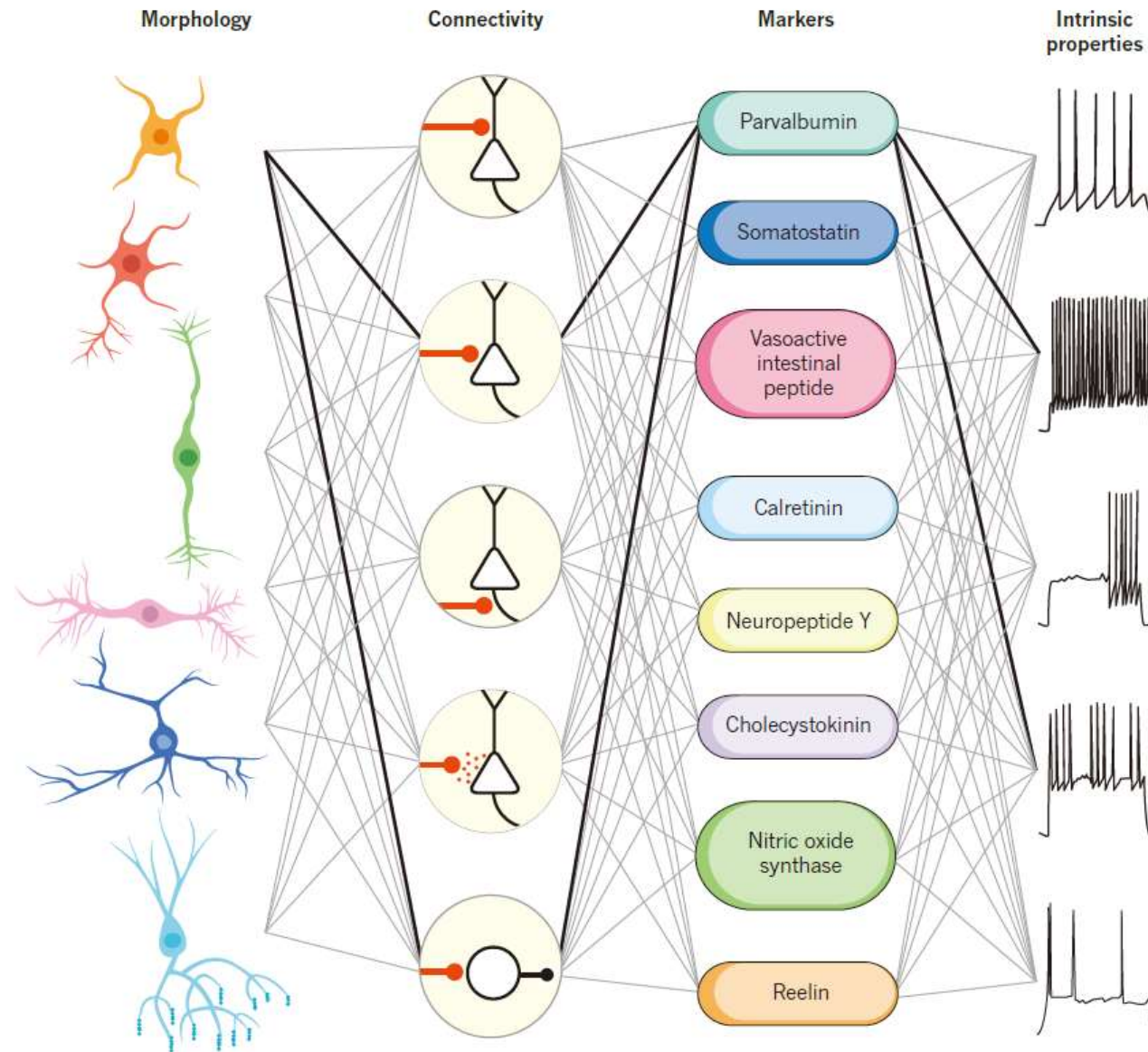
- PFA不能过度固定
- 标记完的组织不能脱水，一脱水就，没有细胞形态了，震荡切，封片避免脑片干掉效果最好
- 脑子没用PFA固定，非常软，切片碎的严重
- 目前在尝试Dil标记后，再用PFA固定，看是否能够保持脑片完整，观察沟回部RG及oRG形态差异



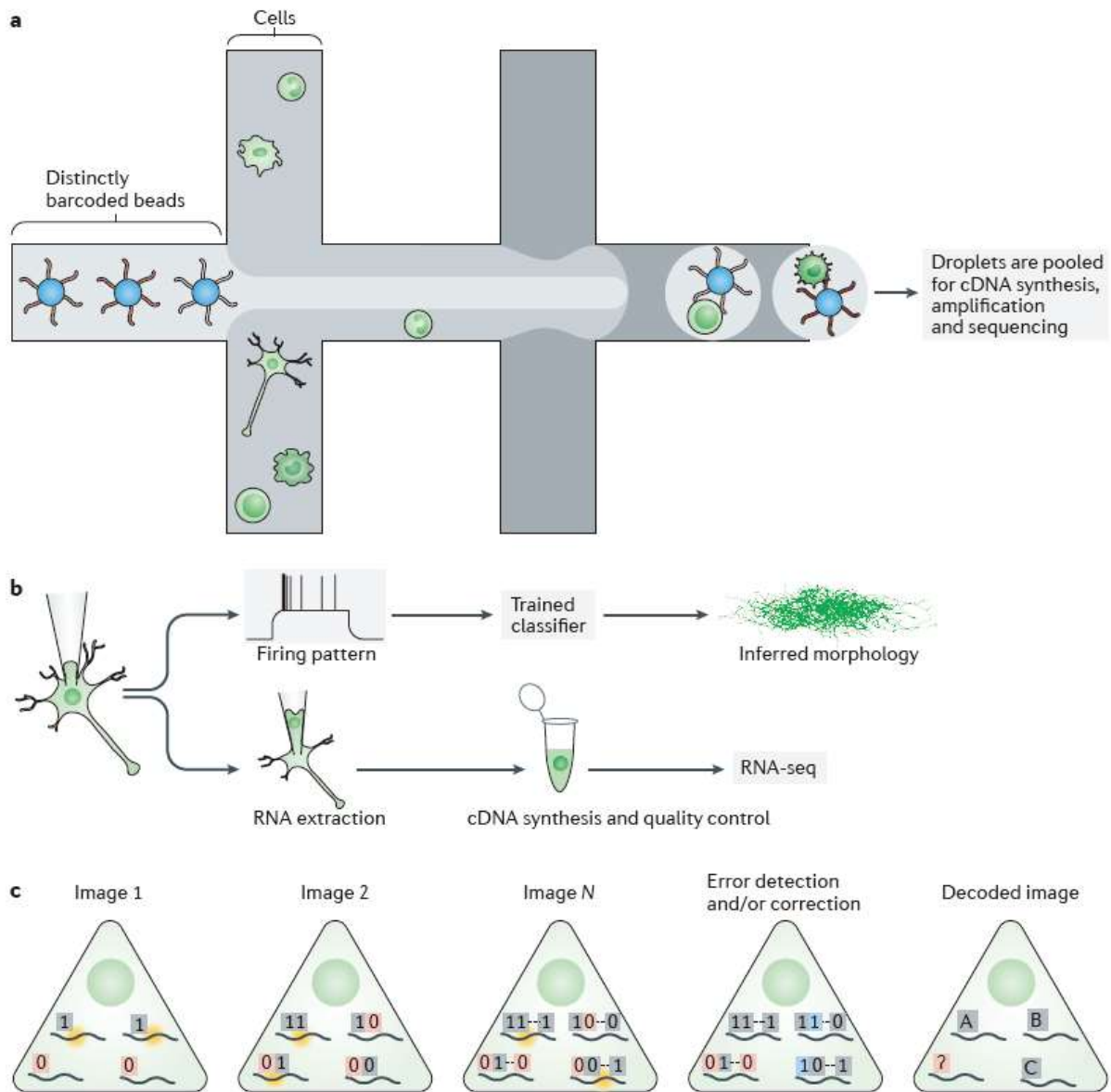
Interneuron Classification

Zhou Ying

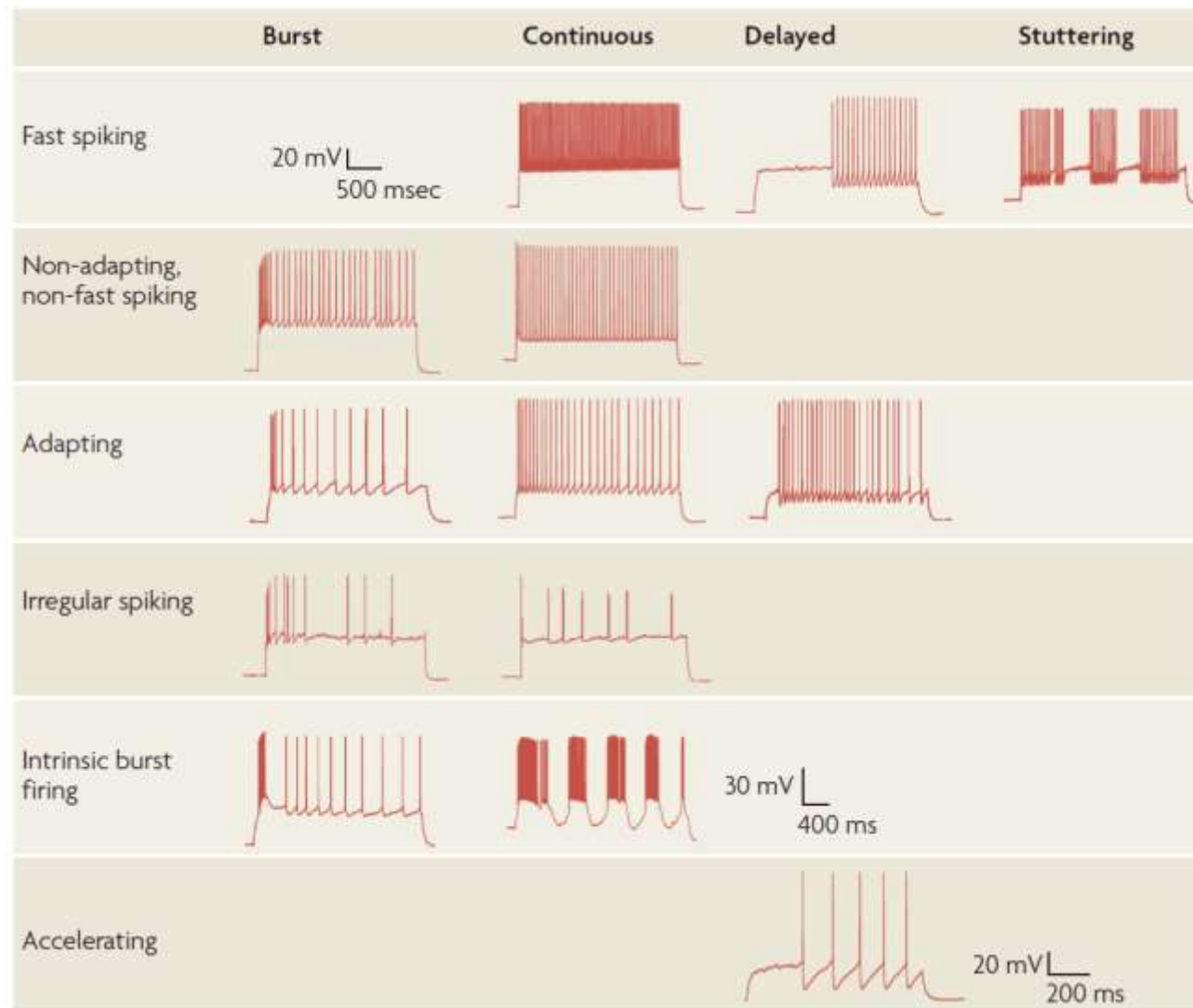
18th Dec. 2018



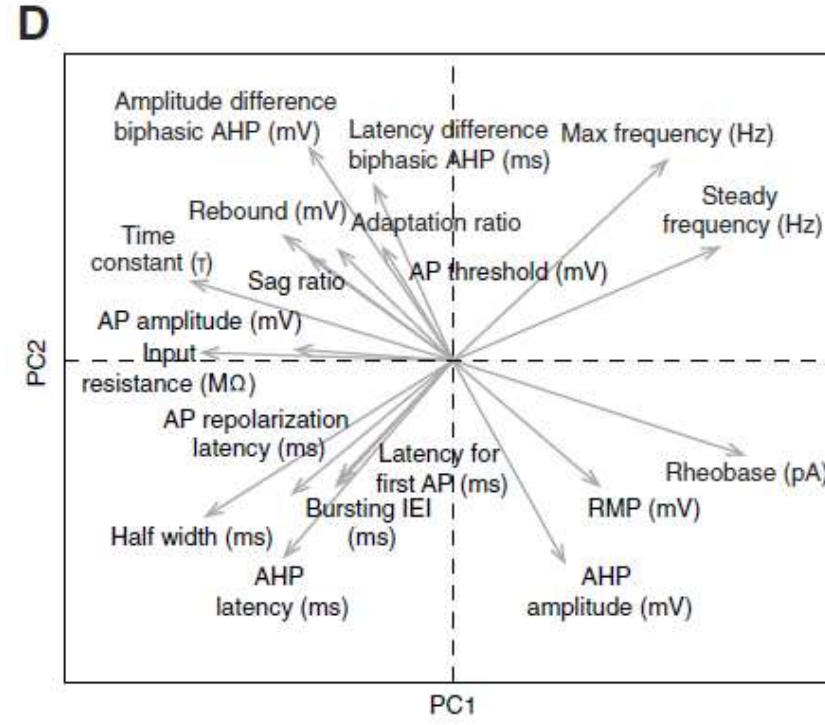
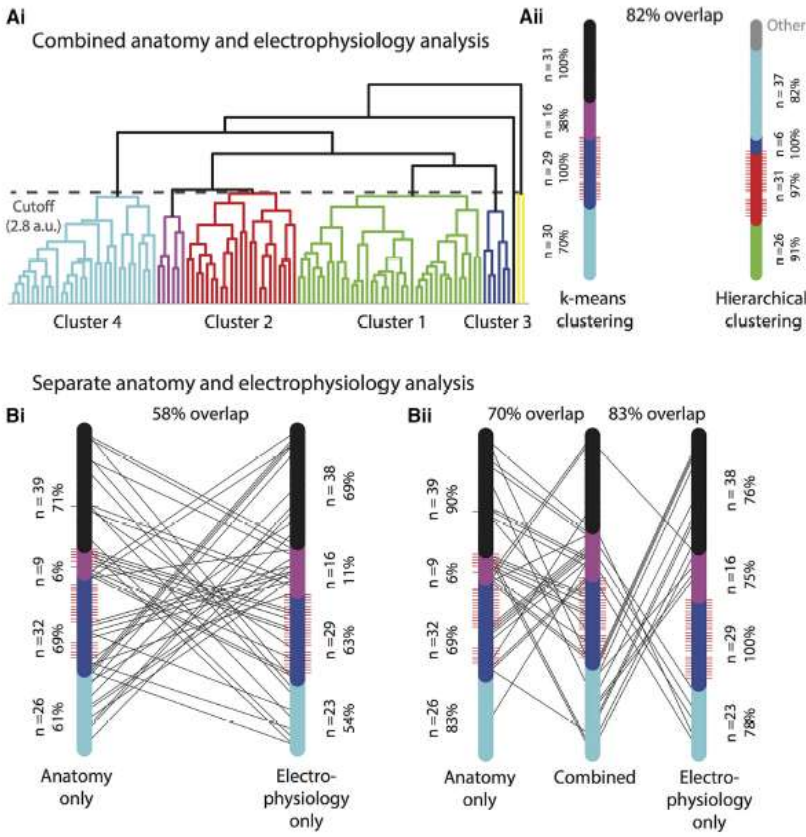
Adam Kepecs¹& Gordon Fishell et al.(2014) Nat.Reviews



- The data dimensionality for interneuron classification is increasing.
- It is necessary to filter out irrelevant information from high-dimensional data to extract valuable insights.



*The Petilla Interneuron Nomenclature Group
(PING)*



Joan José Martínez et al.(2017)eNeuro

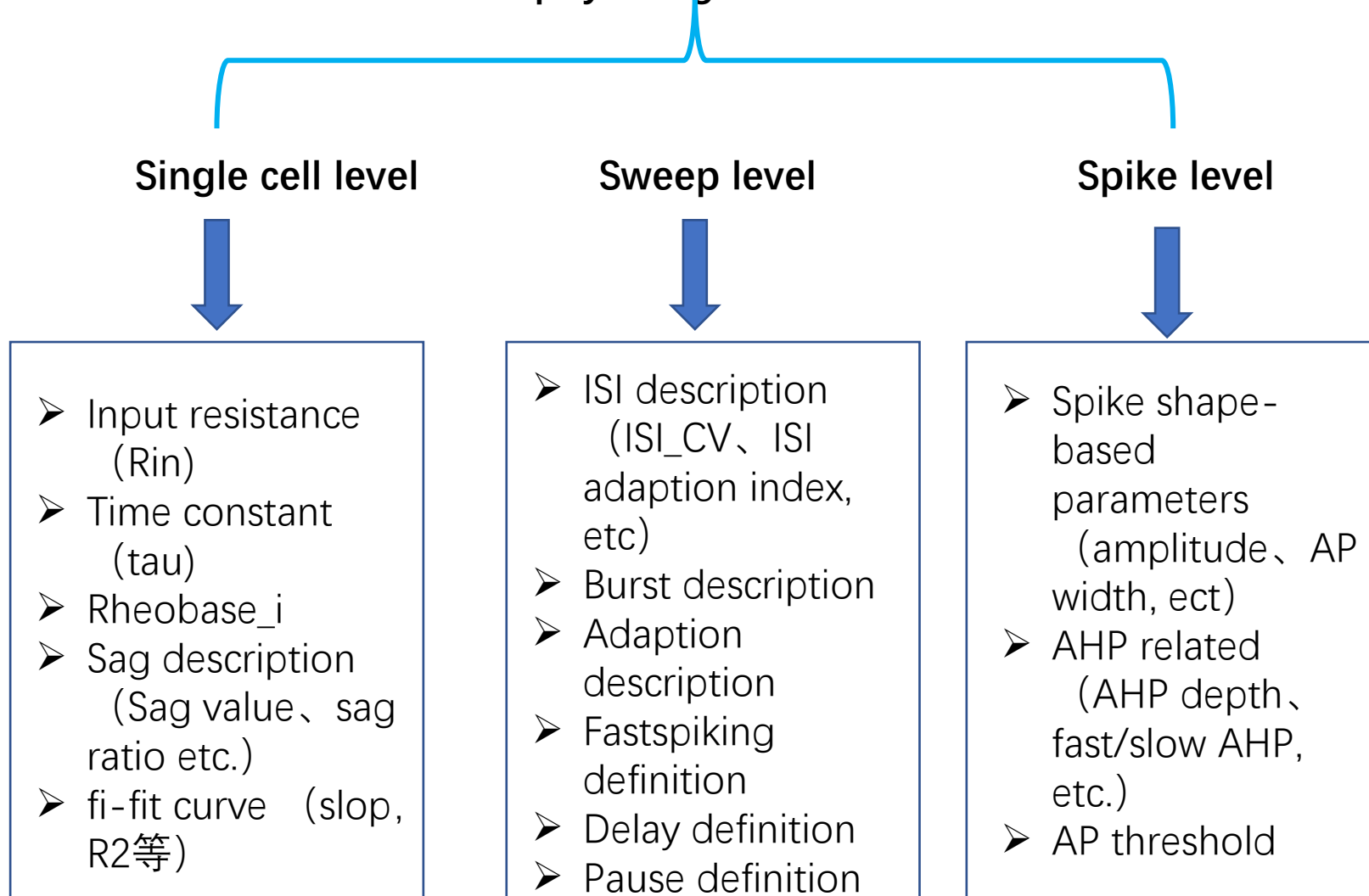
Ana B. Munoz-Manchado et al.(2018)cell report

- For interneuron electrophysiological classification, either assigning a name based on waveform or conducting single-dimensional clustering analysis based on selected parameters is common.
- there is a lack of detailed parameter screening based on dataset characteristics.

Purposes

- 分析比对中间神经元电生理特性，选择适合于中间神经元分类的电生理特性参数(尤其在于ISI之间关系上的描述)
- 使用迭代PCA根据所选择参数对数据集进行聚类
- 使用随机森林对于聚类结果验证并构建自动分类训练模型

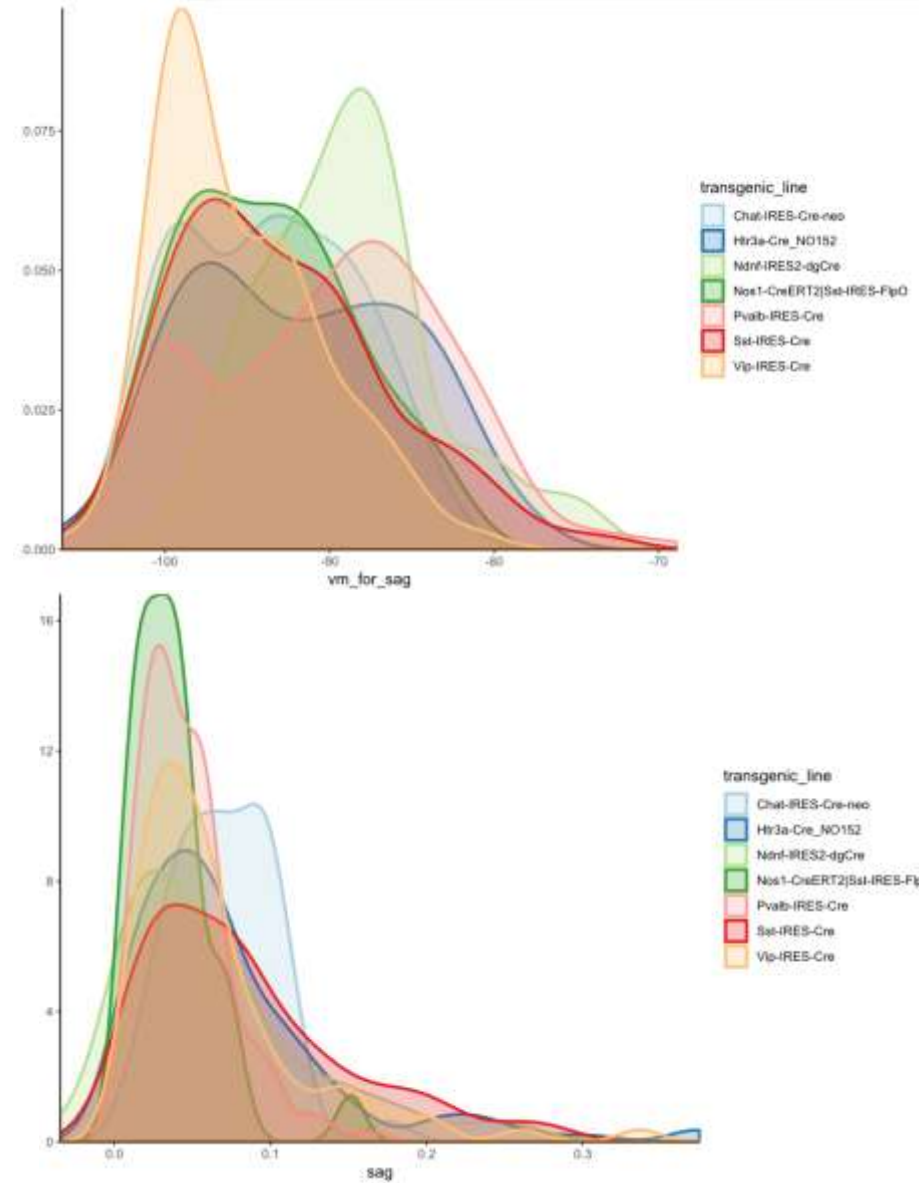
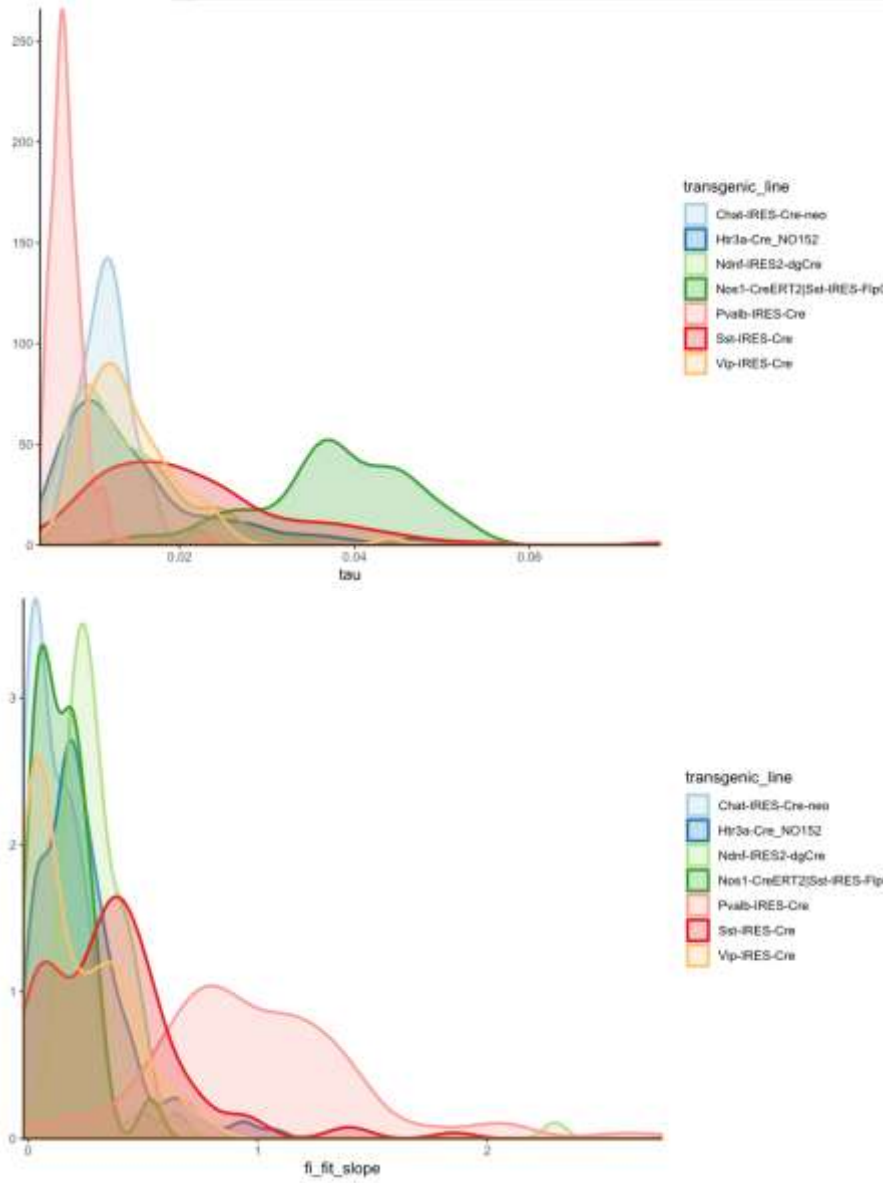
Whole-cell patch-clamp electrophysiological data



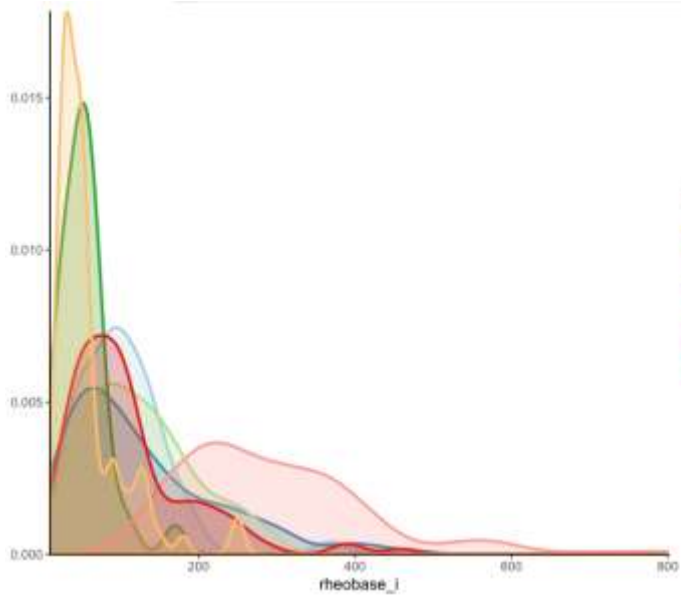
Parameters filtration

- Calculate parameters at different levels.
- Analyze the distribution of each parameter.
- Perform PCA for dimensionality reduction and use biplot to analyze the correlation between parameters.
- Select parameters with significant classification contributions and remove highly correlated duplicates.

Cell level parameters

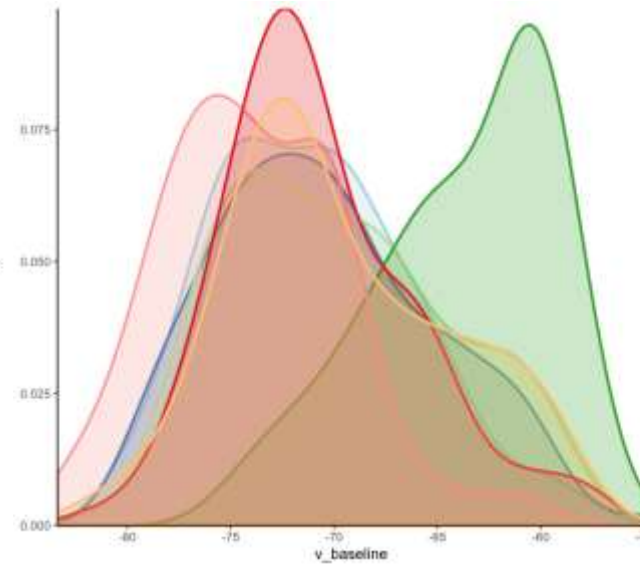


Cell level parameters



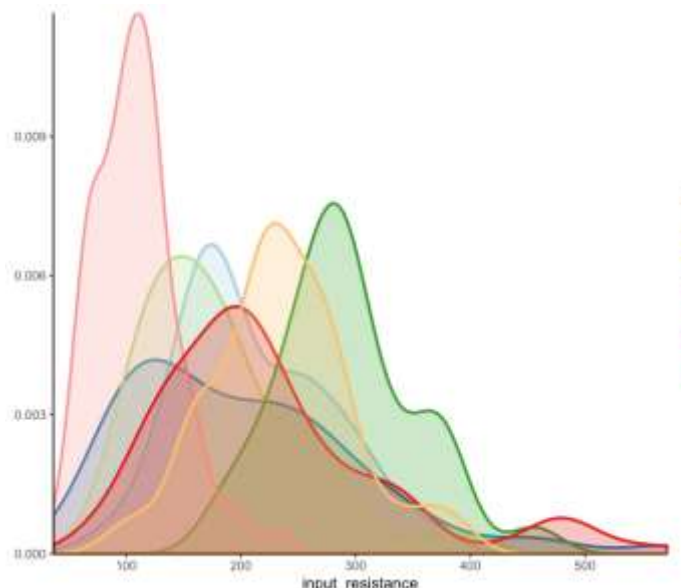
transgenic_line

- Chat-IRES-Cre-neo
- Htr3a-Cre_NO152
- Ndnf-IRES2-dgCre
- Nos1-CreERT2|Sst-IRES-FlpO
- Pvalb-IRES-Cre
- Sst-IRES-Cre
- Vip-IRES-Cre



transgenic_line

- Chat-IRES-Cre-neo
- Htr3a-Cre_NO152
- Ndnf-IRES2-dgCre
- Nos1-CreERT2|Sst-IRES-FlpO
- Pvalb-IRES-Cre
- Sst-IRES-Cre
- Vip-IRES-Cre



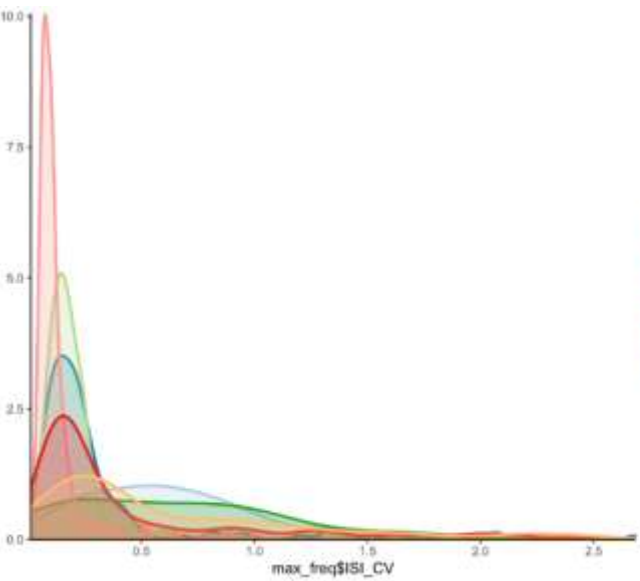
transgenic_line

- Chat-IRES-Cre-neo
- Htr3a-Cre_NO152
- Ndnf-IRES2-dgCre
- Nos1-CreERT2|Sst-IRES-FlpO
- Pvalb-IRES-Cre
- Sst-IRES-Cre
- Vip-IRES-Cre

Summary

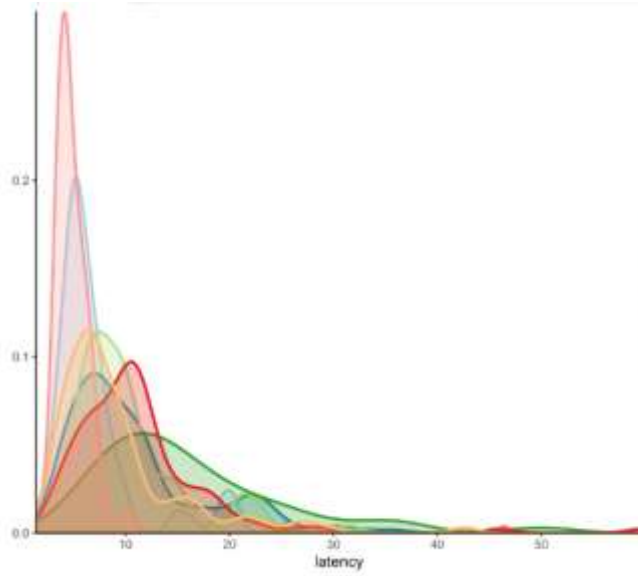
- At the cellular level, parameters pv exhibit significant differences in distribution compared to other types.
- Parameters such as tau, fi_fit_slope, Rin, and Rheobase_i show substantial differences in distribution across various types.
- On the other hand, parameters like Vm_for_sag and sag show relatively dispersed distributions, with minimal differences observed among various types.

Sweep level parameters



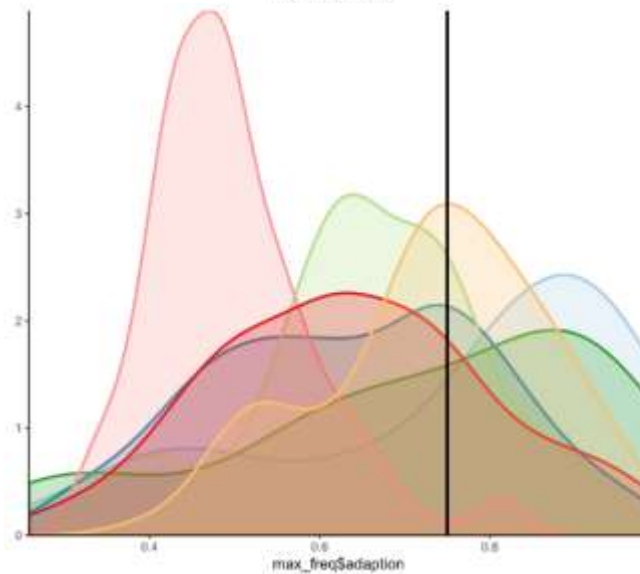
transgenic_line

- Chat-IRES-Cre-neo
- Htr3a-Cre_NO152
- Ndnf-IRES2-dgCre
- Nos1-CreERT2|Sel-IRES
- Pvalb-IRES-Cre
- Sel-IRES-Cre
- Vip-IRES-Cre



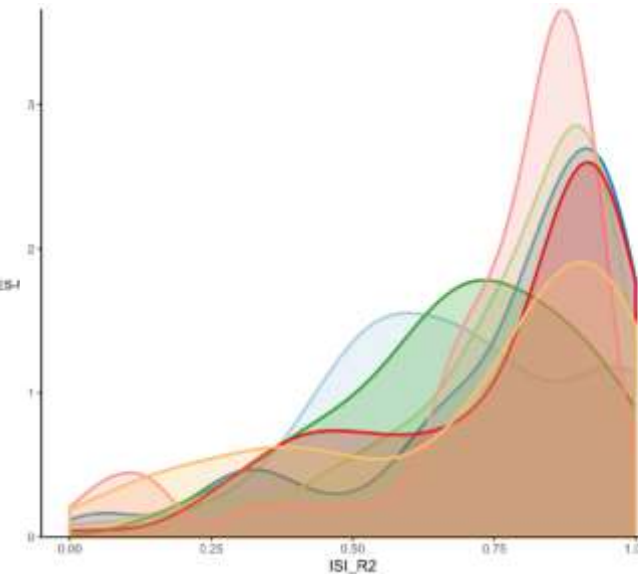
transgenic_line

- Chat-IRES-Cre-neo
- Htr3a-Cre_NO152
- Ndnf-IRES2-dgCre
- Nos1-CreERT2|Sel-IRES-FlpO
- Pvalb-IRES-Cre
- Sel-IRES-Cre
- Vip-IRES-Cre



transgenic_line

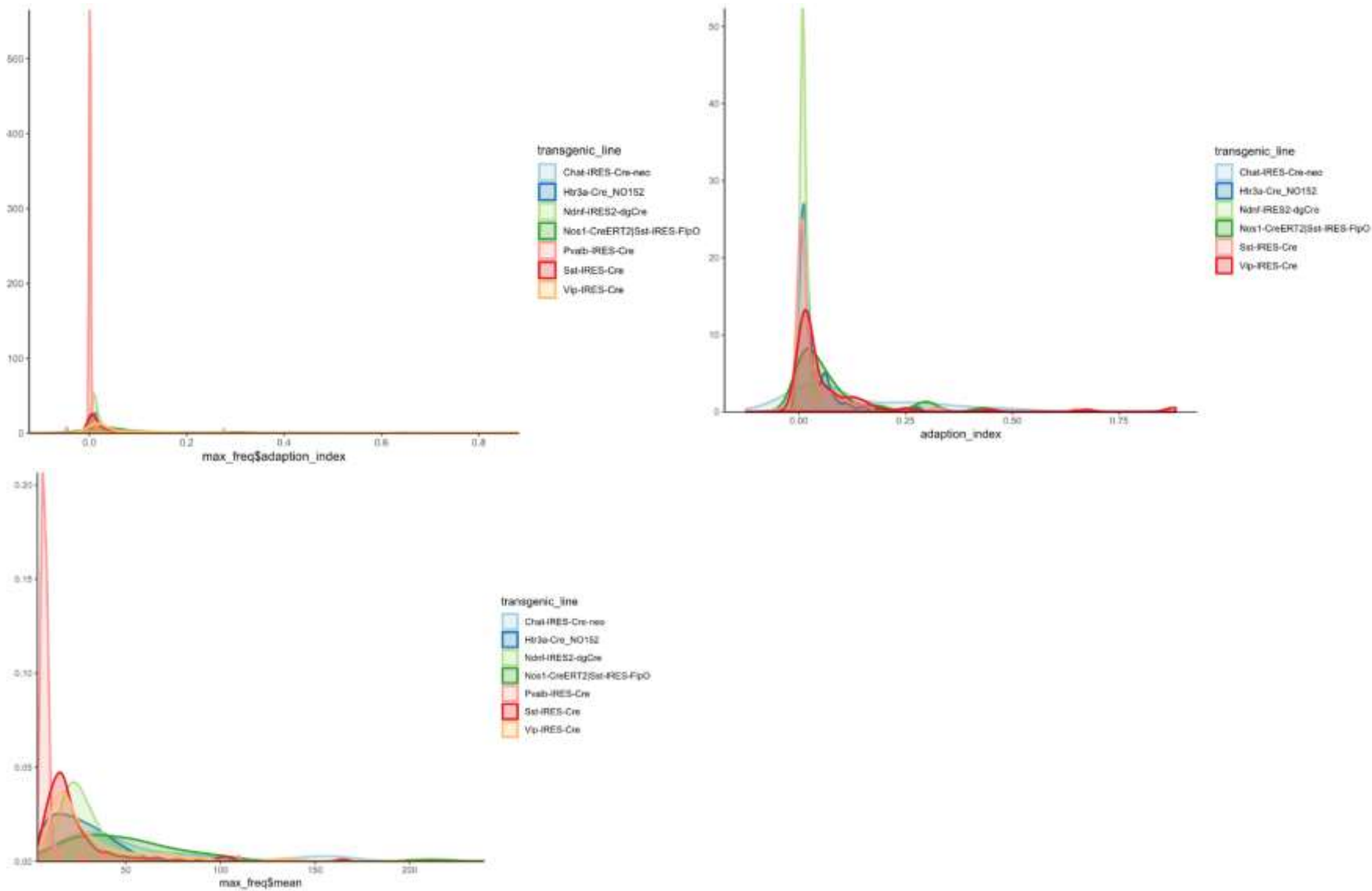
- Chat-IRES-Cre-neo
- Htr3a-Cre_NO152
- Ndnf-IRES2-dgCre
- Nos1-CreERT2|Sel-IRES
- Pvalb-IRES-Cre
- Sel-IRES-Cre
- Vip-IRES-Cre



transgenic_line

- Chat-IRES-Cre-neo
- Htr3a-Cre_NO152
- Ndnf-IRES2-dgCre
- Nos1-CreERT2|Sel-IRES-FlpO
- Pvalb-IRES-Cre
- Sel-IRES-Cre
- Vip-IRES-Cre

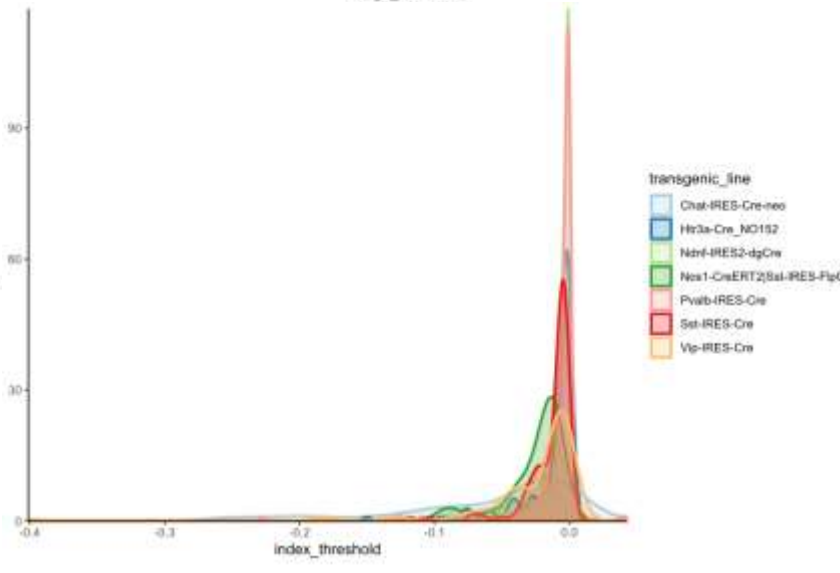
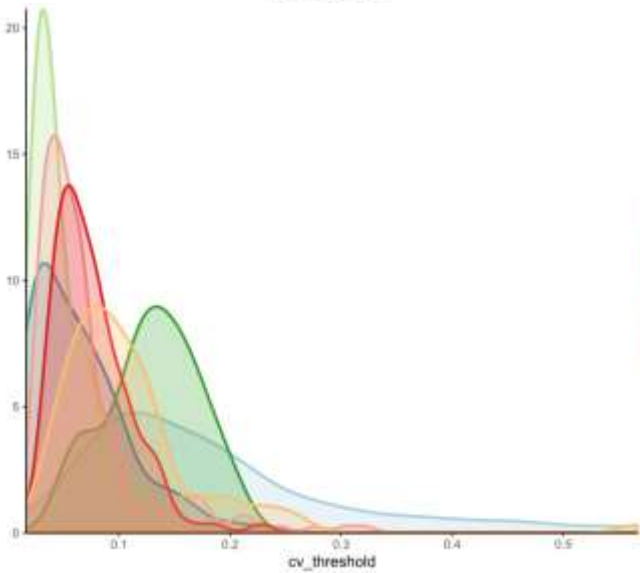
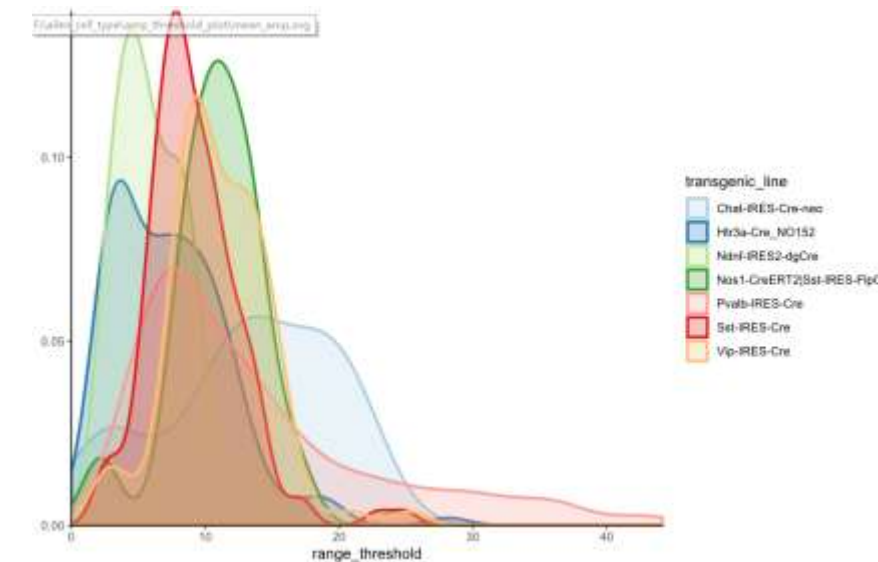
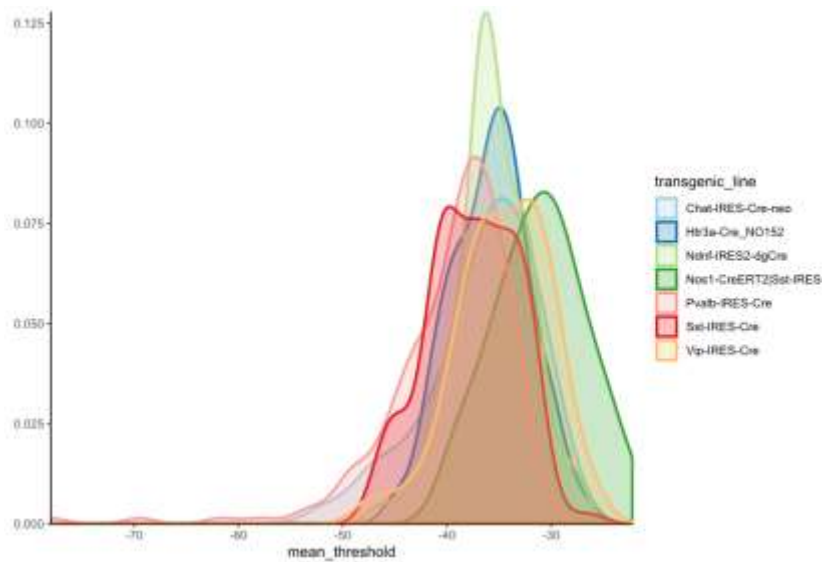
Sweep level parameters



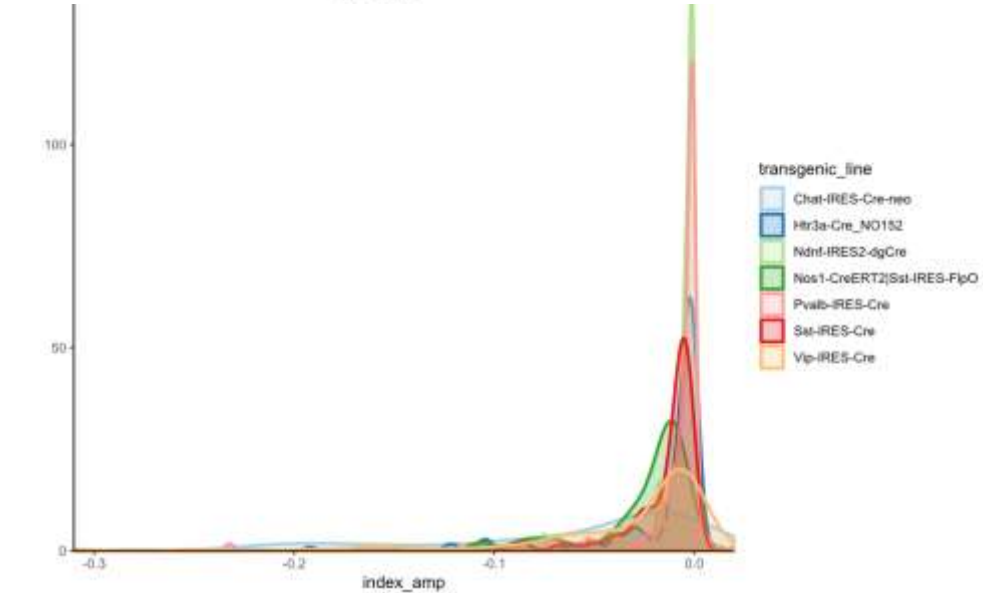
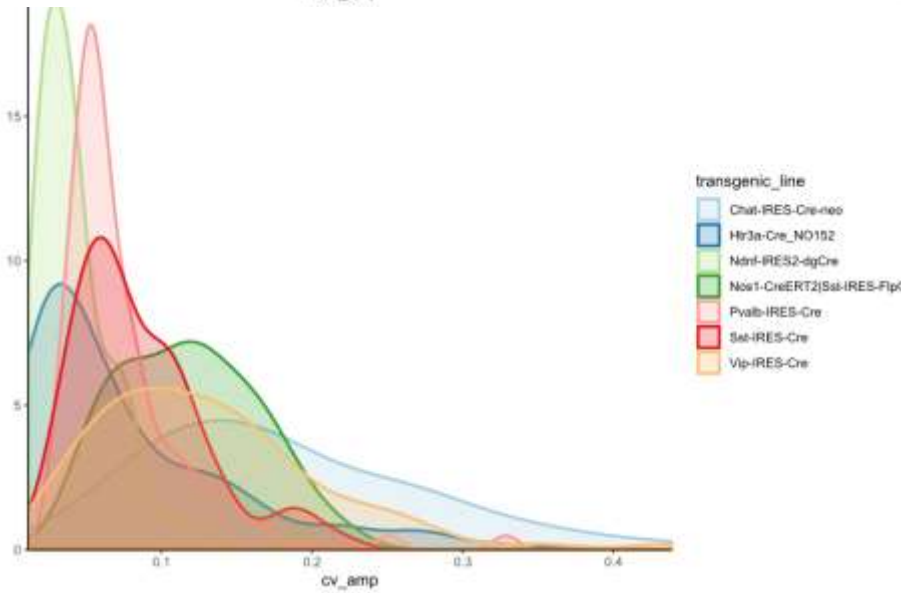
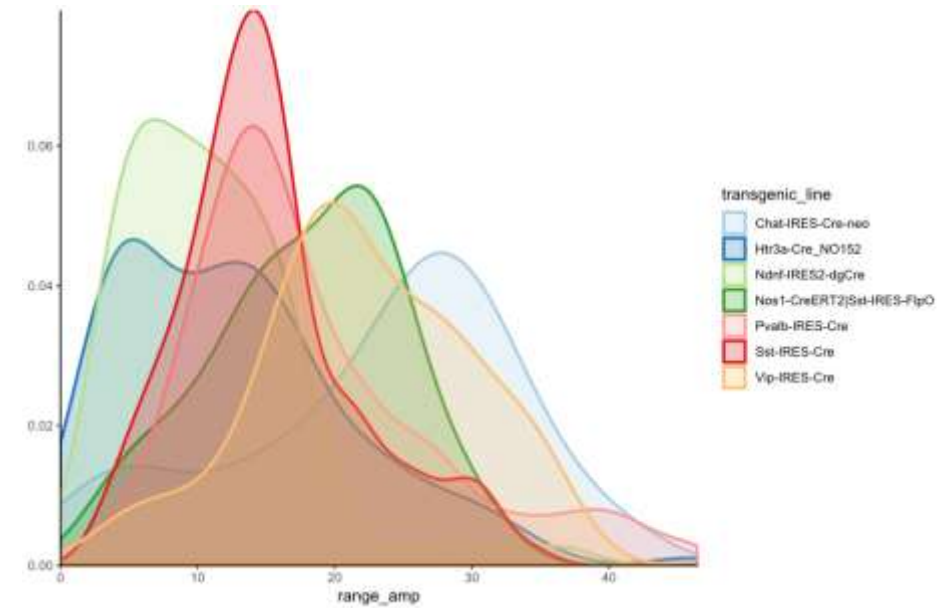
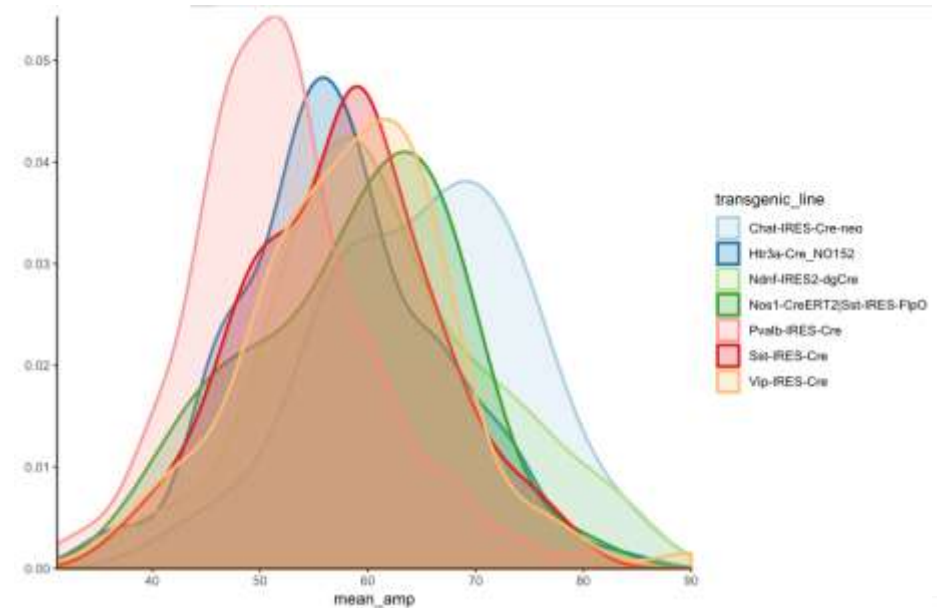
Summary

- At the sweep level, parameters pv are more concentrated compared to other types.
- ISI_cv exhibits highly scattered distributions, particularly in chat, vip, and sst|nos1, with almost no peaks. Currently, we are examining the ISI_cv information before reaching the maximum discharge frequency, which needs to be incorporated.
- The differences in Latency are smaller than expected, possibly due to the lack of correlation with the cell's own ISI. We can attempt to use the ratio between latency and mean_ISI as a descriptive parameter.

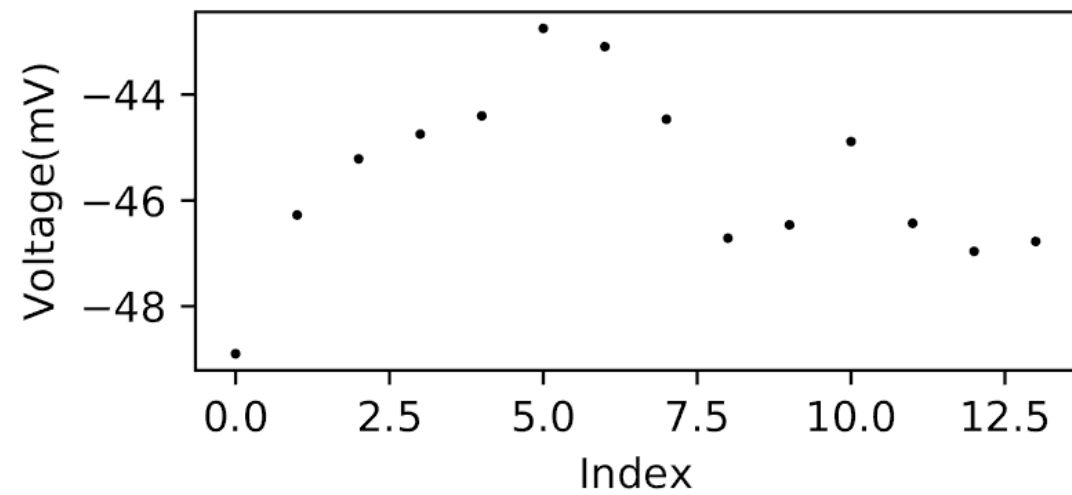
AP level parameters-threshold and amplitude



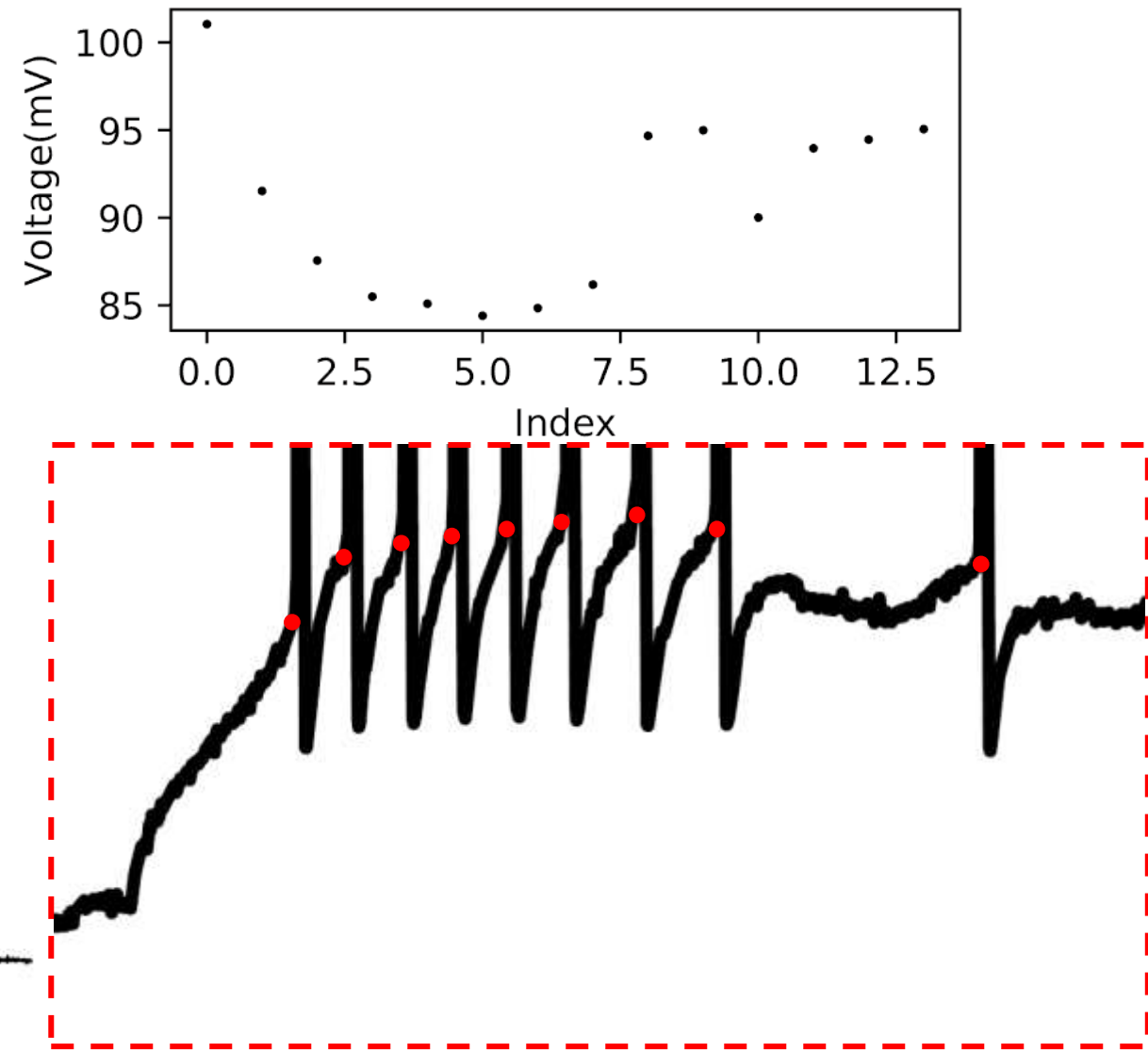
AP level parameters-threshold and amplitude



20180907N2AP7_threshold 2



20180907N2AP7_AP_amp 2

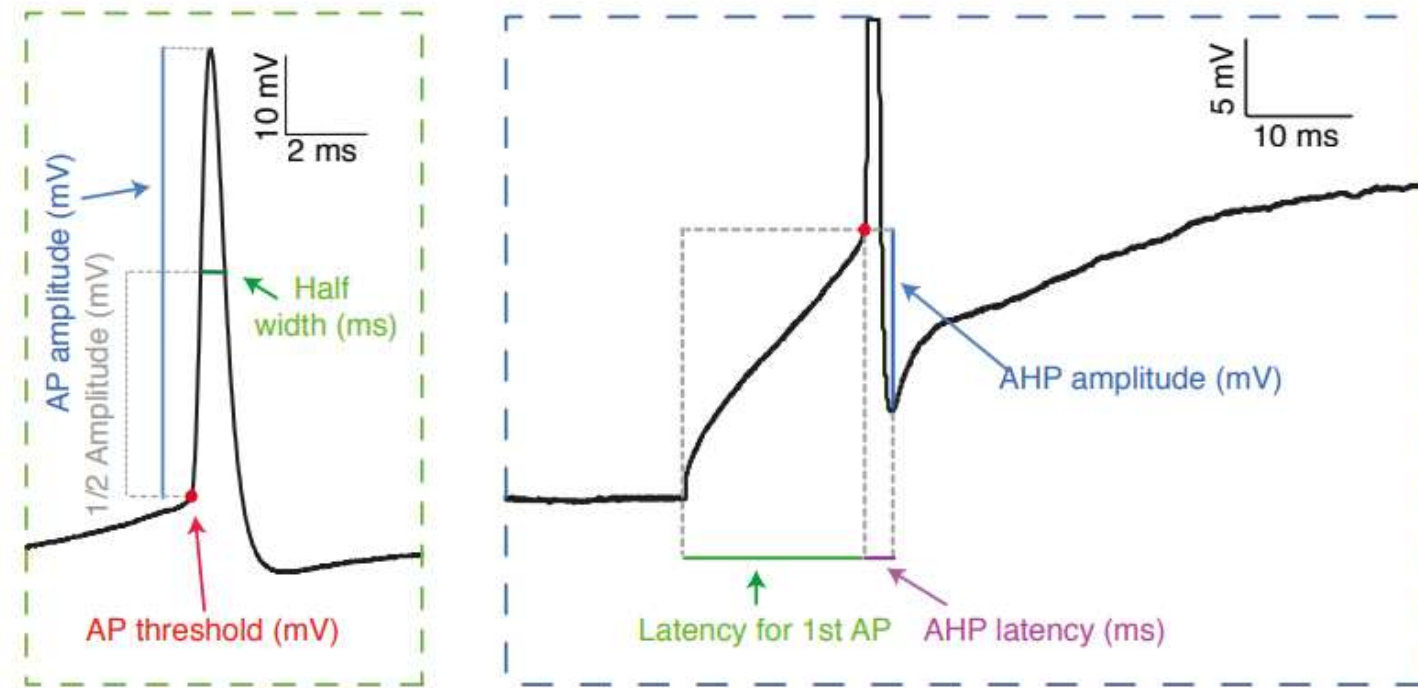


少娜师姐数据

Summary

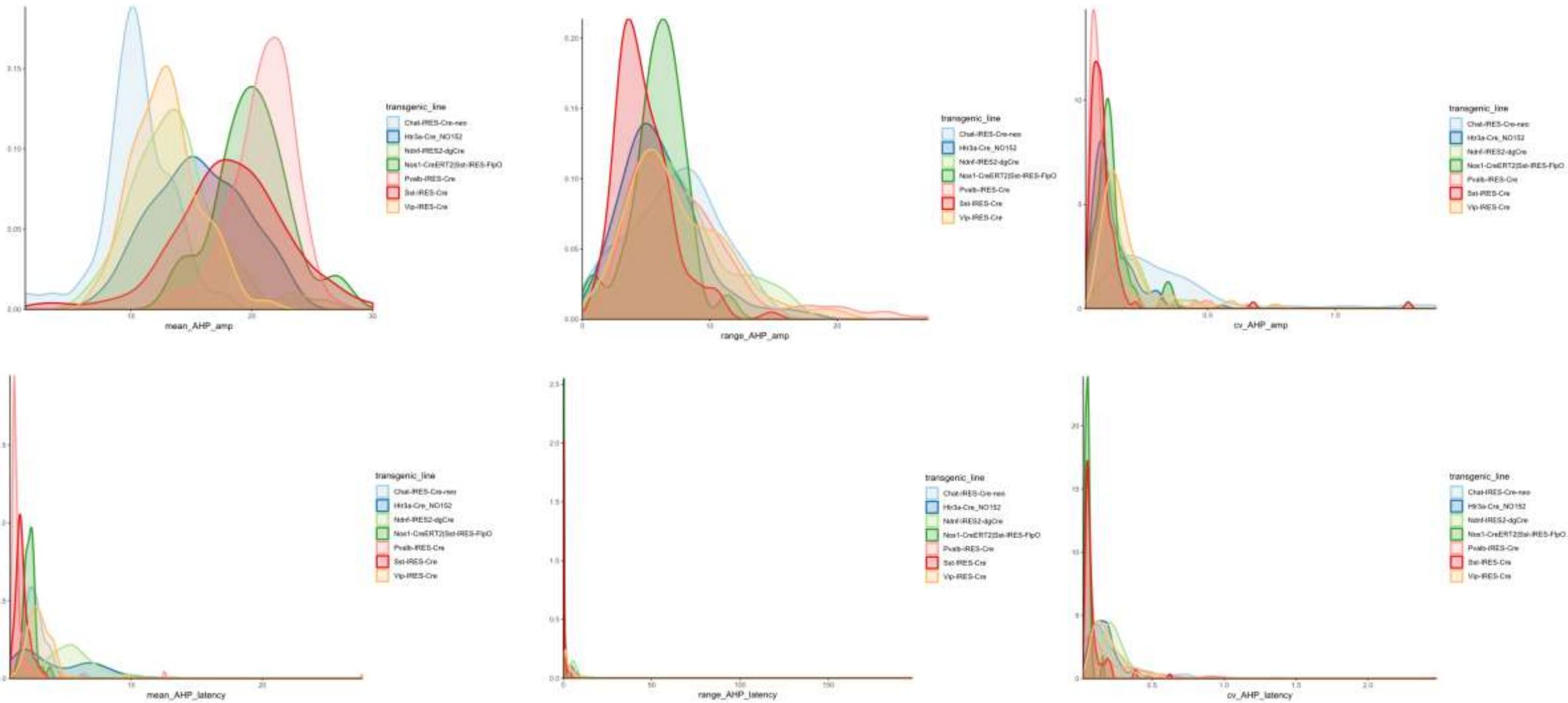
- The differences in Mean_Amplitude and Mean_threshold are much smaller than expected, but CV and range exhibit significant differences. This indicates that different action potentials within a single sweep have considerable differences in these two parameters. Therefore, the average values cannot adequately describe the AP_shape.
- Upon examining these parameters for individual sweeps, it appears that there are considerable variations within bursts. **Therefore, descriptive statistics are needed to characterize this phenomenon.**
- Statistical analysis of shape-related parameters for the first action potential can help describe the differences in single AP shapes.

AP level parameters-AHP related (latency , amplitude)

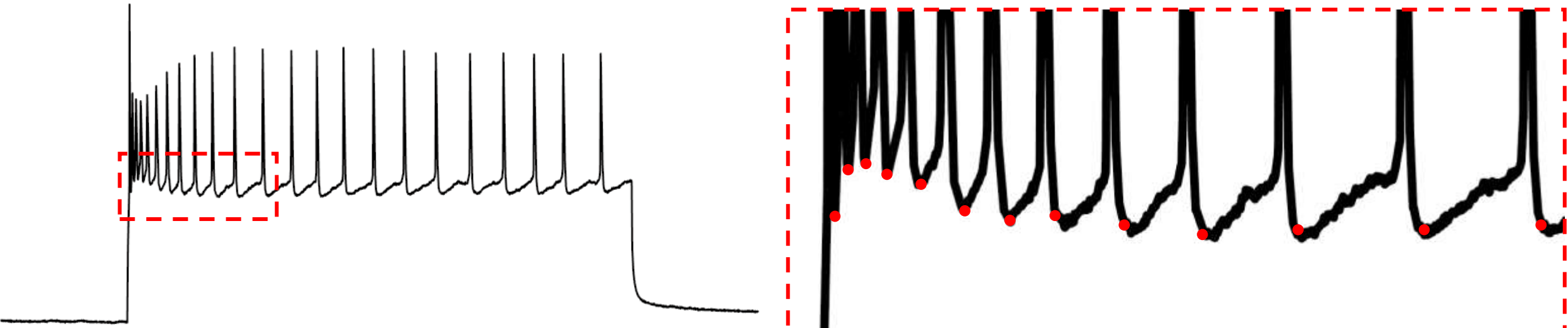


Ana B. Mun~oz-Manchado et al.(2018)cell report

AP level parameters-AHP related(latency, amplitude)



AP level parameters-AHP related(latency, amplitude)

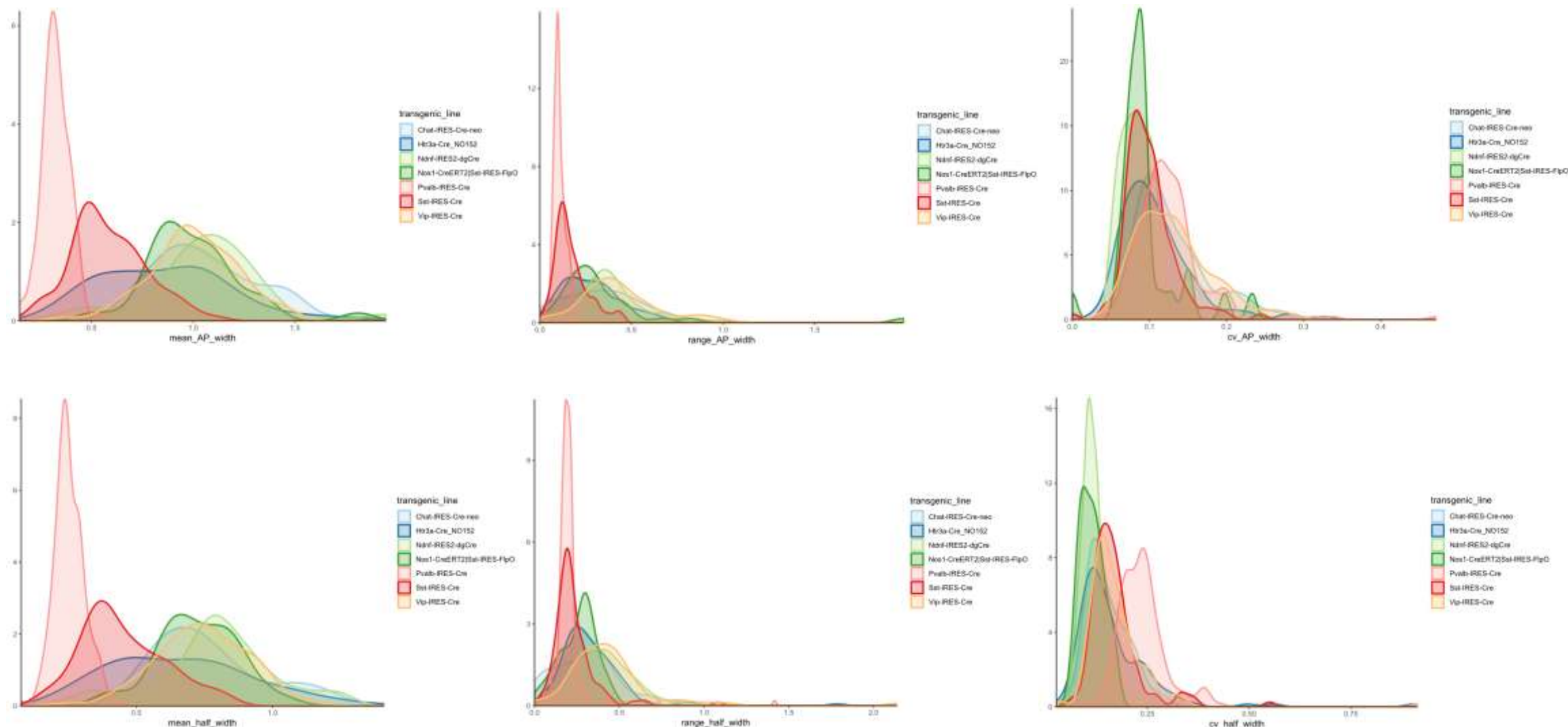


少娜师姐数据

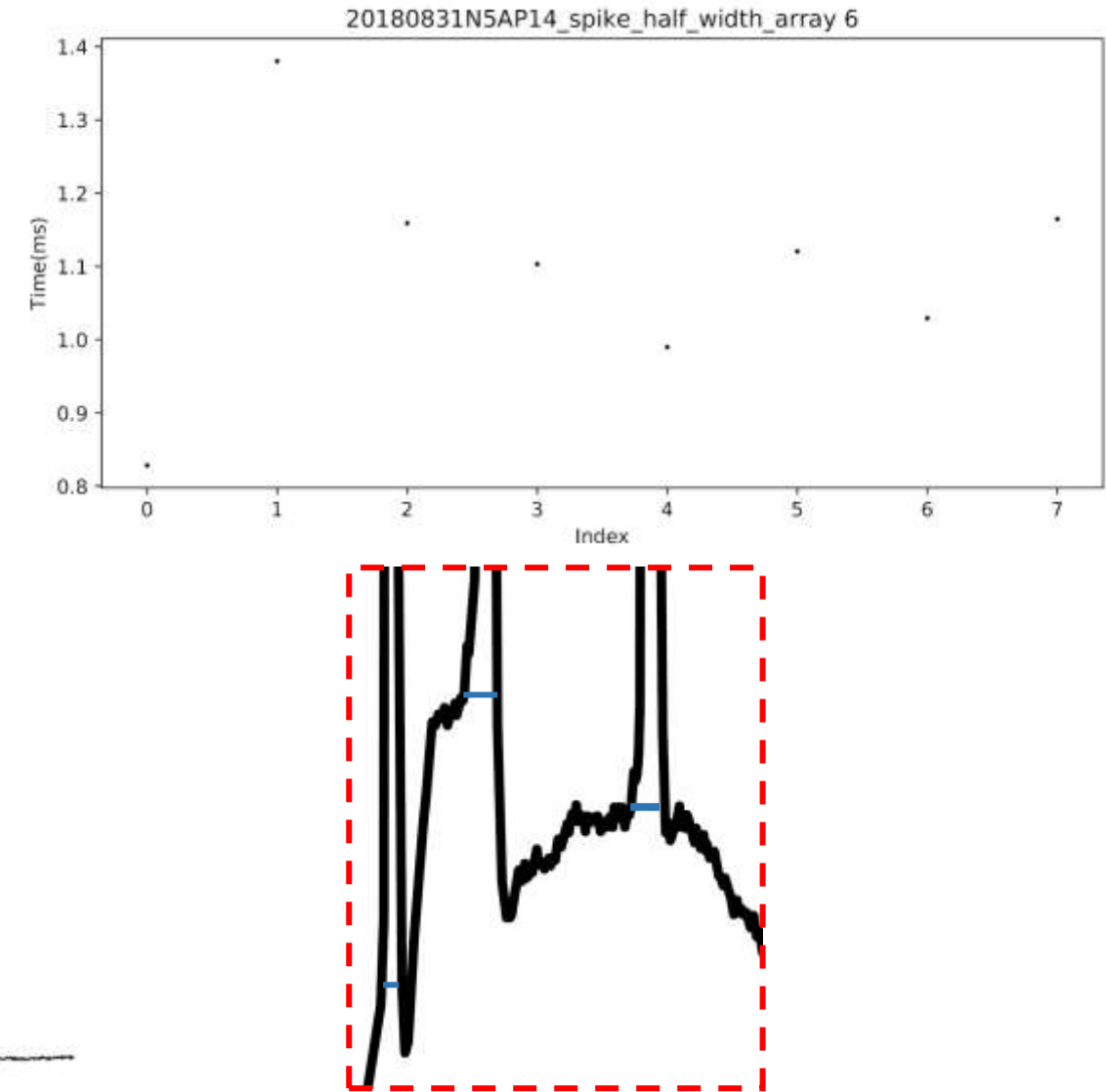
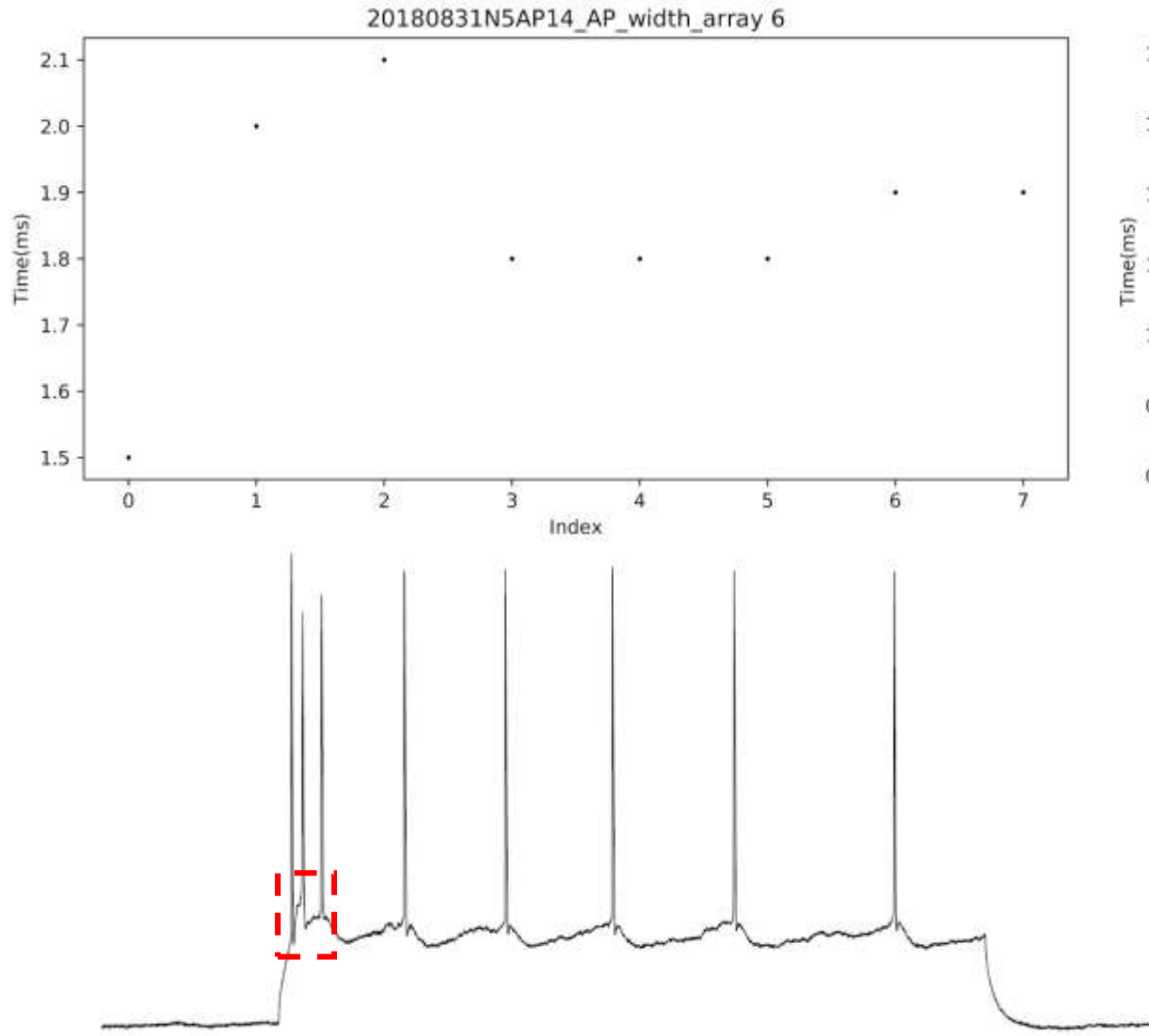
Summary

- Mean_AHP_amp and Mean_AHP_latency exhibit differences in distribution across various classes, with CV and range also showing differences. This suggests variations in these two parameters among different action potentials within a single sweep.
- Upon examining these parameters for individual sweeps, it appears that there are significant variations within bursts. **Therefore, descriptive statistics are needed to characterize this phenomenon.**
- Statistical analysis of shape-related parameters for the first action potential can help describe the differences in single AP shapes.

AP level parameters-width related (AP_width, AP_half_width)



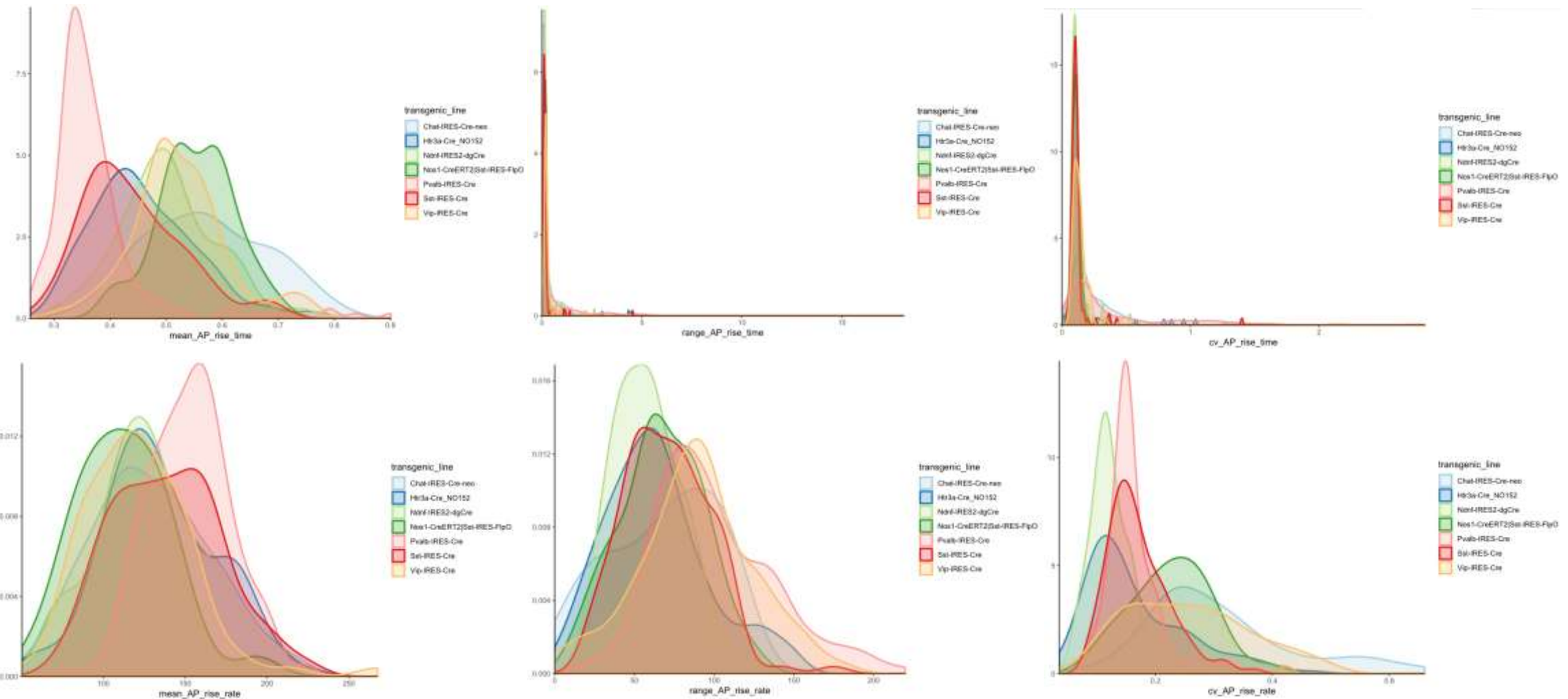
AP level parameters-width related(AP_width, AP_half_width)



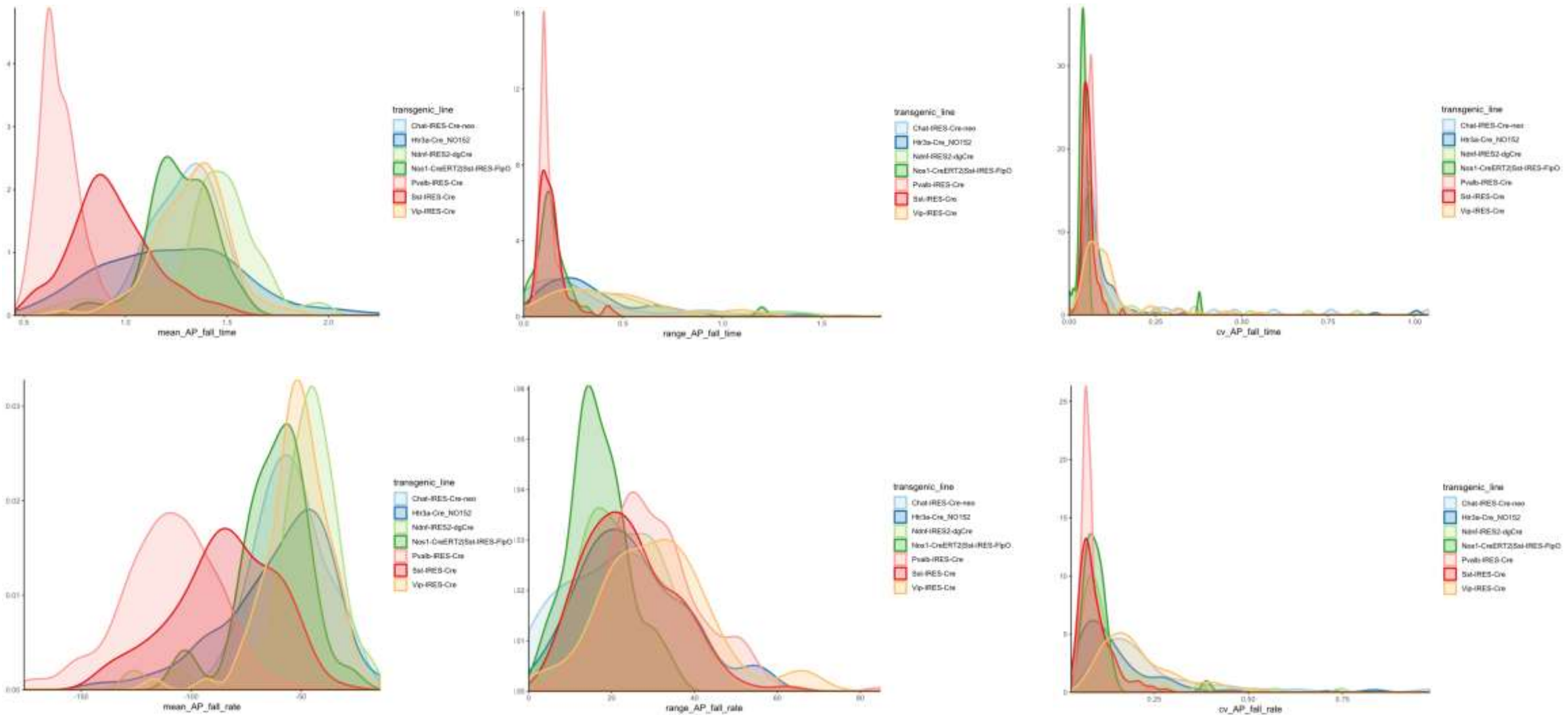
Summary

- Mean_AP_width and Mean_half_width exhibit differences in distribution across various classes, with CV and range also showing differences. This suggests variations in these two parameters among different action potentials within a single sweep.
- Upon examining these parameters for individual sweeps, it appears that there are significant variations within bursts. **Therefore, descriptive statistics are needed to characterize this phenomenon.**
- While the distributions of AP_width and half_width are nearly identical, the trend in individual APs is more pronounced for AP_width. Therefore, half_width can be used as a descriptive parameter.

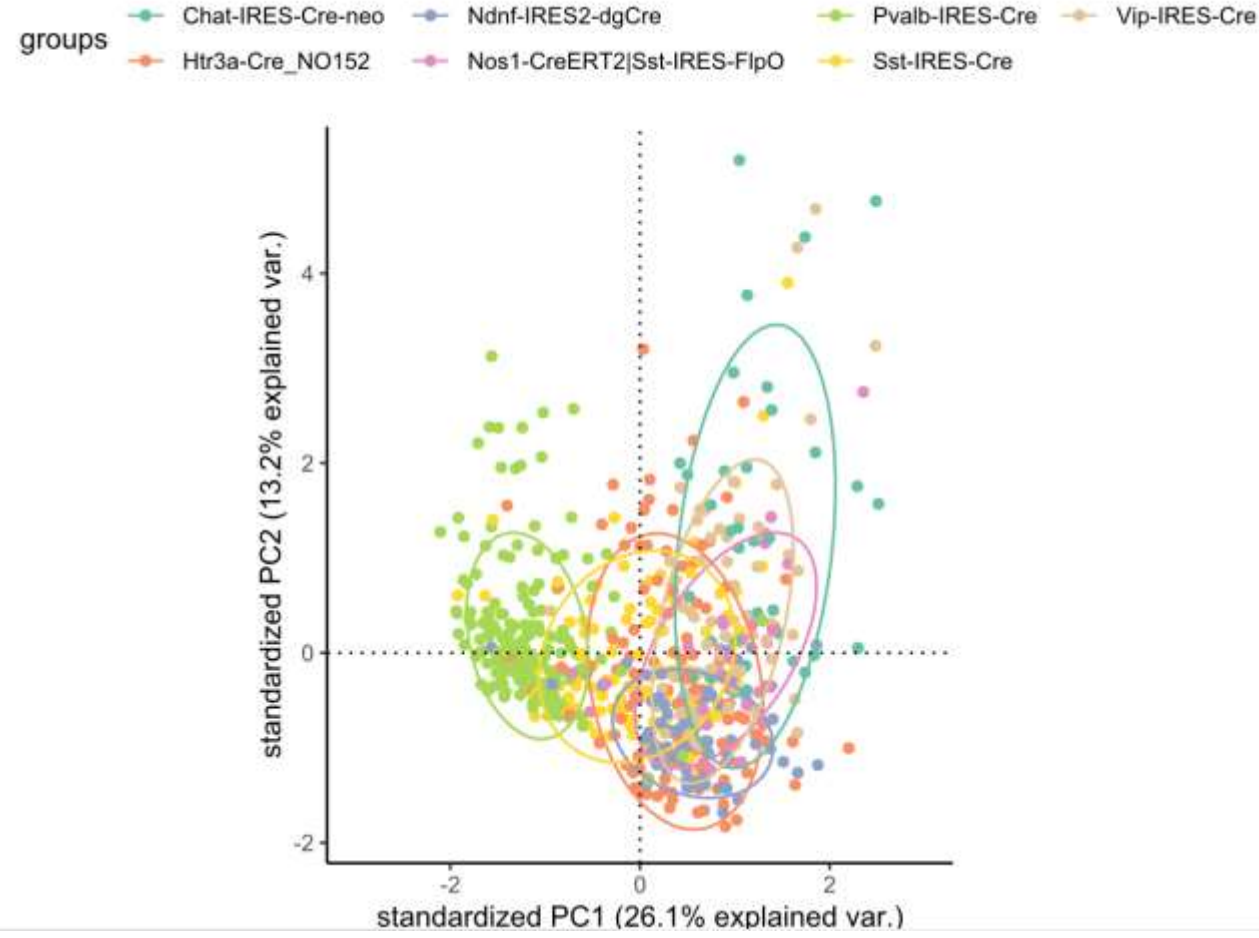
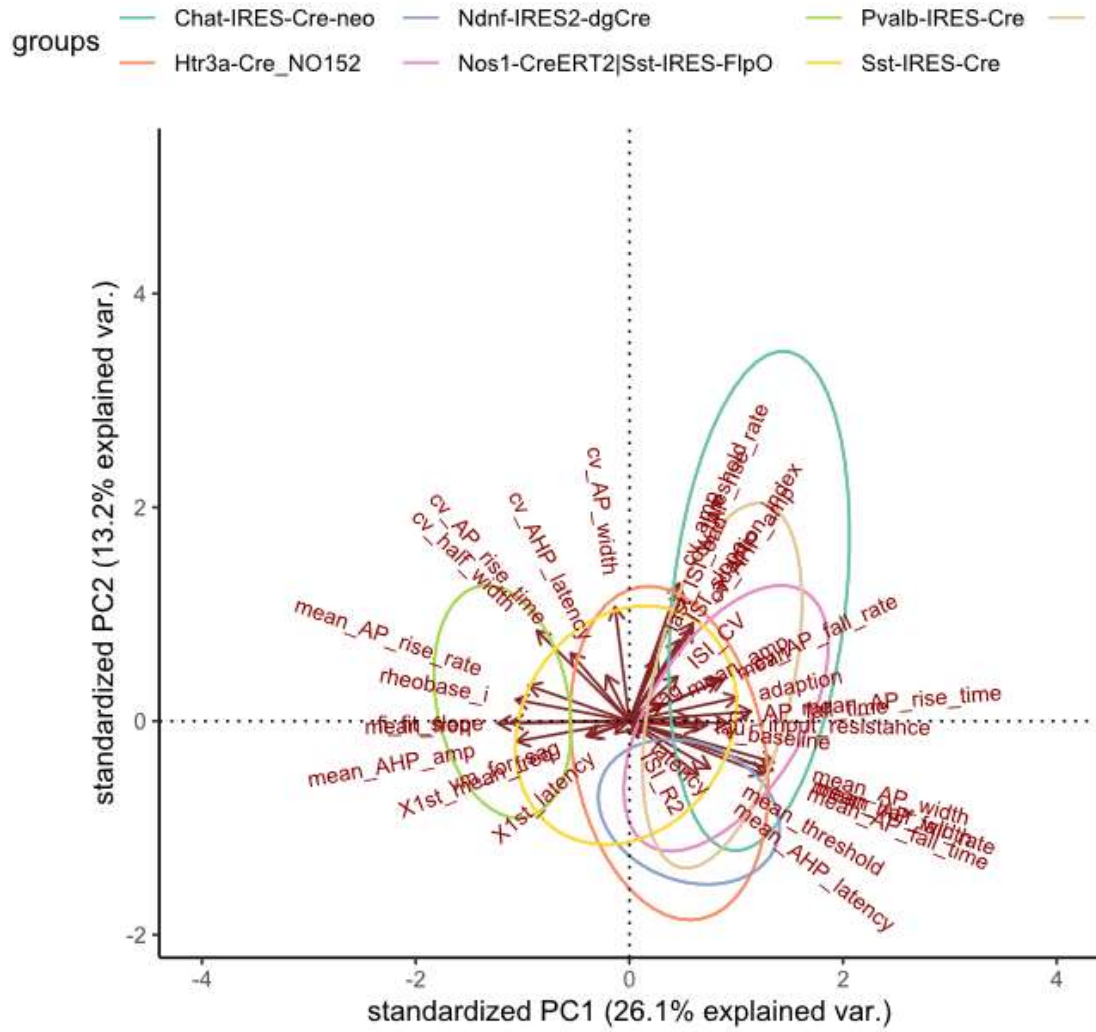
AP level parameters- Rise part correlation (rise_time, rise_rate)



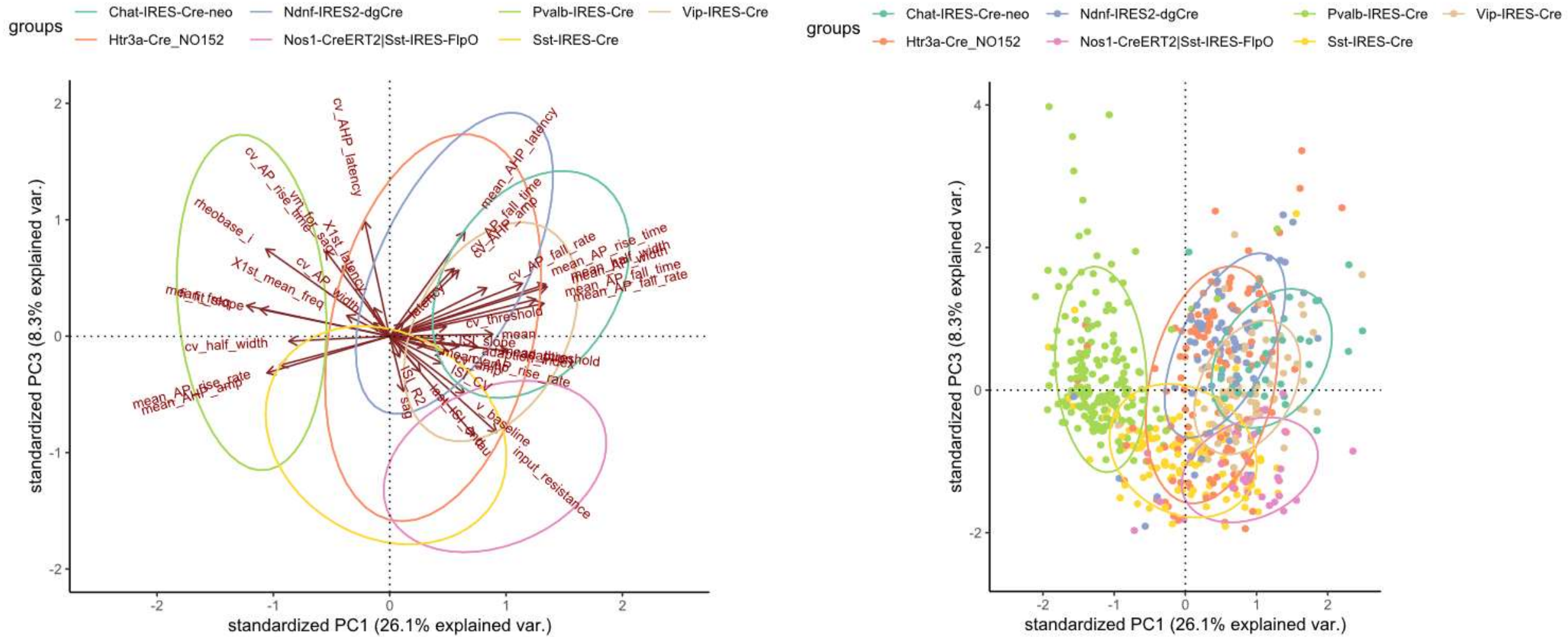
AP level parameter-Down part(rise_time, rise_rate)



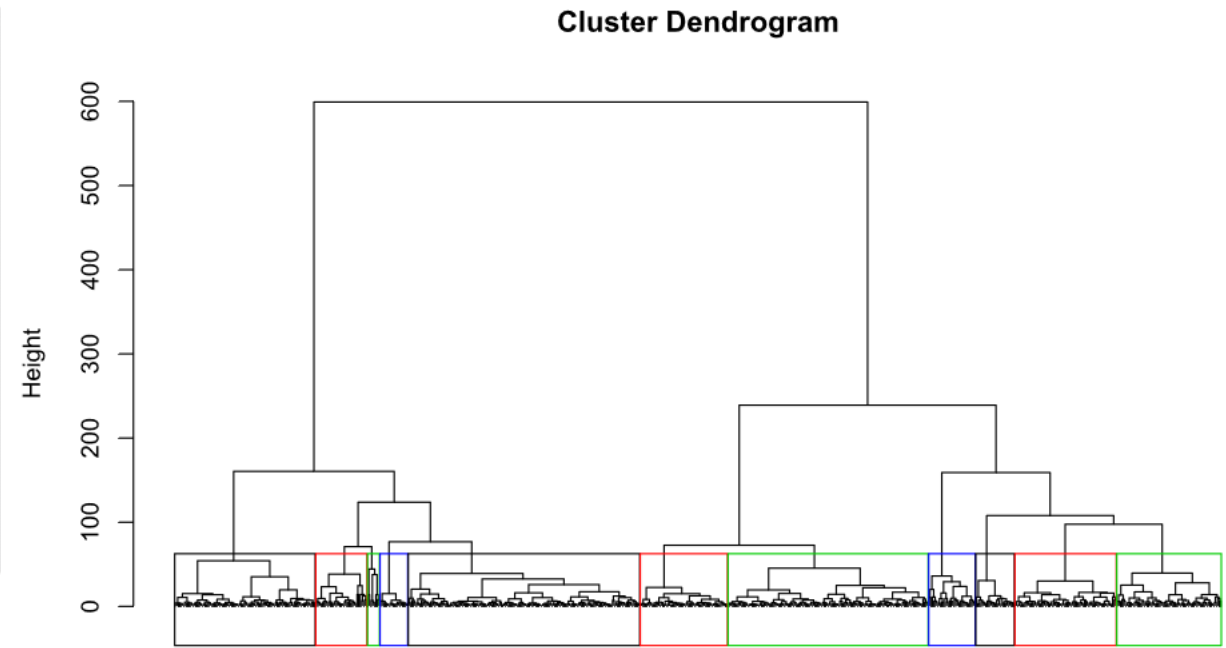
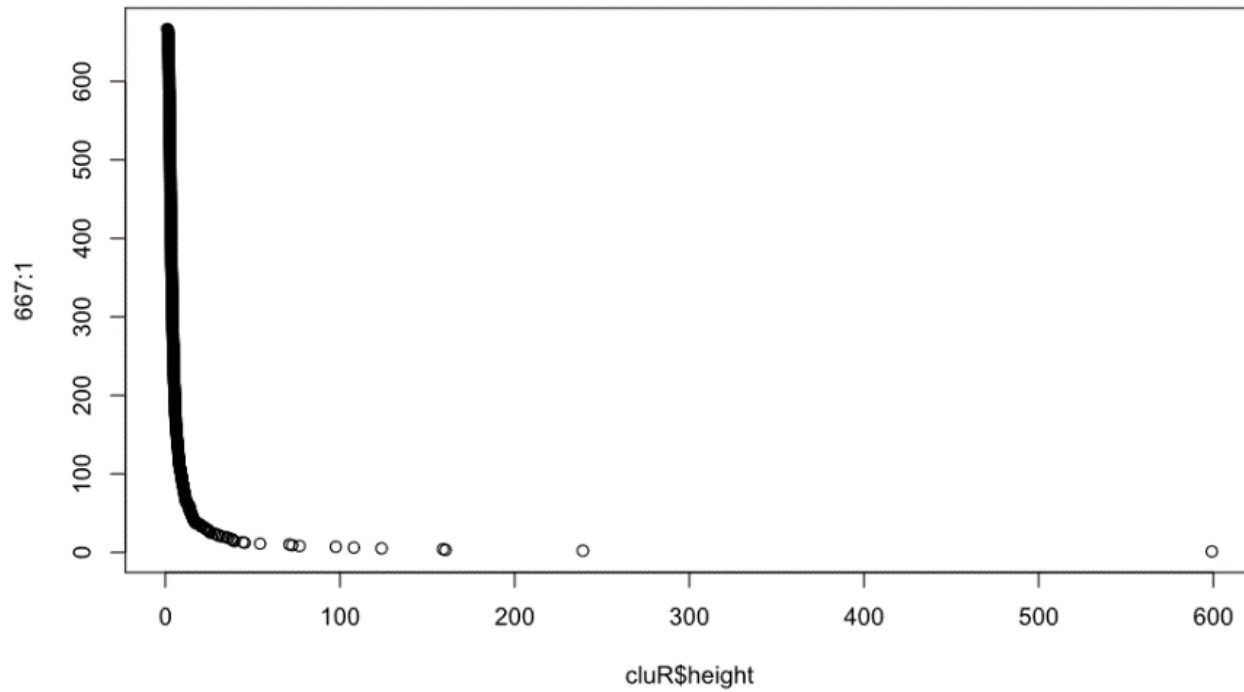
PCA parameter correlation analysis



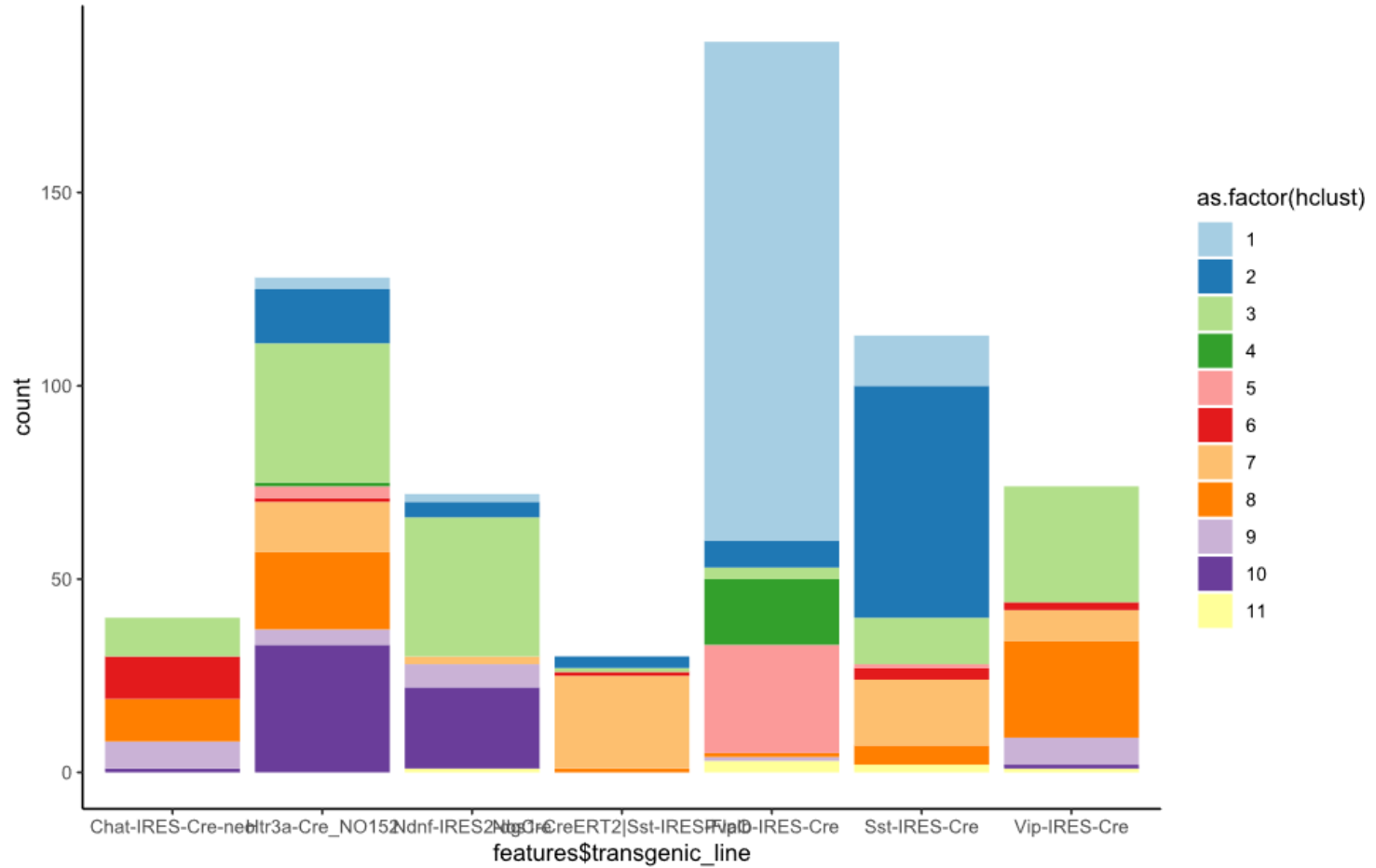
PCA parameter correlation analysis



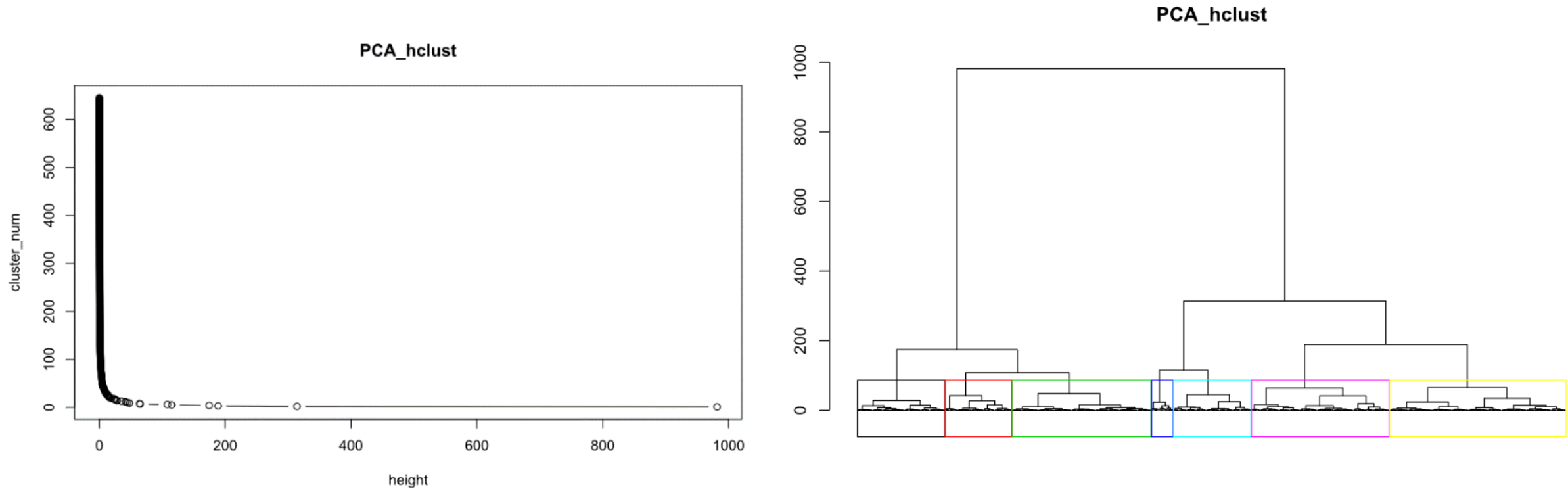
hclust classification with all parameters



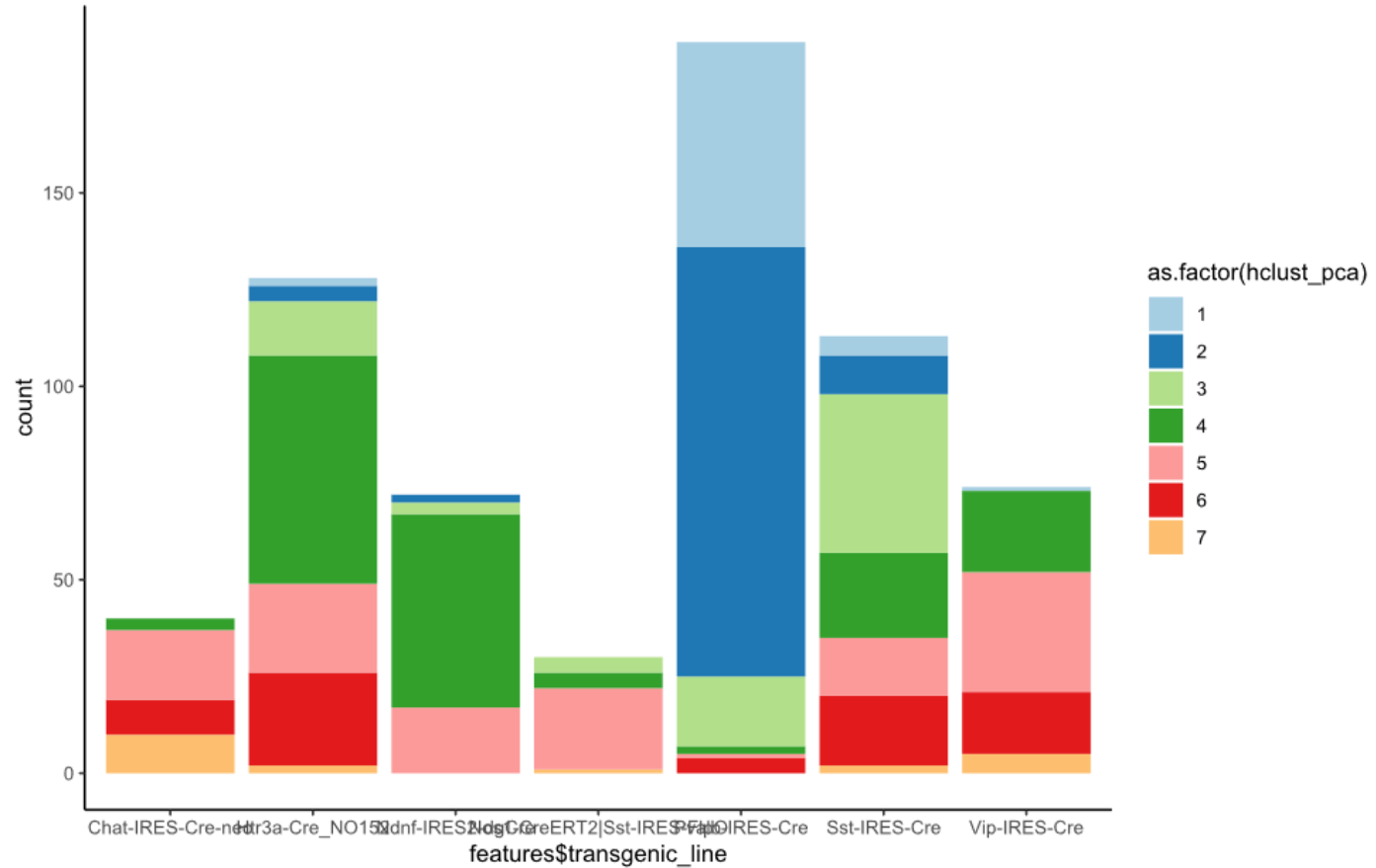
hclust classification with all parameters



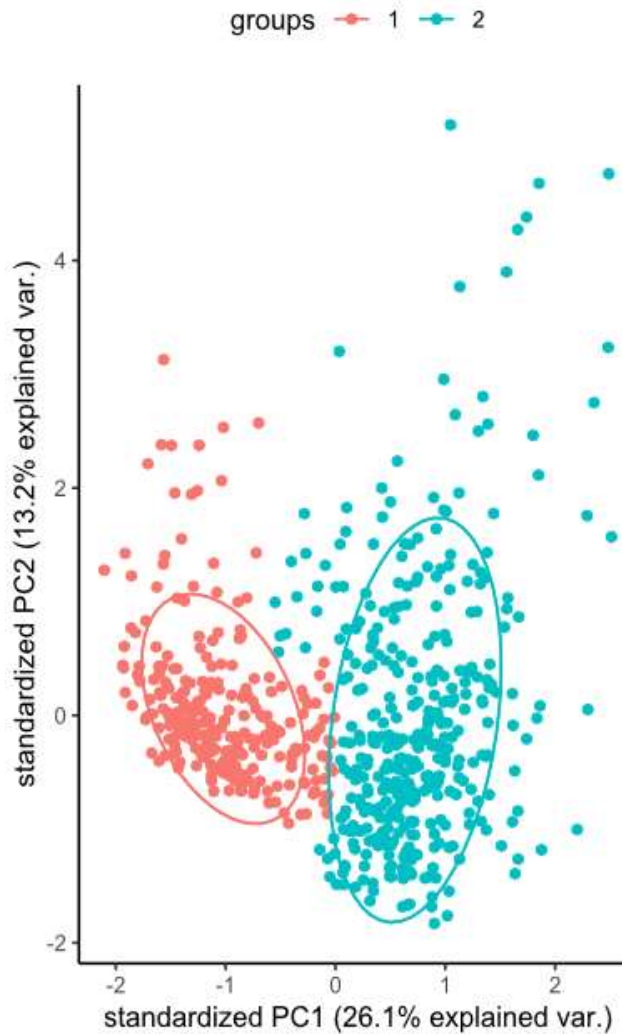
Using PCA-derived PCs for hclust clustering



hclust classification with all parameters

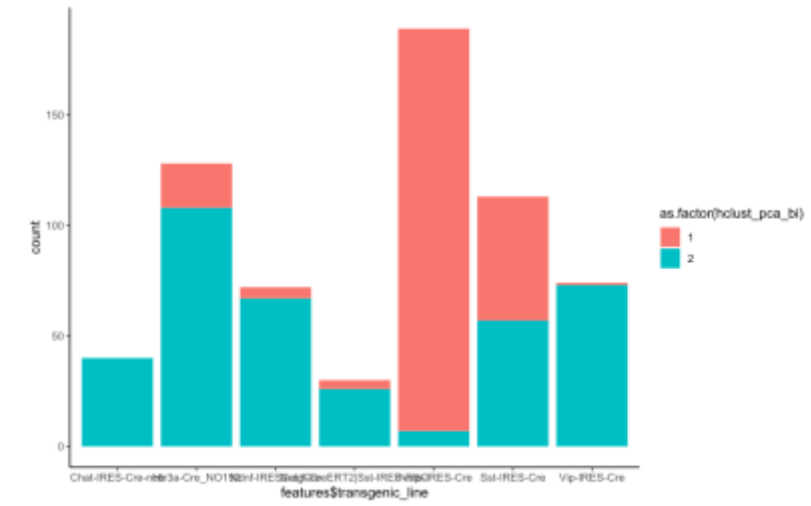
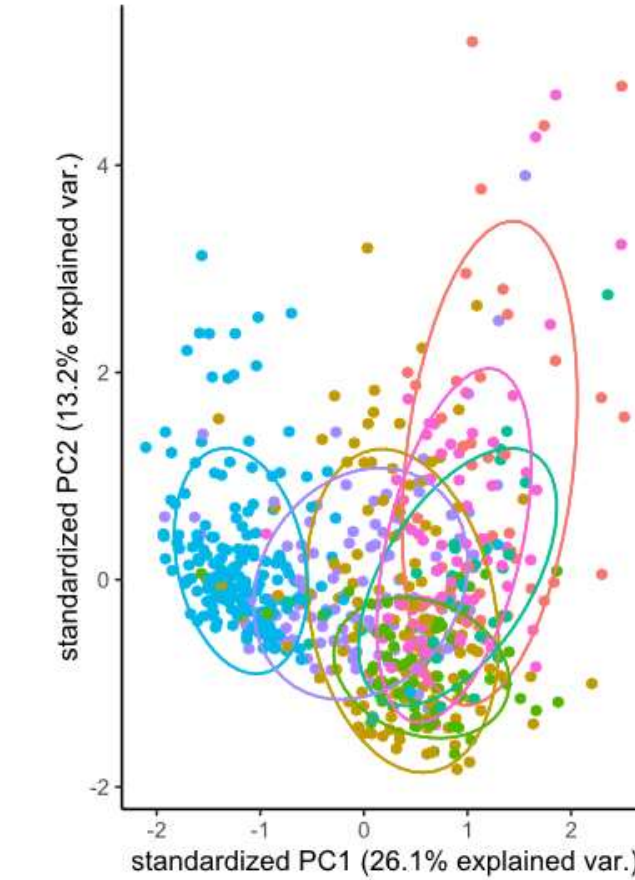


Two PCA_hclust divisions (first division)

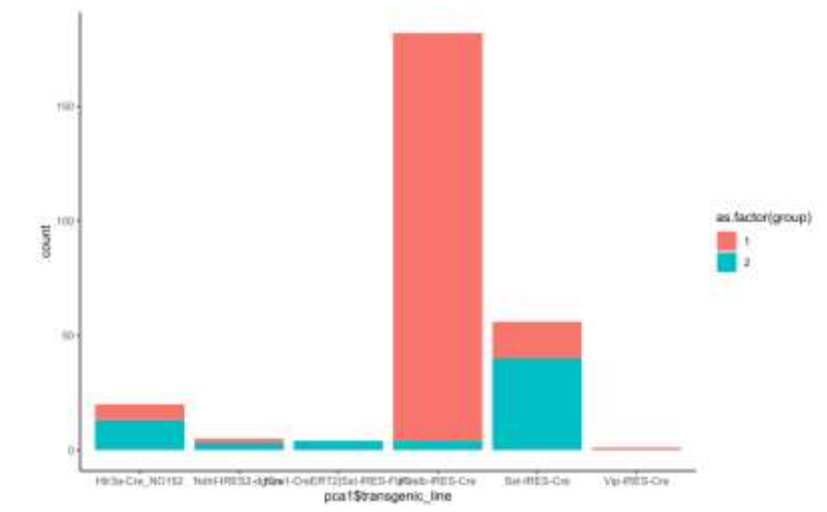
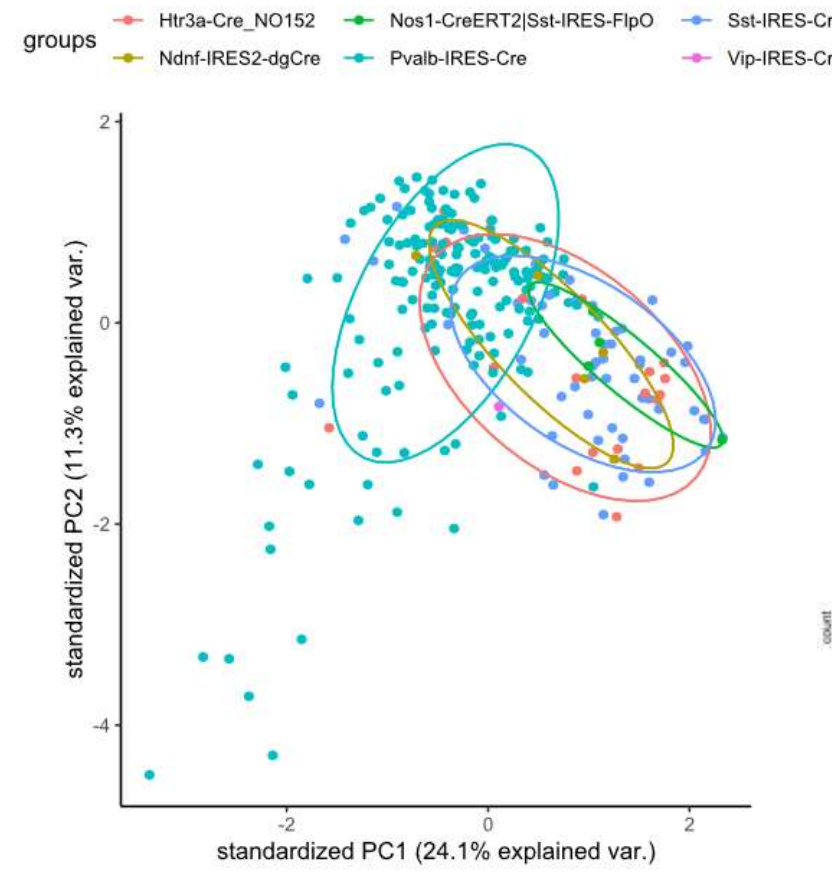
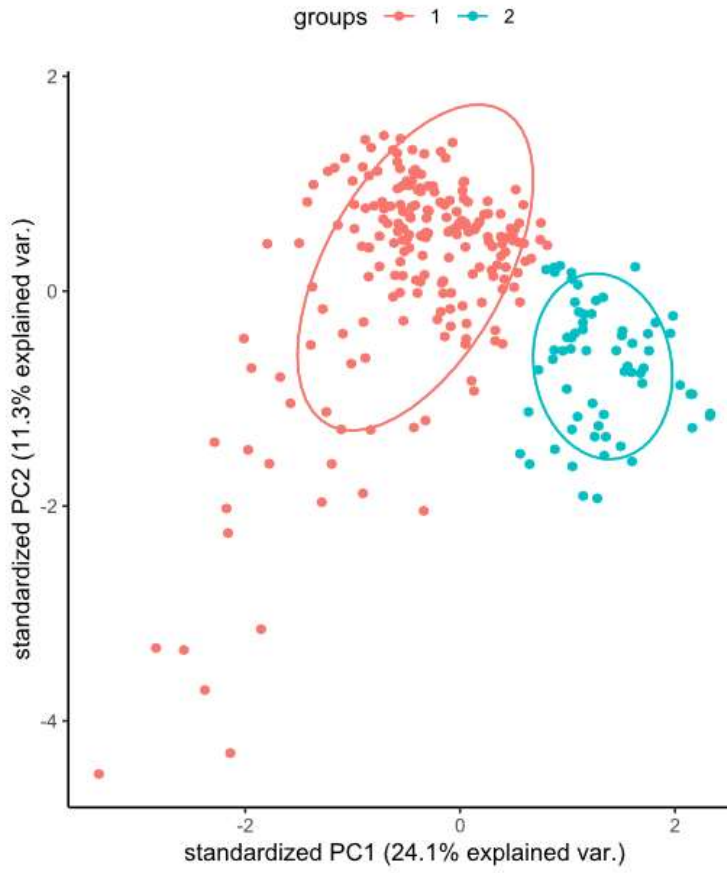


groups

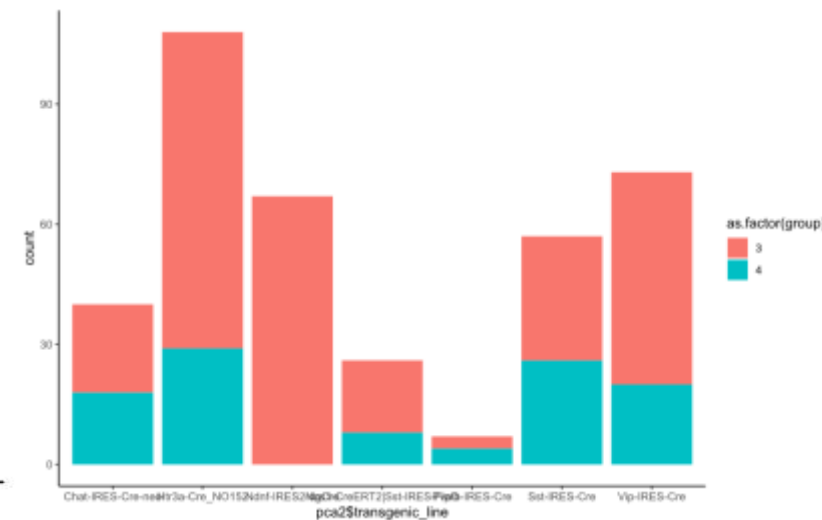
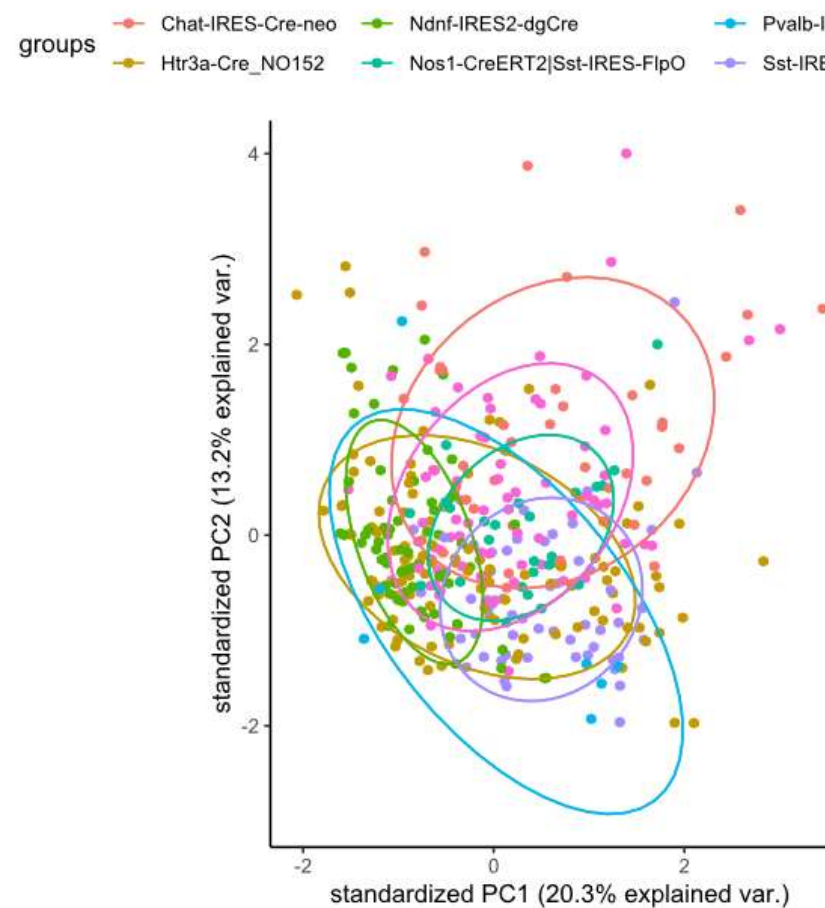
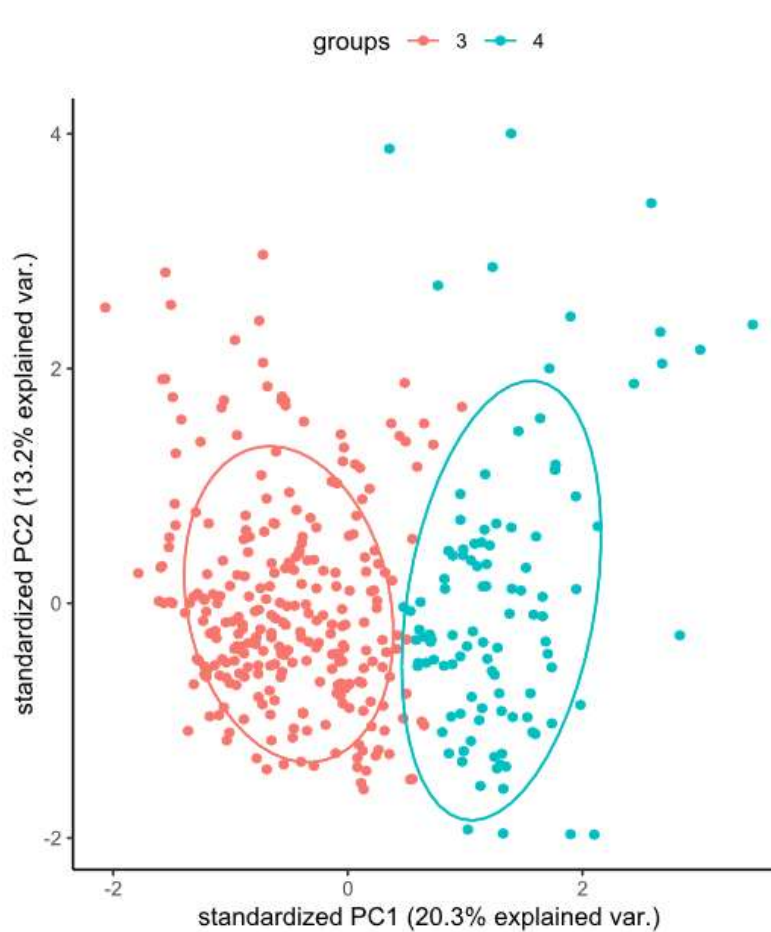
- Chat-IRES-Cre-neo
- Htr3a-Cre_NO152
- Ndnf-IRES2-dgCre
- Nos1-CreERT2|Sst-IRES-FlpO
- Pvalb-IRES-Cre
- Sst-IRES-Cre
- Vip-IRES-Cre

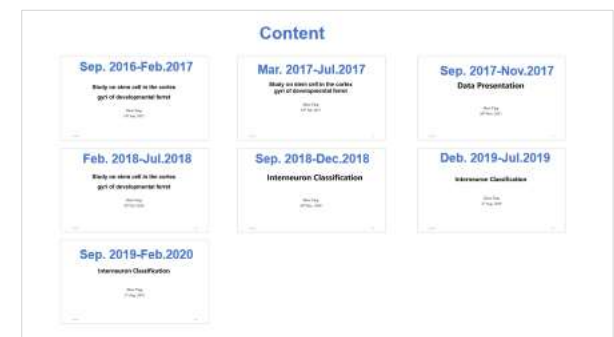
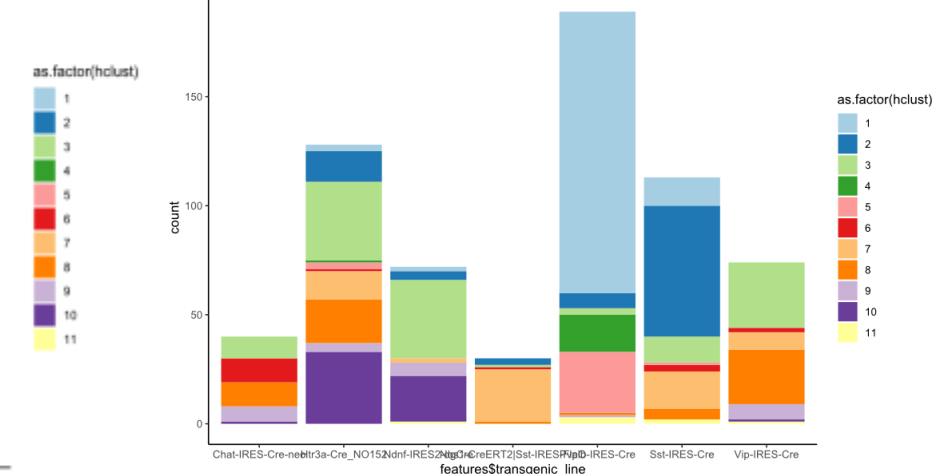
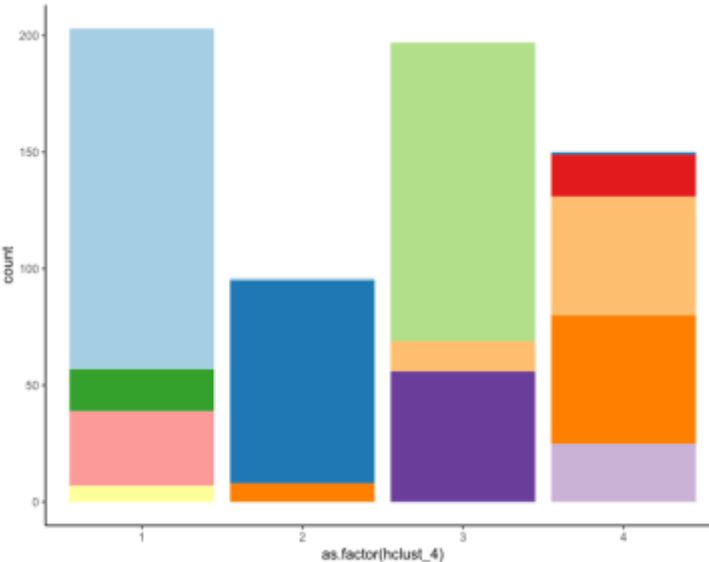
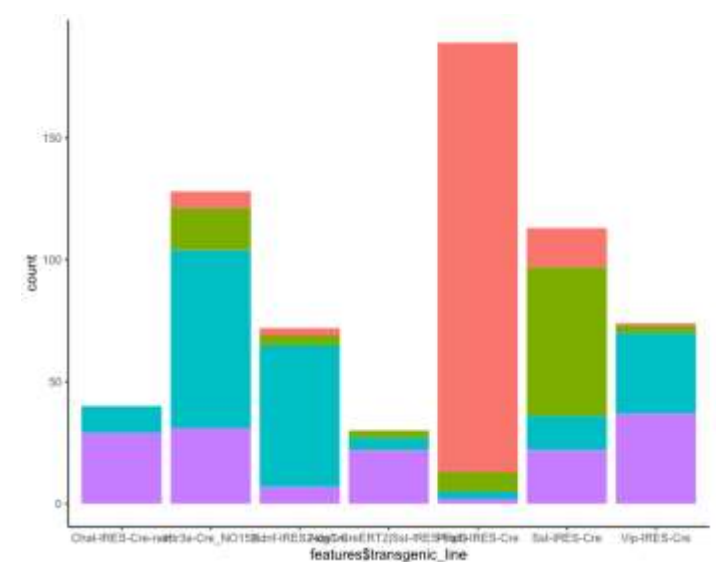


Two PCA_hclust two divisions (second division)



Two PCA_hclust two divisions (second division)





Interneuron Classification

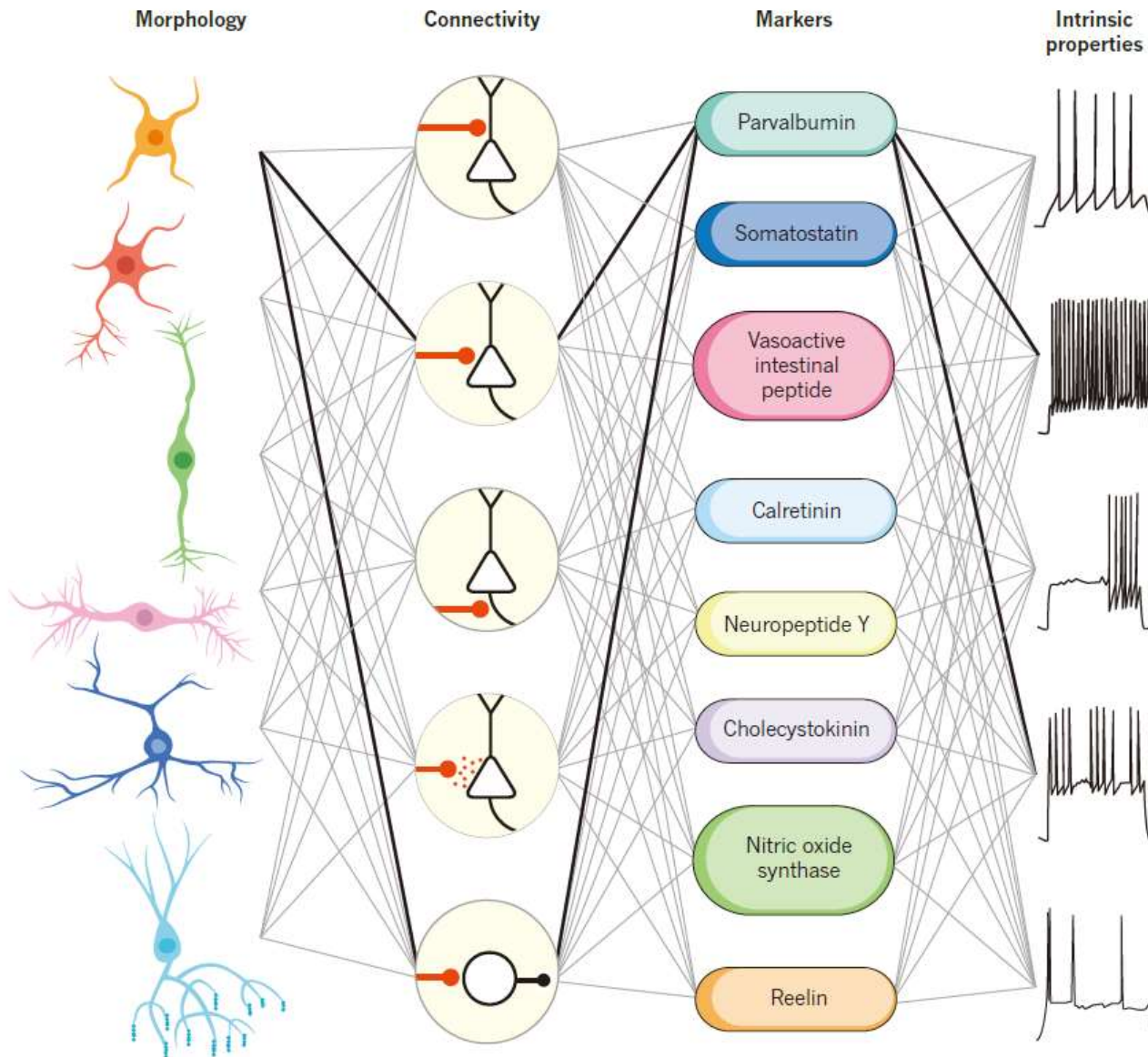
Zhou Ying

2st Aug. 2019

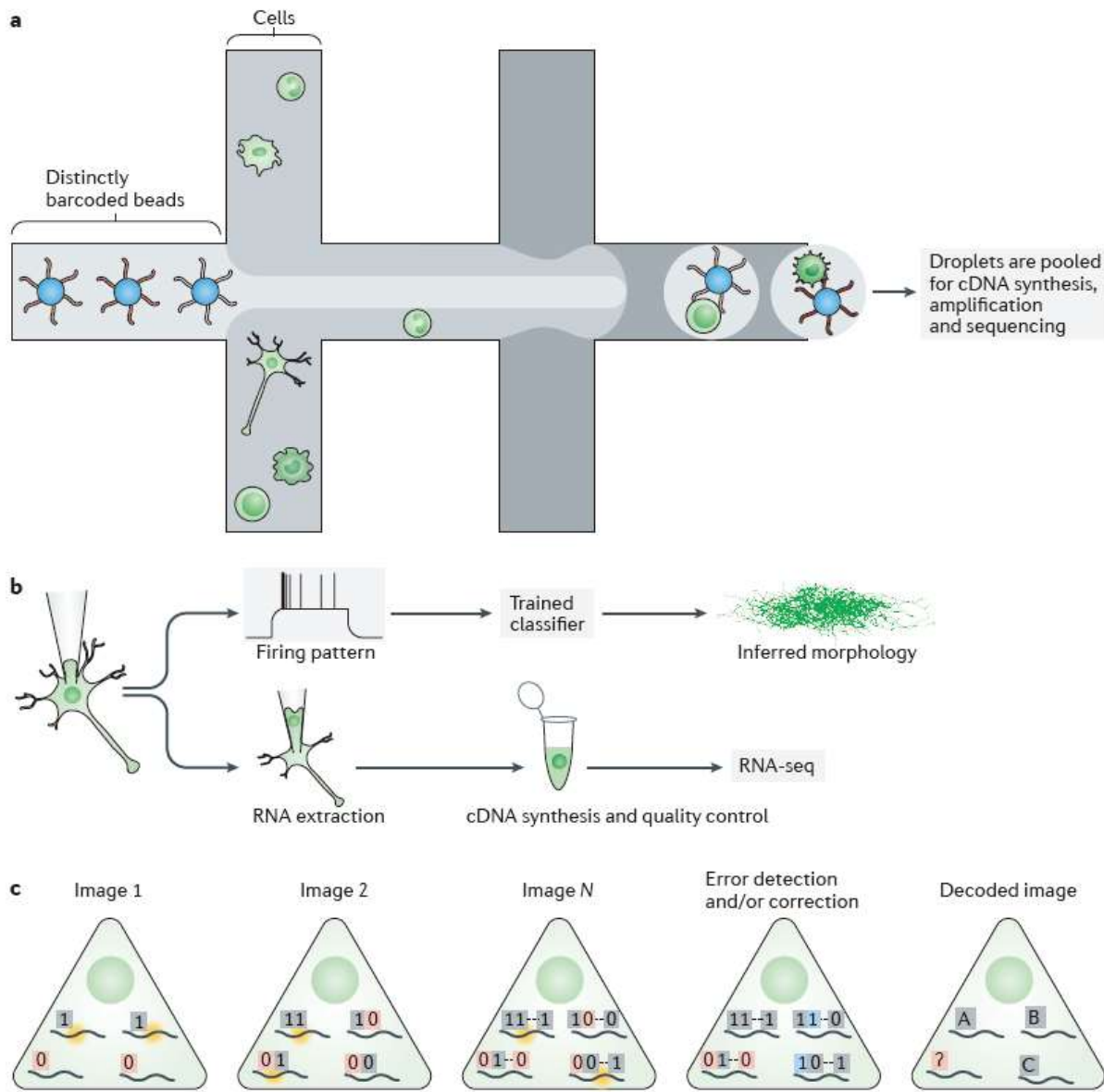
Content

- Background
- Electrophysiological quantification and cluster analysis
- Morphological quantitative parameter extraction
- Simple association analysis and complex network analysis
- Complex network module analysis
- Current problems and next plan

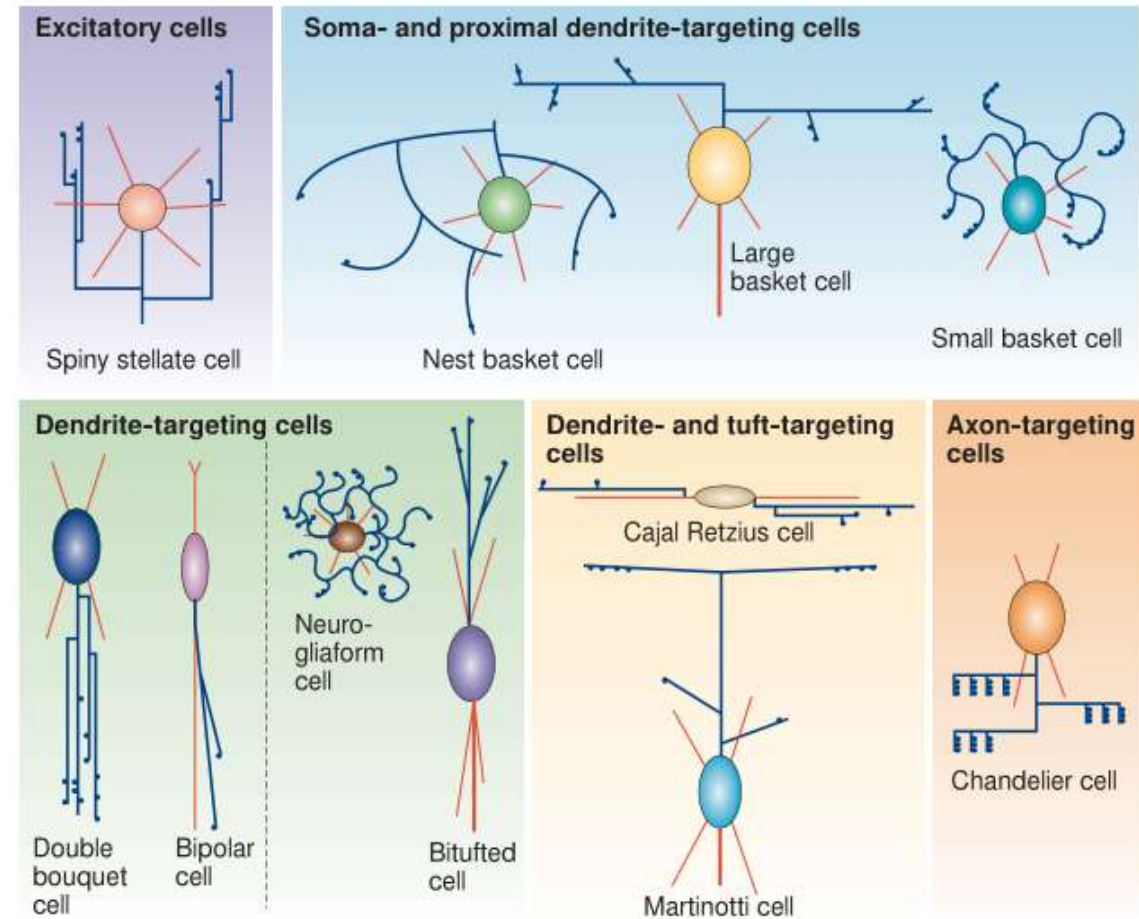
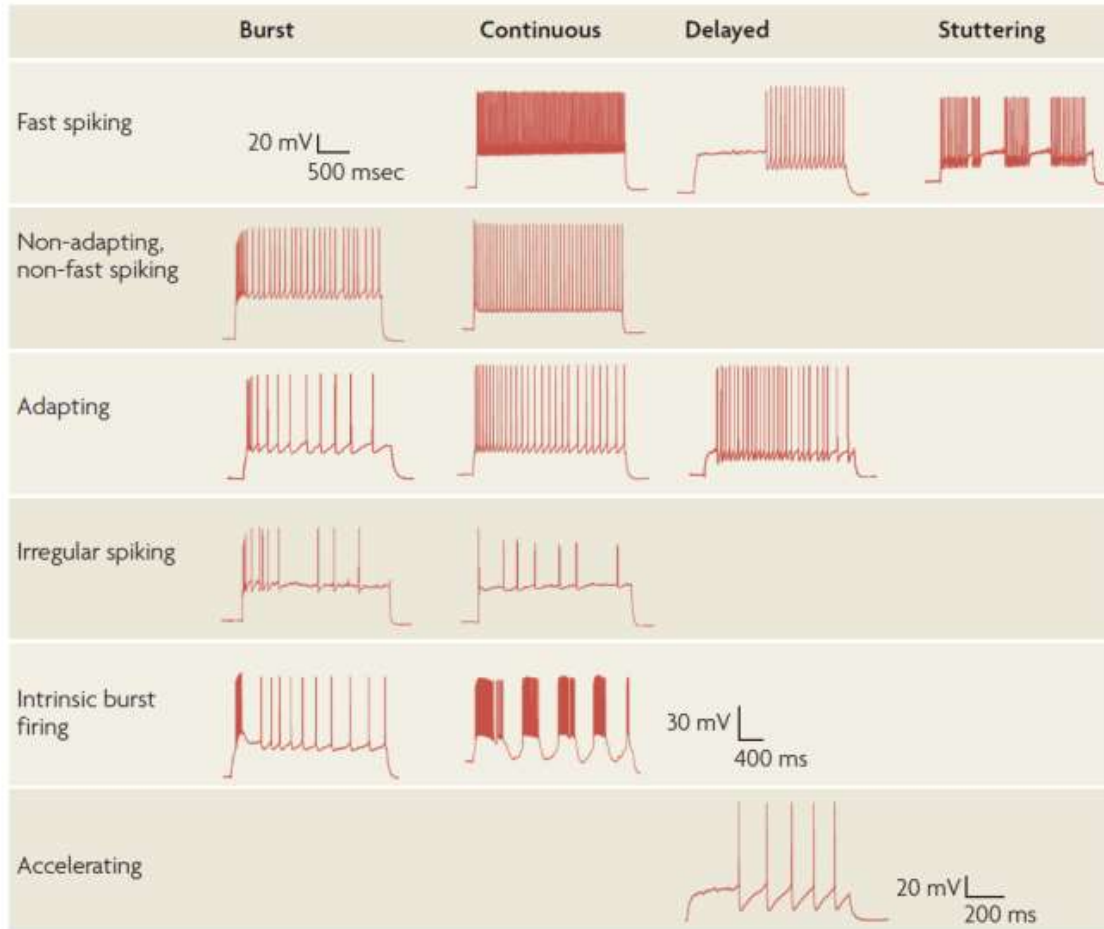
Background



Interneurons have complex diversity in multi-level characteristics. The research of interneurons needs to synthesize multi-level information for classification, and the essence is to correlate multi-level information

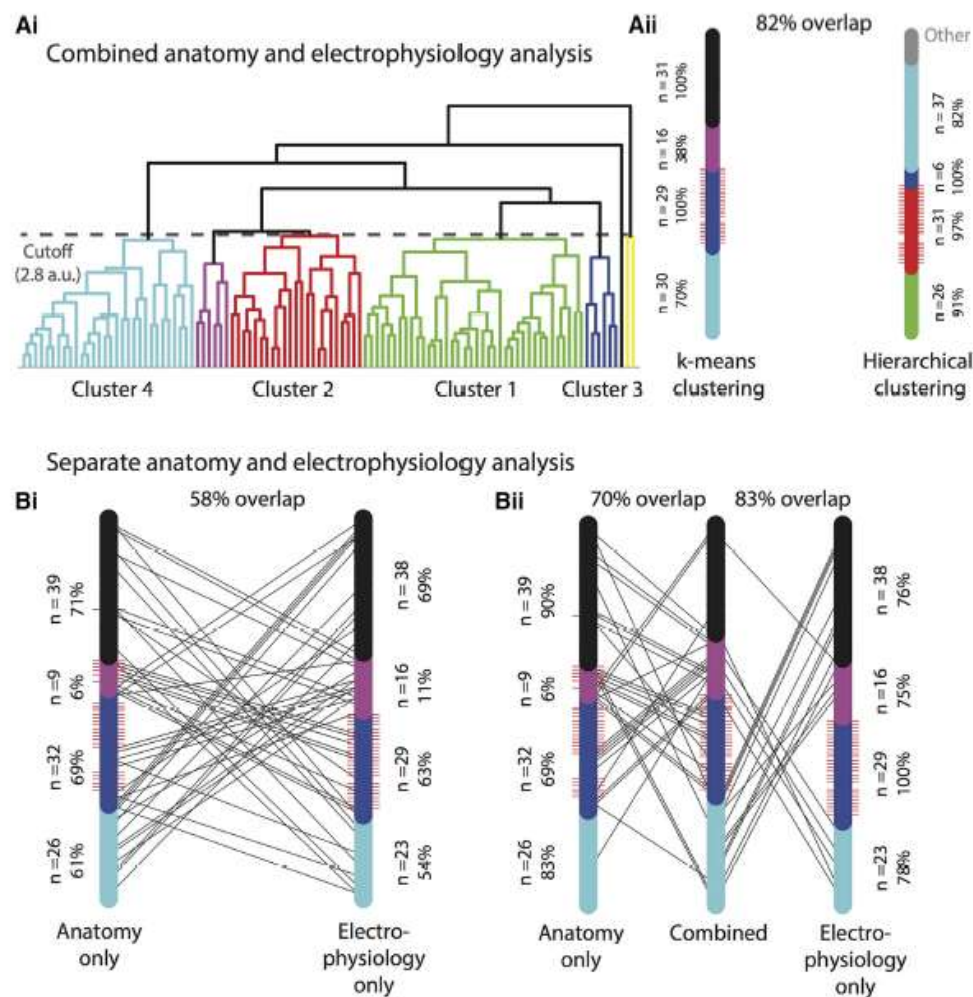


With the development of high-throughput experimental technology, more and more information is collected, and the amount of data is gradually accumulated, and the requirements for high-dimensional data analysis are getting higher and higher

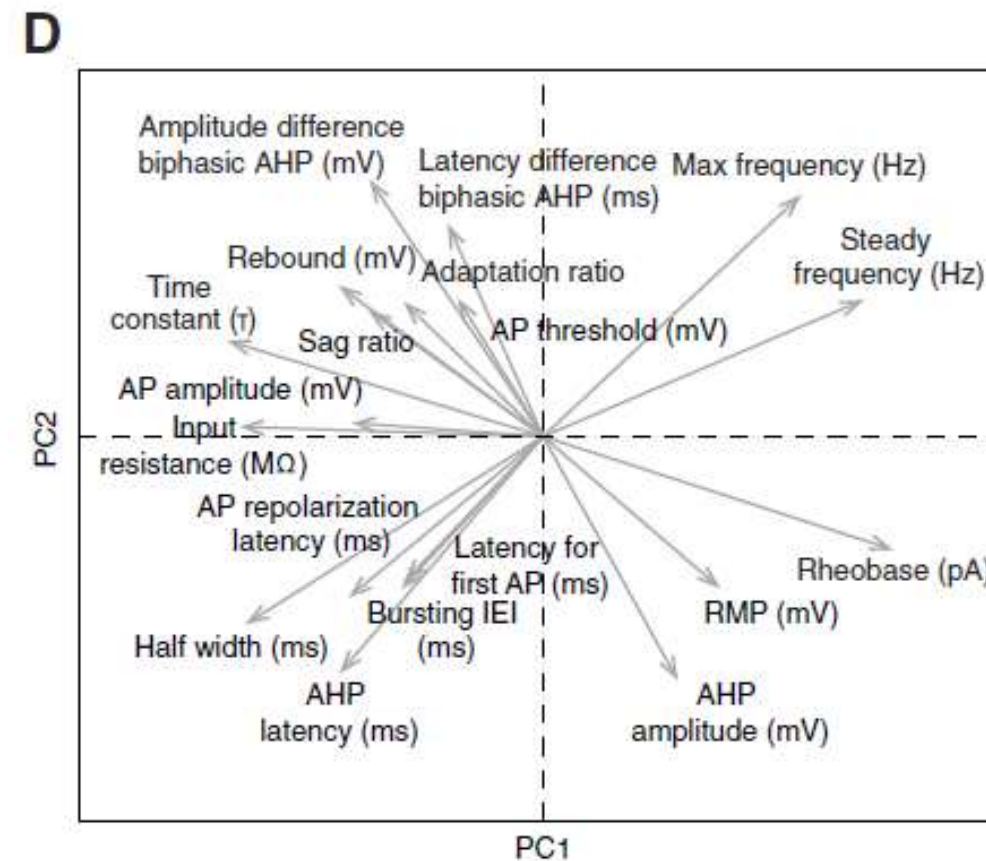


The Petilla Interneuron Nomenclature Group (PING)

In the early stage, the classification characteristics of interneurons were defined through qualitative description. Although the naming could be unified to a certain extent, human factors interfered with the qualitative description. Meanwhile, the qualitative description was not conducive to complex mathematical calculation and multi-level information integration.

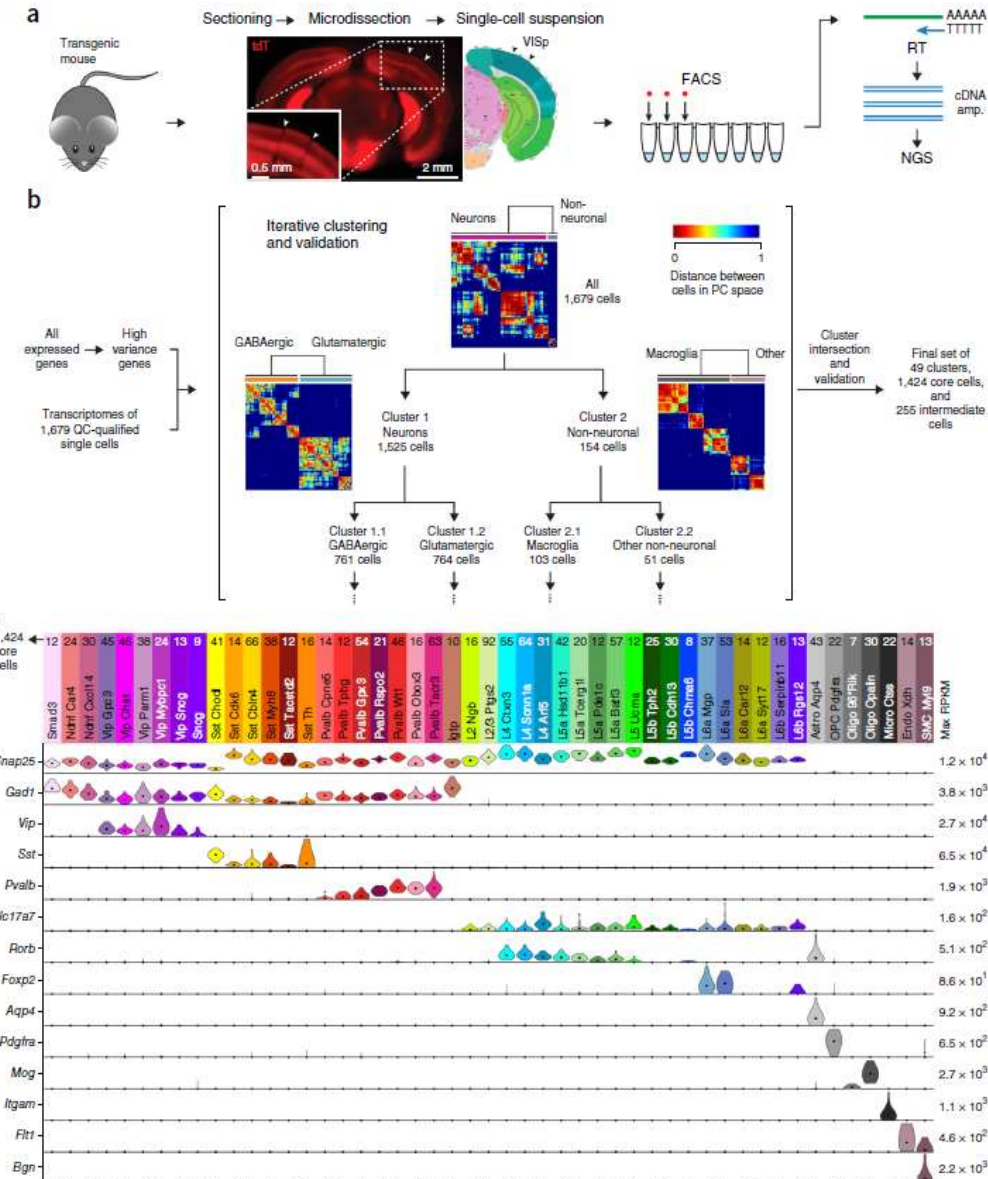


Quantitative calculation has gradually become the trend of interneuron classification



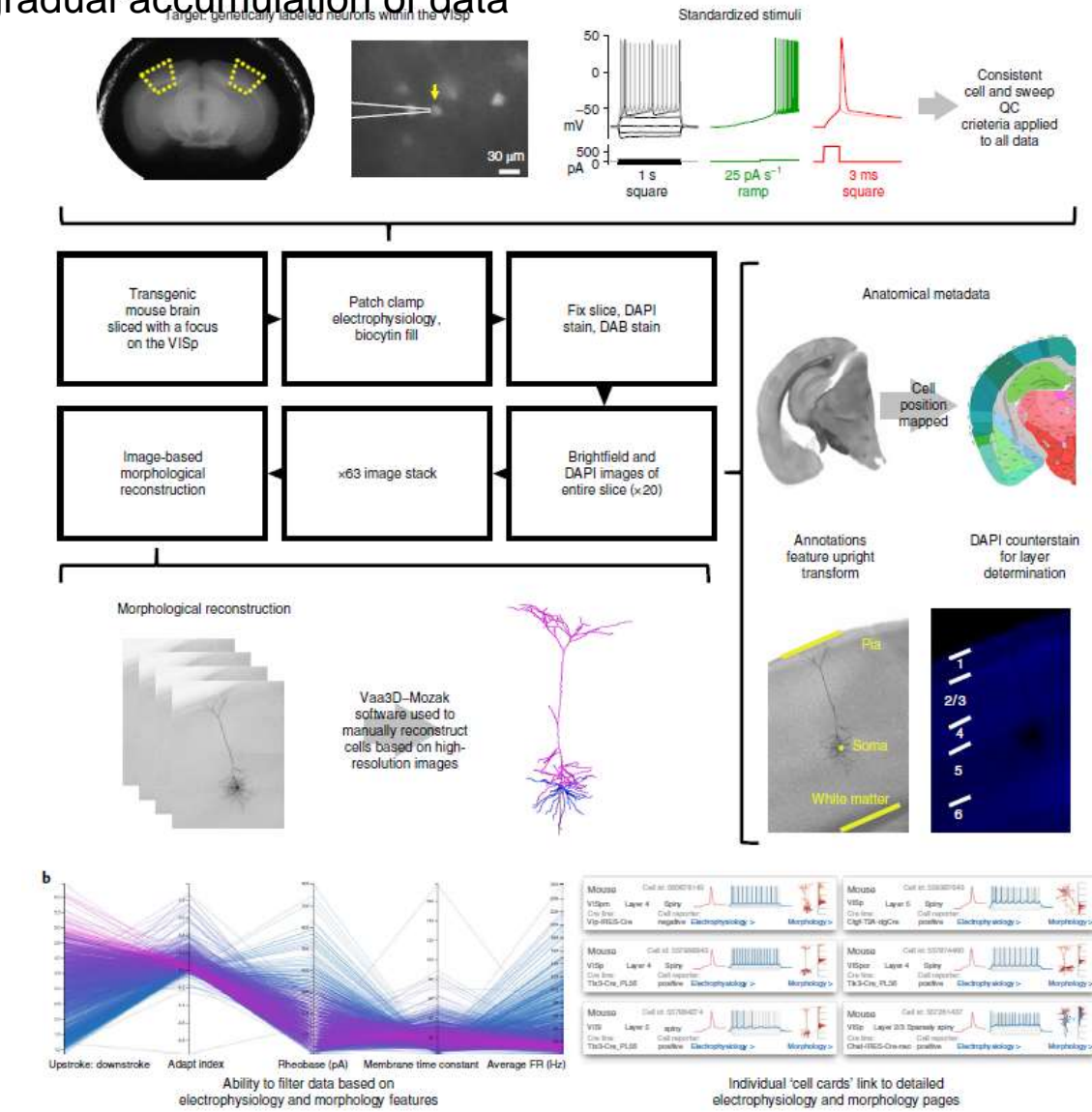
Joan José Martínez et al.(2017)eNeuro

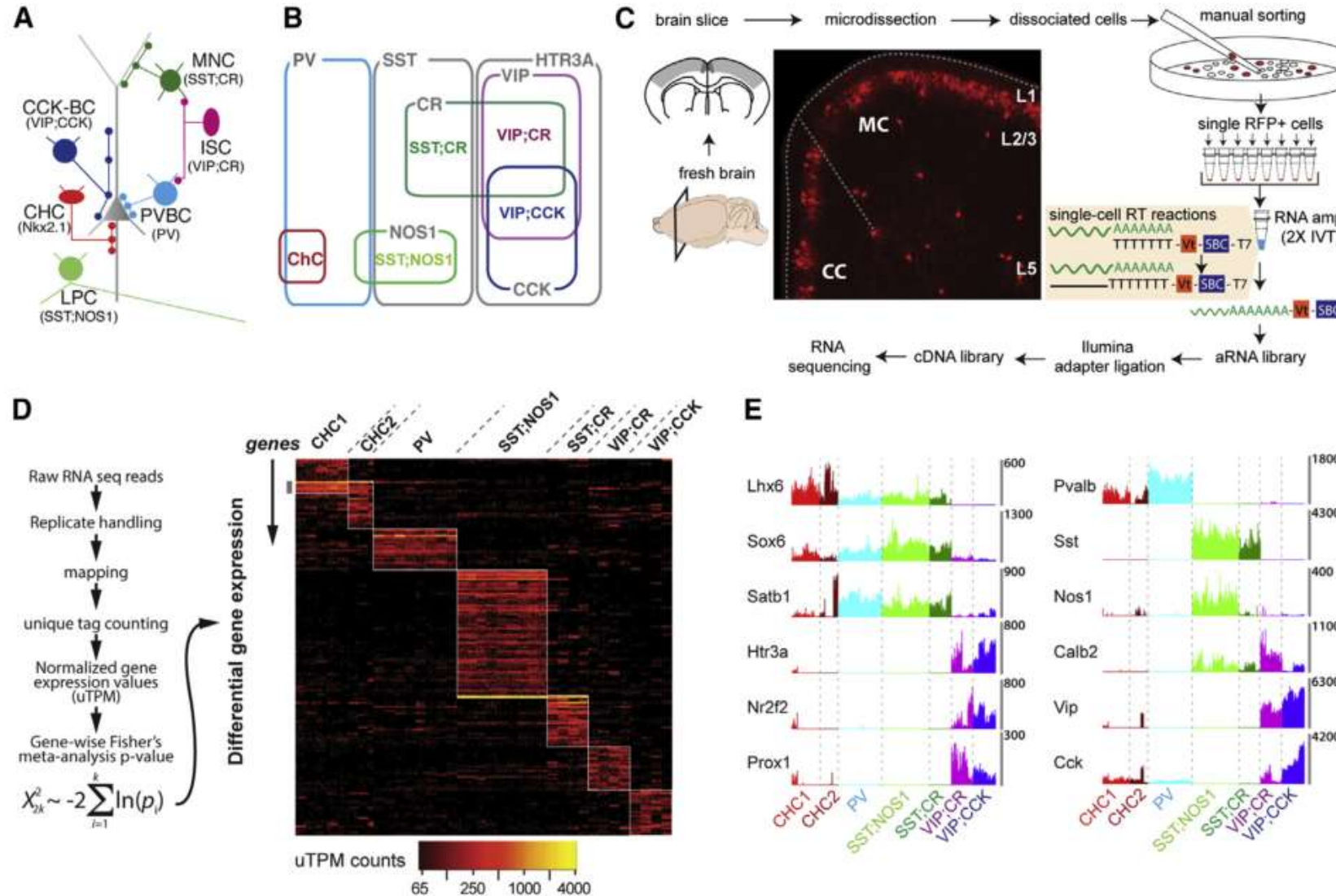
Ana B. Munoz-Manchado et al.(2018)cell report



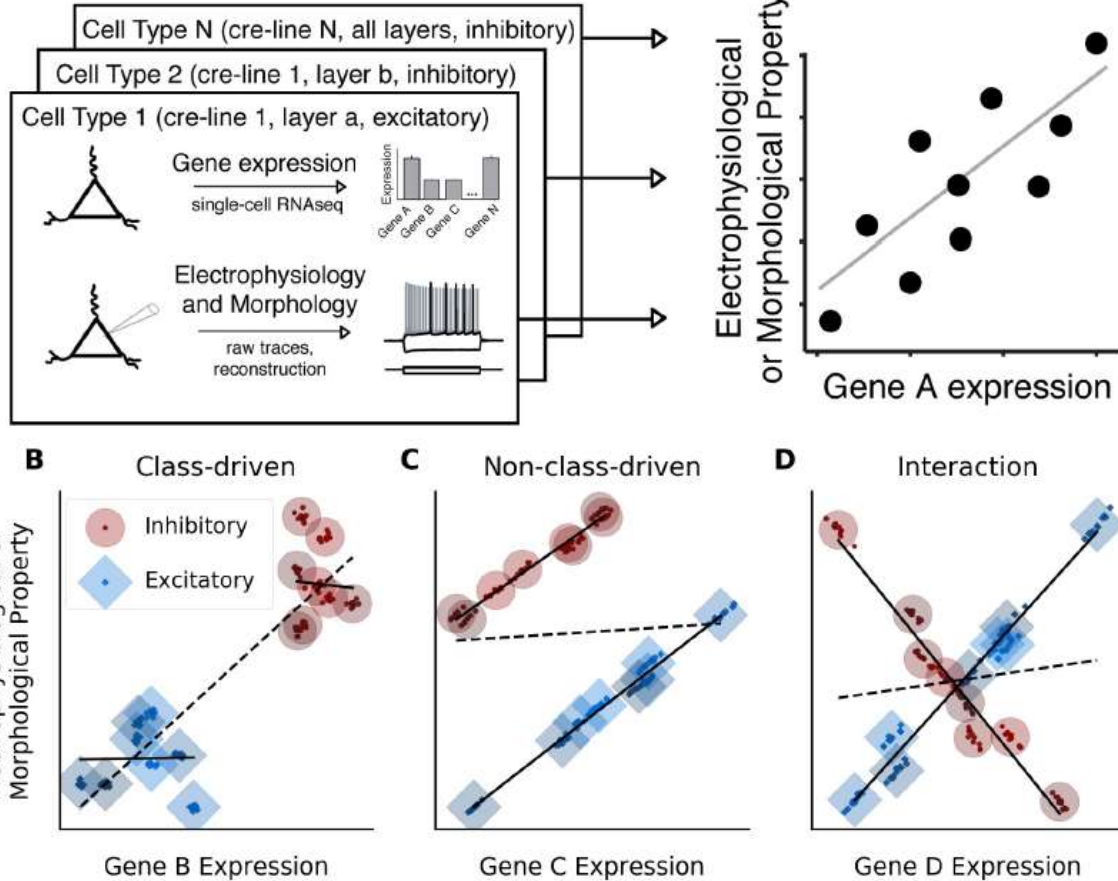
Build a standardized database and discover the rules through the

gradual accumulation of data





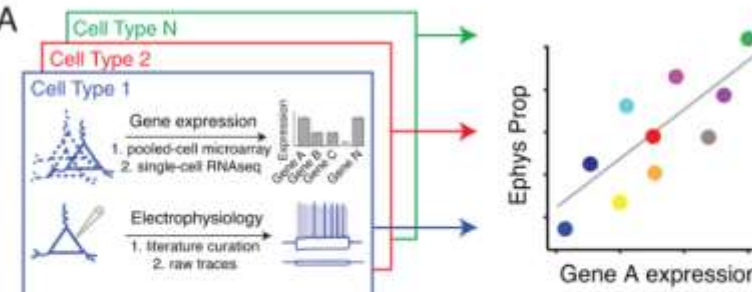
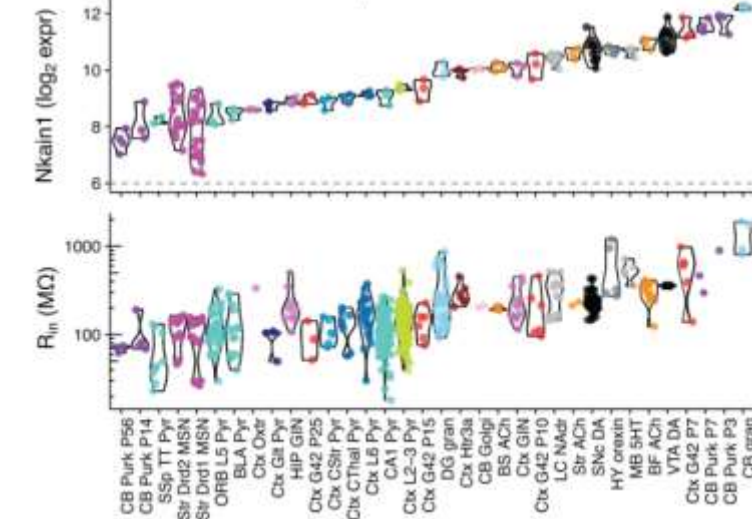
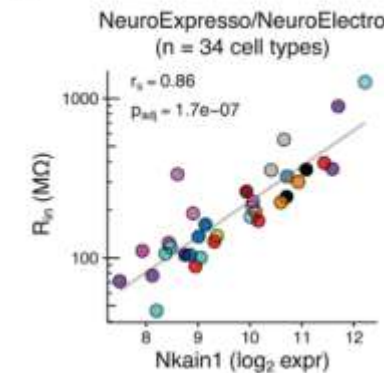
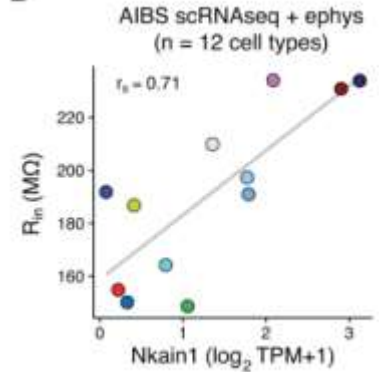
At present, both single-cell sequencing, morphological and electrophysiological data collection are based on transgenic mice, and the known marker phenotypes of transgenic mice are used to narrow the research scope

A

Claire Bomkamp et al. (2019) PLOS

By integrating morphological, electrophysiological and transcriptome data sets obtained from cells labeled with different transgenic mice, the association possibility was inferred, and direct experimental verification was conducted by patch-PCR, patch-seq and other low-throughput techniques that directly correlated multidimensional information

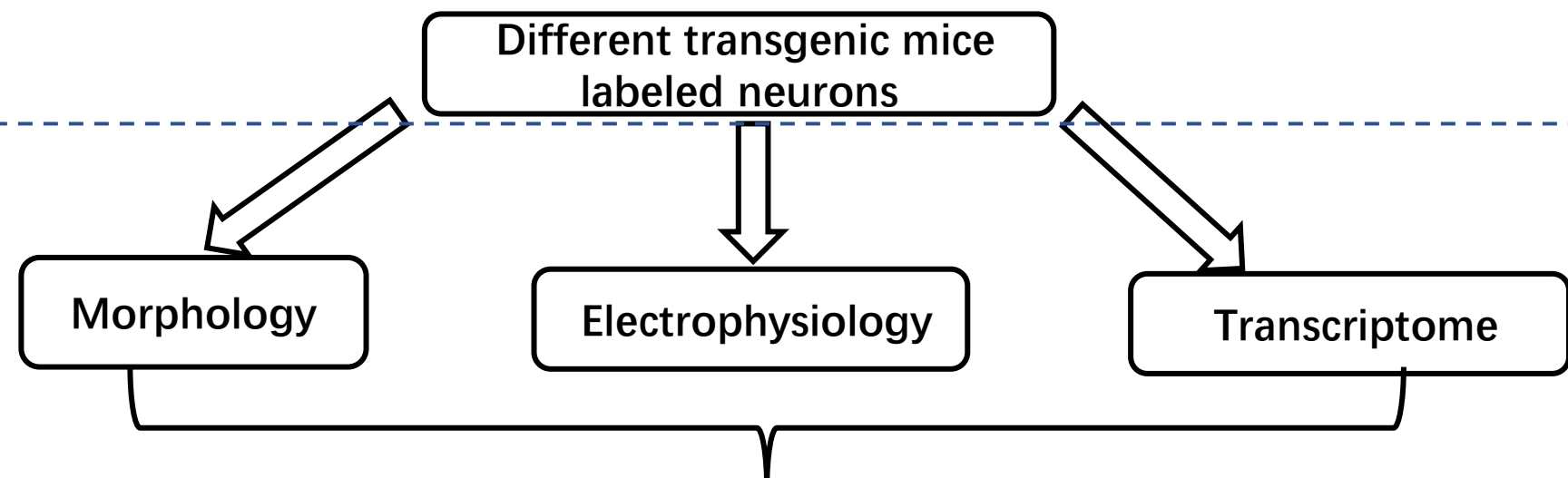
2024/4/7

A**B****C****D**

Shreejoy J. Tripathy et al. (2017) PLOS

192

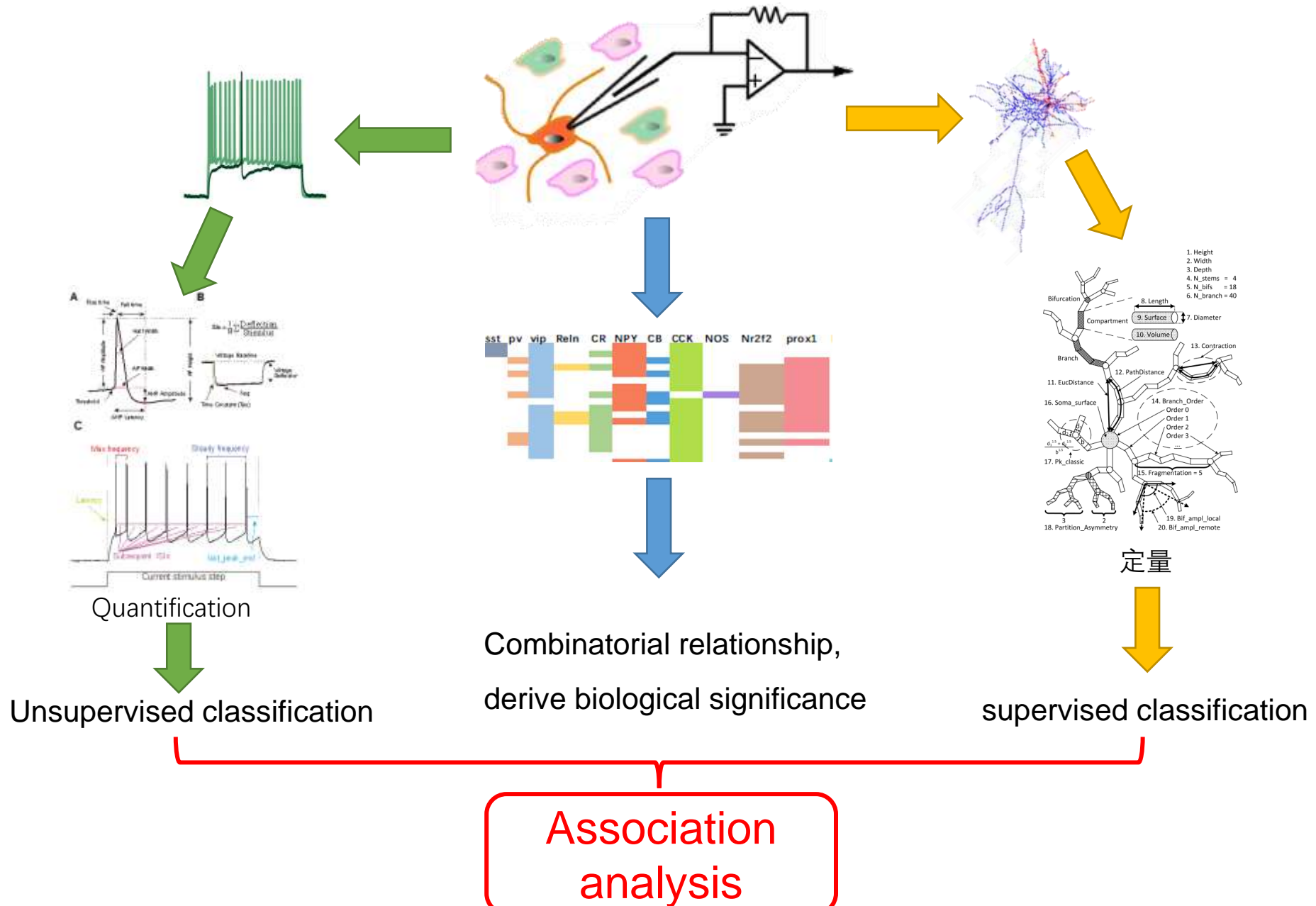
Build
standardized
databases to
accumulate
large amounts
of data through
separate
records and
high-
throughput
technology

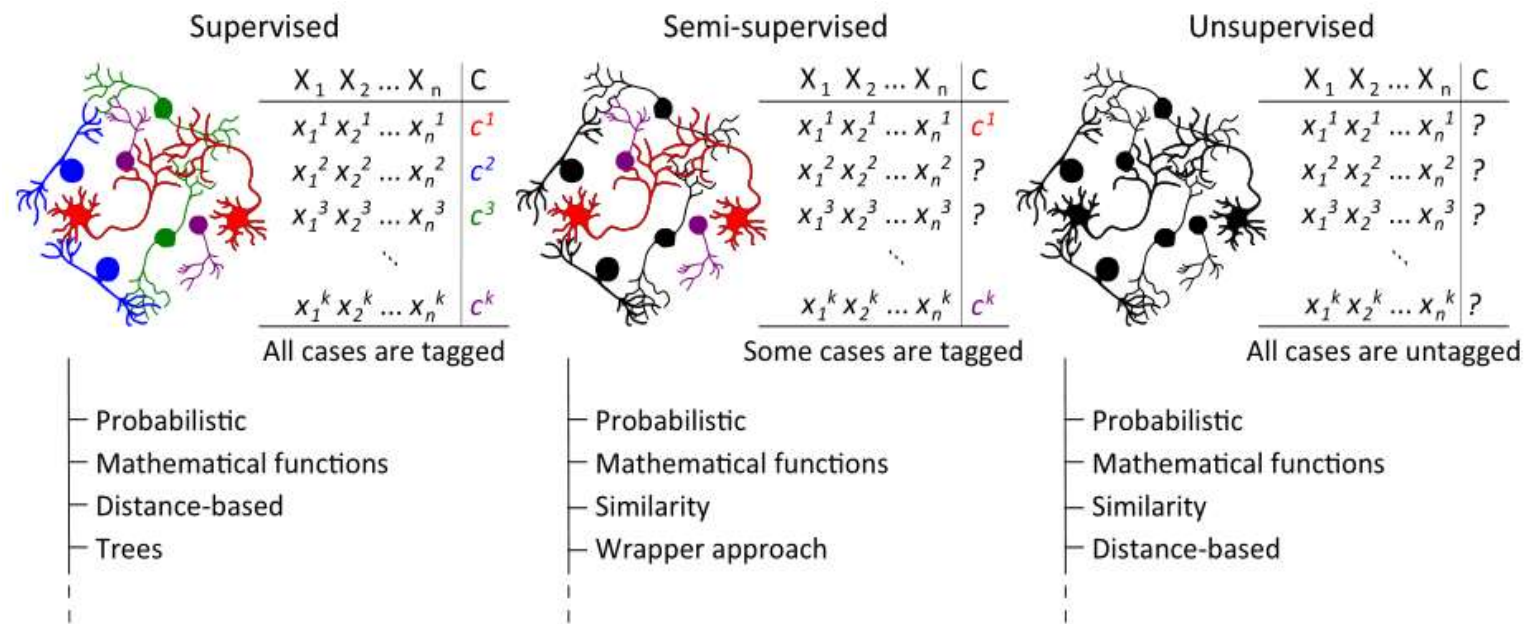


- **The throughput of Patch-PCR is too low, which is currently unfavorable for the broad coverage of intermediate neurons in the project**
- **The project's direct use of patch-PCR determines the biological significance based on marker selection, which needs to be carefully considered.**

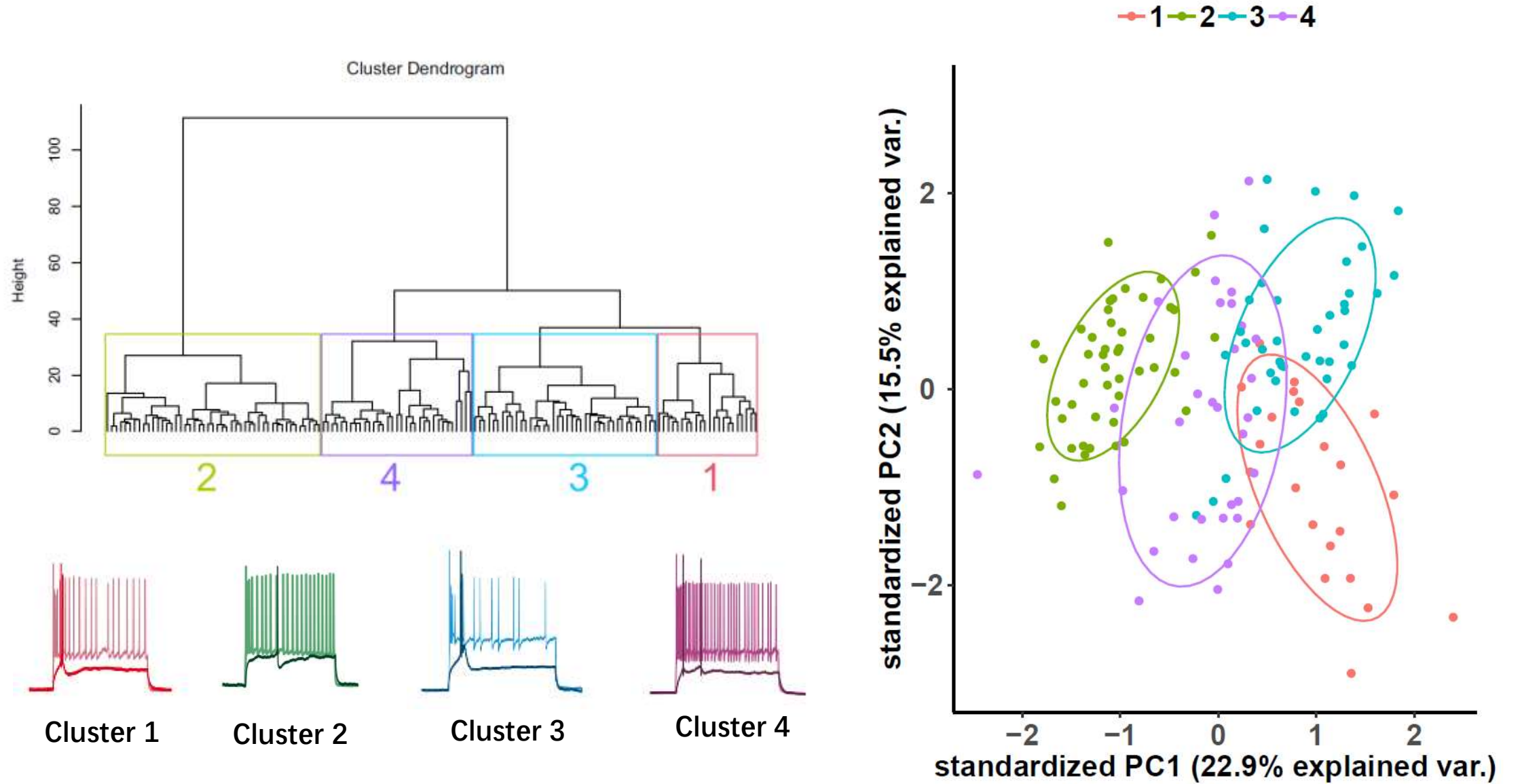
Prediction of the relationship between phenotype and gene expression

According to the new phenotype and gene relationship, the new characteristic markers were made for further study and derivation



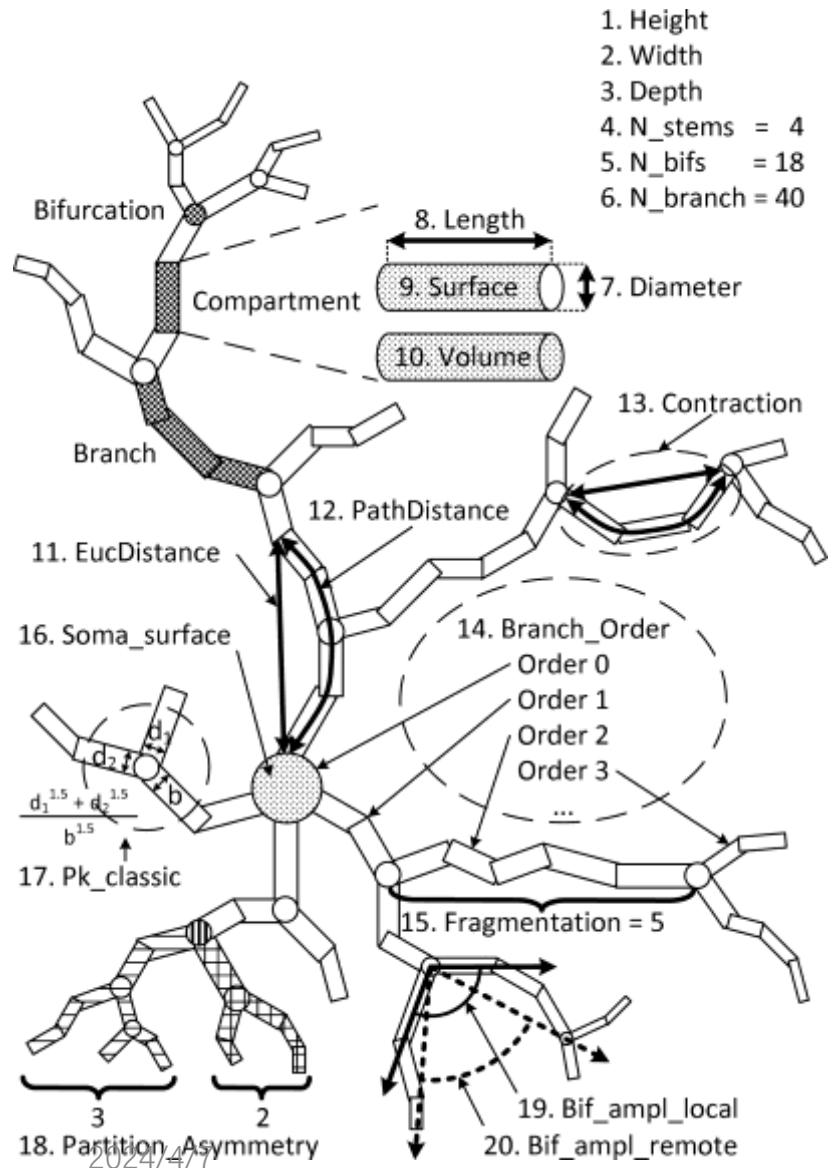


- Electrophysiological data is easily clustered by machines due to its natural clustering properties.
- Electrophysiological data is sensitive to recording conditions, and using publicly available database data to construct a training set can affect classification due to recording conditions.
- Morphological data is complex, and relying solely on machine-driven natural clustering can result in significant bias.
- There is limited morphological data, which is not conducive to natural clustering.
- Therefore, electrophysiological data is processed through unsupervised classification, while morphological data is used to build classifiers through supervised classification using publicly available datasets.



少娜师姐数据

Morphological quantization parameter extraction



mouse strain	Reconstruction cell numbers
Chat	21
Htr3a	37
Ndnf	16
PV	61
Vip	15
Sst	39
Nos1 Sst	16
Total	205

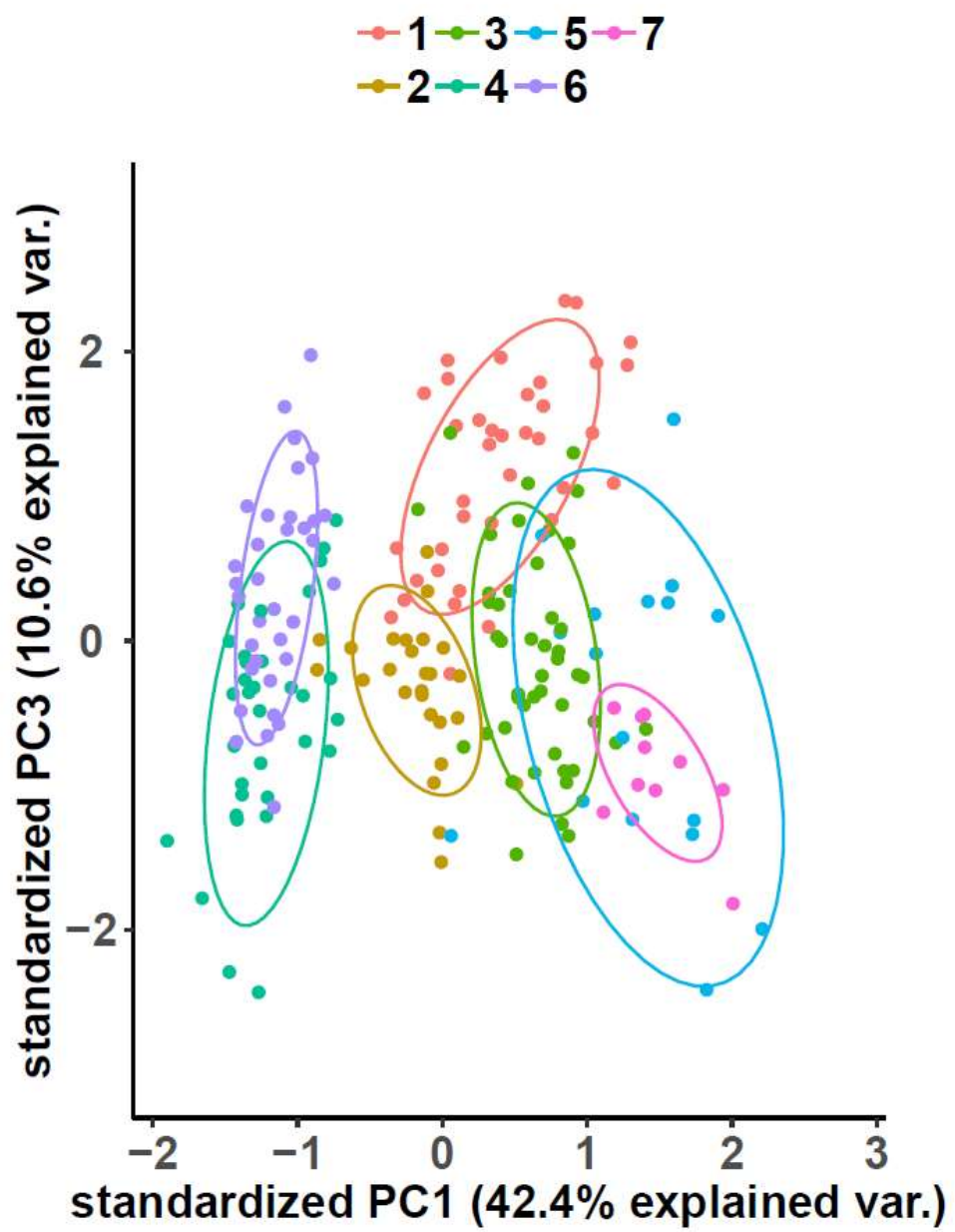
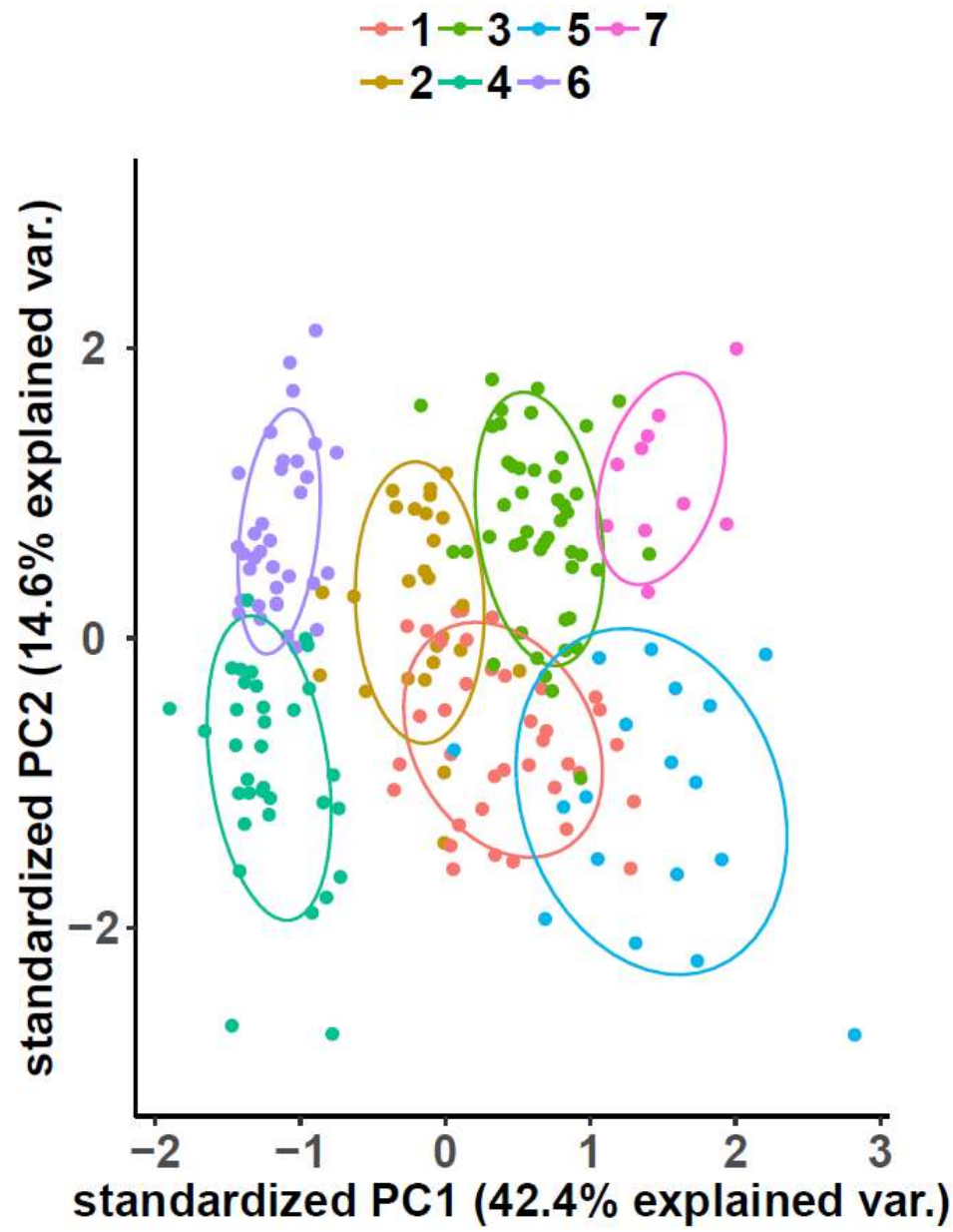
NeuroM

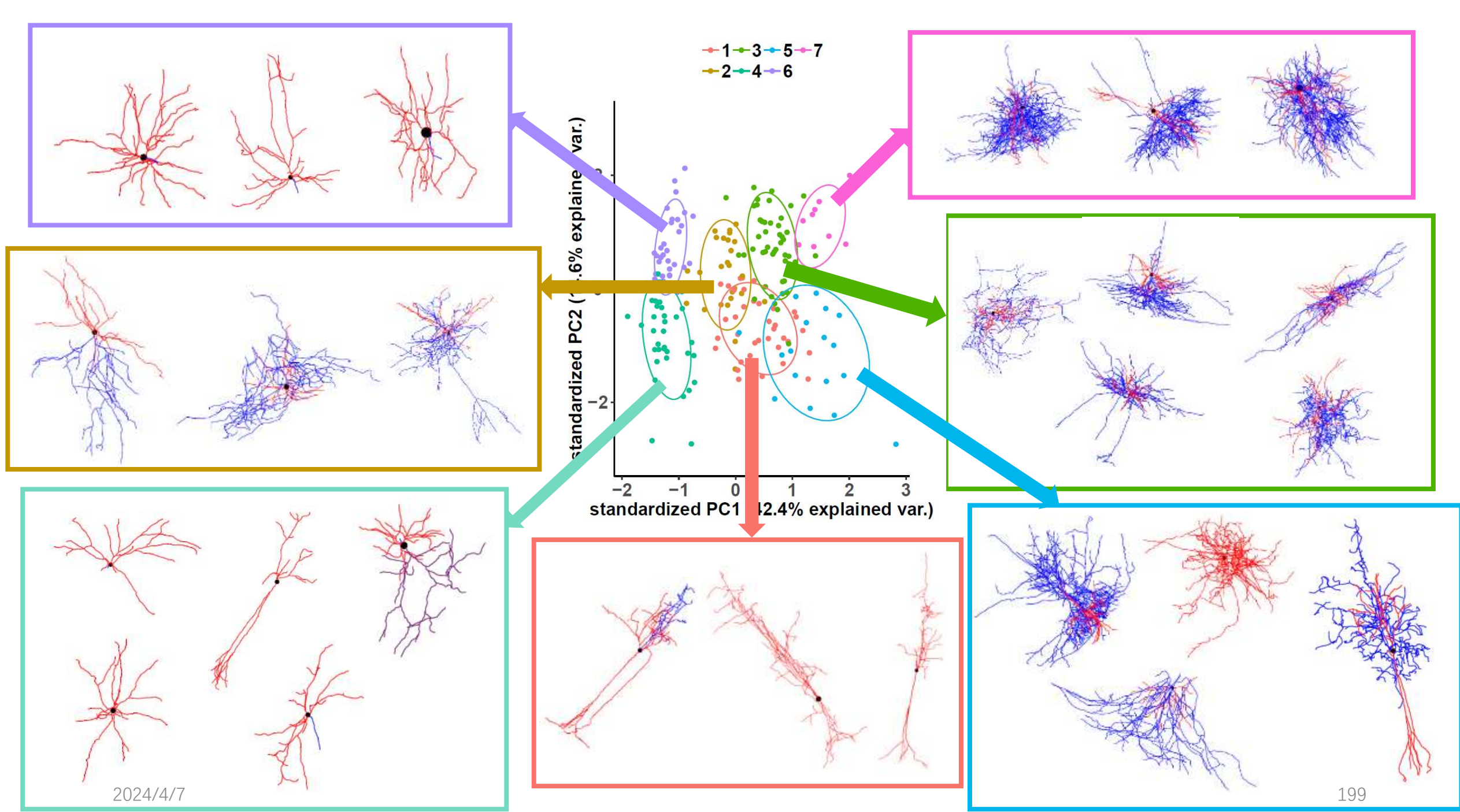
```

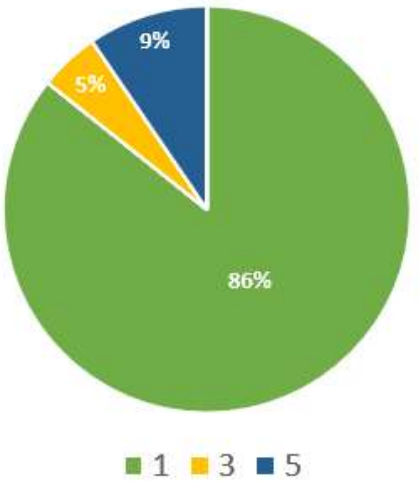
INFO: =====
INFO: File: 313861608.swc
INFO: Is single tree PASS
INFO: Has soma points PASS
INFO: Has sequential ids PASS
INFO: Has increasing ids PASS
INFO: Has valid soma PASS
INFO: Has valid neurites PASS
INFO: Has basal dendrite PASS
INFO: Has axon PASS
ERROR: Has apical dendrite FAIL
INFO: Has all nonzero segment lengths PASS
INFO: Has all nonzero section lengths PASS
INFO: Has all nonzero neurite radii PASS
ERROR: Has all monotonic neurites FAIL
INFO: Has nonzero soma radius PASS
ERROR: ALL FAIL
INFO: =====

```

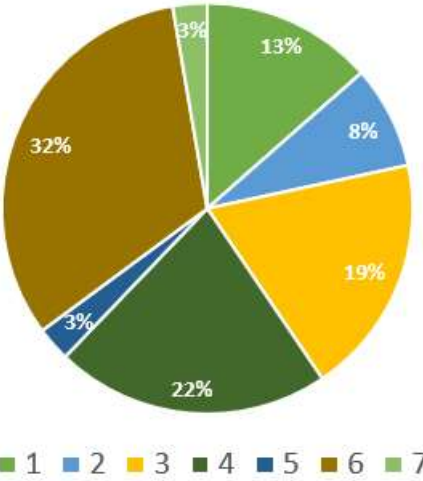




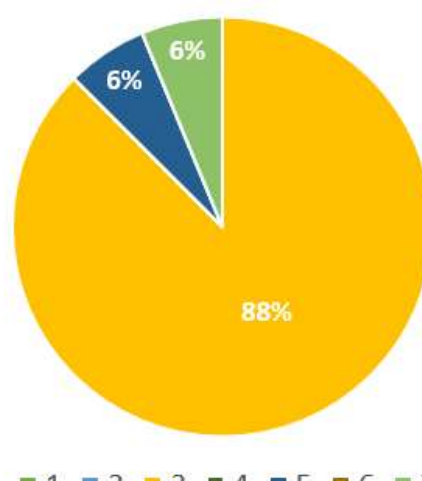




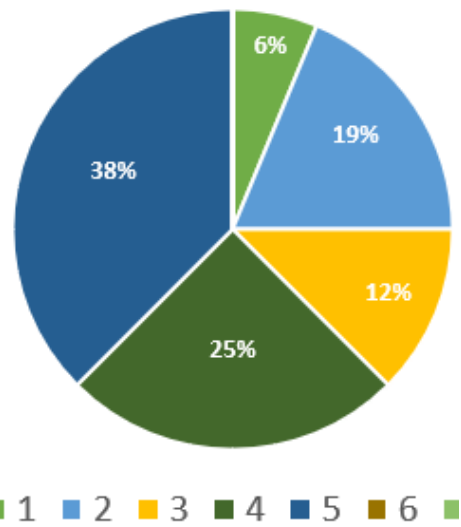
Chat



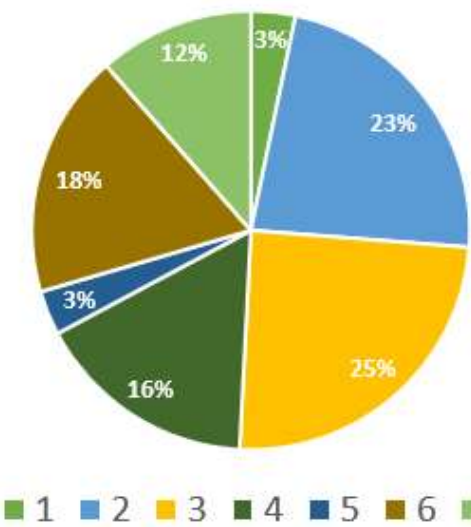
Htr3a



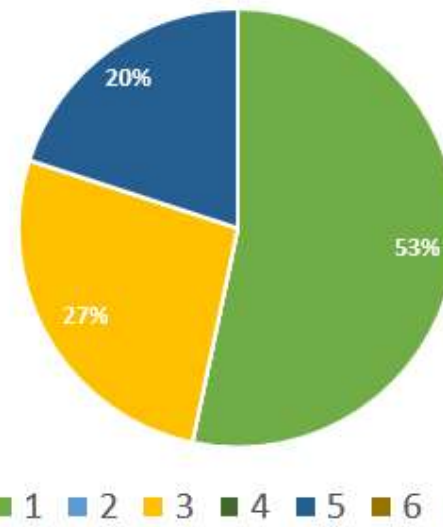
Ndnf



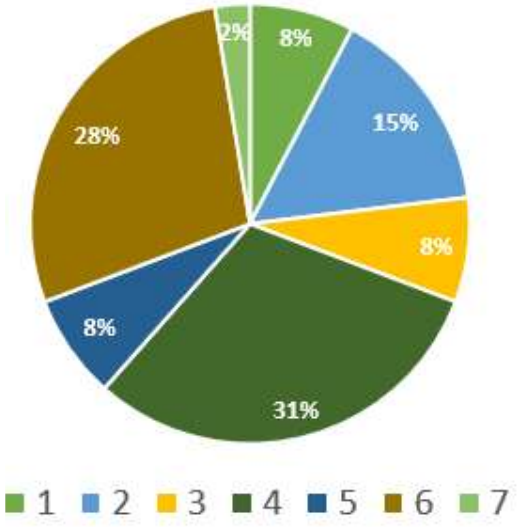
Nos1|Sst



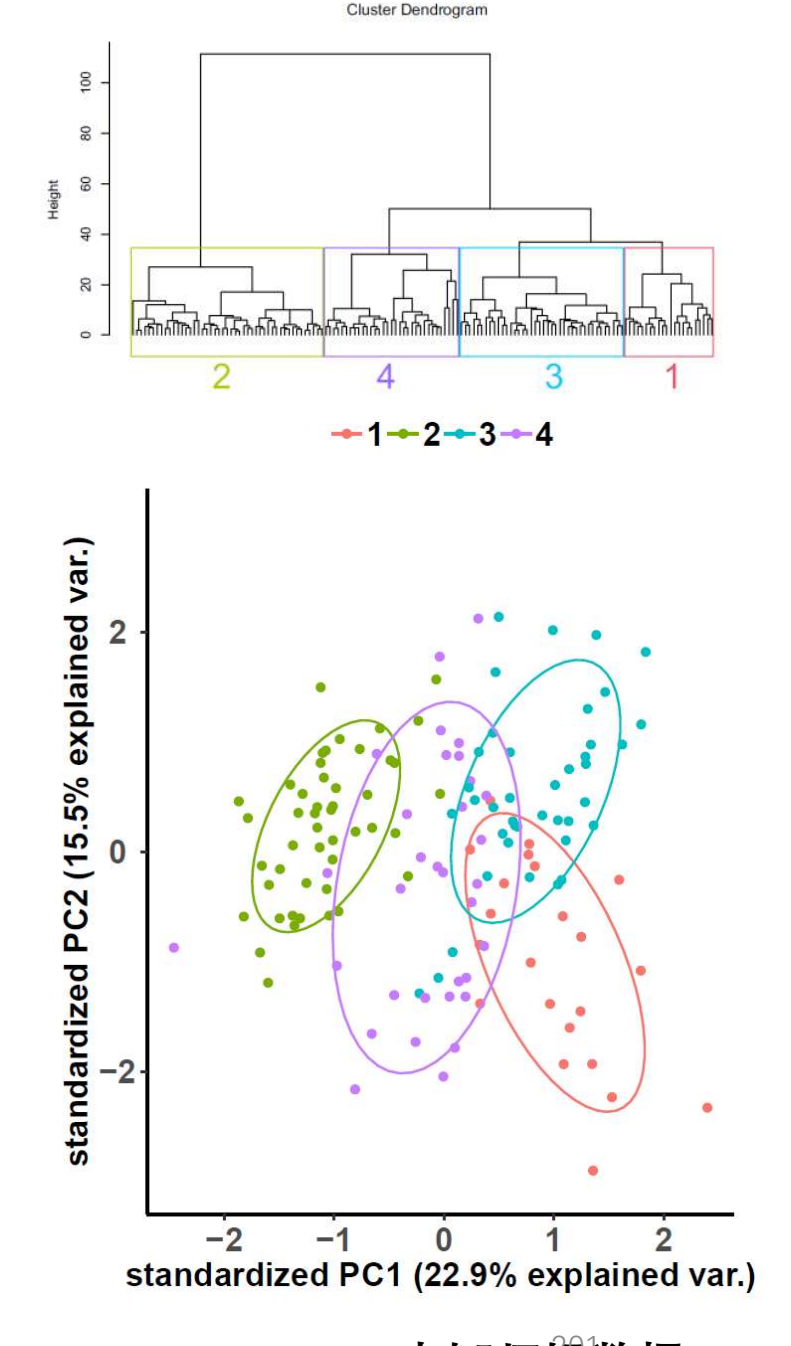
PV



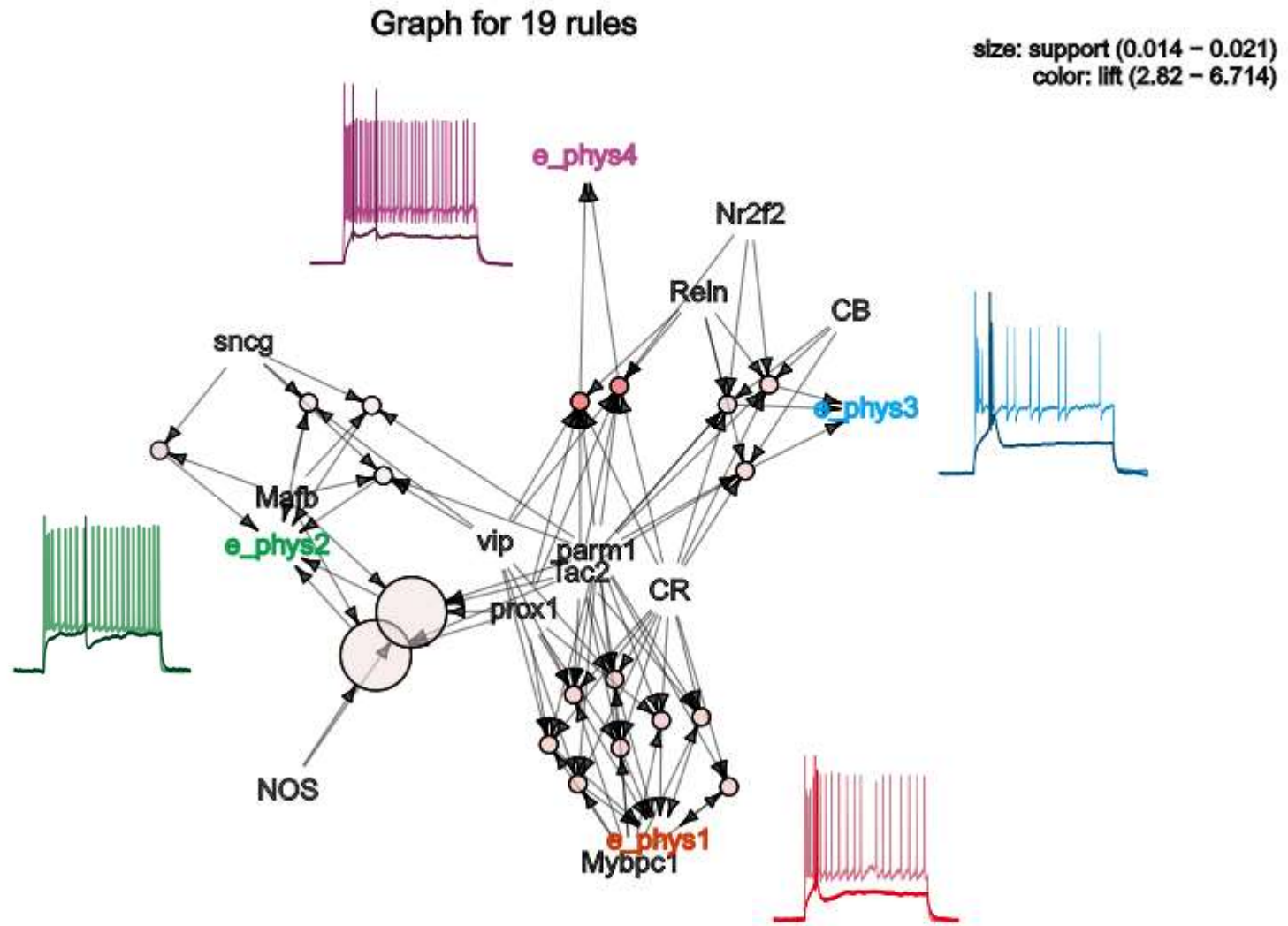
Vip



Sst



Apriori association analysis

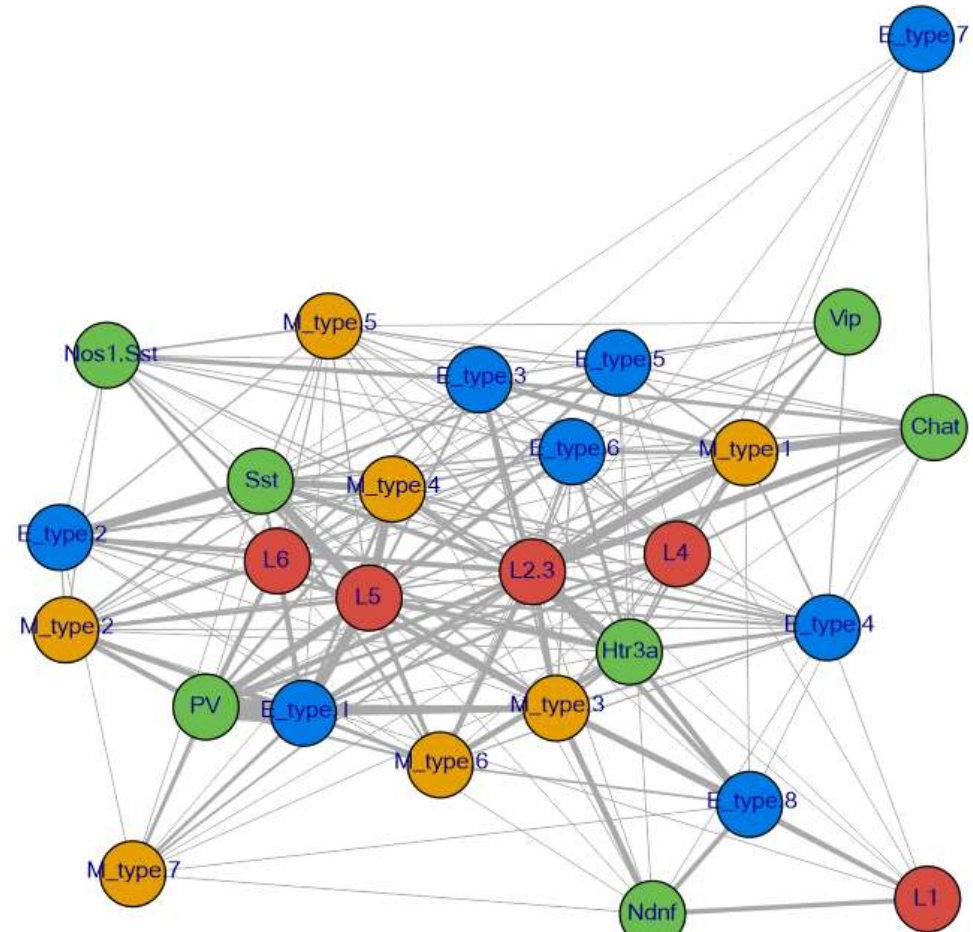


lhs	rhs
CR,parm1,Mybpc1	e_phys1
CR,Tac2,parm1,Mybpc1	e_phys1
vip,CR,parm1,Mybpc1	e_phys1
CR,prox1,parm1,Mybpc1	e_phys1
vip,CR,Tac2,parm1,Mybpc1	e_phys1
CR,prox1,Tac2,parm1,Mybpc1	e_phys1
vip,CR,prox1,parm1,Mybpc1	e_phys1
vip,CR,prox1,Tac2,parm1,Mybpc1	e_phys1
Mafb,sncg	e_phys2
Mafb,parm1,sncg	e_phys2
vip,Mafb,sncg	e_phys2
NOS,prox1,Mafb,Tac2	e_phys2
vip,Mafb,parm1,sncg	e_phys2
NOS,prox1,Mafb,Tac2,parm1	e_phys2
Reln,CR,CB,Nr2f2,parm1	e_phys3
Reln,CR,CB,Tac2,parm1	e_phys3
Reln,CR,CB,Nr2f2,Tac2,parm1	e_phys3
vip,Reln,CR,prox1,Tac2,parm1	e_phys4
vip,Reln,CR,Nr2f2,prox1,Tac2,parm1	e_phys4

少娜师姐数据

- The support distribution of the current data is very low.
- Due to the numerous variables and the multitude of possible rule combinations, the repetition of each rule is insufficient to support its authenticity. It may require more data to establish the validity of the rules.

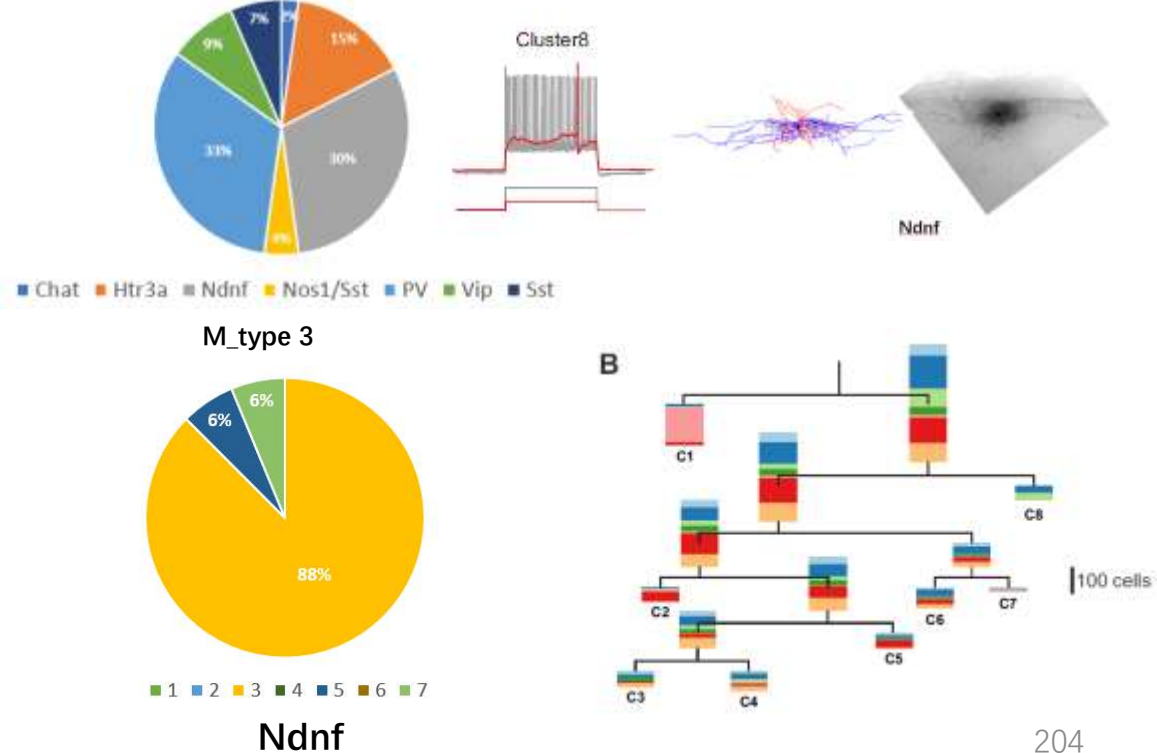
Complex network analysis



General diagram of morphology, electrophysiology,
Marker, layer distribution network

2024/4/7

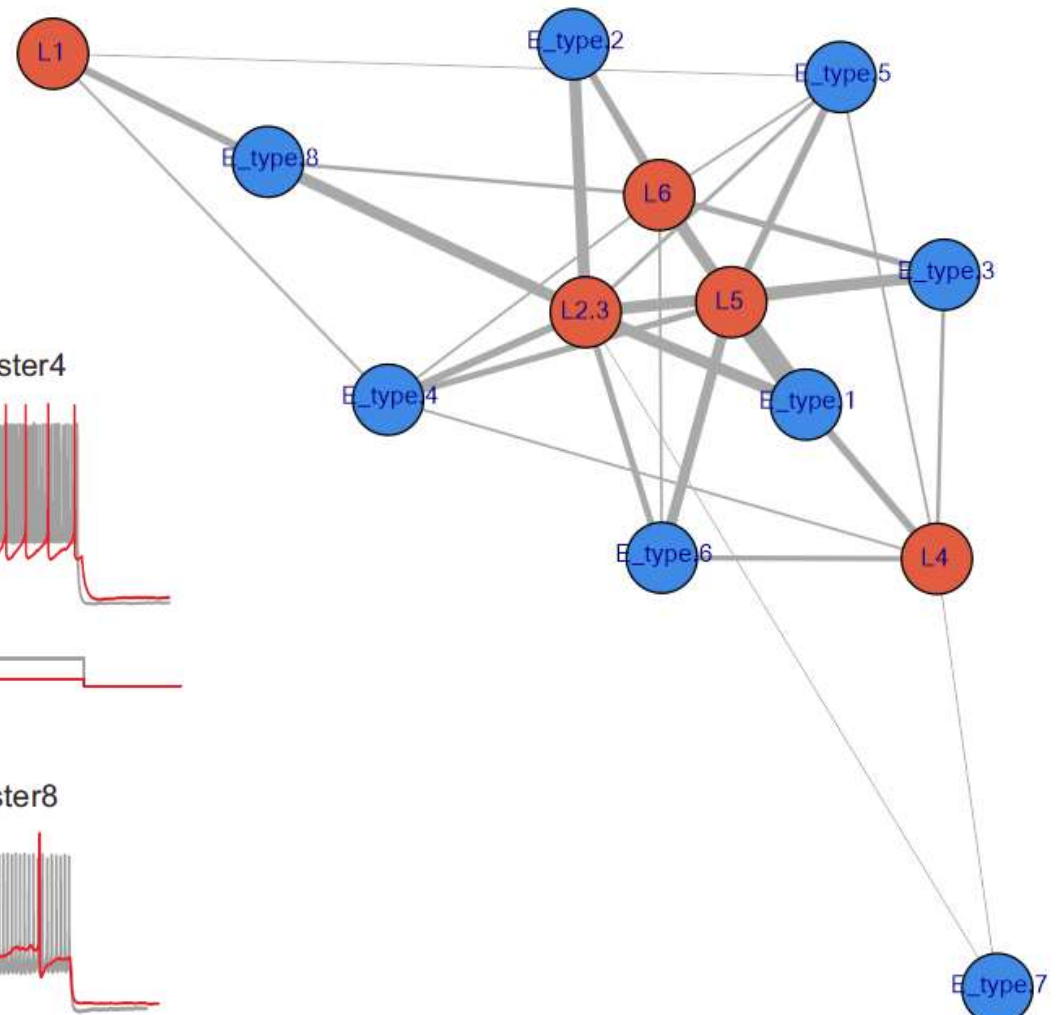
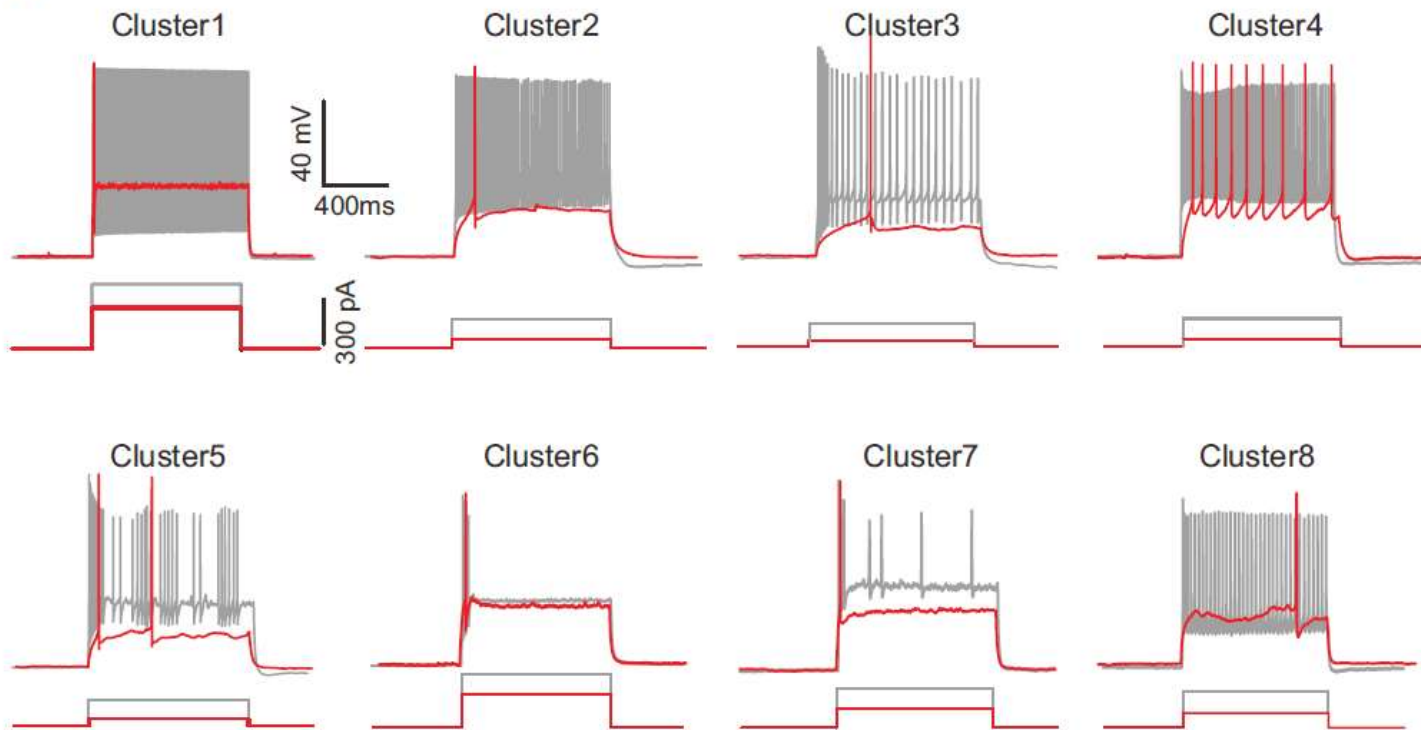
From a layer perspective, L1 being distant from the central network indicates that the neurons in L1 are relatively purer in terms of layer distribution, markers, electrophysiology, and morphology compared to other layers. In terms of weights, there is a tendency towards Ndnf, E_type 8, and M_type 3.

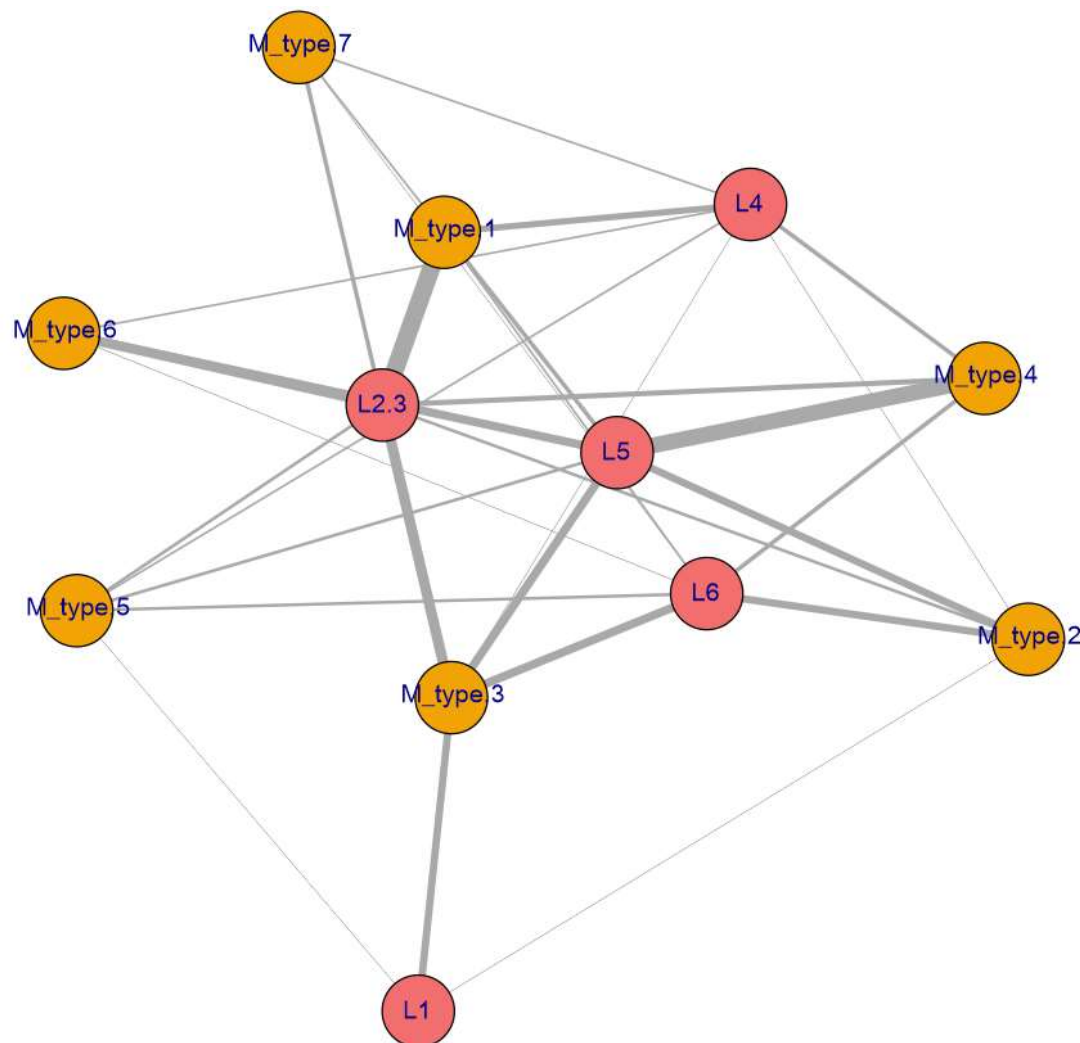


204

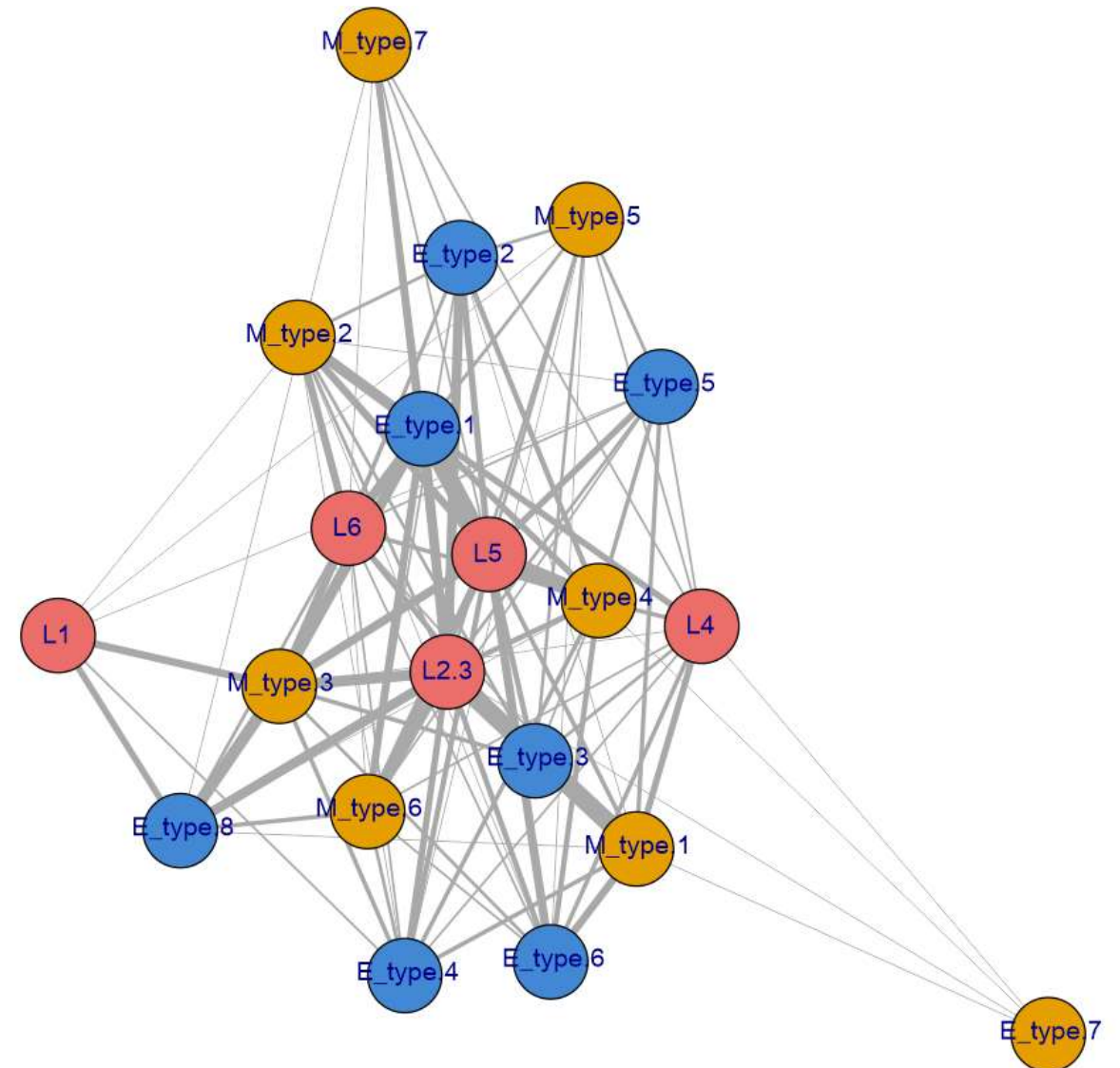
Electrophysiological, layer distribution network diagram

B



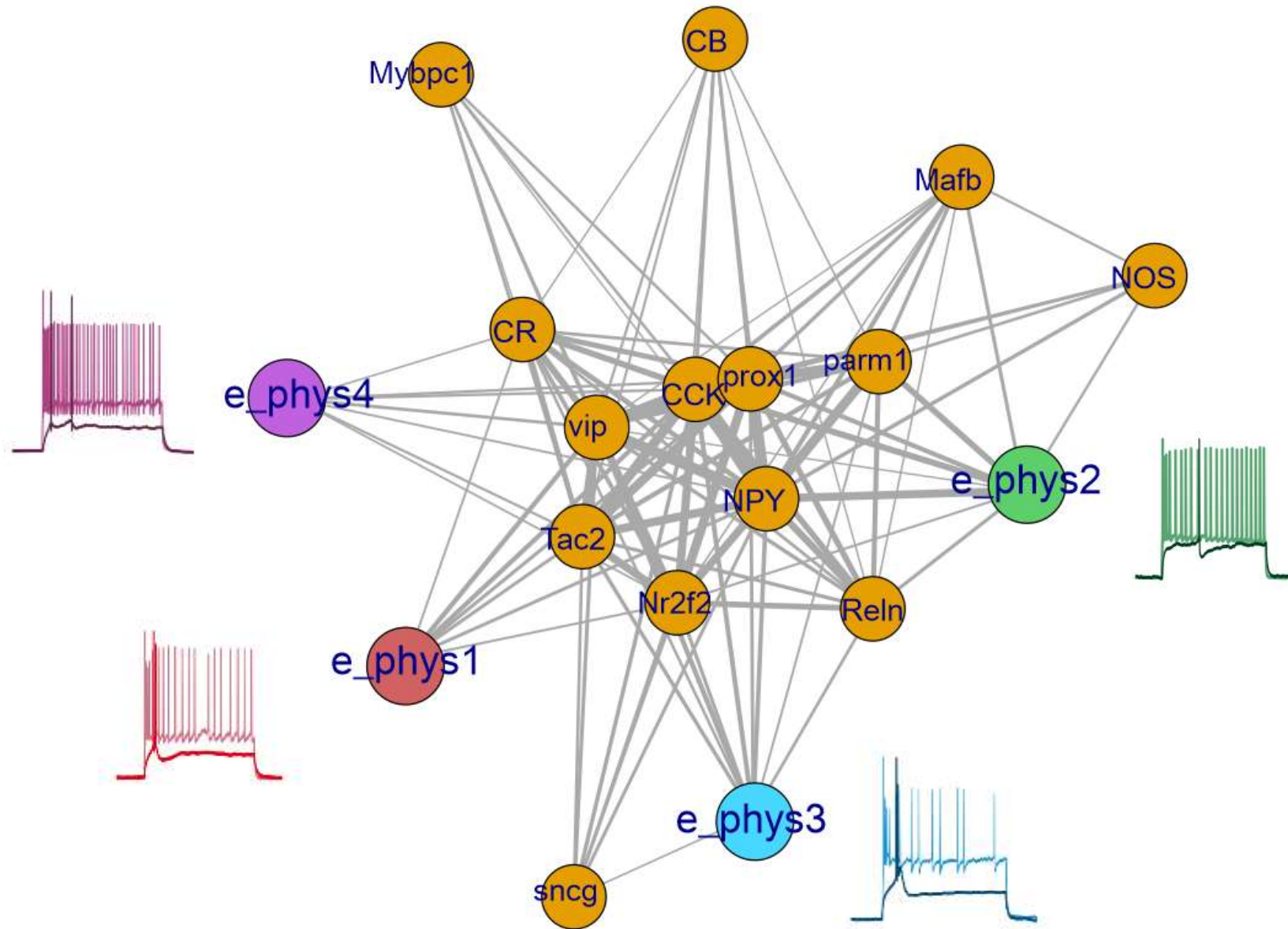


Morphology, layer distribution network diagram



Electrophysiology, morphology, layer distribution network diagram

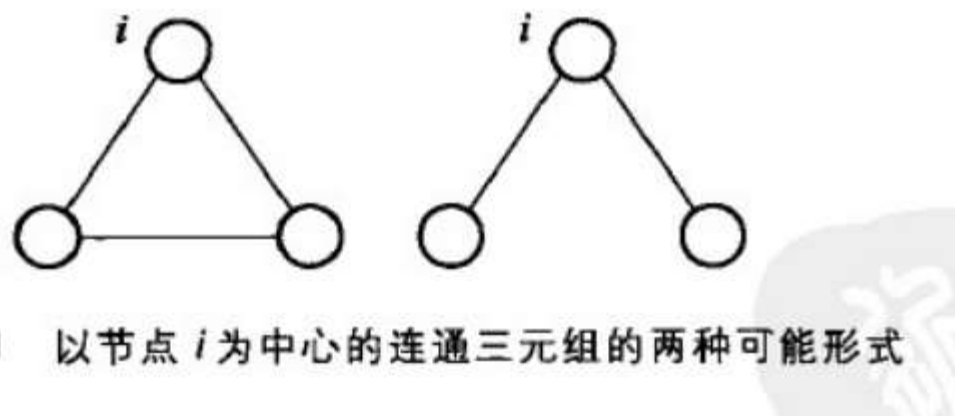
- In comparison to Apriori association analysis, complex network analysis is more suitable for the current situation.
- Complex network analysis requires further filtering of connections with low weights.
- It is necessary to further quantify the constructed network, and describe the relationships between different levels of information through network quantification.



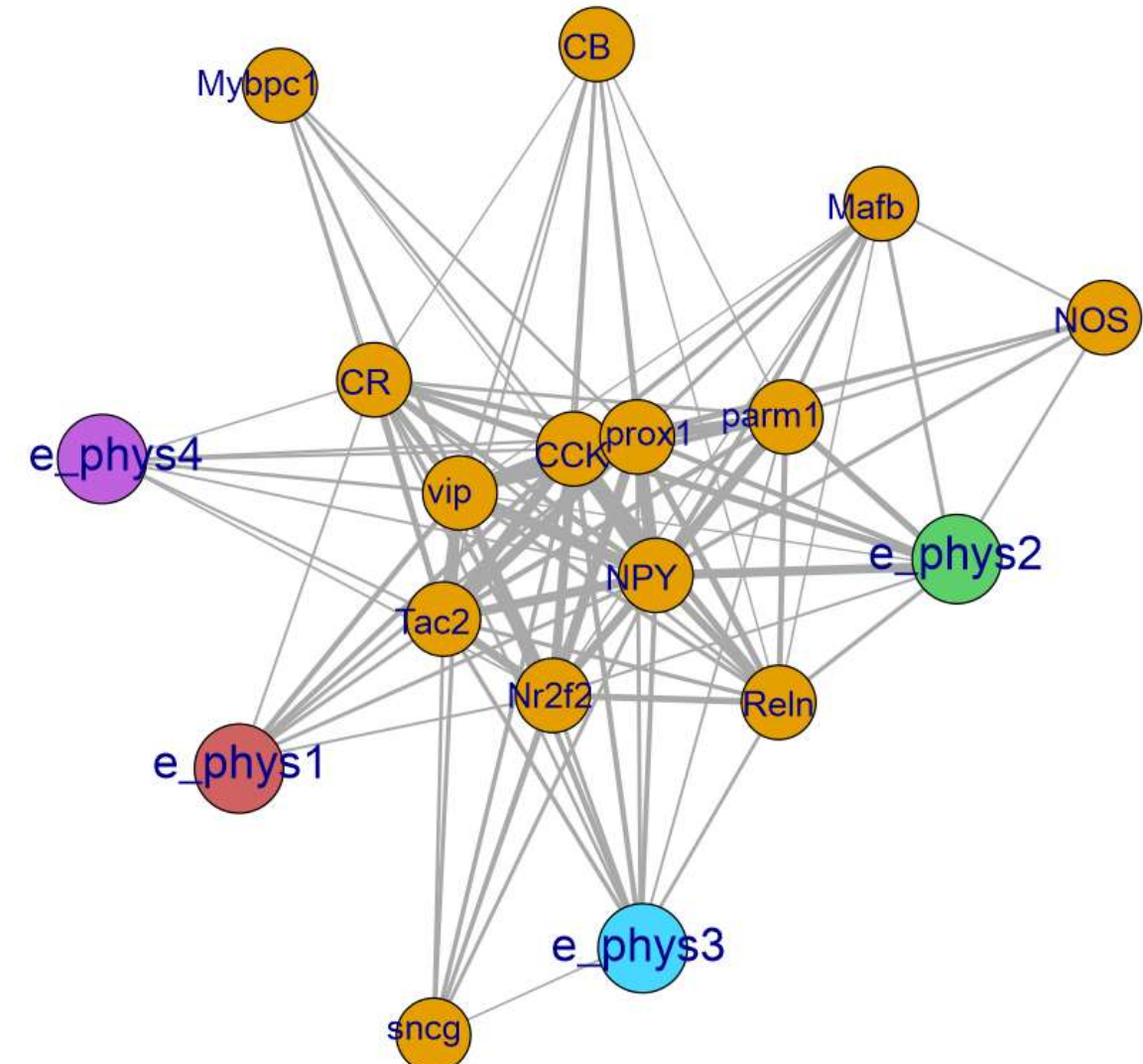
少娜师姐数据 (过滤了连接数低于10的边)

Clustering coefficient

$$C_i = \frac{\text{包含节点 } i \text{ 的三角形的数目}}{\text{以节点 } i \text{ 为中心的连通三元组的数目}}$$

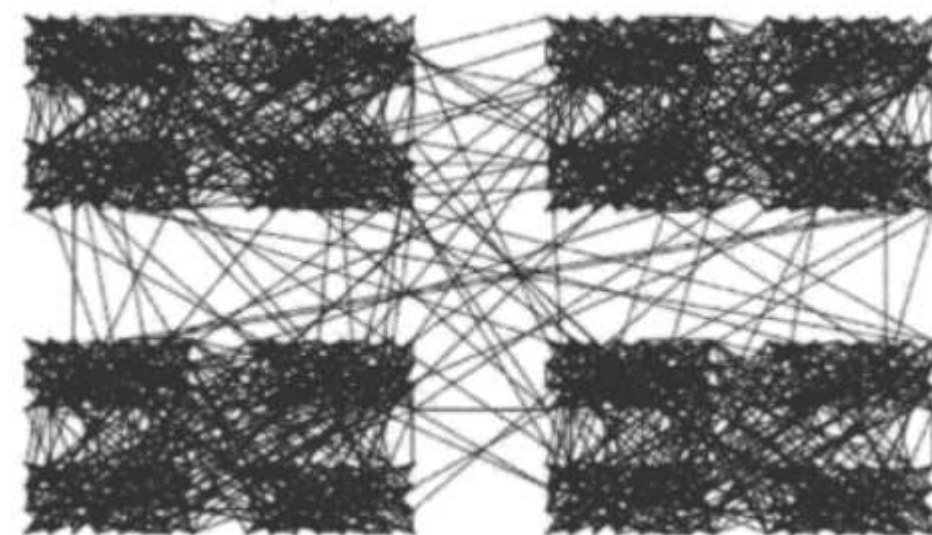
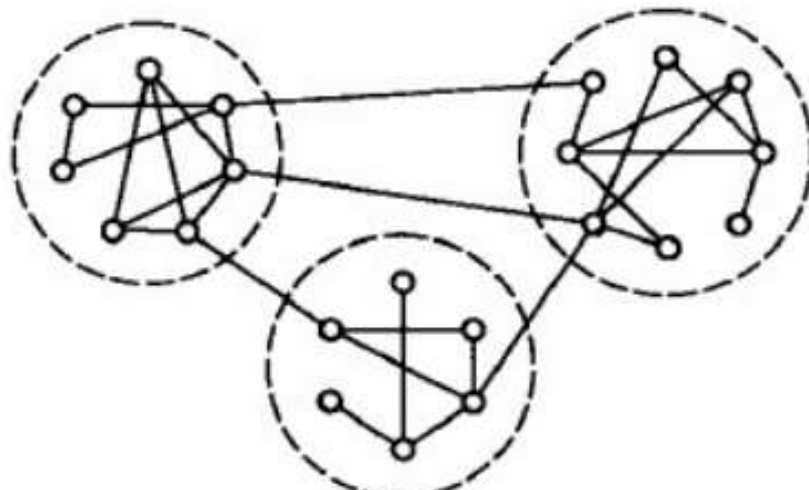


$$\tilde{C}_i = \frac{1}{k_i(k_i - 1)} \sum_{j,k} \omega_{ijk} a_{ij} a_{ik} a_{jk}.$$

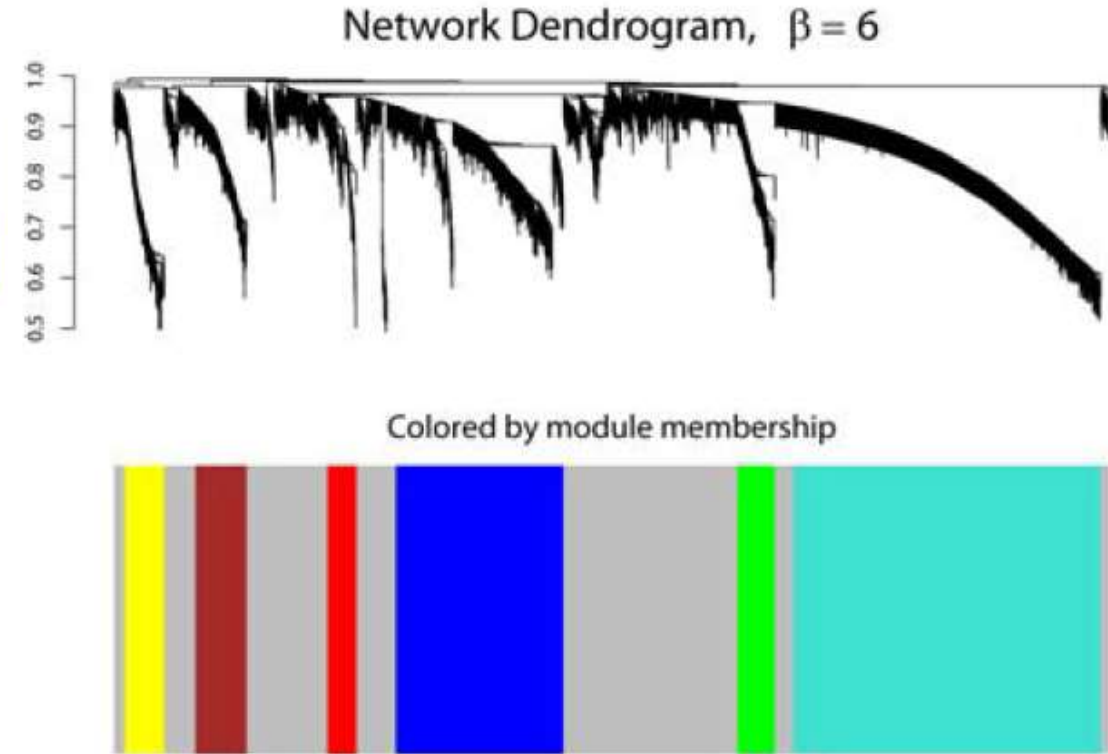
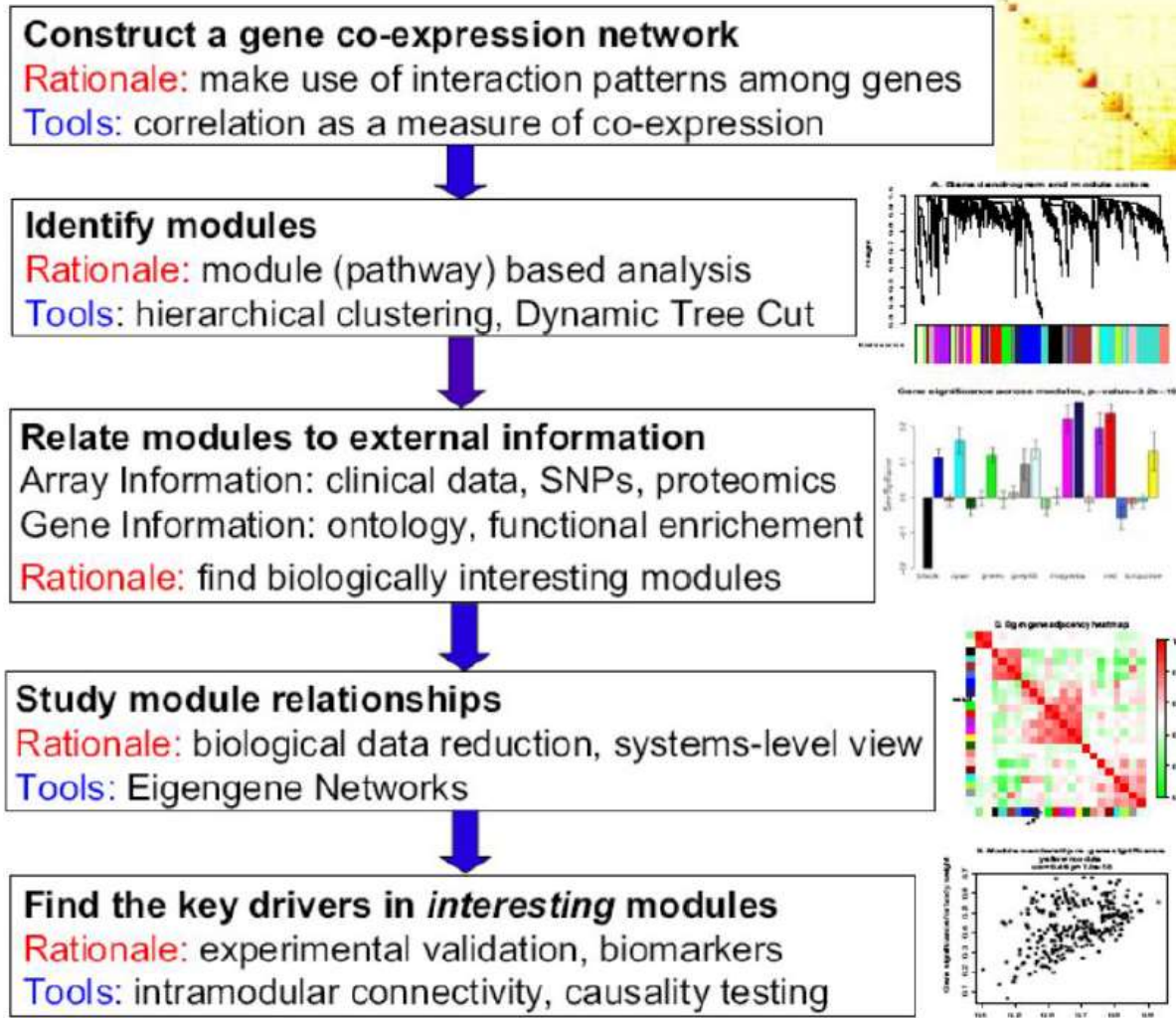


Complex network module analysis

Module analysis: It is commonly believed that networks may consist of multiple modules, where a module is a subnetwork characterized by dense internal connections and sparse connections between modules.



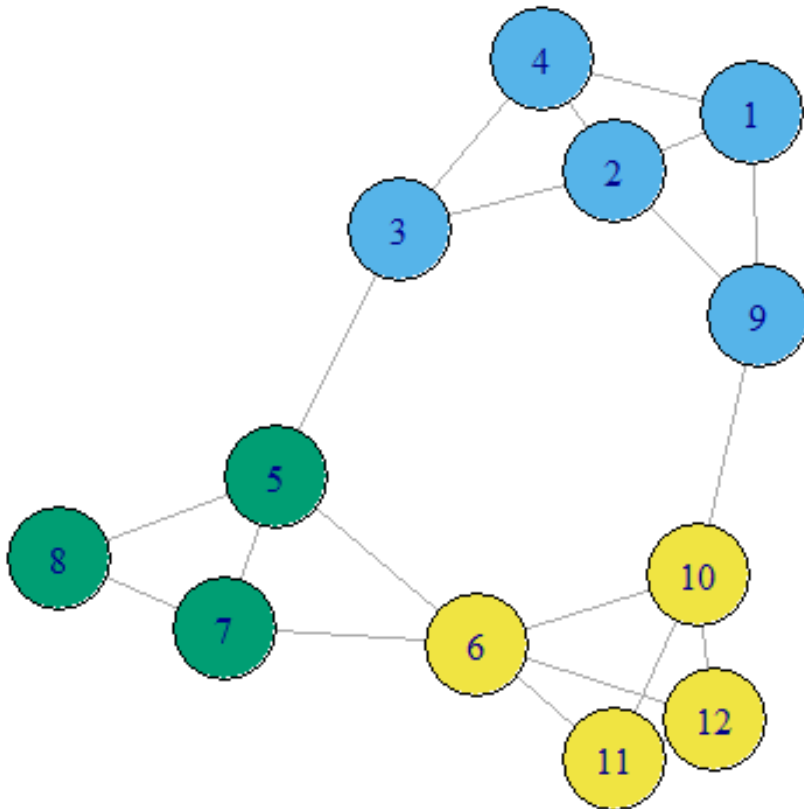
Overview of WGCNA methodology



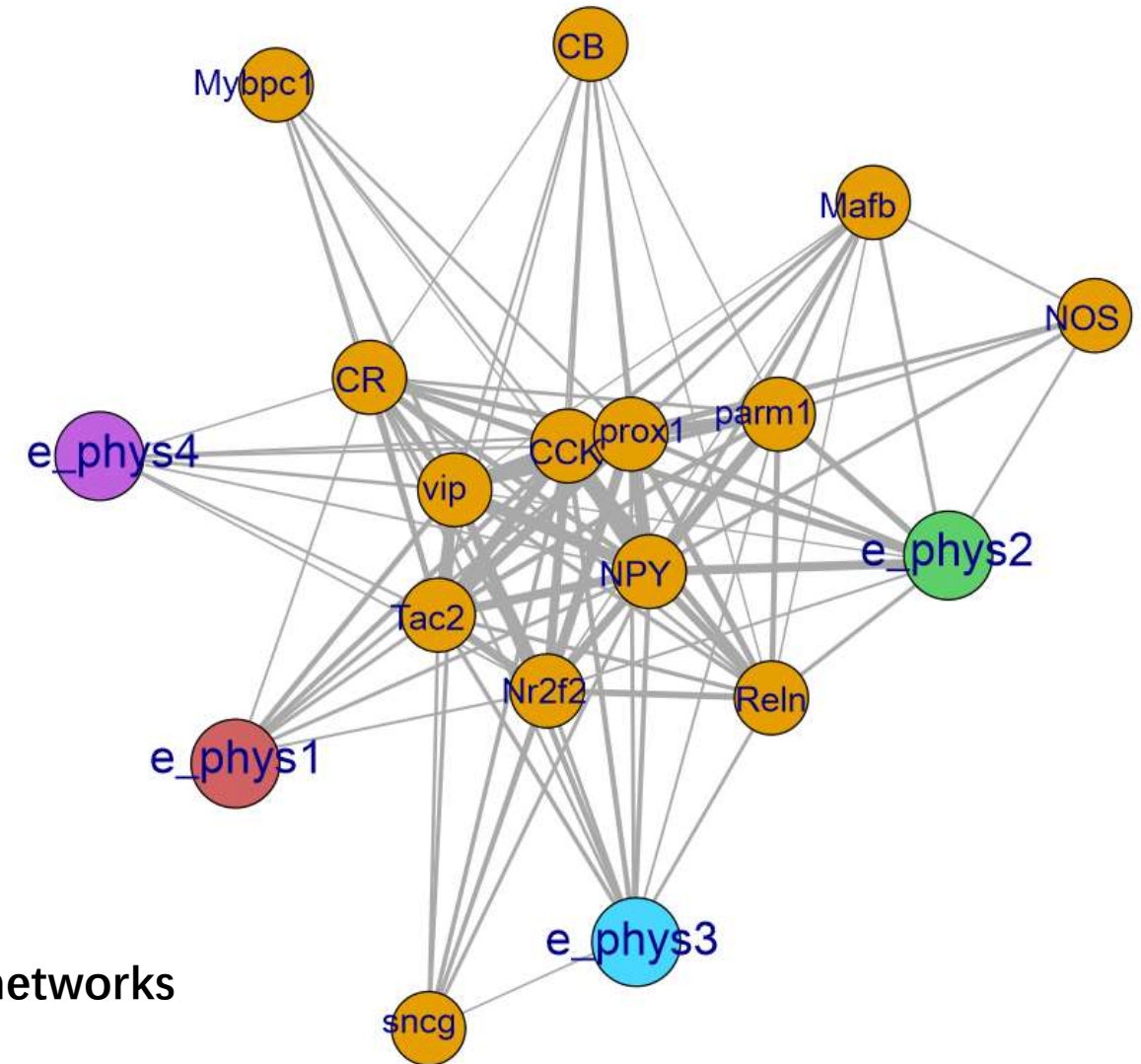
WGCNA (Weighted Co-Expression Network Analysis) is the idea of complex network module analysis

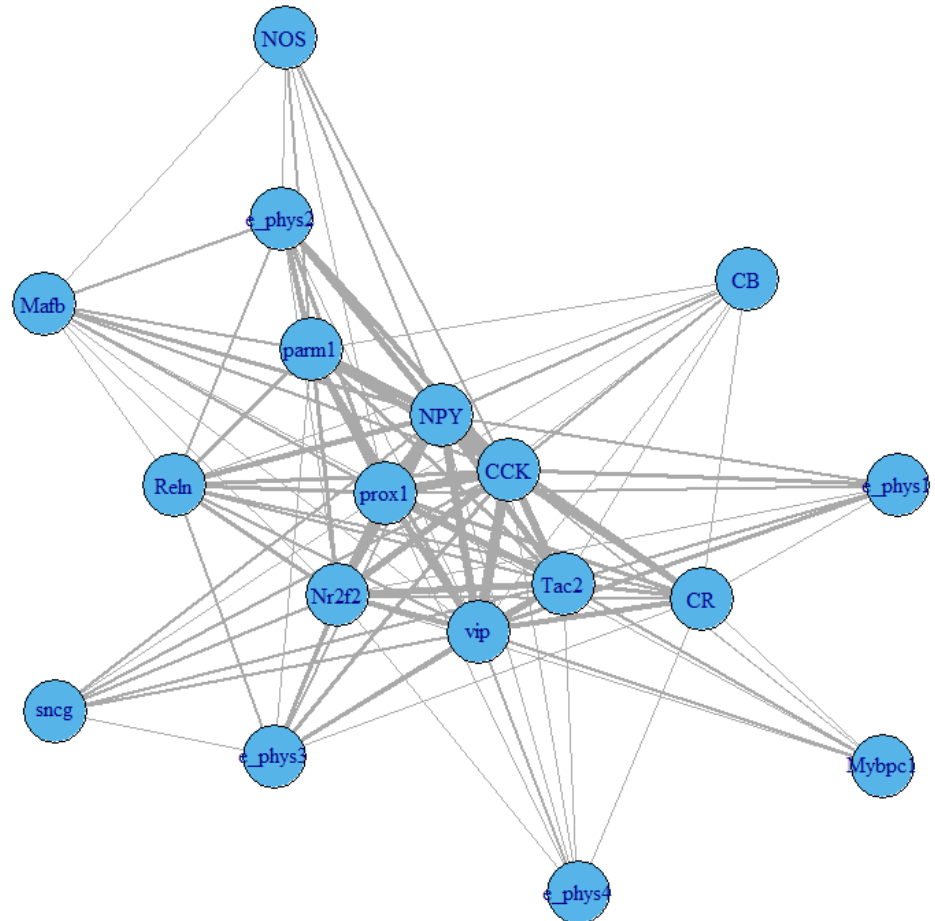
Current module partitioning algorithm

- **Edge.betweenness:** Module partitioning based on edge betweenness centrality.
- **Leading.eigenvector:** Module partitioning based on the module spectral strategy.
- **Fastgreedy:** F-N partitioning algorithm based on module degree score optimization.
- **Spinglass:** Partitioning algorithm based on positive and negative connections.
- **Walktrap:** Partitioning algorithm based on random walk.

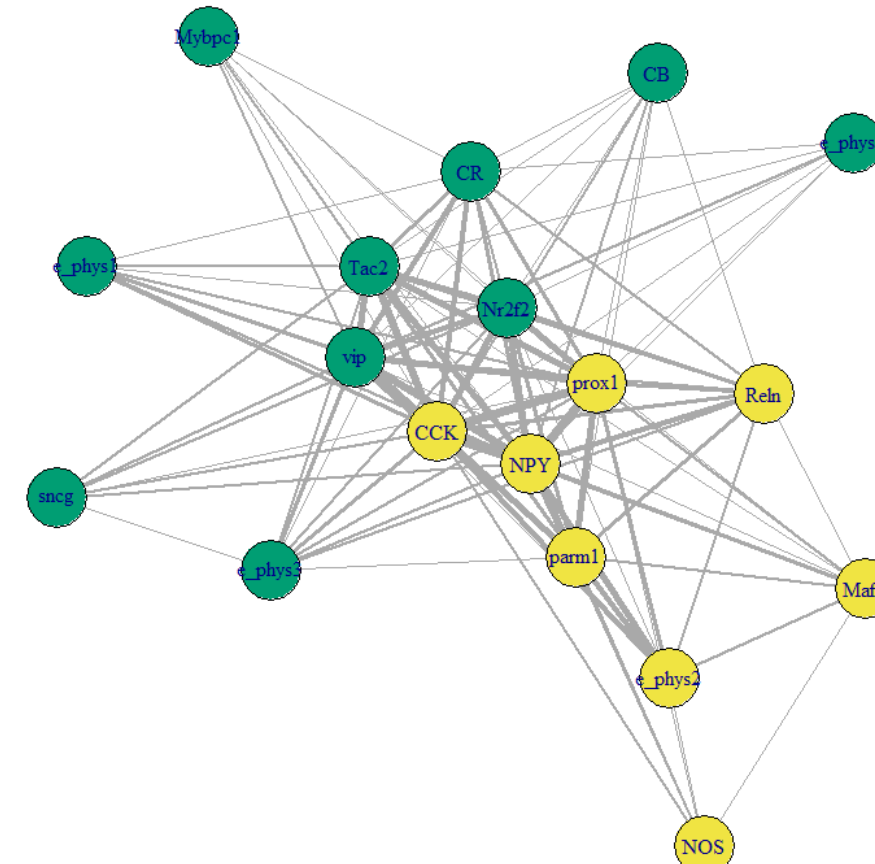


Edge.betweenness analysis of simple unweighted networks

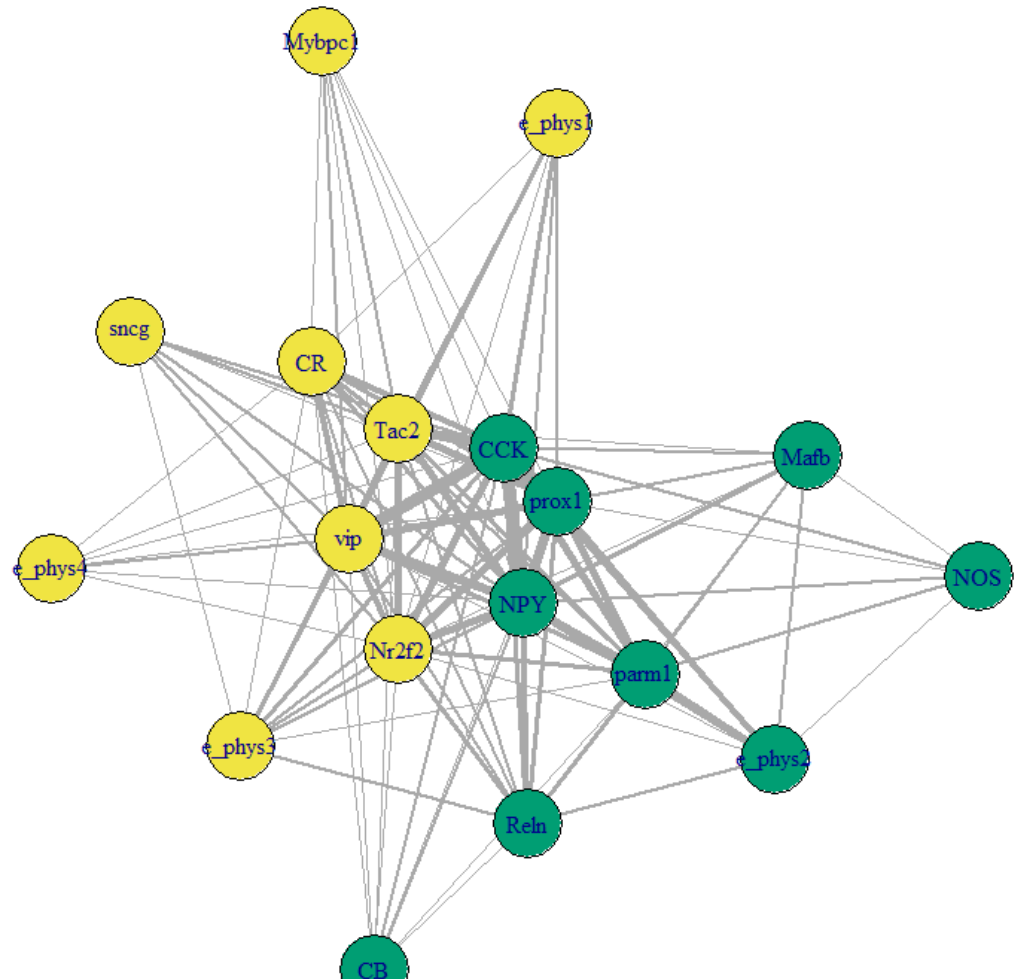




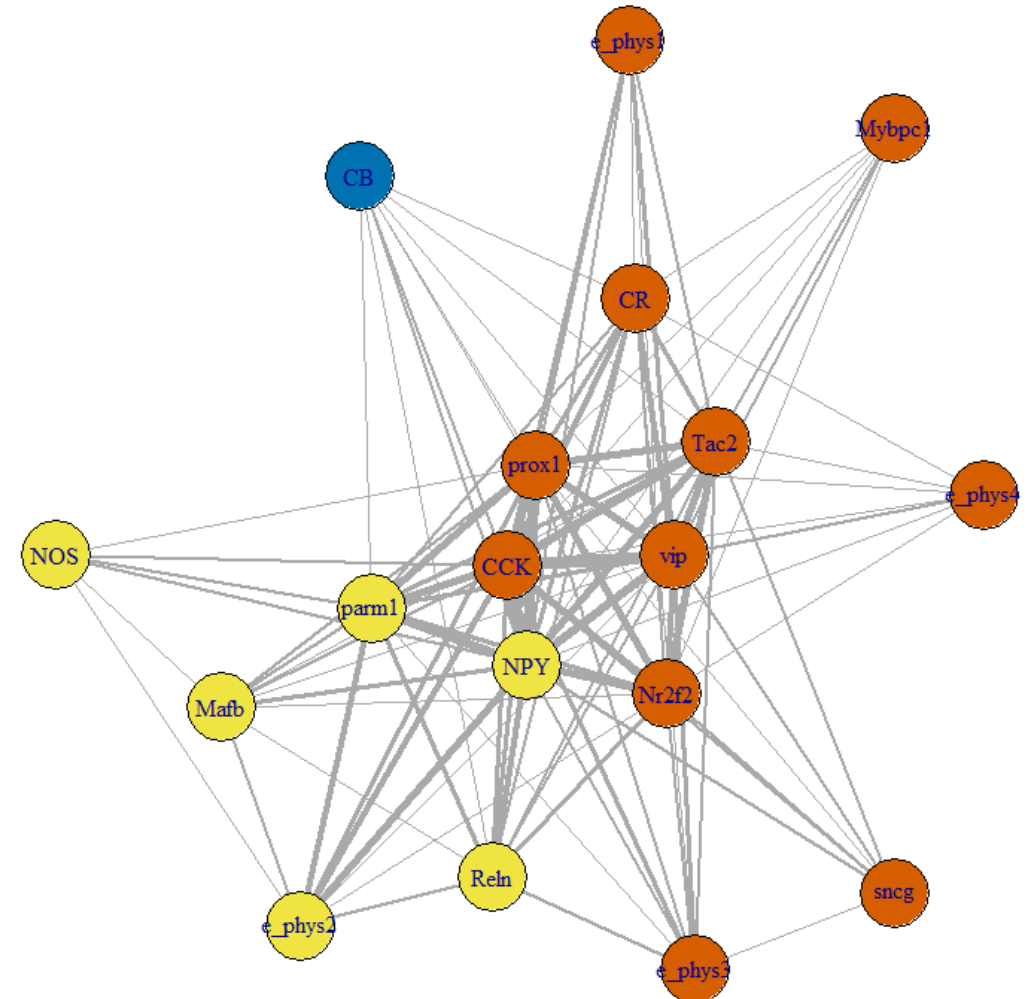
Edge.betweenness



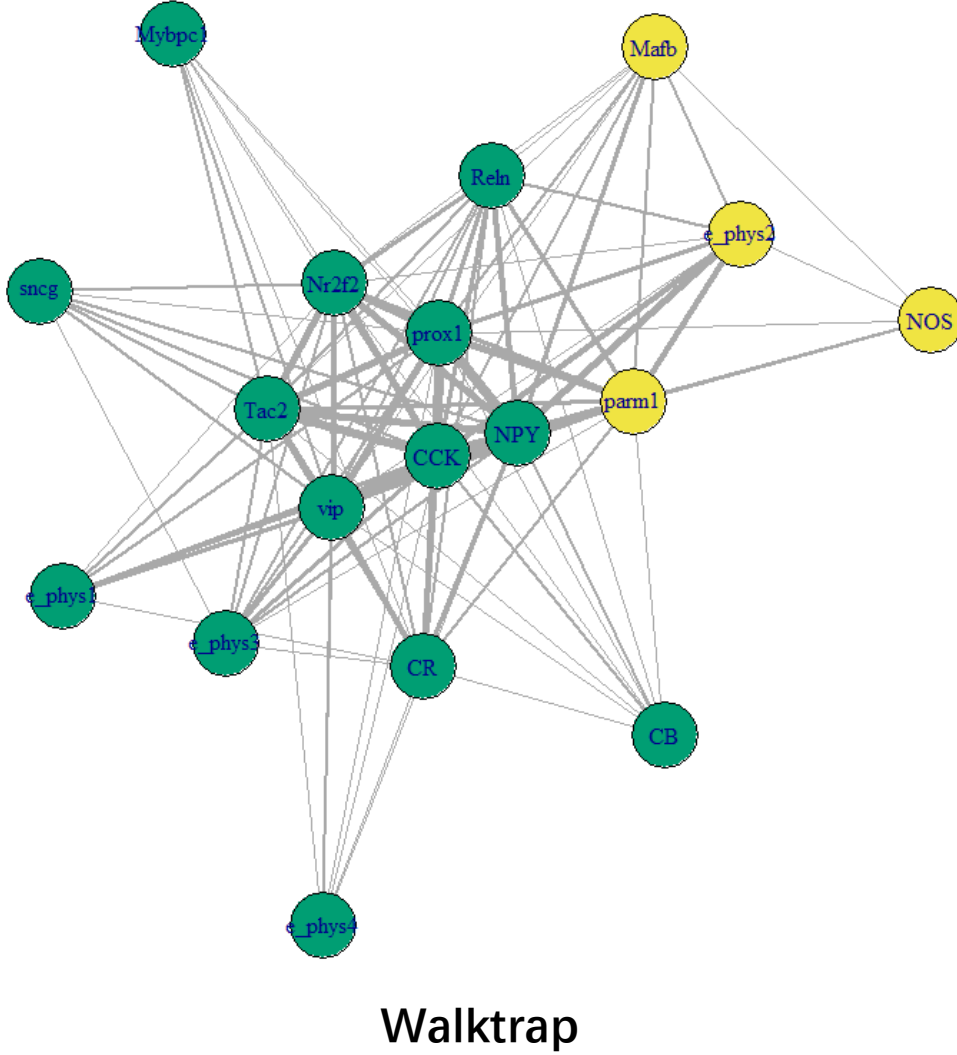
Leading.eigenvector



fastgreedy



Spinglass

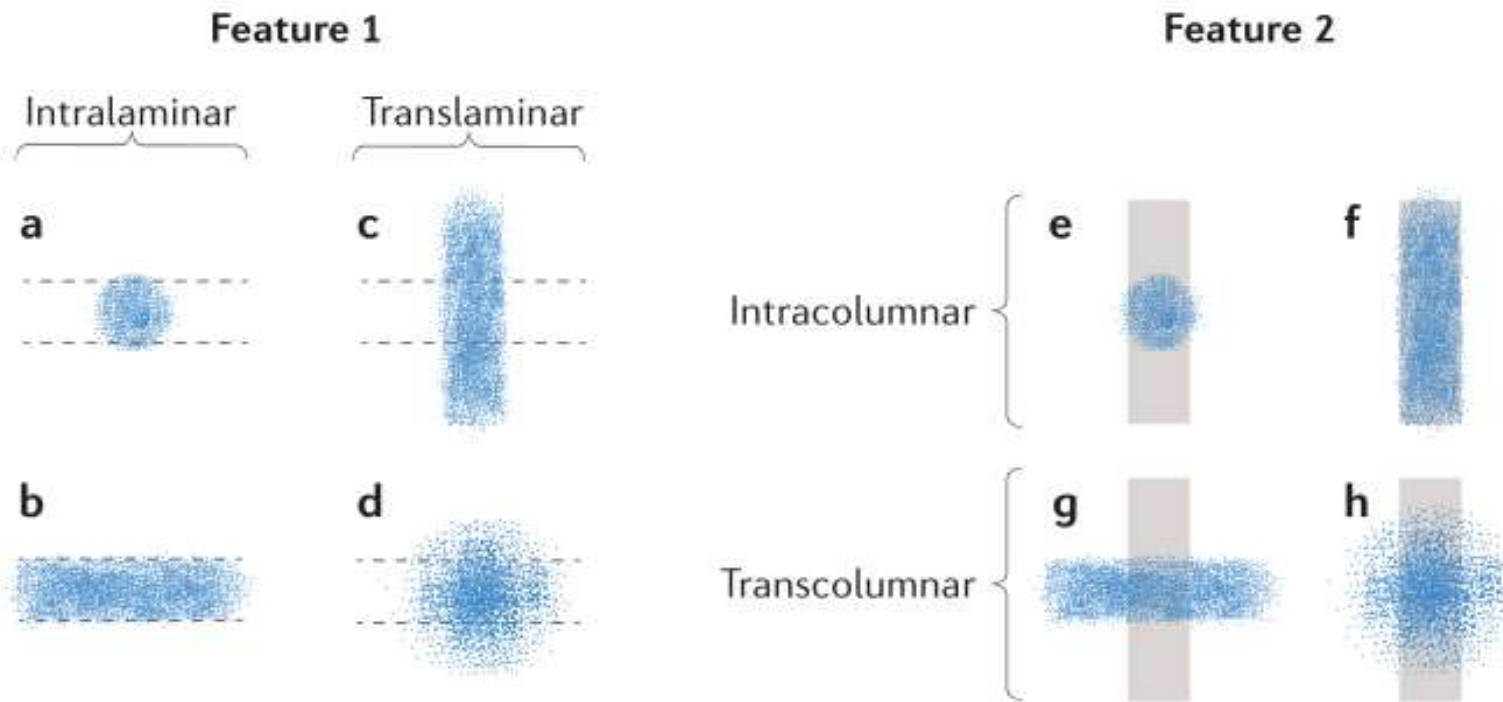


- Edge.betweenness: Unable to distinguish
- Leading.eigenvector: e_phys2、Reln、NPY、CCK、NOS、prox1、Mafb、parm1
- fastgreedy: e_phys2、Reln、NPY、CB、CCK、NOS、prox1、Mafb、parm1
- Spinglass: e_phys2、Reln、NPY、NOS、Mafb、parm1; CB is divided into a separate category
- Walktrap: e_phys2、NOS、Mafb、parm1

Current problems and possible solutions

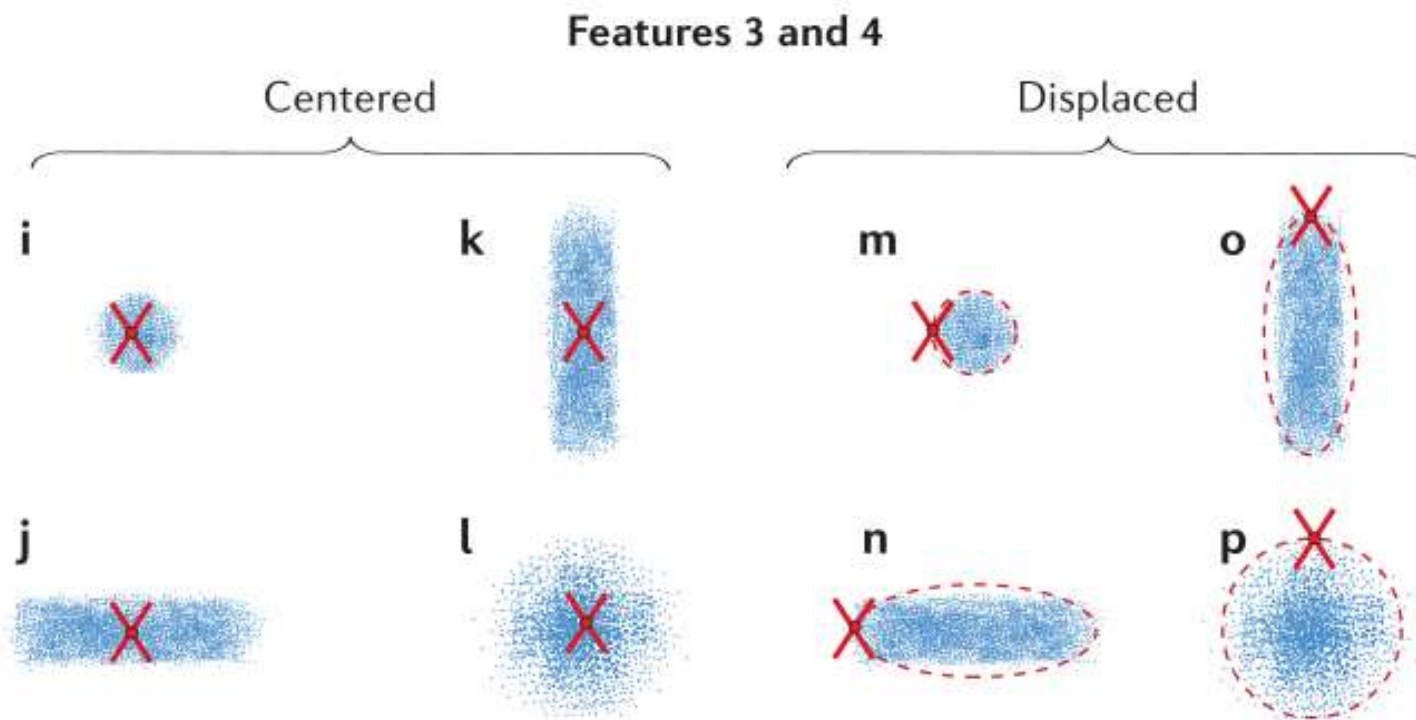
- The construction of the morphology dataset requires careful selection of data.
- Methods for distinguishing axon from dendrite and extracting parameters, as well as calculations and refinements of other descriptive parameters, are needed.
- Further quantification of the correlation between information at different levels is required for network analysis.

Morphological fuzzy classification concepts (relative descriptive features)



- **Feature1:** Define intralaminar and translaminar based on the relationship between the area covered by axons and the layer.
- **Feature2:** Define intracolumn as axon coverage with a diameter smaller than 300 μm around the cell body, considering 300 μm as a column, and define transcolumn as axon coverage with a diameter larger than 300 μm .

The relative position of the dendrite domain and axon domain



- **Feature3:** Define "centered" as the location where the cell body and dendritic domain are positioned near the center of the axonal domain.
- **Feature4:** Define "displaced" as the location where the cell body and dendritic domain are positioned outside of the axonal domain.

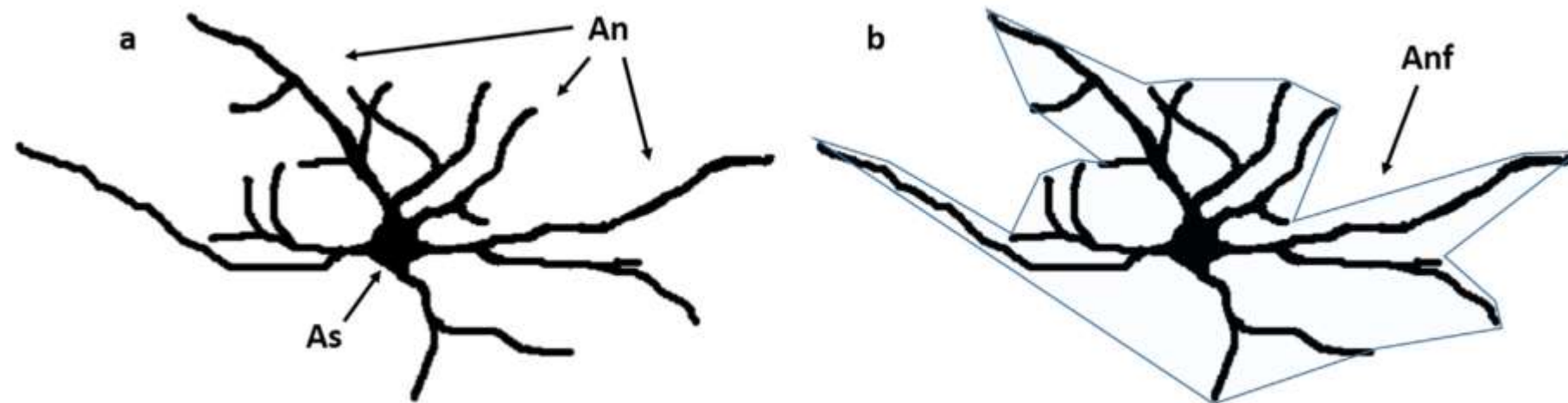


Fig. 3. Calculation of surface parameters (explanations are given in the text).

As: Area occupied by the neuron cell body

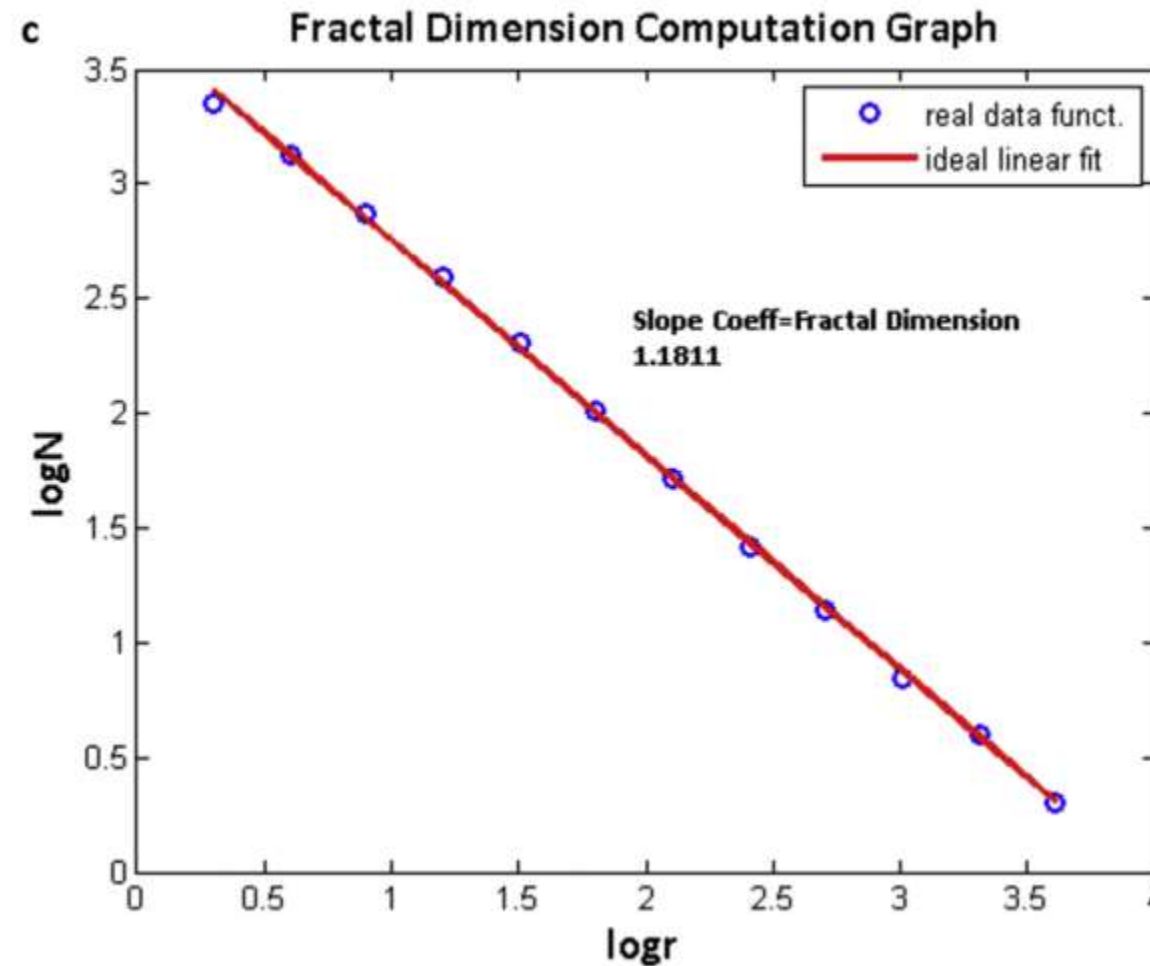
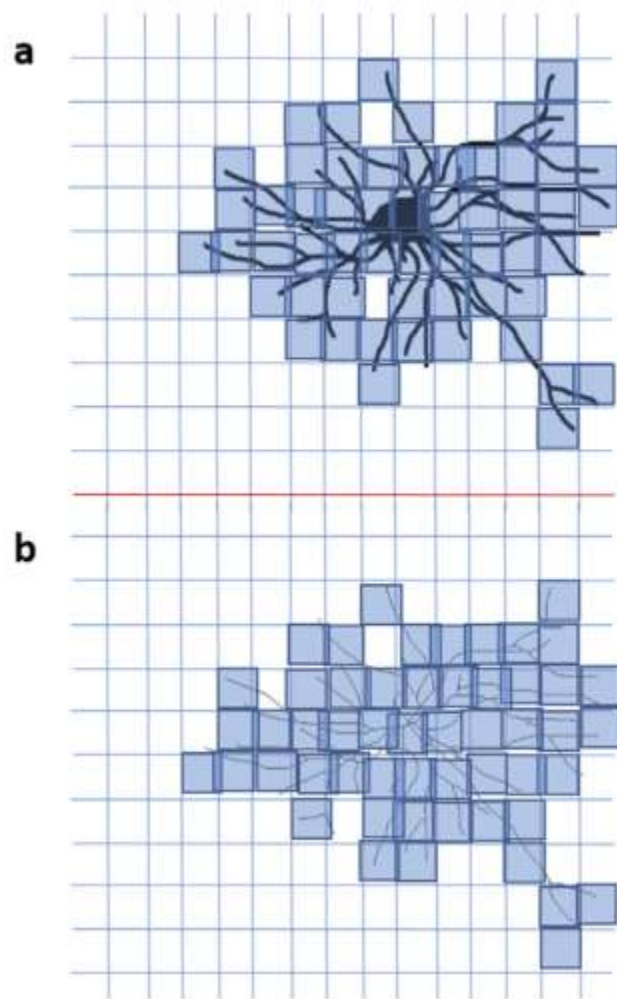
An: Actual area occupied by the neuron

Adt: An-As Area occupied by the dendrites, subtracting the area occupied by the cell body

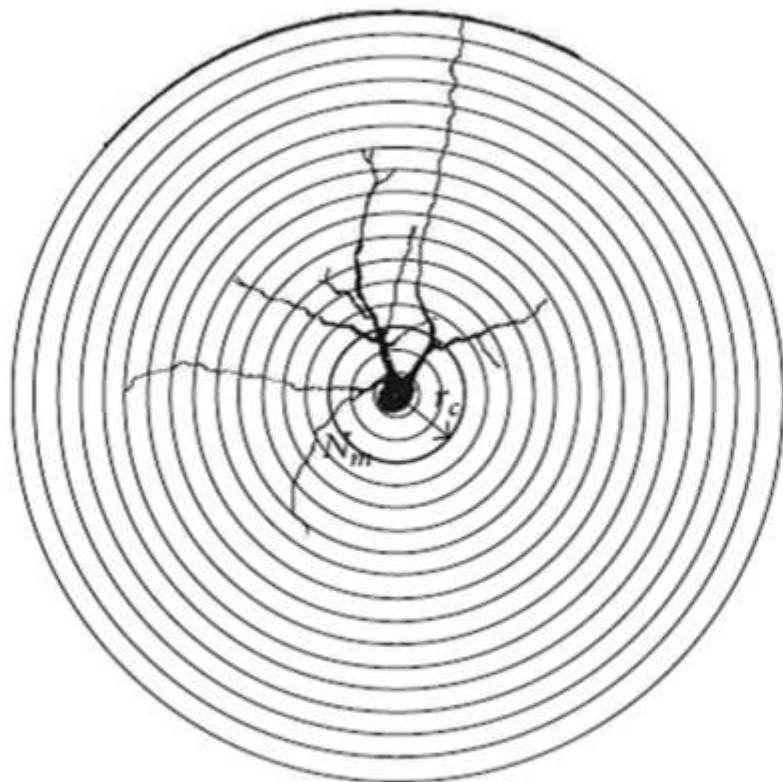
Anf: Minimum area occupied by the neuron, described by measuring the endpoints of dendrites and connecting them to form a polygon

Adf: Minimum area occupied by the dendrites, calculated by subtracting the actual cell body area from the minimum neuron area, $Adf=Anf-As$

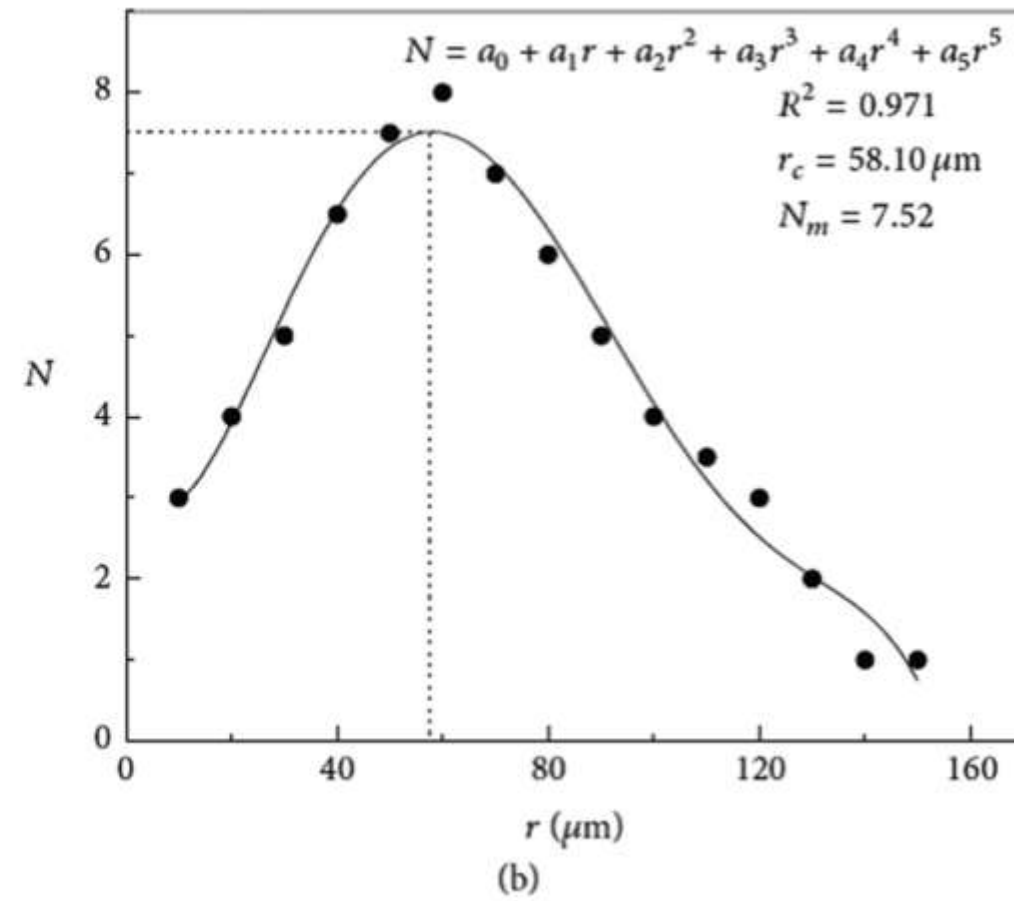
Apns: Area of the neuropil surface, representing the surface between dendrites, calculated by subtracting the actual neuron area from the entire neuron field area, $Apns=Anf-An$



Calculating the dimensional features of neuron typing through box classification of 2D neuron images may potentially avoid compartmental variation.

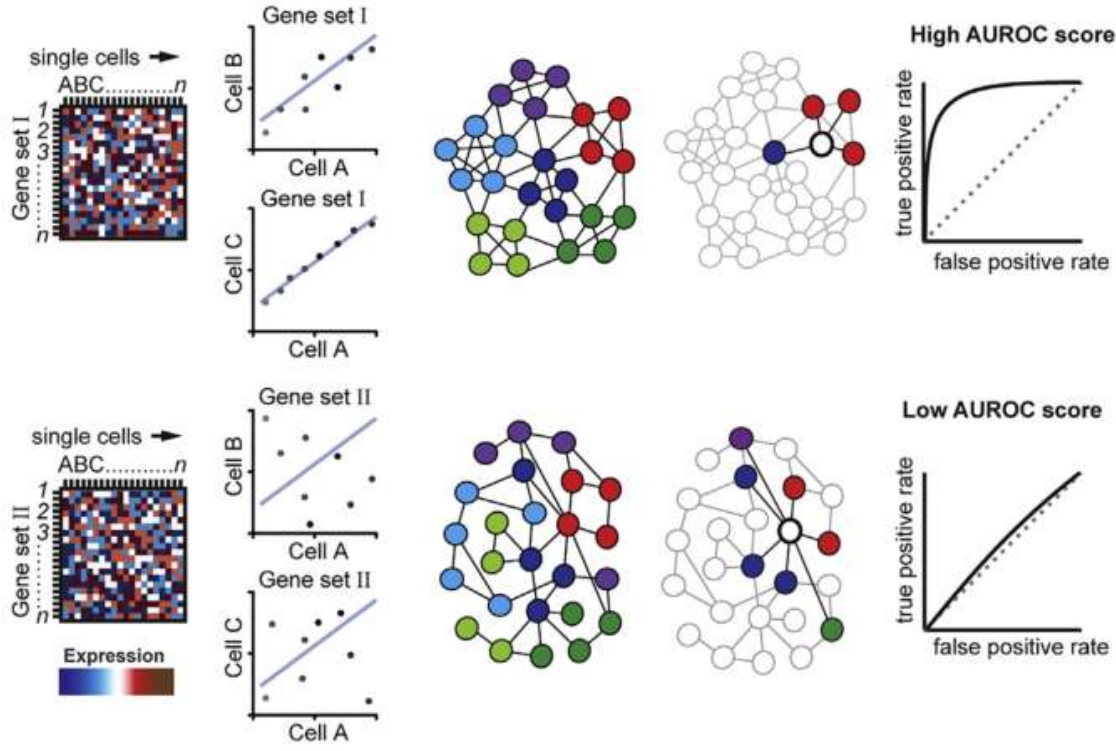


(a)

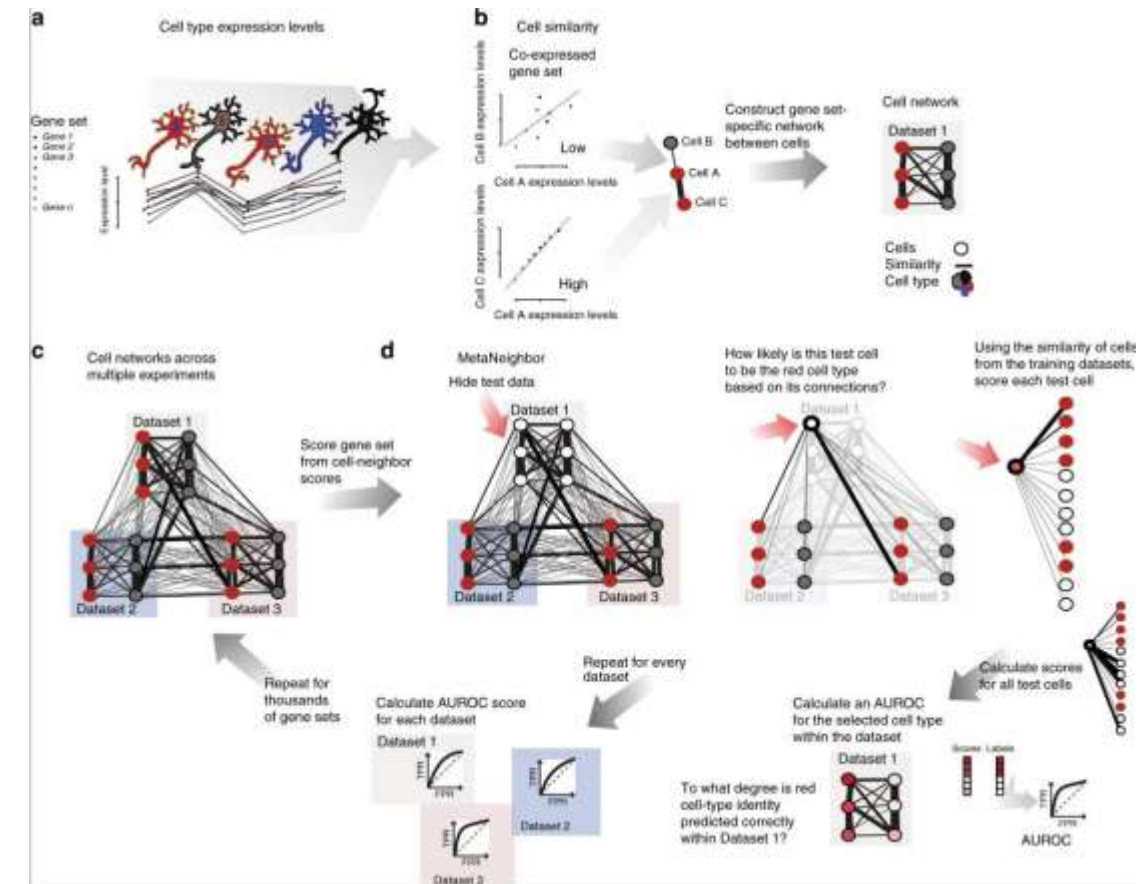


Network analysis for further quantification of relationships

- Understand several alternative methods for module analysis, adjust the algorithms accordingly, and experiment with them.
- Refer to the algorithms used in WGCNA.
- Refer to the algorithms used in MetaNeighbor.



Anirban Paul et al. (2017) Cell



Crow, M. et al.(2018) Nat. Commun.

Next Plan

- Focus on correlation analysis
- Constructing morphological data set
- Implementation of several macroscopic descriptions of morphological data
- Analysis of all integrated data

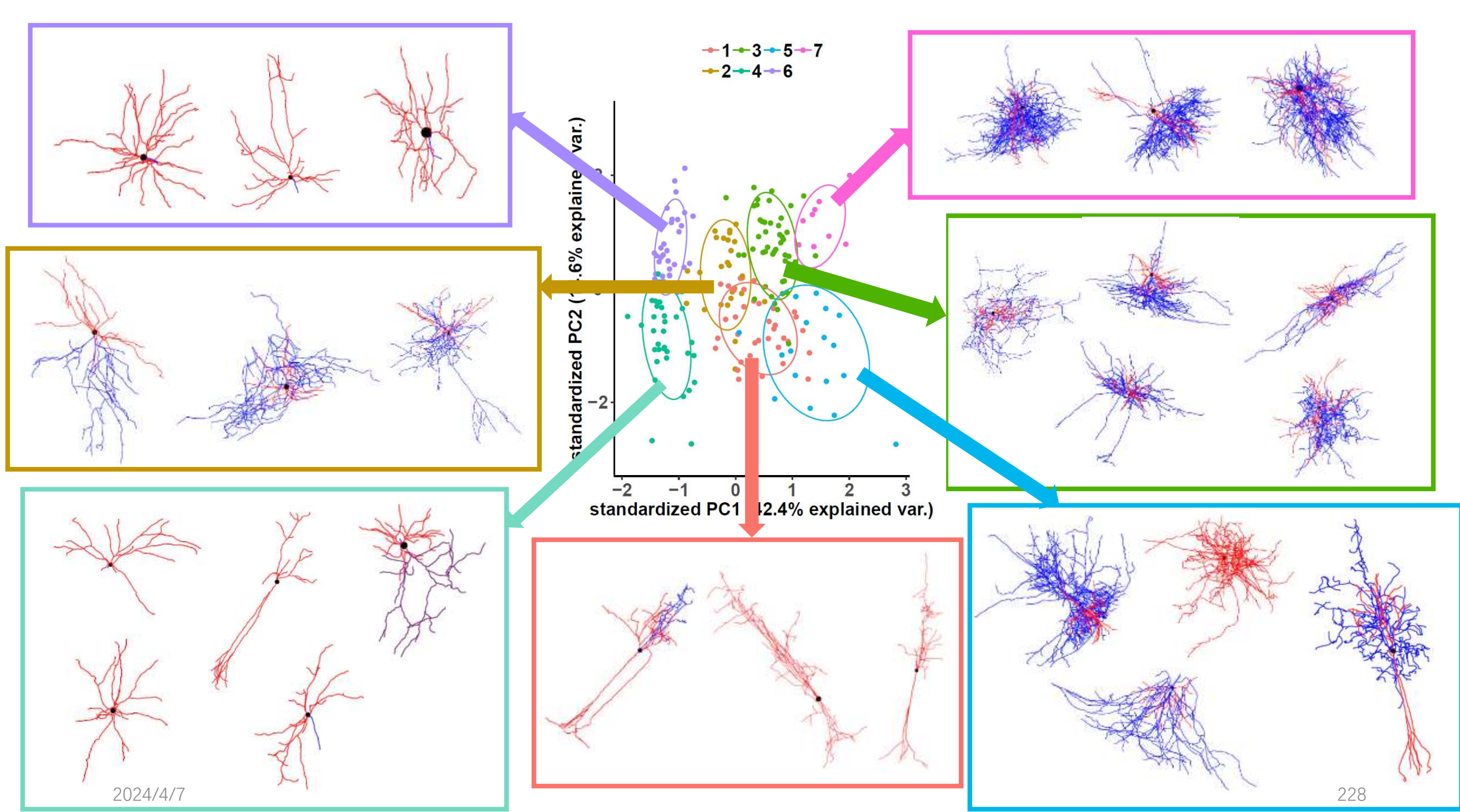
Interneuron classification

Zhou Ying

17th Oct. 2019

Content

- Morphological dataset construction
- Morphological quantization parameter system
- Morphological classification model was constructed in random forest
- Current issues and next plan



Morphological dataset construction

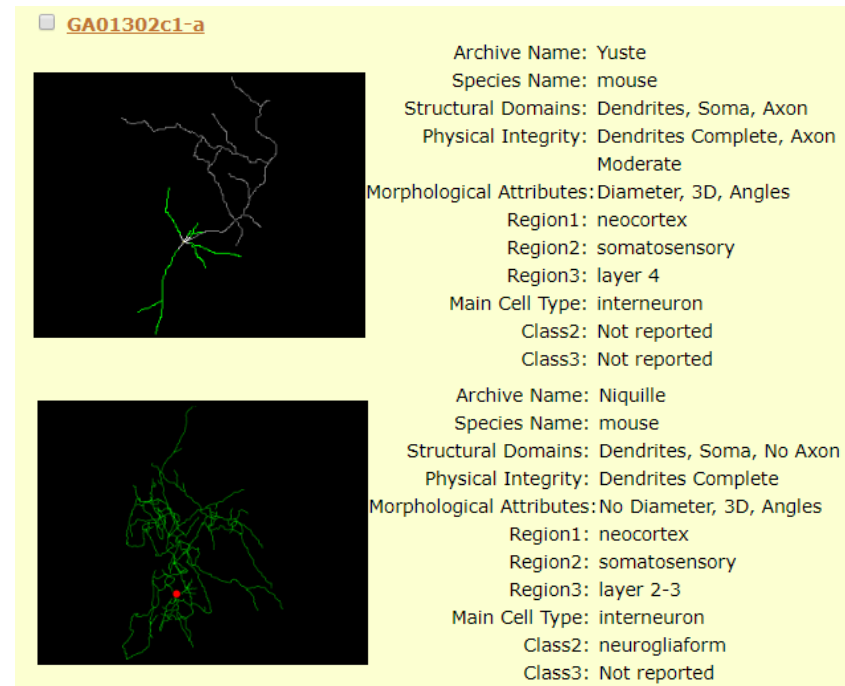


The screenshot shows the NeuroMorpho.Org homepage. At the top left is a stylized brain icon. To its right is the text "NeuroMorpho.Org" in large green letters. Below it is a smaller brain icon. The page header includes the text "Version 7.8 - Released: 08/19/2019 - Content: 112244 neurons". Below the header is a navigation bar with links: HOME (highlighted), BROWSE, SEARCH, LITERATURE COVERAGE, TERMS OF USE, and HELP. The "BROWSE" link has a small orange square icon with a downward arrow and the number "0" next to it. Below the navigation bar is a breadcrumb trail: "Home > Homepage". In the center, there are two sections: "Reconstructions from 721 cell types" and "Reconstructions from 317 brain regions", each accompanied by three small images of reconstructed neurons.

Reconstructions from 721 cell types Reconstructions from 317 brain regions

NeuroMorpho.Org is a centrally curated inventory of **digitally reconstructed neurons** associated with peer-reviewed publications. It contains contributions from over 500 laboratories worldwide and is continuously updated as new morphological reconstructions are collected, published, and shared. To date, NeuroMorpho.Org is the largest collection of publicly accessible 3D neuronal reconstructions and associated metadata.

Mouse Interneuron	6319
Basket cell	292
Bipolar cell	474
Bitufted cell	21
Chandelier cell	49
Double bouquet cell	9
Martinotti cell	91
Neurogilaform cell	100



GA01302c1-a

Archive Name: Yuste
Species Name: mouse
Structural Domains: Dendrites, Soma, Axon
Physical Integrity: Dendrites Complete, Axon Moderate
Morphological Attributes: Diameter, 3D, Angles
Region1: neocortex
Region2: somatosensory
Region3: layer 4
Main Cell Type: interneuron
Class2: Not reported
Class3: Not reported

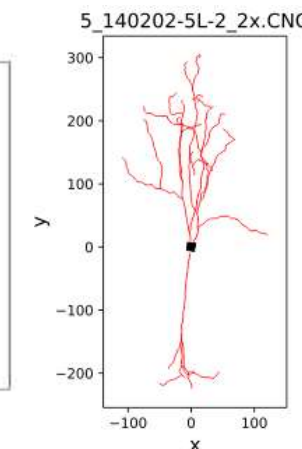
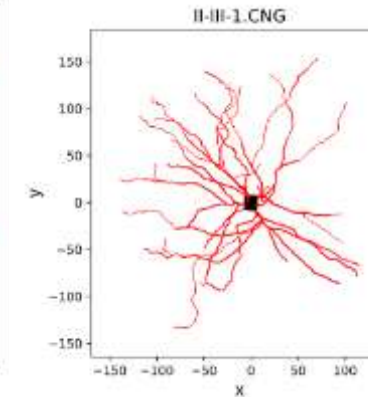
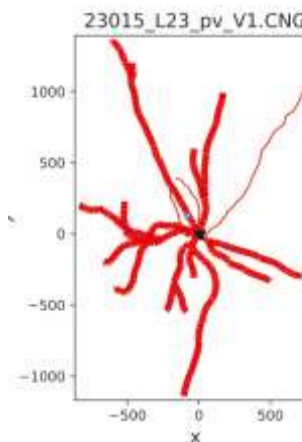
Archive Name: Niquille
Species Name: mouse
Structural Domains: Dendrites, Soma, No Axon
Physical Integrity: Dendrites Complete
Morphological Attributes: No Diameter, 3D, Angles
Region1: neocortex
Region2: somatosensory
Region3: layer 2-3
Main Cell Type: interneuron
Class2: neurogliaform
Class3: Not reported

Morphological dataset construction

preliminary filtering conditions

- **age:** >P21
- **Brain region:** neocortex
- **Cell type:** interneuron

Download 851 morphological data

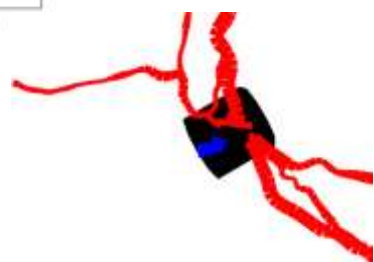
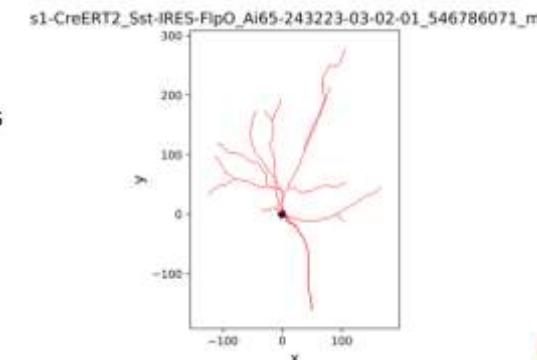


Neurom checks all the data

- Removing incomplete data
- The cell body is not recognized
- No axon information
- No dendrite information

swc was converted into reconstructed image to check the quality

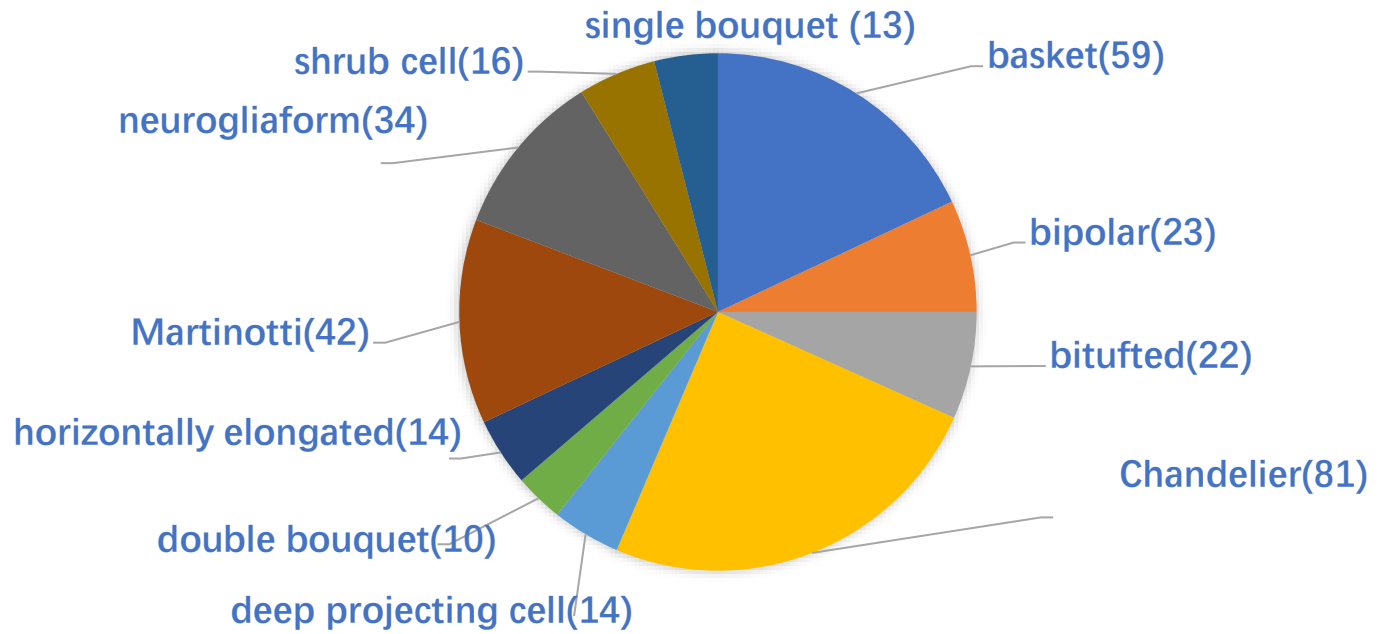
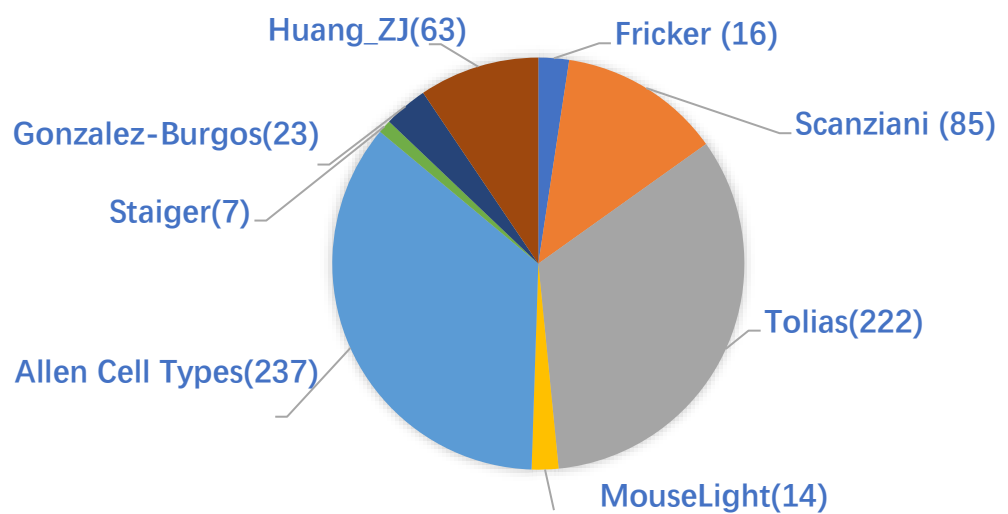
- Incomplete reconstruction
- Reconstruction roughness



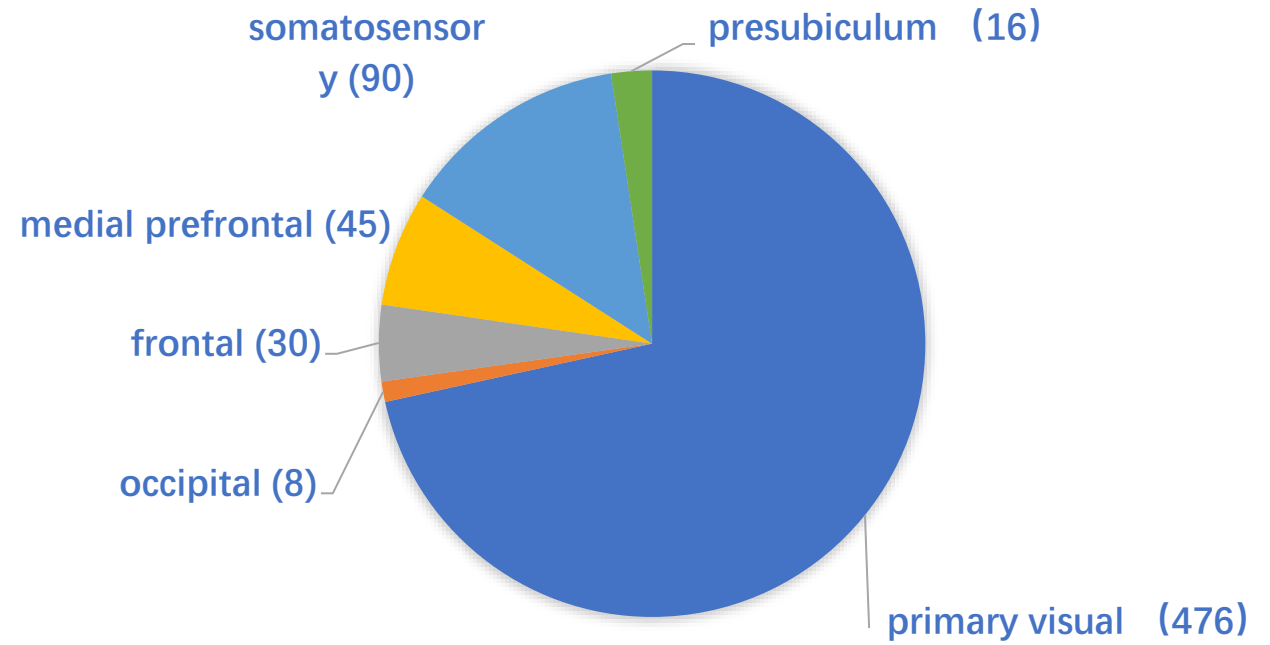
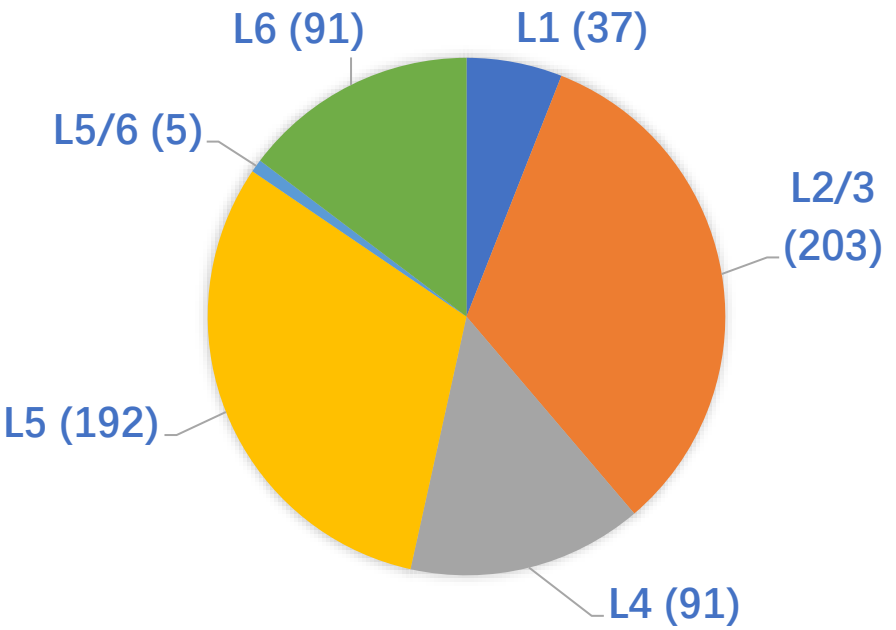
Morphological dataset construction

Resources	Molecule	Morphological labels	Layers	Regions
Fricker	Chat	basket	L1	primary visual
Scanziani	Chrna	bipolar	L2/3	frontal
Tolias	Htr3a	bitufted	L4	medial prefrontal
MouseLight	PV	Chandelier	L5	somatosensory
Allen Cell Types	SST	deep projecting cell	L5/6	occipital
Staiger	Ndnf	double bouquet	L6	presubiculum
Gonzalez-Burgos	Nos1/SST	horizontally elongated	620	665
Huang_ZJ	Vip	Martinotti		
		neurogliaform		
		shrub cell		
		single bouquet		
		323		
665	207			

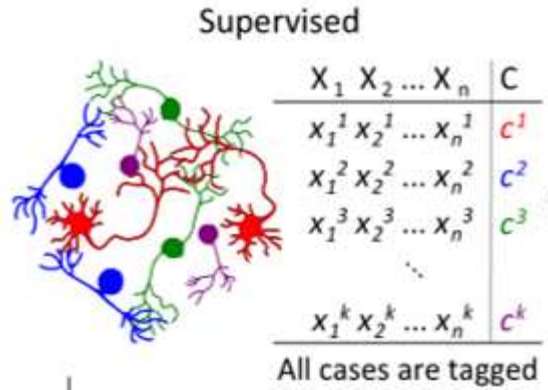
Morphological dataset construction



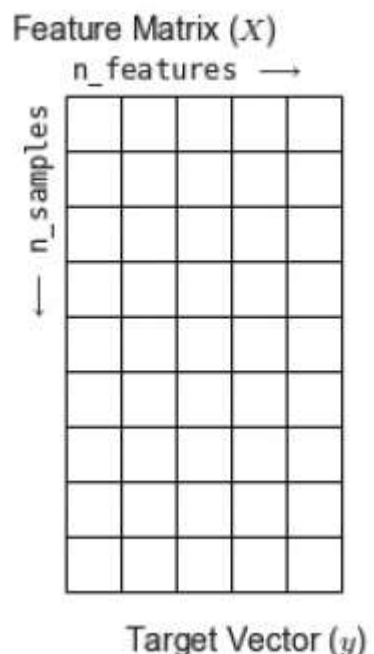
Morphological dataset construction



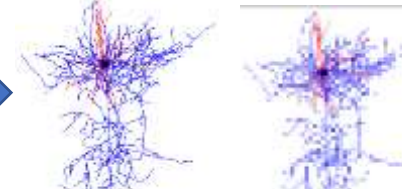
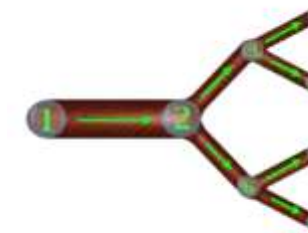
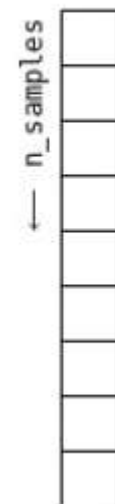
Morphological quantization parameter system



- Probabilistic
- Mathematical functions
- Distance-based
- Trees

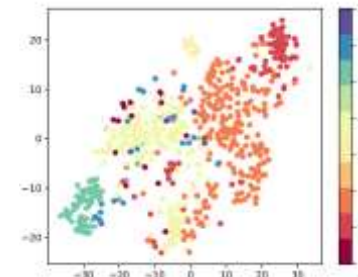
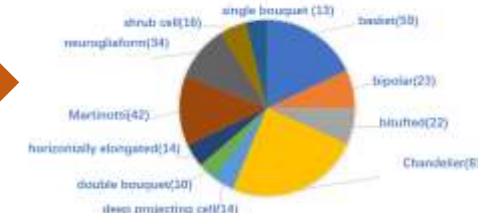
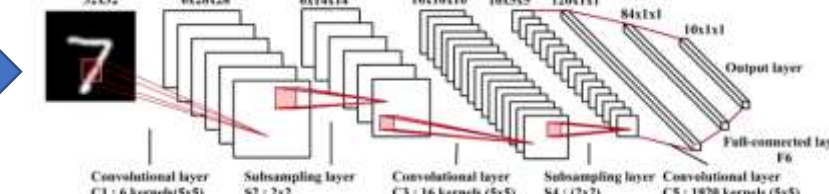
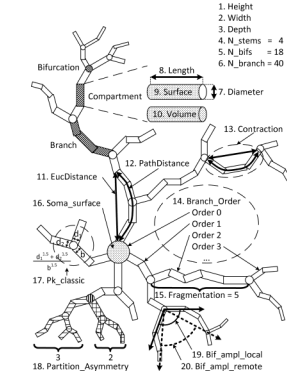


Target Vector (y)



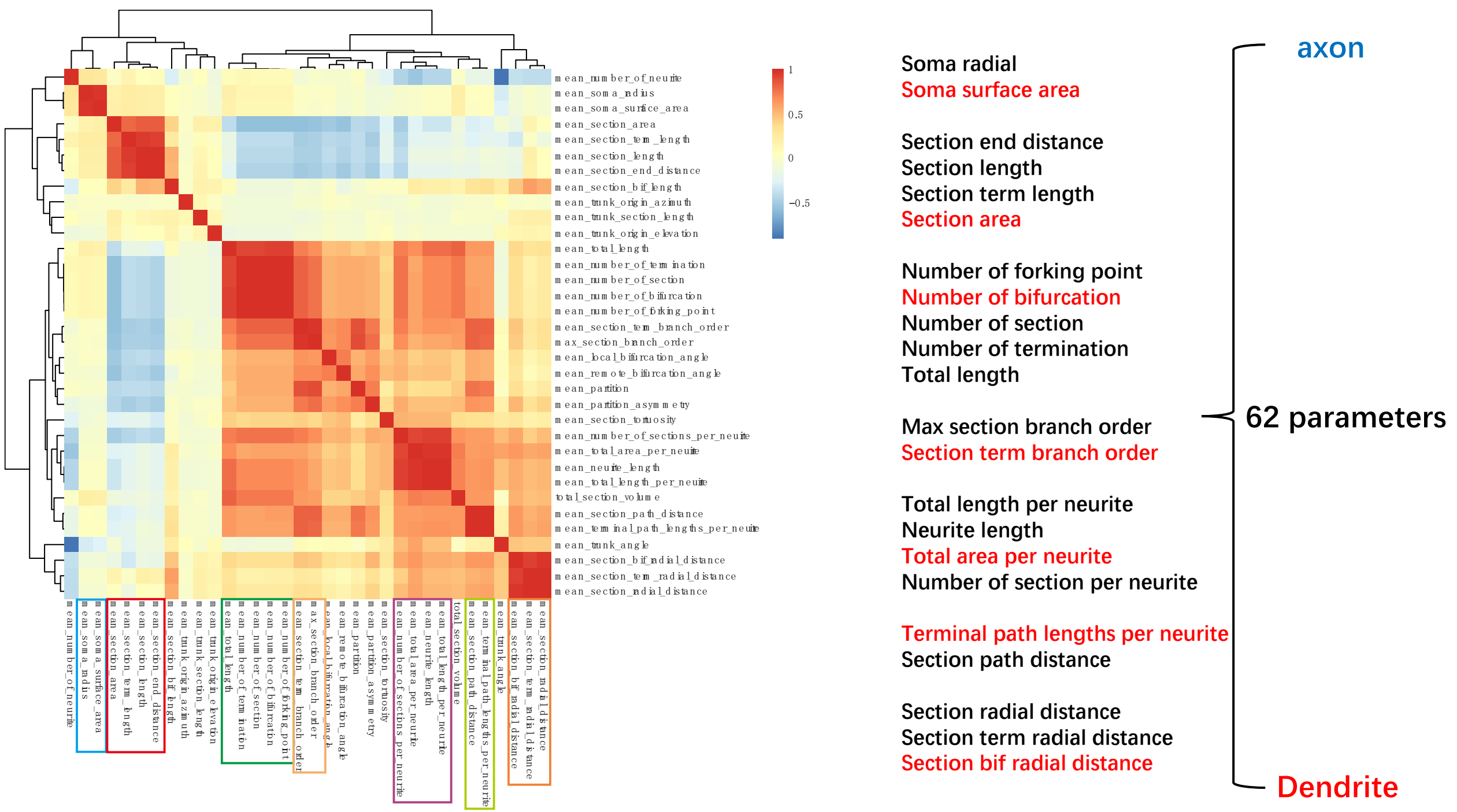
1	2	3	4	5	6	7	8
0	0	0	0	0	0	0	0
1	0	0	0	0	0	0	0
0	1	0	0	0	0	0	0
0	0	1	0	0	0	0	0
0	0	0	1	0	0	0	0
0	1	0	0	0	0	0	0
0	0	0	0	0	1	0	0
0	0	0	0	0	0	1	0

adjacency matrix dA

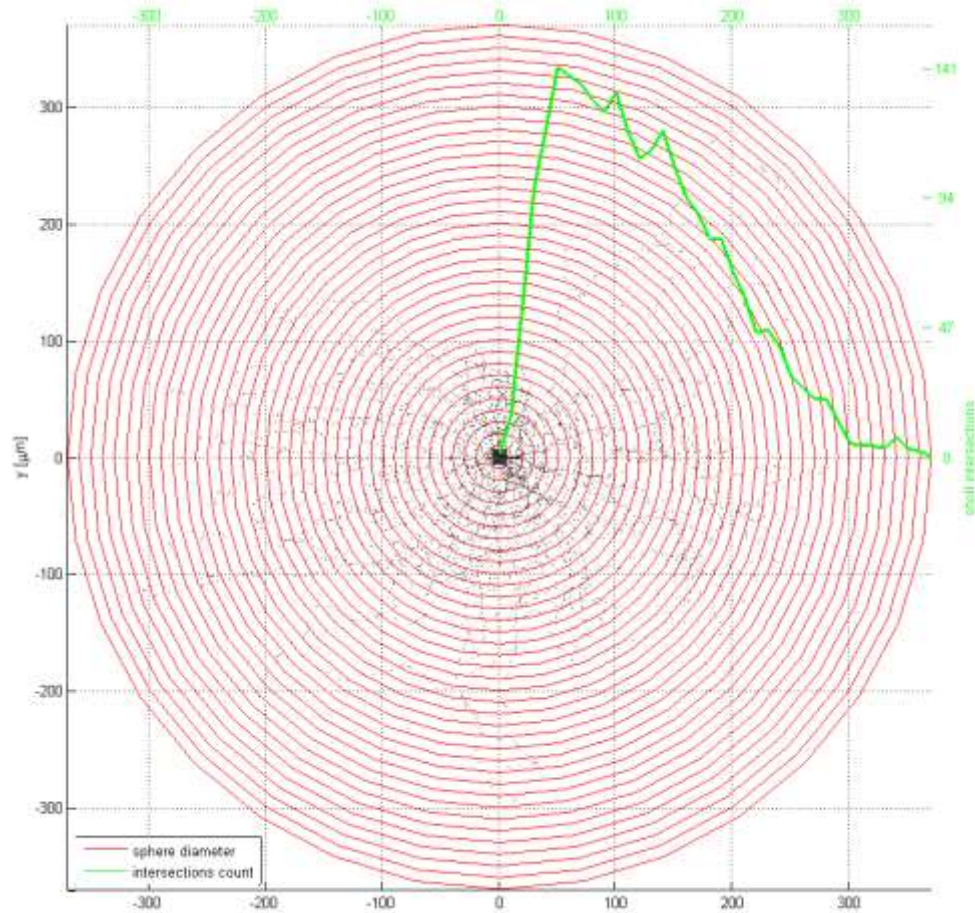


Use existing labels in the dataset

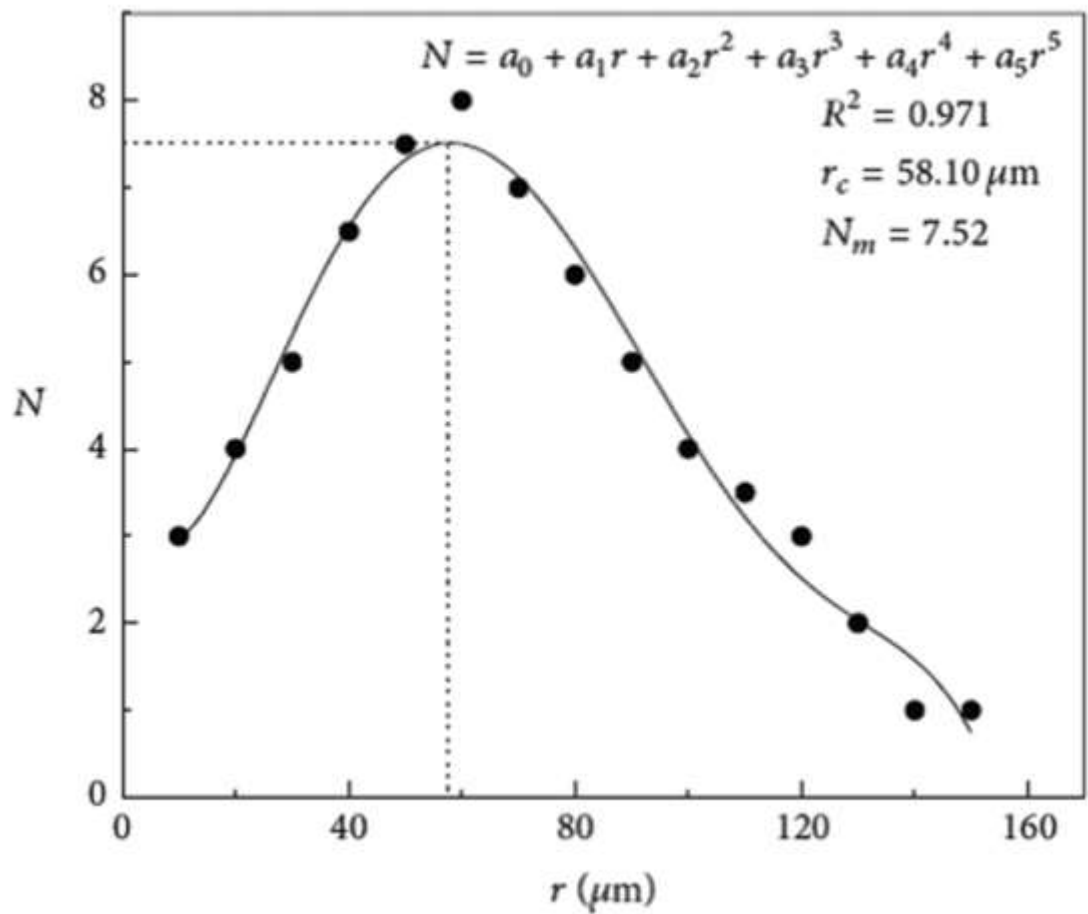
First, natural clustering is used, and the clustering results are used as classification labels



Morphological quantization parameter system

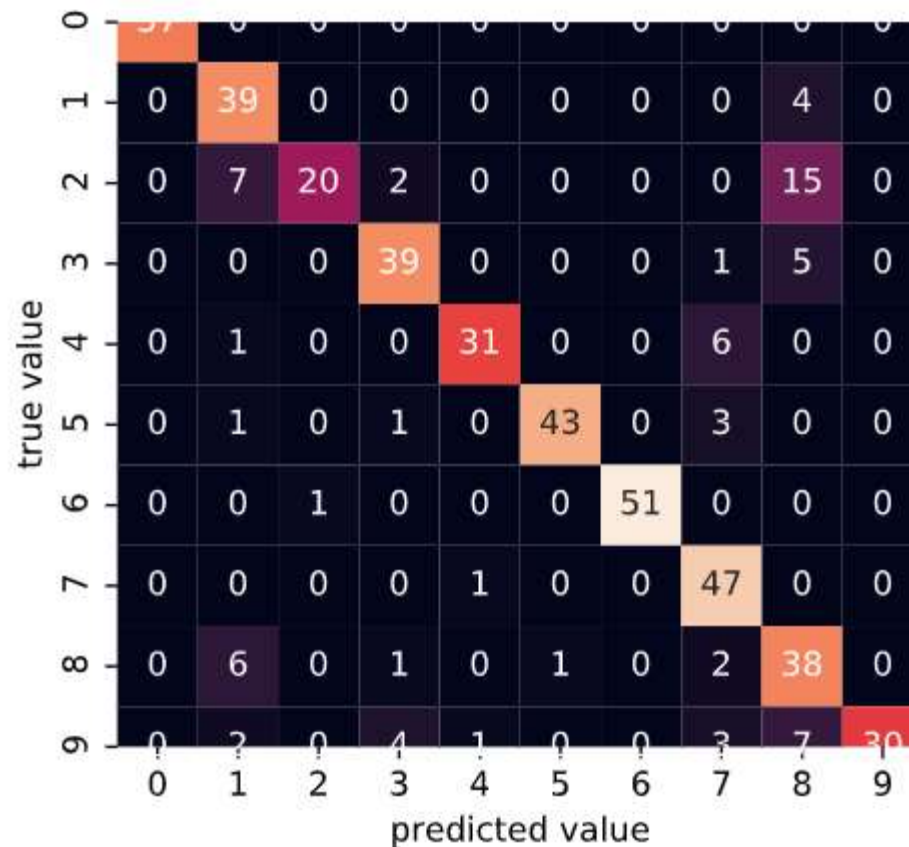


Tolias L5 neurogliaform



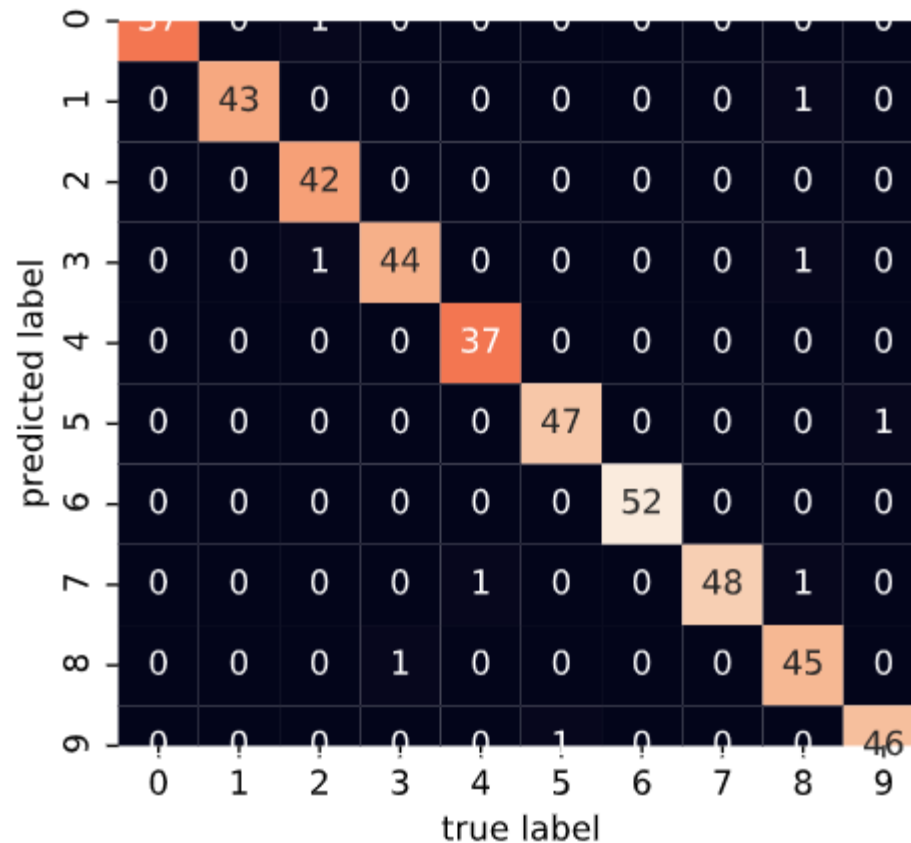
Gaussian naive Bayes classification model

	precision	recall	f1-score	support
0	1.00	1.00	1.00	37
1	0.91	0.70	0.79	56
2	0.45	0.95	0.62	21
3	0.87	0.83	0.85	47
4	0.82	0.94	0.87	33
5	0.90	0.98	0.93	44
6	0.98	1.00	0.99	51
7	0.98	0.76	0.85	62
8	0.79	0.55	0.65	69
9	0.64	1.00	0.78	30
accuracy		0.83	0.83	450
macro avg	0.83	0.87	0.83	450
weighted avg	0.86	0.83	0.83	450

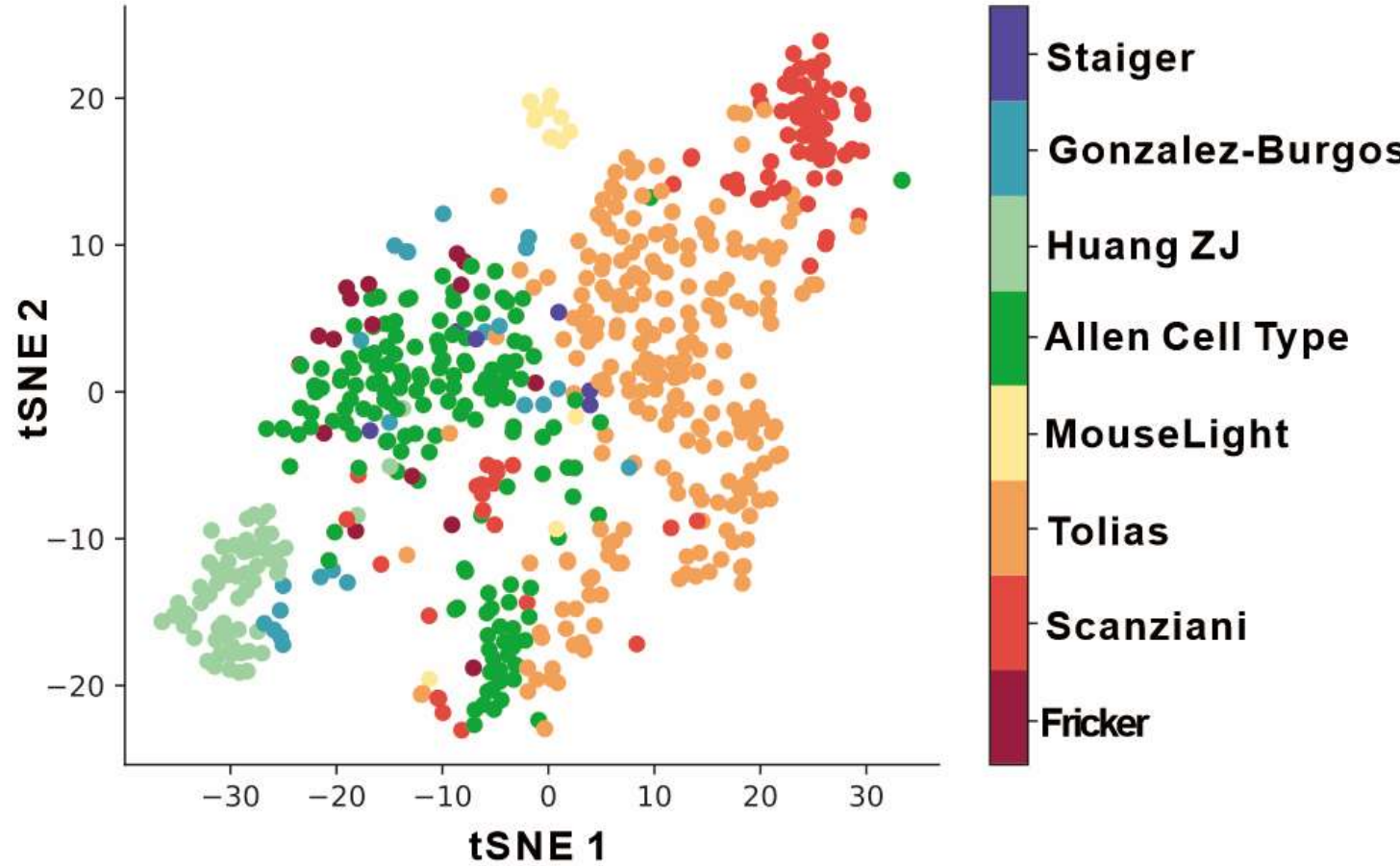


Random forest classification model

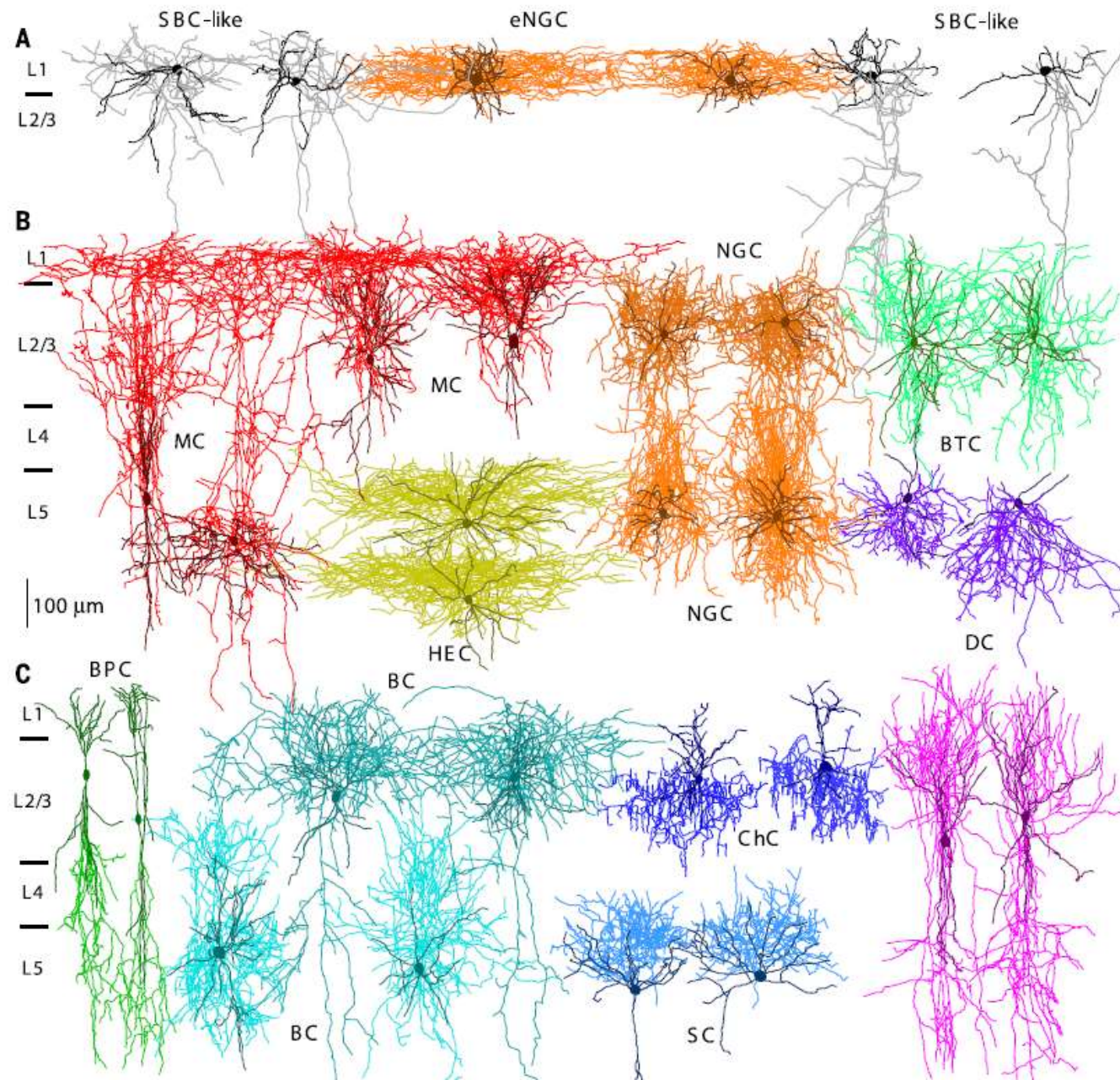
	precision	recall	f1-score	support
0	1.00	0.97	0.99	38
1	1.00	0.98	0.99	44
2	0.95	1.00	0.98	42
3	0.98	0.96	0.97	46
4	0.97	1.00	0.99	37
5	0.98	0.98	0.98	48
6	1.00	1.00	1.00	52
7	1.00	0.96	0.98	50
8	0.94	0.98	0.96	46
9	0.98	0.98	0.98	47
accuracy			0.98	450
macro avg	0.98	0.98	0.98	450
weighted avg	0.98	0.98	0.98	450



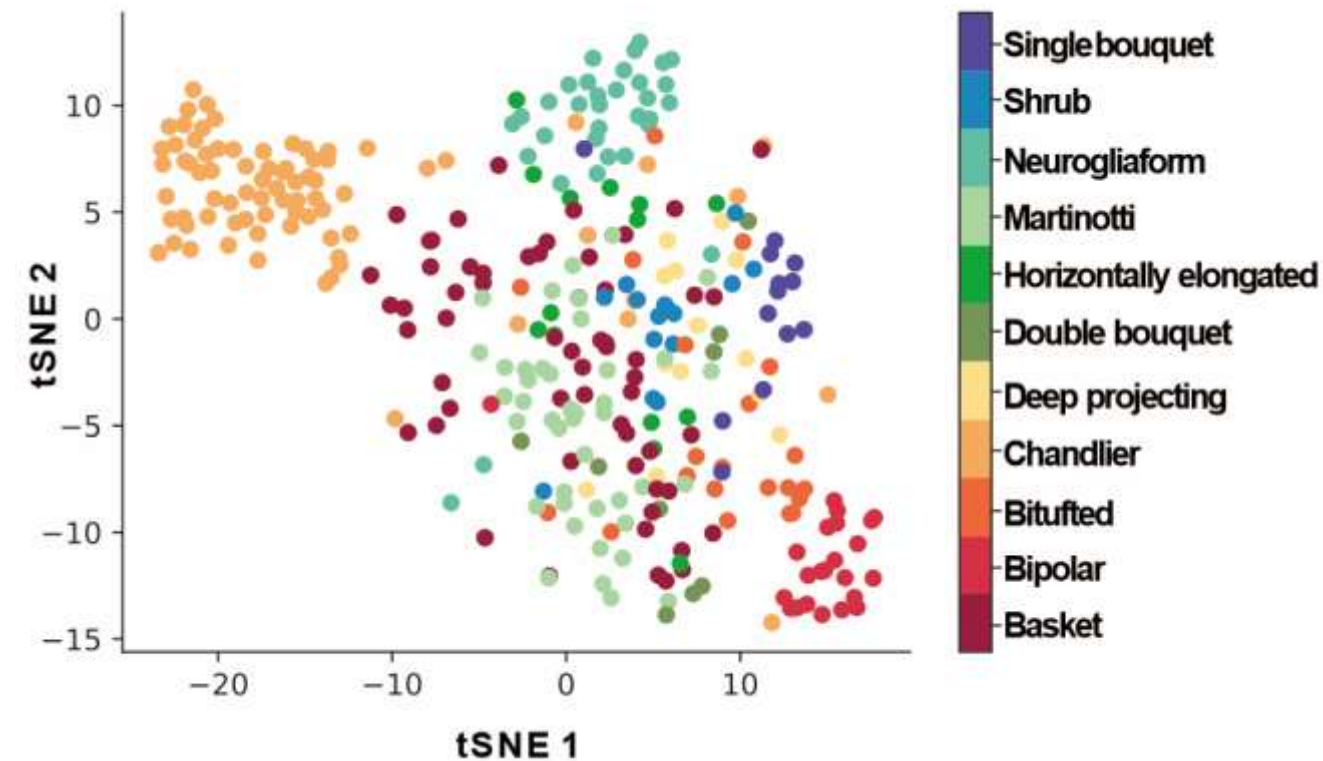
Morphological classification model was constructed in random forest



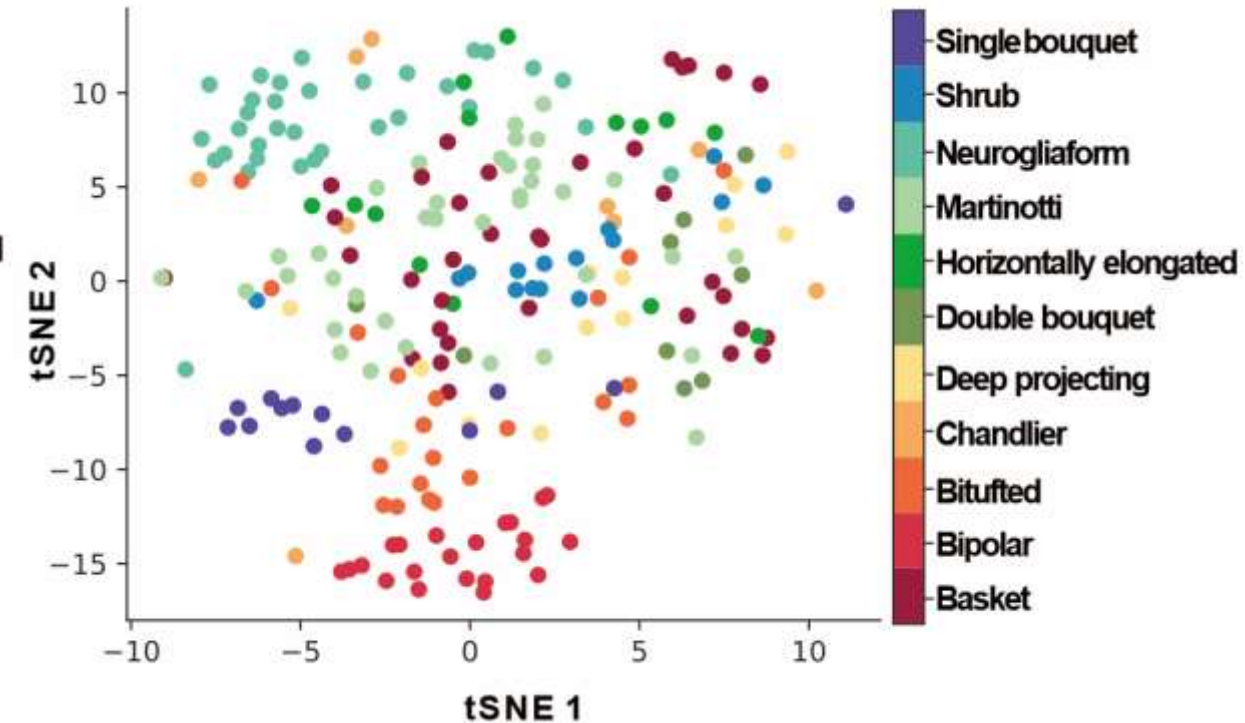
- The data from different laboratories tend to cluster, indicating that differences in data processing methods between laboratories can affect classification results.
- Therefore, there is a need for a method to standardize morphological data from different laboratories in order to facilitate comparison of data from different laboratories.



Morphological classification model was constructed in random forest

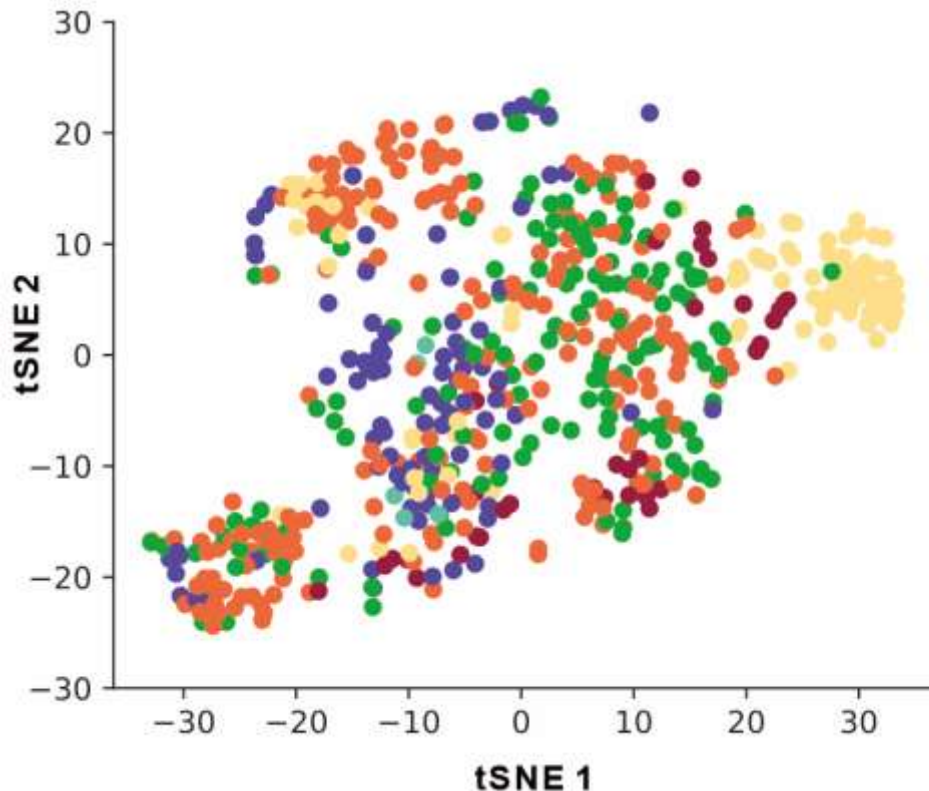


所有有形态学命名标签的数据

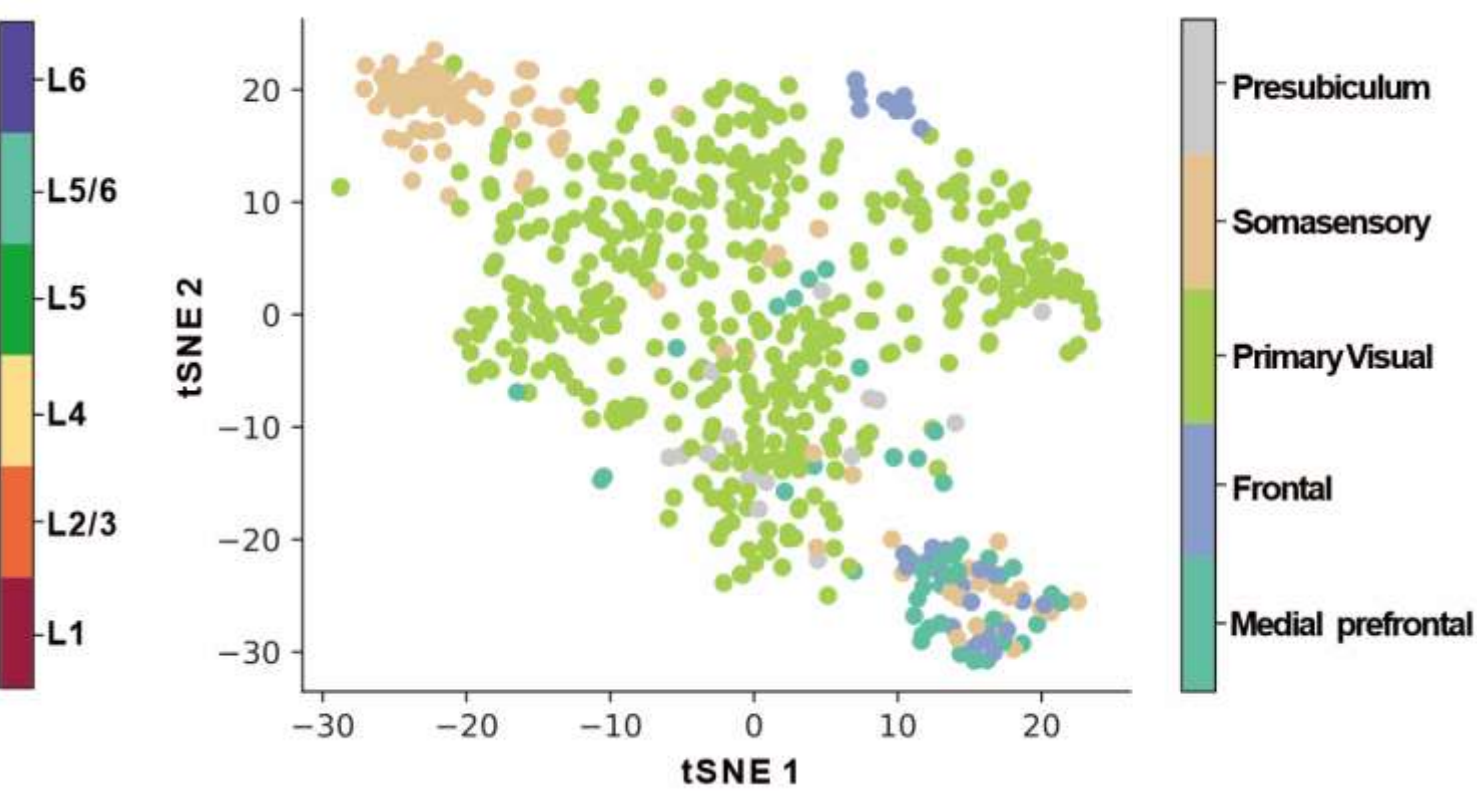


Tolias实验室的数据

Morphological classification model was constructed in random forest



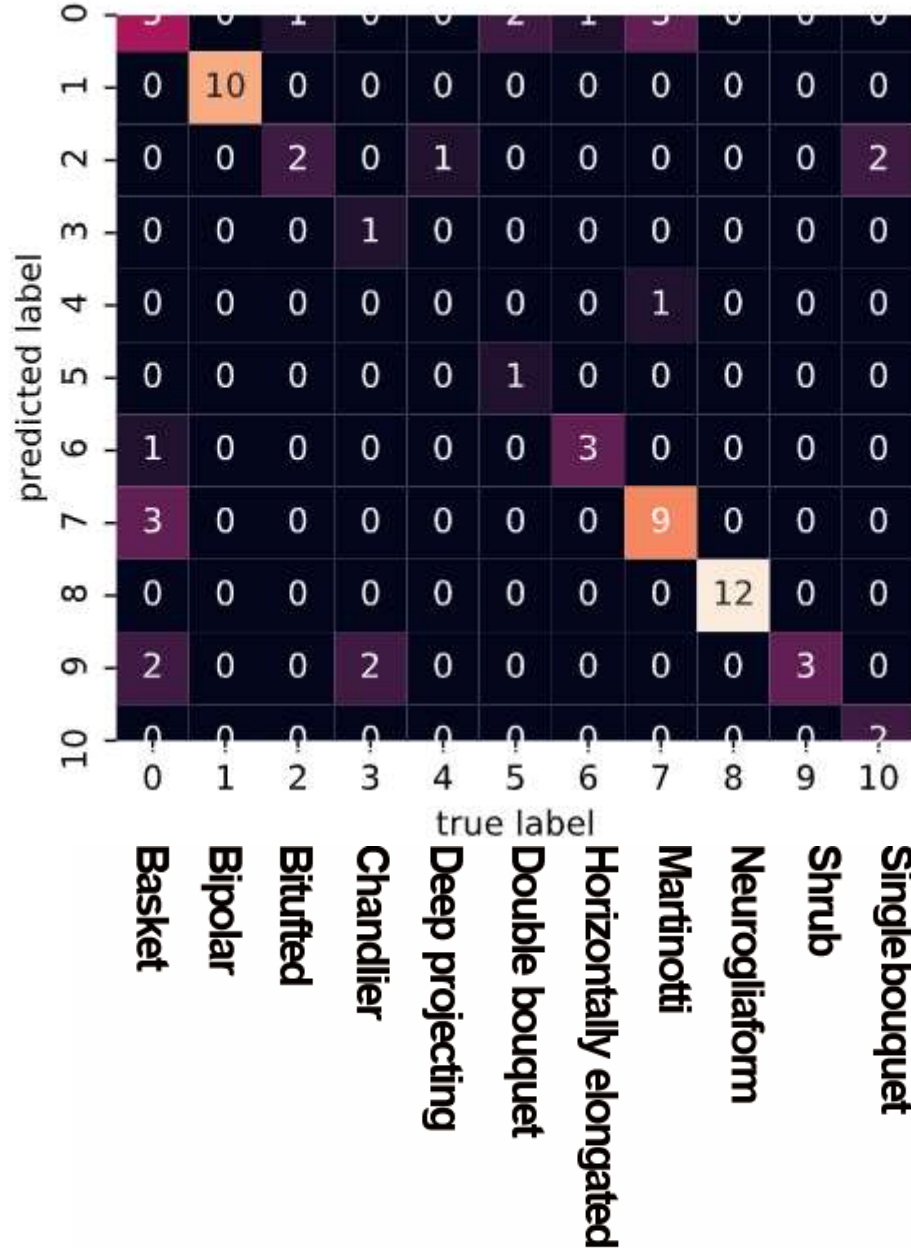
形态的层分布



不同脑区的形态

Morphological classification model was constructed in random forest

	precision	recall	f1-score	support	
0	0.45	0.42	0.43	12	
1	1.00	1.00	1.00	10	
2	0.67	0.40	0.50	5	
3	0.33	1.00	0.50	1	
4	0.00	0.00	0.00	1	
5	0.33	1.00	0.50	1	
6	0.75	0.75	0.75	4	
7	0.69	0.75	0.72	12	
8	1.00	1.00	1.00	12	
9	1.00	0.43	0.60	7	
10	0.50	1.00	0.67	2	
accuracy				67	
macro avg	0.61	0.70	0.61	67	
weighted avg	0.76	0.72	0.71	67	



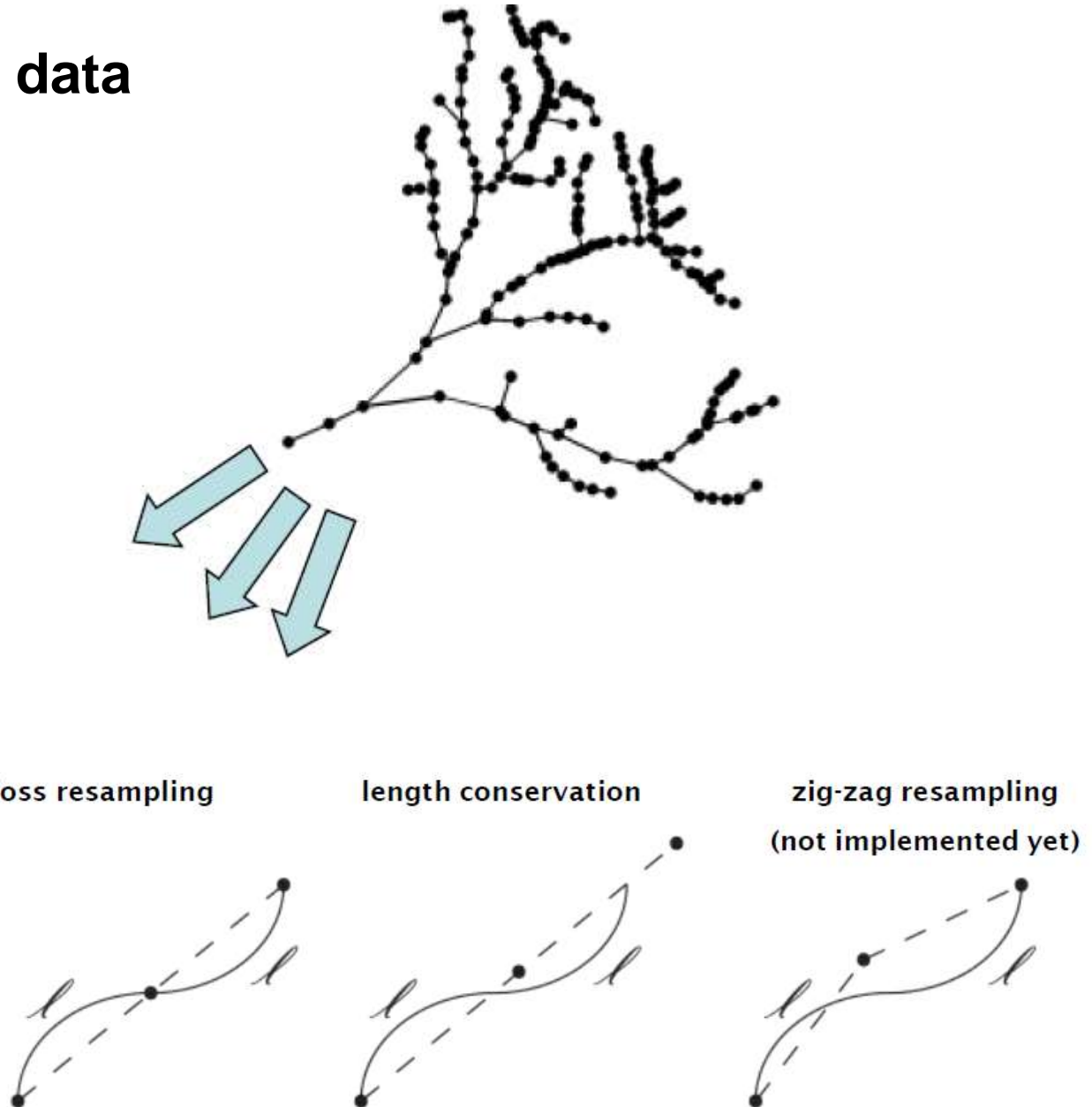
Resampling the reconstructed data

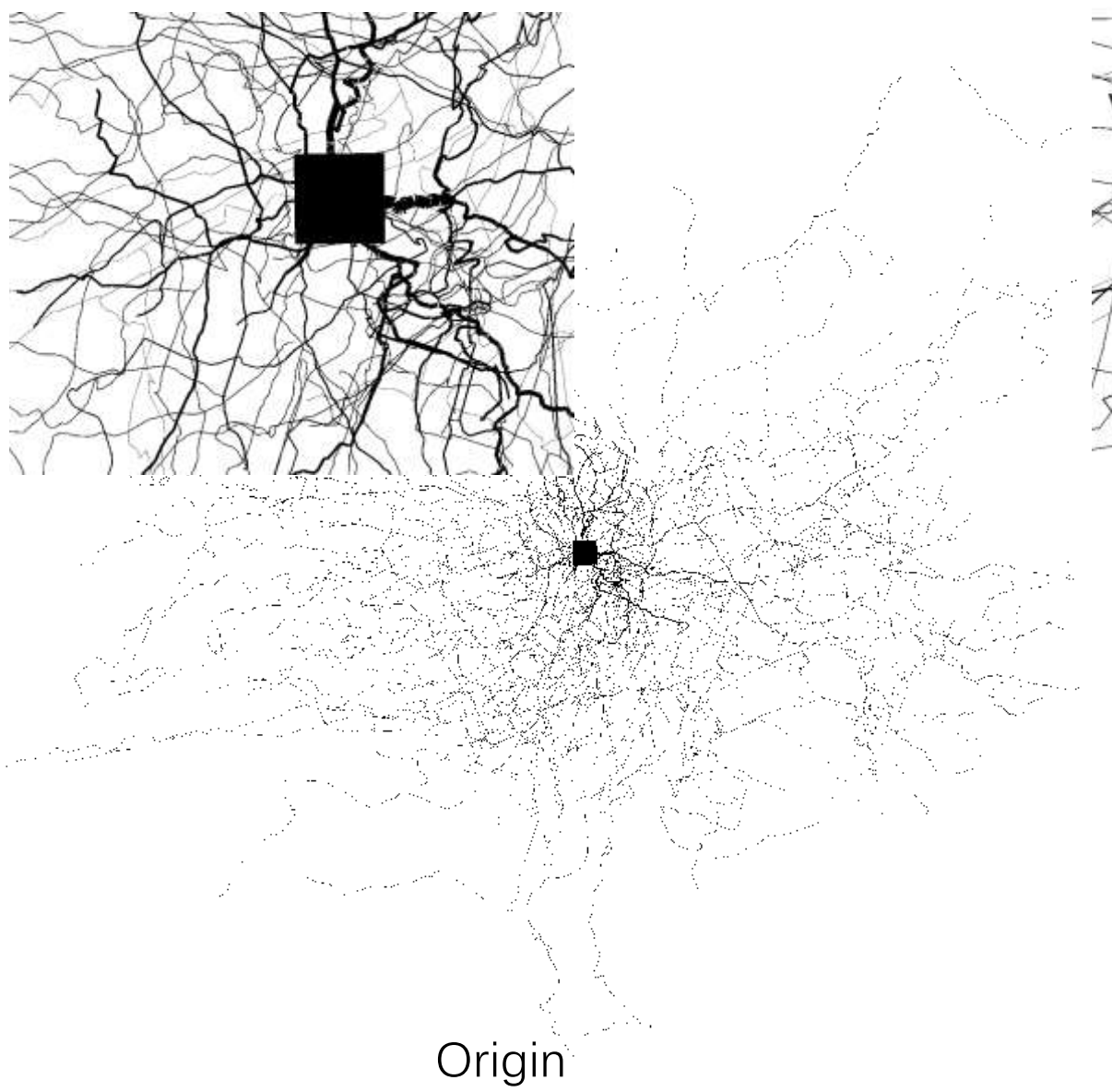


10 μm resampling



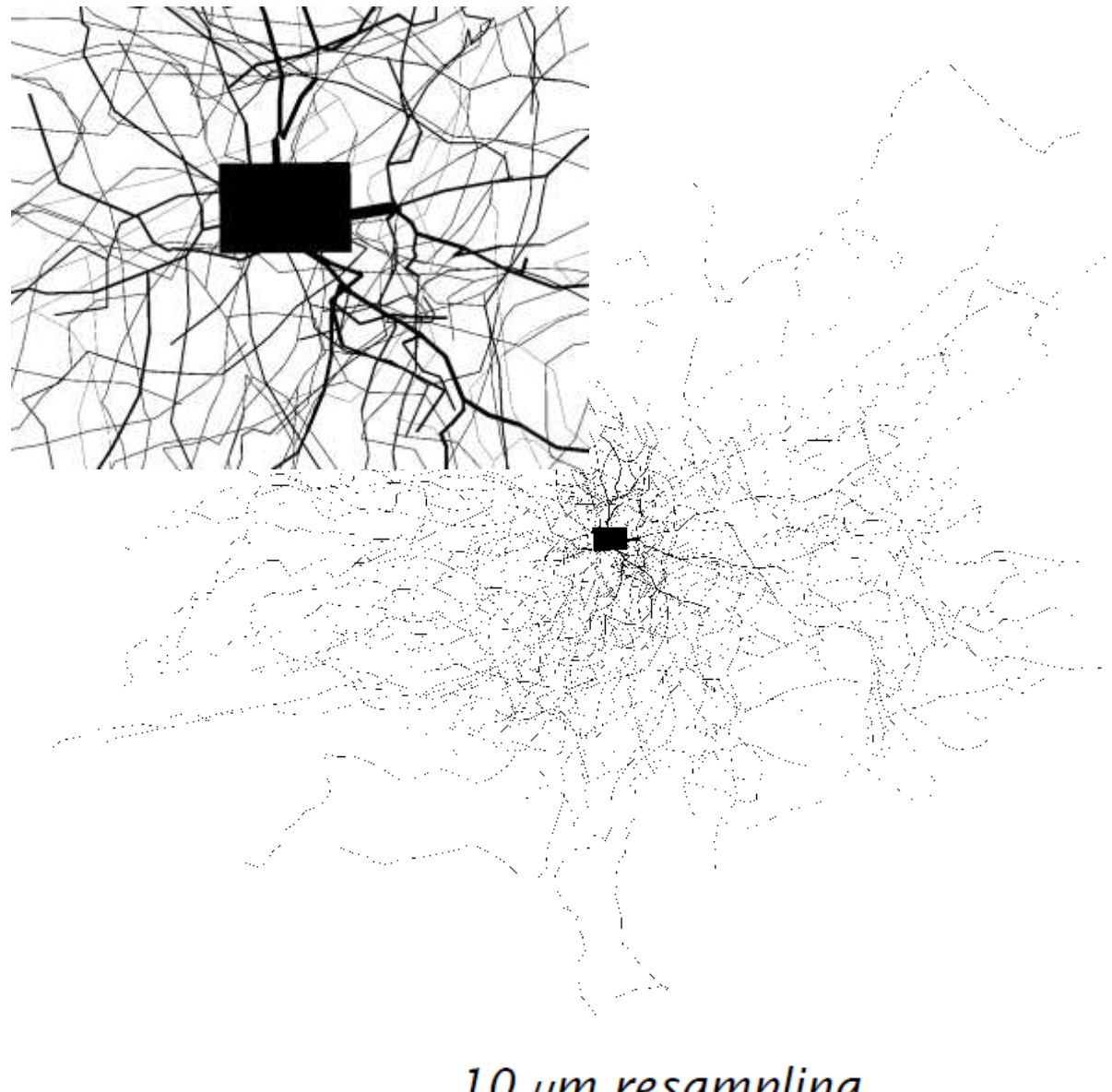
20 μm resampling





Origin

Tolias L5 neurogliaform



10 μm resampling

Current issues and next plan

- Based on the parameters extracted from the SWC file, it may be too detailed. Further integration of parameters is needed, while also attempting to construct a feature matrix using bitmap method for modeling.
- There are certain systematic differences in data from different laboratories, which need to be standardized.
- Testing the method of resampling is a priority. Since the total sample size is not large, direct division leads to excessively small testing samples.
- It is necessary to find a data division method suitable for small samples and retrain the model. After the construction of the model, the focus of the next stage will be on correlation analysis.

